POWER SYSTEM STABILITY AND CONTROL

P. KUNDUR

Vice-President, Power Engineering
Powertech Labs Inc., Surrey, British Columbia

Formerly Manager
Analytical Methods and Specialized Studies Department
Power System Planning Division, Ontario Hydro, Toronto

and

Adjunct Professor
Department of Electrical and Computer Engineering
University of Toronto, Toronto, Ontario

Edited by

Neal J. Balu
Mark G. Lauby
Power System Planning and Operations Program
Electrical Systems Division
Electric Power Research Institute
3412 Hillview Avenue
Palo Alto, California

McGraw-Hill, Inc.
New York San Francisco Washington, D.C. Auckland Bogotá
Caracas Lisbon London Madrid Mexico City Milan
Montreal New Delhi San Juan Singapore
Sydney Tokyo Toronto

Contents

PART II EQUIPMENT CHARACTERISTICS AND MODELLING

PART III SYSTEM STABILITY: physical aspects, analysis, and improvement

Foreword

To paraphrase the renowned electrical engineer, Charles Steinmetz, the North American interconnected power system is the largest and most complex machine ever devised by man. It is truly amazing that such a system has operated with a high degree of reliability for over a century.

The robustness of a power system is measured by the ability of the system to operate in a state of equilibrium under normal and perturbed conditions. Power system stability deals with the study of the behavior of power systems under conditions such as sudden changes in load or generation or short circuits on transmission lines. A power system is said to be stable if the interconnected generating units remain in synchronism.

The ability of a power system to maintain stability depends to a large extent on the controls available on the system to damp the electromechanical oscillations. Hence, the study and design of controls are very important.

Of all the complex phenomena on power systems, power system stability is the most intricate to understand and challenging to analyze. Electric power systems of the 21st century will present an even more formidable challenge as they are forced to operate closer to their stability limits.

I cannot think of a more qualified person than Dr. Prabha Kundur to write a book on power system stability and control. Dr. Kundur is an internationally recognized authority on power system stability. His expertise and practical experience in developing solutions to stability problems is second to none. Dr. Kundur not only has a thorough grasp of the fundamental concepts but also has worked on solving electric utility system stability problems worldwide. He has taught many courses, made excellent presentations at professional society and industry committee meetings,

and has written numerous technical papers on power system stability and control.

It gives me great pleasure to write the Foreword for this timely book, which I am confident will be of great value to practicing engineers and students in the field of power engineering.

Dr. Neal J. Balu
Program Manager
Power System Planning and Operations
Electrical Systems Division
Electric Power Research Institute

Preface

This book is concerned with understanding, modelling, analyzing, and mitigating power system stability and control problems. Such problems constitute very important considerations in the planning, design, and operation of modern power systems. The complexity of power systems is continually increasing because of the growth in interconnections and use of new technologies. At the same time, financial and regulatory constraints have forced utilities to operate the systems nearly at stability limits. These two factors have created new types of stability problems. Greater reliance is, therefore, being placed on the use of special control aids to enhance system security, facilitate economic design, and provide greater flexibility of system operation. In addition, advances in computer technology, numerical analysis, control theory, and equipment modelling have contributed to the development of improved analytical tools and better system-design procedures. The primary motivation for writing this book has been to describe these new developments and to provide a comprehensive treatment of the subject.

The text presented in this book draws together material on power system stability and control from many sources: graduate courses I have taught at the University of Toronto since 1979, several EPRI research projects (RP1208, RP2447, RP3040, RP3141, RP4000, RP849, and RP997) with which I have been closely associated, and a vast number of technical papers published by the IEEE, IEE, and CIGRE.

This book is intended to meet the needs of practicing engineers associated with the electric utility industry as well as those of graduate students and researchers. Books on this subject are at least 15 years old; some well-known books are 30 to 40 years old. In the absence of a comprehensive text, courses on power system stability

often tend to address narrow aspects of the subject with emphasis on special analytical techniques. Moreover, both the teaching staff and students do not have ready access to information on the practical aspects. Since the subject requires an understanding of a wide range of areas, practicing engineers just entering this field are faced with the formidable task of gathering the necessary information from widely scattered sources.

This book attempts to fill the gap by providing the necessary fundamentals, explaining the practical aspects, and giving an integrated treatment of the latest developments in modelling techniques and analytical tools. It is divided into three parts. Part I provides general background information in two chapters. Chapter 1 describes the structure of modern power systems and identifies different levels of control. Chapter 2 introduces the stability problem and provides basic concepts, definitions, and classification.

Part II of the book, comprising Chapters 3 to 11, is devoted to equipment characteristics and modelling. System stability is affected by the characteristics of every major element of the power system. A knowledge of the physical characteristics of the individual elements and their capabilities is essential for the understanding of system stability. The representation of these elements by means of appropriate mathematical models is critical to the analysis of stability. Chapters 3 to 10 are devoted to generators, excitation systems, prime movers, ac and dc transmission, and system loads. Chapter 11 describes the principles of active power and reactive power control and develops models for the control equipment.

Part III, comprising Chapters 12 to 17, considers different categories of power system stability. Emphasis is placed on physical understanding of many facets of the stability phenomena. Methods of analysis along with control measures for mitigation of stability problems are described in detail.

The notions of power system stability and power system control are closely related. The overall controls in a power system are highly distributed in a hierarchical structure. System stability is strongly influenced by these controls.

In each chapter, the theory is developed from simple beginnings and is gradually evolved so that it can be applied to complex practical situations. This is supplemented by a large number of illustrative examples. Wherever appropriate, historical perspectives and past experiences are highlighted.

Because this is the first edition, it is likely that some aspects of the subject may not be adequately covered. It is also likely that there may be some errors, typographical or otherwise. I welcome feedback on such errors as well as suggestions for improvements in the event that a second edition should be published.

I am indebted to many people who assisted me in the preparation of this book. Baofu Gao and Sainath Moorty helped me with many of the calculations and computer simulations included in the book. Kip Morison, Solomon Yirga, Meir Klein, Chi Tang, and Deepa Kundur also helped me with some of the results presented.

Atef Morched, Kip Morison, Ernie Neudorf, Graham Rogers, David Wong, Hamid Hamadanizadeh, Behnam Danai, Saeed Arabi, and Lew Rubino reviewed various chapters of the book and provided valuable comments.

David Lee reviewed Chapters 8 and 9 and provided valuable comments and suggestions. I have worked very closely with Mr. Lee for the last 22 years on a number of complex power system stability-related problems; the results of our joint effort are reflected in various parts of the book.

Carson Taylor reviewed the manuscript and provided many helpful suggestions for improving the text. In addition, many stimulating discussions I have had with Mr. Taylor, Dr. Charles Concordia, and with Mr. Yakout Mansour helped me develop a better perspective of current and future needs of power system stability analysis.

Patti Scott and Christine Hebscher edited the first draft of the manuscript. Janet Kibblewhite edited the final draft and suggested many improvements.

I am deeply indebted to Lei Wang and his wife, Xiaolu Meng, for their outstanding work in the preparation of the manuscript, including the illustrations.

I wish to take this opportunity to express my gratitude to Mr. Paul L. Dandeno for the encouragement he gave me and the confidence he showed in me during the early part of my career at Ontario Hydro. It is because of him that I joined the electric utility industry and then ventured into the many areas of power system dynamic performance covered in this book.

I am grateful to the Electric Power Research Institute for sponsoring this book. In particular, I am thankful to Dr. Neal Balu and Mr. Mark Lauby for their inspiration and support. Mark Lauby also reviewed the manuscript and provided many helpful suggestions.

I wish to express my appreciation to Liz Doherty and Patty Jones for helping me with the correspondence and other business matters related to this book.

Finally, I wish to thank my wife, Geetha Kundur, for her unfailing support and patience during the many months I worked on this book.

Prabha Shankar Kundur

PART I

GENERAL BACKGROUND

Chapter 1

General Characteristics of Modern Power Systems

The purpose of this introductory chapter is to provide a general description of electric power systems beginning with a historical sketch of their evolution. The basic characteristics and structure of modern power systems are then identified. The performance requirements of a properly designed power system and the various levels of controls used to meet these requirements are also described.

This chapter, together with the next, provides general background information and lays the groundwork for the remainder of the book.

1.1 EVOLUTION OF ELECTRIC POWER SYSTEMS

The commercial use of electricity began in the late 1870s when arc lamps were used for lighthouse illumination and street lighting.

The first complete electric power system (comprising a generator, cable, fuse, meter, and loads) was built by Thomas Edison - the historic Pearl Street Station in New York City which began operation in September 1882. This was a dc system consisting of a steam-engine-driven dc generator supplying power to 59 customers within an area roughly 1.5 km in radius. The load, which consisted entirely of incandescent lamps, was supplied at 110 V through an underground cable system. Within a few years similar systems were in operation in most large cities throughout the world. With the development of motors by Frank Sprague in 1884, motor loads were added to such systems. This was the beginning of what would develop into one of the largest industries in the world.

In spite of the initial widespread use of dc systems, they were almost completely superseded by ac systems. By 1886, the limitations of dc systems were becoming increasingly apparent. They could deliver power only a short distance from the generators. To keep transmission power losses (RI^2) and voltage drops to acceptable levels, voltage levels had to be high for long-distance power transmission. Such high voltages were not acceptable for generation and consumption of power; therefore, a convenient means for voltage transformation became a necessity.

The development of the transformer and ac transmission by L. Gaulard and J.D. Gibbs of Paris, France, led to ac electric power systems. George Westinghouse secured rights to these developments in the United States. In 1886, William Stanley, an associate of Westinghouse, developed and tested a commercially practical transformer and ac distribution system for 150 lamps at Great Barrington, Massachusetts. In 1889, the first ac transmission line in North America was put into operation in Oregon between Willamette Falls and Portland. It was a single-phase line transmitting power at 4,000 V over a distance of 21 km.

With the development of polyphase systems by Nikola Tesla, the ac system became even more attractive. By 1888, Tesla held several patents on ac motors, generators, transformers, and transmission systems. Westinghouse bought the patents to these early inventions, and they formed the basis of the present-day ac systems.

In the 1890s, there was considerable controversy over whether the electric utility industry should be standardized on dc or ac. There were passionate arguments between Edison, who advocated dc, and Westinghouse, who favoured ac. By the turn of the century, the ac system had won out over the dc system for the following reasons:

- Voltage levels can be easily transformed in ac systems, thus providing the flexibility for use of different voltages for generation, transmission, and consumption.

- AC generators are much simpler than dc generators.

- AC motors are much simpler and cheaper than dc motors.

The first three-phase line in North America went into operation in 1893 - a 2,300 V, 12 km line in southern California. Around this time, ac was chosen at Niagara Falls because dc was not practical for transmitting power to Buffalo, about 30 km away. This decision ended the ac versus dc controversy and established victory for the ac system.

In the early period of ac power transmission, frequency was not standardized. Many different frequencies were in use: 25, 50, 60, 125, and 133 Hz. This posed a problem for interconnection. Eventually 60 Hz was adopted as standard in North America, although many other countries use 50 Hz.

The increasing need for transmitting larger amounts of power over longer distances created an incentive to use progressively higher voltage levels. The early ac

systems used 12, 44, and 60 kV (RMS line-to-line). This rose to 165 kV in 1922, 220 kV in 1923, 287 kV in 1935, 330 kV in 1953, and 500 kV in 1965. Hydro Quebec energized its first 735 kV in 1966, and 765 kV was introduced in the United States in 1969.

To avoid the proliferation of an unlimited number of voltages, the industry has standardized voltage levels. The standards are 115, 138, 161, and 230 kV for the high voltage (HV) class, and 345, 500 and 765 kV for the extra-high voltage (EHV) class [1,2].

With the development of mercury arc valves in the early 1950s, high voltage dc (HVDC) transmission systems became economical in special situations. The HVDC transmission is attractive for transmission of large blocks of power over long distances. The cross-over point beyond which dc transmission may become a competitive alternative to ac transmission is around 500 km for overhead lines and 50 km for underground or submarine cables. HVDC transmission also provides an asynchronous link between systems where ac interconnection would be impractical because of system stability considerations or because nominal frequencies of the systems are different. The first modern commercial application of HVDC transmission occurred in 1954 when the Swedish mainland and the island of Gotland were interconnected by a 96 km submarine cable.

With the advent of thyristor valve converters, HVDC transmission became even more attractive. The first application of an HVDC system using thyristor valves was at Eel River in 1972 - a back-to-back scheme providing an asynchronous tie between the power systems of Quebec and New Brunswick. With the cost and size of conversion equipment decreasing and its reliability increasing, there has been a steady increase in the use of HVDC transmission.

Interconnection of neighbouring utilities usually leads to improved system security and economy of operation. Improved security results from the mutual emergency assistance that the utilities can provide. Improved economy results from the need for less generating reserve capacity on each system. In addition, the interconnection permits the utilities to make economy transfers and thus take advantage of the most economical sources of power. These benefits have been recognized from the beginning and interconnections continue to grow. Almost all the utilities in the United States and Canada are now part of one interconnected system. The result is a very large system of enormous complexity. The design of such a system and its secure operation are indeed challenging problems.

1.2 STRUCTURE OF THE POWER SYSTEM

Electric power systems vary in size and structural components. However, they all have the same basic characteristics:

- Are comprised of three-phase ac systems operating essentially at constant voltage. Generation and transmission facilities use three-phase equipment.

Industrial loads are invariably three-phase; single-phase residential and commercial loads are distributed equally among the phases so as to effectively form a balanced three-phase system.

- Use synchronous machines for generation of electricity. Prime movers convert the primary sources of energy (fossil, nuclear, and hydraulic) to mechanical energy that is, in turn, converted to electrical energy by synchronous generators.

- Transmit power over significant distances to consumers spread over a wide area. This requires a transmission system comprising subsystems operating at different voltage levels.

Figure 1.1 illustrates the basic elements of a modern power system. Electric power is produced at generating stations (GS) and transmitted to consumers through a complex network of individual components, including transmission lines, transformers, and switching devices.

It is common practice to classify the transmission network into the following subsystems:

1. Transmission system
2. Subtransmission system
3. Distribution system

The *transmission system* interconnects all major generating stations and main load centres in the system. It forms the backbone of the integrated power system and operates at the highest voltage levels (typically, 230 kV and above). The generator voltages are usually in the range of 11 to 35 kV. These are stepped up to the transmission voltage level, and power is transmitted to transmission substations where the voltages are stepped down to the subtransmission level (typically, 69 kV to 138 kV). The generation and transmission subsystems are often referred to as the *bulk power system.*

The *subtransmission system* transmits power in smaller quantities from the transmission substations to the distribution substations. Large industrial customers are commonly supplied directly from the subtransmission system. In some systems, there is no clear demarcation between subtransmission and transmission circuits. As the system expands and higher voltage levels become necessary for transmission, the older transmission lines are often relegated to subtransmission function.

The *distribution system* represents the final stage in the transfer of power to the individual customers. The primary distribution voltage is typically between 4.0 kV and 34.5 kV. Small industrial customers are supplied by primary feeders at this voltage level. The secondary distribution feeders supply residential and commercial customers at 120/240 V.

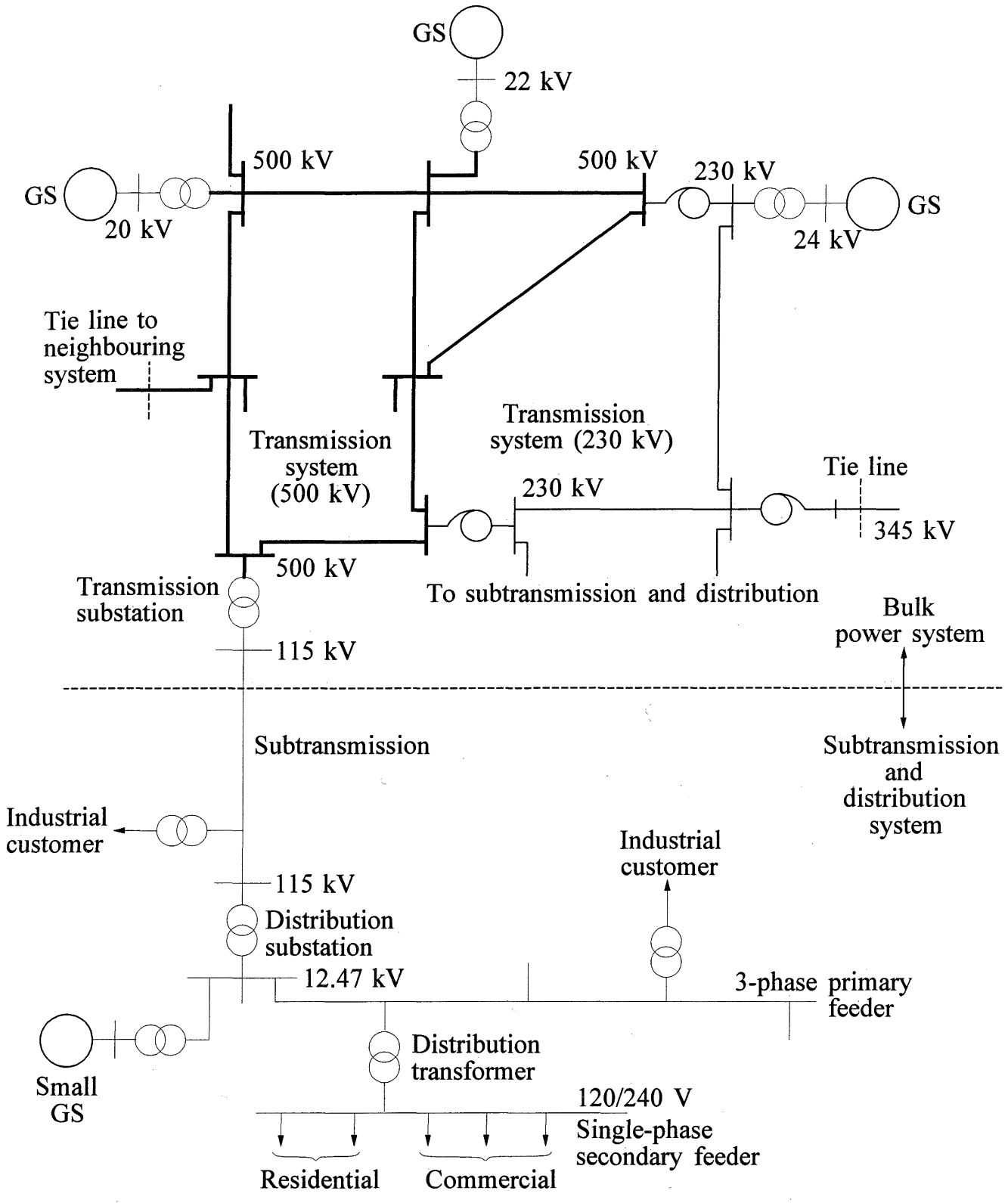

Figure 1.1 Basic elements of a power system

Small generating plants located near the load are often connected to the subtransmission or distribution system directly.

Interconnections to neighbouring power systems are usually formed at the transmission system level.

The overall system thus consists of multiple generating sources and several layers of transmission networks. This provides a high degree of structural redundancy that enables the system to withstand unusual contingencies without service disruption to the consumers.

1.3 POWER SYSTEM CONTROL

The function of an electric power system is to convert energy from one of the naturally available forms to the electrical form and to transport it to the points of consumption. Energy is seldom consumed in the electrical form but is rather converted to other forms such as heat, light, and mechanical energy. The advantage of the electrical form of energy is that it can be transported and controlled with relative ease and with a high degree of efficiency and reliability. A properly designed and operated power system should, therefore, meet the following fundamental requirements:

1. The system must be able to meet the continually changing load demand for active and reactive power. Unlike other types of energy, electricity cannot be conveniently stored in sufficient quantities. Therefore, adequate "spinning" reserve of active and reactive power should be maintained and appropriately controlled at all times.

2. The system should supply energy at minimum cost and with minimum ecological impact.

3. The "quality" of power supply must meet certain minimum standards with regard to the following factors:

   (a) constancy of frequency;

   (b) constancy of voltage; and

   (c) level of reliability.

Several levels of controls involving a complex array of devices are used to meet the above requirements. These are depicted in Figure 1.2 which identifies the various subsystems of a power system and the associated controls. In this overall structure, there are controllers operating directly on individual system elements. In a generating unit these consist of prime mover controls and excitation controls. The prime mover controls are concerned with speed regulation and control of energy supply system variables such as boiler pressures, temperatures, and flows. The function of the

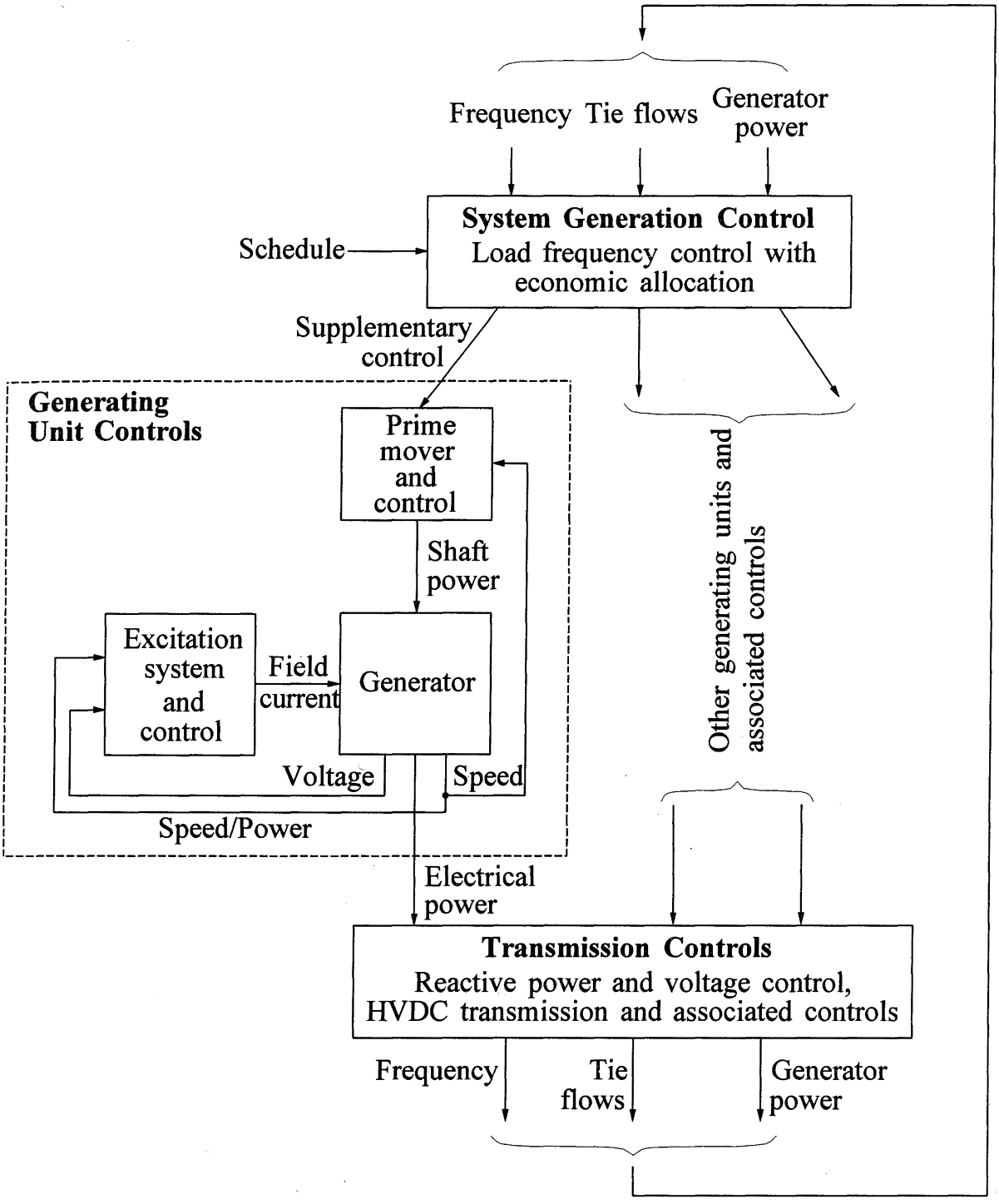

Figure 1.2 Subsystems of a power system and associated controls

excitation control is to regulate generator voltage and reactive power output. The desired MW outputs of the individual generating units are determined by the system-generation control.

The primary purpose of the system-generation control is to balance the total system generation against system load and losses so that the desired frequency and power interchange with neighbouring systems (tie flows) is maintained.

The transmission controls include power and voltage control devices, such as static var compensators, synchronous condensers, switched capacitors and reactors, tap-changing transformers, phase-shifting transformers, and HVDC transmission controls.

The controls described above contribute to the satisfactory operation of the power system by maintaining system voltages and frequency and other system variables within their acceptable limits. They also have a profound effect on the dynamic performance of the power system and on its ability to cope with disturbances.

The control objectives are dependent on the operating state of the power system. Under normal conditions, the control objective is to operate as efficiently as possible with voltages and frequency close to nominal values. When an abnormal condition develops, new objectives must be met to restore the system to normal operation.

Major system failures are rarely the result of a single catastrophic disturbance causing collapse of an apparently secure system. Such failures are usually brought about by a combination of circumstances that stress the network beyond its capability. Severe natural disturbances (such as a tornado, severe storm, or freezing rain), equipment malfunction, human error, and inadequate design combine to weaken the power system and eventually lead to its breakdown. This may result in cascading outages that must be contained within a small part of the system if a major blackout is to be prevented.

Operating states of a power system and control strategies [3,4]

For purposes of analyzing power system security and designing appropriate control systems, it is helpful to conceptually classify the system-operating conditions into five states: normal, alert, emergency, *in extremis*, and restorative. Figure 1.3 depicts these operating states and the ways in which transition can take place from one state to another.

In the *normal state*, all system variables are within the normal range and no equipment is being overloaded. The system operates in a secure manner and is able to withstand a contingency without violating any of the constraints.

The system enters the *alert state* if the security level falls below a certain limit of adequacy, or if the possibility of a disturbance increases because of adverse weather conditions such as the approach of severe storms. In this state, all system variables are still within the acceptable range and all constraints are satisfied. However, the system has been weakened to a level where a contingency may cause

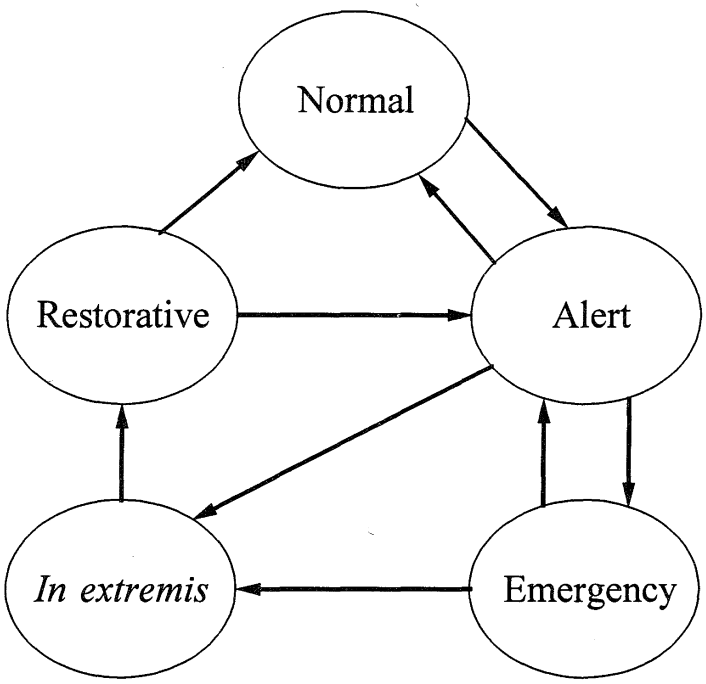

Figure 1.3 Power system operating states

an overloading of equipment that places the system in an emergency state. If the disturbance is very severe, the *in extremis* (or extreme emergency) state may result directly from the alert state.

Preventive action, such as generation shifting (security dispatch) or increased reserve, can be taken to restore the system to the normal state. If the restorative steps do not succeed, the system remains in the alert state.

The system enters the *emergency state* if a sufficiently severe disturbance occurs when the system is in the alert state. In this state, voltages at many buses are low and/or equipment loadings exceed short-term emergency ratings. The system is still intact and may be restored to the alert state by the initiating of emergency control actions: fault clearing, excitation control, fast-valving, generation tripping, generation run-back, HVDC modulation, and load curtailment.

If the above measures are not applied or are ineffective, the system is *in extremis*; the result is cascading outages and possibly a shut-down of a major portion of the system. Control actions, such as load shedding and controlled system separation, are aimed at saving as much of the system as possible from a widespread blackout.

The *restorative state* represents a condition in which control action is being taken to reconnect all the facilities and to restore system load. The system transits from this state to either the alert state or the normal state, depending on the system conditions.

Characterization of the system conditions into the five states as described above provides a framework in which control strategies can be developed and operator actions identified to deal effectively with each state.

For a system that has been disturbed and that has entered a degraded operating state, power system controls assist the operator in returning the system to a normal state. If the disturbance is small, power system controls by themselves may be able to achieve this task. However, if the disturbance is large, it is possible that operator actions such as generation rescheduling or element switching may be required for a return to the normal state.

The philosophy that has evolved to cope with the diverse requirements of system control comprises a hierarchial structure as shown in Figure 1.4. In this structure, there are controllers operating directly on individual system elements such as excitation systems, prime movers, boilers, transformer tap changers, and dc converters. There is usually some form of overall plant controller that coordinates the controls of closely linked elements. The plant controllers are in turn supervised by system controllers at the operating centres. The system-controller actions are coordinated by pool-level master controllers. The overall control system is thus highly distributed, and relies on many different types of telemetering and control signals. Supervisory Control and Data Acquisition (SCADA) systems provide information to indicate the system status. State estimation programs filter monitored data and provide an accurate picture of the system's condition. The human operator is an important link at various levels in this control hierarchy and at key locations on the system. The primary function of the operator is to monitor system performance and manage resources so as to ensure economic operation while maintaining the required quality

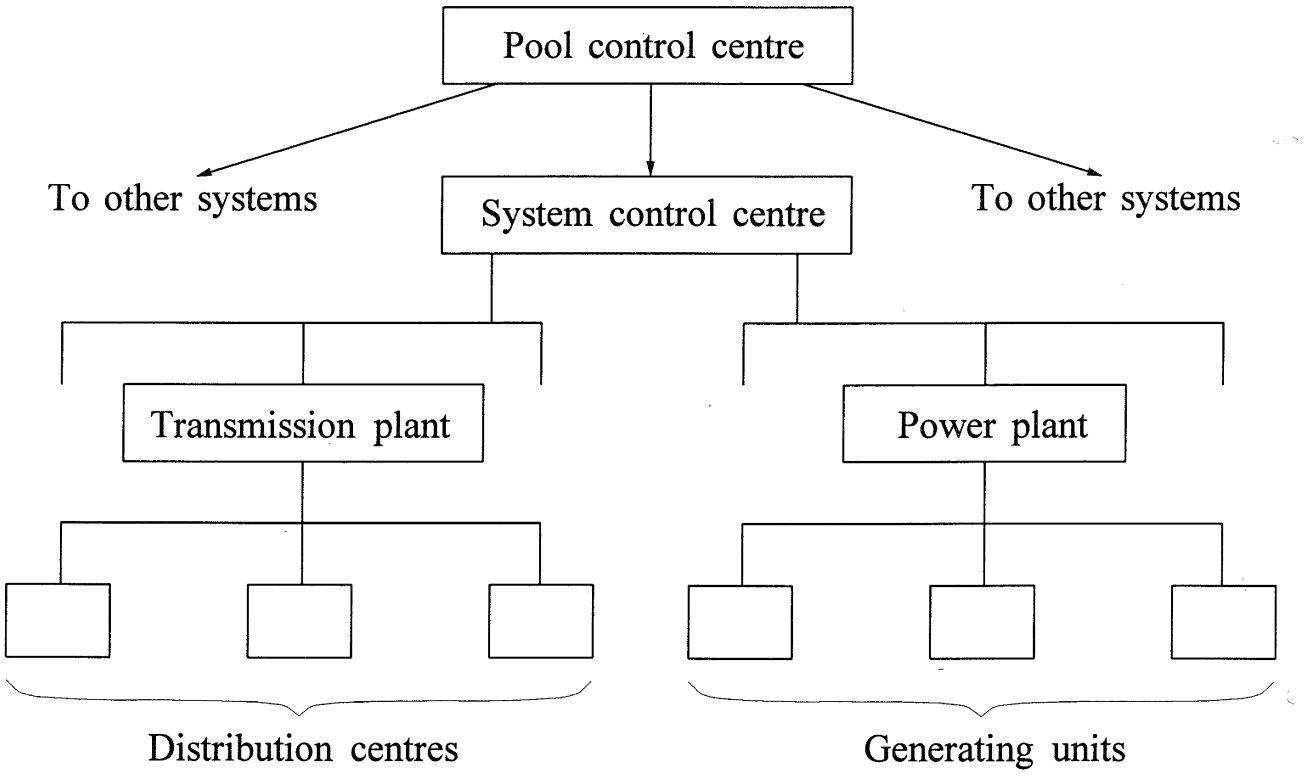

Figure 1.4 Power system control hierarchy

and reliability of power supply. During system emergencies, the operator plays a key role by coordinating related information from diverse sources and developing corrective strategies to restore the system to a more secure state of operation.

1.4 DESIGN AND OPERATING CRITERIA FOR STABILITY

For reliable service, a bulk electricity system must remain intact and be capable of withstanding a wide variety of disturbances. Therefore, it is essential that the system be designed and operated so that the more probable contingencies can be sustained with no loss of load (except that connected to the faulted element) and so that the most adverse possible contingencies do not result in uncontrolled, widespread and cascading power interruptions.

The November 1965 blackout in the northeastern part of the United States and Ontario had a profound impact on the electric utility industry, particularly in North America. Many questions were raised relating to design concepts and planning criteria. These led to the formation of the National Electric Reliability Council in 1968. The name was later changed to the North American Electric Reliability Council (NERC). Its purpose is to augment the reliability and adequacy of bulk power supply in the electricity systems of North America. NERC is composed of nine regional reliability councils and encompasses virtually all the power systems in the United States and Canada. Reliability criteria for system design and operation have been established by each regional council. Since differences exist in geography, load pattern, and power sources, criteria for the various regions differ to some extent [5].

Design and operating criteria play an essential role in preventing major system disturbances following severe contingencies. The use of criteria ensures that, for all frequently occurring contingencies, the system will, at worst, transit from the normal state to the alert state, rather than to a more severe state such as the emergency state or the *in extremis* state. When the alert state is entered following a contingency, operators can take actions to return the system to the normal state.

The following example of design and operating criteria related to system stability is based on those of the Northeast Power Coordinating Council (NPCC) [6]. It does not attempt to provide an exact reproduction of the NPCC criteria but gives an indication of the types of contingencies considered for stability assessment.

Normal design contingencies

The criteria require that the stability of the bulk power system be maintained during and after the most severe of the contingencies specified below, with due regard to reclosing facilities. These contingencies are selected on the basis that they have a significant probability of occurrence given the large number of elements comprising the power system.

The normal design contingencies include the following:

(a) A permanent three-phase fault on any generator, transmission circuit, transformer or bus section, with normal fault clearing and with due regard to reclosing facilities.

(b) Simultaneous permanent phase-to-ground faults on different phases of each of two adjacent transmission circuits on a multiple-circuit tower, cleared in normal time.

(c) A permanent phase-to-ground fault on any transmission circuit, transformer, or bus section with delayed clearing because of malfunction of circuit breakers, relay, or signal channel.

(d) Loss of any element without a fault.

(e) A permanent phase-to-ground fault on a circuit breaker, cleared in normal time.

(f) Simultaneous permanent loss of both poles of a dc bipolar facility.

The criteria require that, following any of the above contingencies, the stability of the system be maintained, and voltages and line and equipment loadings be within applicable limits.

These requirements apply to the following two basic conditions:

(1) All facilities in service.

(2) A critical generator, transmission circuit, or transformer out of service, assuming that the area generation and power flows are adjusted between outages by use of ten minute reserve.

Extreme contingency assessment

The extreme contingency assessment recognizes that the interconnected bulk power system can be subjected to events that exceed in severity the normal design contingencies. The objective is to determine the effects of extreme contingencies on system performance in order to obtain an indication of system strength and to determine the extent of a widespread system disturbance even though extreme contingencies do have very low probabilities of occurrence. After an analysis and assessment of extreme contingencies, measures are to be utilized, where appropriate, to reduce the frequency of occurrence of such contingencies or to mitigate the consequences that are indicated as a result of simulating for such contingencies.

The extreme contingencies include the following:

(a) Loss of the entire capability of a generating station.

(b) Loss of all lines emanating from a generating station, switching station or substation.

(c) Loss of all transmission circuits on a common right-of-way.

(d) A permanent three-phase fault on any generator, transmission circuit, transformer, or bus section, with delayed fault clearing and with due regard to reclosing facilities.

(e) The sudden dropping of a large-load or major-load centre.

(f) The effect of severe power swings arising from disturbances outside the NPCC interconnected systems.

(g) Failure or misoperation of a special protection system, such as a generation rejection, load rejection, or transmission cross-tripping scheme.

System design for stability

The design of a large interconnected system to ensure stable operation at minimum cost is a very complex problem. The economic gains to be realized through the solution to this problem are enormous. From a control theory point of view, the power system is a very high-order multivariable process, operating in a constantly changing environment. Because of the high dimensionality and complexity of the system, it is essential to make simplifying assumptions and to analyze specific problems using the right degree of detail of system representation. This requires a good grasp of the characteristics of the overall system as well as of those of its individual elements.

The power system is a highly nonlinear system whose dynamic performance is influenced by a wide array of devices with different response rates and characteristics. System stability must be viewed not as a single problem, but rather in terms of its different aspects. The next chapter describes the different forms of power system stability problems.

Characteristics of virtually every major element of the power system have an effect on system stability. A knowledge of these characteristics is essential for the understanding and study of power system stability. Therefore, equipment characteristics and modelling will be discussed in Part II. Intricacies of the physical aspects of various categories of the system stability, methods of their analysis, and special measures for enhancing stability performance of the power system will be presented in Part III.

REFERENCES

[1] H.M. Rustebakke (editor), *Electric Utility Systems and Practices*, John Wiley & Sons, 1983.

[2] C.A. Gross, *Power System Analysis*, Second Edition, John Wiley & Sons, 1986.

[3] L.H. Fink and K. Carlsen, "Operating under Stress and Strain," *IEEE Spectrum,* pp. 48-53, March 1978.

[4] EPRI Report EL 6360-L, "Dynamics of Interconnected Power Systems: A Tutorial for System Dispatchers and Plant Operators," Final Report of Project 2473-15, prepared by Power Technologies Inc., May 1989.

[5] IEEE Special Publication 77 CH 1221-1-PWR, *Symposium on Reliability Criteria for System Dynamic Performance*, 1977.

[6] Northeast Power Coordinating Council, "Basic Criteria for Design and Operation of Interconnected Power Systems," October 26, 1990 revision.

Chapter 2

Introduction to the Power System Stability Problem

This chapter presents a general introduction to the power system stability problem including physical concepts, classification, and definition of related terms. Analysis of elementary power system configurations by means of idealized models illustrates some of the fundamental stability properties of power systems. In addition, a historical review of the emergence of different forms of stability problems as power systems evolved and of the developments in the associated methods of analysis is presented. The objective is to provide an overview of the power system stability phenomena and to lay a foundation based on relatively simple physical reasoning. This will help prepare for a detailed treatment of the various aspects of the subject in subsequent chapters.

2.1 BASIC CONCEPTS AND DEFINITIONS

Power system stability may be broadly defined as that property of a power system that enables it to remain in a state of operating equilibrium under normal operating conditions and to regain an acceptable state of equilibrium after being subjected to a disturbance.

Instability in a power system may be manifested in many different ways depending on the system configuration and operating mode. Traditionally, the stability problem has been one of maintaining synchronous operation. Since power systems

rely on synchronous machines for generation of electrical power, a necessary condition for satisfactory system operation is that all synchronous machines remain in synchronism or, colloquially, "in step." This aspect of stability is influenced by the dynamics of generator rotor angles and power-angle relationships.

Instability may also be encountered without loss of synchronism. For example, a system consisting of a synchronous generator feeding an induction motor load through a transmission line can become unstable because of the collapse of load voltage. Maintenance of synchronism is not an issue in this instance; instead, the concern is stability and control of voltage. This form of instability can also occur in loads covering an extensive area supplied by a large system.

In the evaluation of stability the concern is the behaviour of the power system when subjected to a transient *disturbance*. The disturbance may be small or large. Small disturbances in the form of load changes take place continually, and the system adjusts itself to the changing conditions. The system must be able to operate satisfactorily under these conditions and successfully supply the maximum amount of load. It must also be capable of surviving numerous disturbances of a severe nature, such as a short-circuit on a transmission line, loss of a large generator or load, or loss of a tie between two subsystems. The system response to a disturbance involves much of the equipment. For example, a short-circuit on a critical element followed by its isolation by protective relays will cause variations in power transfers, machine rotor speeds, and bus voltages; the voltage variations will actuate both generator and transmission system voltage regulators; the speed variations will actuate prime mover governors; the change in tie line loadings may actuate generation controls; the changes in voltage and frequency will affect loads on the system in varying degrees depending on their individual characteristics. In addition, devices used to protect individual equipment may respond to variations in system variables and thus affect the system performance. In any given situation, however, the responses of only a limited amount of equipment may be significant. Therefore, many assumptions are usually made to simplify the problem and to focus on factors influencing the specific type of stability problem. The understanding of stability problems is greatly facilitated by the classification of stability into various categories.

The following sections will explore different forms of power system instability and associated concepts by considering, where appropriate, simple power system configurations. Analysis of such systems using idealized models will help identify fundamental properties of each form of stability problem.

2.1.1 Rotor Angle Stability

Rotor angle stability is the ability of interconnected synchronous machines of a power system to remain in synchronism. The stability problem involves the study of the electromechanical oscillations inherent in power systems. A fundamental factor in this problem is the manner in which the power outputs of synchronous machines vary as their rotors oscillate. A brief discussion of synchronous machine characteristics is helpful as a first step in developing the related basic concepts.

Synchronous machine characteristics

The characteristics and modelling of synchronous machines will be covered in considerable detail in Chapters 3, 4, and 5. Here discussion is limited to the basic characteristics associated with synchronous operation.

A synchronous machine has two essential elements: the field and the armature. Normally, the field is on the rotor and the armature is on the stator. The field winding is excited by direct current. When the rotor is driven by a prime mover (turbine), the rotating magnetic field of the field winding induces alternating voltages in the three-phase armature windings of the stator. The frequency of the induced alternating voltages and of the resulting currents that flow in the stator windings when a load is connected depends on the speed of the rotor. The frequency of the stator electrical quantities is thus synchronized with the rotor mechanical speed: hence the designation "synchronous machine."

When two or more synchronous machines are interconnected, the stator voltages and currents of all the machines must have the same frequency and the rotor mechanical speed of each is synchronized to this frequency. Therefore, the rotors of all interconnected synchronous machines must be in synchronism.

The physical arrangement (spatial distribution) of the stator armature windings is such that the time-varying alternating currents flowing in the three-phase windings produce a rotating magnetic field that, under steady-state operation, rotates at the same speed as the rotor (see Chapter 3, Section 3.1.3). The stator and rotor fields react with each other and an electromagnetic torque results from the tendency of the two fields to align themselves. In a generator, this electromagnetic torque opposes rotation of the rotor, so that mechanical torque must be applied by the prime mover to sustain rotation. The electrical torque (or power) output of the generator is changed only by changing the mechanical torque input by the prime mover. The effect of increasing the mechanical torque input is to advance the rotor to a new position relative to the revolving magnetic field of the stator. Conversely, a reduction of mechanical torque or power input will retard the rotor position. Under steady-state operating conditions, the rotor field and the revolving field of the stator have the same speed. However, there is an angular separation between them depending on the electrical torque (or power) output of the generator.

In a synchronous motor, the roles of electrical and mechanical torques are reversed compared to those in a generator. The electromagnetic torque sustains rotation while mechanical load opposes rotation. The effect of increasing the mechanical load is to retard the rotor position with respect to the revolving field of the stator.

In the above discussion, the terms *torque* and *power* have been used interchangeably. This is common practice in the power system stability literature, since the average rotational velocity of the machines is constant even though there may be small momentary excursions above and below synchronous speed. The per unit values of torque and power are, in fact, very nearly equal.

Power versus angle relationship

An important characteristic that has a bearing on power system stability is the relationship between interchange power and angular positions of the rotors of synchronous machines. This relationship is highly nonlinear. To illustrate this let us consider the simple system shown in Figure 2.1(a). It consists of two synchronous machines connected by a transmission line having an inductive reactance X_L but negligible resistance and capacitance. Let us assume that machine 1 represents a generator feeding power to a synchronous motor represented by machine 2.

The power transferred from the generator to the motor is a function of angular separation (δ) between the rotors of the two machines. This angular separation is due to three components: generator internal angle δ_G (angle by which the generator rotor leads the revolving field of the stator); angular difference between the terminal voltages of the generator and motor (angle by which the stator field of the generator leads that of the motor); and the internal angle of the motor (angle by which the rotor lags the revolving stator field). Figure 2.1(b) shows a model of the system that can be used to determine the power versus angle relationship. A simple model comprising an internal voltage behind an effective reactance is used to represent each synchronous machine. The value of the machine reactance used depends on the purpose of the study. For analysis of steady-state performance, it is appropriate to use the synchronous reactance with the internal voltage equal to the excitation voltage. The basis for such a model and the approximations associated with it are presented in Chapter 3.

A phasor diagram identifying the relationships between generator and motor voltages is shown in Figure 2.1(c). The power transferred from the generator to the motor is given by

$$P = \frac{E_G E_M}{X_T} \sin\delta \tag{2.1}$$

where

$$X_T = X_G + X_L + X_M$$

The corresponding power versus angle relationship is plotted in Figure 2.1(d). With the somewhat idealized models used for representing the synchronous machines, the power varies as a sine of the angle: a highly nonlinear relationship. With more accurate machine models including the effects of automatic voltage regulators, the variation in power with angle would deviate significantly from the sinusoidal relationship; however, the general form would be similar. When the angle is zero, no power is transferred. As the angle is increased, the power transfer increases up to a maximum. After a certain angle, nominally 90°, a further increase in angle results in a decrease in power transferred. There is thus a maximum steady-state power that can be transmitted between the two machines. The magnitude of the maximum power is

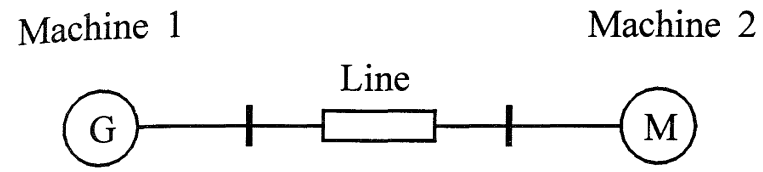

(a) Single-line diagram

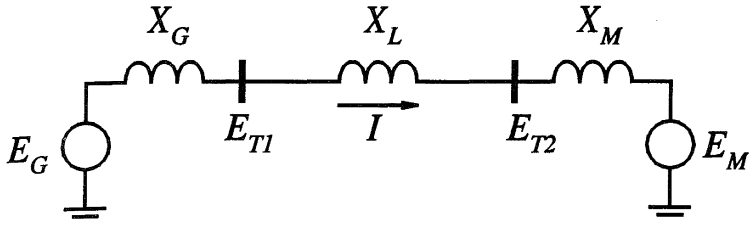

(b) Idealized model

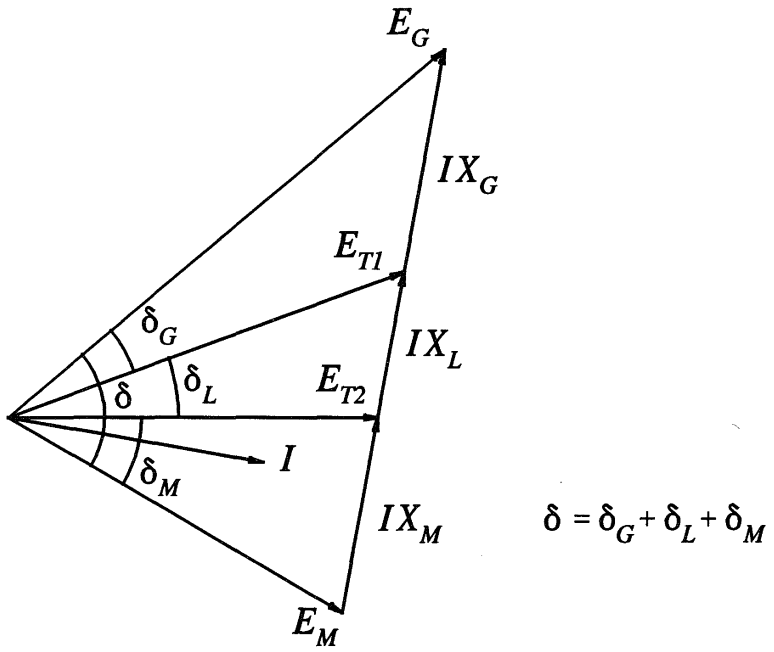

(c) Phasor diagram

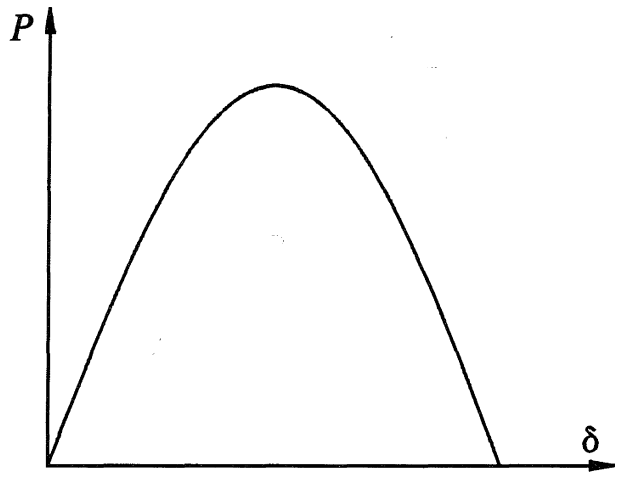

(d) Power-angle curve

Figure 2.1 Power transfer characteristic of a two-machine system

directly proportional to the machine internal voltages and inversely proportional to the reactance between the voltages, which includes reactance of the transmission line connecting the machines and the reactances of the machines.

When there are more than two machines, their relative angular displacements affect the interchange of power in a similar manner. However, limiting values of power transfers and angular separation are a complex function of generation and load distribution. An angular separation of 90° between any two machines (the nominal limiting value for a two-machine system) in itself has no particular significance.

The stability phenomena

Stability is a condition of equilibrium between opposing forces. The mechanism by which interconnected synchronous machines maintain synchronism with one another is through restoring forces, which act whenever there are forces tending to accelerate or decelerate one or more machines with respect to other machines. Under steady-state conditions, there is equilibrium between the input mechanical torque and the output electrical torque of each machine, and the speed remains constant. If the system is perturbed this equilibrium is upset, resulting in acceleration or deceleration of the rotors of the machines according to the laws of motion of a rotating body. If one generator temporarily runs faster than another, the angular position of its rotor relative to that of the slower machine will advance. The resulting angular difference transfers part of the load from the slow machine to the fast machine, depending on the power-angle relationship. This tends to reduce the speed difference and hence the angular separation. The power-angle relationship, as discussed above, is highly nonlinear. Beyond a certain limit, an increase in angular separation is accompanied by a decrease in power transfer; this increases the angular separation further and leads to instability. For any given situation, the stability of the system depends on whether or not the deviations in angular positions of the rotors result in sufficient restoring torques.

When a synchronous machine loses synchronism or "falls out of step" with the rest of the system, its rotor runs at a higher or lower speed than that required to generate voltages at system frequency. The "slip" between rotating stator field (corresponding to system frequency) and the rotor field results in large fluctuations in the machine power output, current, and voltage; this causes the protection system to isolate the unstable machine from the system.

Loss of synchronism can occur between one machine and the rest of the system or between groups of machines. In the latter case synchronism may be maintained within each group after its separation from the others.

The synchronous operation of interconnected synchronous machines is in some ways analogous to several cars speeding around a circular track while joined to each other by elastic links or rubber bands. The cars represent the synchronous machine rotors and the rubber bands are analogous to transmission lines. When all the cars run side by side, the rubber bands remain intact. If force applied to one of the cars causes it to speed up temporarily, the rubber bands connecting it to the other cars will

stretch; this tends to slow down the faster car and speed up the other cars. A chain reaction results until all the cars run at the same speed once again. If the pull on one of the rubber bands exceeds its strength, it will break and one or more cars will pull away from the other cars.

With electric power systems, the change in electrical torque of a synchronous machine following a perturbation can be resolved into two components:

$$\Delta T_e = T_S \Delta\delta + T_D \Delta\omega \tag{2.2}$$

where

$T_S\Delta\delta$ is the component of torque change in phase with the rotor angle perturbation $\Delta\delta$ and is referred to as the *synchronizing torque* component; T_S is the synchronizing torque coefficient.

$T_D\Delta\omega$ is the component of torque in phase with the speed deviation $\Delta\omega$ and is referred to as the *damping torque* component; T_D is the damping torque coefficient.

System stability depends on the existence of both components of torque for each of the synchronous machines. Lack of sufficient synchronizing torque results in instability through an *aperiodic drift* in rotor angle. On the other hand, lack of sufficient damping torque results in *oscillatory instability.*

For convenience in analysis and for gaining useful insight into the nature of stability problems, it is usual to characterize the rotor angle stability phenomena in terms of the following two categories:

(a) *Small-signal (or small-disturbance) stability* is the ability of the power system to maintain synchronism under small disturbances. Such disturbances occur continually on the system because of small variations in loads and generation. The disturbances are considered sufficiently small for linearization of system equations to be permissible for purposes of analysis. Instability that may result can be of two forms: (i) steady increase in rotor angle due to lack of sufficient synchronizing torque, or (ii) rotor oscillations of increasing amplitude due to lack of sufficient damping torque. The nature of system response to small disturbances depends on a number of factors including the initial operating, the transmission system strength, and the type of generator excitation controls used. For a generator connected radially to a large power system, in the absence of automatic voltage regulators (i.e., with constant field voltage) the instability is due to lack of sufficient synchronizing torque. This results in instability through a non-oscillatory mode, as shown in Figure 2.2(a). With continuously acting voltage regulators, the small-disturbance stability problem is one of ensuring sufficient damping of system oscillations. Instability is normally through oscillations of increasing amplitude. Figure 2.2(b) illustrates

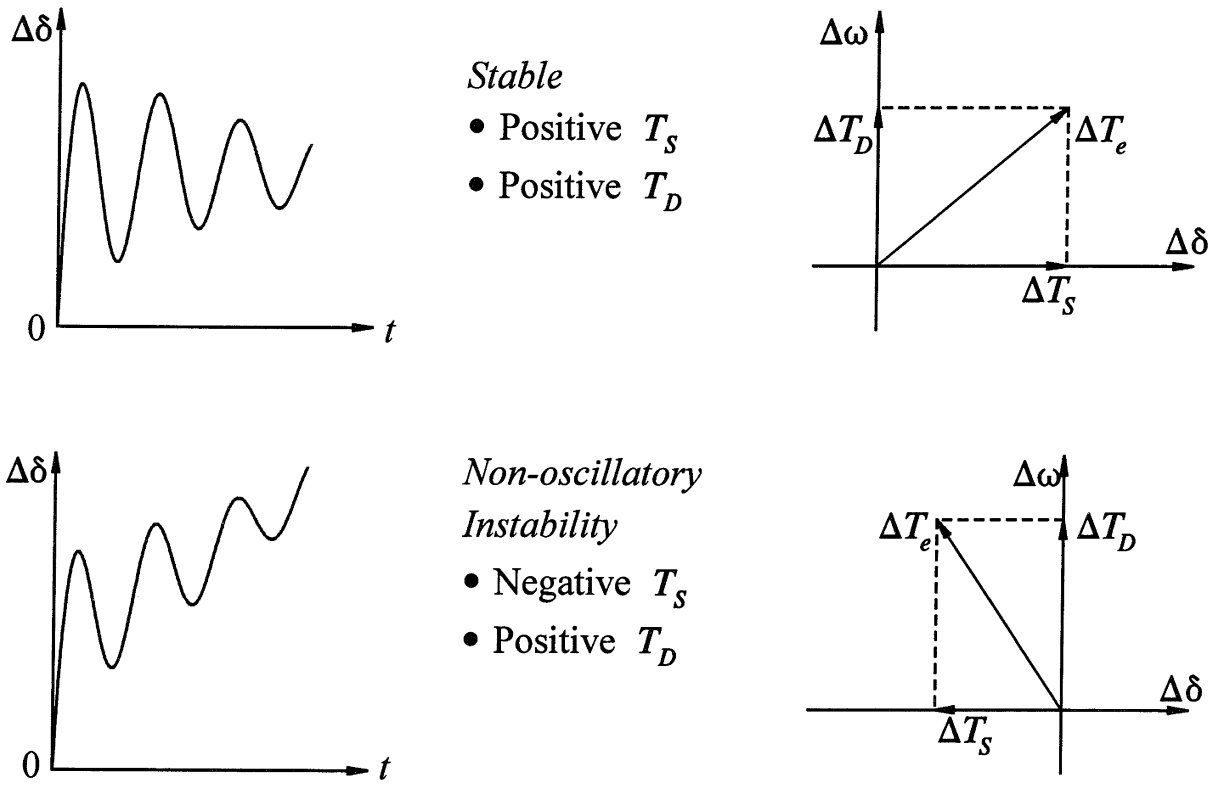

(a) With constant field voltage

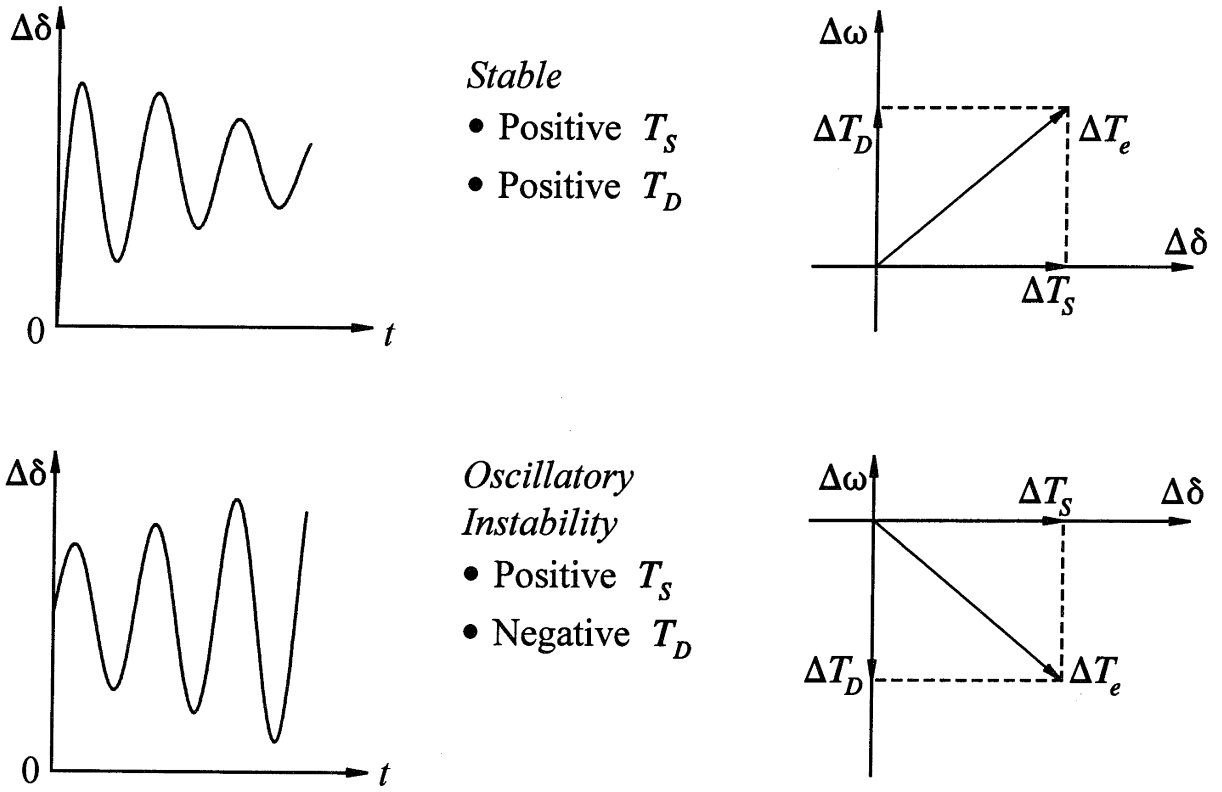

(b) With excitation control

Figure 2.2 Nature of small-disturbance response

the nature of generator response with automatic voltage regulators.

In today's practical power systems, small-signal stability is largely a problem of insufficient damping of oscillations. The stability of the following types of oscillations is of concern:

- *Local modes or machine-system modes* are associated with the swinging of units at a generating station with respect to the rest of the power system. The term *local* is used because the oscillations are localized at one station or a small part of the power system.
- *Interarea modes* are associated with the swinging of many machines in one part of the system against machines in other parts. They are caused by two or more groups of closely coupled machines being interconnected by weak ties.
- *Control modes* are associated with generating units and other controls. Poorly tuned exciters, speed governors, HVDC converters and static var compensators are the usual causes of instability of these modes.
- *Torsional modes* are associated with the turbine-generator shaft system rotational components. Instability of torsional modes may be caused by interaction with excitation controls, speed governors, HVDC controls, and series-capacitor-compensated lines.

(b) *Transient stability* is the ability of the power system to maintain synchronism when subjected to a severe transient disturbance. The resulting system response involves large excursions of generator rotor angles and is influenced by the nonlinear power-angle relationship. Stability depends on both the initial operating state of the system and the severity of the disturbance. Usually, the system is altered so that the post-disturbance steady-state operation differs from that prior to the disturbance.

Disturbances of widely varying degrees of severity and probability of occurrence can occur on the system. The system is, however, designed and operated so as to be stable for a selected set of contingencies. The contingencies usually considered are short-circuits of different types: phase-to-ground, phase-to-phase-to-ground, or three-phase. They are usually assumed to occur on transmission lines, but occasionally bus or transformer faults are also considered. The fault is assumed to be cleared by the opening of appropriate breakers to isolate the faulted element. In some cases, high-speed reclosure may be assumed.

Figure 2.3 illustrates the behaviour of a synchronous machine for stable and unstable situations. It shows the rotor angle responses for a stable case and for two unstable cases. In the stable case (Case 1), the rotor angle increases to a

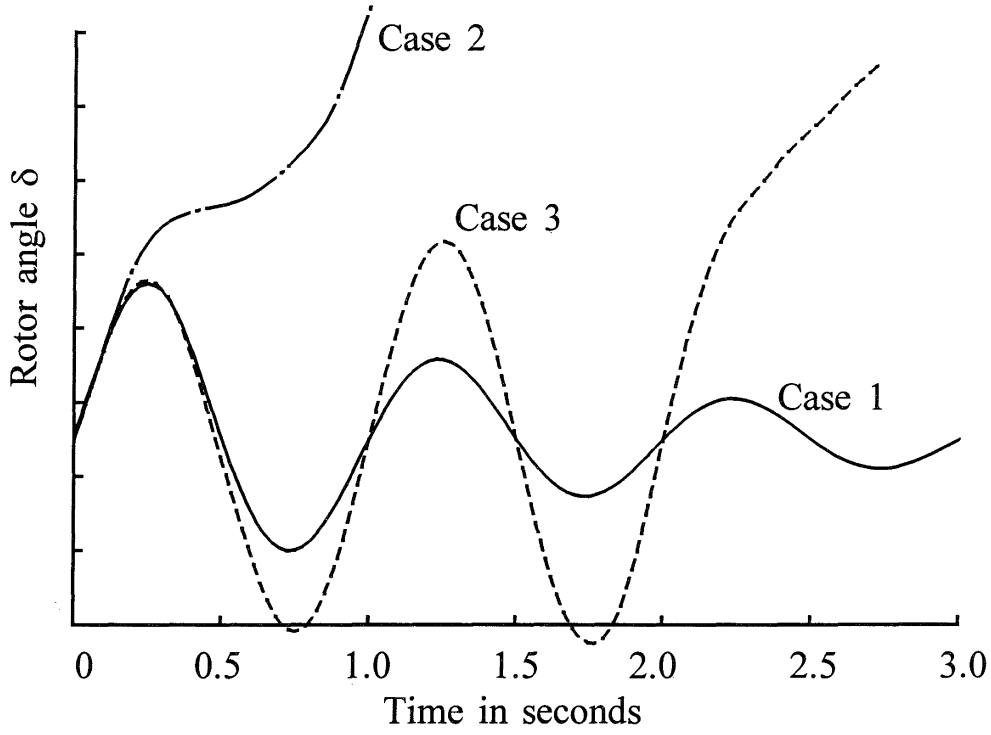

Figure 2.3 Rotor angle response to a transient disturbance

maximum, then decreases and oscillates with decreasing amplitude until it reaches a steady state. In Case 2, the rotor angle continues to increase steadily until synchronism is lost. This form of instability is referred to as *first-swing* instability and is caused by insufficient synchronizing torque. In Case 3, the system is stable in the first swing but becomes unstable as a result of growing oscillations as the end state is approached. This form of instability generally occurs when the postfault steady-state condition itself is "small-signal" unstable, and not necessarily as a result of the transient disturbance.

In large power systems, transient instability may not always occur as first-swing instability; it could be the result of the superposition of several modes of oscillation causing large excursions of rotor angle beyond the first swing.

In transient stability studies the study period of interest is usually limited to 3 to 5 seconds following the disturbance, although it may extend to about ten seconds for very large systems with dominant interarea modes of oscillation.

The term *dynamic stability* has also been widely used in the literature as a class of rotor angle stability. However, it has been used to denote different aspects of the phenomenon by different authors. In North American literature, it has been used mostly to denote small-signal stability in the presence of automatic control devices (primarily generator voltage regulators) as distinct from the classical steady-state stability without automatic controls [1,2]. In the French and German literature, it has been used to denote what we have termed here *transient stability*. Since much confusion has resulted from use of the term *dynamic stability*, both CIGRE and IEEE

have recommended that it not be used [3,4].

2.1.2 Voltage Stability and Voltage Collapse

Voltage stability is the ability of a power system to maintain steady acceptable voltages at all buses in the system under normal operating conditions and after being subjected to a disturbance. A system enters a state of voltage instability when a disturbance, increase in load demand, or change in system condition causes a progressive and uncontrollable drop in voltage. The main factor causing instability is the inability of the power system to meet the demand for reactive power. The heart of the problem is usually the voltage drop that occurs when active power and reactive power flow through inductive reactances associated with the transmission network [5-7].

A criterion for voltage stability is that, at a given operating condition for every bus in the system, the bus voltage magnitude increases as the reactive power injection at the same bus is increased. A system is voltage unstable if, for at least one bus in the system, the bus voltage magnitude (V) decreases as the reactive power injection (Q) at the same bus is increased. In other words, a system is voltage stable if V-Q sensitivity is positive for every bus and voltage unstable if V-Q sensitivity is negative for at least one bus.

Progressive drop in bus voltages can also be associated with rotor angles going out of step. For example, the gradual loss of synchronism of machines as rotor angles between two groups of machines approach or exceed 180° would result in very low voltages at intermediate points in the network (see Chapter 13, Section 13.5.3). In contrast, the type of sustained fall of voltage that is related to voltage instability occurs where rotor angle stability is not an issue.

Voltage instability is essentially a local phenomenon; however, its consequences may have a widespread impact. *Voltage collapse* is more complex than simple voltage instability and is usually the result of a sequence of events accompanying voltage instability leading to a low-voltage profile in a significant part of the power system.

Voltage instability may occur in several different ways. In its simple form it can be illustrated by considering the two terminal network of Figure 2.4 [5]. It consists of a constant voltage source (E_S) supplying a load (Z_{LD}) through a series impedance (Z_{LN}). This is representative of a simple radial feed to load or a load area served by a large system through a transmission line.

The expression for current $\tilde{I}$ in Figure 2.4 is

$$\tilde{I} = \frac{\tilde{E}_S}{\tilde{Z}_{LN}+\tilde{Z}_{LD}} \tag{2.3}$$

where $\tilde{I}$ and $\tilde{E}_S$ are phasors, and

$$\tilde{Z}_{LN} = Z_{LN}\angle\theta, \quad \tilde{Z}_{LD} = Z_{LD}\angle\phi$$

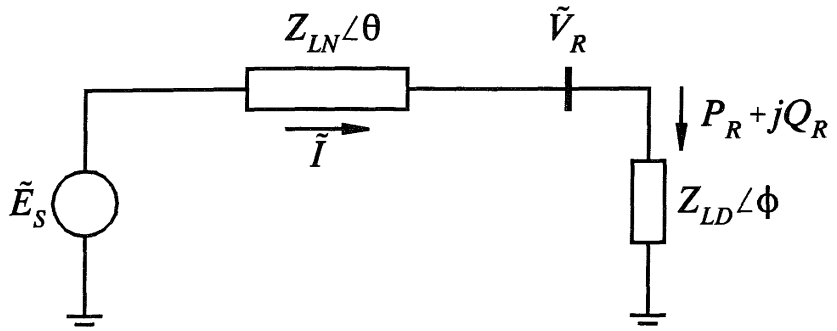

Figure 2.4 A simple radial system for illustration of voltage stability phenomenon

The magnitude of the current is given by

$$I = \frac{E_S}{\sqrt{(Z_{LN}\cos\theta + Z_{LD}\cos\phi)^2 + (Z_{LN}\sin\theta + Z_{LD}\sin\phi)^2}}$$

This may be expressed as

$$I = \frac{1}{\sqrt{F}} \frac{E_S}{Z_{LN}} \tag{2.4}$$

where

$$F = 1 + \left(\frac{Z_{LD}}{Z_{LN}}\right)^2 + 2\left(\frac{Z_{LD}}{Z_{LN}}\right)\cos(\theta - \phi)$$

The magnitude of the receiving end voltage is given by

$$\begin{aligned} V_R &= Z_{LD} I \\ &= \frac{1}{\sqrt{F}} \frac{Z_{LD}}{Z_{LN}} E_S \end{aligned} \tag{2.5}$$

The power supplied to the load is

$$\begin{aligned} P_R &= V_R I \cos\phi \\ &= \frac{Z_{LD}}{F}\left(\frac{E_S}{Z_{LN}}\right)^2 \cos\phi \end{aligned} \tag{2.6}$$

Plots of I, V_R, and P_R are shown in Figure 2.5 as a function of Z_{LN}/Z_{LD}, for the case with $\tan\theta = 10.0$ and $\cos\phi = 0.95$. To make the results applicable to any value of Z_{LN}, the values of I, V_R, and P_R are appropriately normalized.

As the load demand is increased by decreasing Z_{LD}, P_R increases rapidly at first and then slowly before reaching a maximum, after which it decreases. There is thus a maximum value of active power that can be transmitted through an impedance from a constant voltage source.

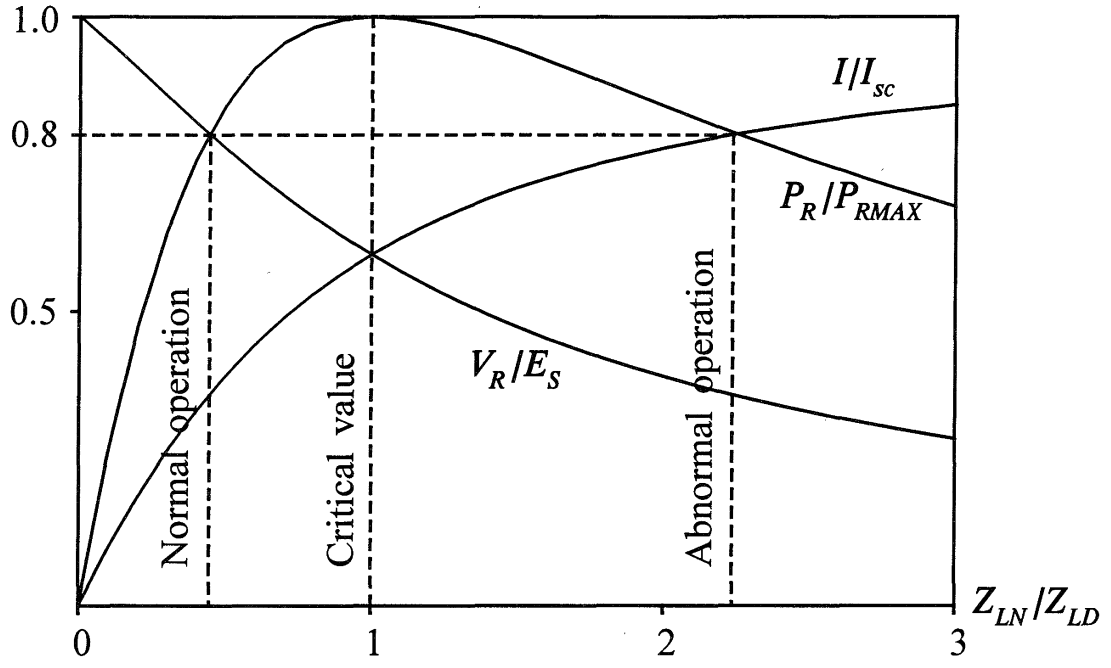

Figure 2.5 Receiving end voltage, current and power as a function of load demand for the system of Figure 2.4 ($I_{sc}=E_S/Z_{LN}$; $\cos\phi=0.95$ lag; $\tan\theta=10.0$)

The power transmitted is maximum when the voltage drop in the line is equal in magnitude to V_R, that is when $Z_{LN}/Z_{LD}=1$. As Z_{LD} is decreased gradually, I increases and V_R decreases. Initially, at high values of Z_{LD}, the increase in I dominates over the decrease in V_R, and hence P_R increases rapidly with decrease in Z_{LD}. As Z_{LD} approaches Z_{LN}, the effect of the decrease in I is only slightly greater than that of the decrease in V_R. When Z_{LD} is less than Z_{LN}, the decrease in V_R dominates over the increase in I, and the net effect is a decrease in P_R.

The critical operating condition corresponding to maximum power represents the limit of satisfactory operation. For higher load demand, control of power by varying load would be unstable; that is, a decrease in load impedance reduces power. Whether voltage will progressively decrease and the system will become unstable depends on the load characteristics. With a constant-impedance static load characteristic, the system stabilizes at power and voltage levels lower than the desired values. On the other hand, with a constant-power load characteristic, the system

becomes unstable through collapse of the load bus voltage. With other characteristics, the voltage is determined by the composite characteristic of the transmission line and load. If the load is supplied by transformers with automatic underload tap-changing (ULTC), the tap-changer action will try to raise the load voltage. This has the effect of reducing the effective Z_{LD} as seen from the system. This in turn lowers V_R still further and leads to a progressive reduction of voltage. This is a simple and pure form of voltage instability.

From the viewpoint of voltage stability, the relationship between P_R and V_R is of interest. This is shown in Figure 2.6 for the system under consideration when the load power factor is equal to 0.95 lag.

From Equations 2.5 and 2.6, we see that the load-power factor has a significant effect on the power-voltage characteristics of the system. This is to be expected since the voltage drop in the transmission line is a function of active as well as reactive power transfer. Voltage stability, in fact, depends on the relationships between P, Q and V. The traditional forms displaying these relationships are shown in Figures 2.7 and 2.8.

Figure 2.7 shows, for the power system of Figure 2.4, curves of the V_R-P_R relationship for different values of load power factor. The locus of critical operating points is shown by the dotted line in the figure. Normally, only the operating points above the critical points represent satisfactory operating conditions. A sudden reduction in power factor (increase in Q_R) can thus cause the system to change from a stable operating condition to an unsatisfactory, and possibly unstable, operating condition represented by the lower part of a V-P curve.

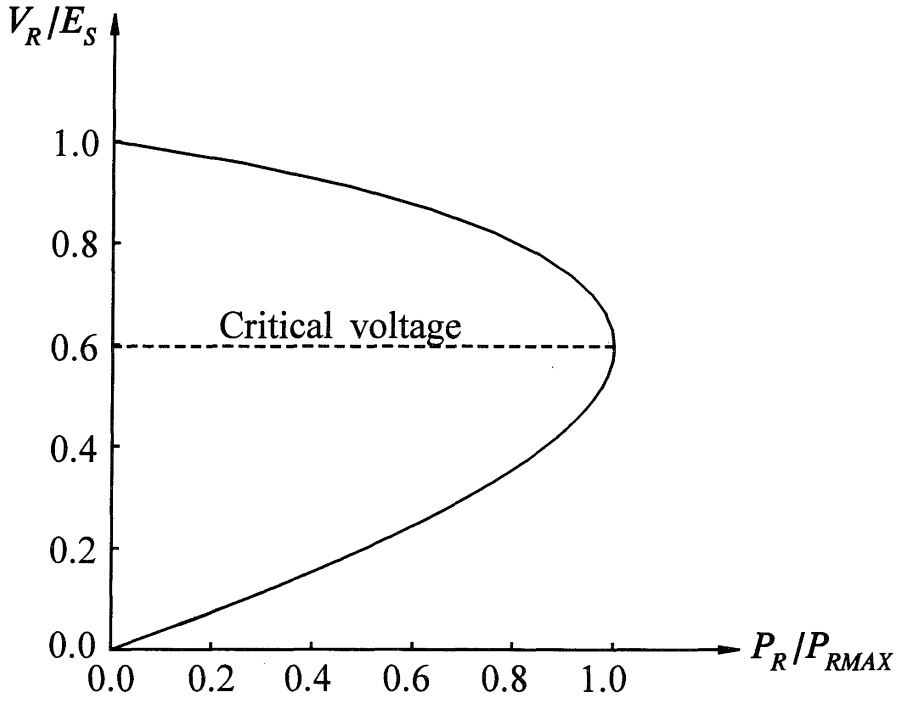

Figure 2.6 Power-voltage characteristics of the system of Figure 2.4 ($\cos\phi = 0.95$ lag; $\tan\theta = 10.0$)

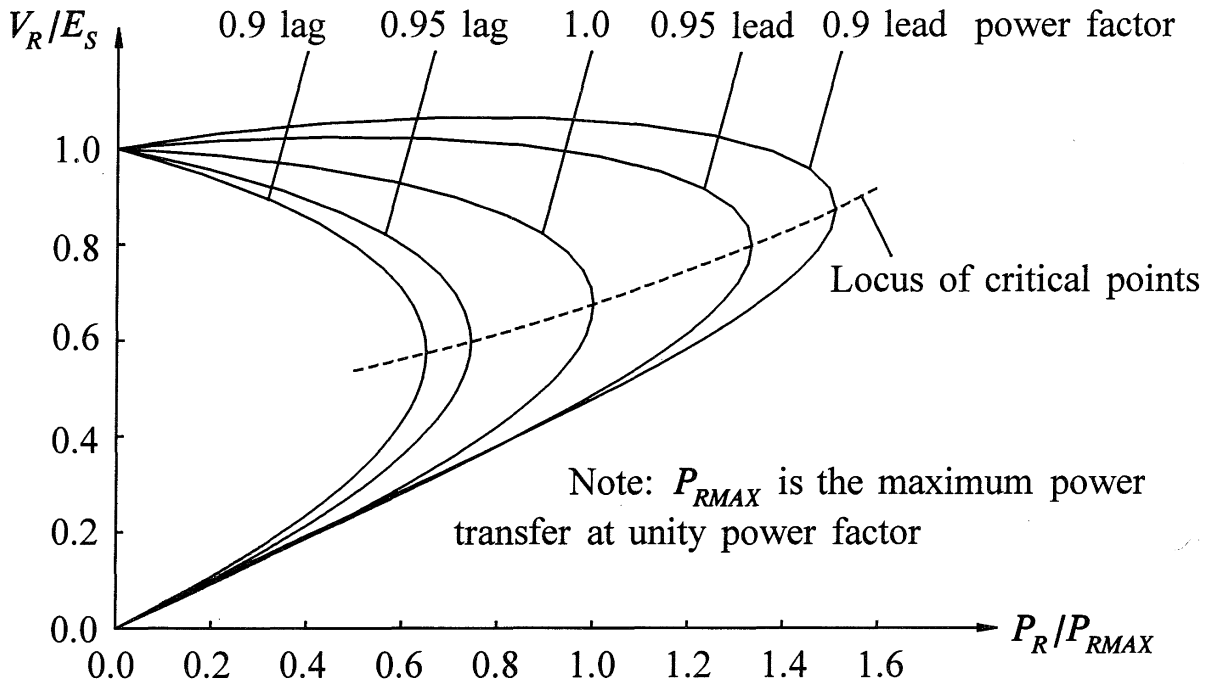

Figure 2.7 V_R-P_R characteristics of the system of Figure 2.4 with different load-power factors

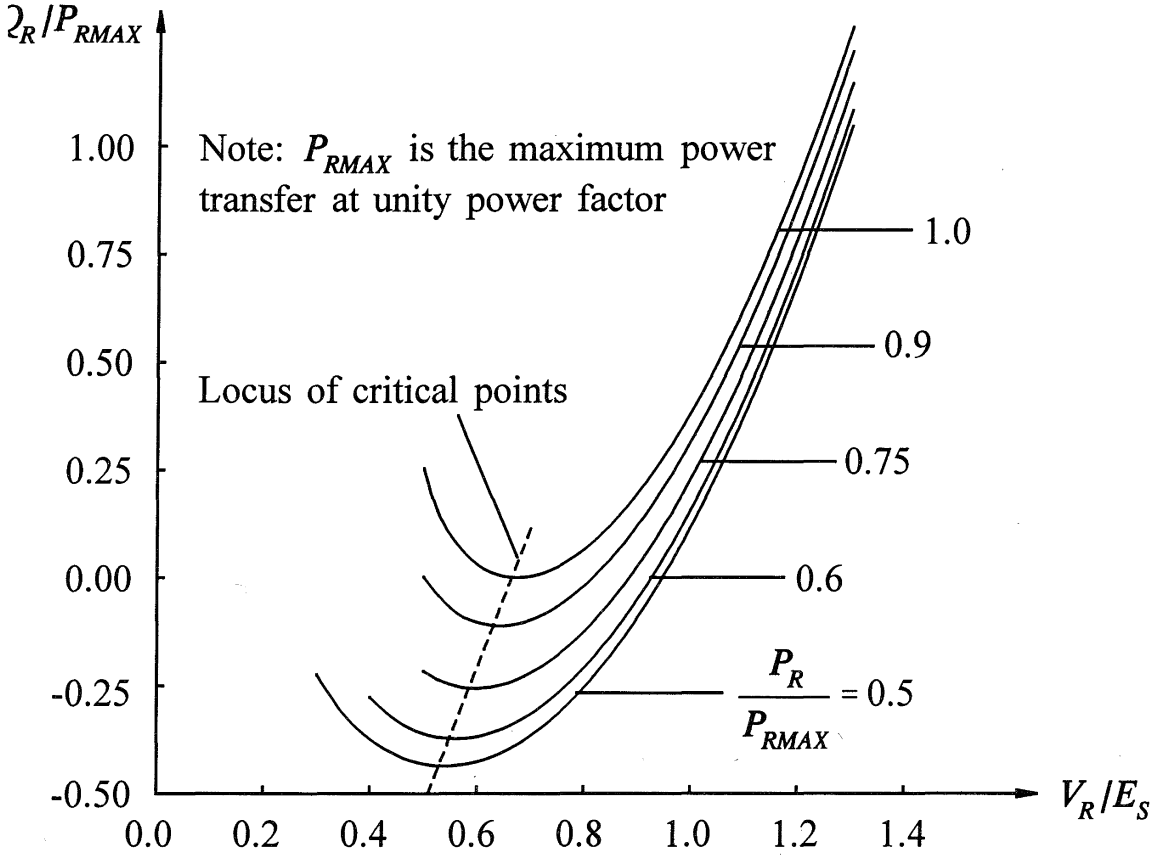

Figure 2.8 V_R-Q_R characteristics of the system of Figure 2.4 with different P_R/P_{RMAX} ratio

The influence of the reactive power characteristics of the devices at the receiving end (loads and compensating devices) is more apparent in Figure 2.8. It shows a family of curves applicable to the power system of Figure 2.4, each of which represents the relationship between V_R and Q_R for a fixed value of P_R. The system is stable in the region where the derivative dQ_R/dV_R is positive. The voltage stability limit (critical operating point) is reached when the derivative is zero. Thus the parts of the Q-V curves to the right of the minima represent stable operation, and the parts to the left represent unstable operation. Stable operation in the region where dQ_R/dV_R is negative can be achieved only with a regulated reactive power compensation having sufficient control range and a high Q/V gain with a polarity opposite to that of the normal.

The above description of the voltage stability phenomenon is basic and intended to help classification and understanding of different aspects of power system stability. Analysis has been limited to a radial system because it presents a simple, yet clear, picture of the voltage stability problem. In complex practical power systems, many factors contribute to the process of system collapse because of voltage instability: strength of transmission system; power-transfer levels; load characteristics; generator reactive power capability limits; and characteristics of reactive power compensating devices. In some cases, the problem is compounded by uncoordinated action of various controls and protective systems.

For purposes of analysis, it is useful to classify voltage stability into the following two subclasses:

(a) *Large-disturbance voltage stability* is concerned with a system's ability to control voltages following large disturbances such as system faults, loss of generation, or circuit contingencies. This ability is determined by the system-load characteristics and the interactions of both continuous and discrete controls and protections. Determination of large-disturbance stability requires the examination of the nonlinear dynamic performance of a system over a period of time sufficient to capture the interactions of such devices as ULTCs and generator field-current limiters. The study period of interest may extend from a few seconds to tens of minutes. Therefore, long-term dynamic simulations are required for analysis.

A criterion for large-disturbance voltage stability is that, following a given disturbance and following system-control actions, voltages at all buses reach acceptable steady-state levels.

(b) *Small-disturbance voltage stability* is concerned with a system's ability to control voltages following small perturbations such as incremental changes in system load. This form of stability is determined by the characteristics of load, continuous controls, and discrete controls *at a given instant of time*. This concept is useful in determining, at any instant, how the system voltage will respond to small system changes.

The basic processes contributing to small-disturbance voltage instability are essentially of a steady-state nature. Therefore, static analysis can be effectively used to determine stability margins, identify factors influencing stability, and examine a wide range of system conditions and a large number of post-contingency scenarios [8].

A criterion for small-disturbance voltage stability is that, at a given operating condition for every bus in the system, the bus voltage magnitude increases as the reactive power injection at the same bus is increased. A system is voltage-unstable if, for at least one bus in the system, the bus voltage magnitude (V) decreases as the reactive power injection (Q) at the same bus is increased. In other words, a system is voltage-stable if V-Q sensitivity is positive for every bus and unstable if V-Q sensitivity is negative for at least one bus.

Voltage instability does not always occur in its pure form. Often the angle and voltage instabilities go hand in hand. One may lead to the other and the distinction may not be clear. However, a distinction between angle stability and voltage stability is important for understanding of the underlying causes of the problems in order to develop appropriate design and operating procedures.

A more detailed discussion of voltage stability, including analytical techniques and methods of preventing voltage collapse, is presented in Chapter 14. A comprehensive treatment of the subject, with an in-depth analysis of the problem, is presented in the companion book *Power System Voltage Stability* by C.W. Taylor.

2.1.3 Mid-Term and Long-Term Stability

The terms *long-term stability* and *mid-term stability* are relatively new to the literature on power system stability. They were introduced as a result of the need to deal with problems associated with the dynamic response of power systems to severe upsets [9-13]. Severe system upsets result in large excursions of voltage, frequency, and power flows that thereby invoke the actions of slow processes, controls, and protections not modelled in conventional transient stability studies. The characteristic times of the processes and devices activated by the large voltage and frequency shifts will range from a matter of seconds (the responses of devices such as generator controls and protections) to several minutes (the responses of devices such as prime mover energy supply systems and load-voltage regulators) [10,14].

Long-term stability analysis assumes that inter-machine synchronizing power oscillations have damped out, the result being uniform system frequency [3,11,15]. The focus is on the slower and longer-duration phenomena that accompany large-scale system upsets and on the resulting large, sustained mismatches between generation and consumption of active and reactive power. These phenomena include: boiler dynamics of thermal units, penstock and conduit dynamics of hydro units, automatic generation control, power plant and transmission system protection/controls, transformer saturation, and off-nominal frequency effects on loads and the network.

The mid-term response represents the transition between short-term and long-term responses. In *mid-term stability* studies, the focus is on synchronizing power oscillations between machines, including the effects of some of the slower phenomena, and possibly large voltage or frequency excursions.

Typical ranges of time periods are as follows:

Short-term or transient: 0 to 10 seconds
Mid-term: 10 seconds to a few minutes
Long-term: a few minutes to 10's of minutes

It should, however, be noted that the distinction between mid-term and long-term stability is primarily based on the phenomena being analyzed and the system representation used, particularly with regard to fast transients and inter-machine oscillations, rather than the time period involved.

Generally, the long-term and mid-term stability problems are associated with inadequacies in equipment responses, poor coordination of control and protection equipment, or insufficient active/reactive power reserves.

Long-term stability is usually concerned with system response to major disturbances that involve contingencies beyond the normal system design criteria. This may entail cascading and splitting of the power system into a number of separate islands with the generators in each island remaining in synchronism. *Stability in this case is a question of whether or not each island will reach an acceptable state of operating equilibrium with minimal loss of load.* It is determined by the overall response of the island as evidenced by its mean frequency, rather than the relative motion of machines. In an extreme case, the system and unit protections may compound the adverse situation and lead to a collapse of the island as a whole or in part.

Other applications of long-term and mid-term stability analysis include dynamic analysis of voltage stability requiring simulation of the effects of transformer tap-changing, generator overexcitation protection and reactive power limits, and thermostatic loads. In this case, inter-machine oscillations are not likely to be important. However, care should be exercised not to neglect some of the fast dynamics.

There is limited experience and literature related to the analysis of long-term and mid-term stability. As more experience is gained and improved analytical techniques for simulation of slow as well as fast dynamics become available, the distinction between mid-term and long-term stability becomes less significant.

2.2 CLASSIFICATION OF STABILITY

Power system stability is a single problem; however, it is impractical to study it as such. As seen in the previous section, instability of a power system can take different forms and can be influenced by a wide range of factors. Analysis of stability

problems, identification of essential factors that contribute to instability, and formation of methods of improving stable operation are greatly facilitated by classification of stability into appropriate categories. These are based on the following considerations:

- The physical nature of the resulting instability;
- The size of the disturbance considered;
- The devices, processes, and time span that must be taken into consideration in order to determine stability; and
- The most appropriate method of calculation and prediction of stability.

Figure 2.9 gives an overall picture of the power system stability problem, identifying its classes and subclasses in terms of the categories described in the previous section. As a practical necessity, the classification has been based on a number of diverse considerations, making it difficult to select clearly distinct categories and to provide definitions that are rigorous and yet convenient for practical use. For example, there is some overlap between mid-term/long-term stability and voltage stability. With appropriate models for loads, on-load transformer tap changers and generator reactive power limits, mid-term/long-term stability simulations are ideally suited for dynamic analysis of voltage stability. Similarly, there is overlap between transient, mid-term and long-term stability: all three use similar analytical techniques for simulation of the nonlinear time domain response of the system to large disturbances. Although the three categories are concerned with different aspects of the stability problem, in terms of analysis and simulation they are really extensions of one another without clearly defined boundaries.

While classification of power system stability is an effective and convenient means to deal with the complexities of the problem, the overall stability of the system should always be kept in mind. Solutions to stability problems of one category should not be at the expense of another. It is essential to look at all aspects of the stability phenomena and at each aspect from more than one viewpoint. This requires the development and wise use of different kinds of analytical tools. In this regard, some degree of overlap in the phenomena being analyzed is in fact desirable.

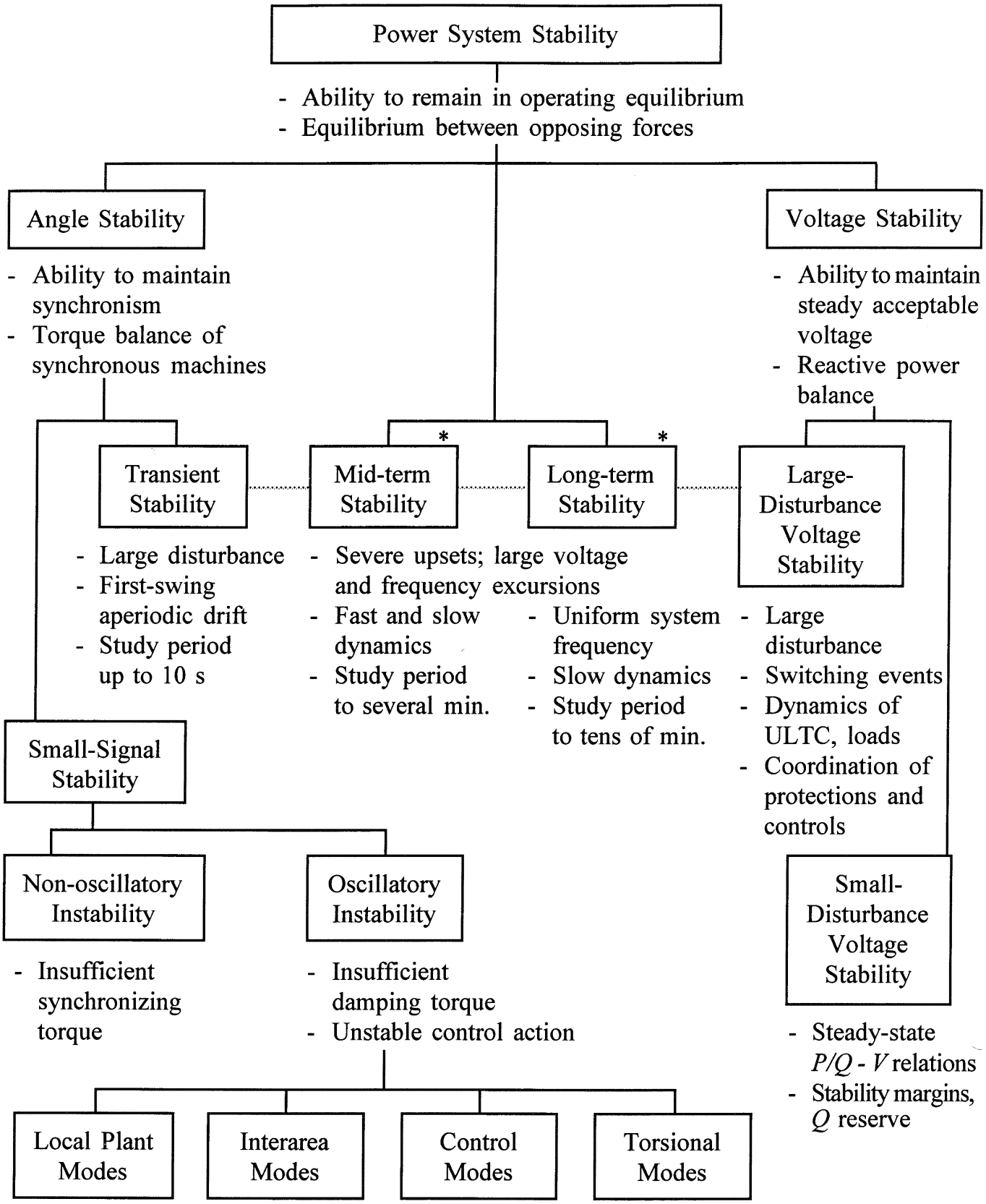

* With availability of improved analytical techniques providing unified approach for analysis of fast and slow dynamics, distinction between mid-term and long-term stability has become less significant.

Figure 2.9 Classification of power system stability

2.3 HISTORICAL REVIEW OF STABILITY PROBLEMS

Power system stability is a complex subject that has challenged power system engineers for many years. A review of the history of the subject is useful for a better understanding of present-day stability problems.

The stability of power systems was first recognized as an important problem in 1920 [16]. Results of the first laboratory tests on miniature systems were reported in 1924 [17]; the first field tests on the stability on a practical power system were conducted in 1925 [18,19].

Early stability problems were associated with remote hydroelectric generating stations feeding into metropolitan load centres over long-distance transmission. For economic reasons, such systems were operated close to their steady- state stability limits. In a few instances, instability occurred during steady-state operation, but it occurred more frequently following short-circuits and other system disturbances [20]. The stability problem was largely influenced by the strength of the transmission system, with instability being the result of insufficient synchronizing torque. The fault-clearing times were slow, being in the order of 0.5 to 2.0 seconds or longer.

The methods of analysis and the models used were dictated by developments in the art of computation and the stability theory of dynamic systems. Slide rules and mechanical calculators were used; hence, the models and methods of analysis had to be simple. In addition, graphical techniques such as the equal-area criterion and circle diagrams were developed. Such techniques were adequate for the analysis of the simple systems that could be treated effectively as two-machine systems. Steady-state and transient stability were treated separately. The former was related to the slope and peak of the power-angle curve; it was taken for granted that damping was positive.

As power systems evolved and interconnections between independent systems were found to be economically attractive, the complexity of the stability problems increased. Systems could no longer be treated as two-machine systems. A significant step towards the improvement of stability calculations was the development in 1930 of the network analyzer (or the ac calculating board). A network analyzer is essentially a scaled model of an ac power system with adjustable resistors, reactors and capacitors to represent transmission network and loads, voltage sources whose magnitude and angle can be adjusted to represent generators, and meters to measure voltages, currents, and power anywhere in the network. This development permitted power-flow analysis of multimachine systems; however, the equation of motion or the swing equation still had to be solved by hand using step-by-step numerical integration.

The theoretical work carried out in the 1920s and early 1930s laid the foundation for the industry's basic understanding of the power system stability phenomena. The principal developments and knowledge of power system stability in this early period came about as a result of the study of long-distance transmission, rather than as an extension of synchronous machine theory. The emphasis was on the network; the generators were viewed as simple voltage sources behind fixed reactances, and loads were considered as constant impedances. This was a practical

necessity since the computational tools available during this period were suited for solution of algebraic equations, but not differential equations.

Improvements to system stability came about by way of faster-fault clearing and continuous-acting voltage regulators with no dead band. The benefits of an excitation system with a high degree of response for increasing steady-state stability were in fact recognized in the early 1920s; however, initially this region of "dynamic stability" was not recommended for normal operation but was treated as additional margin in determining operating limits. With the increased realization of the potential benefits of faster-responding excitation systems in limiting first-swing transient instability as well as increasing steady-state power transfer limits, their use became more commonplace. However, the use of high-response exciters in some cases resulted in decreased damping of power swings. Oscillatory instability thus became a cause for concern, while steady-state monotonic instability was virtually eliminated. These trends required better analytical tools. Synchronous machine and excitation system representation had to be more detailed and simulations had to be carried out for longer time periods.

In the early 1950s, electronic analog computers were used for analysis of special problems requiring detailed modelling of the synchronous machine, excitation system, and speed governor. Such simulations were suited for a detailed study of the effects of equipment characteristics rather than the overall behaviour of multimachine systems. The 1950s also saw the development of digital computers: the first digital computer program for power system stability analysis was developed about 1956. The models used in the early stability programs were similar to those of network analyzer studies. It was soon recognized that digital computer programs would allow improvements over network analyzer methods in both the size of the network that could be simulated and the modelling of equipment dynamic characteristics. They would provide the ideal means for the study of stability problems associated with growth in interconnections between formerly separate power systems.

In the 1960s, most of the power systems in the United States and Canada were joined as part of one of two large interconnected systems, one in the east and the other in the west. In 1967, low capacity HVDC ties were also established between the east and west systems. At present, the power systems in the United States and Canada form virtually one large system. While interconnections result in operating economy and increased reliability through mutual assistance, they also contribute to increased complexity of stability problems and increase the consequences of instability. The northeast blackout of November 9, 1965 made this abundantly clear; it brought the problem of stability and the importance of power system reliability beyond the focus of engineers and to the attention of the public and of the regulatory agencies [25].

Much of the industry effort and interest related to system stability since the 1960s has been concentrated on *transient stability*. Power systems are designed and operated to criteria concerning transient stability. As a consequence, the principal tool for stability analysis in power system design and operation has been the transient stability program. Very powerful programs have been developed, with facilities for representing very large systems and detailed equipment models. This has been greatly

facilitated by developments in numerical methods and digital computer technology. There have also been significant developments in equipment modelling and testing, particularly for synchronous machines, excitation systems, and loads. In addition, significant improvements in transient stability performance of power systems have been achieved through use of high-speed fault-clearing, high initial-response exciters, series capacitors, and special stability aids.

Accompanying the above trends has been an increased tendency of power systems to exhibit oscillatory instability. Higher-response exciters, while improving transient stability, adversely affect small-signal stability associated with *local plant modes of oscillation* by introducing negative damping. The effects of fast exciters are compounded by the decreasing strength of transmission systems relative to the size of generating stations. Such problems have been solved through use of power system stabilizers (see Chapter 12).

Another source of the oscillatory instability problem has been the formation, as a consequence of growth in interconnections among power systems, of large groups of closely coupled machines connected by weak links. With heavy power transfers, such systems exhibit *interarea modes of oscillation* of low frequency. In many situations, the stability of these modes has become a source of concern.

Present trends in the planning and operation of power systems have resulted in new kinds of stability problems. Financial and regulatory conditions have caused electric utilities to build power systems with less redundancy and operate them closer to transient stability limits. Interconnections are continuing to grow with more use of new technologies such as multiterminal HVDC transmission. More extensive use is being made of shunt capacitors. Composition and characteristics of loads are changing. These trends have contributed to significant changes in the dynamic characteristics of modern power systems. Modes of instability are becoming increasingly more complex and require a comprehensive consideration of the various aspects of system stability. In particular, voltage instability and low-frequency interarea oscillations have become greater sources of concern than in the past. Whereas these problems used to occur in isolated situations, they have now become more commonplace. The need for analyzing the long-term dynamic response following major upsets and ensuring proper coordination of protection and control systems is also being recognized.

Significant research and development work has been undertaken in the last few years to gain a better insight into physical aspects of these new stability problems and to develop analytical tools for their analysis and better system design. Developments in control system theory and numerical methods have had a significant influence on this work. The following chapters describe these new developments and provide a comprehensive treatment of the subject of power system stability.

REFERENCES

[1] D.N. Ewart and F.P. deMello, "A Digital Computer Program for the Automatic Determination of Dynamic Stability Limits," *IEEE Trans.,* Vol. PAS-86, pp. 867-875, July 1967.

[2] H.M. Rustebakke (editor), *Electric Utility Systems and Practices*, John Wiley & Sons, 1983.

[3] CIGRE Working Group 32-03, "Tentative Classification and Terminologies Relating to Stability Problems of Power Systems," *Electra,* No. 56, 1978.

[4] IEEE Task Force, "Proposed Terms and Definitions for Power System Stability," *IEEE Trans.,* Vol. PAS-101, pp. 1894-1898, July 1982.

[5] C. Barbier and J.P. Barret, "An Analysis of Phenomena of Voltage Collapse on Transmission System," *Revue Generale d'Electricite,* pp. 672-690, October 1980.

[6] CIGRE Task Force 38-01-03, "Planning against Voltage Collapse," *Electra,* No. 111, pp. 55-75, March 1987.

[7] IEEE Special Publication, *Voltage Stability of Power Systems: Concepts, Analytical Tools, and Industry Experience*, 90TH0358-2-PWR, 1990.

[8] B. Gao, G.K. Morison, and P. Kundur, "Voltage Stability Evaluation Using Modal Analysis," *IEEE Trans.,* Vol. PWRS-7, No. 4, pp. 1529-1542, November 1992.

[9] D.R. Davidson, D.N. Ewart, and L.K. Kirchmayer, "Long Term Dynamic Response of Power Systems - An Analysis of Major Disturbances," *IEEE Trans.,* Vol. PAS-94, pp. 819-826, May/June 1975.

[10] C. Concordia, D.R. Davidson, D.N. Ewart, L.K. Kirchmayer, and R.P. Schulz, "Long Term Power System Dynamics - A New Planning Dimension," CIGRE Paper 32-13, 1976.

[11] EPRI Report EL-596, "Midterm Simulation of Electric Power Systems," Project RP745, June 1979.

[12] EPRI Report EL-983, "Long Term Power System Dynamics, Phase III," Research Project 764-2, May 1982.

[13] R.P. Schulz, "Capabilities of System Simulation Tools for Analyzing Severe Upsets," *Proceedings of International Symposium on Power System Stability,* Ames, Iowa, pp. 209-215, May 13-15, 1985.

[14] E.G. Cate, K. Hemmaplardh, J.W. Manke, and D.P. Gelopulos, "Time Frame Notion and Time Response of the Methods in Transient, Mid-Term and Long-Term Stability Programs," *IEEE Trans.,* Vol. PAS-103, pp. 143-151, January 1984.

[15] K. Hemmaplardh, J.W. Manke, W.R. Pauly, and J.W. Lamont, "Considerations for a Long Term Dynamics Simulation Program," *IEEE Trans.,* Vol. PWRS-1, pp. 129-135, February 1986.

[16] C.P. Steinmetz, "Power Control and Stability of Electric Generating Stations," *AIEE Trans.,* Vol. XXXIX, Part II, pp. 1215, July-December, 1920.

[17] R.D. Evans and R.C. Bergvall, "Experimental Analysis of Stability and Power Limitations," *AIEE Trans.,* pp. 39-58, 1924.

[18] R. Wilkins, "Practical Aspects of System Stability," *AIEE Trans.,* pp. 41-50, 1926.

[19] R.D. Evans and C.F. Wagner, "Further Studies of Transmission System Stability," *AIEE Trans.,* pp. 51-80, 1926.

[20] AIEE Subcommittee on Interconnections and Stability Factors, "First Report of Power System Stability," *AIEE Trans.,* pp. 261-282, February 1937.

[21] S.B. Crary, *Power System Stability, Vol. I: Steady-State Stability*, John Wiley & Sons, 1945.

[22] E.W. Kimbark, *Power System Stability, Vol. I: Elements of Stability Calculations*, John Wiley & Sons, 1948.

[23] Westinghouse Electric Corporation, *Electric Transmission and Distribution Reference Book*, East Pittsburgh, Pa., 1964.

[24] C. Concordia, "Power System Stability," *Proceedings of the International Symposium on Power System Stability,* Ames, Iowa, pp. 3-5, May 13-15, 1985.

[25] G.S. Vassell, "Northeast Blackout of 1965," *IEEE Power Engineering Review,* pp. 4-8, January 1991.

PART II

EQUIPMENT CHARACTERISTICS AND MODELLING

Chapter 3

Synchronous Machine Theory and Modelling

Synchronous generators form the principal source of electric energy in power systems. Many large loads are driven by synchronous motors. Synchronous condensers are sometimes used as a means of providing reactive power compensation and controlling voltage. These devices operate on the same principle and are collectively referred to as synchronous machines. As discussed in Chapter 2, the power system stability problem is largely one of keeping interconnected synchronous machines in synchronism. Therefore, an understanding of their characteristics and accurate modelling of their dynamic performance are of fundamental importance to the study of power system stability.

The modelling and analysis of the synchronous machine has always been a challenge. The problem was worked on intensely in the 1920s and 1930s [1,2,3], and has been the subject of several more recent investigations [4-9]. The theory and performance of synchronous machines have also been covered in a number of books [10-14].

In this chapter, we will develop in detail the mathematical model of a synchronous machine and briefly review its steady-state and transient performance characteristics.

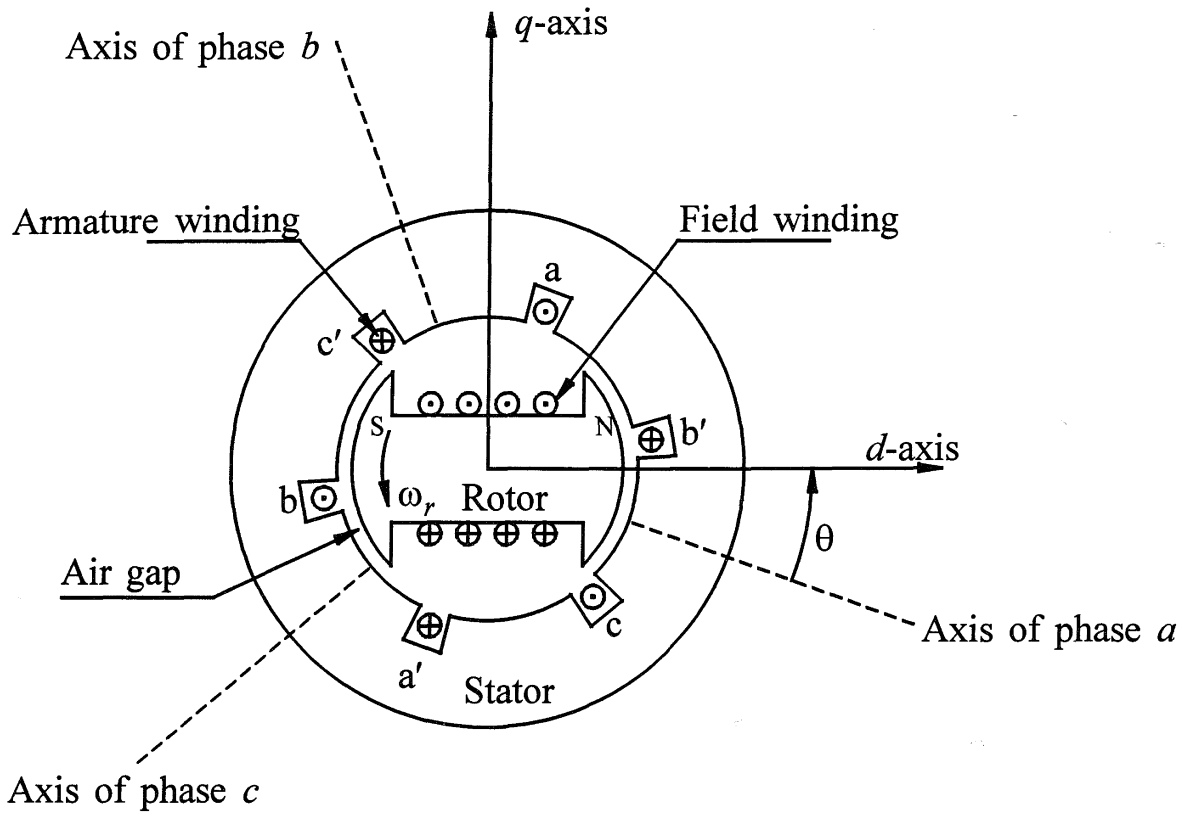

Figure 3.1 Schematic diagram of a three-phase synchronous machine

3.1 PHYSICAL DESCRIPTION

Figure 3.1 shows the schematic of the cross section of a three-phase synchronous machine with one pair of field poles. The machine consists of two essential elements: the field and the armature. The field winding carries direct current and produces a magnetic field which induces alternating voltages in the armature windings.

3.1.1 Armature and Field Structure

The armature windings usually operate at a voltage that is considerably higher than that of the field and thus they require more space for insulation. They are also subject to high transient currents and must have adequate mechanical strength. Therefore, normal practice is to have the armature on the stator. The three-phase windings of the armature are distributed 120° apart in *space* so that, with uniform rotation of the magnetic field, voltages displaced by 120° in *time* phase will be produced in the windings. Because the armature is subjected to a varying magnetic flux, the stator iron is built up of thin laminations to reduce eddy current losses.

When carrying balanced three-phase currents, the armature will produce a magnetic field in the air-gap rotating at synchronous speed (this will be formally shown in Section 3.1.3). The field produced by the direct current in the rotor winding, on the other hand, revolves with the rotor. For production of a steady torque, the fields of stator and rotor must rotate at the same speed. Therefore, the rotor must run at precisely the synchronous speed.

The number of field poles is determined by the mechanical speed of the rotor and electric frequency of stator currents. The synchronous speed is given by

$$n = \frac{120f}{p_f} \tag{3.1}$$

where n is the speed in rev/min, f is the frequency in Hz, and p_f is the number of field poles.

There are two basic rotor structures used, depending on speed. Hydraulic turbines operate at low speeds and hence a relatively large number of poles are required to produce the rated frequency. A rotor with salient or projecting poles and concentrated windings is better suited mechanically to this situation. Such rotors often have damper windings or amortisseurs in the form of copper or brass rods embedded in the pole face. These bars are connected to end rings to form short-circuited windings similar to those of a squirrel cage induction motor, as shown in Figure 3.2(a). They are intended to damp out speed oscillations. The damper windings may also be non-continuous, being wound only about the pole pieces as shown in Figure 3.2(b). The space harmonics of the armature magnetomotive force (mmf) contribute to surface eddy current losses; therefore, pole faces of salient pole machines are usually laminated.

Steam and gas turbines, on the other hand, operate at high speeds. Their generators have round (or cylindrical) rotors made up of solid steel forgings. They have two or four field poles, formed by distributed windings placed in slots milled in the solid rotor and held in place by steel wedges. They often do not have special

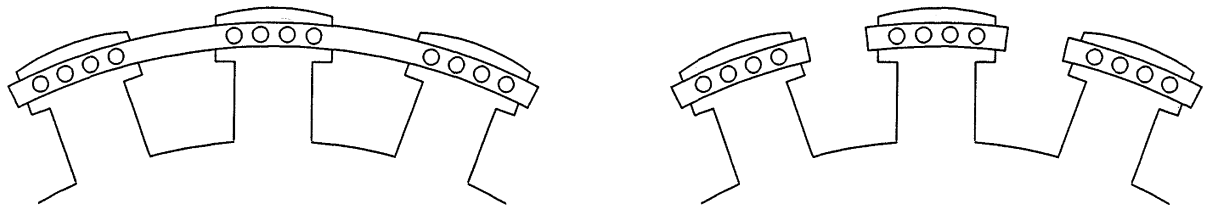

(a) Continuous damper (b) Non-continuous damper

Figure 3.2 Salient pole rotor construction

damper windings, but the solid steel rotor offers paths for eddy currents which have effects equivalent to amortisseur currents. Some manufacturers provide for additional damping effects and negative-sequence current capability by using metal wedges in the field winding slots as damper bars and interconnecting them to form a damper cage, or by providing separate copper rods underneath the wedges. Figure 3.3 illustrates the rotor structure.

Under steady-state conditions, the only rotor current that exists is the direct current in the field winding. However, under dynamic conditions eddy currents are induced on the rotor surface and slot walls, and in slot wedges or damper windings (if used to produce additional damping). Figure 3.4 shows the rotor current paths of a steam turbine generator.

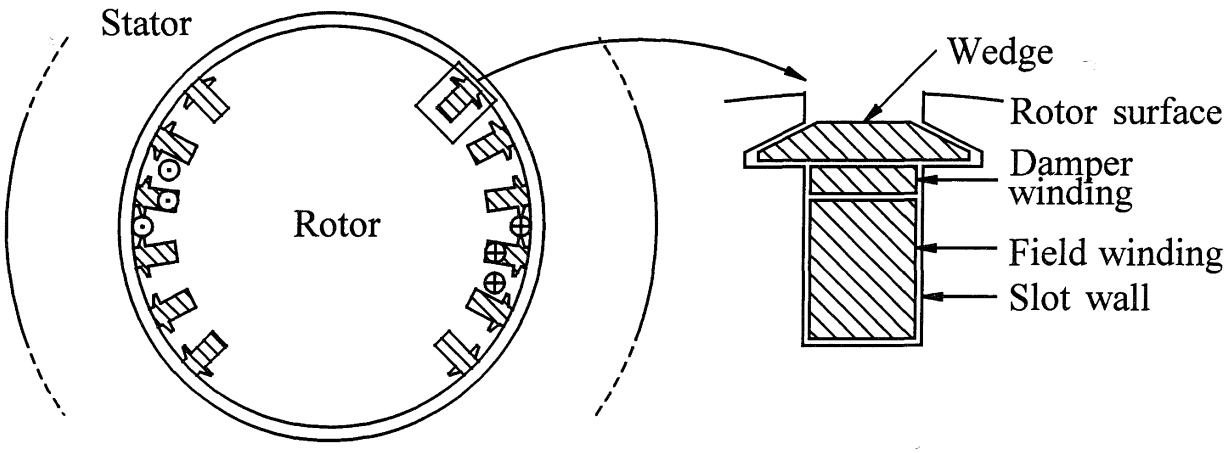

(a) Rotor structure (b) Rotor slot and windings

Figure 3.3 Solid round rotor construction

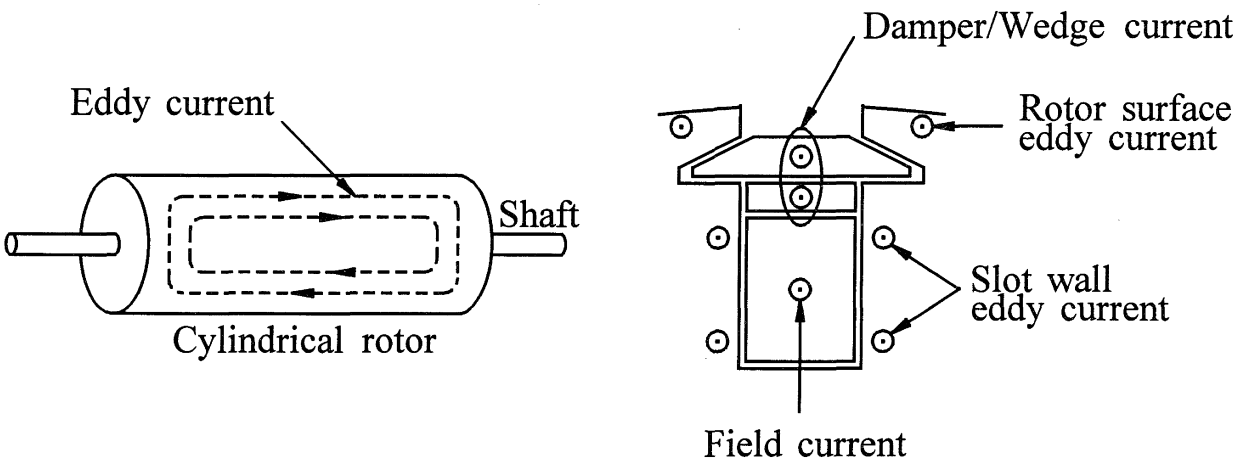

(a) Current paths (b) Components of currents associated with an individual rotor slot

Figure 3.4 Current paths in a round rotor

3.1.2 Machines with Multiple Pole Pairs

Machines with more than one pair of field poles will have stator windings made up of a corresponding multiple set of coils. For purposes of analysis, it is convenient to consider only a single pair of poles and recognize that conditions associated with other pole pairs are identical to those for the pair under consideration. Therefore, angles are normally measured in electrical radians or degrees. The angle covered by one pole pair is 2π radians or 360 electrical degrees. The relationship between angle θ in electrical units and the corresponding angle θ_m in mechanical units is

$$\theta = \frac{p_f}{2}\theta_m \tag{3.2}$$

3.1.3 MMF Waveforms

In practice, the armature windings and round rotor machine field windings are distributed in many slots so that the resulting mmf and flux waveforms have nearly sinusoidal space distribution. In the case of salient pole machines, which have field windings concentrated at the poles, shaping of the pole faces is used to minimize harmonics in the flux produced.

First, let us consider the mmf waveform due to the armature windings only. The mmf produced by current flowing in only one coil in phase *a* is illustrated in Figure 3.5, in which the cross section of the stator has been cut open and rolled out in order to develop a view of the mmf wave.

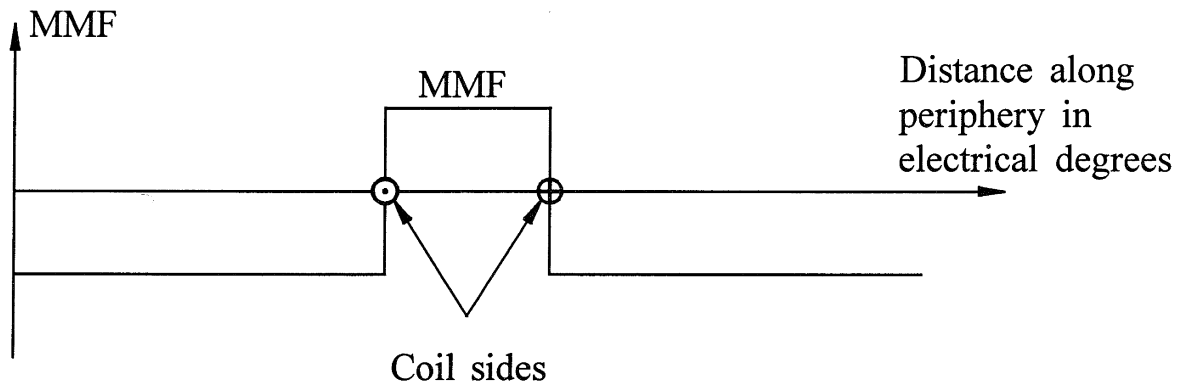

Figure 3.5 MMF waveform due to a single coil

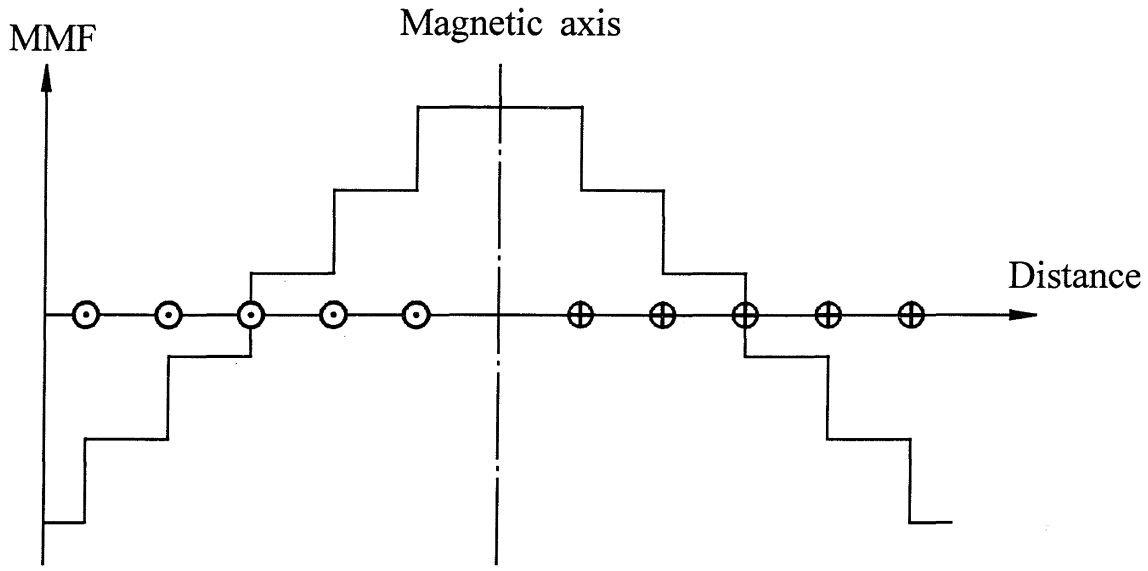

Figure 3.6 MMF waveform due to a number of coils

By adding more coils, the mmf wave distribution shown in Figure 3.6 may be obtained. We see that the mmf waveform is progressing from a square wave toward a sine wave as coils are added. Through use of fractional-pitch windings, the space harmonics can be made small [12]. Machine design aims at minimizing harmonics and, for most analyses of machine performance, it is reasonable to assume that each phase winding produces a sinusoidally distributed mmf wave. The windings are then said to be sinusoidally distributed. The harmonics may be considered as secondary from the viewpoint of machine performance. In addition to causing rotor surface eddy current losses, harmonics contribute to armature leakage reactances.

Rotating magnetic field

Let us now determine the net mmf wave due to the three-phase windings in the stator. Figure 3.7 shows the mmf wave of phase *a*.

With γ representing the angle along the periphery of the stator with respect to the centre of phase *a*, the mmf wave due to the three phases may be described as follows:

$$MMF_a = Ki_a\cos\gamma$$

$$MMF_b = Ki_b\cos(\gamma - \frac{2\pi}{3})$$

$$MMF_c = Ki_c\cos(\gamma + \frac{2\pi}{3})$$

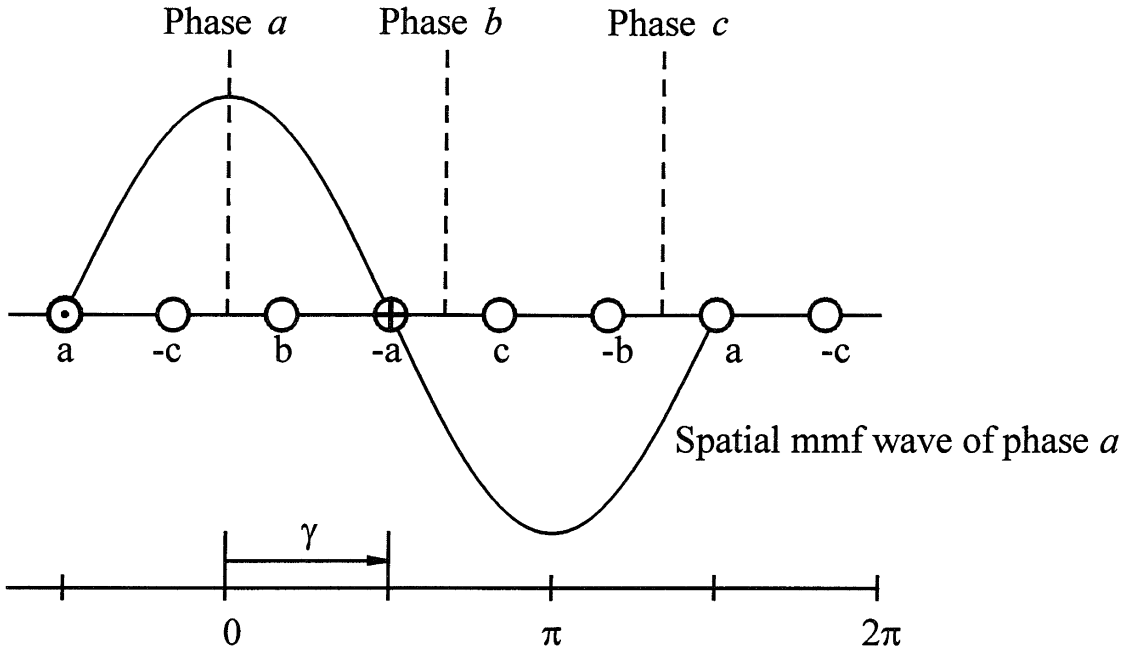

Figure 3.7 Spatial mmf wave of phase *a*

where i_a, i_b and i_c are the instantaneous values of the phase currents and K is a constant. Each winding produces a stationary mmf wave whose magnitude changes as the instantaneous value of the current through the winding changes. The three mmf waves due to the three phases are displaced 120 electrical degrees apart in space.

With balanced phase currents, and time origin arbitrarily chosen as the instant when i_a is maximum, we have

$$\begin{aligned} i_a &= I_m \cos(\omega_s t) \\ i_b &= I_m \cos(\omega_s t - \frac{2\pi}{3}) \\ i_c &= I_m \cos(\omega_s t + \frac{2\pi}{3}) \end{aligned} \tag{3.3}$$

where $\omega_s = 2\pi f$ = angular frequency of stator currents in electrical rad/s.

The total mmf due to the three phases is given by

$$\begin{aligned} MMF_{total} &= MMF_a + MMF_b + MMF_c \\ &= KI_m[\cos(\omega_s t)\cos\gamma + \cos(\omega_s t - \frac{2\pi}{3})\cos(\gamma - \frac{2\pi}{3}) + \\ &\qquad \cos(\omega_s t + \frac{2\pi}{3})\cos(\gamma + \frac{2\pi}{3})] \\ &= \frac{3}{2}KI_m\cos(\gamma - \omega_s t) \end{aligned} \tag{3.4}$$

This is the equation of a *travelling wave*. At any instant in time, the total mmf has a sinusoidal spatial distribution. It has a constant amplitude and a space-phase angle $\omega_s t$, which is a function of time. Thus, the entire mmf wave moves at the constant angular velocity of ω_s electrical rad/s. For a machine with p_f field poles, the speed of rotation of the stator field is

$$\omega_{sm} = \frac{2}{p_f}\omega_s \qquad \text{mech. rad/s} \tag{3.5a}$$

or

$$n_s = \frac{60\omega_{sm}}{2\pi} = \frac{120f}{p_f} \qquad \text{r/min} \tag{3.5b}$$

This is the same as the synchronous speed of the rotor given by Equation 3.1. Therefore, for balanced operation the mmf wave due to stator currents is stationary with respect to the rotor.

The stator and rotor mmf waves are shown in Figure 3.8 relative to the rotor structure, again with both stator and rotor cross sections rolled out.

The magnitude of the stator mmf wave and its relative angular position with respect to the rotor mmf wave depend on the synchronous machine load (output). The electromagnetic torque on the rotor acts in a direction so as to bring the magnetic fields into alignment. If the rotor field leads the armature field, the torque acts in opposition to the rotation with the machine acting as a generator. On the other hand, if the rotor field lags the armature field, the torque acts in the direction of rotation with the machine acting as a motor. In other words, for generator action, the rotor field leads the armature field by the forward torque of a prime mover; for motor action, the rotor field lags behind the armature field due to the retarding torque of shaft load (mechanical).

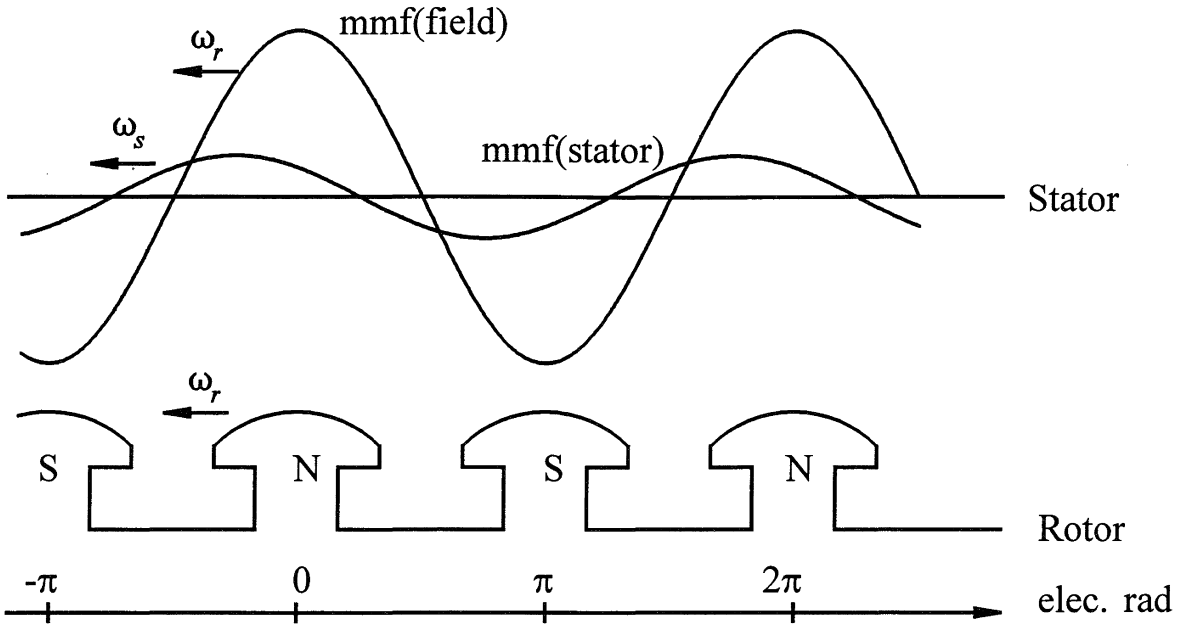

Figure 3.8 Stator and rotor mmf wave shapes

3.1.4 Direct and Quadrature Axes

We see that the magnetic circuits and all rotor windings are symmetrical with respect to both polar axis and the inter-polar axis. Therefore, for the purpose of identifying synchronous machine characteristics, two axes are defined as shown in Figure 3.1:

- The direct (*d*) axis, centred magnetically in the centre of the north pole;
- The quadrature (*q*) axis, 90 electrical degrees ahead of the *d*-axis.

The position of the rotor relative to the stator is measured by the angle θ between the *d*-axis and the magnetic axis of phase *a* winding.

The selection of the *q*-axis as leading the *d*-axis is purely arbitrary. This convention is based on the IEEE standard definition [15], and is widely used. Alternatively, the *q*-axis could be chosen to lag the *d*-axis by 90 degrees [16,17].

3.2 MATHEMATICAL DESCRIPTION OF A SYNCHRONOUS MACHINE

In developing equations of a synchronous machine, the following assumptions are made:

(a) The stator windings are sinusoidally distributed along the air-gap as far as the mutual effects with the rotor are concerned.

(b) The stator slots cause no appreciable variation of the rotor inductances with rotor position.

(c) Magnetic hysteresis is negligible.

(d) Magnetic saturation effects are negligible.

Assumptions (a), (b), and (c) are reasonable. The principal justification comes from the comparison of calculated performances based on these assumptions and actual measured performances. Assumption (d) is made for convenience in analysis. With magnetic saturation neglected, we are required to deal with only linear coupled circuits, making superposition applicable. However, saturation effects are important, and methods of accounting for their effects separately in an approximate manner will be discussed in Section 3.8. The machine equations will be developed first by assuming linear flux-current relationships.

Figure 3.9 shows the circuits involved in the analysis of a synchronous machine. The stator circuits consist of three-phase armature windings carrying alternating currents. The rotor circuits comprise field and amortisseur windings. The field winding is connected to a source of direct current. For purposes of analysis, the currents in the amortisseur (solid rotor and/or damper windings) may be assumed to flow in two sets of closed circuits: one set whose flux is in line with that of the field along the d-axis and the other set whose flux is at right angles to the field axis or along the q-axis. The amortisseur circuits, as discussed previously, take different forms and distinct, electrically independent circuits may not exist. In machine design analysis, a large number of circuits are used to represent amortisseur effects. For system analysis, where the characteristics of the machine as seen from its stator and rotor terminals are of interest, a limited number of circuits may be used. The type of rotor construction and the frequency range over which the model should accurately represent the machine characteristics determine the number of rotor circuits. For system stability studies, it is seldom necessary to represent more than two or three rotor circuits in each axis. In Figure 3.9, for the sake of simplicity only one amortisseur circuit is assumed in each axis, and we will write the machine equations based on this assumption. However, we implicitly consider an arbitrary number of such circuits; the subscript k is used to denote this.

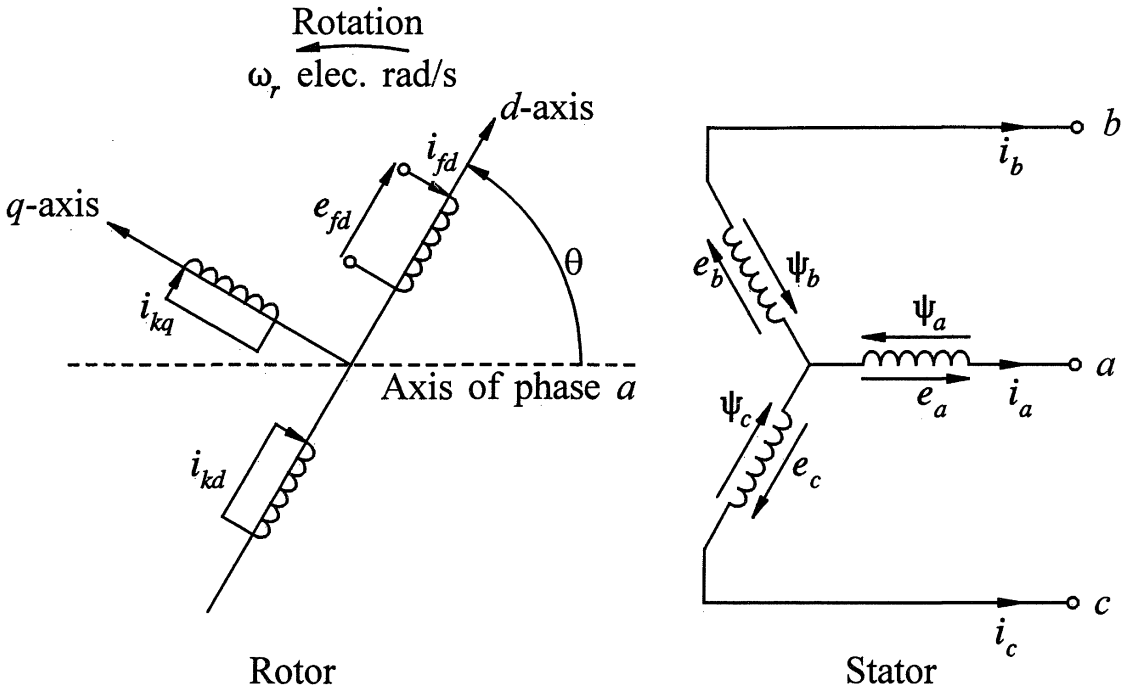

a, b, c : Stator phase windings
fd : Field winding
kd : *d*-axis amortisseur circuit
kq : *q*-axis amortisseur circuit
k = 1, 2, ... n; n = no. of amortisseur circuits
θ = Angle by which *d*-axis leads the magnetic axis of phase *a* winding, electrical rad
ω_r = Rotor angular velocity, electrical rad/s

Figure 3.9 Stator and rotor circuits of a synchronous machine

In Figures 3.1 and 3.9, θ is defined as the angle by which the *d*-axis leads the centreline of phase *a* winding in the direction of rotation. Since the rotor is rotating with respect to the stator, angle θ is continuously increasing and is related to the rotor angular velocity ω_r and time t as follows:

$$\theta = \omega_r t$$

The electrical performance equations of a synchronous machine can be developed by writing equations of the coupled circuits identified in Figure 3.9. Before we attempt to do this, it is useful to review how the equations of simple circuits may be written.

3.2.1 Review of Magnetic Circuit Equations

Single excited circuit

Consider first the elementary circuit of Figure 3.10, comprising a single exciting coil. The coil has N turns and a resistance of r. It is assumed to have a linear flux-mmf relationship. According to Faraday's law, the induced voltage e_i is

$$e_i = \frac{d\psi}{dt} \tag{3.6}$$

where ψ is the instantaneous value of flux linkage and t is time. The terminal voltage e_1 is given by

$$e_1 = \frac{d\psi}{dt} + ri \tag{3.7}$$

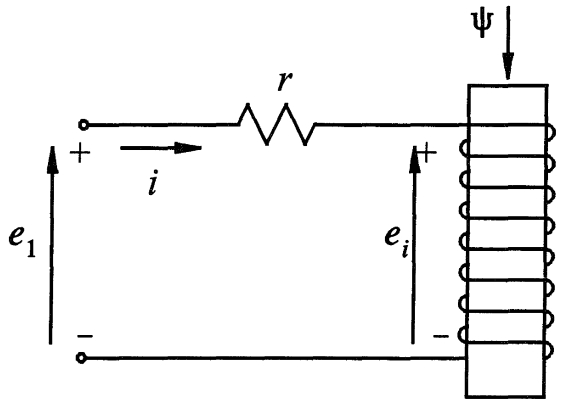

Figure 3.10 Single-excited magnetic circuit

The flux linkage may be expressed in terms of the inductance L of the circuit:

$$\psi = Li \tag{3.8}$$

The inductance, by definition, is equal to flux linkage per unit current. Therefore,

$$\begin{aligned} L &= N\frac{\Phi}{i} \\ &= N^2\mathrm{P} \end{aligned} \tag{3.9}$$

where

P = permeance of magnetic path

Φ = flux = $(MMF)\mathrm{P} = Ni\mathrm{P}$

Coupled circuits

Let us next consider the circuit shown in Figure 3.11, consisting of two magnetically coupled windings. The windings have turns N_1 and N_2, and resistances r_1 and r_2, respectively; the magnetic path is assumed to have a linear flux-mmf relationship. The winding currents i_1 and i_2 are considered positive into the windings, as shown in the figure. The terminal voltages are

$$e_1 = \frac{d\psi_1}{dt} + r_1 i_1 \tag{3.10}$$

$$e_2 = \frac{d\psi_2}{dt} + r_2 i_2 \tag{3.11}$$

The magnetic field is determined by currents in both windings. Therefore, ψ_1 and ψ_2 are the flux linkages with the respective windings produced by the total effect of both currents. Thus

$$\psi_1 = N_1(\Phi_{m1} + \Phi_{l1}) + N_1\Phi_{m2} \tag{3.12}$$

$$\psi_2 = N_2(\Phi_{m2} + \Phi_{l2}) + N_2\Phi_{m1} \tag{3.13}$$

where

Φ_{m1} = mutual flux linking both windings due to current in winding 1 acting alone
Φ_{l1} = leakage flux linking winding 1 only
Φ_{m2} = mutual flux linking both windings due to current in winding 2 acting alone
Φ_{l2} = leakage flux linking winding 2 only

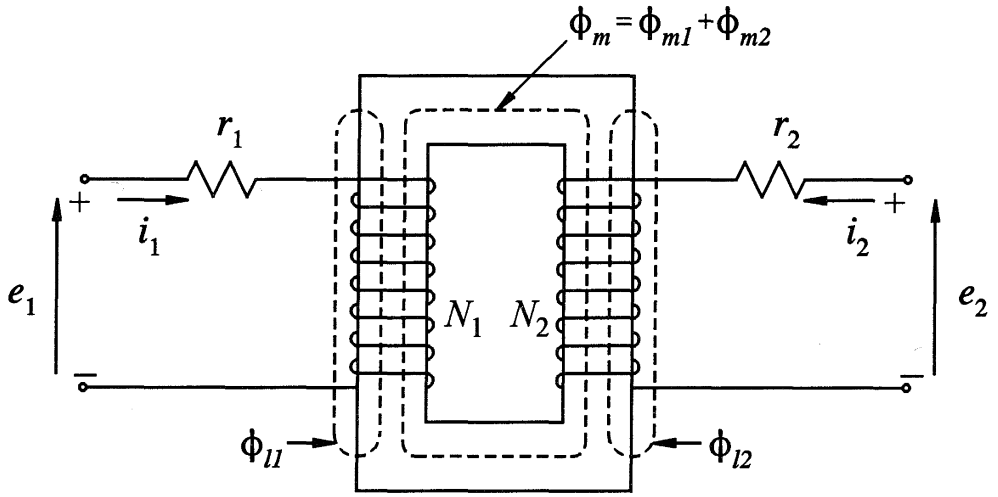

Figure 3.11 Magnetically coupled circuits

The flux linkages can be expressed in terms of self and mutual inductances whose expressions are given below.

Self inductance, by definition, is the flux linkage per unit current in the same winding. Accordingly, the self inductances of windings 1 and 2 are, respectively,

$$L_{11} = N_1(\Phi_{m1}+\Phi_{l1})/i_1 \tag{3.14}$$

$$L_{22} = N_2(\Phi_{m2}+\Phi_{l2})/i_2 \tag{3.15}$$

or

$$L_{11} = L_{m1}+L_{l1} \tag{3.16}$$

$$L_{22} = L_{m2}+L_{l2} \tag{3.17}$$

where L_{m1} and L_{m2} are the magnetizing inductances, and L_{l1} and L_{l2} the leakage inductances, of the respective windings.

Mutual inductance between two windings, by definition, is the flux linkage with one winding per unit current in the other winding. Therefore, the mutual inductances between windings 1 and 2 are

$$L_{12} = N_1\Phi_{m2}/i_2 \tag{3.18}$$

and

$$L_{21} = N_2\Phi_{m1}/i_1 \tag{3.19}$$

If P is the permeance of the mutual flux path,

$$\Phi_{m1} = N_1 i_1 \mathrm{P} \tag{3.20}$$

$$\Phi_{m2} = N_2 i_2 \mathrm{P} \tag{3.21}$$

From Equations 3.18, 3.19, 3.20 and 3.21, we see that

$$L_{12} = L_{21} = N_1 N_2 \mathrm{P} \tag{3.22}$$

Substitution of Equations 3.16 to 3.19 in Equations 3.12 and 3.13 gives the following expressions for flux linking windings 1 and 2 in terms of self and mutual inductances:

$$\psi_1 = L_{11}i_1 + L_{12}i_2 \tag{3.23}$$

$$\psi_2 = L_{21}i_1 + L_{22}i_2 \tag{3.24}$$

In the above equations, it is important to recognize the relative directions of self and mutual flux linkages by the use of an appropriate algebraic sign for the mutual inductance. The mutual inductance is positive if positive currents in the two windings produce self and mutual fluxes in the same direction (i.e., the fluxes add up); otherwise it is negative.

Equations 3.10 and 3.11 for voltage together with Equations 3.23 and 3.24 for flux linkage give the performance equations of the linear static coupled circuits of Figure 3.11. In this form of representation, the self and mutual inductances of the windings are used as parameters. An inductance represents the proportionality between a flux linkage and a current. As seen from Equations 3.9 and 3.22, an inductance is directly proportional to the permeance of the associated flux path.

In developing the equations of magnetic circuits in this section, we have not explicitly specified units of system quantities. These equations are valid in any consistent system of units.

Finally, before we turn to synchronous machine equations, a comment about notation used is appropriate. In circuit analysis, the symbol λ is commonly used to denote flux linkage, whereas in most of the literature on synchronous machines and power system stability the symbol ψ is used. Here we have followed the latter practice, in order to correspond with the published literature and to avoid confusion in later chapters where we use λ to denote eigenvalues.

3.2.2 Basic Equations of a Synchronous Machine

The same general form of the equations derived in the previous section applies to the coupled circuits of Figure 3.9. We will, however, use the generator convention for polarities so that the positive direction of a stator winding current is assumed to be out of the machine. The positive direction of field and amortisseur currents is assumed to be into the machine.

In addition to the large number of circuits involved, the fact that the mutual and self inductances of the stator circuits vary with rotor position complicates the synchronous machine equations. The variations in inductances are caused by the variations in the permeance of the magnetic flux path due to non-uniform air-gap. This is pronounced in a salient pole machine in which the permeances in the two axes are significantly different. Even in a round rotor machine there are differences in the two axes due mostly to the large number of slots associated with the field winding.

The flux produced by a stator winding follows a path through the stator iron, across the air-gap, through the rotor iron, and back across the air-gap. The variations in permeance of this path as a function of the rotor position can be approximated as

$$P = P_0 + P_2 \cos 2\alpha \tag{3.25}$$

In the above equation, α is the angular distance from the *d*-axis along the periphery as shown in Figure 3.12.

A double frequency variation is produced, since the permeances of the north and south poles are equal. Higher order even harmonics of permeance exist but are small enough to be neglected.

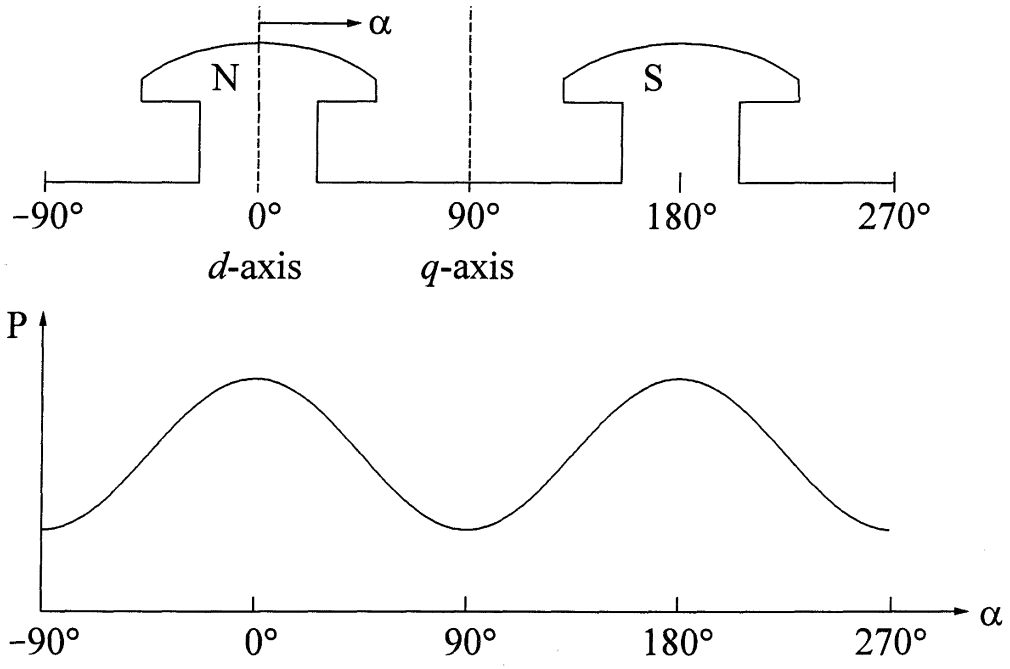

Figure 3.12 Variation of permeance with rotor position

We will use the following notation in writing the equations for the stator and rotor circuits:

e_a, e_b, e_c	= instantaneous stator phase to neutral voltages
i_a, i_b, i_c	= instantaneous stator currents in phases *a, b, c*
e_{fd}	= field voltage
i_{fd}, i_{kd}, i_{kq}	= field and amortisseur circuit currents
R_{fd}, R_{kd}, R_{kq}	= rotor circuit resistances
l_{aa}, l_{bb}, l_{cc}	= self-inductances of stator windings
l_{ab}, l_{bc}, l_{ca}	= mutual inductances between stator windings
$l_{afd}, l_{akd}, l_{akq}$	= mutual inductances between stator and rotor windings
$l_{ffd}, l_{kkd}, l_{kkq}$	= self-inductances of rotor circuits
R_a	= armature resistance per phase
p	= differential operator d/dt

Stator circuit equations

The voltage equations of the three phases are

$$e_a = \frac{d\psi_a}{dt} - R_a i_a = p\psi_a - R_a i_a \tag{3.26}$$

$$e_b = p\psi_b - R_a i_b \tag{3.27}$$

$$e_c = p\psi_c - R_a i_c \tag{3.28}$$

The flux linkage in the phase a winding at any instant is given by

$$\psi_a = -l_{aa} i_a - l_{ab} i_b - l_{ac} i_c + l_{afd} i_{fd} + l_{akd} i_{kd} + l_{akq} i_{kq} \tag{3.29}$$

Similar expressions apply to flux linkages of windings b and c. The units used are webers, henrys, and amperes. The negative sign associated with the stator winding currents is due to their assumed direction.

As shown below, all the inductances in Equation 3.29 are functions of the rotor position and are thus time-varying.

Stator self-inductances

The self-inductance l_{aa} is equal to the ratio of flux linking phase a winding to the current i_a, with currents in all other circuits equal to zero. The inductance is directly proportional to the permeance, which as indicated earlier has a second harmonic variation. The inductance l_{aa} will be a maximum for $\theta=0°$, a minimum for $\theta=90°$, a maximum again for $\theta=180°$, and so on.

Neglecting space harmonics, the mmf of phase a has a sinusoidal distribution in space with its peak centred on the phase a axis. The peak amplitude of the mmf wave is equal to $N_a i_a$, where N_a is the effective turns per phase. As shown in Figure 3.13, this can be resolved into two other sinusoidally distributed mmf's, one centred on the d-axis and the other on the q-axis.

The peak values of the two component waves are

$$\text{peak } MMF_{ad} = N_a i_a \cos\theta \tag{3.30}$$

$$\text{peak } MMF_{aq} = N_a i_a \cos(\theta+90°) = -N_a i_a \sin\theta \tag{3.31}$$

The reason for resolving the mmf into the d- and q-axis components is that each acts on specific air-gap geometry of defined configuration. Air-gap fluxes per pole along the two axes are

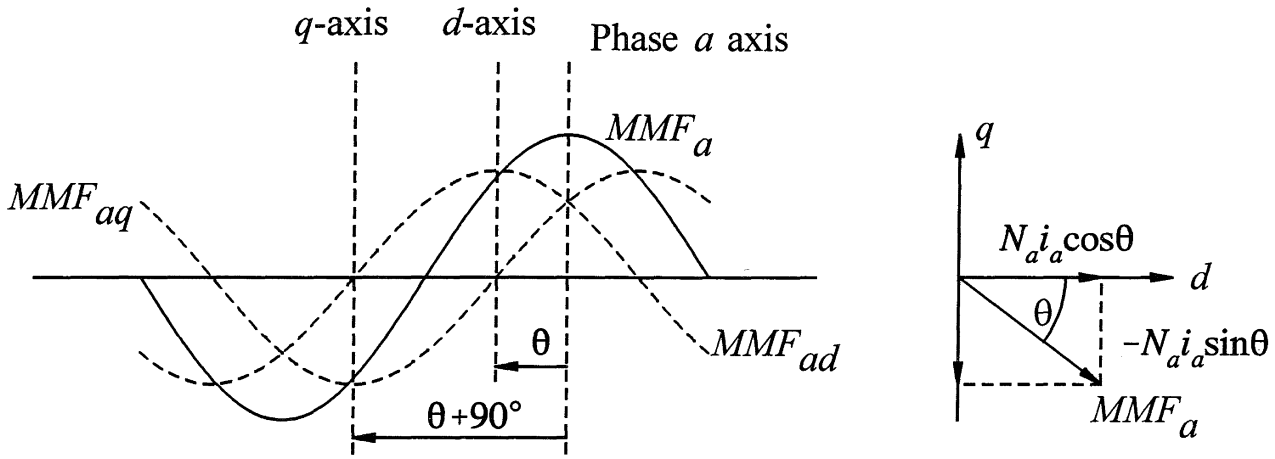

Figure 3.13 Phase a mmf wave and its components

$$\Phi_{gad} = (N_a i_a \cos\theta) P_d \tag{3.32}$$

$$\Phi_{gaq} = (-N_a i_a \sin\theta) P_q \tag{3.33}$$

In the above, P_d and P_q are the permeance coefficients of the d- and q-axis, respectively. In addition to the actual permeance, they include factors required to relate flux per pole with peak value of the mmf wave.

The total air-gap flux linking phase a is

$$\begin{aligned}\Phi_{gaa} &= \Phi_{gad}\cos\theta - \Phi_{gaq}\sin\theta \\ &= N_a i_a (P_d \cos^2\theta + P_q \sin^2\theta) \\ &= N_a i_a \left(\frac{P_d + P_q}{2} + \frac{P_d - P_q}{2} \cos 2\theta \right)\end{aligned} \tag{3.34}$$

The self-inductance l_{gaa} of phase a due to air-gap flux is

$$\begin{aligned}l_{gaa} &= \frac{N_a \Phi_{gaa}}{i_a} \\ &= N_a^2 \left(\frac{P_d + P_q}{2} + \frac{P_d - P_q}{2} \cos 2\theta \right) \\ &= L_{g0} + L_{aa2} \cos 2\theta\end{aligned} \tag{3.35}$$

The total self-inductance l_{aa} is given by adding to the above the leakage inductance L_{al} which represents the leakage flux not crossing the air-gap:

$$\begin{aligned} l_{aa} &= L_{al}+l_{gaa} \\ &= L_{al}+L_{g0}+L_{aa2}\cos 2\theta \\ &= L_{aa0}+L_{aa2}\cos 2\theta \end{aligned} \tag{3.36}$$

Since the windings of phases b and c are identical to that of phase a and are displaced from it by 120° and 240° respectively, we have

$$l_{bb} = L_{aa0}+L_{aa2}\cos 2(\theta-\frac{2\pi}{3}) \tag{3.37}$$

$$l_{cc} = L_{aa0}+L_{aa2}\cos 2(\theta+\frac{2\pi}{3}) \tag{3.38}$$

The variation of l_{aa} with θ is shown in Figure 3.14.

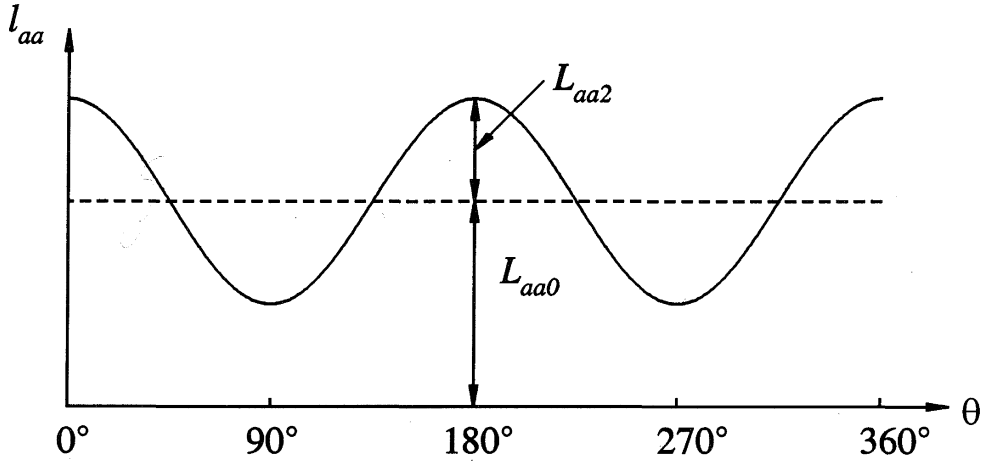

Figure 3.14 Variation of self-inductance of a stator phase

In Equations 3.36, 3.37 and 3.38, the stator self-inductances have a fixed plus second harmonic terms. Higher order harmonic terms have been neglected. In a well designed machine in which the stator and rotor windings produce nearly sinusoidally distributed mmf and flux waves, these higher order harmonic terms are negligible.

Stator mutual inductances

The mutual inductance between any two stator windings also exhibits a second harmonic variation because of the rotor shape. It is always negative, and has the greatest absolute value when the north and south poles are equidistant from the centres of the two windings concerned. For example, l_{ab} has maximum absolute value when $\theta=-30°$ or $\theta=150°$.

The mutual inductance l_{ab} can be found by evaluating the air-gap flux Φ_{gba} linking phase b when only phase a is excited. As we wish to find the flux linking phase b due to mmf of phase a, θ is replaced by $\theta-2\pi/3$ in Equation 3.34.

$$\begin{aligned}\Phi_{gba} &= \Phi_{gad}\cos(\theta-\frac{2\pi}{3})-\Phi_{gaq}\sin(\theta-\frac{2\pi}{3})\\ &= N_a i_a\left[P_d\cos\theta\cos(\theta-\frac{2\pi}{3})+P_q\sin\theta\sin(\theta-\frac{2\pi}{3})\right]\\ &= N_a i_a\left[-\frac{P_d+P_q}{4}+\frac{P_d-P_q}{2}\cos(2\theta-\frac{2\pi}{3})\right]\end{aligned} \tag{3.39}$$

The mutual inductance between phases a and b due to the air-gap flux is

$$\begin{aligned}l_{gba} &= \frac{N_a\Phi_{gba}}{i_a}\\ &= -\frac{1}{2}L_{g0}+L_{ab2}\cos(2\theta-\frac{2\pi}{3})\end{aligned} \tag{3.40}$$

where L_{g0} has the same meaning as in the expression for self-inductance l_{gaa} given by Equation 3.35. There is a very small amount of mutual flux around the ends of windings which does not cross the air-gap. With this flux included, the mutual inductance between phases a and b can be written as

$$\begin{aligned}l_{ab} = l_{ba} &= -L_{ab0}+L_{ab2}\cos(2\theta-\frac{2\pi}{3})\\ &= -L_{ab0}-L_{ab2}\cos(2\theta+\frac{\pi}{3})\end{aligned} \tag{3.41}$$

Similarly,

$$l_{bc} = l_{cb} = -L_{ab0}-L_{ab2}\cos(2\theta-\pi) \tag{3.42}$$

$$l_{ca} = l_{ac} = -L_{ab0}-L_{ab2}\cos(2\theta-\frac{\pi}{3}) \tag{3.43}$$

From the above equations, it can be readily seen that $L_{ab2}=L_{aa2}$. This is to be expected since the same variation in permeance produces the second harmonic terms in self and mutual inductances. It can also be seen that L_{ab0} is nearly equal to $L_{aa0}/2$.

The variation of mutual inductance between phases a and b as a function of θ is illustrated in Figure 3.15.

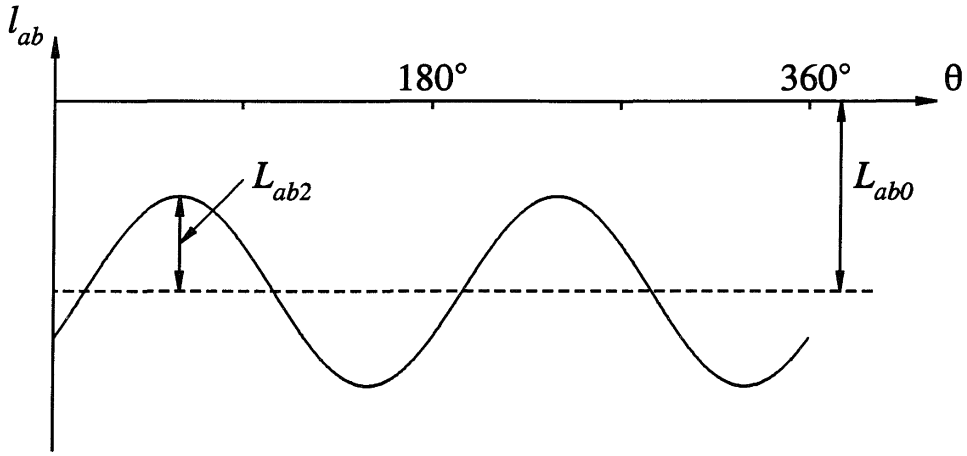

Figure 3.15 Variation of mutual inductance between stator windings

Mutual inductance between stator and rotor windings

With the variations in air-gap due to stator slots neglected, the rotor circuits see a constant permeance. Therefore, the situation in this case is not one of variation of permeance; instead, the variation in the mutual inductance is due to the relative motion between the windings themselves.

When a stator winding is lined up with a rotor winding, the flux linking the two windings is maximum and the mutual inductance is maximum. When the two windings are displaced by 90°, no flux links the two circuits and the mutual inductance is zero.

With a sinusoidal distribution of mmf and flux waves,

$$l_{afd} = L_{afd}\cos\theta \tag{3.44}$$

$$l_{akd} = L_{akd}\cos\theta \tag{3.45}$$

$$\begin{aligned} l_{akq} &= L_{akq}\cos(\theta+\frac{\pi}{2}) \\ &= -L_{akq}\sin\theta \end{aligned} \tag{3.46}$$

For considering the mutual inductance between phase b winding and the rotor circuits, θ is replaced by $\theta-2\pi/3$; for phase c winding θ is replaced by $\theta+2\pi/3$.

We now have the expressions for all the inductances that appear in the stator voltage equations. On substituting the expressions for these inductances into Equation 3.29, we obtain

$$\begin{aligned}\psi_a &= -i_a[L_{aa0}+L_{aa2}\cos 2\theta]+i_b[L_{ab0}+L_{aa2}\cos(2\theta+\frac{\pi}{3})]\\ &+i_c[L_{ab0}+L_{aa2}\cos(2\theta-\frac{\pi}{3})]+i_{fd}L_{afd}\cos\theta\\ &+i_{kd}L_{akd}\cos\theta-i_{kq}L_{akq}\sin\theta\end{aligned} \tag{3.47}$$

Similarly,

$$\begin{aligned}\psi_b &= i_a[L_{ab0}+L_{aa2}\cos(2\theta+\frac{\pi}{3})]-i_b[L_{aa0}+L_{aa2}cos2(\theta-\frac{2\pi}{3})]\\ &+i_c[L_{ab0}+L_{aa2}\cos(2\theta-\pi)]+i_{fd}L_{afd}\cos(\theta-\frac{2\pi}{3})\\ &+i_{kd}L_{akd}\cos(\theta-\frac{2\pi}{3})-i_{kq}L_{akq}\sin(\theta-\frac{2\pi}{3})\end{aligned} \tag{3.48}$$

and

$$\begin{aligned}\psi_c &= i_a[L_{ab0}+L_{aa2}\cos(2\theta-\frac{\pi}{3})]+i_b[L_{ab0}+L_{aa2}\cos(2\theta-\pi)]\\ &-i_c[L_{aa0}+L_{aa2}\cos 2(\theta+\frac{2\pi}{3})]+i_{fd}L_{afd}\cos(\theta+\frac{2\pi}{3})\\ &+i_{kd}L_{akd}\cos(\theta+\frac{2\pi}{3})-i_{kq}L_{akq}\sin(\theta+\frac{2\pi}{3})\end{aligned} \tag{3.49}$$

Rotor circuit equations

The rotor circuit voltage equations are

$$e_{fd} = p\psi_{fd}+R_{fd}i_{fd} \tag{3.50}$$

$$0 = p\psi_{kd}+R_{kd}i_{kd} \tag{3.51}$$

$$0 = p\psi_{kq}+R_{kq}i_{kq} \tag{3.52}$$

The rotor circuits see constant permeance because of the cylindrical structure of the stator. Therefore, the self-inductances of rotor circuits and mutual inductances between each other do not vary with rotor position. Only the rotor to stator mutual inductances vary periodically with θ as given by Equations 3.44, 3.45 and 3.46.

The rotor circuit flux linkages may be expressed as follows:

$$\psi_{fd} = L_{ffd}i_{fd}+L_{fkd}i_{kd}-L_{afd}[i_a\cos\theta+i_b\cos(\theta-\frac{2\pi}{3})+i_c\cos(\theta+\frac{2\pi}{3})] \quad (3.53)$$

$$\psi_{kd} = L_{fkd}i_{fd}+L_{kkd}i_{kd}-L_{akd}[i_a\cos\theta+i_b\cos(\theta-\frac{2\pi}{3})+i_c\cos(\theta+\frac{2\pi}{3})] \quad (3.54)$$

$$\psi_{kq} = L_{kkq}i_{kq}+L_{akq}[i_a\sin\theta+i_b\sin(\theta-\frac{2\pi}{3})+i_c\sin(\theta+\frac{2\pi}{3})] \quad (3.55)$$

3.3 THE *dq0* TRANSFORMATION

Equations 3.26 to 3.28 and Equations 3.47 to 3.49 associated with the stator circuits, together with Equations 3.50 to 3.55 associated with the rotor circuits, completely describe the electrical performance of a synchronous machine. However, these equations contain inductance terms which vary with angle θ which in turn varies with time. This introduces considerable complexity in solving machine and power system problems. A much simpler form leading to a clearer physical picture is obtained by appropriate transformation of stator variables.

We see from Equations 3.53 to 3.55 that stator currents combine into convenient forms in each axis. This suggests the transformation of the stator phase currents into new variables as follows:

$$i_d = k_d\left[i_a\cos\theta+i_b\cos(\theta-\frac{2\pi}{3})+i_c\cos(\theta+\frac{2\pi}{3})\right] \quad (3.56)$$

$$i_q = -k_q\left[i_a\sin\theta+i_b\sin(\theta-\frac{2\pi}{3})+i_c\sin(\theta+\frac{2\pi}{3})\right] \quad (3.57)$$

The constants k_d and k_q are arbitrary and their values may be chosen to simplify numerical coefficients in performance equations. In most of the literature on synchronous machine theory [3,10,11,12,13,19], k_d and k_q are taken as 2/3, and this choice will be followed here. An alternative transformation with $k_d=k_q=\sqrt{2/3}$ is discussed in Section 3.4.8.

With k_d and k_q equal to 2/3, for balanced sinusoidal conditions, the peak values of i_d and i_q are equal to the peak value of the stator current as shown below.

For the balanced condition,

$$i_a = I_m \sin\omega_s t$$

$$i_b = I_m \sin(\omega_s t - \frac{2\pi}{3})$$

$$i_c = I_m \sin(\omega_s t + \frac{2\pi}{3})$$

Substituting in Equation 3.56 gives

$$i_d = k_d\left[I_m \sin\omega_s t\cos\theta + I_m \sin(\omega_s t - \frac{2\pi}{3})\cos(\theta - \frac{2\pi}{3}) + I_m \sin(\omega_s t + \frac{2\pi}{3})\cos(\theta + \frac{2\pi}{3})\right]$$

$$= k_d \frac{3}{2} I_m \sin(\omega_s t - \theta)$$

For the peak value of i_d to be equal to I_m, k_d should equal 2/3.

Similarly from Equation 3.57, for the balanced condition

$$i_q = -k_q \frac{3}{2} I_m \cos(\omega_s t - \theta)$$

Again, k_q=2/3 results in the maximum value of i_q being equal to the peak value of stator current.

To give a complete degree of freedom, a third component must be defined so that the three-phase currents are transformed into three variables. Since the two current components i_d and i_q together produce a field identical to that produced by the original set of phase currents, the third component must produce no space field in the air-gap. Therefore, a convenient third variable is the zero sequence current i_0, associated with the symmetrical components:

$$i_0 = \frac{1}{3}(i_a + i_b + i_c) \tag{3.58}$$

Under balanced conditions $i_a+i_b+i_c=0$ and, therefore, $i_0=0$.

The transformation from the *abc* phase variables to the *dq0* variables can be written in the following matrix form:

$$\begin{bmatrix} i_d \\ i_q \\ i_0 \end{bmatrix} = \frac{2}{3} \begin{bmatrix} \cos\theta & \cos(\theta-\frac{2\pi}{3}) & \cos(\theta+\frac{2\pi}{3}) \\ -\sin\theta & -\sin(\theta-\frac{2\pi}{3}) & -\sin(\theta+\frac{2\pi}{3}) \\ \frac{1}{2} & \frac{1}{2} & \frac{1}{2} \end{bmatrix} \begin{bmatrix} i_a \\ i_b \\ i_c \end{bmatrix} \tag{3.59}$$

The inverse transformation is given by

$$\begin{bmatrix} i_a \\ i_b \\ i_c \end{bmatrix} = \begin{bmatrix} \cos\theta & -\sin\theta & 1 \\ \cos(\theta-\frac{2\pi}{3}) & -\sin(\theta-\frac{2\pi}{3}) & 1 \\ \cos(\theta+\frac{2\pi}{3}) & -\sin(\theta+\frac{2\pi}{3}) & 1 \end{bmatrix} \begin{bmatrix} i_d \\ i_q \\ i_0 \end{bmatrix} \tag{3.60}$$

The above transformations also apply to stator flux linkages and voltages.

Stator flux linkages in dq0 components

Using the expressions for ψ_a, ψ_b and ψ_c given by Equations 3.47, 3.48 and 3.49, transforming the flux linkages and currents into *dq0* components (Equation 3.59), and with suitable reduction of terms involving trigonometric terms, we obtain the following expressions:

$$\psi_d = -(L_{aa0}+L_{ab0}+\frac{3}{2}L_{aa2})i_d+L_{afd}i_{fd}+L_{akd}i_{kd}$$

$$\psi_q = -(L_{aa0}+L_{ab0}-\frac{3}{2}L_{aa2})i_q+L_{akq}i_{kq}$$

$$\psi_0 = -(L_{aa0}-2L_{ab0})i_0$$

Defining the following new inductances

$$L_d = L_{aa0}+L_{ab0}+\frac{3}{2}L_{aa2} \tag{3.61}$$

$$L_q = L_{aa0}+L_{ab0}-\frac{3}{2}L_{aa2} \tag{3.62}$$

$$L_0 = L_{aa0}-2L_{ab0} \tag{3.63}$$

the flux linkage equations become

$$\psi_d = -L_d i_d+L_{afd} i_{fd}+L_{akd} i_{kd} \tag{3.64}$$

$$\psi_q = -L_q i_q+L_{akq} i_{kq} \tag{3.65}$$

$$\psi_0 = -L_0 i_0 \tag{3.66}$$

The *dq0* components of stator flux linkages are seen to be related to the components of stator and rotor currents through constant inductances.

Rotor flux linkages in dq0 components

Substitution of the expressions for i_d, i_q in Equations 3.53 to 3.55 gives

$$\psi_{fd} = L_{ffd} i_{fd}+L_{fkd} i_{kd}-\frac{3}{2}L_{afd} i_d \tag{3.67}$$

$$\psi_{kd} = L_{fkd} i_{fd}+L_{kkd} i_{kd}-\frac{3}{2}L_{akd} i_d \tag{3.68}$$

$$\psi_{kq} = L_{kkq} i_{kq}-\frac{3}{2}L_{akq} i_q \tag{3.69}$$

Again, all the inductances are seen to be constant, i.e., they are independent of the rotor position. It should, however, be noted that the saturation effects are not considered here. The variations in inductances due to saturation are of a different nature and this will be treated separately.

It is interesting to note that i_0 does not appear in the rotor flux linkage equations. This is because zero sequence components of armature current do not produce net mmf across the air-gap.

While the *dq0* transformation has resulted in constant inductances in Equations 3.64 to 3.69, the mutual inductances between stator and rotor quantities are not reciprocal. For example, the mutual inductance associated with the flux linking the field winding due to current i_d flowing in the *d*-axis stator winding from Equation

3.67 is $(3/2)L_{afd}$, whereas from Equation 3.64 the mutual inductance associated with flux linking the *d*-axis stator winding due to field current is L_{afd}. As discussed in Section 3.4, this problem is overcome by appropriate choice of the per unit system for the rotor quantities.

Stator voltage equations in dq0 components

Equations 3.26 to 3.28 are basic equations for phase voltages in terms of phase flux linkages and currents. By applying the *dq0* transformation of Equation 3.59, the following expressions in terms of transformed components of voltages, flux linkages and currents result:

$$e_d = p\psi_d - \psi_q p\theta - R_a i_d \tag{3.70}$$

$$e_q = p\psi_q + \psi_d p\theta - R_a i_q \tag{3.71}$$

$$e_0 = p\psi_0 - R_a i_0 \tag{3.72}$$

The angle θ, as defined in Figure 3.9, is the angle between the axis of phase *a* and the *d*-axis. The term $p\theta$ in the above equations represents the angular velocity ω_r of the rotor. For a 60 Hz system under steady-state conditions $p\theta = \omega_r = \omega_s = 2\pi 60 = 377$ electrical rad/s.

The above equations have a form similar to those of a static coil, except for the $\psi_q p\theta$ and $\psi_d p\theta$ terms. They result from the transformation from a stationary to a rotating reference frame, and represent the fact that a flux wave rotating in synchronism with the rotor will create voltages in the stationary armature coil. The $\psi_q p\theta$ and $\psi_d p\theta$ terms are referred to as *speed voltages* (due to flux change in space) and the terms $p\psi_d$ and $p\psi_q$ as the *transformer voltages* (due to flux change in time).

The speed voltage terms are the dominant components of the stator voltage. Under steady-state conditions, the transformer voltage terms $p\psi_d$ and $p\psi_q$ are in fact equal to zero; there are many transient conditions where the transformer voltage terms can be dropped from the stator voltage equations without causing errors of any significance. However, in other situations they could be important. This will be discussed further in Sections 3.7 and 5.1.

The signs associated with the speed voltage terms in Equations 3.70 and 3.71 are related to the sign conventions assumed for the voltage and flux linkage relationship and to the assumed relative positions of *d*- and *q*- axes. Since we have assumed that the *q*-axis leads the *d*-axis by 90°, the voltage e_q in the *q*-axis is induced by the flux in the *d*-axis. Similarly, the voltage e_d is induced by a flux in an axis lagging the *d*-axis by 90°, i.e., the negative *q*-axis. Therefore, the voltage induced in the *q*-axis due to rotation is $+\omega\psi_d$ and that in the *d*-axis is $-\omega\psi_q$.

Electrical power and torque

The instantaneous three-phase power output of the stator is

$$P_t = e_a i_a + e_b i_b + e_c i_c$$

Eliminating phase voltages and currents in terms of *dq0* components, we have

$$P_t = \frac{3}{2}(e_d i_d + e_q i_q + 2e_0 i_0) \tag{3.73}$$

Under balanced operation, $e_0 = i_0 = 0$ and the expression for power is given by

$$P_t = \frac{3}{2}(e_d i_d + e_q i_q)$$

The electromagnetic torque may be determined from the basic consideration of forces acting on conductors as being the product of currents and the flux. Alternatively, it can be derived by developing an expression for the power transferred across the air-gap.

Using Equations 3.70 to 3.72 to express the voltage components in terms of flux linkages and currents, by recognizing ω_r as the rotor speed $d\theta/dt$, and rearranging, we have

$$\begin{aligned} P_t = \frac{3}{2}[&(i_d p\psi_d + i_q p\psi_q + 2i_0 p\psi_0) \\ &+ (\psi_d i_q - \psi_q i_d)\omega_r \\ &- (i_d^2 + i_q^2 + 2i_0^2) R_a] \end{aligned} \tag{3.74}$$

= (Rate of change of armature magnetic energy)
+(power transferred across the air-gap)
-(armature resistance loss)

The air-gap torque T_e is obtained by dividing the power transferred across the air-gap (i.e., power corresponding to the speed voltages) by the rotor speed in mechanical radians per second.

$$\begin{aligned} T_e &= \frac{3}{2}(\psi_d i_q - \psi_q i_d)\frac{\omega_r}{\omega_{mech}} \\ &= \frac{3}{2}(\psi_d i_q - \psi_q i_d)\frac{p_f}{2} \end{aligned} \tag{3.75}$$

The flux-linkage equations 3.64 to 3.69 associated with the stator and rotor circuits, together with the voltage equations 3.70 to 3.72 for the stator, the voltage equations 3.50 to 3.52 for the rotor, and the torque equation 3.75, describe the electrical dynamic performance of the machine in terms of the *dq0* components. These equations are usually referred to as Park's equations in honour of R.H. Park who developed the concepts on which the equations are based [3]. The *dq0* transformation given by Equation 3.59 is referred to as Park's transformation. It is based on the two-reaction theory originally developed by Blondel [1] and the further exposition of the concept by Doherty and Nickle [2].

Physical interpretation of dq0 transformation

In Section 3.1.3, we saw that the combined mmf wave due to the currents in the three armature phases travels along the periphery of the stator at a velocity of ω_s rad/s. This is also the velocity of the rotor. Therefore, for balanced synchronous operation, the armature mmf wave appears stationary with respect to the rotor and has a sinusoidal space distribution. Since a sine function can be expressed as a sum of two sine functions, the mmf due to stator windings can be resolved into two sinusoidally distributed mmf waves stationary with respect to the rotor, so that one has its peak over the *d*-axis and the other has its peak over the *q*-axis. Therefore, i_d may be interpreted as the instantaneous current in a fictitious armature winding which rotates at the same speed as the rotor, and remains in such a position that its axis always coincides with the *d*-axis. The value of the current in this winding is such that it results in the same mmf on the *d*-axis as do actual phase currents flowing in the armature windings. A similar interpretation applies to i_q, except that it acts on the *q*-axis instead of the *d*-axis.

The mmfs due to i_d and i_q are stationary with respect to the rotor and act on paths of constant permeance. Therefore, the corresponding inductances L_d and L_q are constant.

For balanced steady-state conditions, the phase currents may be written as follows:

$$i_a = I_m \sin(\omega_s t + \phi) \tag{3.76}$$

$$i_b = I_m \sin(\omega_s t + \phi - \frac{2\pi}{3}) \tag{3.77}$$

$$i_c = I_m \sin(\omega_s t + \phi + \frac{2\pi}{3}) \tag{3.78}$$

where $\omega_s = 2\pi f$ is the angular frequency of stator currents. Using the *dq0* transformation,

$$i_d = I_m \sin(\omega_s t + \phi - \theta) \tag{3.79}$$

$$i_q = -I_m \cos(\omega_s t + \phi - \theta) \tag{3.80}$$

$$i_0 = 0 \tag{3.81}$$

For synchronous operation, the rotor speed ω_r is equal to the angular frequency ω_s of the stator currents. Hence,

$$\theta = \omega_r t = \omega_s t$$

Therefore,

$$i_d = I_m \sin\phi = \text{constant}$$

$$i_q = -I_m \cos\phi = \text{constant}$$

For balanced steady-state operation, i_d and i_q are constant. In other words, alternating phase currents in the *abc* reference frame appear as direct currents in the *dq0* reference frame.

The *dq0* transformation may be viewed as a means of referring the stator quantities to the rotor side. This is analogous to referring secondary side quantities in a transformer to the primary side by means of the turns ratio. The inverse transformation (Equation 3.60) can similarly be viewed as referring the rotor quantities to the stator side.

The analysis of synchronous machine equations in terms of *dq0* variables is considerably simpler than in terms of phase quantities, for the following reasons:

- The dynamic performance equations have constant inductances.
- For balanced conditions, zero sequence quantities disappear.
- For balanced steady-state operation, the stator quantities have constant values. For other modes of operation they vary with time. Stability studies involve slow variations having frequencies below 2 to 3 Hz.
- The parameters associated with *d*- and *q*-axes may be directly measured from terminal tests.

We will show in Section 3.6 that, under balanced steady-state conditions, the *dq0* transformation is equivalent to the use of phasors to represent alternating stator phase quantities. In many ways, the advantages of using *d,q* variables are similar to those of using phasors (instead of dealing directly with time varying sinusoidal quantities) for steady-state analysis of ac circuits.

3.4 PER UNIT REPRESENTATION

In power system analysis, it is usually convenient to use a per unit system to normalize system variables. Compared to the use of physical units (amperes, volts, ohms, webers, henrys, etc.), the per unit system offers computational simplicity by eliminating units and expressing system quantities as dimensionless ratios. Thus,

$$\text{quantity in per unit} = \frac{\text{actual quantity}}{\text{base value of quantity}}$$

A well-chosen per unit system can minimize computational effort, simplify evaluation, and facilitate understanding of system characteristics. Some base quantities may be chosen independently and quite arbitrarily, while others follow automatically depending on fundamental relationships between system variables. Normally, the base values are chosen so that the principal variables will be equal to one per unit under rated condition.

In the case of a synchronous machine, the per unit system may be used to remove arbitrary constants and simplify mathematical equations so that they may be expressed in terms of equivalent circuits. The basis for selection of the per unit system for the stator is straightforward, whereas it requires careful consideration for the rotor. Several alternative per unit systems have been proposed in the literature for the selection of base rotor quantities [18,19]. Only one system will be discussed here as it offers several advantages over others and has found wide acceptance. This system is referred to as *the L_{ad}-base reciprocal per unit system.*

In this section, for the purpose of defining per unit values and showing their relationships to the values in natural units, a superbar will be used to identify per unit quantities. We will, however, drop this convention for subsequent general use to simplify the notation.

3.4.1 Per Unit System for the Stator Quantities

The universal practice is to use the machine ratings as the base values for the stator quantities. In the machine equations developed so far, the stator currents and voltages have been expressed as instantaneous values; where they were sinusoidal quantities, they have been expressed in terms of the peak values and sinusoidal functions of time and frequency.

Let us choose the following base quantities for the stator (denoted by subscript *s*):

e_{sbase} = peak value of rated line-to-neutral voltage, V
i_{sbase} = peak value of rated line current, A
f_{base} = rated frequency, Hz

The base values of the remaining quantities are automatically set and depend on the above as follows:

$$\omega_{base} = 2\pi f_{base}, \text{ elec. radians/second}$$

$$\omega_{m\,base} = \omega_{base}\left(\frac{2}{p_f}\right), \text{ mech. radians/second}$$

$$Z_{s\,base} = \frac{e_{s\,base}}{i_{s\,base}}, \text{ ohms}$$

$$L_{s\,base} = \frac{Z_{s\,base}}{\omega_{base}}, \text{ henrys}$$

$$\psi_{s\,base} = L_{s\,base} i_{s\,base}$$

$$= \frac{e_{s\,base}}{\omega_{base}}, \text{ weber-turns}$$

$$\text{3-phase VA}_{base} = 3E_{RMS\,base} I_{RMS\,base}$$

$$= 3\frac{e_{s\,base}}{\sqrt{2}}\frac{i_{s\,base}}{\sqrt{2}}$$

$$= \frac{3}{2} e_{s\,base} i_{s\,base}, \text{ volt-amperes}$$

$$\text{Torque base} = \frac{\text{3-phase VA}_{base}}{\omega_{m\,base}}$$

$$= \frac{3}{2}\left(\frac{p_f}{2}\right)\psi_{s\,base} i_{s\,base}, \text{ newton-meters}$$

3.4.2 Per Unit Stator Voltage Equations

From Equation 3.70,

$$e_d = p\psi_d - \psi_q \omega_r - R_a i_d$$

Dividing throughout by $e_{s\,base}$, and noting that $e_{s\,base} = i_{s\,base} Z_{s\,base} = \omega_{base} \psi_{s\,base}$, we get

$$\frac{e_d}{e_{s\,base}} = p\left(\frac{1}{\omega_{s\,base}}\frac{\psi_d}{\psi_{s\,base}}\right) - \frac{\psi_q}{\psi_{s\,base}}\frac{\omega_r}{\omega_{base}} - \frac{R_a}{Z_{s\,base}}\frac{i_d}{i_{s\,base}} \tag{3.82}$$

Expressed in per unit notation,

$$\bar{e}_d = \frac{1}{\omega_{base}} p\bar{\psi}_d - \bar{\psi}_q \bar{\omega}_r - \bar{R}_a \bar{i}_d \tag{3.83}$$

The unit of time in the above equation is seconds. Time can also be expressed in per unit (or radians) with the base value equal to the time required for the rotor to move one electrical radian at synchronous speed:

$$t_{base} = \frac{1}{\omega_{base}} = \frac{1}{2\pi f_{base}} \tag{3.84}$$

With time in per unit, Equation 3.83 may be written as

$$\bar{e}_d = \bar{p}\bar{\psi}_d - \bar{\psi}_q \bar{\omega}_r - \bar{R}_a \bar{i}_d \tag{3.85}$$

Comparing Equation 3.70 and Equation 3.85, we see that the form of the original equation is unchanged, when all quantities involved are expressed in per unit.

Similarly, the per unit forms of Equations 3.71 and 3.72 are

$$\bar{e}_q = \bar{p}\bar{\psi}_q + \bar{\psi}_d \bar{\omega}_r - \bar{R}_a \bar{i}_q \tag{3.86}$$

$$\bar{e}_0 = \bar{p}\bar{\psi}_0 - \bar{R}_a \bar{i}_0 \tag{3.87}$$

The per unit time derivative $\bar{p}$ appearing in the above equations is given by

$$\bar{p} = \frac{d}{d\bar{t}} = \frac{1}{\omega_{base}} \frac{d}{dt} = \frac{1}{\omega_{base}} p \tag{3.88}$$

3.4.3 Per Unit Rotor Voltage Equations

From Equation 3.50, dividing throughout by $e_{fd\,base} = \omega_{base} \psi_{fd\,base} = Z_{fd\,base} i_{fd\,base}$, the per unit field voltage equation may be written as

$$\bar{e}_{fd} = \bar{p}\bar{\psi}_{fd} + \bar{R}_{fd} \bar{i}_{fd} \tag{3.89}$$

Similarly, the per unit forms of Equations 3.51 and 3.52 are

$$0 = \bar{p}\bar{\psi}_{kd} + \bar{R}_{kd}\bar{i}_{kd} \tag{3.90}$$

$$0 = \bar{p}\bar{\psi}_{kq} + \bar{R}_{kq}\bar{i}_{kq} \tag{3.91}$$

The above equations show the form of the rotor circuit voltage equations. However, we have not yet developed a basis for the choice of the rotor base quantities.

3.4.4 Stator Flux Linkage Equations

Using the basic relationship $\psi_{s\,base} = L_{s\,base}\, i_{s\,base}$, the per unit forms of Equations 3.64, 3.65 and 3.66 may be written as

$$\bar{\psi}_d = -\bar{L}_d\bar{i}_d + \bar{L}_{afd}\bar{i}_{fd} + \bar{L}_{akd}\bar{i}_{kd} \tag{3.92}$$

$$\bar{\psi}_q = -\bar{L}_q\bar{i}_q + \bar{L}_{akq}\bar{i}_q \tag{3.93}$$

$$\bar{\psi}_0 = -\bar{L}_0\bar{i}_0 \tag{3.94}$$

where by definition,

$$\bar{L}_{afd} = \frac{L_{afd}}{L_{s\,base}}\frac{i_{fd\,base}}{i_{s\,base}} \tag{3.95}$$

$$\bar{L}_{akd} = \frac{L_{akd}}{L_{s\,base}}\frac{i_{kd\,base}}{i_{s\,base}} \tag{3.96}$$

$$\bar{L}_{akq} = \frac{L_{akq}}{L_{s\,base}}\frac{i_{kq\,base}}{i_{s\,base}} \tag{3.97}$$

3.4.5 Rotor Flux Linkage Equations

Similarly, in per unit form Equations 3.67, 3.68 and 3.69 become

$$\bar{\psi}_{fd} = \bar{L}_{ffd}\bar{i}_{fd} + \bar{L}_{fkd}\bar{i}_{kd} - \bar{L}_{fda}\bar{i}_d \tag{3.98}$$

$$\bar{\psi}_{kd} = \bar{L}_{kdf}\bar{i}_{fd} + \bar{L}_{kkd}\bar{i}_{kd} - \bar{L}_{kda}\bar{i}_d \tag{3.99}$$

$$\bar{\psi}_{kq} = \bar{L}_{kkq}\bar{i}_{kq} - \bar{L}_{kqa}\bar{i}_q \tag{3.100}$$

where by definition,

$$\bar{L}_{fda} = \frac{3}{2}\frac{L_{afd}}{L_{fdbase}}\frac{i_{sbase}}{i_{fdbase}} \tag{3.101}$$

$$\bar{L}_{fkd} = \frac{L_{fkd}}{L_{fdbase}}\frac{i_{kdbase}}{i_{fdbase}} \tag{3.102}$$

$$\bar{L}_{kda} = \frac{3}{2}\frac{L_{akd}}{L_{kdbase}}\frac{i_{sbase}}{i_{kdbase}} \tag{3.103}$$

$$\bar{L}_{kdf} = \frac{L_{fkd}}{L_{kdbase}}\frac{i_{fdbase}}{i_{kdbase}} \tag{3.104}$$

$$\bar{L}_{kqa} = \frac{3}{2}\frac{L_{akq}}{L_{kqbase}}\frac{i_{sbase}}{i_{kqbase}} \tag{3.105}$$

By appropriate choice of per unit system, we have eliminated the factor 3/2 in the rotor flux equations. However, we have not yet tied down the values of the rotor base voltages and currents, which we will proceed to do next.

3.4.6 Per Unit System for the Rotor

The rotor circuit base quantities will be chosen so as to make the flux linkage equations simple by satisfying the following:

(a) The per unit mutual inductances between different windings are to be reciprocal; for example, $\bar{L}_{afd}=\bar{L}_{fda}$. This will allow the synchronous machine model to be represented by equivalent circuits.

(b) All per unit mutual inductances between stator and rotor circuits in each axis are to be equal; for example, $\bar{L}_{afd}=\bar{L}_{akd}$.

In order to have $\bar{L}_{fkd}$ equal to $\bar{L}_{kdf}$ so that reciprocity is achieved, from Equations 3.102 and 3.104, it is necessary to have

$$\frac{L_{fkd}}{L_{fdbase}}\frac{i_{kdbase}}{i_{fdbase}} = \frac{L_{fkd}}{L_{kdbase}}\frac{i_{fdbase}}{i_{kdbase}}$$

or

$$L_{kdbase}i_{kdbase}^2 = L_{fdbase}i_{fdbase}^2 \tag{3.106}$$

Multiplying by ω_{base} gives

$$\omega_{base} L_{kdbase} i_{kdbase}^2 = \omega_{base} L_{fdbase} i_{fdbase}^2$$

Since $\omega_{base} L_{base} i_{base} = e_{base}$,

$$e_{kdbase} i_{kdbase} = e_{fdbase} i_{fdbase} \tag{3.107}$$

Therefore, in order for the rotor circuit mutual inductances to be equal, their volt-ampere bases must be equal.

For mutual inductances $\bar{L}_{afd}$ and $\bar{L}_{fda}$ to be equal, from Equations 3.95 and 3.101,

$$\frac{L_{afd}}{L_{sbase}} \frac{i_{fdbase}}{i_{sbase}} = \frac{3}{2} \frac{L_{afd}}{L_{fdbase}} \frac{i_{sbase}}{i_{fdbase}}$$

or

$$L_{fdbase} i_{fdbase}^2 = \frac{3}{2} L_{sbase} i_{sbase}^2$$

Multiplying by ω_{base} and noting that $\omega Li = e$, we get

$$\begin{aligned} e_{fdbase} i_{fdbase} &= \frac{3}{2} e_{sbase} i_{sbase} \\ &= 3\text{-phase VA base for stator} \end{aligned} \tag{3.108}$$

Similarly in order for $\bar{L}_{akd} = \bar{L}_{kda}$ and $\bar{L}_{akq} = \bar{L}_{kqa}$,

$$e_{kdbase} i_{kdbase} = \frac{3}{2} e_{sbase} i_{sbase} \tag{3.109}$$

and

$$e_{kqbase} i_{kqbase} = \frac{3}{2} e_{sbase} i_{sbase} \tag{3.110}$$

These equations imply that in order to satisfy requirement (a) above, the volt-ampere base in all rotor circuits must be the same and equal to the stator three-phase VA base.

So far, we have specified only the product of base voltage and base current for the rotor circuits. The next step is to specify either the base voltage or the base current for these circuits.

The stator self inductances $\bar{L}_d$ and $\bar{L}_q$ are associated with the total flux linkages due to i_d and i_q, respectively. They can be split into two parts: the leakage inductance due to flux that does not link any rotor circuit and the mutual inductance due to flux that links the rotor circuits. As shown in Figure 3.16, the stator leakage flux is made up of the slot leakage, end turn leakage and air-gap leakage. The stator

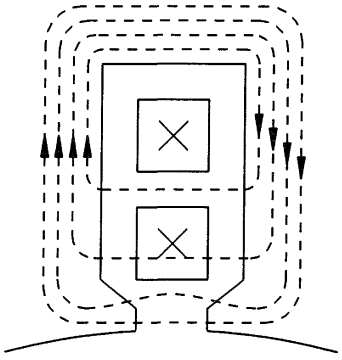

(a) Leakage flux within the slot

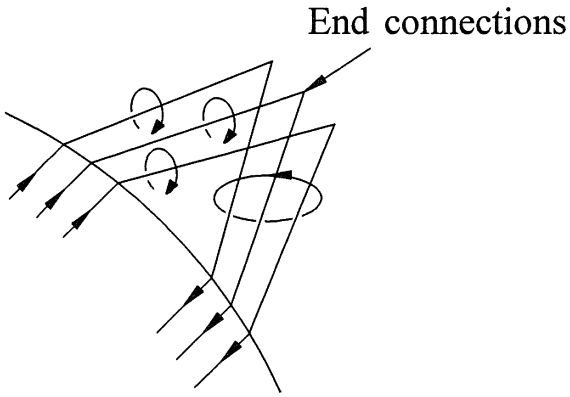

(b) Leakage flux around the end connection

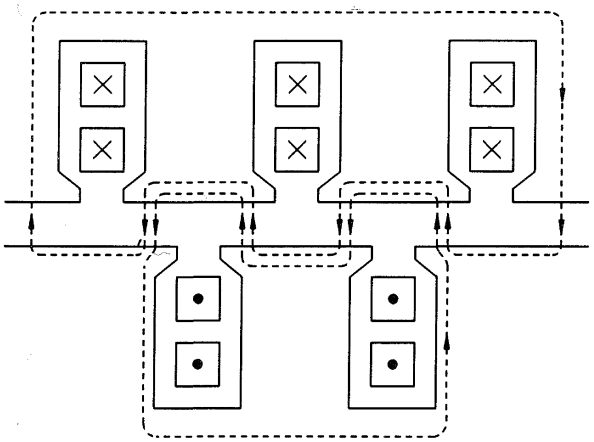

(c) Leakage flux following zigzag path between stator and rotor tooth faces along the air-gap

Figure 3.16 Stator leakage flux patterns

leakage inductances in the two axes are nearly equal. Denoting the leakage inductance $\bar{L}_l$ and the mutual inductances by $\bar{L}_{ad}$ and $\bar{L}_{aq}$:

$$\bar{L}_d = \bar{L}_l + \bar{L}_{ad} \tag{3.111}$$

and

$$\bar{L}_q = \bar{L}_l + \bar{L}_{aq} \tag{3.112}$$

In order to make all the per unit mutual inductances between the stator and rotor circuits in the *d*-axis equal, from Equations 3.95 and 3.96 it follows that

$$\bar{L}_{ad} = \frac{L_{ad}}{L_{sbase}} = \bar{L}_{afd} = \frac{L_{afd}}{L_{sbase}} \frac{i_{fdbase}}{i_{sbase}}$$

$$= \bar{L}_{akd} = \frac{L_{akd}}{L_{sbase}} \frac{i_{kdbase}}{i_{sbase}}$$

Therefore,

$$i_{fdbase} = \frac{L_{ad}}{L_{afd}} i_{sbase} \tag{3.113}$$

$$i_{kdbase} = \frac{L_{ad}}{L_{akd}} i_{sbase} \tag{3.114}$$

Similarly, for the *q*-axis mutual inductances $\bar{L}_{aq}$ and $\bar{L}_{akq}$ to be equal,

$$i_{kqbase} = \frac{L_{aq}}{L_{akq}} i_{sbase} \tag{3.115}$$

This completes the choice of rotor base quantities.

As stated before, the per unit system used here is referred to as the L_{ad}-base reciprocal per unit system. In this system, the base current in any rotor circuit is defined as that which induces in each phase a per unit voltage equal to per unit $\bar{L}_{ad}$, that is, the same voltage as balanced three-phase unit-peak armature currents.

3.4.7 Per Unit Power and Torque

From Equation 3.73, the instantaneous power at the machine terminal is

$$P_t = \frac{3}{2}(e_d i_d + e_q i_q + 2e_0 i_0)$$

Dividing by the base three-phase VA $=(3/2)e_{s\,base}\, i_{s\,base}$, the expression for per unit may be written as

$$\bar{P}_t = \bar{e}_d \bar{i}_d + \bar{e}_q \bar{i}_q + 2\bar{e}_0 \bar{i}_0 \tag{3.116}$$

Similarly, with base torque $= \frac{3}{2}\left(\frac{p_f}{2}\right)\psi_{s base} i_{s base}$, the per unit form of Equation 3.75 is

$$\bar{T}_e = \bar{\psi}_d \bar{i}_q - \bar{\psi}_q \bar{i}_d \tag{3.117}$$

3.4.8 Alternative Per Unit Systems and Transformations

Several different alternative per unit systems have been proposed in the literature for the analysis of synchronous machines [4,13,16]. Some analysts, notably Lewis [20], have also suggested the use of an alternative form of transformation from the *abc* reference frame to the *dq0* reference frame, which is similar to that of Equation 3.59, but with factors k_d and k_q equal to $\sqrt{2/3}$ instead of 2/3 and with zero-sequence coefficients equal to $1/\sqrt{2}$. The alternative transformation equations are given by

$$\begin{bmatrix} i_d \\ i_q \\ i_0 \end{bmatrix} = \sqrt{\frac{2}{3}} \begin{bmatrix} \cos\theta & \cos(\theta - \frac{2\pi}{3}) & \cos(\theta + \frac{2\pi}{3}) \\ -\sin\theta & -\sin(\theta - \frac{2\pi}{3}) & -\sin(\theta + \frac{2\pi}{3}) \\ \sqrt{\frac{1}{2}} & \sqrt{\frac{1}{2}} & \sqrt{\frac{1}{2}} \end{bmatrix} \begin{bmatrix} i_a \\ i_b \\ i_c \end{bmatrix} \tag{3.118}$$

and the inverse transformation by

$$\begin{bmatrix} i_a \\ i_b \\ i_c \end{bmatrix} = \sqrt{\frac{2}{3}} \begin{bmatrix} \cos\theta & -\sin\theta & \sqrt{\frac{1}{2}} \\ \cos(\theta-\frac{2\pi}{3}) & -\sin(\theta-\frac{2\pi}{3}) & \sqrt{\frac{1}{2}} \\ \cos(\theta+\frac{2\pi}{3}) & -\sin(\theta+\frac{2\pi}{3}) & \sqrt{\frac{1}{2}} \end{bmatrix} \begin{bmatrix} i_d \\ i_q \\ i_0 \end{bmatrix} \tag{3.119}$$

Such a transformation is orthogonal; i.e., the inverse of the transformation matrix is equal to its transpose. This also means that the transformation is power invariant:

$$\begin{aligned} P_t &= e_a i_a + e_b i_b + e_c i_c \\ &= e_d i_d + e_q i_q + e_0 i_0 \end{aligned}$$

In addition, with this transformation, all mutual inductances would be reciprocal. However, as discussed in reference 19 by Harris, Lawrenson and Stephenson, such a transformation has several fundamental disadvantages which appear to override the advantages. The orthogonal transformation does not correspond to any particular meaningful physical situation. With k_d and k_q equal to $\sqrt{2/3}$, the equivalent *d*- and *q*-axis coils would have $\sqrt{3/2}$ times the number of turns as *abc* coils. This removes the unit-to-unit relationship between *abc* and *dq0* variables that exists with the original transformation of Equation 3.59.

Reference 19 provides a thorough and comprehensive analysis of the alternative per unit and transformation systems. It concludes that the transformation of Equation 3.59 together with the L_{ad}-base reciprocal per unit system leads to a system which reflects most closely the physical features of the machine. In addition, the inductances in the resulting equivalent circuits correspond to those normally calculated by machine designers. In view of these advantages, this system is widely used by the electrical utility industry and generator manufacturers.

3.4.9 Summary of Per Unit Equations

Base quantities

Stator base quantities:

3-phase VA_{base} = volt-ampere rating of machine, VA

e_{sbase} = peak phase-to-neutral rated voltage, V

$$f_{base} = \text{rated frequency, Hz}$$

$$i_{sbase} = \text{peak line current, A}$$

$$= \frac{3\text{-phase VA}_{base}}{(3/2)\,e_{sbase}}$$

$$Z_{sbase} = \frac{e_{sbase}}{i_{sbase}}, \Omega$$

$$\omega_{base} = 2\pi f_{base}, \text{ elec. rad/s}$$

$$\omega_{mbase} = \omega_{base}\frac{2}{p_f}, \text{ mech. rad/s}$$

$$L_{sbase} = \frac{Z_{sbase}}{\omega_{base}}, \text{ H}$$

$$\psi_{sbase} = L_{sbase} i_{sbase}, \text{ Wb·turns}$$

Rotor base quantities:

$$i_{fdbase} = \frac{L_{ad}}{L_{afd}} i_{sbase}, \text{ A}$$

$$i_{kdbase} = \frac{L_{ad}}{L_{akd}} i_{sbase}, \text{ A}$$

$$i_{kqbase} = \frac{L_{aq}}{L_{akq}} i_{sbase}, \text{ A}$$

$$e_{fdbase} = \frac{3\text{-phase VA}_{base}}{i_{fdbase}}, \text{ V}$$

$$Z_{fdbase} = \frac{e_{fdbase}}{i_{fdbase}}, \Omega$$

$$= \frac{3\text{-phase VA}_{base}}{i^2_{fdbase}}$$

$$Z_{kdbase} = \frac{3\text{-phase VA}_{base}}{i^2_{kdbase}}, \Omega$$

$$Z_{kqbase} = \frac{3\text{-phase VA}_{base}}{i^2_{kqbase}}, \Omega$$

$$L_{fdbase} = \frac{Z_{fdbase}}{\omega_{base}}, \text{ H}$$

$$L_{kd\,base} = \frac{Z_{kd\,base}}{\omega_{base}}, \text{ H}$$

$$L_{kq\,base} = \frac{Z_{kq\,base}}{\omega_{base}}, \text{ H}$$

$$t_{base} = \frac{1}{\omega_{base}}, \text{ s}$$

$$T_{base} = \frac{3\text{-phase VA}_{base}}{\omega_{m\,base}}, \text{ N·m}$$

Complete set of electrical equations in per unit

In view of the L_{ad}-base per unit system chosen, in per unit

$$L_{afd} = L_{fda} = L_{akd} = L_{kda} = L_{ad}$$

$$L_{akq} = L_{kqa} = L_{aq}$$

$$L_{fkd} = L_{kdf}$$

In the following equations, two q-axis amortisseur circuits are considered, and the subscripts $1q$ and $2q$ are used (in place of kq) to identify them. Only one d-axis amortisseur circuit is considered, and it is identified by the subscript $1d$. **Since all quantities are in per unit, we drop the superbar notation.**

Per unit stator voltage equations:

$$e_d = p\psi_d - \psi_q\omega_r - R_a i_d \tag{3.120}$$

$$e_q = p\psi_q + \psi_d\omega_r - R_a i_q \tag{3.121}$$

$$e_0 = p\psi_0 - R_a i_0 \tag{3.122}$$

Per unit rotor voltage equations:

$$e_{fd} = p\psi_{fd} + R_{fd} i_{fd} \tag{3.123}$$

$$0 = p\psi_{1d} + R_{1d} i_{1d} \tag{3.124}$$

$$0 = p\psi_{1q} + R_{1q} i_{1q} \tag{3.125}$$

$$0 = p\psi_{2q} + R_{2q} i_{2q} \tag{3.126}$$

Per unit stator flux linkage equations:

$$\psi_d = -(L_{ad}+L_l)i_d+L_{ad}i_{fd}+L_{ad}i_{1d} \tag{3.127}$$

$$\psi_q = -(L_{aq}+L_l)i_q+L_{aq}i_{1q}+L_{aq}i_{2q} \tag{3.128}$$

$$\psi_0 = -L_0 i_0 \tag{3.129}$$

Per unit rotor flux linkage equations:

$$\psi_{fd} = L_{ffd}i_{fd}+L_{f1d}i_{1d}-L_{ad}i_d \tag{3.130}$$

$$\psi_{1d} = L_{f1d}i_{fd}+L_{11d}i_{1d}-L_{ad}i_d \tag{3.131}$$

$$\psi_{1q} = L_{11q}i_{1q}+L_{aq}i_{2q}-L_{aq}i_q \tag{3.132}$$

$$\psi_{2q} = L_{aq}i_{1q}+L_{22q}i_{2q}-L_{aq}i_q \tag{3.133}$$

Per unit air-gap torque:

$$T_e = \psi_d i_q-\psi_q i_d \tag{3.134}$$

In writing Equations 3.132 and 3.133, we have assumed that the per unit mutual inductance L_{12q} is equal to L_{aq}. This implies that the stator and rotor circuits in the q-axis all link a single mutual flux represented by L_{aq}. This is acceptable because the rotor circuits represent the overall rotor body effects, and actual windings with physically measurable voltages and currents do not exist.

For power system stability analysis, the machine equations are normally solved with all quantities expressed in per unit, with the exception of time. Usually time t is expressed in seconds, in which case the per unit p in Equations 3.120 to 3.126 is replaced by $(1/\omega_{base})p$.

Per unit reactances

If the frequency of the stator quantities is equal to the base frequency, the per unit reactance of a winding is numerically equal to the per unit inductance. For example,

$$X_d = 2\pi f L_d \quad \Omega$$

Dividing by $Z_{s\,base}=2\pi f_{base} L_{s\,base}$,

$$\frac{X_d}{Z_{sbase}} = \frac{2\pi f}{2\pi f_{base}} \frac{L_d}{L_{sbase}}$$

If $f=f_{base}$, per unit values of X_d and L_d are equal. For this reason, in the literature on synchronous machines, symbols associated with reactances are often used to denote per unit inductances.

3.5 EQUIVALENT CIRCUITS FOR DIRECT AND QUADRATURE AXES

While Equations 3.120 to 3.133 can be used directly to determine synchronous machine performance, it is a common practice to use equivalent circuits to provide a visual description of the machine model.

Before we develop an equivalent circuit to represent complete electrical characteristics of the machine, let us first consider only the d-axis flux linkage. Figure 3.17 shows an equivalent circuit which represents the d-axis stator and rotor flux linkage equations 3.127, 3.130 and 3.131. In this figure, the currents appear as loop currents.

A similar equivalent circuit can be developed for the q-axis flux linkage and current relationships. At this point, it is helpful to introduce the following rotor circuit per unit leakage inductances:

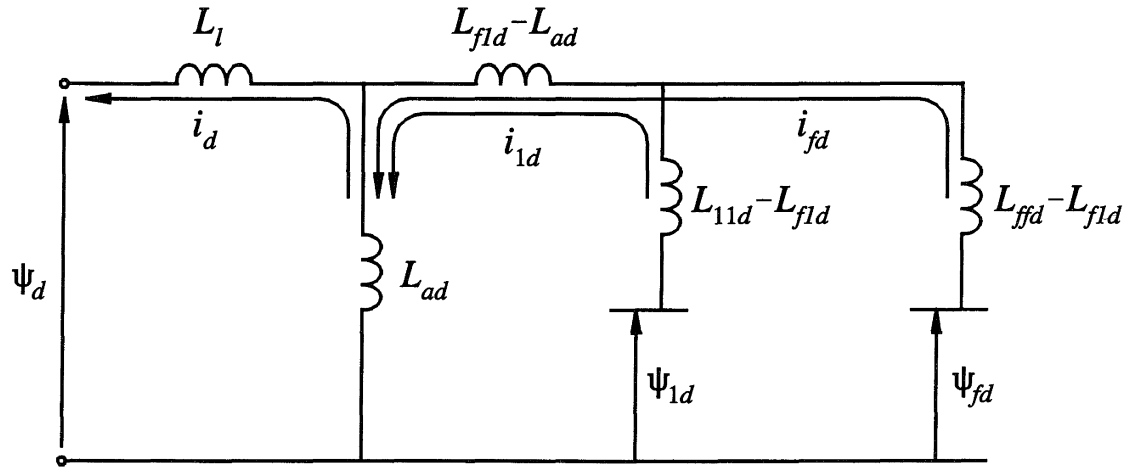

Figure 3.17 The d-axis equivalent circuit illustrating ψ-i relationship

$$L_{fd} = L_{ffd} - L_{f1d} \tag{3.135}$$

$$L_{1d} = L_{11d} - L_{f1d} \tag{3.136}$$

$$L_{1q} = L_{11q} - L_{aq} \tag{3.137}$$

$$L_{2q} = L_{22q} - L_{aq} \tag{3.138}$$

Equivalent circuits representing the complete characteristics, including the voltage equations, are shown in Figure 3.18. In these equivalent circuits, voltages as well as flux linkages appear. Therefore, flux linkages are shown in terms of their time derivatives.

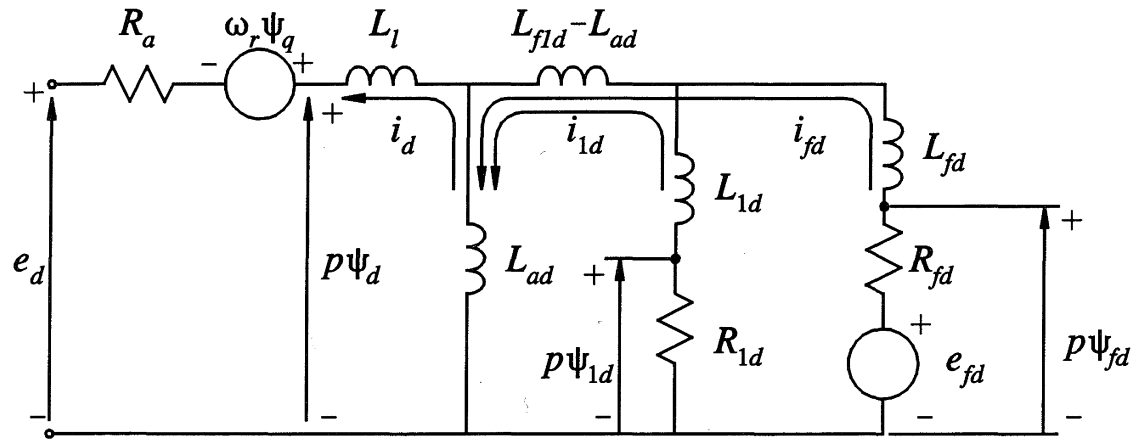

(a) *d*-axis equivalent circuit

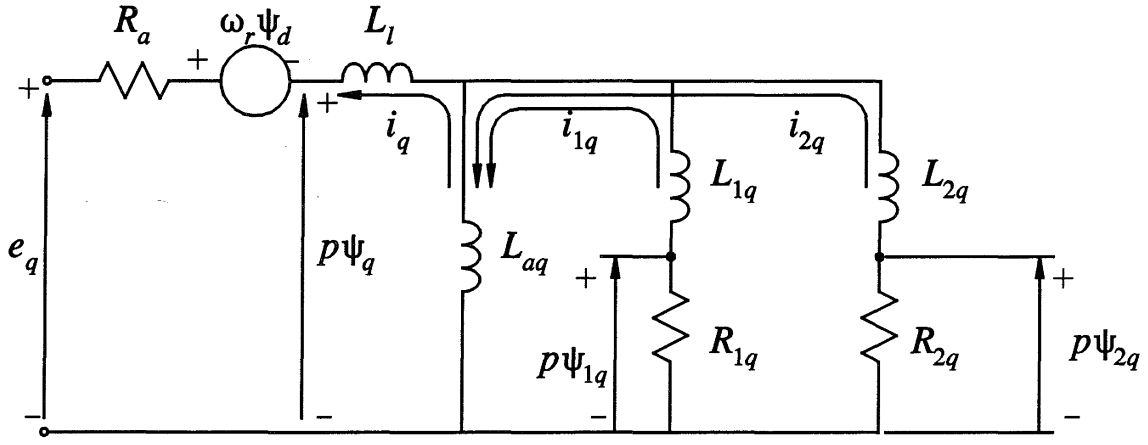

(b) *q*-axis equivalent circuit

Figure 3.18 Complete *d*- and *q*-axis equivalent circuits

In the *d*-axis equivalent circuit, the series inductance L_{fld}-L_{ad} represents the flux linking both the field winding and the amortisseur, but not the armature. It is a very common practice to neglect this series inductance on the grounds that the flux linking the damper circuit is very nearly equal to that linking the armature, because the damper windings are near the air-gap. This would be true in practice if the damper circuits were fully pitched. For short-pitched damper circuits and solid rotor iron paths, this approximation is not strictly valid [19]. In recent years, there has been some emphasis on including the series inductance L_{fld}-L_{ad}, particularly for detailed studies where the identity of the field circuit is to be retained [5,21].

In the case of the *q*-axis, there is no field winding and the amortisseurs represent the overall effects of the damper windings and eddy current paths. Therefore, it is reasonable to assume (as has been done in the development of the *q*-axis equivalent circuit of Figure 3.18 and the related equations) that the armature and damper circuits all link a single ideal mutual flux represented by L_{aq}.

In the literature, it is a widely accepted practice to simplify the *d*- and *q*-axis equivalent circuits as shown in Figure 3.19 which do not show the stator resistance

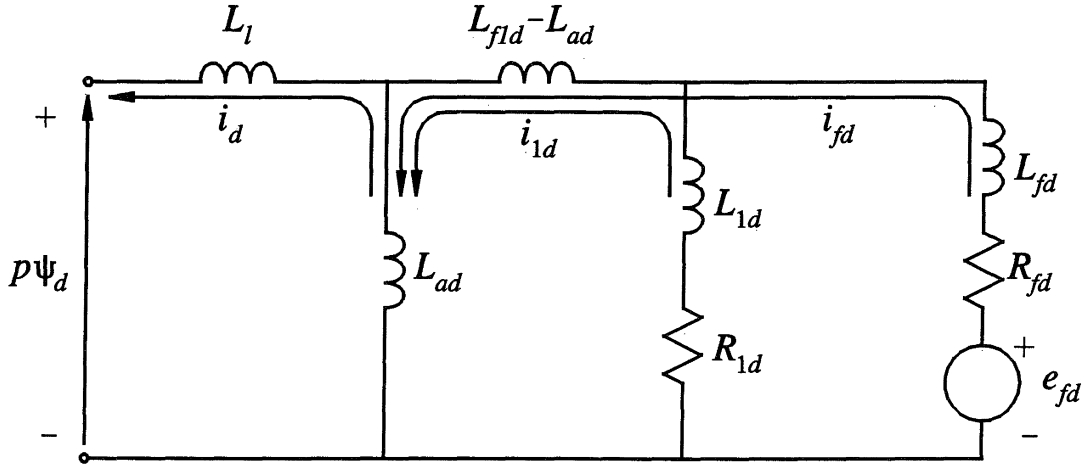

(a) *d*-axis equivalent circuit

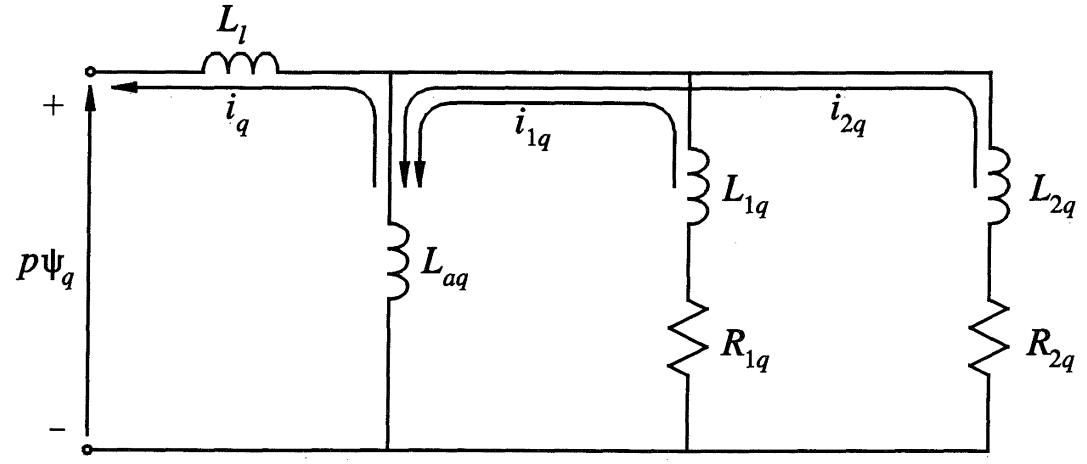

(b) *q*-axis equivalent circuit

Figure 3.19 Commonly used simplified equivalent circuits

voltage drops and the speed voltage terms. These equivalent circuits are adequate for determining ψ_d and ψ_q, including their time derivatives.

The equivalent circuits in Figure 3.19 represent rotor flux linkage and voltage equations. So far as the stator is concerned they merely establish ψ_d, ψ_q in terms of i_d, i_q and rotor variables.

Example 3.1

A 555 MVA, 24 kV, 0.9 p.f., 60 Hz, 3 phase, 2 pole synchronous generator has the following inductances and resistances associated with the stator and field windings:

$$
\begin{aligned}
l_{aa} &= 3.2758+0.0458\cos(2\theta) \text{ mH} \\
l_{ab} &= -1.6379-0.0458\cos(2\theta+\pi/3) \text{ mH} \\
l_{afd} &= 40.0\cos\theta \text{ mH} \\
L_{ffd} &= 576.92 \text{ mH} \\
R_a &= 0.0031\ \Omega \\
R_{fd} &= 0.0715\ \Omega
\end{aligned}
$$

a. Determine L_d and L_q in henrys.

b. If the stator leakage inductance L_l is 0.4129 mH, determine L_{ad} and L_{aq} in henrys.

c. Using the machine rated values as the base values for the stator quantities, determine the per unit values of the following in the L_{ad}-base reciprocal per unit system:

$$L_l,\ L_{ad},\ L_{aq},\ L_d,\ L_q,\ L_{afd},\ L_{ffd},\ L_{fd},\ R_a,\ R_{fd}$$

Solution

a. From Equations 3.61 and 3.62,

$$
\begin{aligned}
L_d &= L_{aa0}+L_{ab0}+\frac{3}{2}L_{aa2} \\
&= 3.2758+1.6379+\frac{3}{2}\times 0.0458 \\
&= 4.9825 \text{ mH}
\end{aligned}
$$

$$
\begin{aligned}
L_q &= L_{aa0}+L_{ab0}-\frac{3}{2}L_{aa2} \\
&= 3.2758+1.6379-\frac{3}{2}\times 0.0458 \\
&= 4.8451 \text{ mH}
\end{aligned}
$$

b.

$$L_{ad} = L_d - L_l$$
$$= 4.9825 - 0.4129$$
$$= 4.5696 \text{ mH}$$

$$L_{aq} = L_q - L_l$$
$$= 4.845 - 0.4129$$
$$= 4.432 \text{ mH}$$

c. The base values of stator and rotor quantities are as follows:

3-phase VA base = 555 MVA

E_{sbase}(RMS) = $24/\sqrt{3}$ = 13.856 kV

e_{sbase}(peak) = $\sqrt{2}\times 13.856$ = 19.596 kV

$$I_{sbase}(\text{RMS}) = \frac{555\times 10^6}{3\times 13.856\times 10^3} = 13{,}351.2 \text{ A}$$

i_{sbase}(peak) = $\sqrt{2}\times 13{,}351.2$ = 18,881.5 A

$$Z_{sbase} = \frac{13.856\times 10^3}{13{,}351.2} = 1.03784\ \Omega$$

ω_{base} = $2\pi 60$ = 377 elec. rad/s

$$L_{sbase} = \frac{1.03784}{377}\times 10^3 = 2.753 \text{ mH}$$

$$i_{fdbase} = \frac{L_{ad}}{L_{afd}} i_{sbase}$$
$$= \frac{4.5696}{40.0}\times 18{,}881.5$$
$$= 2158.0 \text{ A}$$

$$e_{fdbase} = \frac{555\times 10^6}{2158} = 257.183 \text{ kV}$$

$$Z_{fdbase} = \frac{257.183}{2158.0} = 119.18\ \Omega$$

$$L_{fdbase} = \frac{119.18}{377}\times 10^3 = 316.12 \text{ mH}$$

The per unit values are

$$L_l = \frac{0.4129}{2.753} = 0.15 \text{ pu}$$

$$L_{ad} = \frac{4.5696}{2.753} = 1.66 \text{ pu}$$

$$L_{aq} = \frac{4.432}{2.753} = 1.61 \text{ pu}$$

$$L_d = L_{ad}+L_l = 1.66+0.15 = 1.81 \text{ pu}$$

$$L_q = L_{aq}+L_l = 1.61+0.15 = 1.76 \text{ pu}$$

$$L_{afd} = \frac{L_{afd}}{L_{sbase}}\frac{i_{fdbase}}{i_{sbase}}$$

$$= \frac{40.0}{2.753}\times\frac{2158}{18{,}881.5} = 1.66 \text{ pu}$$

$$L_{ffd} = \frac{576.92}{316.12} = 1.825 \text{ pu}$$

$$L_{fd} = L_{ffd}-L_{ad}$$

$$= 1.825-1.66 = 0.165 \text{ pu}$$

$$R_a = \frac{0.0031}{1.03784} = 0.003 \text{ pu}$$

$$R_{fd} = \frac{0.0715}{119.18} = 0.0006 \text{ pu}$$ ■

3.6 STEADY-STATE ANALYSIS

The performance of synchronous machines under balanced steady-state conditions may be readily analyzed by applying the per unit equations summarized in Section 3.4.9.

3.6.1 Voltage, Current, and Flux Linkage Relationships

As has been shown in Section 3.3, the *dq0* transformation applied to balanced steady-state armature phase currents results in steady direct currents. This is also true of stator voltages and flux linkages. Since rotor quantities are also constant under steady state, all time derivative terms drop out of machine equations. In addition, zero-sequence components are absent and $\omega_r=\omega_s=1$ pu.

With $p\psi$ terms set to zero in Equations 3.124, 3.125 and 3.126,

$$R_{1d}i_{1d} = R_{1q}i_{1q} = R_{2q}i_{2q} = 0$$

Therefore, all amortisseur currents are zero. This is to be expected since, under steady state, the rotating magnetic field due to the stator currents is stationary with respect to the rotor. As the amortisseurs are closed circuits with no applied voltage, currents are induced in them only when the magnetic field due to the stator windings or the field winding is changing.

The per unit machine equations (3.120 to 3.134), under balanced steady-state conditions, become

$$e_d = -\omega_r \psi_q - R_a i_d \tag{3.139}$$

$$e_q = \omega_r \psi_d - R_a i_q \tag{3.140}$$

$$e_{fd} = R_{fd} i_{fd} \tag{3.141}$$

$$\psi_d = -L_d i_d + L_{ad} i_{fd} \tag{3.142}$$

$$\psi_q = -L_q i_q \tag{3.143}$$

$$\psi_{fd} = L_{ffd} i_{fd} - L_{ad} i_d \tag{3.144}$$

$$\psi_{1d} = L_{f1d} i_{fd} - L_{ad} i_d \tag{3.145}$$

$$\psi_{1q} = \psi_{2q} = -L_{aq} i_q \tag{3.146}$$

Field current

From Equation 3.142,

$$i_{fd} = \frac{\psi_d + L_d i_d}{L_{ad}}$$

Substituting for ψ_d in terms of e_d, i_q from Equation 3.140,

$$i_{fd} = \frac{e_q + R_a i_q + \omega_r L_d i_d}{\omega_r L_{ad}}$$

Replacing the product of synchronous speed and inductance L by the corresponding reactance X,

$$i_{fd} = \frac{e_q + R_a i_q + X_d i_d}{X_{ad}} \tag{3.147}$$

The above equation is useful in computing the steady-state value of the field current for any specified operating condition. The inductances/reactances appearing in Equations 3.139 to 3.147 are saturated values. This will be discussed in Section 3.8.

3.6.2 Phasor Representation

For balanced steady-state operation, the stator phase voltages may be written as

$$e_a = E_m\cos(\omega_s t+\alpha) \tag{3.148}$$

$$e_b = E_m\cos(\omega_s t-\frac{2\pi}{3}+\alpha) \tag{3.149}$$

$$e_c = E_m\cos(\omega_s t+\frac{2\pi}{3}+\alpha) \tag{3.150}$$

where ω_s is the angular frequency and α is the phase angle of e_a with respect to the time origin.

Applying the *dq* transformation gives

$$e_d = E_m\cos(\omega_s t+\alpha-\theta) \tag{3.151}$$

$$e_q = E_m\sin(\omega_s t+\alpha-\theta) \tag{3.152}$$

The angle θ by which the *d*-axis leads the axis of phase *a* is given by

$$\theta = \omega_r t+\theta_0 \tag{3.153}$$

where θ_0 is the value of θ at t=0.

With ω_r equal to ω_s at synchronous speed, substitution for θ in Equations 3.151 and 3.152 yields

$$e_d = E_m\cos(\alpha-\theta_0) \tag{3.154}$$

$$e_q = E_m\sin(\alpha-\theta_0) \tag{3.155}$$

In the above equations, E_m is the peak value of phase voltage. In steady-state analysis, we are interested in RMS values and phase displacements rather than instantaneous or peak values. Using E_t to denote per unit RMS value of armature terminal voltage and noting that in per unit RMS and peak values are equal,

$$e_d = E_t\cos(\alpha-\theta_0) \tag{3.156}$$

$$e_q = E_t\sin(\alpha-\theta_0) \tag{3.157}$$

The *dq* components of armature voltage are scalar quantities. However, in view of the trigonometric relationship between them, they can be expressed as phasors in

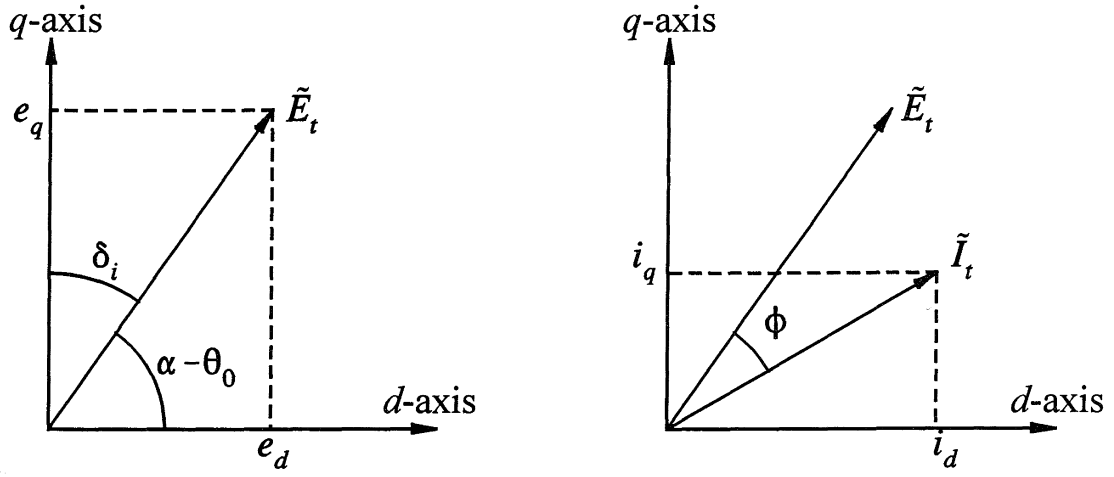

(a) Voltage components (b) Current components

Figure 3.20 Representation of *dq* components of armature voltage and current as phasors

a complex plane having *d*- and *q*-axes as coordinates. This is illustrated in Figure 3.20 and is conceptually similar to phasor representation of alternating quantities varying sinusoidally with respect to time. Thus the armature terminal voltage may be expressed in complex form as

$$\tilde{E}_t = e_d + je_q \tag{3.158}$$

By denoting δ_i as the angle by which the *q*-axis leads the phasor $\tilde{E}_t$, Equations 3.156 and 3.157 become

$$e_d = E_t \sin\delta_i \tag{3.159}$$

$$e_q = E_t \cos\delta_i \tag{3.160}$$

Similarly, the *dq* components of armature terminal current I_t can be expressed as phasors. If ϕ is the power factor angle, we can write

$$i_d = I_t \sin(\delta_i + \phi) \tag{3.161}$$

$$i_q = I_t \cos(\delta_i + \phi) \tag{3.162}$$

and

$$\tilde{I}_t = i_d + j i_q \tag{3.163}$$

From the above analysis, it is clear that in phasor form with dq axes as reference, the RMS armature phase current and voltage can be treated the same way as is done with phasor representation of alternating voltages and currents. This provides the link between the steady-state values of dq components of armature quantities and the phasor representation used in conventional ac circuit analysis.

The relationships between dq components of armature terminal voltage and current are defined by Equations 3.139, 3.140, 3.142 and 3.143. Thus

$$\begin{aligned} e_d &= -\omega_r \psi_q - R_a i_d \\ &= \omega_r L_q i_q - R_a i_d \\ &= X_q i_q - R_a i_d \end{aligned} \tag{3.164}$$

$$\begin{aligned} e_q &= \omega_r \psi_d - R_a i_q \\ &= -X_d i_d + X_{ad} i_{fd} - R_a i_q \end{aligned} \tag{3.165}$$

The reactances X_d and X_q are called the direct- and quadrature-axis synchronous reactances, respectively. They represent the inductive effects of the armature mmf wave by separately accounting for its d- and q-axis components. These and other reactances of a synchronous machine will be discussed in detail in a later section.

We have not yet developed a means of identifying the d- and q-axis positions relative to $\tilde{E}_t$. In order to assist us in this regard, let us define a voltage $\tilde{E}_q$ as

$$\begin{aligned} \tilde{E}_q &= \tilde{E}_t + (R_a + j X_q)\tilde{I}_t \\ &= (e_d + j e_q) + (R_a + j X_q)(i_d + j i_q) \end{aligned} \tag{3.166}$$

Substitution of Equations 3.164 and 3.165, followed by reduction of the resulting expression, yields the following expression for $\tilde{E}_q$ in phasor form with d, q axes as reference:

$$\tilde{E}_q = j[X_{ad} i_{fd} - (X_d - X_q) i_d] \tag{3.167}$$

The corresponding phasor diagram is shown in Figure 3.21. We see that the phasor $\tilde{E}_q$ lies along the q-axis. The position of the q-axis with respect to $\tilde{E}_t$ can be identified by computing $\tilde{E}_q$, the voltage behind $R_a + j X_q$.

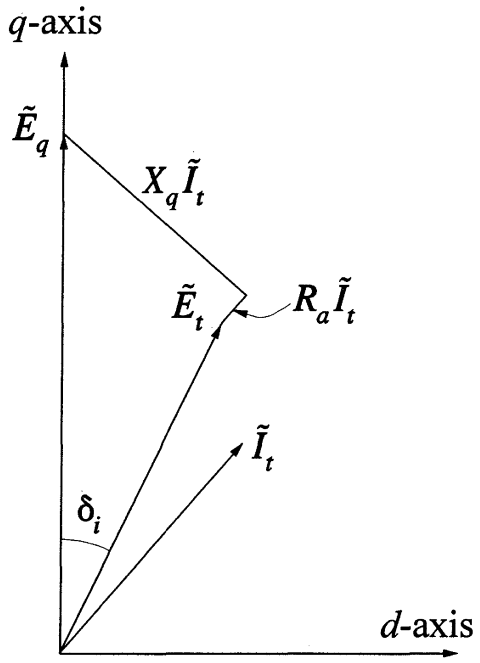

Figure 3.21 Phasor $\tilde{E}_q$ in *dq* complex plane

3.6.3 Rotor Angle

Under no-load or open-circuit conditions, $i_d=i_q=0$. Substituting in Equations 3.139, 3.140, 3.142 and 3.143 yields

$$\psi_d = L_{ad} i_{fd}$$

$$\psi_q = 0$$

$$e_d = 0$$

$$e_q = X_{ad} i_{fd}$$

Therefore,

$$\begin{aligned} \tilde{E}_t &= e_d + j e_q \\ &= j X_{ad} i_{fd} \end{aligned} \tag{3.168}$$

Under no-load conditions, $\tilde{E}_t$ has only the *q*-axis component and hence $\delta_i=0$. As the machine is loaded, δ_i increases. Therefore, the angle δ_i is referred to as the *internal rotor angle* or *load angle*. The relationship between power output and the rotor angle is nonlinear and is of fundamental importance in power system stability studies.

The angle δ_i represents the angle by which the q-axis leads the stator terminal voltage phasor $\tilde{E}_t$, and it is given by

$$\delta_i = 90° - (\alpha - \theta_0) \tag{3.169}$$

where α is the phase angle of e_a and θ_0 is the value of θ with respect to the time origin. Therefore, δ_i depends on the angle between the stator and rotor magnetic fields. For any given machine power output, either α or θ_0 may be arbitrarily chosen, but not both.

3.6.4 Steady-State Equivalent Circuit

If saliency is neglected,

$$X_d = X_q = X_s$$

where X_s is the synchronous reactance. Therefore,

$$\tilde{E}_q = \tilde{E}_t + (R_a + jX_s)\tilde{I}_t \tag{3.170}$$

With $X_d = X_q$, from Equation 3.167, the magnitude of $\tilde{E}_q$ is given by

$$E_q = X_{ad} i_{fd} \tag{3.171}$$

The corresponding equivalent circuit is shown in Figure 3.22. The resistance R_a is usually very small and may be neglected.

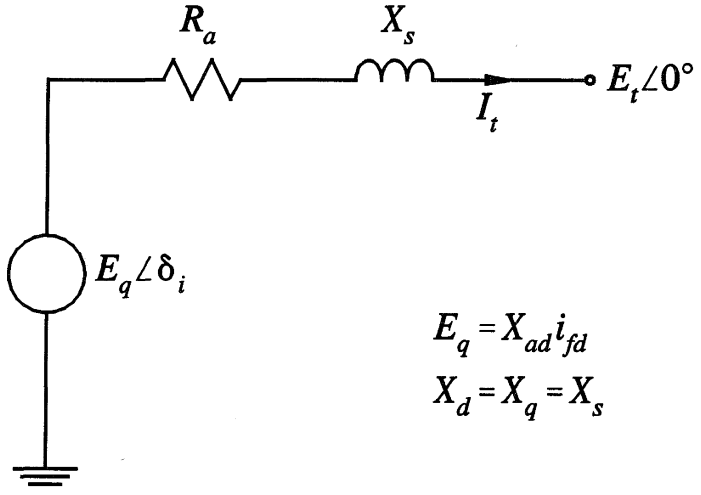

Figure 3.22 Steady-state equivalent circuit with saliency neglected

The voltage E_q may be considered as the effective internal voltage. It is equal in magnitude to $X_{ad}i_{fd}$ and hence represents the excitation voltage due to the field current. The synchronous reactance X_s accounts for the flux produced by the stator currents, i.e., the effect of armature reaction. For a round rotor machine, X_d is nearly equal to X_q and therefore the above equivalent circuit provides a satisfactory representation.

For salient pole machines, X_d is not equal to X_q. The effect of saliency is, however, not very significant so far as the relationships between terminal voltage, armature current, power and excitation over the normal operating range are concerned. The approximate equivalent often provides sufficient insight into the steady-state characteristics. Only at small excitations will the effect of saliency become significant. The approximation also neglects the reluctance torque due to saliency. With modern computing facilities, there is little difficulty in accounting for saliency; therefore, the approximation associated with round rotor theory is not used in detailed calculations.

Active and reactive power

$$\begin{aligned} S &= \tilde{E}_t \tilde{I}_t^* \\ &= (e_d+je_q)(i_d-ji_q) \\ &= (e_d i_d+e_q i_q)+j(e_q i_d-e_d i_q) \end{aligned}$$

$$P_t = e_d i_d+e_q i_q \tag{3.172}$$

$$Q_t = e_q i_d-e_d i_q \tag{3.173}$$

Steady-state torque is given by

$$\begin{aligned} T_e &= \psi_d i_q-\psi_q i_d \\ &= (e_d i_d+e_q i_q)+R_a(i_d^2+i_q^2) \\ &= P_t+R_a I_t^2 \end{aligned} \tag{3.174}$$

3.6.5 Procedure for Computing Steady-State Values

For stability analysis, it is necessary to find the initial steady-state values of machine variables as a function of specified terminal quantities. The following steps summarize the procedure for computing these values. It is assumed that all quantities are expressed in per unit.

(a) Normally, terminal active power P_t, reactive power Q_t, and magnitude of voltage E_t are specified. The corresponding terminal current I_t and power factor angle ϕ are computed as follows:

$$I_t = \frac{\sqrt{P_t^2+Q_t^2}}{E_t}$$

$$\phi = \cos^{-1}\left(\frac{P_t}{E_t I_t}\right)$$

(b) The next step is to compute the internal rotor angle δ_i. Since $\tilde{E}_q$ lies along the q-axis, as illustrated in Figure 3.23, the internal angle is given by

$$\delta_i = \tan^{-1}\left(\frac{X_q I_t\cos\phi - R_a I_t\sin\phi}{E_t + R_a I_t\cos\phi + X_q I_t\sin\phi}\right)$$

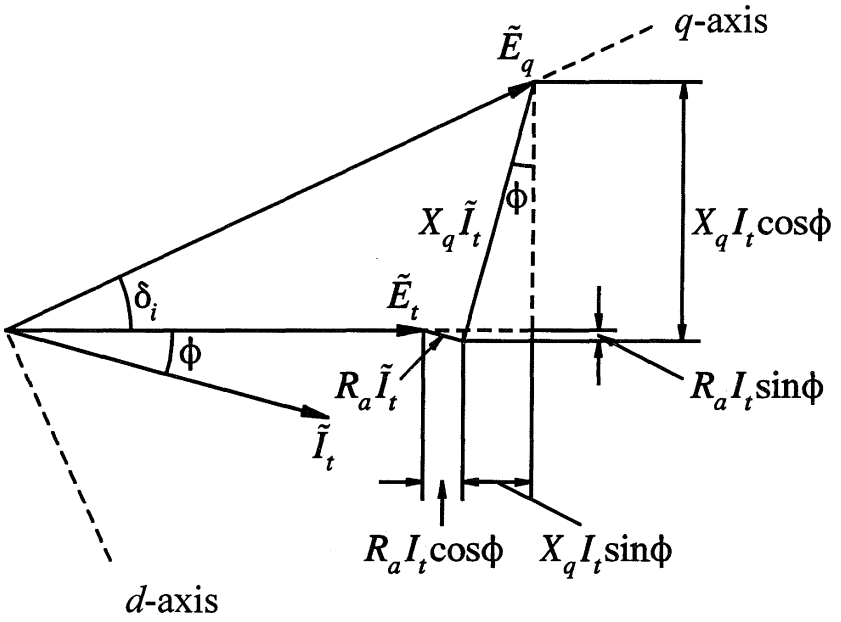

Figure 3.23 Steady-state phasor diagram

(c) With δ_i known, the dq components of stator voltage and current are given by

$$e_d = E_t\sin\delta_i$$

$$e_q = E_t\cos\delta_i$$

$$i_d = I_t\sin(\delta_i+\phi)$$

$$i_q = I_t\cos(\delta_i+\phi)$$

(d) The remaining machine quantities are computed as follows:

$$\psi_d = e_q + R_a i_q$$

$$\psi_q = -e_d - R_a i_d$$

$$i_{fd} = \frac{e_q + R_a i_q + X_d i_d}{X_{ad}}$$

$$e_{fd} = R_{fd} i_{fd}$$

$$\psi_{fd} = (L_{ad} + L_{fd}) i_{fd} - L_{ad} i_d$$

$$\psi_{1d} = L_{ad}(i_{fd} - i_d)$$

$$\psi_{1q} = \psi_{2q} = -L_{aq} i_q$$

$$T_e = P_t + R_a I_t^2$$

So far we have not discussed the effect of magnetic saturation. It is, however, important to recognize that the inductances L_{ad}, L_{aq}, L_d, L_q and the corresponding reactances vary with saturation and should be accounted for in computing the steady-state machine quantities. The method of accounting for saturation will be discussed in Section 3.8.

Example 3.2

The following are the parameters in per unit on machine rating of a 555 MVA, 24 kV, 0.9 p.f., 60 Hz, 3600 RPM turbine-generator[1]:

$L_{ad} = 1.66$	$L_{aq} = 1.61$	$L_l = 0.15$	$R_a = 0.003$
$L_{fd} = 0.165$	$R_{fd} = 0.0006$	$L_{1d} = 0.1713$	$R_{1d} = 0.0284$
$L_{1q} = 0.7252$	$R_{1q} = 0.00619$	$L_{2q} = 0.125$	$R_{2q} = 0.02368$

L_{fkd} is assumed to be equal to L_{ad}.

(a) When the generator is delivering rated MVA at 0.9 p.f. (lag) and rated terminal voltage, compute the following:

---

[1] This generator is same as that of Example 3.1, except that amortisseurs are considered here. We will consider this generator in many other examples throughout the book to illustrate different aspects of generator characteristics and stability performance.

(i) Internal angle δ_i in electrical degrees

(ii) Per unit values of e_d, e_q, i_d, i_q, i_{1d}, i_{1q}, i_{2q}, i_{fd}, e_{fd}, ψ_{fd}, ψ_{1d}, ψ_{1q}, ψ_{2q}

(iii) Air-gap torque T_e in per unit and in newton-meters

Assume that the effect of magnetic saturation at the given operating condition is to reduce L_{ad} and L_{aq} to 83.5% of the values given above.

(b) Compute the internal angle δ_i and field current i_{fd} for the above operating condition, using the approximate equivalent circuit of Figure 3.22. Neglect R_a.

Solution

(a) With the given operating condition, the per unit values of terminal quantities are

$$P=0.9, \qquad Q=0.436, \qquad E_t=1.0, \qquad I_t=1.0, \qquad \phi=25.84^\circ$$

The saturated values of the inductances are

$$L_{ad} = 0.835\times1.66 = 1.386$$
$$L_{aq} = 0.835\times1.61 = 1.344$$
$$L_d = L_{ad}+L_l = 1.386+0.15 = 1.536$$
$$L_q = L_{aq}+L_l = 1.344+0.15 = 1.494$$

Following the procedure outlined in Section 3.6.5,

(i) $$\delta_i = \tan^{-1}\left(\frac{1.494\times1.0\times0.9-0.003\times1.0\times0.436}{1.0+0.003\times1.0\times0.9+1.494\times1.0\times0.436}\right)$$
$$= \tan^{-1}(0.812) = 39.1 \quad \text{electrical degrees}$$

(ii) $$e_d = E_t\sin\delta_i = 1.0\sin39.1 = 0.631 \quad \text{pu}$$
$$e_q = E_t\cos\delta_i = 1.0\cos39.1 = 0.776 \quad \text{pu}$$
$$i_d = I_t\sin(\delta_i+\phi) = 1.0\sin(39.1+25.84) = 0.906 \quad \text{pu}$$
$$i_q = I_t\cos(\delta_i+\phi) = 1.0\cos(39.1+25.84) = 0.423 \quad \text{pu}$$
$$i_{fd} = \frac{e_q+R_a i_q-X_d i_d}{X_{ad}}$$
$$= \frac{0.776+0.003\times0.423+1.536\times0.906}{1.386}$$
$$= 1.565 \quad \text{pu}$$

$$e_{fd} = R_{fd} i_{fd} = 0.0006 \times 1.565$$

$$= 0.000939 \quad \text{pu}$$

$$\psi_{fd} = (L_{ad} + L_{fd}) i_{fd} - L_{ad} i_d$$

$$= (1.386 + 0.165) \times 1.565 - 1.386 \times 0.907$$

$$= 1.17 \quad \text{pu}$$

$$\psi_{1d} = L_{ad}(i_{fd} - i_d)$$

$$= 1.386 \times (1.565 - 0.906)$$

$$= 0.913 \quad \text{pu}$$

$$\psi_{1q} = \psi_{2q} = -L_{aq} i_q = -1.344 \times 0.423$$

$$= -0.569 \quad \text{pu}$$

Under steady state,

$$i_{1d} = i_{1q} = i_{2q} = 0$$

(iii) Air-gap torque

$$T_e = P_t + I_t^2 R_a$$

$$= 0.9 + 1.0^2 \times 0.003$$

$$= 0.903 \quad \text{pu}$$

$$T_{base} = \frac{\text{MVA}_{\text{base}} \times 10^6}{\omega_{m\,base}}$$

$$= \frac{555 \times 10^6}{2\pi 60} = 1.472 \times 10^6 \quad \text{N·m}$$

Therefore,

$$T_e = 0.903 \times 1.472 \times 10^6$$

$$= 1.329 \times 10^6 \quad \text{N·m}$$

(b) Using the saturated value of X_{ad},

$$E_q = X_{ad} i_{fd} = 1.386 i_{fd}$$

and

$$X_s = X_{ad}+X_l = 1.386+0.15 = 1.536$$

From the equivalent circuit of Figure 3.22, with $\tilde{E}_t$ as reference phasor,

$$\begin{aligned}\tilde{E}_q &= \tilde{E}_t+jX_s\tilde{I}_t \\ &= 1.0+j1.536(0.9-j0.436) \\ &= 1.670+j1.382 \\ &= 2.17\angle 39.6^\circ \quad \text{pu}\end{aligned}$$

$$\delta_i = 39.6^\circ$$

Therefore,

$$i_{fd} = \frac{E_q}{X_{ad}} = \frac{2.17}{1.386} = 1.566 \quad \text{pu}$$

The values of δ_i and i_{fd} computed using the approximate representation are seen to be in good agreement with the accurate calculation. This is to be expected, since X_q is nearly equal to X_d and we are considering rated operating condition. ■

3.7 ELECTRICAL TRANSIENT PERFORMANCE CHARACTERISTICS

This section examines the fundamental electrical transient characteristics of a synchronous machine by considering the response to a three-phase short-circuit at the terminals. Such an analysis, in addition to providing insight into the machine transient performance, is useful in identifying some of the approximations necessary for its representation in large scale stability studies. We will first consider a simple *RL* circuit, as it helps in understanding of the nature of transient response of a synchronous machine.

3.7.1 Short-Circuit Current in a Simple *RL* Circuit

Consider the *RL* circuit shown in Figure 3.24, with

$$e = E_m\sin(\omega t+\alpha) \tag{3.175}$$

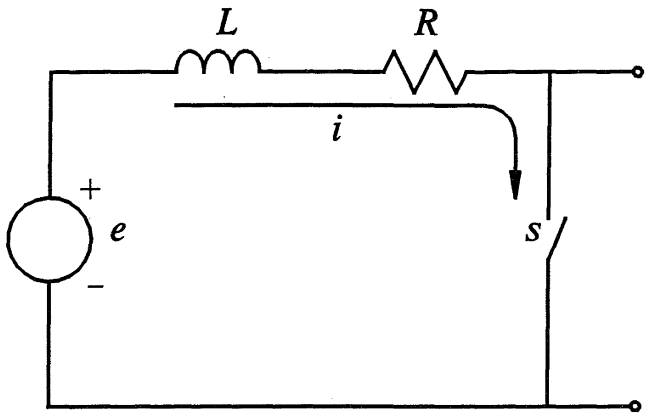

Figure 3.24 *RL* circuit

If the switch s is closed at time t=0, the current i is given by

$$e = L\frac{di}{dt} + Ri \tag{3.176}$$

Solving for i,

$$i = Ke^{-\frac{R}{L}t} + \frac{E_m}{Z}\sin(\omega t + \alpha - \phi) \tag{3.177}$$

with

$$Z = \sqrt{R^2 + \omega^2 L^2}$$

$$\phi = \tan^{-1}\left(\frac{\omega L}{R}\right)$$

In Equation 3.177, K is such that i at t=0$^+$ is the same as that at t=0$^-$. If i is equal to i_0 at t=0$^-$,

$$K = i_0 - \frac{E_m}{Z}\sin(\alpha - \phi) \tag{3.178}$$

From Equation 3.177 the short circuit current has two components: a transient unidirectional component and a steady-state alternating component. The presence of the unidirectional component of the short circuit current ensures that the current does not change instantaneously. The unidirectional component decays to zero with a time constant of L/R.

3.7.2 Three-Phase Short-Circuit at the Terminals of a Synchronous Machine

If a bolted three-phase fault is suddenly applied to a synchronous machine, the three phase currents are as shown in Figure 3.25.

In general, the fault current in each phase has two distinct components:

(a) A fundamental frequency component, which decays initially very rapidly (in a few cycles) and then relatively slowly (in several seconds) to a steady-state value.

(b) A unidirectional component (or a dc offset), which decays exponentially in several cycles.

This is similar to the short-circuit current in the case of the simple *RL* circuit considered in the previous section. However, in the case of a synchronous machine the amplitude of the ac component is not constant because the internal voltage, which is a function of the rotor flux linkages, is not constant. The initial rapid decay of the

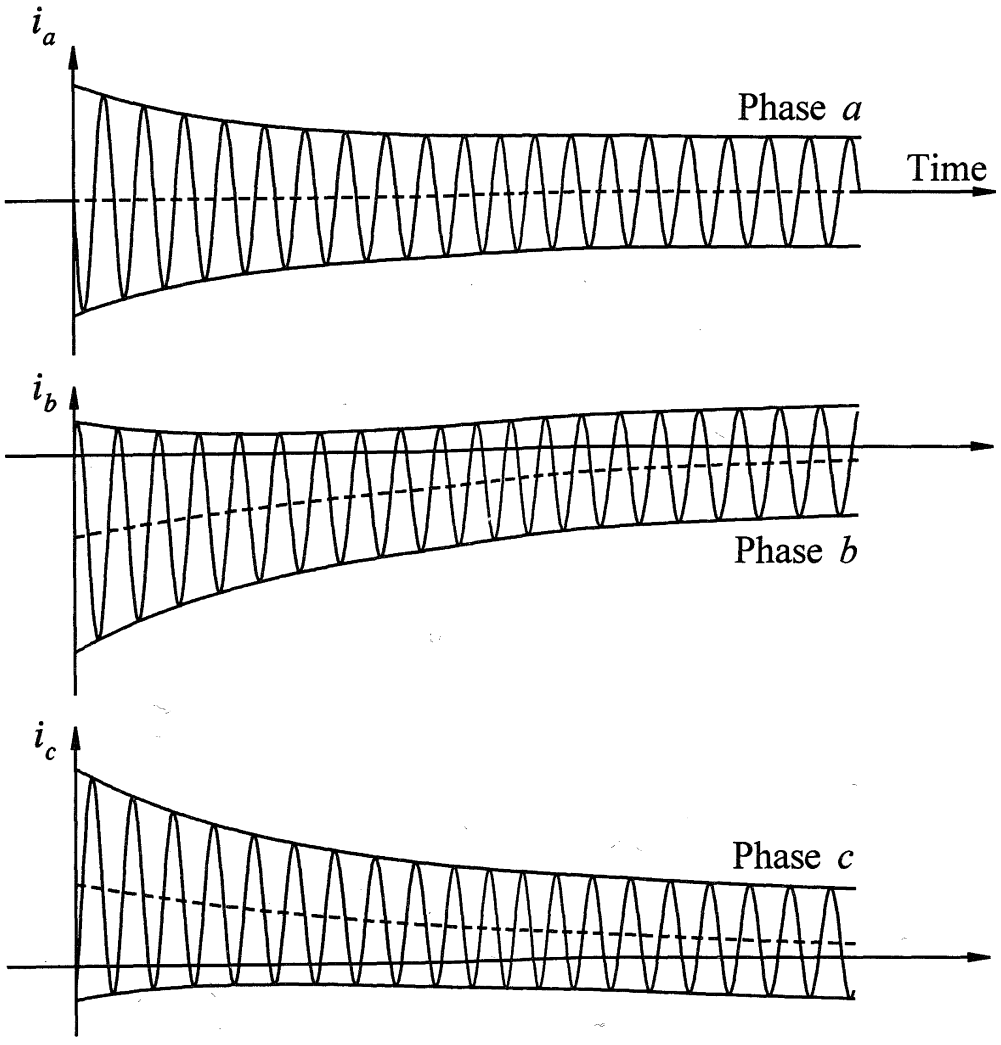

Figure 3.25 Short-circuit currents in the three phases

ac component of the short circuit current is due to the rapid decay of flux linking the subtransient circuits (*1d* and *2q* in Figures 3.18 and 3.19). The slowly decaying part of the ac component is due to the relatively slow decay of flux linking the transient circuits (field and *1q*).

The dc components have different magnitudes in the three phases and decay with a time constant T_a, the armature time constant. This time constant is equal to the ratio of the effective armature inductance (with the unidirectional currents in the armature) to the armature resistance.

In addition to the fundamental frequency and dc components, the short circuit armature currents contain second harmonic components, which depend on subtransient saliency ($X_q''-X_d''$) [10]. The amplitudes of these components are very small and are usually of little significance.

The currents during short-circuits (either balanced or unbalanced) or any other disturbance can be computed by solving Equations 3.26 to 3.51 in terms of the phase (*abc*) variables, or the corresponding Equations 3.120 to 3.133 in terms of the transformed *dq0* variables. The fundamental frequency components of phase currents are reflected as unidirectional components in the transformed currents i_d and i_q. The dc offset associated with the phase currents is reflected as fundamental frequency components in i_d and i_q.

The field current following the short-circuit is shown in Figure 3.26. It consists of a unidirectional component and an alternating component, corresponding to the ac component and the dc component in the armature phase, respectively.

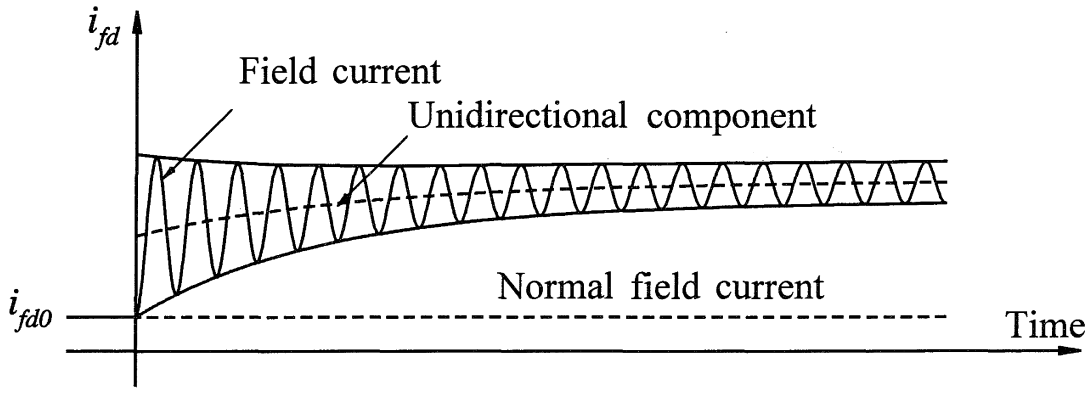

Figure 3.26 Field current response following a stator short-circuit

3.7.3 Elimination of DC Offset in Short-Circuit Current

The analysis of power system performance with the effects of both fundamental frequency and unidirectional components of phase currents included would be complex and computationally very involved. For many classes of power system problems, computation is much simpler if the effects of dc offset in the phase current are either neglected or treated separately. This also makes it easier to

distinguish between the important and the unimportant factors influencing the dynamic performance of power systems.

The effects of dc offset in the stator phase currents may be eliminated by neglecting the transformer voltage terms ($p\psi_d$, $p\psi_q$) in the stator voltage equations 3.120 and 3.121:

$$e_d = p\psi_d - \omega_r\psi_q - R_a i_d$$

$$e_q = p\psi_q + \omega_r\psi_d - R_a i_q$$

The transformer voltage terms represent the stator transients and prevent ψ_d and ψ_q from changing instantaneously. It is this fact that produces the dc offset in the phase currents. Omission of $p\psi_d$, $p\psi_q$ terms would therefore eliminate the dc offset and its related effects on the dynamic performance of the machine. By neglecting the $p\psi$ terms, we are not assuming that ψ_d and ψ_q remain constant; on the contrary, we are assuming that they change instantly following a perturbation.

If the stator transients (accounted for by the $p\psi$ terms) are neglected, the resulting armature short circuit current is as shown in Figure 3.27.

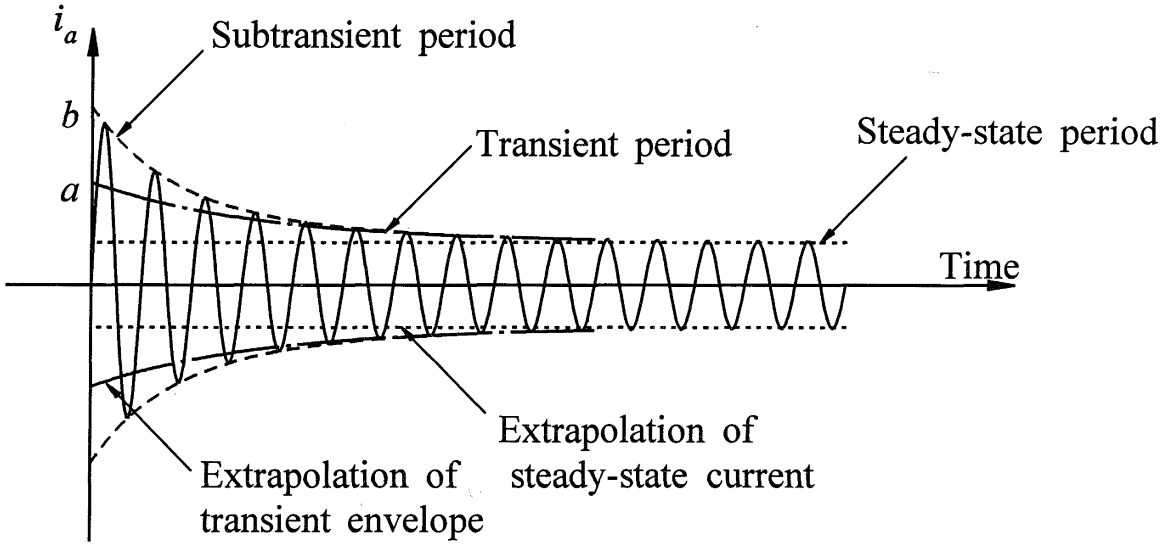

Figure 3.27 Fundamental frequency component of armature current

We see that the resulting current consists of only the fundamental frequency component. The waveform of the current may be divided into three distinct time periods: the *subtransient period*, lasting only for the first few cycles, during which the amplitude decays rapidly; the *transient period*, spanning a longer time, during which the amplitude decays considerably more slowly; and finally the *steady-state period*, during which the amplitude of the current remains constant. The parameters of the synchronous machine that determine the amplitudes of the short-circuit waveform during the three time periods and the rates of decay during the first two periods will be discussed in the next section.

To summarize the results of this section, we have discussed the response of the electrical circuits associated with a synchronous machine by considering a three-phase short circuit. We have identified the significance of neglecting the transformer voltage terms ($p\psi_d$, $p\psi_q$) in the stator voltage equations. This provides valuable guides to the representation of synchronous machines in power system analysis. It is also helpful in understanding the basis for and the significance of parameters widely used to identify the machine parameters.

The need for and the effects of neglecting the transformer voltage terms in power system stability studies will be discussed in Chapter 5.

3.8 MAGNETIC SATURATION

In the development of basic equations of the synchronous machine and the analysis of its characteristics so far, we have ignored the effects of stator and rotor iron saturation. As noted in Section 3.2, this was done to make the analysis simple and manageable. A rigorous treatment of synchronous machine performance including saturation effects is a futile exercise. Any practical method of accounting for saturation effects must be based on semi-heuristic reasoning and judiciously chosen approximations, with due consideration to simplicity of model structure, data availability, and accuracy of results.

Before we discuss the methods of representing saturation in stability studies, it is useful to briefly review the characteristics of synchronous machines with stator terminals open and shorted.

3.8.1 Open-Circuit and Short-Circuit Characteristics

Magnetic circuit data essential to the treatment of saturation are given by the open-circuit characteristic.

Under no-load rated speed conditions, as seen in Section 3.6.3, we have

$$i_d = i_q = \psi_q = e_d = 0$$

and

$$E_t = e_q = \psi_d = L_{ad} i_{fd}$$

Therefore, the open-circuit characteristic (OCC) relating E_t and i_{fd} gives the saturation characteristic of the d-axis.

A typical OCC is shown in Figure 3.28. The straight line tangent to the lower part of the curve is the *air-gap line* indicating the field current (or mmf) required to overcome the reluctance of the air-gap. The departure of the OCC from the air-gap line is an indication of the degree of saturation in the rotor and stator iron.

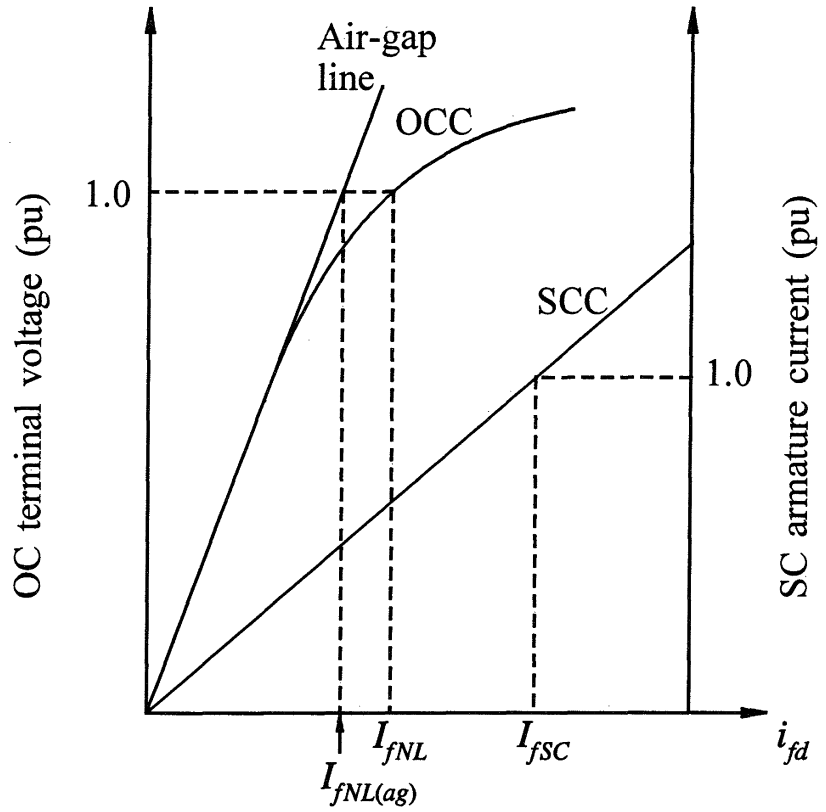

Figure 3.28 Open-circuit and short-circuit characteristics

The short-circuit characteristic (SCC) is also shown in Figure 3.28. This is a plot of the armature current vs. the field current, with the generator operating at rated speed in the steady state and with a three-phase short-circuit placed on the armature terminals. The SCC is linear up to and well beyond the rated armature current, since there is very little or no saturation in the iron under rated short-circuit conditions due to the demagnetizing effect of the armature reaction.

From Figure 3.22, it can be seen that the internally generated voltage is equal to the product of the short-circuit current and synchronous reactance (R_a is much much smaller than X_s and hence can be neglected). When the short-circuit current is one per unit, this voltage is proportional to I_{fSC} as shown in Figure 3.28. Hence,

$$KI_{fSC} = 1.0X_{s(unsat)}$$

Corresponding to the one per unit voltage on the air-gap line,

$$KI_{fNL(ag)} = 1.0$$

Therefore, the unsaturated value of X_s is given by

$$X_{s(unsat)} = \frac{I_{fSC}}{I_{fNL(ag)}} \tag{3.179}$$

The saturated value of X_s corresponding to rated voltage is given by

$$X_{s(sat)} = \frac{I_{fSC}}{I_{fNL}} \tag{3.180}$$

where I_{fNL} and I_{fSC} are the values of field current required to give rated terminal voltage on the OCC and rated armature current on the SCC, respectively.

The *short-circuit ratio* (SCR) is defined as the ratio of the field current required to produce rated voltage at rated speed and no load to the field current required to produce rated armature current under a steady three-phase short-circuit condition. That is,

$$SCR = \frac{I_{fNL}}{I_{fSC}} = \frac{1}{X_{s(sat)}} \tag{3.181}$$

If there were no saturation, the SCR would be equal to the reciprocal of the unsaturated value of synchronous reactance. The SCR reflects the degree of saturation and therefore has significance with respect to both the performance of the machine and its cost. A lower SCR is indicative of a larger change in field current required to maintain constant terminal voltage for a given change in load. Therefore, a machine with a low SCR requires an excitation system that is able to provide large changes of field current to maintain system stability.

On the other hand, when the SCR is lower, the size, weight and cost of the machine are lower. With improvements in excitation systems and the associated controls, there has been a trend toward the use of generators of lower SCR and, consequently, lower cost.

3.8.2 Representation of Saturation in Stability Studies

In the representation of magnetic saturation for stability studies, the following assumptions are usually made:

(a) The leakage inductances are independent of saturation. The leakage fluxes are in air for a considerable portion of their paths so that they are not significantly affected by saturation of the iron portion. As a result, the only elements of the equivalent circuits of Figure 3.18 that saturate are the mutual inductances L_{ad} and L_{aq}.

(b) The leakage fluxes do not contribute to the iron saturation. The leakage fluxes are usually small and their paths coincide with that of the main flux for only a small part of its path. By this assumption, saturation is determined by the air-gap flux linkage.

(c) The saturation relationship between the resultant air-gap flux and the mmf under loaded conditions is the same as under no-load conditions. This allows the saturation characteristics to be represented by the open-circuit saturation curve, which is usually the only saturation data readily available.

(d) There is no magnetic coupling between the *d*- and *q*-axes as a result of nonlinearities introduced by saturation; i.e., currents in the windings of one axis do not produce flux that link with the windings of the other axis.

With the above assumptions, the effects of saturation may be represented as

$$L_{ad} = K_{sd} L_{adu} \tag{3.182}$$

$$L_{aq} = K_{sq} L_{aqu} \tag{3.183}$$

where L_{adu} and L_{aqu} are the unsaturated values of L_{ad} and L_{aq}. The saturation factors K_{sd} and K_{sq} identify the degrees of saturation in the *d*- and *q*-axis, respectively. We will first discuss how *d*-axis saturation is represented and then consider saturation of the *q*-axis.

According to assumption (c) above, the degree of *d*-axis saturation is determined from the OCC. Referring to Figure 3.29, for an operating point defined by point "a" on the OCC, the saturation factor K_{sd} is given by

$$K_{sd} = \frac{\psi_{at}}{\psi_{at0}} \tag{3.184}$$

It can be shown by simple proportion that K_{sd} is also given by

$$K_{sd} = \frac{I_0}{I} \tag{3.185}$$

In our representation of saturation, we will use the expression given by Equation 3.184. This gives the degree of saturation for any specified value of air-gap flux linkage or voltage.

Our next step is to identify a convenient way of mathematically representing the deviation of OCC from the air-gap line.

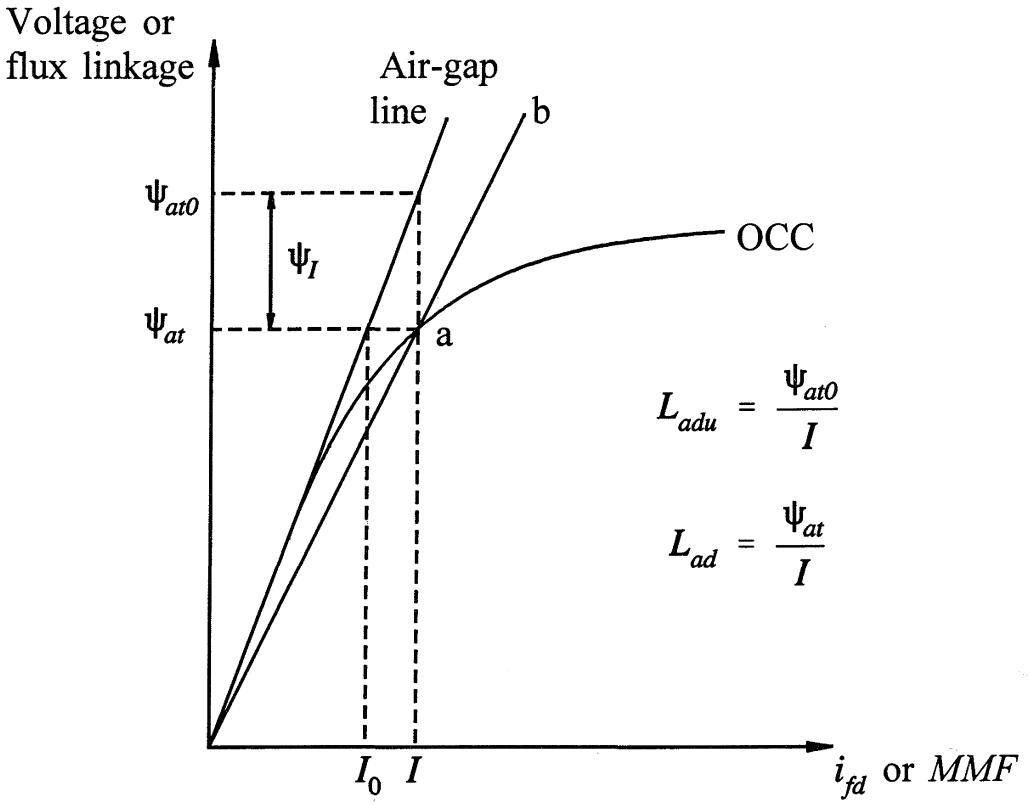

Figure 3.29 Open-circuit characteristic showing effects of saturation

Defining

$$\psi_I = \psi_{at0} - \psi_{at} \tag{3.186}$$

the expression for the saturation factor becomes

$$K_{sd} = \frac{\psi_{at}}{\psi_{at} + \psi_I} \tag{3.187}$$

The saturation curve may be divided into three segments: unsaturated segment I, nonlinear segment II, and fully saturated linear segment III. The threshold values ψ_{T1} and ψ_{T2} define the boundaries of the three segments as shown in Figure 3.30.

For segment I defined by $\psi_{at} \leq \psi_{T1}$

$$\psi_I = 0 \tag{3.188}$$

For segment II defined by $\psi_{T1} < \psi_{at} \leq \psi_{T2}$, ψ_I can be expressed by a suitable mathematical function. Here we will use an exponential function:

$$\psi_I = A_{sat} e^{B_{sat}(\psi_{at} - \psi_{T1})} \tag{3.189}$$

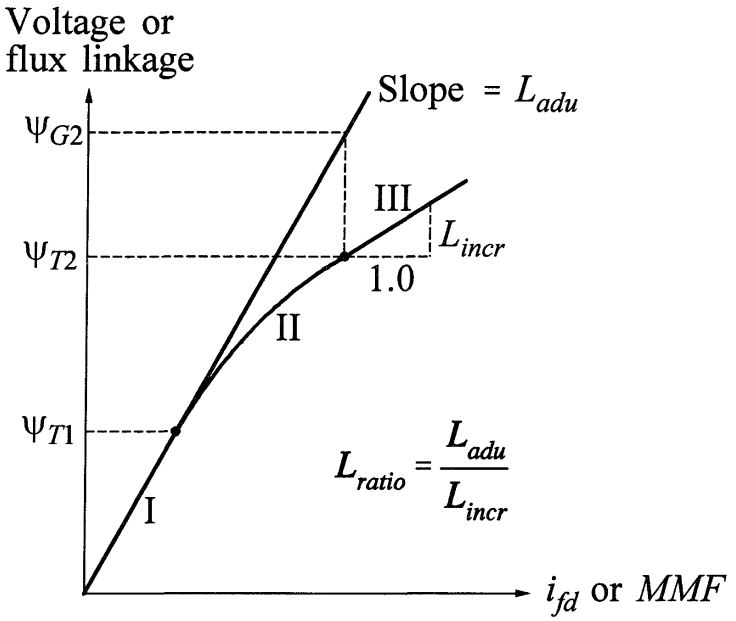

Figure 3.30 Representation of saturation characteristic

where A_{sat} and B_{sat} are constants depending on the saturation characteristic in the segment II portion.

When $\psi_{at}=\psi_{T1}$, from Equation 3.189, $\psi_I=A_{sat}$. Hence, this representation results in a small discontinuity at the junction of segments I and II. However, A_{sat} is normally very small and the discontinuity is inconsequential.

For segment III defined by $\psi_{at}>\psi_{T2}$,

$$\psi_I = \psi_{G2}+L_{ratio}(\psi_{at}-\psi_{T2})-\psi_{at} \tag{3.190}$$

where L_{ratio}, as defined in Figure 3.30, is the ratio of the slope of the air-gap line to the incremental slope of segment III of the OCC.

With the above method of representation, the saturation characteristic for any given machine is completely specified by ψ_{T1}, ψ_{T2}, ψ_{G2}, A_{sat}, B_{sat} and L_{ratio}.

The value of K_{sd}, for any given operating condition, is computed as a function of the corresponding air-gap flux linkage given by

$$\psi_{at} = \sqrt{\psi_{ad}^2+\psi_{aq}^2} \tag{3.191}$$

where ψ_{ad} and ψ_{aq} are the d- and q-axis components of air-gap or mutual flux linkages, identified in Figure 3.31.

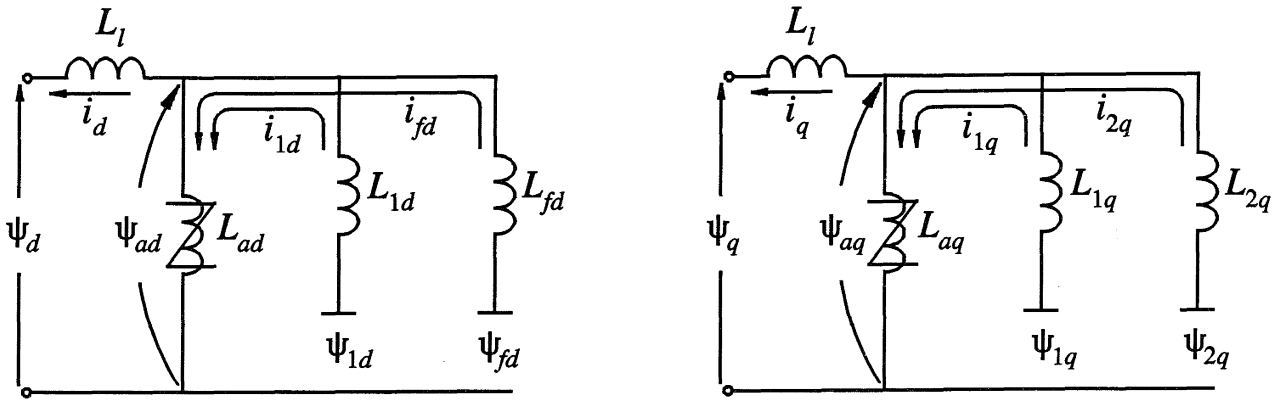

(a) d-axis (b) q-axis

Figure 3.31 Equivalent circuits identifying nonlinear elements and air-gap flux linkages

The d- and q-axis air-gap flux linkages are given by

$$\psi_{ad} = \psi_d + L_l i_d = (e_q + R_a i_q) + L_l i_d \tag{3.192}$$

$$\psi_{aq} = \psi_q + L_l i_q = (-e_d - R_a i_d) + L_l i_q \tag{3.193}$$

Therefore, ψ_{at} in per unit is equal to the air-gap voltage

$$\tilde{E}_a = \tilde{E}_t + (R_a + jX_l)\tilde{I}_t \tag{3.194}$$

The saturation factor K_{sd} can thus be determined, for any given values of terminal voltage and current, by first computing $\tilde{E}_a$ and then using Equations 3.187 and 3.188, 3.189 or 3.190.

For salient pole machines, because the path for q-axis flux is largely in air, L_{aq} does not vary significantly with saturation of the iron portion of the path. Therefore, K_{sq} is assumed to be equal to 1.0 for all loading conditions.

In the case of round rotor machines, there is magnetic saturation in both axes. The saturation factor K_{sq} can be determined from the no-load saturation characteristic of the q-axis. However, q-axis saturation data is usually not available; hence, K_{sq} is assumed to be equal to K_{sd}. This is equivalent to assuming that the reluctance of the magnetic path is homogeneous around the rotor periphery. Improved saturation modelling using q-axis saturation characteristics derived from finite-element analysis or tests on loaded machines is discussed in the following section.

3.8.3 Improved Modelling of Saturation

The method of representing saturation described in the previous section is based on a number of idealizing assumptions. For accurate representation under all loading conditions these assumptions are not strictly valid. Several improvements in saturation modelling have been proposed in the literature to overcome these limitations. These include consideration of the following effects:

(a) Power and load angle dependency of the direct and quadrature axis saturation [4,7,22]. This variation occurs because of higher saturation of rotor iron under load and variation in permeance in the air-gap with load angle. The mutual fluxes in the stator at no-load and loaded conditions are similar because the stator voltage is close to rated value under both conditions. On the other hand, due to large excitation under loaded conditions, particularly when overexcited, the rotor flux is considerably more dense and hence saturation is considerably higher than under no-load. For a given stator terminal voltage and active power output, L_{ad} is smaller when overexcited and larger when underexcited. In contrast, L_{aq} is smaller when underexcited since the corresponding load angle is higher. Accurate representation of saturation effects including power and load angle dependency requires a significant amount of computational effort, which cannot be justified for stability studies.

(b) Cross coupling between *d*- and *q*-axes [6,9,23]. Due to the nonlinearity introduced by saturation, the permeability pattern is not symmetric around the *d*-axis. This results in dissymmetry in flux linkages; that is, *d*-axis currents produce *q*-axis flux linkages and vice versa. The cross coupling phenomenon in fact invalidates the fundamental assumption on which Park's *dq0* transformation is based. However, the use of a rigorous mathematical model of a synchronous machine including nonlinear effects is neither practical nor justified. The cross-coupling effects are of a secondary nature and may be represented approximately or neglected altogether.

(c) Quadrature-axis saturation [5,6,9,24]. For round rotor machines, experience has shown that the *q*-axis saturates appreciably more than the *d*-axis. This is due to the presence of rotor teeth in the magnetic path of the *q*-axis. For accurate prediction of steady-state rotor angle and field excitation, it would be necessary to account for the *q*-axis saturation characteristic as distinct from the *d*-axis characteristic. The errors introduced by assuming the *q*-axis saturation to be same as the *d*-axis open-circuit curve are shown in Figure 3.32. The figure shows the differences between measured and computed values of rotor angle and field current as a function of reactive power output of a 500 MW generator at the Lambton coal-fired generating station in Ontario [5]. The error in field current is greater in the overexcited region with the highest error being on the order of 4%; the error in rotor angle is higher in the underexcited region with the highest value being as high as 10°.

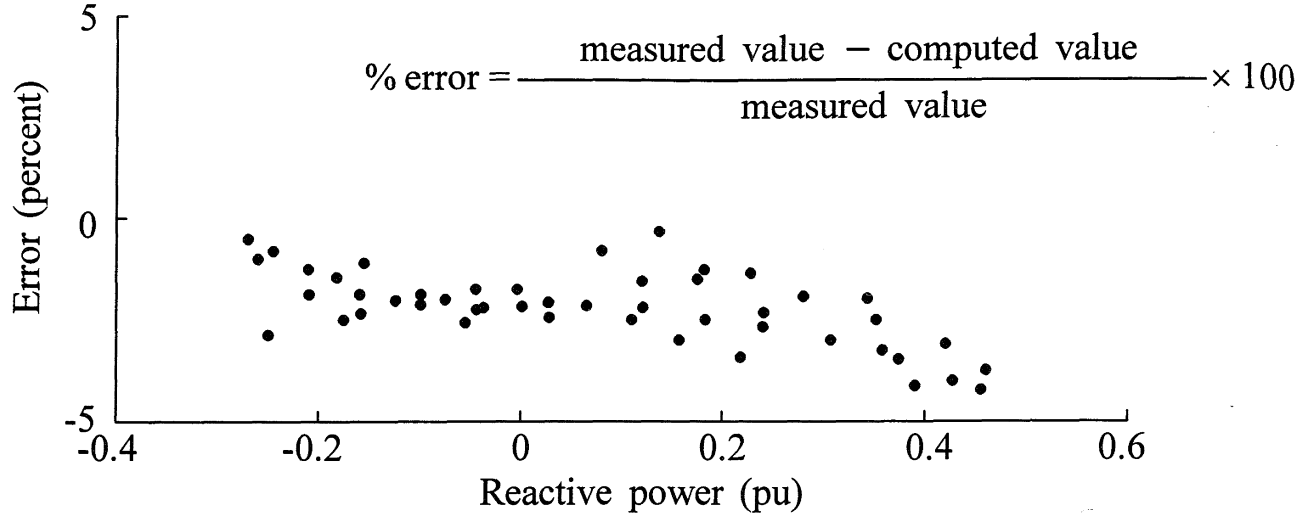

(a) Field current error

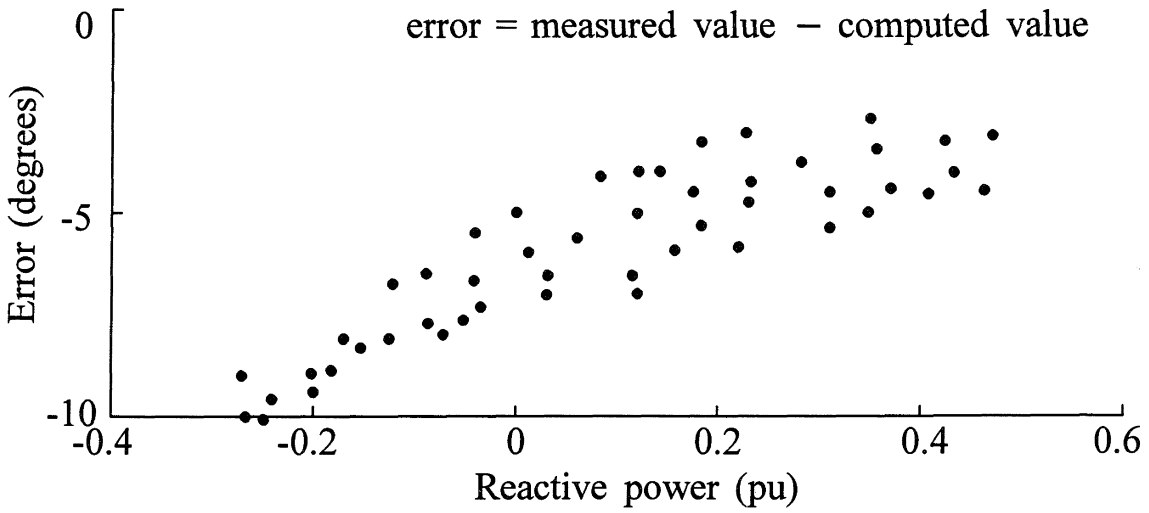

(b) Internal angle error

Figure 3.32 Field current and internal angle errors with conventional saturation representation

The q-axis saturation characteristic is not readily available from the generator manufacturers. It can, however, be easily determined from steady-state measurements of field current and rotor angle at different values of terminal voltage, active and reactive power output. These measurements also provide the d-axis saturation characteristics under load, which should be more accurate than using the open-circuit saturation curves. Figure 3.33 shows the d- and q-axis saturation characteristics derived from steady-state measurements on the Lambton unit [5].

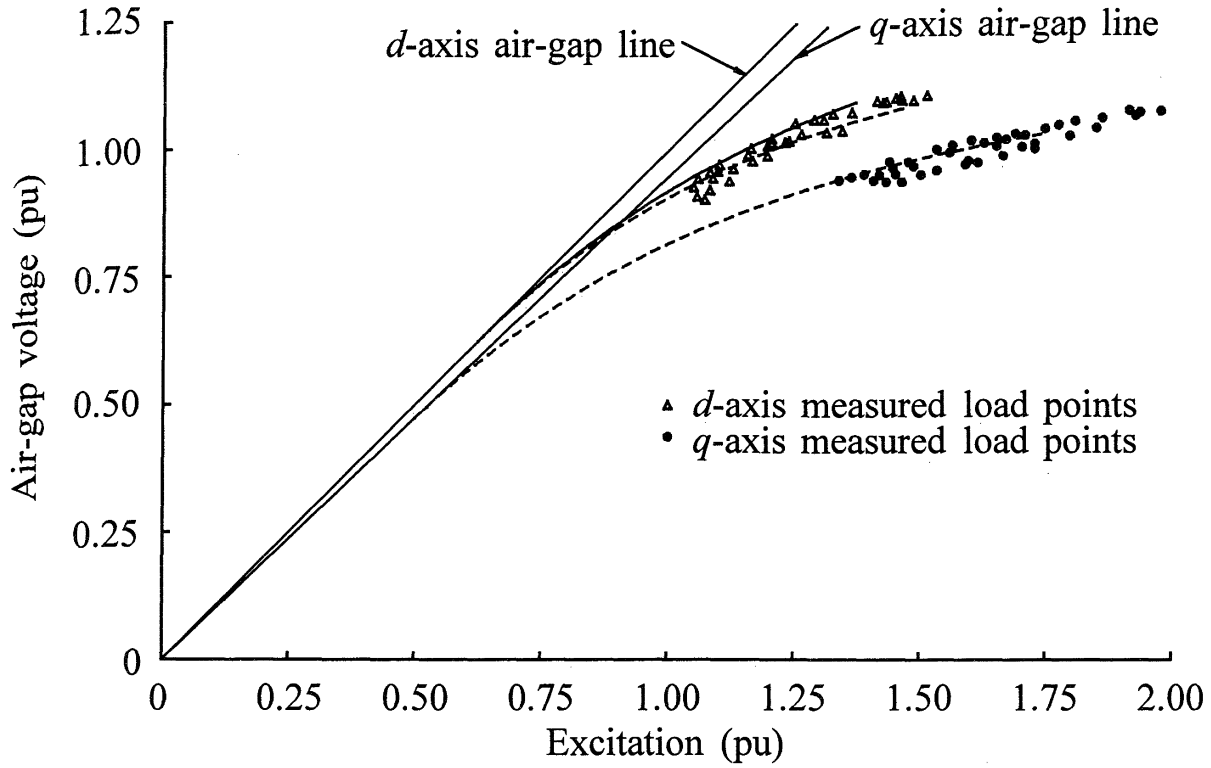

Figure 3.33 Lambton saturation curves derived from steady-state field current and rotor angle measurements

An accurate method of saturation representation including the effects of cross coupling and q-axis saturation, based on finite element analysis, is presented in references 6 and 9. The overall effect of this improved representation on system stability is assessed in reference 8. The beneficial effect of using such a representation appears to be only marginal for the case investigated.

In general, very complex saturation models based on specially developed data are not justified for stability studies. The approach described in Section 3.8.2 using readily available data should be adequate in most situations. In critical cases, the best approach is to use d- and q-axis saturation characteristics based on simple measurement under steady-state on-load conditions, such as those shown in Figure 3.33.

Use of Potier reactance[1]

The voltage E_p behind the Potier reactance (X_p) is often used in place of E_a to identify the saturation level. The use of X_p, instead of X_l, is believed to make an empirical allowance for the difference between the load saturation and open-circuit

[1] For a description of the Potier reactance and its physical significance, see references 12 and 14.

characteristic. An important factor causing the discrepancy between the load and no-load saturation is the difference in the field leakage flux under the two conditions. The Potier reactance accounts for this difference and is higher than the stator leakage reactance due to the appreciably higher field leakage under loaded conditions.

The use of E_p, because of the manner in which X_p is computed, gives accurate values of field current under steady-state loaded conditions. However, its use to represent saturation under transient conditions, when the amortisseur effects are included, leads to unrealistic results in some situations. Its use in stability studies is, therefore, not recommended.

Example 3.3

The open-circuit saturation curve of the 555 MVA generator considered in Examples 3.1 and 3.2 is shown in Figure E3.1. The per unit resistance and inductances associated with the stator circuits are as follows:

$$R_a = 0.003 \qquad L_l = 0.15 \qquad L_{adu} = 1.66 \qquad L_{aqu} = 1.61$$

(a) If the field current required to generate rated E_t on the air-gap line is 1300 amperes, determine the base values of the field current and field voltage. Compare with the values computed in Example 3.1.

(b) If segment II of the saturation curve is to be represented by the function defined by Equation 3.189, determine the constants A_{sat} and B_{sat}.

(c) With the armature terminal voltage at rated value, for each of the following generator output conditions expressed in per unit of the MVA rating:

(i) $P_t=0,\ Q_t=0$

(ii) $P_t=0.4,\ Q_t=0.2$ (overexcited)

(iii) $P_t=0.9,\ Q_t=0.436$

(iv) $P_t=0.9,\ Q_t=0$

(v) $P_t=0.9,\ Q_t=-0.2$ (underexcited)

compute the air-gap voltage E_a, saturation factor K_{sd}, internal rotor angle δ_i, and field current i_{fd}. Assume that the open-circuit curve represents the saturation characteristics of both d- and q-axis. Comment on the effect of reactive power output on δ_i and i_{fd}.

(d) How would the results of (c) change if the q-axis saturation characteristic differs from that of the d-axis as shown in Figure E3.2?

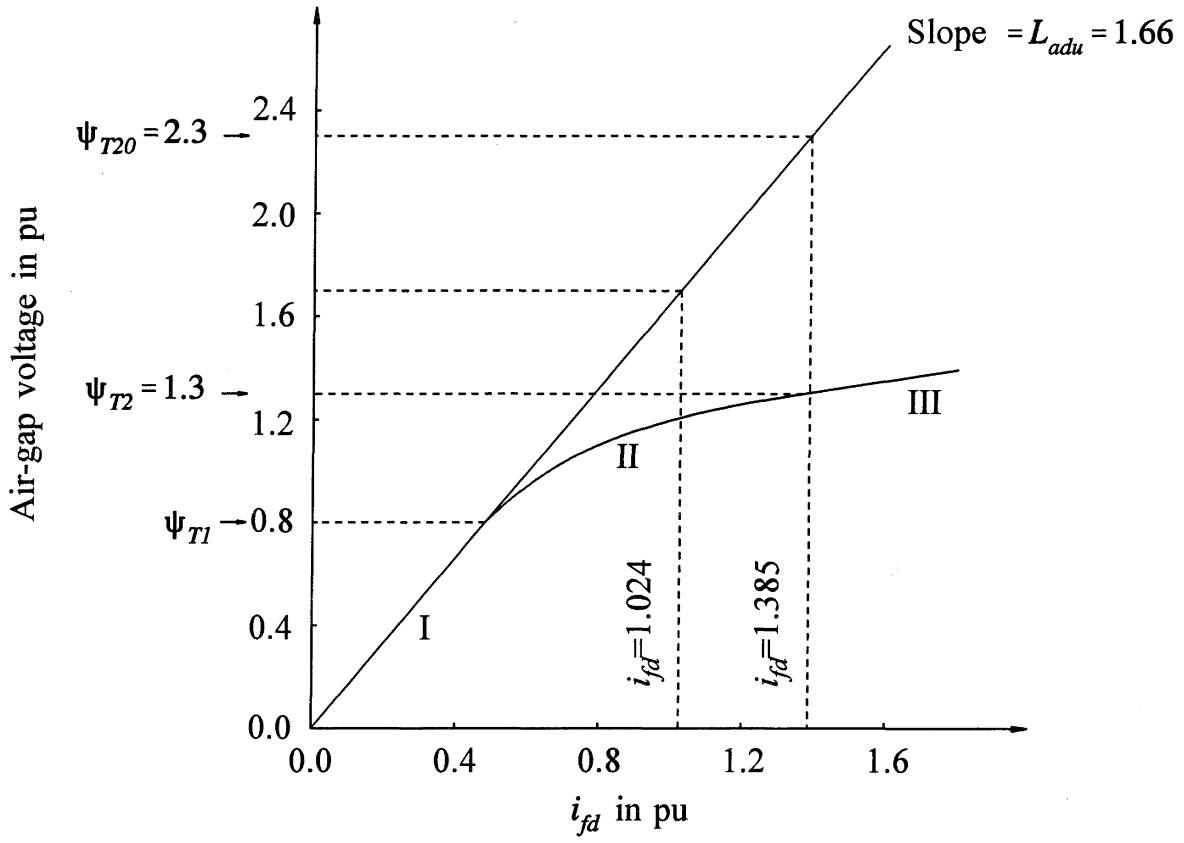

Figure E3.1 Open-circuit saturation curve

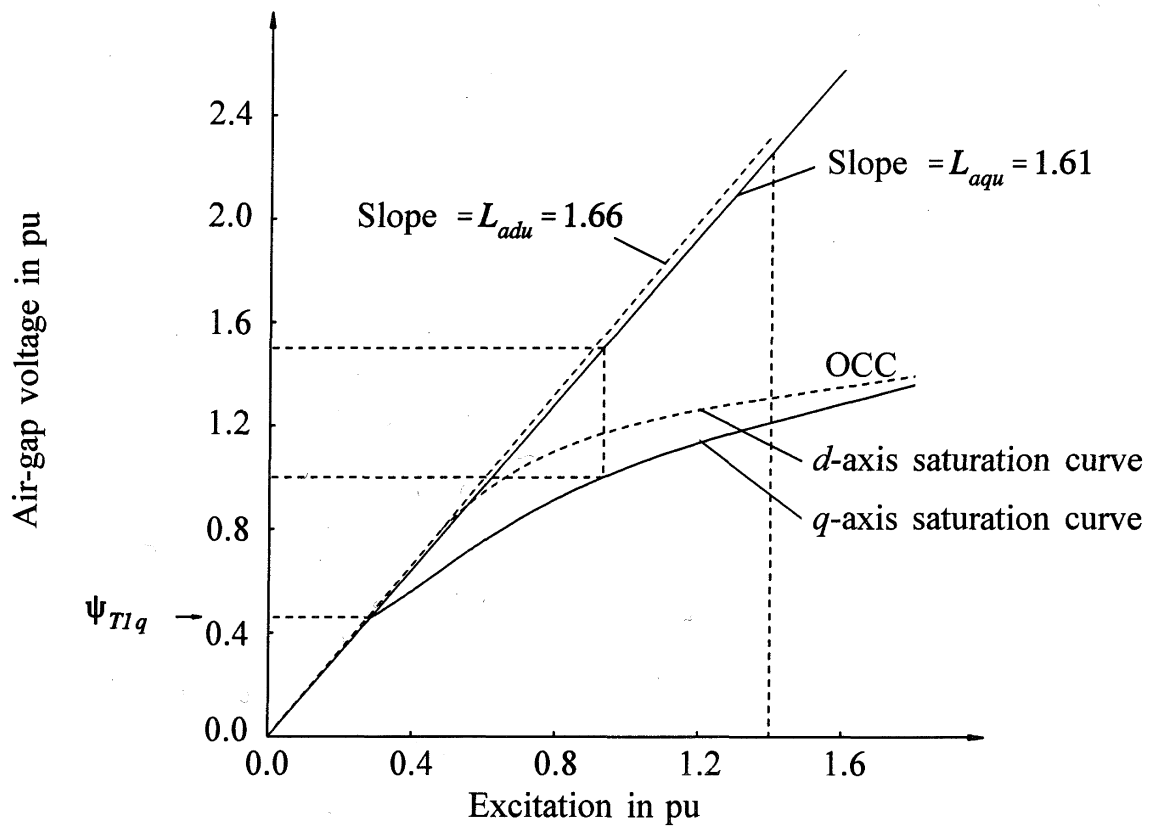

Figure E3.2 The d- and q-axis saturation characteristics

Solution

(a) As discussed in Section 3.8.1, under no-load rated speed conditions,

$$E_t = e_q = L_{ad} i_{fd}$$

The slope of the air-gap line represents the unsaturated value of L_{ad}. Therefore, the field current required to produce 1.0 per unit E_t on the air-gap line is

$$i_{fd} = \frac{1.0}{L_{adu}} \quad \text{per unit}$$

$$= \frac{1.0}{1.66} \quad \text{per unit}$$

Since this is equal to 1300 amperes, the base field current is

$$i_{fdbase} = 1300 \times 1.66 = 2158 \quad \text{A}$$

$$e_{fdbase} = \frac{\text{VA rating}}{i_{fdbase}} = \frac{555 \times 10^6}{2158} \quad \text{V}$$

$$= 257.183 \quad \text{kV}$$

As is to be expected, this agrees with the value computed in Example 3.1.

(b) From Equation 3.189,

$$\psi_I = A_{sat} e^{B_{sat}(\psi_{at} - \psi_{TI})}$$

We will compute A_{sat} and B_{sat} by considering two points on the saturation curve corresponding to ψ_{at}=1.2 and 1.3 in Figure E3.1. With ψ_{at}=1.2, ψ_I=1.7−1.2=0.5, and with ψ_{at}=1.3, ψ_I=2.3−1.3=1.0. Therefore,

$$0.5 = A_{sat} e^{B_{sat}(1.2-0.8)}$$

and

$$1.0 = A_{sat} e^{B_{sat}(1.3-0.8)}$$

Solving gives

$$A_{sat} = 0.03125$$

$$B_{sat} = 6.931$$

(c) From the steady-state equations summarized in Section 3.6.5,

$$I_t = \frac{\sqrt{P_t^2+Q_t^2}}{E_t}$$

$$\phi = \cos^{-1}\left(\frac{P_t}{I_t E_t}\right)$$

$$\tilde{E}_a = \tilde{E}_t+(R_a+jX_l)\tilde{I}_t$$

$$\psi_{at} = E_a$$

From Figure E3.1, $\psi_{T1}=0.8$ and $\psi_{T2}=1.3$. For $0.8<\psi_{at}<1.3$,

$$\psi_I = 0.03125e^{6.931(\psi_{at}-0.8)}$$

$$K_{sd} = K_{sq} = \frac{\psi_{at}}{\psi_{at}+\psi_I}$$

$$X_{ad} = K_{sd}X_{adu};\quad X_d = X_{ad}+X_l$$

$$X_{aq} = K_{sq}X_{aqu};\quad X_q = X_{aq}+X_l$$

$$\delta_i = \tan^{-1}\left(\frac{X_q I_t\cos\phi - R_a I_t\sin\phi}{E_t+R_a I_t\cos\phi+X_q I_t\sin\phi}\right)$$

$$e_q = E_t\cos\delta_i$$

$$i_d = I_t\sin(\delta_i+\phi)$$

$$i_q = I_t\cos(\delta_i+\phi)$$

$$i_{fd} = \frac{e_q+R_a i_q+X_d i_d}{X_{ad}}$$

Table E3.1 summarizes the results for the given operating conditions.

Table E3.1

P_t	Q_t	E_a (pu)	K_{sd}	δ_i (deg)	i_{fd} (pu)
0	0	1.0	0.889	0	0.678
0.4	0.2	1.033	0.868	25.3	1.016
0.9	0.436	1.076	0.835	39.1	1.565
0.9	0	1.012	0.882	54.6	1.206
0.9	-0.2	0.982	0.899	64.6	1.089

From the results, the reactive power output is seen to have a significant effect on δ_i as well as i_{fd}. The reason for this is readily apparent from the phasor diagrams shown

in Figure E3.3. These diagrams are based on the simplified model of Figure 3.22, which neglects saliency.

(d) Constants approximating the nonlinear portion (segment II) of the q-axis saturation curve of Figure E3.2, determined by considering two points on the curve corresponding ψ_{at}=1.0 and 1.2, are

$$A_{satq} = 0.077$$
$$B_{satq} = 3.465$$

The threshold value defining the beginning of segment II is

$$\psi_{T1q} = 0.46$$

Corresponding to any air-gap voltage $E_a=\psi_{at}$, the q-axis saturation factor is

$$K_{sq} = \frac{\psi_{at}}{\psi_{at}+\psi_{Iq}}$$

where

$$\psi_{Iq} = 0.077e^{3.465(\psi_{at}-0.46)}$$

The d-axis saturation representation is same as in (c).

Table E3.2 summarizes the results obtained with distinct d- and q-axis saturation representations.

Table E3.2

P_t	Q_t	E_a (pu)	K_{sd}	K_{sq}	δ_i (deg)	i_{fd} (pu)
0	0	1.0	0.889	0.667	0	0.678
0.4	0.2	1.033	0.868	0.648	21.0	1.013
0.9	0.436	1.076	0.835	0.623	34.6	1.559
0.9	0	1.012	0.882	0.660	47.5	1.194
0.9	-0.2	0.982	0.899	0.676	55.9	1.074

By comparing with the results of Table E3.1, the effect of increased q-axis saturation is seen to be quite significant, particularly in the underexcited operating condition.

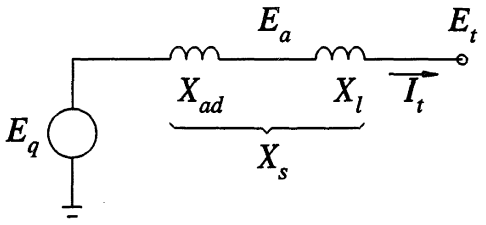

$X_{ad} = K_{sd}X_{adu}$

$E_q = X_{ad}i_{fd}$

(a) Simplified steady-state model

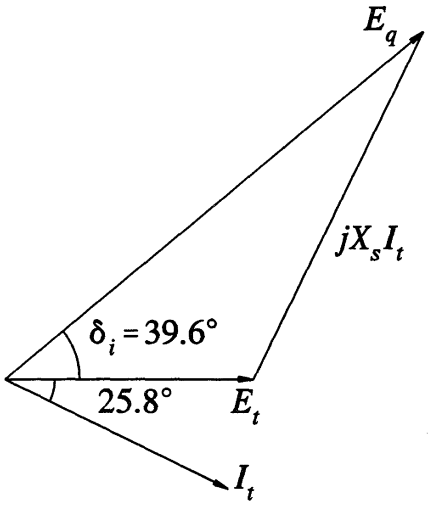

$X_{ad} = 0.835 \times 1.66 = 1.386$

$X_s = 1.386 + 0.15 = 1.536$

$I_t = 0.9 - j0.436$
$= 1.0\angle -25.8°$

$E_q = 1.0 + j1.536(0.9 - j0.436)$
$= 2.17\angle 39.6°$

$i_{fd} = 1.564$

$\delta_i = 39.6°$

(b) Phasor diagram with $P = 0.9$, $Q = 0.436$, $E_t = 1.0$

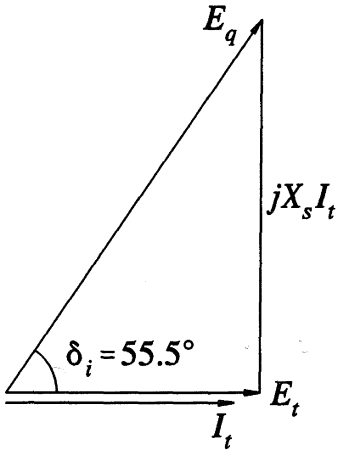

$X_{ad} = 0.882 \times 1.66 = 1.464$

$X_s = 1.614$

$I_t = 0.9\angle 0°$

$E_q = 1.764\angle 55.5°$

$i_{fd} = 1.205$

$\delta_i = 55.5°$

(c) Phasor diagram with $P = 0.9$, $Q = 0$, $E_t = 1.0$

Figure E3.3 Phasor diagrams showing the effect of varying Q on i_{fd} and δ_i

(Continued on next page)

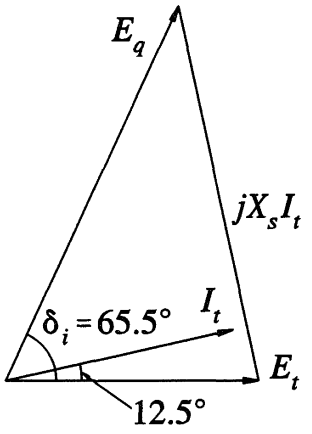

X_{ad} = 0.899×1.66 = 1.492

X_s = 1.64

I_t = 0.92∠12.5°

E_q = 1.62∠65.5°

i_{fd} = 1.086

δ_i = 65.5°

(d) Phasor diagram with $P=0.9$, $Q=-0.2$, $E_t=1.0$

Figure E3.3 (*Continued*) Phasor diagrams showing the effect of varying Q on i_{fd} and δ_i

Example 3.4

For the generator of Example 3.3, determine the steady-state relationship between armature current and field current, with the terminal voltage maintained at rated value and with:

(a) Active power constant at 0, 0.25 pu, 0.5 pu and 0.9 pu

(b) Power factor constant at 0.6 lead, 0.8 lead, 1.0, 0.8 lag, and 0.6 lag

Assume that the *d*- and *q*-axis saturation characteristics are as shown in Figure E3.2. Discuss the characteristics determined.

Solution

(a) With P equal to the specified value, Q is varied between −0.6 and +0.6. For each value of Q, the I_t, E_a, K_{sd}, K_{sq}, δ_i, e_q, i_d, i_q, and i_{fd} values are computed as described in Example 3.3. Curves showing the relationship between armature current and field current for P=0, 0.25, 0.5 and 0.9 pu are in Figure E3.4. These are known as *V curves* because of their characteristic shape.

(b) With power factor at specified value, I_t is varied between 0.0 and 1.5. The corresponding values of Q, P and i_{fd} are computed using the same approach as in (a). The loci of constant power factor are shown as dashed lines in Figure E3.4. These are commonly referred to as *compounding curves.*

For a given P, armature current I_t is a minimum at unity power factor (UPF). Under such a condition the field provides all the magnetizing current required and the armature current is associated with only active power. The generator neither supplies nor absorbs reactive power.

If the field current is increased beyond the value corresponding to UPF, not all of the field current is required to magnetize the generator. The stator current, which now has a reactive component in addition to the active component, increases and lags the stator terminal voltage. The reactive power output Q is positive and the power factor is lagging. The generator under such a condition is said to be overexcited.

If, on the other hand, the field current is decreased beyond the value corresponding to the UPF condition, the field current is insufficient to magnetize the machine, and the balance of magnetizing current is drawn from the system to which the machine is connected. This inductive component of stator current absorbed by the generator increases as the field current is reduced. The magnitude of the total stator current therefore increases. The machine absorbs Q; i.e., the Q output is negative. The stator current leads the stator voltage and hence the power factor is considered to be leading. The generator under these conditions is said to be underexcited.

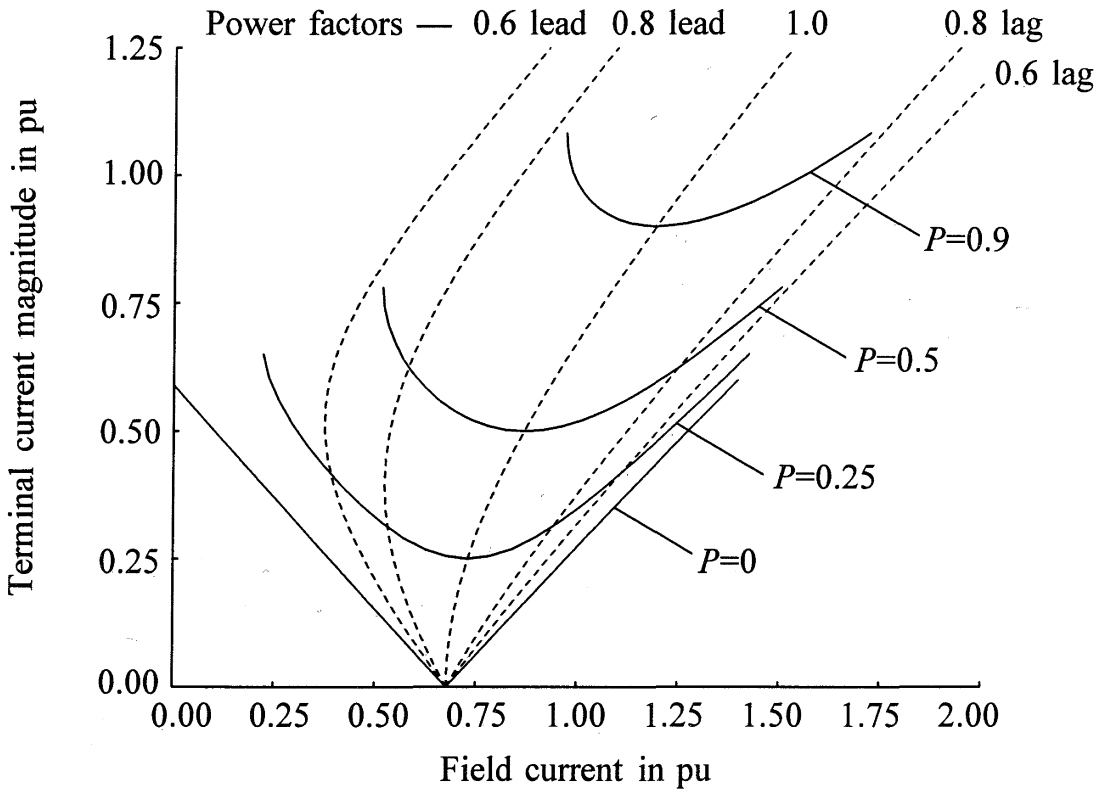

Figure E3.4 Relationship between armature and field current for varying values of P and power factors

3.9 EQUATIONS OF MOTION

The equations of central importance in power system stability analysis are the rotational inertia equations describing the effect of unbalance between the electromagnetic torque and the mechanical torque of the individual machines. In this section, we will develop these equations in *per unit form* and define parameters that are used to represent mechanical characteristics of synchronous machines in stability studies.

3.9.1 Review of Mechanics of Motion

Before we develop the equations of motion of a synchronous machine, it is useful to review the quantities and relationships associated with the mechanics of motion. These are summarized in Table 3.1. Since it is easier to visualize quantities associated with rotation by analogy with those associated with the more familiar linear motion, the latter are also included in the table.

3.9.2 Swing Equation

As we are introducing new per unit equations and parameters, once again we temporarily resort to the use of superbars to identify per unit quantities.

When there is an unbalance between the torques acting on the rotor, the net torque causing acceleration (or deceleration) is

$$T_a = T_m - T_e \tag{3.195}$$

where

T_a = accelerating torque in N·m
T_m = mechanical torque in N·m
T_e = electromagnetic torque in N·m

In the above equation, T_m and T_e are positive for a generator and negative for a motor.

The combined inertia of the generator and prime mover is accelerated by the unbalance in the applied torques. Hence, the equation of motion is

$$J\frac{d\omega_m}{dt} = T_a = T_m - T_e \tag{3.196}$$

where

J = combined moment of inertia of generator and turbine, kg·m^2
ω_m = angular velocity of the rotor, mech. rad/s
t = time, s

Table 3.1

Linear Motion			Rotation		
Quantity	Symbol/ Equation	MKS unit	Quantity	Symbol/ Equation	MKS unit
Length	s	meter (m)	Angular displacement	θ	radian (rad)
Mass	M	kilogram (kg)	Moment of inertia	$J=\int r^2 dm$	kg·m^2
Velocity	$v=ds/dt$	meter/second (m/s)	Angular velocity	$\omega=d\theta/dt$	rad/s
Acceleration	$a=dv/dt$	m/s^2	Angular acceleration	$\alpha=d\omega/dt$	rad/s^2
Force	$F=Ma$	newton (N)	Torque	$T=J\alpha$	newton-meter (N·m) or J/rad
Work	$W=\int Fds$	joule (J)	Work	$W=\int Td\theta$	J, or W·s
Power	$p=dW/dt$ $=Fv$	watt (W)	Power	$p=dW/dt$ $=T\omega$	W

The above equation can be normalized in terms of per unit *inertia constant H*, defined as the kinetic energy in watt-seconds at rated speed divided by the VA base. Using ω_{0m} to denote rated angular velocity in mechanical radians per second, the inertia constant is

$$H = \frac{1}{2}\frac{J\omega_{0m}^2}{\text{VA}_{base}} \tag{3.197}$$

The moment of inertia J in terms of H is

$$J = \frac{2H}{\omega_{0m}^2}\text{VA}_{base}$$

Substituting the above in Equation 3.196 gives

$$\frac{2H}{\omega_{0m}^2}\mathrm{VA}_{base}\frac{d\omega_m}{dt} = T_m - T_e$$

Rearranging yields

$$2H\frac{d}{dt}\left(\frac{\omega_m}{\omega_{0m}}\right) = \frac{T_m - T_e}{\mathrm{VA}_{base}/\omega_{0m}}$$

Noting that $T_{base}=\mathrm{VA}_{base}/\omega_{0m}$, the equation of motion in per unit form is

$$2H\frac{d\bar{\omega}_r}{dt} = \bar{T}_m - \bar{T}_e \tag{3.198}$$

In the above equation,

$$\bar{\omega}_r = \frac{\omega_m}{\omega_{0m}} = \frac{\omega_r/p_f}{\omega_0/p_f} = \frac{\omega_r}{\omega_0}$$

where ω_r is angular velocity of the rotor in electrical rad/s, ω_0 is its rated value, and p_f is number of field poles.

If δ is the angular position of the rotor in electrical radians with respect to a synchronously rotating reference and δ_0 is its value at $t=0$,

$$\delta = \omega_r t - \omega_0 t + \delta_0 \tag{3.199}$$

Taking the time derivative, we have

$$\frac{d\delta}{dt} = \omega_r - \omega_0 = \Delta\omega_r \tag{3.200}$$

and

$$\begin{aligned}\frac{d^2\delta}{dt^2} &= \frac{d\omega_r}{dt} = \frac{d(\Delta\omega_r)}{dt} \\ &= \omega_0\frac{d\bar{\omega}_r}{dt} = \omega_0\frac{d(\Delta\bar{\omega}_r)}{dt}\end{aligned} \tag{3.201}$$

Substituting for $d\bar{\omega}_r/dt$ given by the above equation in Equation 3.198, we get

$$\frac{2H}{\omega_0}\frac{d^2\delta}{dt^2} = \bar{T}_m - \bar{T}_e \tag{3.202}$$

It is often desirable to include a component of damping torque, not accounted for in the calculation of T_e, separately. This is accomplished by adding a term proportional to speed deviation in the above equation as follows:

$$\frac{2H}{\omega_0}\frac{d^2\delta}{dt^2} = \bar{T}_m - \bar{T}_e - K_D\Delta\bar{\omega}_r \tag{3.203}$$

From Equation 3.200,

$$\Delta\bar{\omega}_r = \frac{\Delta\omega_r}{\omega_0} = \frac{1}{\omega_0}\frac{d\delta}{dt}$$

Equation 3.203 represents the equation of motion of a synchronous machine. It is commonly referred to as the *swing equation* because it represents swings in rotor angle δ during disturbances.

Per unit moment of inertia

Substituting in Equation 3.203 gives

$$\frac{2H}{\omega_0}\frac{d^2\delta}{dt^2} = \bar{T}_m - \bar{T}_e - \frac{K_D}{\omega_0}\frac{d\delta}{dt} \tag{3.204}$$

In Equations 3.203 and 3.204, K_D is the damping factor or coefficient in pu torque/pu speed deviation.

If it is desired to use per unit value of time $\bar{t}$, Equation 3.204 becomes

$$2H\omega_0\frac{d^2\delta}{d\bar{t}^2} = \bar{T}_m - \bar{T}_e - K_D\frac{d\delta}{d\bar{t}} \tag{3.205}$$

Some authors (for example, reference 19) refer to $2H\omega_0$ as the per unit moment of inertia $\bar{J}$.

3.9.3 Mechanical Starting Time

From Equation 3.198,

$$\frac{d\bar{\omega}_r}{dt} = \frac{1}{2H}\bar{T}_a$$

Integrating with respect to time gives

$$\bar{\omega}_r = \frac{1}{2H}\int_0^t \bar{T}_a\, dt \tag{3.206}$$

Let T_M be the time required for rated torque to accelerate the rotor from standstill to rated speed. From Equation 3.206, with $\bar{\omega}_r = 1.0$, $\bar{T}_a = 1.0$ and with the starting value of $\bar{\omega}_r = 0$, we have

$$1.0 = \frac{1}{2H}\int_0^{T_M} 1.0\, dt = \frac{T_M}{2H}$$

Therefore,

$$T_M = 2H \quad \text{s}$$

and T_M is called the *mechanical starting time.* The symbol M is also used in the literature to denote this time.

3.9.4 Calculation of Inertia Constant

As defined in Section 3.9.2, the inertia constant is given by

$$H = \frac{\text{stored energy at rated speed in MW·s}}{\text{MVA rating}}$$

Calculation of H from moment of inertia in MKS units

$$\begin{aligned}\text{Stored energy} &= \text{kinetic energy}\\ &= \frac{1}{2}J\omega_{0m}^2 \quad \text{W·s}\\ &= \frac{1}{2}J\omega_{0m}^2 \times 10^{-6} \quad \text{MW·s}\end{aligned}$$

where

$$J = \text{moment of inertia in kg·m}^2$$
$$\omega_{0m} = \text{rated speed in mech. rad/s} = 2\pi\frac{RPM}{60}$$

Therefore,

$$H = \frac{1}{2}\frac{J\omega_{0m}^2\times10^{-6}}{\text{MVA rating}} = \frac{1}{2}\frac{J(2\pi RPM/60)^2\times10^{-6}}{\text{MVA rating}} = 5.48\times10^{-9}\frac{J(RPM)^2}{\text{MVA rating}} \tag{3.207}$$

Calculation of H from WR^2 in English units

Sometimes the moment of inertia of the rotor is given in terms of WR^2, which is equal to the weight of rotating parts multiplied by the square of radians of gyration in lb·ft^2. Then, moment of inertia in slug·ft^2=WR^2/32.2.

The following relationship between MKS units and English units is useful in converting WR^2 to J:

$$1\text{ m} = 3.281\text{ ft}$$
$$1\text{ kg} = 2.205\text{ lb (mass)} = 0.0685\text{ slug}$$
$$1\text{ slug·ft}^2 = \frac{1}{0.0685\times3.281^2} = 1.356\text{ kg·m}^2$$

The moment of inertia J in kg·m^2 is related to WR^2 as follows:

$$J = \frac{WR^2}{32.2}\times1.356$$

Substituting the above expression for J in Equation 3.207 gives

$$H = \frac{5.48\times10^{-9}\times1.356(WR^2)(RPM)^2}{\text{MVA rating}\times32.2}$$
$$= \frac{2.31\times10^{-10}(WR^2)(RPM)^2}{\text{MVA rating}} \quad \text{in MW·s/MVA} \tag{3.208}$$

Typical values of H

Table 3.2 gives the normal range within which the inertia constant H lies, for thermal and hydraulic generating units. The values of H given are in MW·s per MVA rating of the generator, and represent the combined inertia of the generator and the turbine.

Table 3.2

Type of generating unit	H
Thermal unit (a) 3600 r/min (2-pole) (b) 1800 r/min (4-pole)	 2.5 to 6.0 4.0 to 10.0
Hydraulic unit	2.0 to 4.0

Example 3.5

If the WR^2 of the rotor (including the turbine rotor) of the 555 MVA generating unit of Examples 3.1 and 3.2 is 654,158 lb·ft^2, compute the following:

(a) Moment of inertia J, kg·m^2
(b) Inertia constant H, MW·s/MVA rating
(c) Stored energy, MW·s at rated speed
(d) The mechanical starting time, s

Solution

(a) From the relationships developed in Section 3.9.4,

$$J = \frac{\text{WR}^2}{32.2}\times1.356 = \frac{654{,}158\times1.356}{32.2}$$

$$= 27{,}547.8 \quad \text{kg·m}^2$$

(b) Inertia constant

$$H = 5.48\times10^{-9}\frac{J(RPM)^2}{\text{MVA rating}}$$

$$= \frac{5.48\times10^{-9}\times27{,}547.8\times3600^2}{555}$$

$$= 3.525 \quad \text{MW·s/MVA}$$

(c) Stored energy at rated speed

$$E = H\times\text{MVA rating} = 3.525\times555$$

$$= 1956.4 \quad \text{MW·s}$$

(d) Mechanical starting time

$$T_M = 2H = 2\times3.525$$

$$= 7.05 \quad \text{s}$$

■

3.9.5 Representation in System Studies

For analysis of power system dynamic performance, the component models are expressed in the state-space form (see Chapter 12, Section 12.1) or the block diagram form.

The state-space form requires the component models to be expressed as a set of first order differential equations. The swing equation 3.203, expressed as two first order differential equations, becomes

$$\frac{d\Delta\bar{\omega}_r}{dt} = \frac{1}{2H}(\bar{T}_m - \bar{T}_e - K_D\Delta\bar{\omega}_r) \tag{3.209}$$

$$\frac{d\delta}{dt} = \omega_0\Delta\bar{\omega}_r \tag{3.210}$$

In the above equations, time t is in seconds, rotor angle δ is in electrical radians, and ω_0 is equal to $2\pi f$. In later chapters, when we use the above equations we will not use superbars to identify per unit quantities. We will assume the variables $\Delta\omega_r$, T_m and T_e to be in per unit. However, t will be expressed in seconds and ω_0 in electrical radians per second.

The block diagram form representation of Equations 3.209 and 3.210 is shown in Figure 3.34.

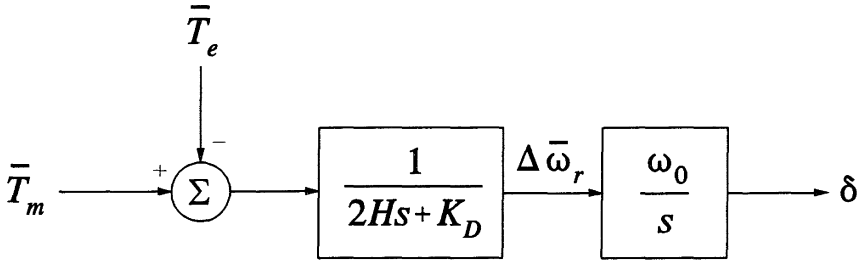

Figure 3.34 Block diagram representation of swing equations

In the block diagram, s is the Laplace operator; it replaces d/dt of Equations 3.209 and 3.210. As noted earlier, symbols T_M and M are often used in place of $2H$.

REFERENCES

[1] A. Blondel, "The Two-Reaction Method for Study of Oscillatory Phenomena in Coupled Alternators," *Revue Générale de L'Electricité*, Vol. 13, pp. 235-251, February 1923; pp. 515-531, March 1923.

[2] R.E. Doherty and C.A. Nickle, "Synchronous Machine I and II," *AIEE Trans.*, Vol. 45, pp. 912-942, 1926.

[3] R.H. Park, "Two-Reaction Theory of Synchronous Machines - Generalized Method of Analysis - Part I," *AIEE Trans.*, Vol. 48, pp. 716-727, 1929; Part II, Vol. 52, pp. 352-355, 1933.

[4] G. Shackshaft and P.B. Henser, "Model of Generator Saturation for Use in Power System Studies," *Proc. IEE* (London), Vol. 126, No. 8, pp. 759-763, 1979.

[5] EPRI Report EL-1424, "Determination of Synchronous Machine Stability Constants," Vol. 2, prepared by Ontario Hydro, December 1980.

[6] EPRI Report EL-3359, "Improvement in Accuracy of Prediction of Electrical Machine Constants, and Generator Model for Subsynchronous Resonance Conditions," Final Report of EPRI Projects RP 1288-1 and RP, Vols. 1, 2 and 3, prepared by General Electric Company, 1984.

[7] D.C. Macdonald, A.B.J. Reece, and P.J. Turner, "Turbine-Generator Steady-State Reactances," *Proc. IEE* (London), Vol. 132, No. 3, pp. 101-108, 1985.

[8] R.P. Schulz, et al., "Benefit Assessment of Finite-Element Based Generator

Saturation Model," *IEEE Trans.*, Vol. PWRS-2, pp. 1027-1033, November 1987.

[9] S.H. Minnich et al., "Saturation Functions for Synchronous Generators from Finite Elements," *IEEE Trans.*, Vol. EC-2, pp. 680-692, December 1987.

[10] C. Concordia, *Synchronous Machines*, John Wiley & Sons, 1951.

[11] E.W. Kimbark, *Power System Stability, Vol. III: Synchronous Machines*, John Wiley & Sons, 1956.

[12] A.E. Fitzgerald and C. Kingsley, *Electric Machinery*, Second Edition, McGraw-Hill, 1961.

[13] B. Adkins, *The General Theory of Electrical Machines*, Chapman and Hall, 1964.

[14] G.R. Slemon, *Magnetoelectric Devices*, John Wiley & Sons, 1966.

[15] ANSI/IEEE Standard 100-1977, *IEEE Standard Dictionary of Electrical and Electronic Terms.*

[16] IEEE Committee Report, "Recommended Phasor Diagram for Synchronous Machines," *IEEE Trans.*, Vol. PAS-88, pp. 1593-1610, 1969.

[17] P.M. Anderson and A.A Fouad, *Power System Control and Stability*, Iowa State University Press, Ames, Iowa, 1977.

[18] A.W. Rankin, "Per-Unit Impedances of Synchronous Machines," *AIEE Trans.*, Vol. 64, Part I, pp. 569-573, August 1945; Part II, pp. 839-845, December 1945.

[19] M.R. Harris, P.J. Lawrenson, and J.M. Stephenson, "Per-Unit Systems with Special Reference to Electric Machines," IEE Monograph, Cambridge University Press, 1970.

[20] W.A. Lewis, "A Basic Analysis of Synchronous Machine - Part I," *AIEE Trans.*, Vol. 77, pp. 436-456, 1958.

[21] I.M. Canay, "Causes of Discrepancies on Calculation of Rotor Quantities and Exact Equivalent Diagram of Synchronous Machines," *IEEE Trans.*, Vol. PAS-88, pp. 1114-1120, July 1969.

[22] E.F. Fuchs and E.A. Erdelyi, "Non-linear Theory of Turbine-Alternators,"

IEEE Trans., Vol. PAS-91, pp. 583-599, 1972.

[23] El-Serafi et al., "Experimental Study of the Saturation and the Cross-Magnetizing Phenomenon in Saturated Synchronous Machines," *IEEE Trans.*, Vol. EC-3, pp. 815-823, 1988.

[24] I.M. Canay, "Extended Synchronous Machine Model for the Calculation of Transient Processes and Stability," *Electrical Machines & Electromechanics*, Vol. 1, pp. 137-150, 1977.

Chapter 4

Synchronous Machine Parameters

The synchronous machine equations developed in Chapter 3 have the inductances and resistances of the stator and rotor circuits as parameters. These are referred to as *fundamental* or *basic parameters* and are identified by the elements of the *d*- and *q*-axis equivalent circuits shown in Figure 3.18. While the fundamental parameters completely specify the machine electrical characteristics, they cannot be directly determined from measured responses of the machine. Therefore, the traditional approach to assigning machine data has been to express them in terms of derived parameters that are related to observed behaviour as viewed from the terminals under suitable test conditions. In this chapter, we will define these derived parameters and develop their relationships to the fundamental parameters.

4.1 OPERATIONAL PARAMETERS

A convenient method of identifying the machine electrical characteristics is in terms of operational parameters relating the armature and field terminal quantities. Referring to Figure 4.1, the relationship between the incremental values of terminal quantities may be expressed in the operational form as follows:

$$\Delta\psi_d(s) = G(s)\Delta e_{fd}(s) - L_d(s)\Delta i_d(s) \tag{4.1}$$

$$\Delta\psi_q(s) = -L_q(s)\Delta i_q(s) \tag{4.2}$$

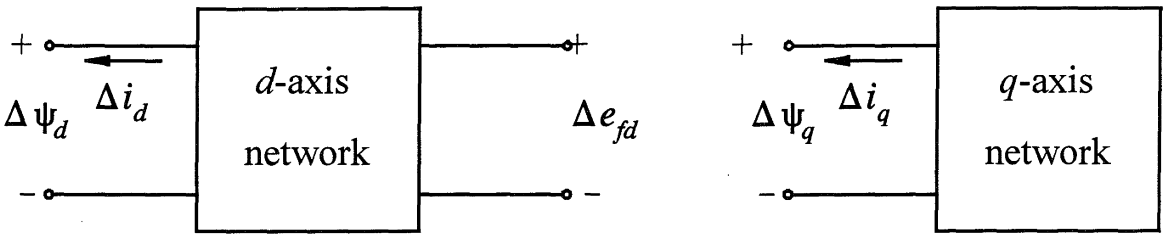

Figure 4.1 The *d*- and *q*-axis networks identifying terminal quantities

where

$G(s)$ is the stator to field transfer function
$L_d(s)$ is the *d*-axis operational inductance
$L_q(s)$ is the *q*-axis operational inductance

In the above equations, s is the familiar Laplace operator and the prefix Δ denotes incremental or perturbed values.

Equations 4.1 and 4.2 are true for any number of rotor circuits. In fact, R.H. Park in his original paper [1] expressed the stator flux equations without specifying the number of rotor circuits. With the equations in operational form, the rotor can be considered as a distributed parameter system. The operational parameters may be determined either from design calculations or more readily from frequency response measurements.

When a finite number of rotor circuits are assumed, the operational parameters can be expressed as a ratio of polynomials in s. The orders of the numerator and denominator polynomials of $L_d(s)$ and $L_q(s)$ are equal to the number of rotor circuits assumed in the respective axes, and $G(s)$ has the same denominator as $L_d(s)$, but a different numerator of order one less than the denominator.

We will develop here the expressions for the operational parameters of the model represented by the equivalent circuits of Figure 4.2. This model structure is generally considered adequate for stability studies and is widely used in large scale stability programs. The rotor characteristics are represented by the field winding and a damper winding in the *d*-axis and two damper windings in the *q*-axis. The mutual inductances L_{fld} and L_{ad} are assumed to be equal; this makes all mutual inductances in the *d*-axis equal. In the next section we will consider the effect of not making this simplifying assumption.

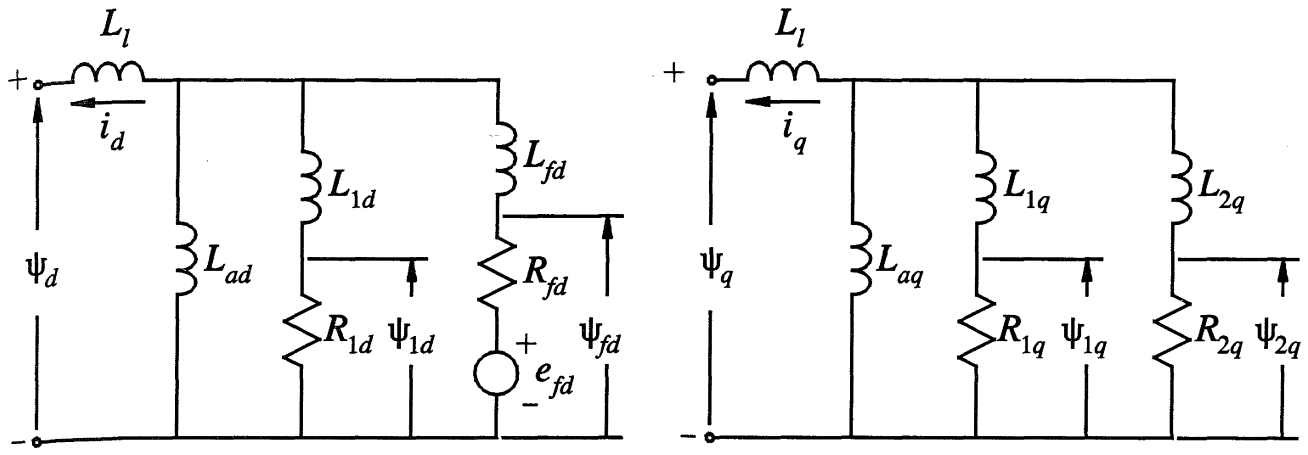

Figure 4.2 Structure of commonly used model

With equal mutual inductances, Equations 3.127, 3.130 and 3.131 for *d*-axis flux linkages in the operational form become

$$\psi_d(s) = -L_d i_d(s) + L_{ad} i_{fd}(s) + L_{ad} i_{1d}(s) \tag{4.3}$$

$$\psi_{fd}(s) = -L_{ad} i_d(s) + L_{ffd} i_{fd}(s) + L_{ad} i_{1d}(s) \tag{4.4}$$

$$\psi_{1d}(s) = -L_{ad} i_d(s) + L_{ad} i_{fd}(s) + L_{11d} i_{1d}(s) \tag{4.5}$$

The operational forms of Equations 3.123 and 3.124 for rotor voltages are

$$e_{fd}(s) = s\psi_{fd}(s) - \psi_{fd}(0) + R_{fd} i_{fd}(s) \tag{4.6}$$

$$0 = s\psi_{1d}(s) - \psi_{1d}(0) + R_{1d} i_{1d}(s) \tag{4.7}$$

where $\psi_d(0)$, $\psi_{fd}(0)$ and $\psi_{1d}(0)$ denote initial values of the flux linkages. It is preferable to express the above equations in terms of incremental values about the initial operating condition so that the initial values drop out; this makes it more convenient to manipulate the operational equations. Substituting for the flux linkages in terms of the currents, the rotor voltage equations in incremental form become

$$\begin{aligned} \Delta e_{fd}(s) &= s\Delta\psi_{fd}(s) + R_{fd}\Delta i_{fd}(s) \\ &= -sL_{ad}\Delta i_d(s) + (R_{fd} + sL_{ffd})\Delta i_{fd}(s) + sL_{ad}\Delta i_{1d}(s) \end{aligned} \tag{4.8}$$

$$\begin{aligned} 0 &= s\Delta\psi_{1d}(s)+R_{1d}\Delta i_{fd}(s) \\ &= -sL_{ad}\Delta i_d(s)+sL_{ad}\Delta i_{fd}(s)+(R_{1d}+sL_{11d})\Delta i_{1d}(s) \end{aligned} \tag{4.9}$$

Our objective is to express the d-axis equations in the form of Equation 4.1, and this can be achieved by eliminating the rotor currents in terms of the terminal quantities e_{fd} and i_d. Accordingly, solution of Equations 4.8 and 4.9 gives

$$\Delta i_{fd}(s) = \frac{1}{D(s)}[(R_{1d}+sL_{11d})\Delta e_{fd}(s)+sL_{ad}(R_{1d}+sL_{1d})\Delta i_d(s)] \tag{4.10}$$

$$\Delta i_{1d}(s) = \frac{1}{D(s)}[-sL_{ad}\Delta e_{fd}(s)+sL_{ad}(R_{fd}+sL_{fd})\Delta i_d(s)] \tag{4.11}$$

where

$$D(s) = s^2(L_{11d}L_{ffd}-L_{ad}^2)+s(L_{11d}R_{fd}+L_{ffd}R_{1d})+R_{1d}R_{fd} \tag{4.12}$$

Given that

$$L_d = L_{ad}+L_l$$

$$L_{ffd} = L_{ad}+L_{fd}$$

$$L_{11d} = L_{ad}+L_{1d}$$

substitution of Equations 4.10 and 4.11 in the incremental form of Equation 4.3 then gives the relationship between the d-axis quantities in the desired form:

$$\Delta\psi_d(s) = G(s)\Delta e_{fd}(s)-L_d(s)\Delta i_d(s)$$

The expressions for the d-axis operational parameters are given by

$$L_d(s) = L_d\frac{1+(T_4+T_5)s+T_4T_6s^2}{1+(T_1+T_2)s+T_1T_3s^2} \tag{4.13}$$

$$G(s) = G_0 \frac{(1+sT_{kd})}{1+(T_1+T_2)s+T_1T_3s^2} \tag{4.14}$$

where

$$\begin{aligned} G_0 &= \frac{L_{ad}}{R_{fd}} & T_{kd} &= \frac{L_{1d}}{R_{1d}} \\ T_1 &= \frac{L_{ad}+L_{fd}}{R_{fd}} & T_2 &= \frac{L_{ad}+L_{1d}}{R_{1d}} \\ T_3 &= \frac{1}{R_{1d}}\left(L_{1d}+\frac{L_{ad}L_{fd}}{L_{ad}+L_{fd}}\right) & T_4 &= \frac{1}{R_{fd}}\left(L_{fd}+\frac{L_{ad}L_l}{L_{ad}+L_l}\right) \\ T_5 &= \frac{1}{R_{1d}}\left(L_{1d}+\frac{L_{ad}L_l}{L_{ad}+L_l}\right) & T_6 &= \frac{1}{R_{1d}}\left(L_{1d}+\frac{L_{ad}L_{fd}L_l}{L_{ad}L_l+L_{ad}L_{fd}+L_{fd}L_l}\right) \end{aligned} \tag{4.15}$$

Equations 4.13 and 4.14 can be expressed in the factored form:

$$L_d(s) = L_d \frac{(1+sT_d')(1+sT_d'')}{(1+sT_{d0}')(1+sT_{d0}'')} \tag{4.16}$$

$$G(s) = G_0 \frac{(1+sT_{kd})}{(1+sT_{d0}')(1+sT_{d0}'')} \tag{4.17}$$

The expression for the q-axis operational inductance may be written by inspection and recognizing the similarities between d- and q-axis equivalent circuits. In the factored form, it is given by

$$L_q(s) = L_q \frac{(1+sT_q')(1+sT_q'')}{(1+sT_{q0}')(1+sT_{q0}'')} \tag{4.18}$$

The time constants associated with the expressions for $L_d(s)$, $L_q(s)$ and $G(s)$ in the factored form as seen in the following section represent important machine parameters.

4.2 STANDARD PARAMETERS

Following a disturbance, currents are induced in the machine rotor circuits. As shown in Section 3.7 for a short-circuit, some of these induced rotor currents decay more rapidly than others. Machine parameters that influence rapidly decaying components are called the *subtransient* parameters, while those influencing the slowly decaying components are called the *transient* parameters and those influencing sustained components are the *synchronous* parameters.

The synchronous machine characteristics of interest are the effective inductances (or reactances) as seen from the terminals of the machine and associated with the fundamental frequency currents during sustained, transient and subtransient conditions. In addition to these inductances, the corresponding time constants which determine the rate of decay of currents and voltages form the *standard parameters* used in specifying synchronous machine electrical characteristics. These standard parameters, as discussed below, can be determined from the expressions for the operational parameters $L_d(s)$, $G(s)$ and $L_q(s)$.

The constants T'_{d0}, T''_{d0}, T'_d and T''_d are the four principal d-axis time constants of the machine. Their relationships to fundamental parameters are determined by equating the respective numerators and denominators of Equations 4.13 and 4.16. Thus,

$$(1+sT'_{d0})(1+sT''_{d0}) = 1+s(T_1+T_2)+s^2(T_1T_3) \tag{4.19}$$

$$(1+sT'_d)(1+sT''_d) = 1+s(T_4+T_5)+s^2(T_4T_6) \tag{4.20}$$

The expressions for the four time constants can be determined accurately by solving the above equations. However, such expressions would be very complex. Simpler expressions can be developed by making some reasonable approximations.

Parameters based on classical definitions

The solution of Equations 4.19 and 4.20 is considerably simplified by recognizing that the value of R_{1d} is very much larger than R_{fd}. This makes T_2 and T_3 very much smaller than T_1, and T_5 and T_6 very much smaller than T_4. Hence

$$(1+sT'_{d0})(1+sT''_{d0}) \approx (1+sT_1)(1+sT_3) \tag{4.21}$$

$$(1+sT'_d)(1+sT''_d) \approx (1+sT_4)(1+sT_6) \tag{4.22}$$

We thus have the following approximate relationships

$$\begin{aligned} T'_{d0} &\approx T_1 \\ T''_{d0} &\approx T_3 \\ T'_d &\approx T_4 \\ T''_d &\approx T_6 \end{aligned} \tag{4.23}$$

The expressions for T_1 to T_6 in terms of the fundamental parameters are given by Equation 4.15. These time constants are in per unit (radians). They have to be divided by rated angular frequency ($\omega_0=2\pi f$) to be converted to seconds. For a 60 Hz system, $\omega_0=376.991$ (usually approximated to be 377) radians per second.

With the stator terminals open ($\Delta i_d=0$), from Equations 4.1 and 4.17, we have

$$\Delta\psi_d(s) = G_0 \frac{1+sT_{kd}}{(1+sT'_{d0})(1+sT''_{d0})} \Delta e_{fd} \tag{4.24}$$

The above indicates that, for open-circuit conditions, the *d*-axis stator flux and hence the terminal voltage respond to a change in field voltage with time constants T'_{d0} and T''_{d0}. Since R_{1d} is much larger than R_{fd}, T''_{d0} is much smaller than T'_{d0}. Thus T''_{d0} is associated with the initial change and is referred to as the *d*-axis open-circuit *subtransient time constant*. The time constant T'_{d0} represents a slow change corresponding to the transient period and is referred to as the *d*-axis open-circuit *transient time constant*. The time constants T'_d and T''_d represent the transient and subtransient short-circuit time constants, respectively.

Let us now examine the effective values of $L_d(s)$ under steady-state, transient, and subtransient conditions.

Under steady-state conditions, with $s=0$ Equation 4.16 becomes

$$L_d(0) = L_d \tag{4.25}$$

This represents the *d*-axis *synchronous inductance*.

During a rapid transient, as s tends to infinity, the limiting value of $L_d(s)$ is given by

$$\begin{aligned} L''_d &= L_d(\infty) \\ &= L_d\left(\frac{T'_d T''_d}{T'_{d0} T''_{d0}}\right) \end{aligned} \tag{4.26}$$

This represents the effective inductance $\Delta\psi_d/\Delta i_d$ immediately following a sudden change and is called the *d*-axis *subtransient inductance.*

In the absence of the damper winding, the limiting value of inductance is

$$\begin{aligned} L'_d &= L_d(\infty) \\ &= L_d\left(\frac{T'_d}{T'_{d0}}\right) \end{aligned} \tag{4.27}$$

This is referred to as the *d*-axis *transient inductance.*

Substitution of the expressions of the time constants from Equations 4.15 and 4.23 in Equations 4.26 and 4.27 gives the following alternative expressions for L''_d and L'_d in terms of the mutual and leakage inductances.

$$L''_d = L_l + \frac{L_{ad}L_{fd}L_{1d}}{L_{ad}L_{fd}+L_{ad}L_{1d}+L_{fd}L_{1d}} \tag{4.28}$$

and

$$L'_d = L_l + \frac{L_{ad}L_{fd}}{L_{ad}+L_{fd}} \tag{4.29}$$

The above expressions for the subtransient and transient inductances can also be derived from the principle of constant flux linkages, which states that the flux linking an inductive circuit with a finite resistance and emf cannot change instantly. Following a disturbance, the rotor flux linkages do not therefore change instantly. For conditions immediately following a disturbance, the equivalent circuit of Figure 3.17, with incremental rotor flux linkages ($\Delta\psi_{fd}$, $\Delta\psi_{1d}$) set to zero, reduces to that shown in Figure 4.3.

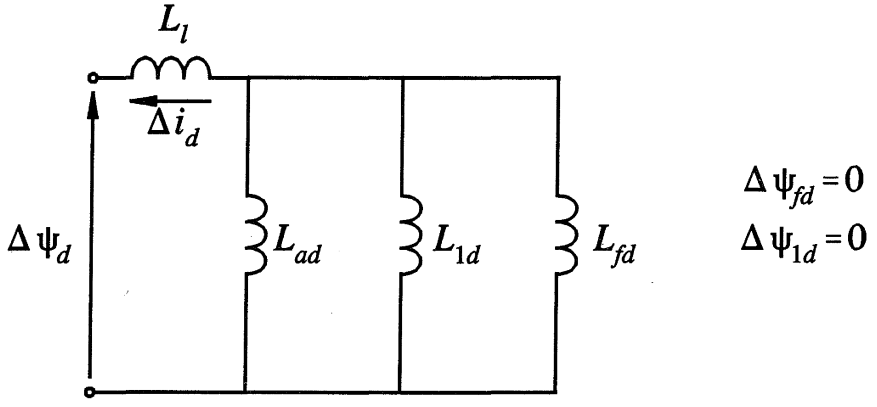

Figure 4.3 Equivalent circuit for incremental values, immediately following a disturbance

From Figure 4.3, the effective inductance $\Delta\psi_d/\Delta i_d$ representing L_d'' is seen to be the same as that given by Equation 4.28. With the damper winding absent ($L_{1d}=\infty$), the effective inductance corresponds to L_d' given by Equation 4.29.

The expression for the q-axis parameters may be readily written by recognizing the similarities in the structure of d- and q-axis equivalent circuits. Thus, the q-axis open-circuit transient and subtransient time constants are given by

$$T_{q0}' = \frac{L_{aq}+L_{1q}}{R_{1q}} \tag{4.30}$$

$$T_{q0}'' = \frac{1}{R_{2q}}\left(L_{2q}+\frac{L_{aq}L_{1q}}{L_{aq}+L_{1q}}\right) \tag{4.31}$$

and the subtransient and transient inductances are given by

$$L_q'' = L_l+\frac{L_{aq}L_{1q}L_{2q}}{L_{aq}L_{1q}+L_{aq}L_{2q}+L_{1q}L_{2q}} \tag{4.32}$$

$$L_q' = L_l+\frac{L_{aq}L_{1q}}{L_{aq}+L_{1q}} \tag{4.33}$$

The q-axis synchronous inductance is given by the steady-state value of $L_q(s)$, which is equal to L_q.

The expressions derived above for the machine standard parameters are based on the assumptions that during the subtransient period $R_{fd}=R_{1q}=0$ and that during the transient period $R_{1d}=R_{2q}=\infty$. These assumptions have been used in the classical theory on synchronous machines [2,3]. However, in recent years there has been some concern [4,5] that significant errors could occur between the values of parameters calculated using the above assumptions and those derived from test measurements such as those described in IEEE Standard 115-1983. Expressions which more closely reflect the definition of the standard parameters are derived below.

Accurate expressions for standard parameters

The exact values of T_{d0}' and T_{d0}'' are given by the poles of $L_d(s)$ and those of T_d' and T_d'' by the zeros of $L_d(s)$. In other words, we need to use the exact solutions of Equations 4.19 and 4.20. From Equation 4.19, the poles of $L_d(s)$ are given by

$$s^2+\frac{T_1+T_2}{T_1T_3}s+\frac{1}{T_1T_3} = 0 \tag{4.34}$$

However, the exact expressions for the poles of $L_d(s)$ become cumbersome and difficult to handle. The expressions can be simplified considerably without much loss of accuracy if it is recognized that $4T_1T_3$ is much less than $(T_1+T_2)^2$. With this simplification, the roots of Equation 4.34 reduce to

$$s_1 = -\frac{1}{T_1+T_2}$$

$$s_2 = -\frac{T_1+T_2}{T_1T_3}$$

The open-circuit time constants are equal to the negatives of the reciprocals of the roots.

$$T'_{d0} = T_1+T_2 \tag{4.35}$$

$$T''_{d0} = \frac{T_1T_3}{T_1+T_2} \tag{4.36}$$

Similarly, by solving for the roots of the numerator of $L_d(s)$, we have

$$T'_d = T_4+T_5 \tag{4.37}$$

$$T''_d = \frac{T_4T_6}{T_4+T_5} \tag{4.38}$$

The transient and subtransient inductances are given by substituting for the above time constants in Equations 4.26 and 4.27. Thus,

$$L'_d = L_d\frac{T_4+T_5}{T_1+T_2} \tag{4.39}$$

$$L''_d = L_d\frac{T_4T_6}{T_1T_3} \tag{4.40}$$

The accurate and approximate (classical) expressions for the standard parameters are summarized in Table 4.1. These expressions apply to a synchronous machine model represented by the equivalent circuit of Figure 4.2 which considers two rotor circuits in each axis with equal mutual inductances.

It should be noted that most stability programs assume that the input data in terms of transient and subtransient parameters are based on the simplifying assumptions from classical theory. However the data provided by some generator manufacturers and those obtained by standard test procedures correspond to the exact values of these parameters. There could thus be some inconsistency associated with the definition and use of standard parameters. As illustrated in Example 4.1, the discrepancies between the two definitions are likely to be significant primarily for the q-axis parameters.

In this book, unless otherwise specified, we will assume the classical definition.

Parameters including unequal mutual effects

In deriving the expressions for the standard parameters above, it is assumed that all mutual inductances in the d-axis are equal. The reciprocal per unit system chosen makes the mutual inductances between the armature and field and between the armature and damper equal. The mutual inductance between field and damper, however, could be different from these mutual inductances.

Although the assumption of all d-axis mutual inductances being equal gives good results in calculating armature quantities, it could lead to significant errors in calculating the field current during transient conditions [6].

The d-axis equivalent circuit including unequal mutual effects and the various mutual and leakage fluxes involved are shown in Figure 4.4.

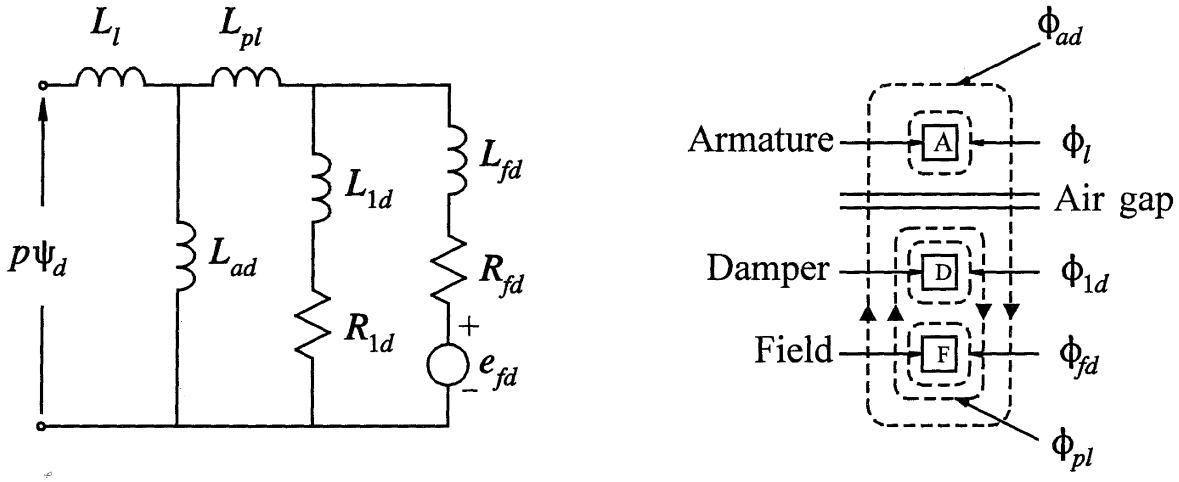

(a) Equivalent circuit (b) Flux paths

Figure 4.4 Unequal mutual effects in d-axis

Table 4.1

Expressions for Standard Parameters of Synchronous Machine

Parameter	Classical Expression	Accurate Expression
T'_{d0}	T_1	T_1+T_2
T'_d	T_4	T_4+T_5
T''_{d0}	T_3	$T_3[T_1/(T_1+T_2)]$
T''_d	T_6	$T_6[T_4/(T_4+T_5)]$
L'_d	$L_d(T_4/T_1)$	$L_d(T_4+T_5)/(T_1+T_2)$
L''_d	$L_d(T_4T_6)/(T_1T_3)$	$L_d(T_4T_6)/(T_1T_3)$

with

$$T_1 = \frac{L_{ad}+L_{fd}}{R_{fd}} \qquad T_2 = \frac{L_{ad}+L_{1d}}{R_{1d}}$$

$$T_3 = \frac{1}{R_{1d}}\left(L_{1d}+\frac{L_{ad}L_{fd}}{L_{ad}+L_{fd}}\right) \qquad T_4 = \frac{1}{R_{fd}}\left(L_{fd}+\frac{L_{ad}L_l}{L_{ad}+L_l}\right)$$

$$T_5 = \frac{1}{R_{1d}}\left(L_{1d}+\frac{L_{ad}L_l}{L_{ad}+L_l}\right) \qquad T_6 = \frac{1}{R_{1d}}\left(L_{1d}+\frac{L_{ad}L_lL_{fd}}{L_{ad}L_l+L_{ad}L_{fd}+L_{fd}L_l}\right)$$

Notes:
1. Similar expressions apply to q-axis parameters.
2. All parameters are in per unit.
3. Time constants in seconds are obtained by dividing the per unit values given in the table by $\omega_0=2\pi f$.
4. All mutual inductances in d-axis assumed equal.

The series inductance, $L_{pl}=L_{fld}-L_{ad}$, corresponds to the peripheral leakage flux (ϕ_{pl}) which links the field and damper, but not the armature.

Assuming that $R_{fd}=0$ during the subtransient period and that $R_{1d}=\infty$ during the transient period, following the approach used previously, the expressions for the standard parameters may be written by inspection of the equivalent circuit as follows:

$$
\begin{aligned}
L_d &= L_{ad}+L_l \\
L'_d &= L_l+\frac{1}{\dfrac{1}{L_{ad}}+\dfrac{1}{L_{fd}+L_{pl}}} = L_l+\frac{L_{ad}(L_{fd}+L_{pl})}{L_{ad}+L_{fd}+L_{pl}} \\
L''_d &= L_l+\frac{L_{1d}L_{fd}L_{ad}+L_{1d}L_{pl}L_{ad}+L_{ad}L_{fd}L_{pl}}{L_{ad}L_{fd}+L_{ad}L_{1d}+L_{1d}L_{fd}+L_{1d}L_{pl}+L_{fd}L_{pl}} \\
T'_{d0} &= \frac{L_{ad}+L_{fd}+L_{pl}}{R_{fd}} \\
T''_{d0} &= \frac{1}{R_{1d}}\left(L_{1d}+\frac{L_{fd}(L_{ad}+L_{pl})}{L_{pl}+L_{fd}+L_{ad}}\right) \\
T'_d &= \frac{1}{R_{fd}}\left(L_{fd}+L_{pl}+\frac{L_{ad}L_l}{L_{ad}+L_l}\right) \\
T''_d &= \frac{1}{R_{1d}}\left(L_{1d}+\frac{L_{ad}L_{pl}L_{fd}+L_lL_{fd}L_{ad}+L_lL_{fd}L_{pl}}{L_{fd}L_{ad}+L_{fd}L_l+L_{pl}L_{ad}+L_{pl}L_l+L_{ad}L_l}\right)
\end{aligned}
\tag{4.41}
$$

The above expressions are based on the approximations associated with the classical definition of the parameters. Accurate expressions applicable to a more complex model structure consisting of these rotor circuits in each axis and unequal *d*-axis mutual inductances are given in reference 7.

Parameters of salient pole machines:

In the discussion of standard parameters so far, we have considered a model structure with two rotor circuits in each axis. This is applicable to a round rotor machine. However, for a laminated salient pole machine, the damper winding is the only rotor circuit in the *q*-axis; therefore, only one *q*-axis rotor circuit (denoted by the subscript 1*q*) is applicable. The parameters of this rotor circuit are such that it represents rapidly decaying subtransient effects. The second rotor circuit (denoted by subscript 2*q*) is ignored and no distinction is made between transient and synchronous

(steady-state) conditions. Hence, the expressions for the q-axis parameters of a salient pole machine are as follows:

$$L_q = L_l + L_{aq}$$

$$L_q'' = L_l + \frac{L_{aq} L_{1q}}{L_{aq} + L_{1q}} \tag{4.42}$$

$$T_{q0}'' = \frac{L_{aq} + L_{1q}}{R_{1q}}$$

The transient parameters L_q' and T_{q0}' are not applicable in this case.

In the d-axis, it is appropriate to consider two rotor circuits (field and damper) and the expressions previously derived are applicable to salient pole machines.

Reactances:

In per unit, the subtransient, transient and synchronous reactances are equal to the corresponding inductances. Hence, common practice is to identify synchronous machine parameters in terms of the reactances, instead of the inductances.

Typical values of standard parameters:

Table 4.2 gives ranges within which generator parameters normally lie.

From the expressions for machine parameters summarized in Table 4.1, it is readily apparent that

$$X_d \geq X_q > X_q' \geq X_d' > X_q'' \geq X_d'' \tag{4.43}$$

$$T_{d0}' > T_d' > T_{d0}'' > T_d'' > T_{kd} \tag{4.44}$$

$$T_{q0}' > T_q' > T_{q0}'' > T_q'' \tag{4.45}$$

Table 4.2

Parameter		Hydraulic Units	Thermal Units
Synchronous Reactance	X_d	0.6 - 1.5	1.0 - 2.3
	X_q	0.4 - 1.0	1.0 - 2.3
Transient Reactance	X'_d	0.2 - 0.5	0.15 - 0.4
	X'_q	-	0.3 - 1.0
Subtransient Reactance	X''_d	0.15 - 0.35	0.12 - 0.25
	X''_q	0.2 - 0.45	0.12 - 0.25
Transient OC Time Constant	T'_{d0}	1.5 - 9.0 s	3.0 - 10.0 s
	T'_{q0}	-	0.5 - 2.0 s
Subtransient OC Time Constant	T''_{d0}	0.01 - 0.05 s	0.02 - 0.05 s
	T''_{q0}	0.01 - 0.09 s	0.02 - 0.05 s
Stator Leakage Inductance	X_l	0.1 - 0.2	0.1 - 0.2
Stator Resistance	R_a	0.002 - 0.02	0.0015 - 0.005

Notes:
1. Reactance values are in per unit with stator base values equal to the corresponding machine rated values.
2. Time constants are in seconds.

Example 4.1

The following are the per unit values of the standard parameters of the 555 MVA, 0.9 p.f., 60 Hz turbine generator considered in the examples of Chapter 3:

$L_d = 1.81$ $L_q = 1.76$ $L_l = 0.15$ $R_a = 0.003$

$L'_d = 0.3$ $L'_q = 0.65$ $L''_d = 0.23$ $L''_q = 0.25$

$T'_{d0} = 8.0$ s $T'_{q0} = 1.0$ s $T''_{d0} = 0.03$ s $T''_{q0} = 0.07$ s

The transient and subtransient parameters are based on the *classical definitions*. The parameters given correspond to unsaturated values of L_{ad} and L_{aq}.

(a) Assuming that $L_{fkd}=L_{ad}$, determine the per unit values of the fundamental parameters, i.e., elements of the d- and q-axis equivalent circuits.

(b) Using the fundamental parameters computed in (a) above, and without making the simplifying assumptions of the classical definitions, calculate the accurate values of the transient and subtransient parameters. How do they compare with the values based on the classical definitions?

(c) If, at the rated output conditions, the effect of magnetic saturation is to reduce L_{ad} and L_{aq} to 83.5% of their unsaturated values, find the corresponding values of the standard parameters based on the classical definitions.

Solution

(a) We first compute the unsaturated mutual inductances

$$L_{ad} = L_d - L_l = 1.81 - 0.15 = 1.66 \quad \text{pu}$$
$$L_{aq} = L_q - L_l = 1.76 - 0.15 = 1.61 \quad \text{pu}$$

We then compute the rotor leakage inductances from the expressions for transient and subtransient inductances. From Equation 4.29, the expression for L'_d based on the classical definition is

$$L'_d = L_l + \frac{L_{ad}L_{fd}}{L_{ad}+L_{fd}}$$

Substituting the respective numerical values gives

$$0.3 = 0.15 + \frac{1.66 \times L_{fd}}{1.66 + L_{fd}}$$

Solving for L_{fd} yields

$$L_{fd} = 0.165 \quad \text{pu}$$

Similarly, from the expression for L'_q given by Equation 4.33, we obtain

$$0.65 = 0.15 + \frac{1.61 \times L_{1q}}{1.61 + L_{1q}}$$

Solving for L_{1q} gives

$$L_{1q} = 0.7252 \quad \text{pu}$$

From Equation 4.28

$$L_d'' = L_l + \frac{L_{ad}L_{fd}L_{1d}}{L_{ad}L_{fd} + L_{ad}L_{1d} + L_{fd}L_{1d}}$$

Substituting the respective numerical values gives

$$0.23 = 0.15 + \frac{1.66 \times 0.165 \times L_{1d}}{1.66 \times 0.165 + 1.66 \times L_{1d} + 0.165 \times L_{1d}}$$

Solving for L_{1d}, we have

$$L_{1d} = 0.1713 \quad \text{pu}$$

Similarly, from the expression for L_q'' given by Equation 4.32, we obtain

$$0.25 = 0.15 + \frac{1.61 \times 0.7252 \times L_{2q}}{1.61 \times 0.7252 + (1.61 + 0.7252) L_{2q}}$$

and solving for L_{2q} yields

$$L_{2q} = 0.125 \quad \text{pu}$$

Next, we compute the rotor resistances from the expressions for the open-circuit time constants. From Equations 4.15 and 4.23, the expressions for T_{d0}' and T_{d0}'', based on the classical definitions, are

$$T_{d0}' = \frac{L_{ad} + L_{fd}}{R_{fd}} \quad \text{pu}$$

and

$$T_{d0}'' = \frac{1}{R_{fd}} \left(L_{1d} + \frac{L_{ad}L_{fd}}{L_{ad} + L_{fd}} \right) \quad \text{pu}$$

Substituting the numerical values and noting that the time constant in per unit is equal to 377 times the time constant in seconds, we obtain

$$R_{fd} = \frac{1.66 + 0.165}{8.0 \times 377}$$

$$= 0.000605 \quad \text{pu}$$

and

$$R_{1d} = \frac{1}{0.03\times377}\left(0.1713+\frac{1.66\times0.165}{1.66+0.165}\right)$$

$$= 0.0284 \quad \text{pu}$$

Similarly, using Equations 4.30 and 4.31 to compute the q-axis rotor circuit resistances, we obtain

$$R_{1q} = 0.0062 \quad \text{pu}$$

and

$$R_{2q} = 0.0237 \quad \text{pu}$$

The following is a summary of the per unit values of the fundamental parameters:

$R_a = 0.003$	$L_l = 0.15$	$L_{ad} = 1.66$	$L_{aq} = 1.61$
$L_{fd} = 0.165$	$R_{fd} = 0.0006$	$L_{1d} = 0.1713$	$R_{1d} = 0.0284$
$L_{1q} = 0.7252$	$R_{1q} = 0.0062$	$L_{2q} = 0.125$	$R_{2q} = 0.0237$

(b) The accurate expressions for the d-axis transient and subtransient constants are summarized in Table 4.1.

Substituting the fundamental parameters computed above in the expressions for the time constants T_1 to T_6 and dividing by 377 to convert to seconds, we obtain

$T_1 = 8.0$ s	$T_2 = 0.171$ s	$T_3 = 0.03$ s
$T_4 = 1.326$ s	$T_5 = 0.0288$ s	$T_6 = 0.023$ s

The accurate value of the d-axis transient inductance is

$$L'_d = L_d\frac{T_4+T_5}{T_1+T_2}$$

$$= 1.81\left(\frac{1.326+0.0288}{8.0+0.171}\right)$$

$$= 0.3 \quad \text{pu}$$

The accurate values of transient and subtransient open-circuit time constants are

$$T'_{d0} = T_1+T_2 = 8.0+0.171$$

$$= 8.171 \text{ s}$$

$$T''_{d0} = \frac{T_1 T_3}{T_1+T_2}$$

$$= \frac{8.0\times0.03}{8.0+0.03}$$

$$= 0.0294 \text{ s}$$

Similarly, for the q-axis, we obtain

$$T_1 = 1.0 \text{ s} \qquad T_2 = 0.1943 \text{ s} \qquad T_3 = 0.07 \text{ s}$$
$$T_4 = 0.3693 \text{ s} \qquad T_5 = 0.0294 \text{ s} \qquad T_6 = 0.0269 \text{ s}$$

The accurate value of the q-axis transient inductance is

$$L'_q = L_q \frac{T_4+T_5}{T_1+T_2}$$

$$= 1.76\frac{0.3693+0.0294}{1.0+0.1943}$$

$$= 0.5875 \text{ pu}$$

The accurate values of the q-axis open-circuit time constants are

$$T'_{q0} = T_1+T_2 = 1.0+0.1943$$

$$= 1.1943 \text{ s}$$

$$T''_{q0} = T_3 \frac{T_1}{T_1+T_2}$$

$$= 0.07\frac{1.0}{1.1943}$$

$$= 0.0586 \text{ s}$$

There are no approximations associated with the classical definitions of the subtransient inductances; hence, accurate values of L''_d and L''_q are the same as the given values.

The following is a comparison of the accurate and approximate values of the parameters.

Parameter	Value based on Classical Definition	Accurate Value
L'_d	0.3	0.3
T'_{d0}	8.0	8.171
T''_{d0}	0.03	0.0294
L'_q	0.65	0.5875
T'_{q0}	1.0	1.1943
T''_{q0}	0.07	0.0586

The differences are significant only for the q-axis.

(c) At the rated output condition, the saturated values of mutual inductances are

$$L_{ad} = 0.835 \times L_{adu} = 0.835 \times 1.66$$

$$= 1.386 \quad \text{pu}$$

$$L_{aq} = 0.835 \times L_{aqu} = 0.835 \times 1.61$$

$$= 1.344 \quad \text{pu}$$

The corresponding values of the standard parameters, based on the classical definitions, are

$$L_d = 1.386 + 0.15 = 1.536 \quad \text{pu}$$

$$L_q = 1.344 + 0.15 = 1.494 \quad \text{pu}$$

$$L'_d = 0.15 + \frac{1.386 \times 0.165}{1.386 + 0.165}$$

$$= 0.2974 \quad \text{pu}$$

$$L''_d = 0.15 + \frac{1.386 \times 0.165 \times 0.1713}{1.386 \times 0.165 + 1.386 \times 0.1713 + 0.165 \times 0.1713}$$

$$= 0.2292 \quad \text{pu}$$

$$L'_q = 0.15 + \frac{1.344 \times 0.7252}{1.344 + 0.7252}$$

$$= 0.621 \quad \text{pu}$$

$$L_q'' = 0.15 + \frac{1.344 \times 0.7252 \times 0.125}{1.344 \times 0.7252 + 1.344 \times 0.125 + 0.7252 \times 0.125}$$

$$= 0.2488 \quad \text{pu}$$

$$T_{d0}' = \frac{1.386 + 0.165}{0.0006 \times 377} = 6.86 \quad \text{s}$$

$$T_{d0}'' = \frac{1}{0.0284 \times 377}\left(0.1713 + \frac{1.386 \times 0.165}{1.386 + 0.165}\right)$$

$$= 0.0298 \quad \text{s}$$

$$T_{q0}' = \frac{1.344 + 0.7252}{0.0062 \times 377} = 0.885 \quad \text{s}$$

$$T_{q0}'' = \frac{1}{0.0237 \times 377}\left(0.125 + \frac{1.344 \times 0.7252}{1.344 + 0.7252}\right)$$

$$= 0.0667 \quad \text{s}$$

■

4.3 FREQUENCY-RESPONSE CHARACTERISTICS

It is of interest to examine the frequency-response characteristics of the operational parameters and relate them to standard parameters. Such characteristics provide useful insight into the dynamic characteristics of the machine and may be readily sketched using the asymptotic approximation.

With the rotor effects represented by two circuits in the d-axis, $L_d(s)$ and $G(s)$ are given by Equations 4.16 and 4.17, respectively. Figure 4.5 shows the magnitude of $L_d(s)$ as a function of frequency. The transient and subtransient time constants and inductances have been used to identify the corner points for the asymptotic approximation. The plot shown is for the generator considered in Example 4.1. The general shape of the frequency response characteristic, however, is applicable to any synchronous machine. The effective inductance is equal to the synchronous inductance L_d at frequencies below 0.02 Hz, the transient inductance L_d' in the range 0.2 Hz to 2 Hz, and the subtransient inductance L_d'' beyond 10 Hz. In stability studies, the frequency range of interest is that corresponding to L_d'.

Figure 4.6 shows the magnitude of $G(s)$ as a function of frequency for the same machine, with G_0 normalized so that it is equal to 1.0. From the plot we see that the effective gain drops off considerably at high frequencies. This indicates that high-frequency variations in field voltage are not reflected in the stator flux linkage and hence other stator quantities.

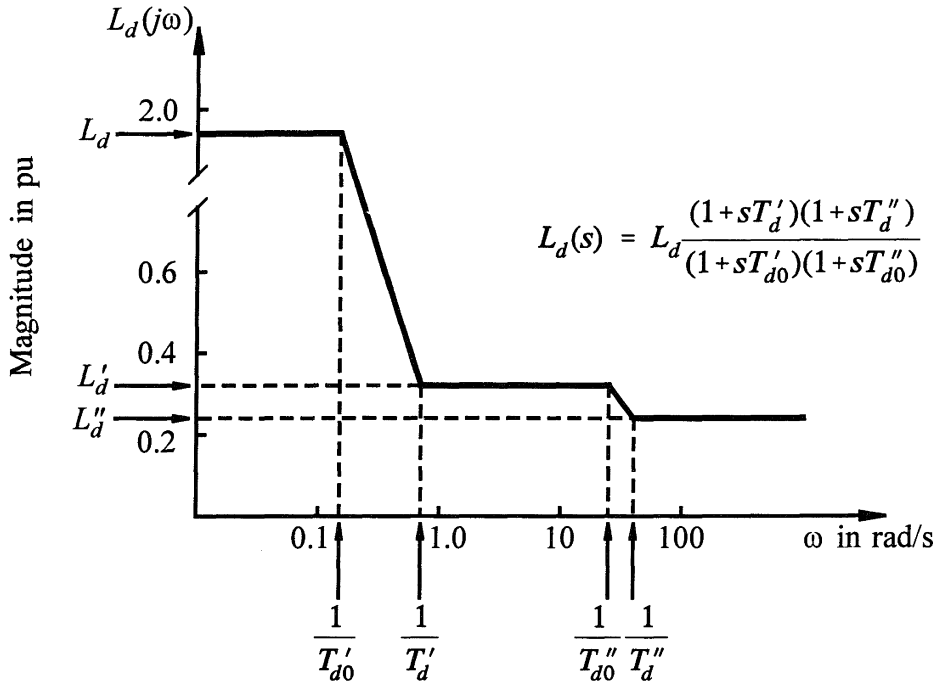

Figure 4.5 Variation of magnitude of $L_d(s)$

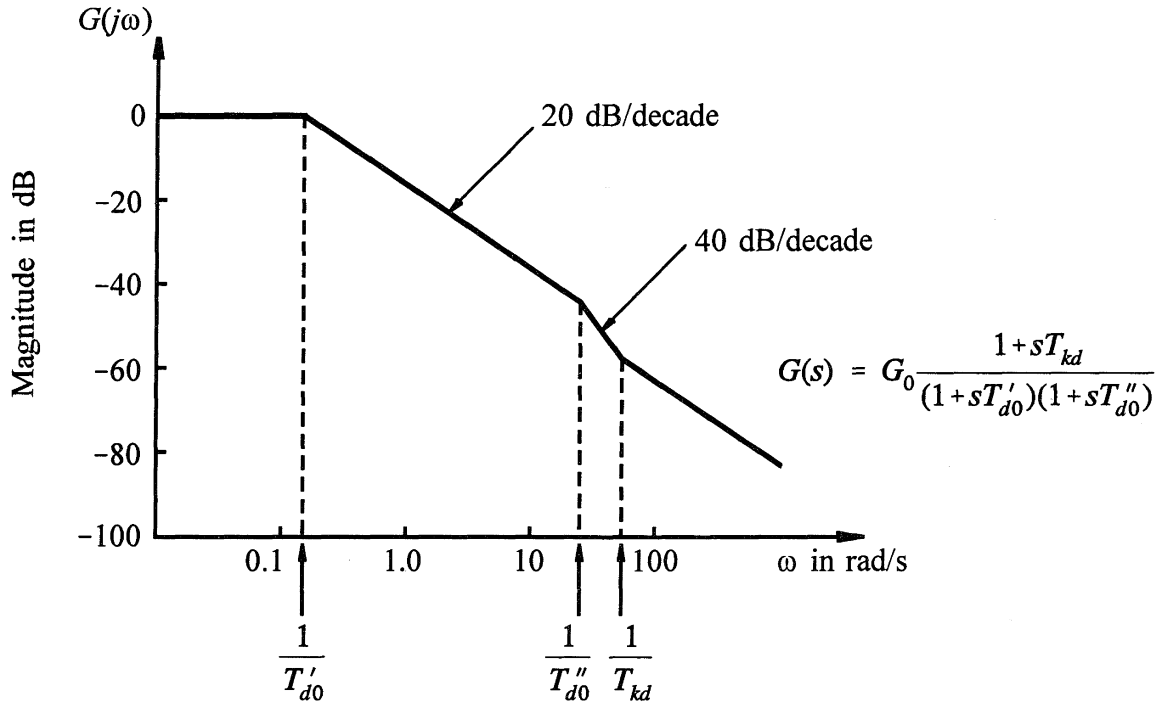

Figure 4.6 Variation of magnitude of $G(s)$ with frequency

Armature time constant

As discussed in Section 3.7.2, the armature time constant, T_a, gives the rate of decay of the unidirectional component (dc offset) of armature phase currents following a three-phase short-circuit at the terminals.

The unidirectional components of currents, which have unequal magnitudes in the three phases, produce a stationary mmf wave. This induces fundamental frequency currents in the rotor circuits, keeping the flux linking with these circuits constant. The flux path due to the direct current in the armature is similar to those corresponding to subtransient inductances L_d'' and L_q''. Since the rotor moves at synchronous speed with respect to the mmf wave produced by the direct currents in the stator, the mmf wave alternately sees conditions corresponding to L_d'' and L_q''. Hence, the effective inductance seen by the direct currents in the armature lies between L_d'' and L_q''. It will be shown later that this is also the inductance L_2, seen by the negative sequence currents applied to the stator windings. Therefore,

$$T_a = \frac{1}{R_a}\left(\frac{L_d'' + L_q''}{2}\right) \quad \text{per unit} \tag{4.46}$$

The value of T_a lies between 0.03 and 0.35 s.

4.4 DETERMINATION OF SYNCHRONOUS MACHINE PARAMETERS

The conventional method of determining synchronous machine parameters is from short-circuit tests on unloaded machines. The test procedures are specified in IEEE Standard 115-1983 [8]. These tests provide X_d, X_q, X_d', X_d'', T_{d0}', T_d', T_{d0}'' and T_d''. They do not, however, provide q-axis transient and subtransient constants. In addition, they do not include measurement of the field circuit during the short-circuit tests, and consequently the field circuit is not specifically identified. The limitations of these procedures for providing data suitable for stability studies have been recognized for some time.

Several alternative testing and analytical methods have been proposed and used to obtain better models:

- Enhanced sudden short-circuit tests;
- Stator decrement test;
- Frequency-response tests
  - — Standstill frequency response,
  - — Open-circuit frequency response,

— On-line frequency response;

- Analysis of design data; and
- Quadrature axis saturation measurements.

The special features of theses methods are briefly discussed below. A detailed description of these methods is, however, beyond the scope of this book. Readers may refer to the references provided for additional information.

Enhanced short-circuit tests

Improved methods of utilizing results from sudden short-circuit tests to determine more accurate *d*-axis parameters are described in references 9 and 10. The most important feature of these methods is the utilization of rotor current measurements during the short-circuit tests to identify the field-circuit characteristics more accurately.

Among the disadvantages of the short-circuit approach are the inability to provide *q*-axis parameters accurately and the necessity of exposing the machine to a severe shock.

Decrement tests

These tests are similar in approach to the sudden short-circuit tests in that the time responses of machine variables following a sudden disturbance are measured to identify machine characteristics. References 10, 11 and 12 use this approach.

In this approach, with operating conditions arranged such that current is flowing only in the direct axis (i_q=0), the unit is tripped and the resulting terminal voltage and field current decay are used to extract parameters for a model in much the same way as with sudden short-circuit data. A similar test is performed with current flowing only in the quadrature axis (i_d=0) to obtain *q*-axis data. To maintain unsaturated conditions, these tests are conducted at partial load and reduced voltage.

These tests provide both *d*- and *q*-axis data. However, they are somewhat difficult and expensive to conduct. For most machines, it is difficult or impossible to attain unsaturated conditions which unfortunately complicates the testing and the analysis of results. The tests require rescheduling of generation and several unit trips, which is often not practical.

Frequency-response tests

a. Standstill frequency response (SSFR):

In the SSFR technique, all tests are conducted with the unit at rest (rotor stationary) and disconnected from the system. The rotor must be aligned to two particular positions with respect to the stator during the tests. With the stator excited

by a low level (±60 A, ±20 V) source over the range of frequencies from 1 mHz to 1 kHz, the following responses are measured:

With the stator winding excited and field shorted

$$sG(s) = \frac{\Delta i_{fd}(s)}{\Delta i_d(s)} \tag{4.47}$$

and

$$Z_d(s) = \frac{\Delta e_d(s)}{\Delta i_d(s)} \tag{4.48}$$

With the stator winding excited (field condition immaterial)

$$Z_q(s) = -\frac{\Delta e_q(s)}{\Delta i_q(s)} \tag{4.49}$$

The latter two, $Z_d(s)$ and $Z_q(s)$, are the d- and q-axis operational impedances as viewed from the armature terminals. The operational inductances are computed by subtracting the armature resistance from these impedances:

$$L_d(s) = \frac{Z_d(s) - R_a}{s} \tag{4.50}$$

and

$$L_q(s) = \frac{Z_q(s) - R_a}{s} \tag{4.51}$$

where R_a is the dc resistance of one armature phase and $s=j\omega$.

The parameters of the d-axis equivalent circuit are obtained using transfer function approximations for the functions $L_d(s)$ and $sG(s)$. The function $sG(s)$ rather than $G(s)$ is used because the former can be measured at the same time as $Z_d(s)$, with the field shorted. The q-axis parameters are obtained using the transfer function for $L_q(s)$. The order of the transfer function depends on the number of rotor circuits assumed in the respective axes.

Because the tests are conducted at very low flux levels, the results must be corrected to bring them from the "toe" of the saturation curve to normal unsaturated levels. This is done by minor adjustment of the mutual reactance in each axis.

This technique has been used in references 7, 13, 14, and 15. In addition, it is

now a "trial use" standard of the IEEE [16]. SSFR testing is relatively easy to perform either in the factory or during a maintenance outage on a unit.

Besides the required adjustment for unsaturated conditions, there are two other limitations to this type of testing, both of which involve rotational effects. Where damper windings are employed, they are often just overlapped and may not form a good connection at standstill. In addition, the extent to which rotation causes the slot wedges to form a low impedance path to the rotor is largely unknown.

At low and high frequencies, the data obtained are expected to be good. In the mid-frequency range it is expected to be good for most machines with no specific damper windings or the equivalent, short dampers and non-magnetic retaining rings [17].

Details of models developed from SSFR tests on three large generators are given in references 7 and 14. The measured $L_d(s)$, $sG(s)$ and $L_q(s)$ characteristics for one of these generators (500 MW, 3800 RPM generator at Lambton GS in Ontario) are shown in Figures 4.7, 4.8 and 4.9. Second- and third-order transfer function approximations to the measured characteristics are also shown in the figures. For this generator, second-order transfer functions are seen to be good approximations for both *d*- and *q*-axis. However, this may not always be the case; depending on the rotor construction, third-order transfer functions may be more appropriate in some cases [7,14].

b. Open-circuit frequency response (OCFR):

Open-circuit frequency-response testing allows confirmation of some of the SSFR data in the middle of the frequency range for the *d*-axis only [7]. For this test, the unit is operated on open-circuit at reduced voltage. The field is excited at various frequencies and the field-to-stator frequency-response measured. The difference between this response and the equivalent one from the standstill tests gives some indication of rotational effects.

The test is normally done at more than one voltage to examine saturation effects. By conducting the test with various signal amplitudes, slot wedge conduction effects can be assessed.

c. On-line frequency response (OLFR):

In many respects, on-line frequency response (OLFR) testing is the "proof in the pudding" as far as small-signal verification of machine models is concerned. Here the machine is tested under the same conditions as those under which the model is expected to perform, although over a restricted operating range.

For this test, the machine is operated near rated (or at reduced) load preferably over a substantial impedance to the system. The excitation is modulated by either sinusoidal or random noise. Components are resolved on the two axes and data similar to those of the SSFR tests are used to derive a model. The frequency range of usable data in this case is more limited than that of the SSFR tests, but the SSFR data are

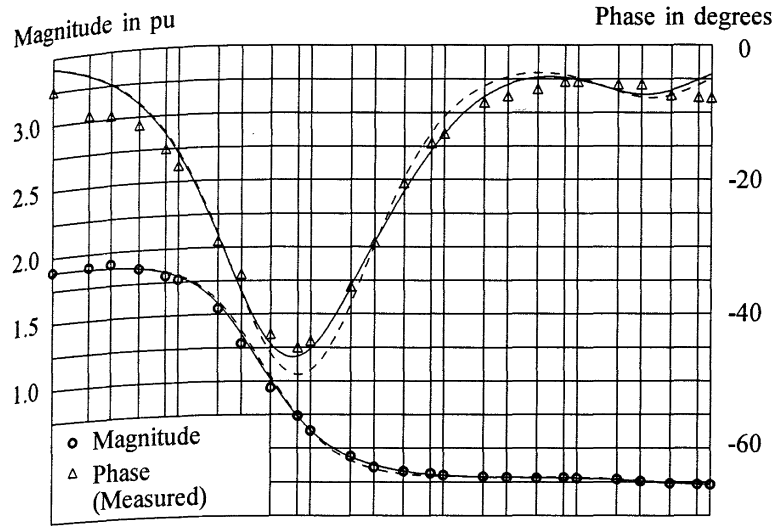

$$\text{——} \quad L_d(s) = 1.89\frac{(1+s1.03)(1+s0.32)(1+s0.0042)}{(1+s5.35)(1+s0.41)(1+s0.0053)}$$

$$\text{- - - -} \quad L_d(s) = 1.89\frac{(1+s0.77)(1+s0.0038)}{(1+s5.06)(1+s0.0049)}$$

Figure 4.7 Lambton GS - Variation of $L_d(s)$ with frequency at standstill with field closed

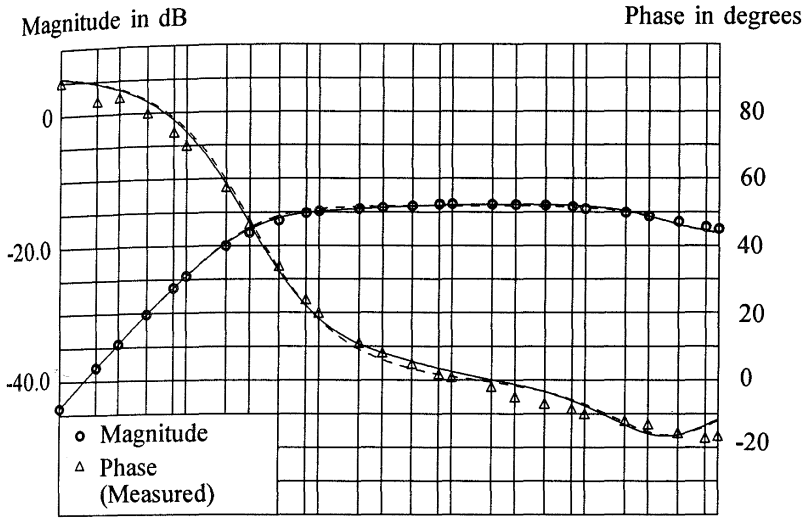

$$\text{——} \quad sG(s) = s4.25\frac{(1+s0.446)(1+s0.003)}{(1+s5.35)(1+s0.41)(1+s0.0053)}$$

$$\text{- - - -} \quad sG(s) = s4.25\frac{(1+s0.0028)}{(1+s5.06)(1+s0.0049)}$$

Figure 4.8 Lambton GS - Variation of $sG(s)$ with frequency at standstill with field closed

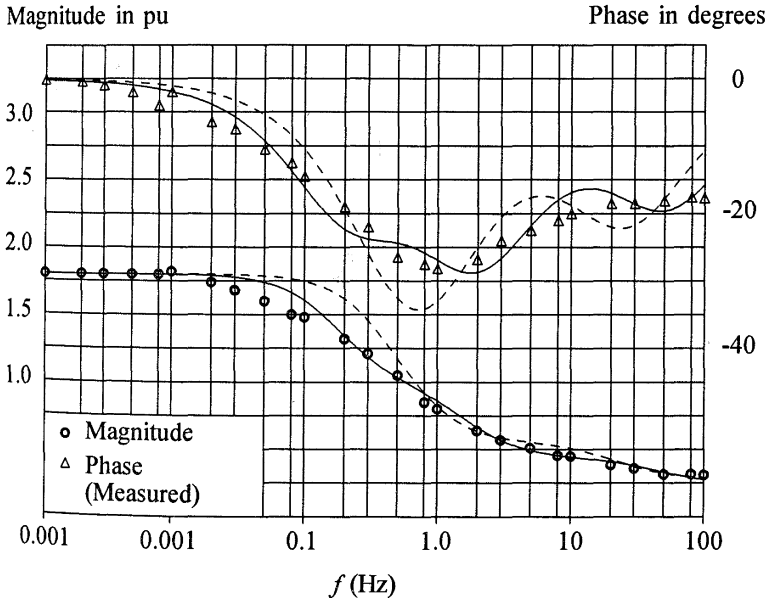

$$\text{——} \quad L_q(s) = 1.8\frac{(1+s0.562)(1+s0.052)(1+s0.0022)}{(1+s1.020)(1+s0.118)(1+s0.0040)}$$

$$\text{- - - -} \quad L_q(s) = 1.8\frac{(1+s0.128)(1+s0.0043)}{(1+s0.417)(1+s0.0086)}$$

Figure 4.9 Lambton GS - Variation of $L_q(s)$ with frequency at standstill

expected to be good at the frequency extremes. The OLFR testing allows the middle of the frequency range to be filled in with data for both axes which include rotational effects. The disadvantage of this test is that it requires testing on an operating unit connected to the system, possibly under special system or unit conditions. In addition, it does not provide large signal response information.

Details of OLFR measurement techniques and model identification procedures are given in reference 18. Results of OLFR tests on two large units and improved models developed from the tests are given in references 7 and 19. In reference 20, models for three large generators based on SSFR and OLFR tests are validated by comparing the results of simulations with measured responses involving line switching. For one generator, models derived from short-circuit tests and decrement tests are also validated.

Calculation of machine parameters from design data

Improved generator models developed from design information are described in reference 21. Reference 22 presents more recent work using finite element analysis.

Work done on two and three dimensional finite element models in the steady state has shown good agreement with measured results. In addition, two dimensional finite element models have been developed which provide frequency response data that compare well with measured results. The degree to which conduction occurs across slot wedges appears to have a significant effect on the model at higher frequencies. The significance of rotational effects and the effect of disturbance amplitude on the model require additional investigation.

REFERENCES

[1] R.H. Park, "Two-Reaction Theory of Synchronous Machines," *AIEE Trans.*, Part I, Vol. 48, pp. 716-730, 1929; Part II, Vol. 52, pp. 352-355, 1933.

[2] C. Concordia, *Synchronous Machines - Theory and Performance*, John Wiley & Sons, 1952.

[3] B. Adkins, *The General Theory of Electric Machines*, Chapman and Hall, 1964.

[4] G. Shackshaft, "New Approach to the Determination of Synchronous Machine Parameters from Tests," *Proc. IEE* (London), Vol. 121, No. 11, pp. 1385-1392, 1974.

[5] IEEE Committee Report, "Supplementary Definitions and Associated Test Methods for Obtaining Parameters for Synchronous Machine Stability Simulations," *IEEE Trans.*, Vol. PAS-99, pp. 1625-1633, July/August 1980.

[6] I.M. Canay, "Causes of Discrepancies on Calculation of Rotor Quantities and Exact Equivalent Diagram of Synchronous Machines," *IEEE Trans.*, Vol. PAS-88, pp. 1114-1120, July 1969.

[7] EPRI Report EL-1424, "Determination of Synchronous Machine Stability Constants," Vol. 2, prepared by Ontario Hydro, December 1980.

[8] ANSI/IEEE Standard 115-1983, *IEEE Guide: Test Procedures for Synchronous Machines.*

[9] Y. Takeda and B. Adkins, "Determination of Synchronous Machine Parameters Allowing for Unequal Mutual Inductances," *Proc. IEE* (London), Vol. 121, No. 12, pp. 1501-1504, December 1974.

[10] G. Shackshaft and A.T. Poray, "Implementation of New Approach to Determination of Synchronous Machine Parameters from Tests," *Proc. IEE* (London), Vol. 124, No. 12, pp. 1170-1178, 1977.

[11] F.P. deMello and J.R. Ribeiro, "Derivation of Synchronous Machine Parameters from Tests," *IEEE Trans.*, Vol. PAS-96, pp. 1211-1218, July/August 1977.

[12] F.P. deMello and L.N. Hannett, "Validation of Synchronous Machine Models and Determination of Model Parameters from Tests," *IEEE Trans.*, Vol. PAS-100, pp. 662-672, February 1981.

[13] M.E. Coultes and W. Watson, "Synchronous Machine Models by Standstill Frequency Response Tests," *IEEE Trans.*, Vol. PAS-100, pp. 1480-1489, April 1981.

[14] P.L. Dandeno and A.T. Poray, "Development of Detailed Turbogenerator Equivalent Circuits from Standstill Frequency Response Measurements," *IEEE Trans.*, Vol. PAS-100, pp. 1646-1653, April 1981.

[15] M.E. Coultes, "Standstill Frequency Response Tests," Presented at the IEEE Symposium on Synchronous Machine Modelling for Power System Studies, IEEE Publication 83TH0101-6-PWR, pp. 26-30.

[16] IEEE Standard 115A-1984, *IEEE Trial Use Standard Procedures for Obtaining Synchronous Machine Parameters by Standstill Frequency Response Testing.*

[17] A.G. Jack and T.J. Bedford, "A Study of the Frequency Response of Turbogenerators with Special Reference to Nanticoke GS," *IEEE Trans.*, Vol.

EC-2, pp. 496-505, September 1987.

[18] M.E. Coultes, P. Kundur and G.J. Rogers, "On-Line Frequency Response Tests and Identification of Generator Models," *IEEE Trans.*, Vol. EC-2, pp. 38-42, September 1987.

[19] P.L. Dandeno, P. Kundur, A.T. Poray, and H.M. Zein El-Din, "Adaptation and Validation of Turbogenerator Model Parameters through On-Line Frequency Response Measurements," *IEEE Trans.*, Vol. EC-2, pp. 1656-1661, September 1987.

[20] P.L. Dandeno, P. Kundur, A.T. Poray, and M.E. Coultes, "Validation of Turbogenerator Stability Models by Comparison with Power System Tests," *IEEE Trans.*, Vol. EC-2, pp. 1637-1645, September 1987.

[21] R.P. Schulz, W.D. Jones, and D.N. Ewart, "Dynamic Models of Turbine Generators Derived from Solid Rotor Equivalent Circuits," *IEEE Trans.*, Vol. PAS-92, pp. 926-933, May/June 1973.

[22] J.W. Dougherty and S.M. Minnich, "Finite Element Modelling of Large Turbine Generators: Calculations versus Load Test Data," *IEEE Trans.*, Vol. PAS-100, pp. 3921-3929, August 1981.

Chapter 5

Synchronous Machine Representation in Stability Studies

The per unit equations summarized in Section 3.4.9 describe completely the electrical dynamic performance of a synchronous machine. However, except for the analysis of very small systems, these equations cannot be used directly for system stability studies. In this chapter the simplifications required for the representation of synchronous machines in stability studies are discussed. Also considered are various degrees of approximations that can be made to simplify the machine model, minimizing data requirements and computational effort.

5.1 SIMPLIFICATIONS ESSENTIAL FOR LARGE-SCALE STUDIES

For stability analysis of large systems, it is necessary to neglect the following from Equations 3.120 and 3.121 for stator voltage:

- The transformer voltage terms, $p\psi_d$ and $p\psi_q$.
- The effect of speed variations.

The reasons for and the effects of these simplifications are discussed below.

5.1.1 Neglect of Stator $p\psi$ Terms

As discussed in Section 3.7, the $p\psi_d$ and $p\psi_q$ terms represent the stator transients. With these terms neglected, the stator quantities contain only fundamental frequency components and the stator voltage equations appear as algebraic equations. This allows the use of steady-state relationships for representing the interconnecting transmission network.

The transients associated with the network decay very rapidly and there is little justification for modelling their effects in stability studies. The network transients cannot be neglected unless machine stator transients are also neglected; otherwise we would have an inconsistent set of equations representing the various elements of the power system. Inclusion of the network transients increases the order of the overall system model considerably, and hence limits the size of the system that can be simulated. In addition, a system representation with machine stator and network transients contains high frequency transients. This requires small time steps for numerical integration, resulting in an enormous increase in computational costs. Also, time responses of system variables containing high frequency components are difficult to analyze and interpret from the viewpoint of system stability. For these reasons, stability analysis of practical power systems consisting of thousands of buses and hundreds of generators would be impossible without the simplification resulting from the neglect of machine stator transients. While we have identified the need for omitting the stator $p\psi$ terms from computational considerations, we have not yet established that the computed machine response with this simplification is acceptable for the study of system stability. This has been investigated in references 1 to 3, and we will discuss the results of one of the cases considered in reference 1.

Figure 5.1 shows the system studied. It consists of a salient-pole generator connected to an infinite bus through two transmission lines. The disturbance applied is a three-phase short-circuit at the sending end of one of the lines, cleared in 0.09 s by isolating the faulted circuit. The responses of generator variables computed with and without inclusion of the stator $p\psi$ terms are compared in Figures 5.2, 5.3 and 5.4.

When the stator $p\psi$ terms are omitted, we see from Figure 5.2 that i_d and i_q have only unidirectional components; these correspond to the fundamental frequency component of phase currents. The resulting air-gap torque is unidirectional and small in magnitude; it is due to the stator resistance losses.

On the other hand, when the $p\psi$ terms are included, i_d and i_q contain fundamental frequency (60 Hz) components, which correspond to the dc offset in the phase currents (discussed in Section 3.7). These in turn result in the following components of air-gap torque:

- A fundamental frequency oscillatory component, due to interaction with the rotor field.

- A unidirectional component, due to rotor resistance losses caused by the fundamental frequency currents induced in the rotor.

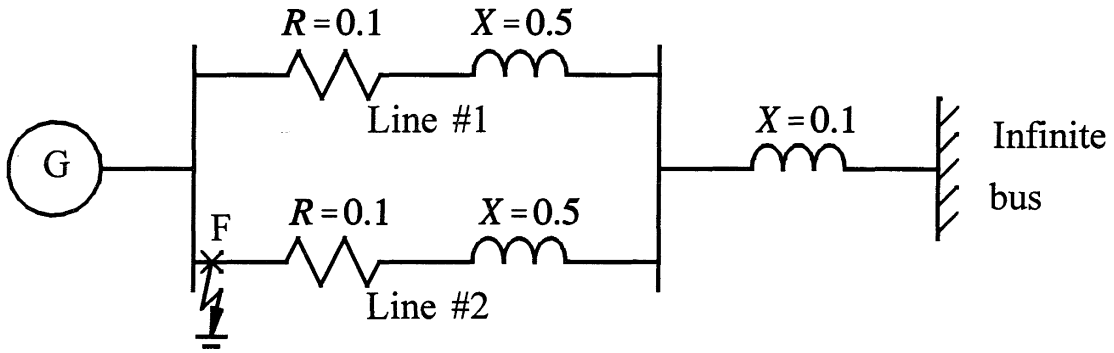

Disturbance:
3-phase fault at F; cleared in 0.09 s by opening line #2

Generator parameters in per unit:

$L_{ad} = 1.0$	$L_{aq} = 0.6$	$L_l = 0.18$	$L_{fd} = 0.13$
$L_{1d} = 0.11$	$L_{1q} = 0.13$	$R_a = 0.005$	$R_{fd} = 0.00075$
$R_{1d} = 0.02$	$R_{1q} = 0.04$	$H = 3.5$	

Figure 5.1 System configuration and parameters

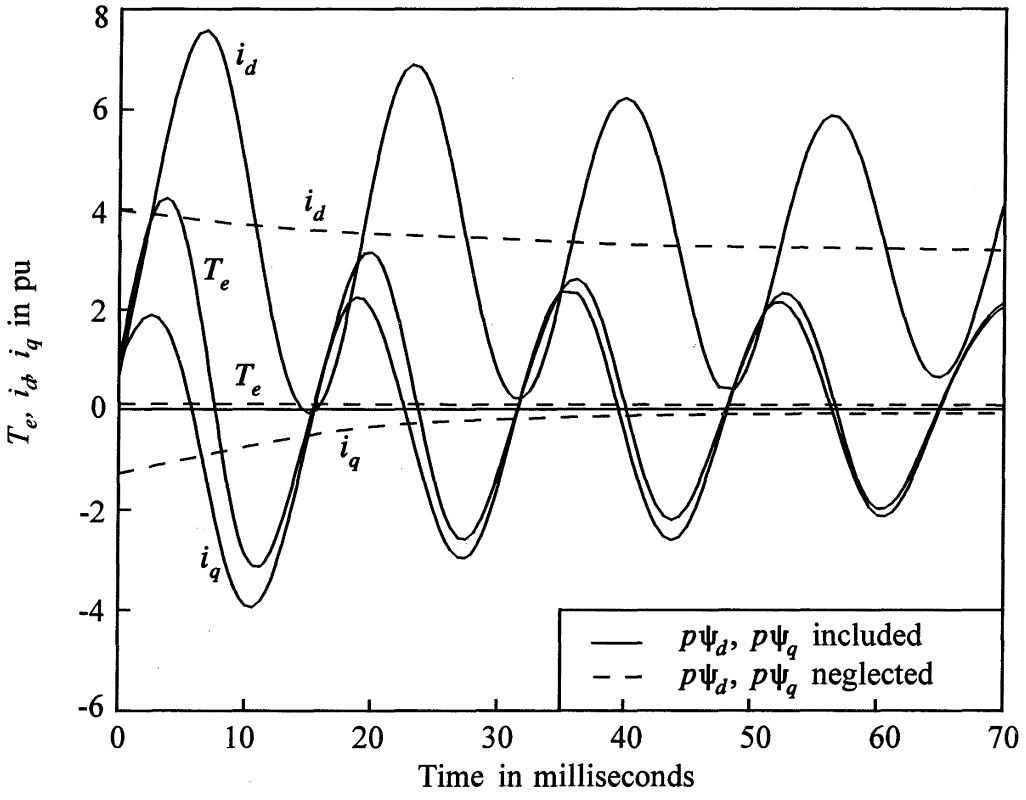

Figure 5.2 Effect of neglecting stator transients on air-gap torque and *d-q* components of stator currents

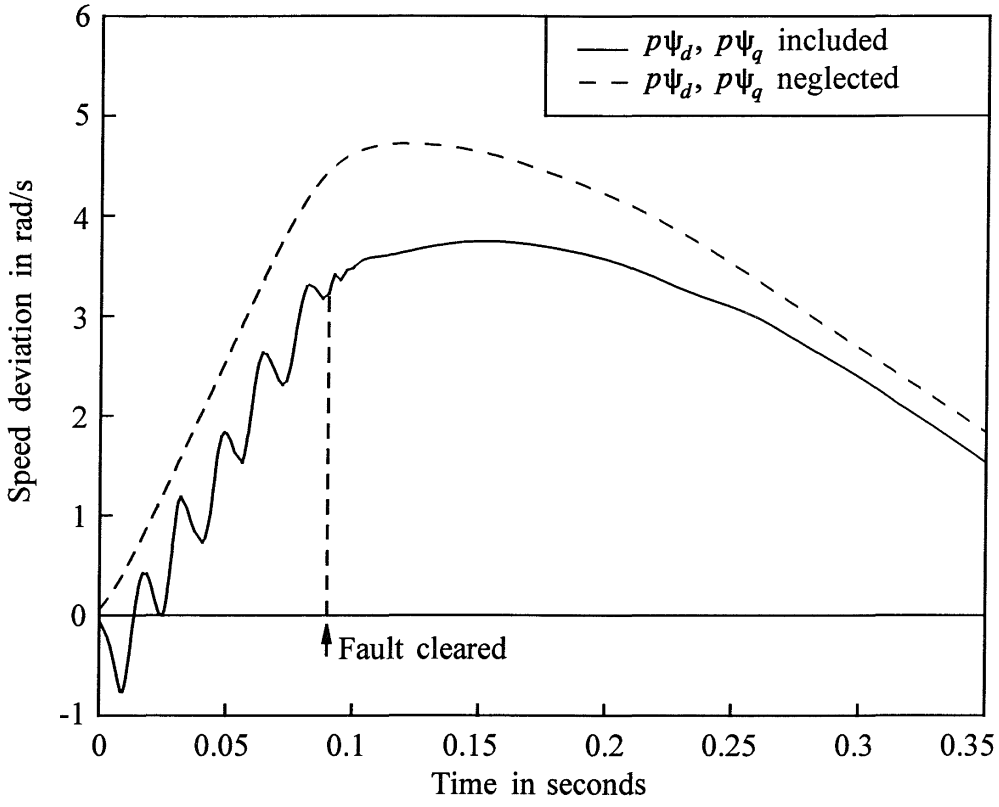

Figure 5.3 Effect of neglecting stator transients on speed deviation

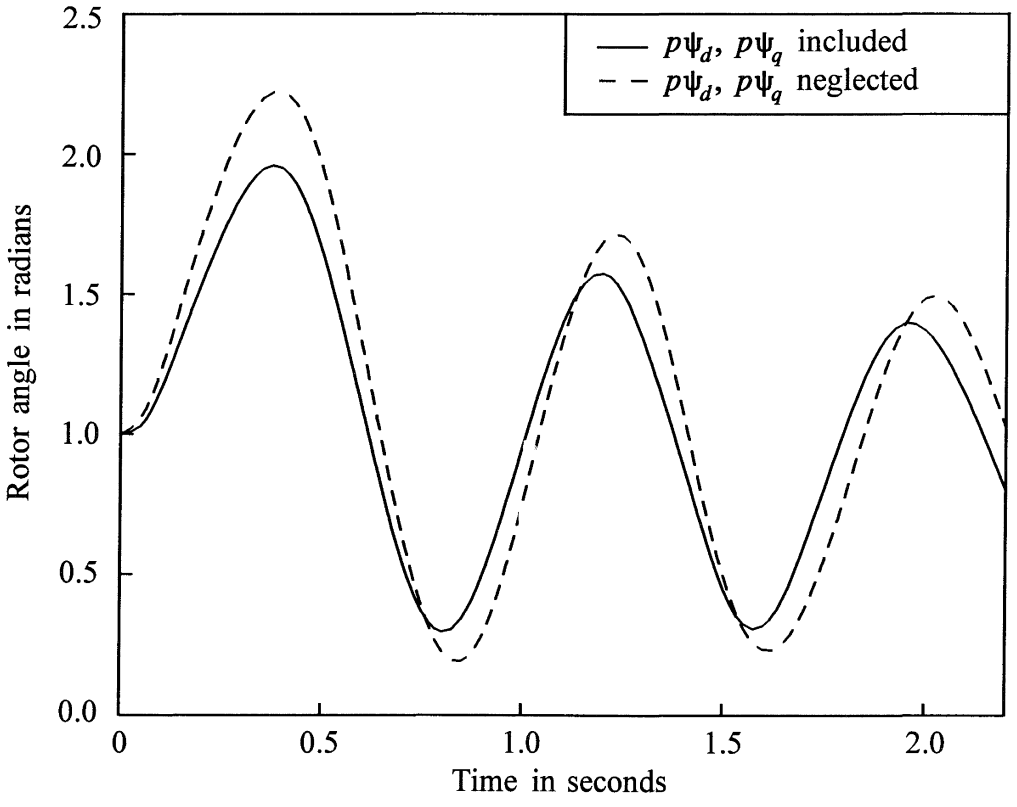

Figure 5.4 Effect of neglecting stator transients on rotor angle swings

The unidirectional component of torque, due to rotor resistive losses, can be quite high and has a braking effect. Therefore, it is referred to as the *dc braking torque*; its effect is to reduce the acceleration of the rotor following the disturbance. The effect of the oscillatory component is to decelerate the rotor during the first half cycle and to accelerate it to near its initial speed during the second half cycle, and so on during subsequent cycles. The net effect of the oscillatory torque is therefore a reduction of the mean speed of the rotor [4]. The overall effect of these two components for a close-up simultaneous three-phase fault could be large enough to initially cause retardation of the rotor or a *back swing*. This could have a significant beneficial effect on system stability as seen from plots of speed deviation and rotor angle in Figures 5.3 and 5.4.

Since, for large-scale stability studies, it is necessary to neglect the $p\psi$ terms, the effects of the unidirectional (dc) braking torque and the oscillatory torque may be estimated and included in the calculations. References 1, 3, 5 and 6 give methods of estimating the unidirectional braking torque, and reference 4 gives a method to account for the oscillatory torque. These would be applicable only to simultaneous three-phase faults and need to be considered only for machines very close to the fault.

However, in practical studies of power system stability, the effects of dc braking and oscillatory torque are not normally included for the following reasons:

(a) Multi-phase faults are mostly sequentially developed; that is, they start as single-phase faults and develop into two-phase or three-phase faults. If each phase were to become involved as its voltage reached the peak of the voltage wave, the short circuit current would lag by 90° and would therefore start as a sinusoidal wave beginning at zero on the sine wave. In such a case, there is no requirement for dc offset in the fault current. Records of oscillograms of actual short circuit currents appear to show very little dc offset in the phase currents. Therefore, one cannot depend on the existence of dc braking to assist in stability.

(b) Even if some dc offset exists, ignoring its effect introduces a slight degree of conservatism.

With the stator transients neglected, the per unit stator voltage Equations 3.120 and 3.121 appear as algebraic equations:

$$e_d = -\psi_q \omega_r - R_a i_d \tag{5.1}$$

$$e_q = \psi_d \omega_r - R_a i_q \tag{5.2}$$

5.1.2 Neglecting the Effect of Speed Variations on Stator Voltages

Another simplifying assumption normally made is that the per unit value of ω_r is equal to 1.0 in the stator voltage equations. This is not the same as saying that speed is constant; it assumes that speed changes are small and do not have a significant effect on the voltage.

The assumption of per unit ω_r=1.0 (i.e., $\omega_r=\omega_0$ rad/s) in the stator voltage equations does not contribute to computational simplicity in itself. The primary reason for making this assumption is that it counterbalances the effect of neglecting $p\psi_d$, $p\psi_q$ terms so far as the low-frequency rotor oscillations are concerned [7,8]. We will demonstrate this in Example 5.1.

With per unit ω_r=1.0, the stator voltage equations reduce to

$$e_d = -\psi_q - R_a i_d \tag{5.3}$$

$$e_q = \psi_d - R_a i_q \tag{5.4}$$

All other equations (3.123 to 3.134) summarized in Section 3.4.9 remain the same. Organization of the machine equations in a form suitable for small-signal and transient stability studies is described in Chapters 12 and 13.

Relationship between per unit P_e and T_e

The terminal electric power in per unit is given by

$$P_t = e_d i_d + e_q i_q$$

Substituting for e_d and e_q from Equations 5.3 and 5.4 gives

$$\begin{aligned} P_t &= (-\psi_q - R_a i_d) i_d + (\psi_d - R_a i_q) i_q \\ &= (\psi_d i_q - \psi_q i_d) - R_a (i_d^2 + i_q^2) \\ &= T_e - R_a I_t^2 \end{aligned} \tag{5.5}$$

The air-gap power, measured behind R_a, is given by

$$\begin{aligned} P_e &= P_t + R_a I_t^2 \\ &= T_e \end{aligned} \tag{5.6}$$

The per unit air-gap power P_e so computed is in fact the power at synchronous speed and is equal to the per unit air-gap torque T_e.

Normally, $P_e=\omega_r T_e$. However, the assumption of $\omega_r=1.0$ pu in the stator voltage equation is also reflected in the torque equation, making $P_e=T_e$. This fact is often overlooked.

Example 5.1

With zero armature resistance, show that for small perturbations the effect of neglecting the speed variations (i.e., assuming $\omega_r=\omega_0$) in the stator voltage equations is to counterbalance the effect of neglecting $p\psi_d$, $p\psi_q$ terms.

Solution

With $R_a=0$ and time t in seconds, the stator voltage Equations 3.120 and 3.121 become

$$e_d = \frac{1}{\omega_0} p\psi_d - \psi_q \frac{\omega_r}{\omega_0} \tag{E5.1}$$

$$e_q = \frac{1}{\omega_0} p\psi_q + \psi_d \frac{\omega_r}{\omega_0} \tag{E5.2}$$

where ω_r and ω_0 are expressed in rad/s.

For small perturbation,

$$\Delta e_d = \frac{1}{\omega_0} p(\Delta\psi_d) - \Delta\psi_q - \psi_{q0} \frac{\Delta\omega_r}{\omega_0} \tag{E5.3}$$

$$\Delta e_q = \frac{1}{\omega_0} p(\Delta\psi_q) + \Delta\psi_d + \psi_{d0} \frac{\Delta\omega_r}{\omega_0} \tag{E5.4}$$

Since

$$e_d = E_t \sin\delta \tag{E5.5}$$

$$e_q = E_t \cos\delta \tag{E5.6}$$

from Equations E5.1, E5.2, at steady state (derivative terms absent) we have

$$e_{d0} = E_t \sin\delta_0 = -\psi_{q0}$$

$$e_{q0} = E_t \cos\delta_0 = \psi_{d0}$$

Hence, for small perturbations, Equations E5.5 and E5.6 become

$$\Delta e_d = (E_t \cos\delta_0)\Delta\delta = \psi_{d0}\Delta\delta \tag{E5.7}$$

$$\Delta e_q = -(E_t \sin\delta_0)\Delta\delta = \psi_{q0}\Delta\delta \tag{E5.8}$$

From Equations E5.3, E5.4, E5.7, and E5.8, with $\Delta\omega_r = p(\Delta\delta)$, we may write

$$\psi_{d0}\Delta\delta = \frac{1}{\omega_0}p(\Delta\psi_d) - \Delta\psi_q - \psi_{q0}\frac{1}{\omega_0}p(\Delta\delta) \tag{E5.9}$$

$$\psi_{q0}\Delta\delta = \frac{1}{\omega_0}p(\Delta\psi_q) + \Delta\psi_d + \psi_{d0}\frac{1}{\omega_0}p(\Delta\delta) \tag{E5.10}$$

We will compare the expressions for Δe_d and Δe_q, as given by Equations E5.7 and E5.8, with and without the effects of $p\Delta\psi$ and $p\Delta\delta$ terms.

(a) With both $p(\Delta\psi)$ and $p(\Delta\delta)$ terms included:

Rearranging Equation E5.9, we have

$$\Delta\delta = \frac{\frac{1}{\omega_0}p(\Delta\psi_d) - \Delta\psi_q}{\psi_{d0} + \frac{\psi_{q0}}{\omega_0}p} \tag{E5.11}$$

From Equation E5.10,

$$\Delta\psi_d = (\psi_{q0} - \frac{\psi_{d0}}{\omega_0}p)\Delta\delta - \frac{1}{\omega_0}p(\Delta\psi_q) \tag{E5.12}$$

Substituting Equation E5.12 in E5.11, rearranging and simplifying, we get

$$\boxed{\psi_{d0}\Delta\delta = -\Delta\psi_q} \tag{E5.13}$$

Similarly, from Equation E5.10,

$$\Delta\delta = \frac{\frac{1}{\omega_0}p(\Delta\psi_q) + \Delta\psi_d}{\psi_{q0} - \frac{\psi_{d0}}{\omega_0}p} \tag{E5.14}$$

and from Equation E5.9,

$$\Delta\psi_q = -(\psi_{d0}+\frac{\psi_{q0}}{\omega_0}p)\Delta\delta+\frac{1}{\omega_0}p(\Delta\psi_d) \tag{E5.15}$$

Substituting Equation E5.15 in E5.14, rearranging and simplifying, we find

$$\boxed{\psi_{q0}\Delta\delta = \Delta\psi_d} \tag{E5.16}$$

(b) With both $p(\Delta\psi)$ and $p(\Delta\delta)$ terms neglected:

Equations E5.9 and E5.10, with $p\Delta\psi_d=p\Delta\psi_q=p\Delta\delta=0$, simplify to

$$\boxed{\psi_{d0}\Delta\delta = -\Delta\psi_q} \tag{E5.17}$$

$$\boxed{\psi_{q0}\Delta\delta = \Delta\psi_d} \tag{E5.18}$$

These are same as Equations E5.13 and E5.16.

(c) With only $p(\Delta\psi)$ terms neglected:

From Equation E5.9, with the $p\psi_d$ term neglected, we have

$$\psi_{d0}\Delta\delta = -\Delta\psi_q-\frac{\psi_{q0}}{\omega_0}p(\Delta\delta)$$

Hence,

$$\Delta\delta = -\frac{\Delta\psi_q}{\psi_{d0}+\frac{\psi_{q0}}{\omega_0}p}$$

Multiplying both sides by ψ_{d0} gives

$$\boxed{\psi_{d0}\Delta\delta = -\Delta\psi_q\left[\frac{\psi_{d0}}{\psi_{d0}+\frac{\psi_{q0}}{\omega_0}p}\right]} \tag{E5.19}$$

Similarly from Equation E5.10, with the $p\psi_q$ term neglected, we can show that

$$\psi_{q0}\Delta\delta = \Delta\psi_d\left[\frac{\psi_{q0}}{\psi_{q0}+\frac{\psi_{d0}}{\omega_0}p}\right] \tag{E5.20}$$

The above two equations differ from Equations E5.13 and E5.16.

(d) With only p(Δδ) terms neglected:

With $p\Delta\delta=0$, from Equation E5.9, we have

$$\psi_{d0}\Delta\delta = \frac{1}{\omega_0}p(\Delta\psi_d)-\Delta\psi_q \tag{E5.21}$$

and from Equation E5.10, we have

$$\psi_{q0}\Delta\delta = \frac{1}{\omega_0}p(\Delta\psi_q)+\Delta\psi_d \tag{E5.22}$$

or

$$\Delta\psi_d = \psi_{q0}\Delta\delta-\frac{1}{\omega_0}p(\Delta\psi_q) \tag{E5.23}$$

Substituting Equation E5.23 into Equation E5.21 yields

$$\psi_{d0}\Delta\delta = \frac{1}{\omega_0}p(\psi_{q0}\Delta\delta-\frac{p}{\omega_0}\Delta\psi_q)-\Delta\psi_q$$

Grouping terms involving Δδ and rearranging, we have

$$\psi_{d0}\Delta\delta = -\Delta\psi_q\left[\psi_{d0}\frac{1+p^2/\omega_0^2}{\psi_{d0}-\psi_{q0}\frac{p}{\omega_0}}\right] \tag{E5.24}$$

Similarly,

$$\psi_{q0}\Delta\delta = \Delta\psi_d\left[\psi_{q0}\frac{1+p^2/\omega_0^2}{\psi_{q0}+\psi_{d0}\frac{p}{\omega_0}}\right] \tag{E5.25}$$

Again, the above equations differ from Equations E5.13 and E5.16.

We see that the expressions for Δe_d (i.e., $\psi_{d0}\Delta\delta$) and Δe_q (i.e., $\psi_{q0}\Delta\delta$) with both $p(\Delta\psi)$ and $p(\Delta\delta)$ terms included equal those with both terms neglected, but not those with only one of these terms neglected. Therefore, the effect of neglecting $p(\Delta\delta)$ terms is to counterbalance the effect of neglecting $p(\Delta\psi)$ terms. ■

5.2 SIMPLIFIED MODEL WITH AMORTISSEURS NEGLECTED

The first order of simplification to the synchronous machine model is to neglect the amortisseur effects. This minimizes data requirements since the machine parameters related to the amortisseurs are often not readily available. In addition, it may contribute to reduction in computational effort by reducing the order of the model and allowing larger integration steps in time-domain simulations.

With the amortisseurs neglected, the stator voltage Equations 5.3 and 5.4 are unchanged. The remaining equations (3.123 to 3.133) simplify as follows.

Flux linkages:

$$\psi_d = -L_d i_d + L_{ad} i_{fd} \tag{5.7}$$

$$\psi_q = -L_q i_q \tag{5.8}$$

$$\psi_{fd} = -L_{ad} i_d + L_{ffd} i_{fd} \tag{5.9}$$

Rotor voltage:

$$e_{fd} = p\psi_{fd} + R_{fd} i_{fd}$$

or

$$p\psi_{fd} = e_{fd} - R_{fd} i_{fd} \tag{5.10}$$

Equation 5.10 is now the only differential equation associated with the electrical characteristics of the machine. In the above equations all quantities, including time, are in per unit.

Alternative form of machine equations

In the literature on synchronous machines, Equations 5.7 to 5.10 are often written in terms of the following variables:

$$E_I = L_{ad} i_{fd} = \text{voltage proportional to } i_{fd}$$

$$E'_q = \frac{L_{ad}}{L_{ffd}} \psi_{fd} = \text{voltage proportional to } \psi_{fd}$$

$$E_{fd} = \frac{L_{ad}}{R_{fd}} e_{fd} = \text{voltage proportional to } e_{fd}$$

In terms of the new variables, Equation 5.7 becomes

$$\psi_d = -L_d i_d + E_I \tag{5.11}$$

Multiplying Equation 5.9 by L_{ad}/L_{ffd} throughout and expressing in terms of the new variables, we get

$$E'_q = -\frac{L_{ad}^2}{L_{ffd}} i_d + E_I \tag{5.12}$$

Since, from Equation 4.29,

$$L'_d = L_l + \frac{L_{ad} L_{fd}}{L_{ad} + L_{fd}}$$

$$= (L_d - L_{ad}) + \frac{L_{ad} L_{fd}}{L_{ad} + L_{fd}}$$

$$= L_d - \frac{L_{ad}^2}{L_{ffd}}$$

then

$$L_d - L'_d = \frac{L_{ad}^2}{L_{ffd}}$$

Substituting in Equation 5.12 gives

$$E'_q = E_I - (L_d - L'_d) i_d \tag{5.13}$$

Multiplying Equation 5.10 by L_{ad}/L_{ffd} throughout, we have

$$p\left(\frac{L_{ad}}{L_{ffd}}\psi_{fd}\right) = \frac{L_{ad}}{R_{fd}}\frac{R_{fd}}{L_{ffd}}e_{fd} - \frac{R_{fd}}{L_{ffd}}L_{ad}i_{fd}$$

Expressing this in terms of the new variables gives

$$pE'_q = \frac{1}{T'_{d0}}(E_{fd} - E_I) \tag{5.14}$$

where T'_{d0} is the open-circuit transient time constant defined in Section 4.2.

The following is a summary of the alternative form of machine equations:

$$\psi_d = -L_d i_d + E_I$$

$$\psi_q = -L_q i_q$$

$$E'_q = E_I - (L_d - L'_d) i_d$$

$$pE'_q = \frac{1}{T'_{d0}}(E_{fd} - E_I)$$

The above form is used to represent synchronous machines in many stability programs, particularly the older programs. In this formulation, E'_q is the state variable instead of ψ_{fd}. In a way, this is a carryover from the techniques used in the network analyzer days. As seen in the following development of the phasor diagram, E'_q is the q-axis component of the voltage behind transient reactance X'_d. Therefore, the use of E'_q as the state variable allows a simple enhancement to the classical model to account for the field circuit dynamics. It should, however, be recognized that the parameters L_d, L_q, L'_d and T'_{d0} which appear in this formulation are functions of magnetic saturation.

Phasor diagram for transient conditions:

As we account for only the fundamental frequency components of stator quantities, we can use phasor representation to illustrate the transient conditions. In order to do this it is first necessary to express E'_q, E_I and E_q in terms of d- and q-axis components of terminal voltage and current.

Since in per unit $X_d = L_d$, from Equations 5.4 and 5.7,

$$e_q = \psi_d - R_a i_q$$

$$= -X_d i_d + X_{ad} i_{fd} - R_a i_q$$

$$= -X_d i_d + E_I - R_a i_q$$

Therefore

$$E_I = e_q + X_d i_d + R_a i_q$$

Multiplying by j, we have

$$jE_I = je_q + jX_d i_d + jR_a i_q$$

In terms of phasor notation,

$$\tilde{E}_I = \tilde{e}_q + jX_d \tilde{i}_d + R_a \tilde{i}_q \tag{5.15}$$

From Equation 5.13, with $X'_d = L'_d$,

$$\begin{aligned} E'_q &= e_q + X_d i_d + R_a i_q - X_d i_d + X'_d i_d \\ &= e_q + X'_d i_d + R_a i_q \end{aligned}$$

Multiplying by j gives

$$jE'_q = je_q + jX'_d i_d + jR_a i_q$$

In phasor notation,

$$\tilde{E}'_q = \tilde{e}_q + jX'_d \tilde{i}_d + R_a \tilde{i}_q \tag{5.16}$$

We see that the phasors $\tilde{E}_I$ and $\tilde{E}'_q$ both lie along the q-axis. In Section 3.6.2, we saw that $\tilde{E}_q$ also lies along the q-axis.

Rearranging Equation 3.167 and substituting E_I for $X_{ad} i_{fd}$, we get

$$\tilde{E}_I = \tilde{E}_q + j(X_d - X_q)\tilde{i}_d \tag{5.17}$$

Figure 5.5 shows the phasor diagram representing $\tilde{E}'_q$, $\tilde{E}_q$ and $\tilde{E}_I$ given by Equations 5.15, 5.16 and 5.17.

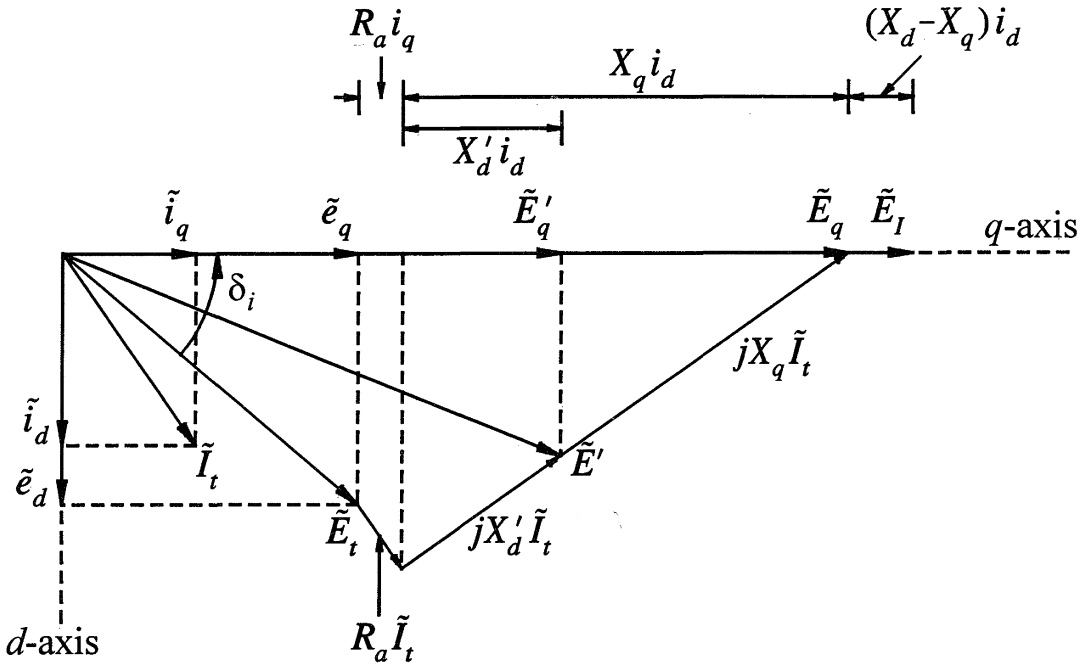

$$
\begin{aligned}
\tilde{E}_t &= e_d + je_q = \tilde{e}_d + \tilde{e}_q \\
\tilde{E}' &= \tilde{E}_t + (R_a + jX'_d)\tilde{I}_t \\
\tilde{E}'_q &= q\text{-axis component of } \tilde{E}' \\
&= \tilde{e}_q + R_a\tilde{i}_q + jX'_d\tilde{i}_d \\
\tilde{E}_q &= \text{Voltage behind } R_a + jX_q \\
&= \tilde{E}_t + (R_a + jX_q)\tilde{I}_t \\
&= \tilde{e}_q + R_a\tilde{i}_q + jX_q\tilde{i}_d \\
\tilde{E}_I &= \tilde{E}_q + j(X_d - X_q)\tilde{i}_d
\end{aligned}
$$

Figure 5.5 Synchronous machine phasor diagram in terms of E_q, E_I, and E'_q

5.3 CONSTANT FLUX LINKAGE MODEL

5.3.1 Classical Model

For studies in which the period of analysis is small in comparison to T'_{d0}, the machine model of Section 5.2 is often simplified by assuming E'_q (or ψ_{fd}) constant throughout the study period. This assumption eliminates the only differential equation associated with the electrical characteristics of the machine.

A further approximation, which simplifies the machine model significantly, is to ignore transient saliency by assuming $X'_d = X'_q$, and to assume that the flux linkage ψ_{1q} (associated with the q-axis rotor circuit corresponding to X'_q) also remains constant. With these assumptions, as shown below, the voltage behind the transient impendence $R_a + jX'_d$ has a constant magnitude.

The d- and q-axis equivalent circuits with only one circuit in each axis are shown in Figure 5.6.

The per unit flux linkages identified in the d-axis are given by

$$\psi_{ad} = -L_{ad} i_d + L_{ad} i_{fd} \tag{5.18}$$

$$\psi_d = \psi_{ad} - L_l i_d \tag{5.19}$$

$$\psi_{fd} = \psi_{ad} + L_{fd} i_{fd} \tag{5.20}$$

From Equation 5.20

$$i_{fd} = \frac{\psi_{fd} - \psi_{ad}}{L_{fd}} \tag{5.21}$$

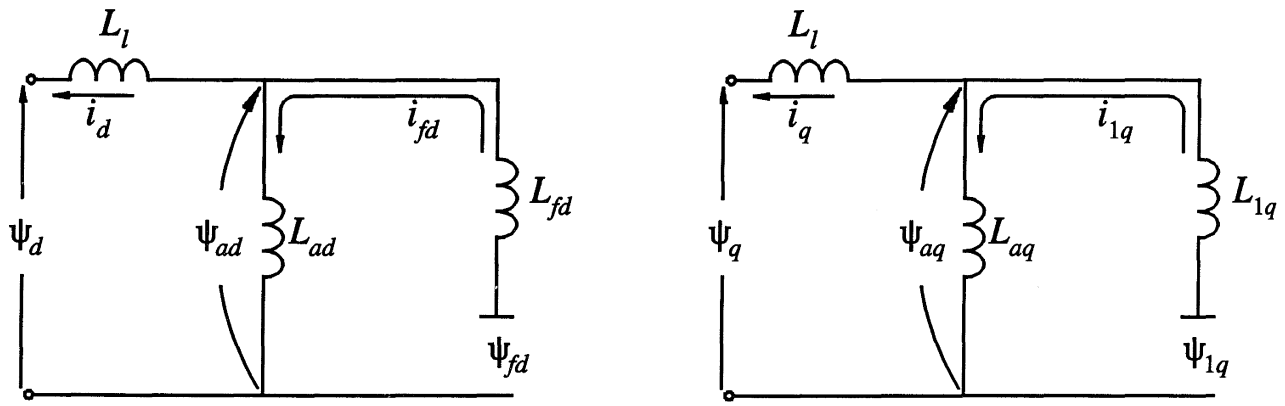

Figure 5.6 The d- and q-axis equivalent circuits with one rotor circuit in each axis

Substituting in Equation 5.18 gives

$$\psi_{ad} = -L_{ad} i_d + \frac{L_{ad}}{L_{fd}} (\psi_{fd} - \psi_{ad})$$

Rearranging to express ψ_{ad} in terms of ψ_{fd}, we find

$$\psi_{ad} = L'_{ad} \left(-i_d + \frac{\psi_{fd}}{L_{fd}} \right) \tag{5.22}$$

where

$$L'_{ad} = \frac{1}{\frac{1}{L_{ad}} + \frac{1}{L_{fd}}} = L'_d - L_l \tag{5.23}$$

Similarly, for the q-axis

$$\psi_{aq} = L'_{aq} \left(-i_q + \frac{\psi_{1q}}{L_{1q}} \right) \tag{5.24}$$

where

$$L_{aq} = L'_d - L_l$$

From Equation 5.1, the d-axis stator voltage is given by

$$\begin{aligned} e_d &= -R_a i_d - \omega \psi_q \\ &= -R_a i_d + \omega (L_l i_q - \psi_{aq}) \end{aligned}$$

where $\omega = \omega_r = \omega_0 = 1.0$ pu. Substituting for ψ_{aq} from Equation 5.24 gives

$$\begin{aligned} e_d &= -R_a i_d + \omega L_l i_q - \omega L'_{aq} \left(-i_q + \frac{\psi_{1q}}{L_{1q}} \right) \\ &= -R_a i_d + \omega (L_l + L'_{aq}) i_q - \omega L'_{aq} \left(\frac{\psi_{1q}}{L_{1q}} \right) \\ &= -R_a i_d + X'_q i_q + E'_d \end{aligned} \tag{5.25}$$

where

$$E'_d = -\omega L'_{aq}\left(\frac{\psi_{1q}}{L_{1q}}\right) \tag{5.26}$$

Similarly, the q-axis stator voltage is given by

$$e_q = -R_a i_q - X'_d i_d + E'_q \tag{5.27}$$

where

$$E'_q = \omega L'_{ad}\left(\frac{\psi_{fd}}{L_{fd}}\right) \tag{5.28}$$

With transient saliency neglected ($X'_d = X'_q$), the stator terminal voltage is

$$\begin{aligned} e_d + je_q &= (E'_d + jE'_q) - R_a(i_d + ji_q) + X'_d(i_q - ji_d) \\ &= (E'_d + jE'_q) - R_a(i_d + ji_q) - jX'_d(i_d + ji_q) \end{aligned}$$

Using phasor notation, we have

$$\tilde{E}_t = \tilde{E}' - (R_a + jX'_d)\tilde{I}_t \tag{5.29}$$

where

$$\begin{aligned} \tilde{E}' &= E'_d + jE'_q \\ &= L'_{ad}\left(-\frac{\psi_{1q}}{L_{1q}} + j\frac{\psi_{fd}}{L_{fd}}\right) \end{aligned}$$

The corresponding equivalent is shown in Figure 5.7.

With rotor flux linkages (ψ_{fd} and ψ_{1q}) constant, E'_d and E'_d are constant. Therefore, the magnitude of E' is constant. As the rotor speed changes, the d- and q-axes move with respect to any general reference coordinate system whose R-I axes rotate at synchronous speed, as shown in Figure 5.8. Hence, the components E'_R and E'_I change.

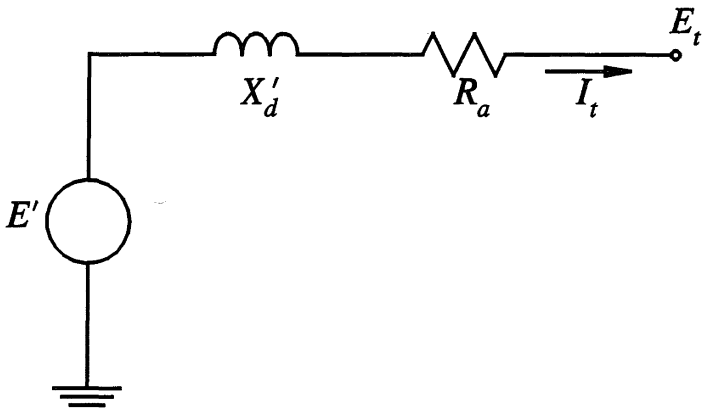

Figure 5.7 Simplified transient model

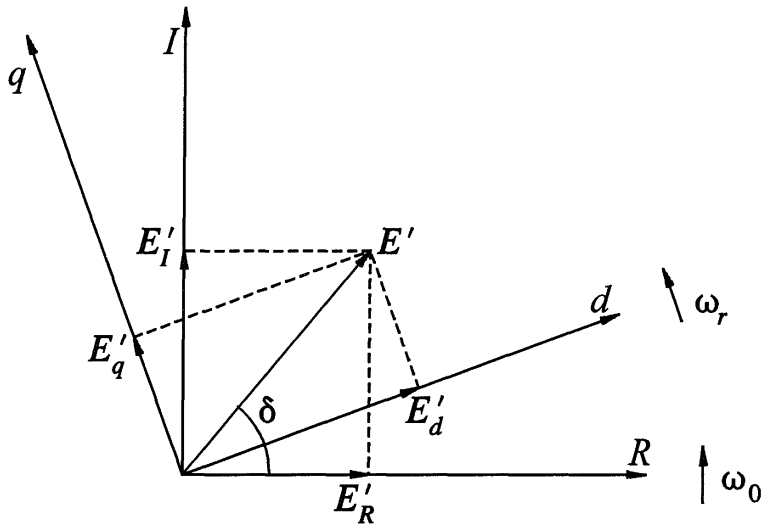

Figure 5.8 The *R-I* and *d-q* coordinate systems

The magnitude of E' can be determined by computing its pre-disturbance value.

$$\tilde{E}' = \tilde{E}_{t0} + (R_a + jX'_d)\tilde{I}_{t0}$$

Its magnitude is then assumed to remain constant throughout the study period. Since R_a is small, it is usual to neglect it.

With the components E'_d and E'_q each having a constant magnitude, E' will have constant orientation with respect to *d*- and *q*-axes, as the rotor speed changes. Therefore, the angle of E' with respect to synchronously rotating reference axes (*R-I*) can be used as a measure of the rotor angle.

This model offers considerable computational simplicity; it allows the transient electrical performance of the machine to be represented by a simple voltage source of fixed magnitude behind an effective reactance. It is commonly referred to as the *classical model*, since it was used extensively in early stability studies.

5.3.2 Constant Flux Linkage Model Including the Effects of Subtransient Circuits

With the subtransient circuits included (see Figure 5.9), the expression developed for the direct axis air-gap flux linkage in the previous section changes as follows:

$$\begin{aligned}\psi_{ad} &= -L_{ad}i_d + L_{ad}i_{fd} + L_{ad}i_{1d} \\ &= -L_{ad}i_d + \frac{L_{ad}}{L_{fd}}(\psi_{fd} - \psi_{ad}) + \frac{L_{ad}}{L_{1d}}(\psi_{1d} - \psi_{ad}) \\ &= L''_{ad}\left(-i_d + \frac{\psi_{fd}}{L_{fd}} + \frac{\psi_{1d}}{L_{1d}}\right)\end{aligned} \tag{5.30}$$

where

$$L''_{ad} = \frac{1}{\frac{1}{L_{ad}} + \frac{1}{L_{fd}} + \frac{1}{L_{1d}}} = L''_d - L_l \tag{5.31}$$

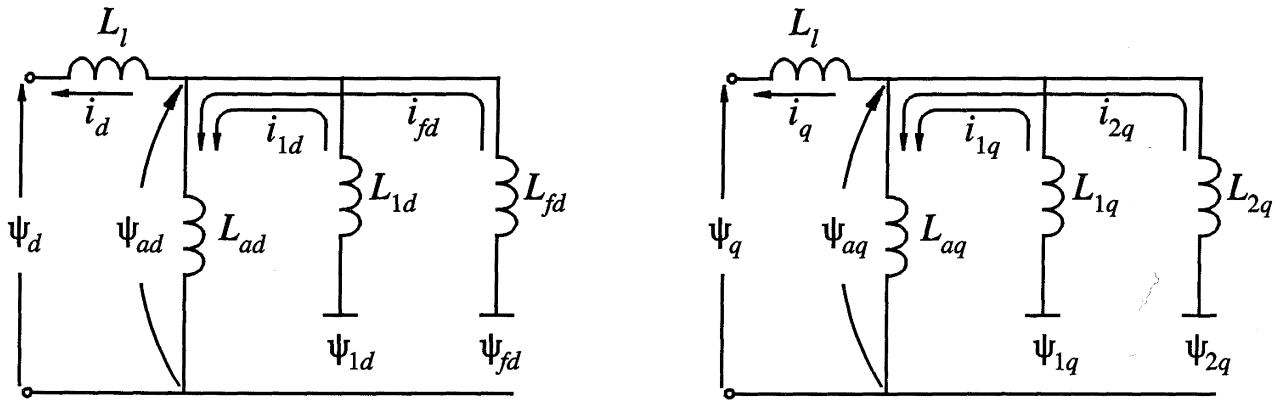

Figure 5.9 Equivalent circuits with subtransient circuits

Similarly, for the q-axis

$$\psi_{aq} = L''_{aq}\left(-i_q + \frac{\psi_{1q}}{L_{1q}} + \frac{\psi_{2q}}{L_{2q}}\right) \tag{5.32}$$

where

$$L''_{aq} = L''_q - L_l$$

The d-axis stator voltage is

$$\begin{aligned} e_d &= -R_a i_d + \omega(L_l i_q - \psi_{aq}) \\ &= -R_a i_d + \omega(L_l + L''_{aq}) i_q - \omega L''_{aq}\left(\frac{\psi_{1q}}{L_{1q}} + \frac{\psi_{2q}}{L_{2q}}\right) \\ &= -R_a i_d + X''_q i_q + E''_d \end{aligned} \tag{5.33}$$

Similarly, the q-axis stator voltage is

$$e_q = -R_a i_q - X''_d i_d + E''_q \tag{5.34}$$

where

$$E''_d = -\omega L''_{aq}\left(\frac{\psi_{1q}}{L_{1q}} + \frac{\psi_{2q}}{L_{2q}}\right) \tag{5.35}$$

$$E''_q = \omega L''_{ad}\left(\frac{\psi_{fd}}{L_{fd}} + \frac{\psi_{1d}}{L_{1d}}\right) \tag{5.36}$$

With subtransient saliency neglected, $X''_d = X''_q$. We then have

$$\begin{aligned} \tilde{E}_t &= e_d + j e_q \\ &= (E''_d + jE''_q) - (R_a + jX''_d)(i_d + ji_q) \\ &= \tilde{E}'' - (R_a + jX''_d)\tilde{I}_t \end{aligned} \tag{5.37}$$

The corresponding equivalent circuit is shown in Figure 5.10. With constant rotor flux linkages, E''_d and E''_q are constant.

This model is used in short-circuit programs for computing the initial value of the fundamental frequency component of short-circuit currents. As the rotor flux linkages cannot change instantaneously, the value E'' is equal to its prefault value.

Such a constant flux linkage model would not be generally acceptable for stability studies, since the subtransient time constants associated with the decay of ψ_{1d} and ψ_{2q} are very small compared to the study period, and hence the assumption of constant rotor flux linkage of all rotor circuits, including the subtransient circuits, is not reasonable. The model, however, is valid if rotor flux linkage variations are accounted for, in which case the magnitude of E'' varies as determined by Equations 3.123 to 3.126.

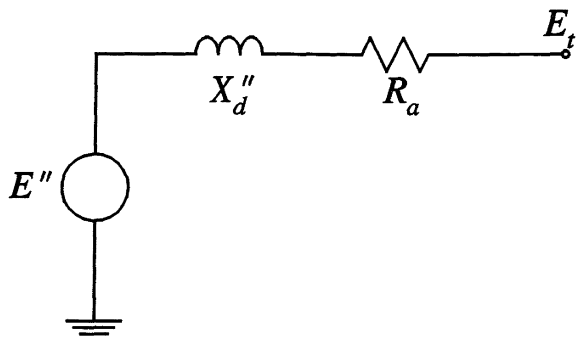

Figure 5.10 Simplified model for subtransient period

5.3.3 Summary of Simple Models for Different Time Frames

Figure 5.11 summarizes the simple models of the synchronous machine applicable to the three time frames: subtransient, transient, and steady state. The model applicable to steady-state conditions was developed in Chapter 3 (Section 3.6.4) and is included here since it has the same structure as the models developed in this chapter for transient and subtransient conditions. The subtransient and transient models assume constant rotor flux linkages, and the steady-state model assumes constant field current. These models neglect saliency effects and stator resistance and offer considerable structural and computational simplicity.

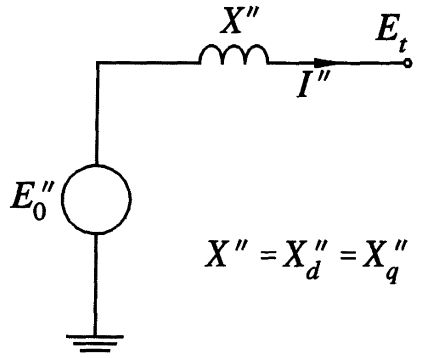

E''_0 is the predisturbance value of internal voltage given by

$$\tilde{E}''_0 = \tilde{E}_{t0} + jX''\tilde{I}_{t0}$$

(a) Subtransient model

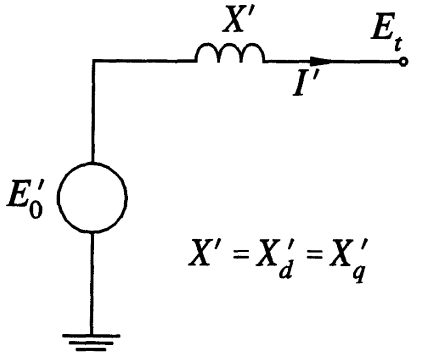

E'_0 is the internal voltage

$$\tilde{E}'_0 = \tilde{E}_{t0} + jX'\tilde{I}_{t0}$$

(b) Transient model

Figure 5.11 Simple synchronous machine models (*Continued on next page*)

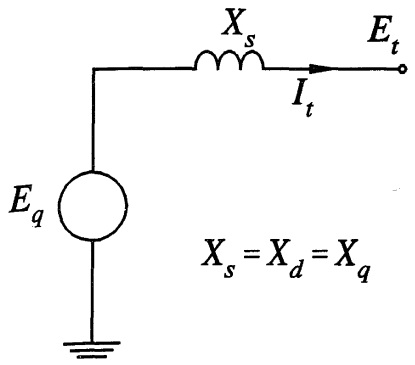

$$\tilde{E}_q = \tilde{E}_{t0} + jX_s\tilde{I}_{t0}$$
$$|E_q| = X_{ad}i_{fd} = E_I$$

(c) Steady-state model

Figure 5.11 (*Continued*) Simple synchronous machine models

5.4 REACTIVE CAPABILITY LIMITS

In voltage stability and long-term stability studies, it is important to consider the reactive capability limits of synchronous machines. In this section, we will develop capability curves which identify these limits.

5.4.1 Reactive Capability Curves

Synchronous generators are rated in terms of the maximum MVA output at a specified voltage and power factor (usually 0.85 or 0.9 lagging) which they can carry continuously without overheating. The active power output is limited by the prime mover capability to a value within the MVA rating. The continuous reactive power output capability is limited by three considerations: armature current limit, field current limit, and end region heating limit.

Armature current limit

The armature current results in an RI^2 power loss, and the energy associated with this loss must be removed so as to limit the increase in temperature of the conductor and its immediate environment. Therefore, one of the limitations on generator rating is the maximum current that can be carried by the armature without exceeding the heating limitations.

The per unit complex output power is

$$S = P + jQ = \tilde{E}_t\tilde{I}_t^*$$
$$= |E_t||I_t|(\cos\phi + j\sin\phi)$$

where ϕ is the power factor angle.

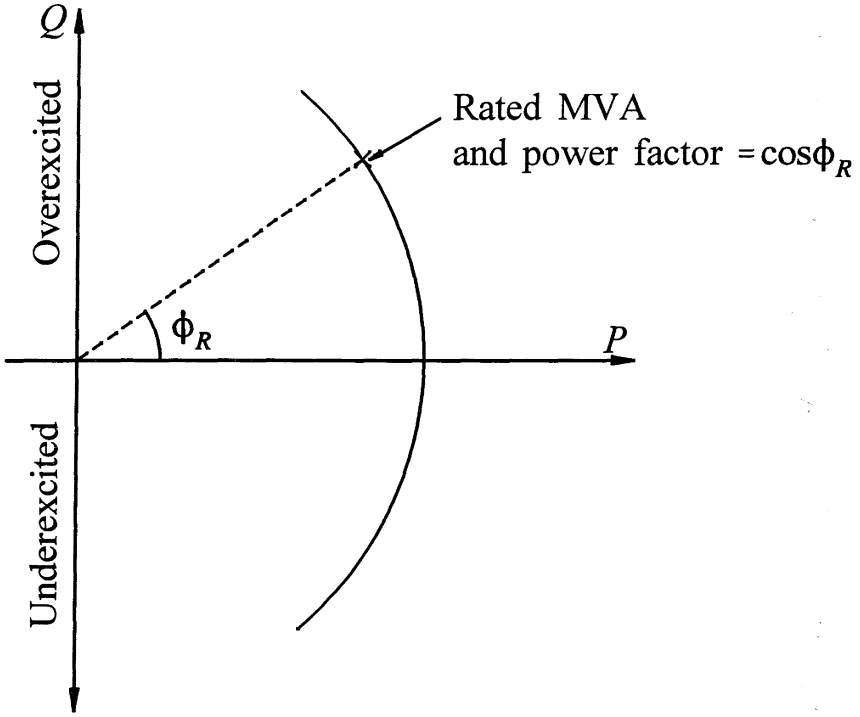

Figure 5.12 Armature current heating limit

Therefore, in the *P-Q* plane the armature current limit, as shown in Figure 5.12, appears as a circle with centre at the origin and radius equal to the MVA rating.

Field current limit

Because of the heat resulting from the $R_{fd}i_{fd}^2$ power loss, the field current imposes a second limit on the operation of the generator.

The constant field current locus may be developed by the steady-state equivalent circuit developed in Section 3.6.4 and reproduced in Section 5.3.3. With $X_d=X_q=X_s$, the equivalent circuit of Figure 5.11(c) gives the relationship between E_t, I_t and E_q (equal to $X_{ad}i_{fd}$). The corresponding phasor diagram, with R_a neglected, is shown in Figure 5.13.

Equating the components along and perpendicular to the phasor $\tilde{E}_t$, we get

$$(X_{ad}i_{fd})\sin\delta_i = X_s I_t\cos\phi \tag{5.38}$$

$$(X_{ad}i_{fd})\cos\delta_i = E_t+X_s I_t\sin\phi \tag{5.39}$$

Rearranging yields

$$I_t\cos\phi = \frac{X_{ad}i_{fd}\sin\delta_i}{X_s}$$

$$I_t\sin\phi = \frac{X_{ad}i_{fd}\cos\delta_i - E_t}{X_s}$$

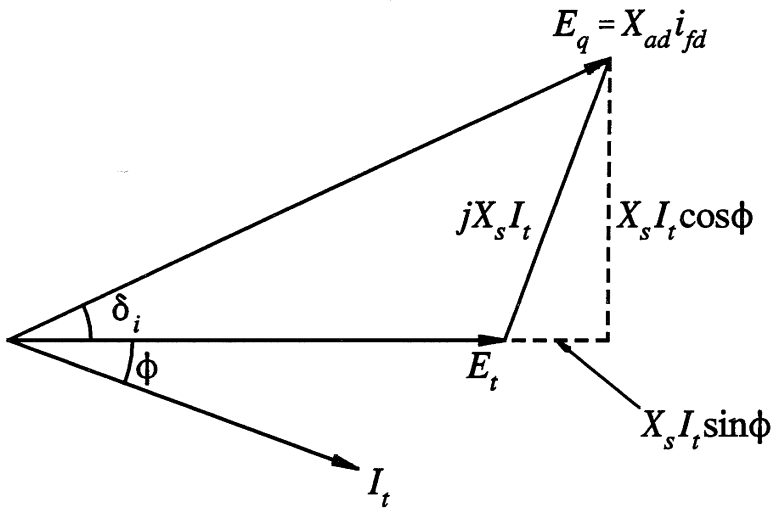

Figure 5.13 Steady-state phasor diagram

Therefore,

$$P = E_t I_t \cos\phi = \frac{X_{ad}}{X_s} E_t i_{fd} \sin\delta_i \tag{5.40}$$

$$Q = E_t I_t \sin\phi = \frac{X_{ad}}{X_s} E_t i_{fd} \cos\delta_i - \frac{E_t^2}{X_s} \tag{5.41}$$

The relationship between the active and reactive powers for a given field current is a circle centred at $-E_t^2/X_s$ on the Q-axis and with $(X_{ad}/X_s)E_t i_{fd}$ as the radius. Therefore, the effect of the maximum field current rating on the capability of the machine may be illustrated on the P-Q plane as shown in Figure 5.14.

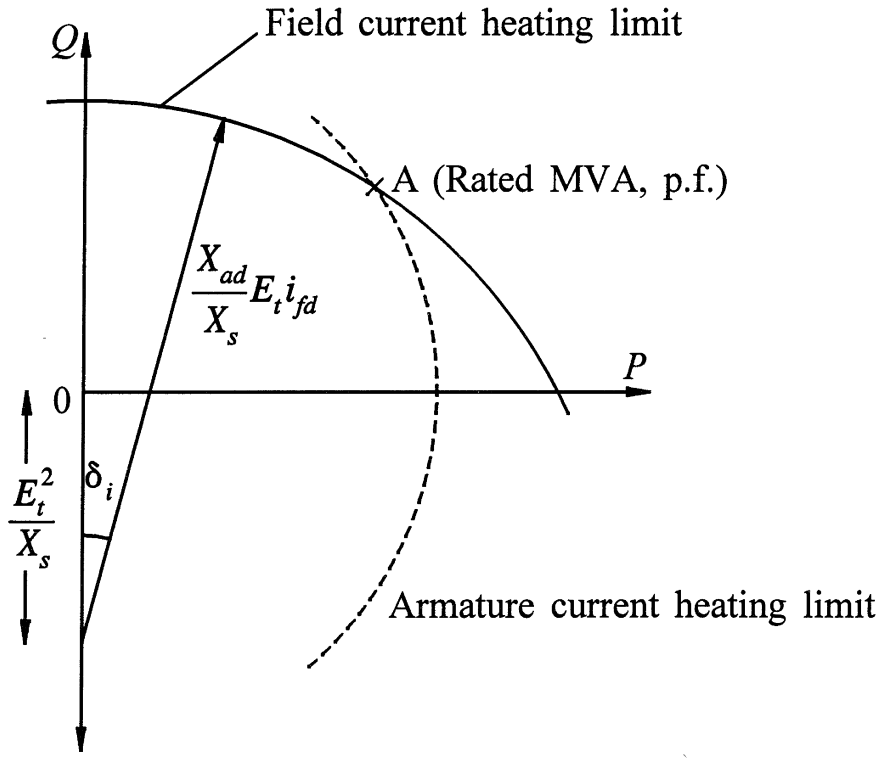

Figure 5.14 Field current heating limit

In any balanced design, the thermal limits for the field and armature intersect at a point A, which represents the machine nameplate MVA and power factor rating.

End region heating limit

The localized heating in the end region of the armature imposes a third limit on the operation of a synchronous machine. As explained below, this limit affects the capability of the machine in the underexcited condition.

Figure 5.15 is a schematic of the end-turn region of a generator. The end-turn leakage flux, as shown in the figure, enters and leaves in a direction perpendicular (axial) to the stator laminations. This causes eddy currents in the laminations, resulting in localized heating in the end region. The high field currents corresponding to the overexcited condition keep the retaining ring saturated, so that end leakage flux is small. However, in the underexcited region the field current is low and the retaining ring is not saturated; this permits an increase in armature end leakage flux [9]. Also, in the underexcited condition, the flux produced by the armature currents adds to the flux produced by the field current; therefore, the end-turn flux enhances the axial flux in the end region and the resulting heating effect may severely limit the generator output, particularly in the case of a round rotor machine. This is illustrated in Figure 5.16, which also includes the limit imposed by the armature current heating effects.

The field current and armature current heating limits when plotted on a P-Q plane depend on the armature voltage. Figure 5.17 shows these limits for a 588 MVA, 22 kV, 0.85 power factor machine at two values of armature voltage, 1.0 pu and 0.95 pu.

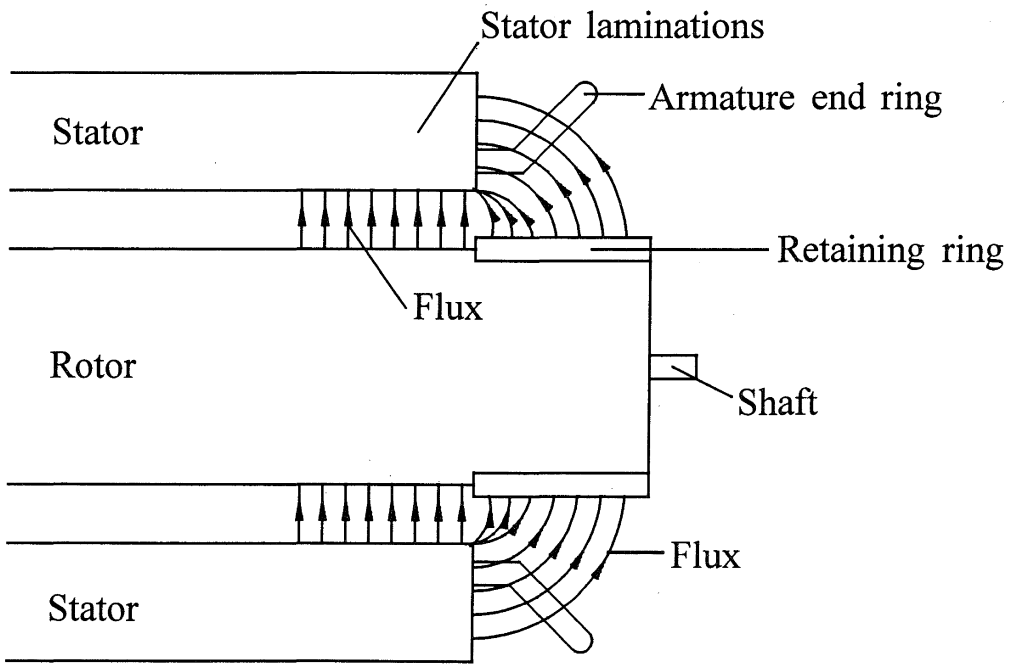

Figure 5.15 Sectional view of end region of a generator

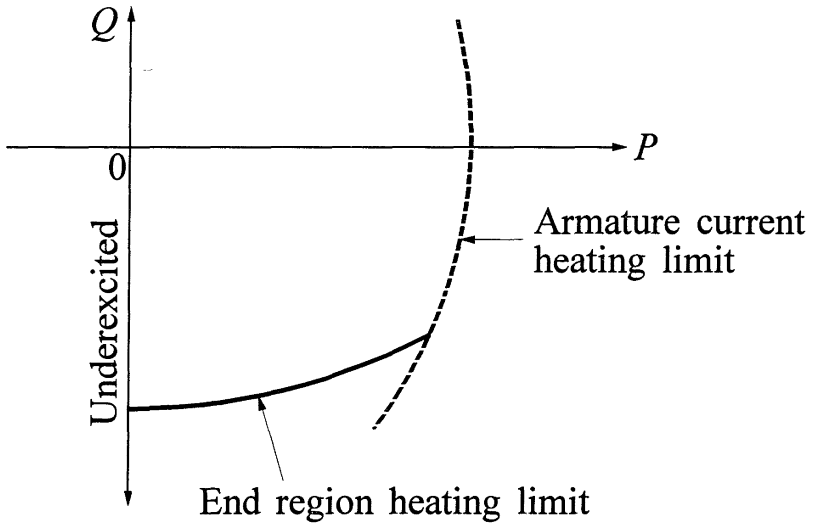

Figure 5.16 End region heating limit

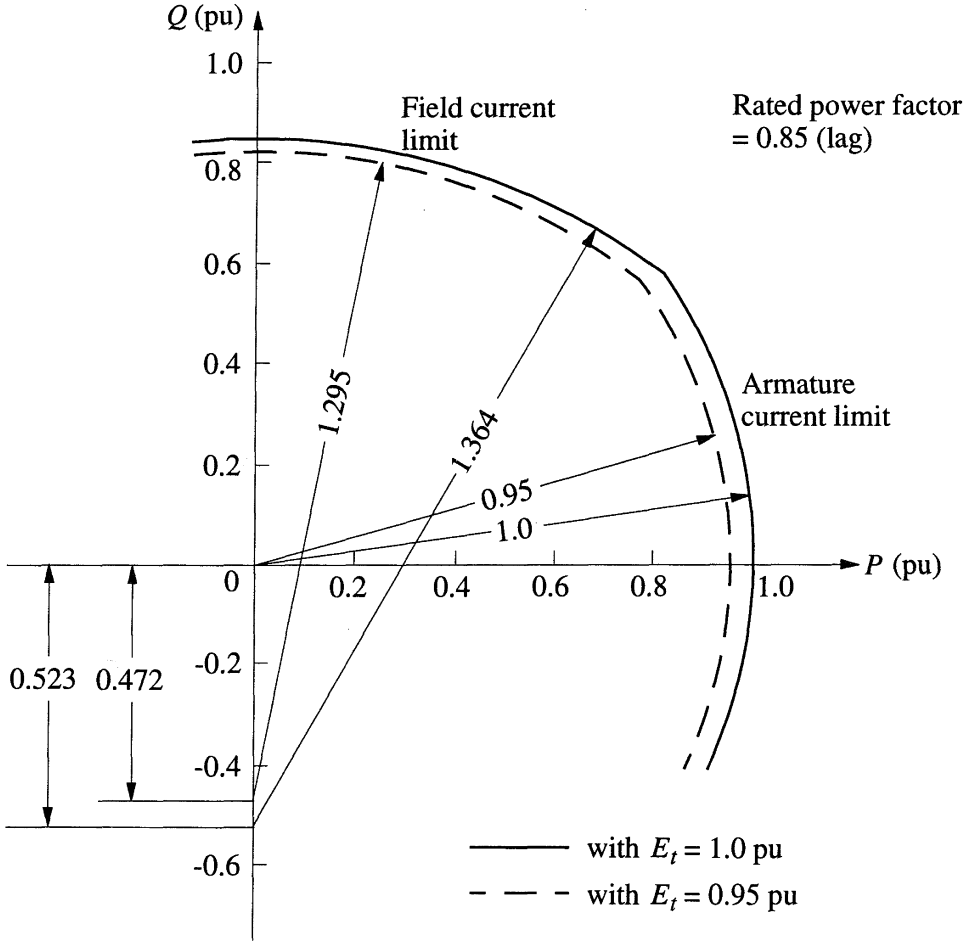

Figure 5.17 Effect of reducing the armature voltage on the generator capability curve

The above limits on the operation of the generator are those imposed by the capabilities of the machine itself and are determined by the design of the machine. Additional limits may be imposed by power system stability limits.

Figure 5.18 shows the reactive capability curves of a 400 MVA hydrogen-cooled steam turbine-driven generator at rated armature voltage. The effectiveness of cooling and hence the allowable machine loading depend on the hydrogen pressure. The base MVA in this case is the rated MVA at 45 PSIG (pounds/square inch gauge) hydrogen pressure. For each pressure, segment AB represents the field heating limit, segment BC the armature heating limit, and segment CD the end region heating limit. Also shown in the figure are the loci of constant power factor.

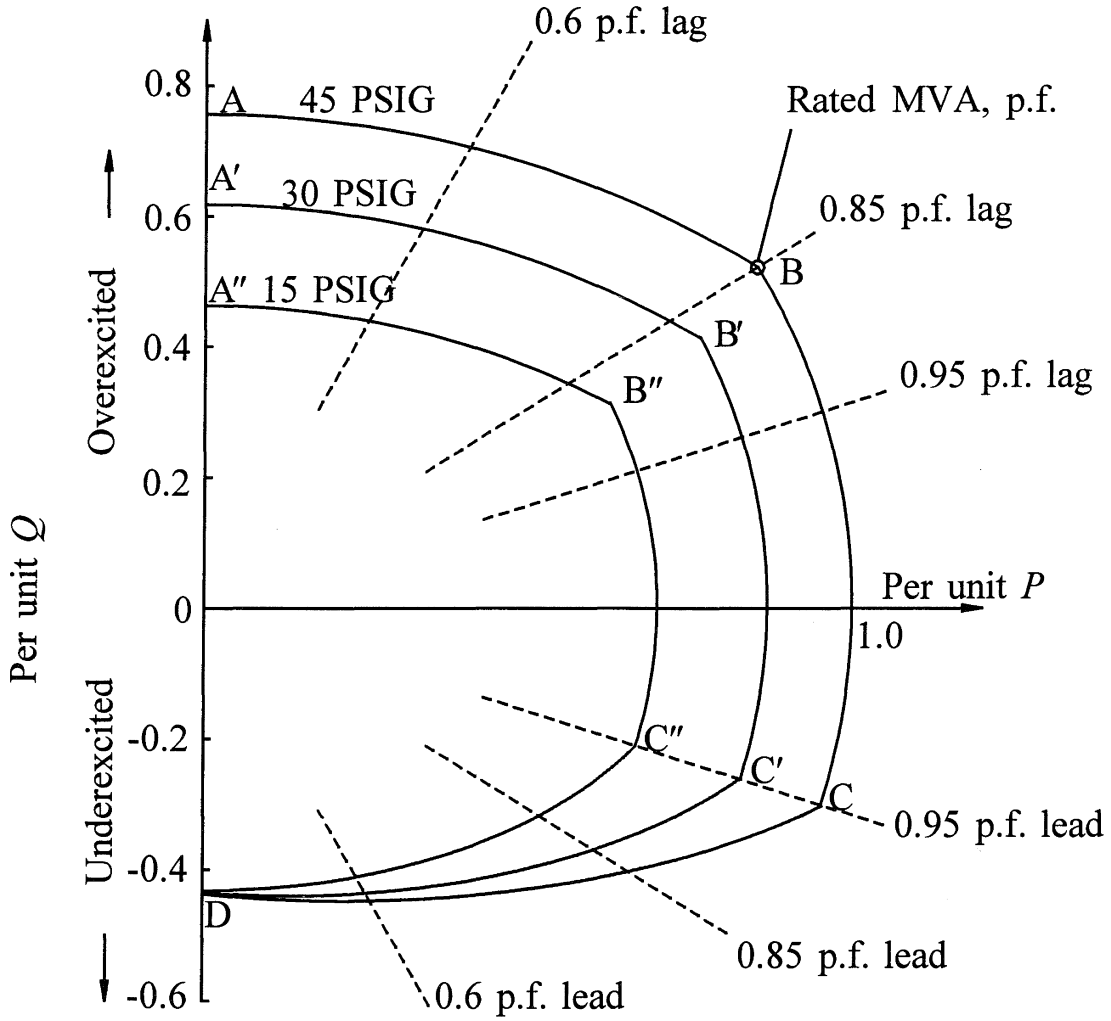

Figure 5.18 Reactive capability curves of a hydrogen-cooled generator at rated voltage

5.4.2 V Curves and Compounding Curves

As discussed in Example 3.4 the curve showing the relation between armature current and field current at a constant terminal voltage and with constant active power output is known as a *V curve*. The V curves for the 400 MVA generator considered

in Section 5.4.1 are shown in Figure 5.19. These are solid curves shown for three values of P (0.5, 0.7, 0.85 pu). The dashed lines are loci of constant power factor and are known as *compounding curves*. Each of these curves shows how field current has to vary in order to maintain a constant power factor.

As illustrated in Example 3.4, V curves and compounding curves can be readily computed using the steady-state equations summarized in Section 3.6.5. They can also be determined approximately by using the equivalent circuit of Figure 5.11(c).

Also shown in Figure 5.19 are the reactive capability limits for one value of hydrogen pressure (45 PSIG). The three segments AB, BC and CD correspond to the field current limit, armature current limit, and end region heating limit, respectively. Since the characteristics shown in Figure 5.19 apply at rated stator terminal voltage, the per unit values of armature current and apparent power output are equal, and hence both are shown along the ordinate. The field current plotted along the abscissa is the normalized value, with 1.0 pu representing the field current corresponding to rated MVA output and power factor.

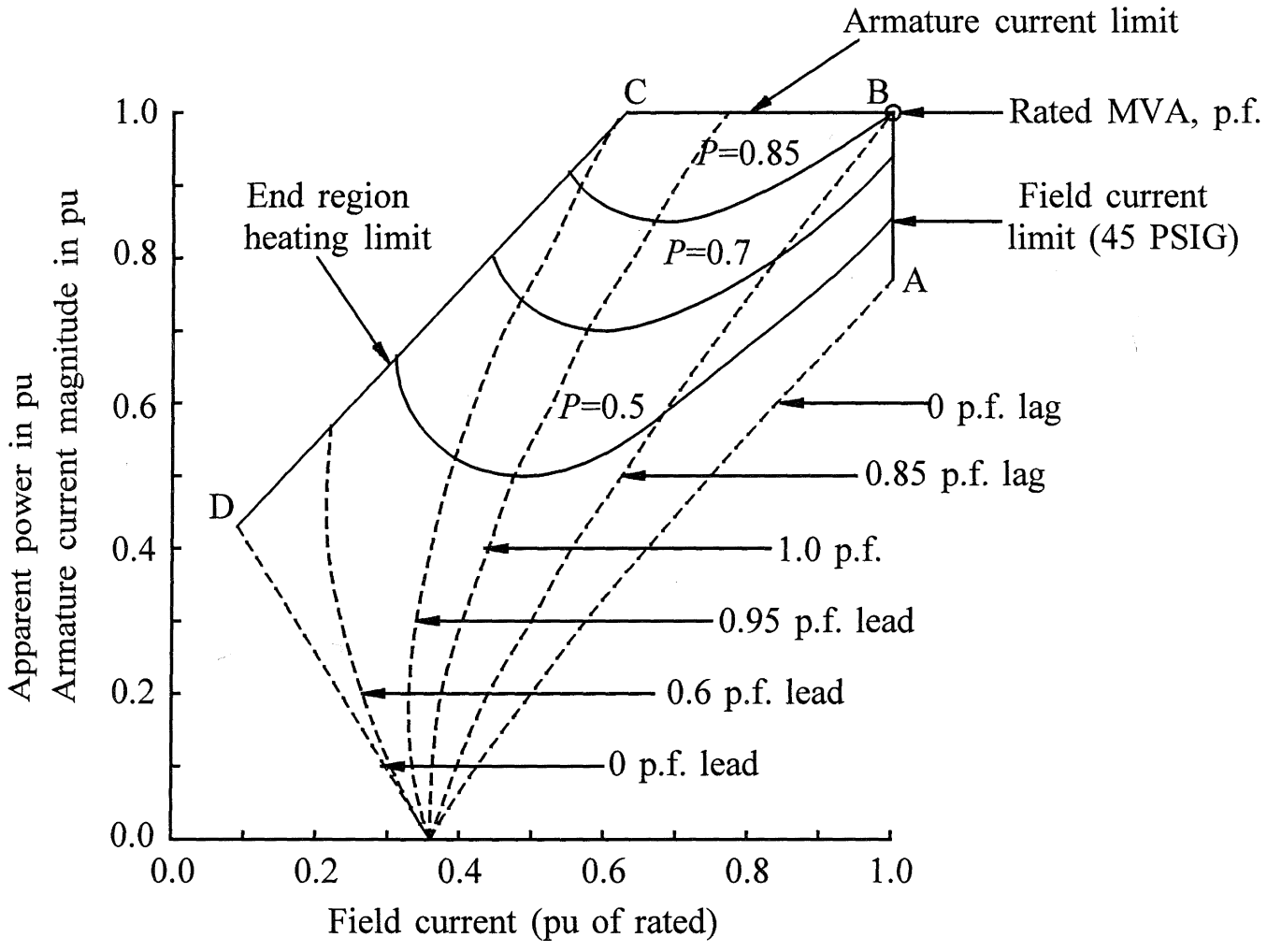

Figure 5.19 The V curves and compounding curves for a generator at rated armature voltage

REFERENCES

[1] Kundur Prabhashankar, "Digital Simulation and Analysis of Power System Dynamic Performance," Ph.D. thesis, University of Toronto, May 1967.

[2] Kundur Prabhashankar and W. Janischewskyj, "Digital Simulation and Analysis of Power System Dynamic Performance - Effects of Synchronous Machine Amortisseur Circuits and Control Mechanisms," Paper CP 94-PWR, presented at the IEEE Winter Power Meeting, January/February 1968.

[3] R.G. Harley and B. Adkins, "Calculation of the Angular Back Swing Following a Short Circuit of a Loaded Alternator," *Proc. IEE*, Vol. 117, No. 2, pp. 377-386, 1970.

[4] G. Shackshaft, "Effect of Oscillatory Torque on the Movement of Generator Rotors," *Proc. IEE*, Vol. 117, No. 10, pp. 1969-1974, 1970.

[5] E.W. Kimbark, *Power System Stability, Vol. III: Synchronous Machines*, John Wiley & Sons, 1956.

[6] D.B. Mehta and B. Adkins, "Transient Torque and Load Angle of a Synchronous Generator Following Several Types of System Disturbance," *Proc. IEE*, Vol. 107A, pp. 61-74, 1960.

[7] G. Kron, Discussion of paper by R.H. Park, "Two-Reaction Theory of Synchronous Machines - Part II," *AIEE Trans.*, Vol. 52, pp. 352-355, June 1933.

[8] D.N. Ewart and R.P. Schulz, "Face Multi-machine Power System Simulator Program," *Proc. PICA Conference*, pp. 133-153, May 1969.

[9] S.B. Farnham and R.W. Swartnout, "Field Excitation in Relation to Machine and System Operation," *AIEE Trans.*, pp. 1215-1223, December 1953.

Chapter 6

AC Transmission

This chapter will review the characteristics and modelling of ac transmission elements and develop methods of power flow analysis in transmission systems.

The focus is on those aspects of the transmission system characteristics that affect system stability and voltage control. Specifically, the objectives are as follows:

(a) To develop performance equations and models for transmission lines;

(b) To examine the power transfer capabilities of transmission lines as influenced by voltage, reactive power, thermal, and system stability considerations;

(c) To develop models for representation of two-winding, three-winding, and phase-shifting transformers;

(d) To examine factors influencing the flow of active power and reactive power through transmission networks; and

(e) To describe analytical techniques for the analysis of power flow in transmission systems.

The above require consideration of balanced steady-state operation of the transmission system. As such, we will model and analyze the performance of transmission elements in terms of their single-phase equivalents.

6.1 TRANSMISSION LINES

Electrical power is transferred from generating stations to consumers through overhead lines and cables.

Overhead lines are used for long distances in open country and rural areas, whereas cables are used for underground transmission in urban areas and for underwater crossings. For the same rating, cables are 10 to 15 times more expensive than overhead lines and they are therefore only used in special situations where overhead lines cannot be used; the distances in such applications are short.

6.1.1 Electrical Characteristics

(a) Overhead lines

A transmission line is characterized by four parameters: series resistance R due to the conductor resistivity, shunt conductance G due to leakage currents between the phases and ground, series inductance L due to magnetic field surrounding the conductors, and shunt capacitance C due to the electric field between conductors.

Detailed derivations from first principles for the line parameters can be found in standard books on power systems [1-7]. References 8 and 9 provide data related to transmission line configurations used in practice. Here, we will briefly summarize salient points relating to line parameters.

Series Resistance (R). The resistances of lines accounting for stranding and skin effect are determined from manufacturers' tables.

Shunt Conductance (G). The shunt conductance represents losses due to leakage currents along insulator strings and corona. In power lines, its effect is small and usually neglected.

Series Inductance (L). The line inductance depends on the partial flux linkages within the conductor cross section and external flux linkages. For overhead lines, the inductances of the three phases are different from each other unless the conductors have equilateral spacing, a geometry not usually adopted in practice. The inductances of the three phases with non-equilateral spacing can be equalized by transposing the lines in such a way that each phase occupies successively all three possible positions.

For a transposed three-phase line, the inductance per phase is [1]

$$L = 2\times10^{-7}\ln\frac{D_{eq}}{D_s} \qquad \text{H/m} \tag{6.1}$$

In the above equation, D_s is the self geometric mean distance, taking into account the conductor composition, stranding, and bundling; it is also called the geometric mean radius. And D_{eq} is the geometric mean of the distances between the conductors of the three phases *a, b,* and *c*:

$$D_{eq} = (d_{ab}d_{bc}d_{ca})^{1/3} \tag{6.2}$$

Shunt Capacitance (C). The potential difference between the conductors of a transmission line causes the conductors to be charged; the charge per unit of potential difference is the capacitance between conductors. When alternating voltages are applied to the conductors, a charging current flows due to alternate charging and discharging of the capacitances. For a three-phase transposed line, the capacitance of each phase to neutral is [1]

$$C = \frac{2\pi k}{\ln(D_{eq}/r)} \quad \text{F/m} \tag{6.3}$$

where r is the conductor radius, D_{eq} is given by Equation 6.2, and k is the permittivity of the dielectric medium. For parallel-circuit lines, the "modified geometric mean distance" of the conductors of the same phase replaces r in Equation 6.3 [1].

The earth presents an equipotential surface and will hence influence the capacitance per phase. This can be accounted for by using the concept of "images" [1-5].

(b) Underground cables [3,4,6,7]

Underground cables have the same basic parameters as overhead lines: series resistance and inductance; shunt capacitance and conductance.

However, the values of the parameters and hence the characteristic of cables differ significantly from those of overhead lines for the following reasons:

1. The conductors in a cable are much closer to each other than are the conductors of overhead lines.

2. The conductors in a cable are surrounded by metallic bodies such as shields, lead or aluminium sheets, and steel pipes.

3. The insulating material between conductors in a cable is usually impregnated paper, low-viscosity oil, or an inert gas.

6.1.2 Performance Equations

In the previous section, we identified the parameters of a transmission line per unit length. These are distributed parameters; that is, the effects represented by the parameters are distributed throughout the length of the line.

If the line is assumed transposed, we can analyze the line performance on a per-phase basis. Figure 6.1 shows the relationship between current and voltage along one phase of the line in terms of the distributed parameters, with

$z = R + j\omega L$ = series impedance per unit length/phase
$y = G + j\omega C$ = shunt admittance per unit length/phase
l = length of the line

The voltages and currents shown are phasors representing sinusoidal time-varying quantities.

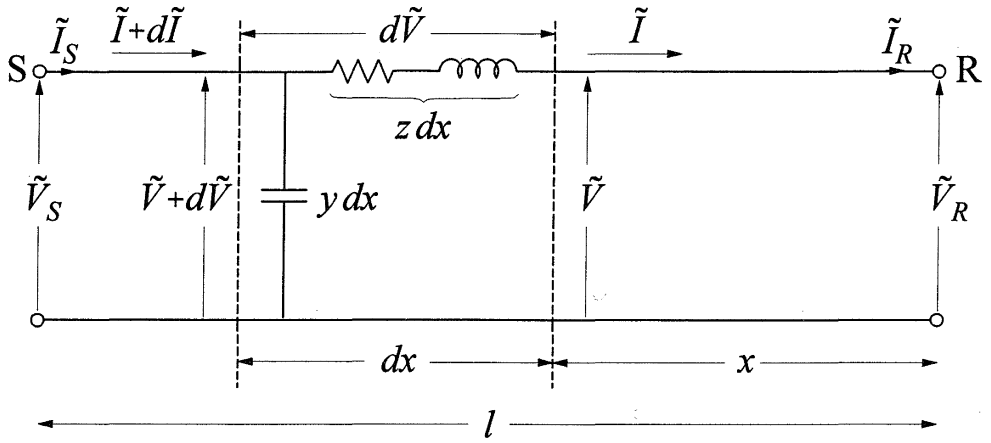

Figure 6.1 Voltage and current relationship of a distributed parameter line

Consider a differential section of the line of length dx at a distance x from the receiving end. The differential voltage across the elemental length is given by

$$d\tilde{V} = \tilde{I}(z\,dx)$$

Hence,

$$\frac{d\tilde{V}}{dx} = \tilde{I}z \tag{6.4}$$

The differential current flowing into the shunt admittance is

$$d\tilde{I} = \tilde{V}(y\,dx)$$

Hence,

$$\frac{d\tilde{I}}{dx} = \tilde{V}y \tag{6.5}$$

Differentiating Equations 6.4 and 6.5 with respect to x, we obtain

$$\frac{d^2\tilde{V}}{dx^2} = z\frac{d\tilde{I}}{dx} = yz\tilde{V} \tag{6.6}$$

and

$$\frac{d^2\tilde{I}}{dx^2} = y\frac{d\tilde{V}}{dx} = yz\tilde{I} \tag{6.7}$$

We will establish the boundary conditions by assuming that voltage V_R and current I_R are known at the receiving end (x=0). The general solution of Equations 6.6 and 6.7 for voltage and current at a distance x from the receiving end is

$$\tilde{V} = \frac{\tilde{V}_R+Z_C\tilde{I}_R}{2}e^{\gamma x} + \frac{\tilde{V}_R-Z_C\tilde{I}_R}{2}e^{-\gamma x} \tag{6.8}$$

$$\tilde{I} = \frac{\tilde{V}_R/Z_C+\tilde{I}_R}{2}e^{\gamma x} - \frac{\tilde{V}_R/Z_C-\tilde{I}_R}{2}e^{-\gamma x} \tag{6.9}$$

where

$$Z_C = \sqrt{z/y} \tag{6.10}$$

$$\gamma = \sqrt{yz} = \alpha + j\beta \tag{6.11}$$

The constant Z_C is called the *characteristic impedance* and γ is called the *propagation constant.*

The constants γ and Z_C are complex quantities. The real part of the propagation constant γ is called the *attenuation constant* α, and the imaginary part the *phase constant* β. Thus the exponential term $e^{\gamma x}$ may be expressed as follows:

$$e^{\gamma x} = e^{(\alpha+j\beta)x} = e^{\alpha x}(\cos\beta x + j\sin\beta x) \tag{6.12}$$

Therefore, the first term in Equation 6.8 increases in magnitude and advances in phase as the distance from the receiving end increases. This term is called the *incident voltage.*

The expanded form of the second exponential term is

$$e^{-\gamma x} = e^{-\alpha x}(\cos\beta x - j\sin\beta x) \tag{6.13}$$

As a result, the second term in Equation 6.8 decreases in magnitude and is retarded in phase from the receiving end toward the sending end. It is called the *reflected voltage*.

At any point along the line, the voltage is equal to the sum of the incident and reflected components at that point. Since Equation 6.9 is similar to Equation 6.8, the current is also composed of incident and reflected components.

If a line is terminated in its characteristic impedance Z_C, V_R is equal to $Z_C I_R$, and there is no reflected wave. Such a line is called a *flat line* or an *infinite line* (since a line of infinite length cannot have a reflected wave). Power lines, unlike communication lines, are not usually terminated in their characteristic impedances.

From Equations 6.12 and 6.13, we see that the incident and reflected components of voltage and current at any instant in time appear as sinusoidal curves or waves along the length of the line. In addition to this variation, the voltage and current components at any point along the line vary in time, since V_R and I_R in Equations 6.8 and 6.9 are phasors representing sinusoidal time-varying quantities. Thus, the incident and reflected components of voltage and current represent travelling waves. They are similar to the travelling waves in water. The total instantaneous voltage and current along the transmission line are not travelling, but they can each be interpreted as the sum of two such travelling waves.

For typical power lines, G is practically zero and $R \ll \omega L$. Therefore,

$$Z_C = \sqrt{\frac{R+j\omega L}{j\omega C}} \approx \sqrt{\frac{L}{C}}\left(1-j\frac{R}{2\omega L}\right) \tag{6.14}$$

$$\gamma = \sqrt{(R+j\omega L)j\omega C} \approx j\omega\sqrt{LC}\left(1-j\frac{R}{2\omega L}\right) \tag{6.15}$$

If losses are completely neglected, Z_C is a real number (i.e., a pure resistance), and γ is an imaginary number.

For a *lossless line*, Equations 6.8 and 6.9 simplify to

$$\tilde{V} = \tilde{V}_R \cos\beta x + jZ_C\tilde{I}_R \sin\beta x \tag{6.16}$$

and

$$\tilde{I} = \tilde{I}_R \cos\beta x + j(\tilde{V}_R/Z_C)\sin\beta x \tag{6.17}$$

Thus, the voltage and current vary harmonically along the line length. A full cycle of voltage and current in space along the line length corresponds to 2π radians. The length corresponding to one full cycle is called the *wavelength* λ. If β is the phase shift in radians per meter, the wavelength in meters is

$$\lambda = \frac{2\pi}{\beta} \tag{6.18}$$

6.1.3 Natural or Surge Impedance Loading

Since G is negligible and R is small, high-voltage lines are assumed to be lossless when we are dealing with lightning and switching surges. Hence, the characteristic impedance Z_C with losses neglected is commonly referred to as the *surge impedance*. It is equal to $\sqrt{L/C}$ and has the dimension of a pure resistance.

The power delivered by a transmission line when it is terminated by its surge impedance is known as the *natural load* or *surge impedance load* (SIL):

$$\text{SIL} = \frac{V_0^2}{Z_C} \quad \text{W} \tag{6.19}$$

where V_0 is the rated voltage of the line. If V_0 is the line-to-neutral voltage, SIL given by the above equation is the per-phase value; if V_0 is the line-to-line value, then SIL is the three-phase value.

From Equations 6.16 and 6.17, the voltage and current along the length of a lossless line at SIL are given by

$$\tilde{V} = \tilde{V}_R e^{\gamma x} \tag{6.20}$$

and

$$\tilde{I} = \tilde{I}_R e^{\gamma x} \tag{6.21}$$

where $\gamma = j\beta = j\omega\sqrt{LC}$.

At SIL, transmission lines (lossless) exhibit the following special characteristics:

- $\tilde{V}$ and $\tilde{I}$ have constant amplitude along the line.
- $\tilde{V}$ and $\tilde{I}$ are in phase throughout the length of the line.
- The phase angle between the sending end and receiving end voltages (currents) is equal to βl (see Figure 6.2).

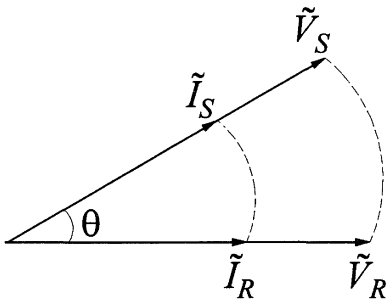

$\theta = \beta l$
l = line length

Figure 6.2 Sending end and receiving end voltage and current relationships of a lossless line at SIL

At the natural load, the reactive power generated by C is equal to the reactive power absorbed by L, for each incremental length of the line. Hence, no reactive power is absorbed or generated at either end of the line, and the voltage and current profiles are flat. This is an optimum condition with respect to control of voltage and reactive power.

As we will see in subsequent sections of this chapter, the natural or surge impedance loading of a line serves as a convenient *reference quantity* for evaluating and expressing its capability.

6.1.4 Equivalent Circuit of a Transmission Line

Equations 6.8 and 6.9 provide a complete description of the performance of transmission lines. However, for purposes of analysis involving interconnection with other elements of the system, it is more convenient to use equivalent circuits which represent the performance of the lines only as seen from their terminals.

By letting $x=l$ in Equation 6.8 and rearranging, we have

$$\begin{aligned}\tilde{V}_S &= \tilde{V}_R\frac{e^{\gamma l}+e^{-\gamma l}}{2}+Z_C\tilde{I}_R\frac{e^{\gamma l}-e^{-\gamma l}}{2} \\ &= \tilde{V}_R\cosh(\gamma l)+Z_C\tilde{I}_R\sinh(\gamma l)\end{aligned} \tag{6.22}$$

Similarly from Equation 6.9, we have

$$\tilde{I}_S = \tilde{I}_R\cosh(\gamma l)+\frac{\tilde{V}_R}{Z_C}\sinh(\gamma l) \tag{6.23}$$

A π circuit with *lumped* parameters, as shown in Figure 6.3, can be used to represent the above relationships.

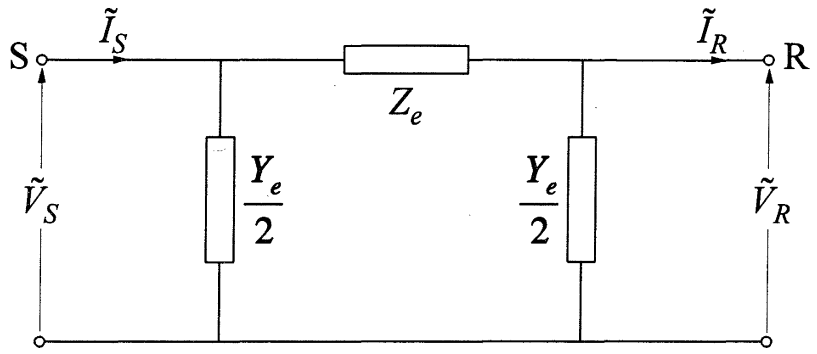

Figure 6.3 Equivalent π circuit of a transmission line

From the equivalent circuit, the sending end voltage is

$$\begin{aligned}\tilde{V}_s &= Z_e\left(\tilde{I}_R+\frac{Y_e}{2}\tilde{V}_R\right)+\tilde{V}_R \\ &= \left(\frac{Z_eY_e}{2}+1\right)\tilde{V}_R+Z_e\tilde{I}_R\end{aligned} \tag{6.24}$$

Comparing Equation 6.24 with 6.22, we have

$$Z_e = Z_C\sinh(\gamma l) \tag{6.25}$$

and

$$\frac{Z_eY_e}{2}+1 = \cosh(\gamma l)$$

Therefore,

$$\begin{aligned}\frac{Y_e}{2} &= \frac{1}{Z_C}\frac{\cosh(\gamma l)-1}{\sinh(\gamma l)} \\ &= \frac{1}{Z_C}\tanh\left(\frac{\gamma l}{2}\right)\end{aligned} \tag{6.26}$$

Equations 6.25 and 6.26 give the elements of the equivalent circuit. These elements reflect the voltage and current relationships given by Equations 6.22 and 6.23 exactly.

Nominal π equivalent circuit

If $\gamma l \ll 1$, the expressions for Z_e and Y_e may be approximated as follows:

$$\begin{aligned} Z_e &= Z_C \sinh(\gamma l) \\ &\approx Z_C(\gamma l) \\ &\approx zl = Z \end{aligned} \tag{6.27}$$

and

$$\begin{aligned} \frac{Y_e}{2} &= \frac{1}{Z_C}\tanh\left(\frac{\gamma l}{2}\right) \\ &\approx \frac{1}{Z_C}\frac{\gamma l}{2} \\ &\approx \frac{yl}{2} = \frac{Y}{2} \end{aligned} \tag{6.28}$$

In Equations 6.27 and 6.28, Z and Y represent the total series impedance (zl) and total shunt admittance (yl), respectively. The resultant circuit model is called the *nominal* π equivalent circuit. Generally, the approximation is good if

l<10,000/f km (170 km at 60 Hz) for overhead lines;
l<3,000/f km (50 km at 60 Hz) for underground cables.

Classification of line length

Overhead lines may be classified according to length, based on the approximations justified in their modelling:

(a) Short lines: lines shorter than about 80 km (50 mi). They have negligible shunt capacitance, and may be represented by their series impedance.

(b) Medium-length lines: lines with lengths in the range of 80 km to about 200 km (125 mi). They may be represented by the nominal π equivalent circuit.

(c) Long lines: lines longer than about 200 km. For such lines the distributed effects of the parameters are significant. They need to be represented by the equivalent π circuit. Alternatively, they may be represented by cascaded sections of shorter lengths, with each section represented by a nominal π equivalent.

6.1.5 Typical Parameters

(a) Overhead lines

Table 6.1 gives typical parameters of overhead lines of nominal voltage ranging from 230 kV to 1,100 kV.

Table 6.1 Typical overhead transmission line parameters

Nominal Voltage	230 kV	345 kV	500 kV	765 kV	1,100 kV
R (Ω/km)	0.050	0.037	0.028	0.012	0.005
$x_L=\omega L$ (Ω/km)	0.488	0.367	0.325	0.329	0.292
$b_C=\omega C$ (μs/km)	3.371	4.518	5.200	4.978	5.544
α (nepers/km)	0.000067	0.000066	0.000057	0.000025	0.000012
β (rad/km)	0.00128	0.00129	0.00130	0.00128	0.00127
Z_C (Ω)	380	285	250	257	230
SIL (MW)	140	420	1000	2280	5260
Charging MVA/km $= V_0^2 b_C$	0.18	0.54	1.30	2.92	6.71

Notes:
1. Rated frequency is assumed to be 60 Hz.
2. Bundled conductors used for all lines listed, except for the 230 kV line.
3. R, x_L, and b_C are per-phase values.
4. SIL and charging MVA are three-phase values.

We see that the surge impedance lies within the range of 230 to 290 Ω for EHV and UHV overhead lines. For a 230 kV line, it is about 380 Ω. The value of β is practically the same for all lines. This is to be expected since $\sqrt{LC}$ is the propagation velocity of electromagnetic waves. For overhead lines it is slightly slower than the velocity of light (300,000 km/s). At 60 Hz, β is nearly equal to 1.27×10^{-3} rad/km. The corresponding wavelength ($\lambda=2\pi/\beta$) is approximately 5,000 km.

An easy-to-remember approximate equivalent circuit applicable to an overhead line of 160 km (100 mi) length and of any voltage rating is shown in Figure 6.4.

For example, for the 500 kV line whose parameters are listed in Table 6.1, with a line length of 160 km, we have

$$X_L = 160\times0.325 = 52.0\ \Omega$$

and

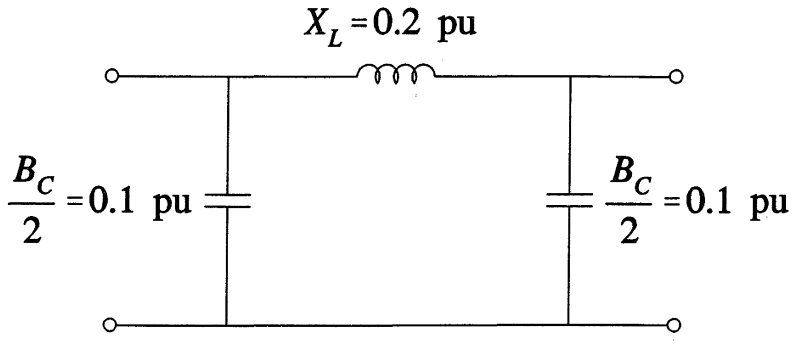

$X_L = \omega Ll$
$B_C = \omega Cl$
$\omega = 2\pi 60$
Base $Z = Z_C$
l = line length = 160 km

Figure 6.4 Approximate equivalent circuit for an overhead line of any voltage rating, with parameters in per unit of surge impedance

$$B_C = 160 \times 5.20 \times 10^{-6} = 8.32 \times 10^{-4} \text{ siemens}$$

Expressed in per unit of Z_C (250 Ω),

$$X_L = 52.0/250 = 0.208 \text{ pu}$$
$$B_C = 8.32 \times 10^{-4} \times 250 = 0.208 \text{ pu}$$

(b) Underground cables

Table 6.2 gives typical parameters of cables. Two types of cables are included: direct-buried paper-insulated lead-covered (PILC) and high-pressure pipe type (PIPE), with nominal voltages of 115, 230, and 500 kV.

Table 6.2 Typical cable parameters

Nominal Voltage	**115 kV**	**115 kV**	**230 kV**	**230 kV**	**500 kV**
Cable Type	PILC	PIPE	PILC	PIPE	PILC
R (Ω/km)	0.0590	0.0379	0.0277	0.0434	0.0128
$x_L = \omega L$ (Ω/km)	0.3026	0.1312	0.3388	0.2052	0.2454
$b_C = \omega C$ (μs/km)	230.4	160.8	245.6	298.8	96.5
α (nepers/km)	0.00081	0.000656	0.000372	0.000824	0.000127
β (rad/km)	0.00839	0.00464	0.00913	0.00787	0.00487
Z_C (Ω)	36.2	28.5	37.1	26.2	50.4
SIL (MW)	365	464	1426	2019	4960
Charging MVA/km $= V_0^2 b_C$	3.05	2.13	13.0	15.8	24.1

From the table we see that underground cables have very high shunt capacitance. The characteristic impedance Z_C of a cable is about one-tenth to one-fifth of that for an overhead line of the same voltage rating.

6.1.6 Performance Requirements of Power Transmission Lines

In Section 6.1.2, we developed the performance equations of transmission lines. The basic equations apply to communication lines as well as power lines. However, the performance requirements of power and communication lines are significantly different.

Communication lines transmit signals of many relatively high frequencies and are very long compared to the wavelengths involved. Fidelity and strength of the signals at the receiving end are the primary considerations. Consequently, termination at the characteristic impedance of the line is the only practical way of operation to avoid distortion on the line. The energy associated with communication lines is small; consequently, efficiency is of minor interest.

In contrast, efficiency, economy and reliability of supply are factors of prime importance in the case of power transmission. There is only one frequency, and distortion is not a problem in the same sense as it is in communication lines. The lengths of most power lines are a fraction of the normal wavelength; hence, the lines can be terminated on equivalent load impedances which are much lower than their characteristic impedances.

If the power line is very long (greater than 500 km), terminating close to the characteristic impedance becomes imperative. To increase power levels that can be transmitted, either the characteristic impedance has to be reduced (by adding compensation) or the transmission voltage has to be increased.

Voltage regulation, *thermal limits*, and *system stability* are the factors that determine the power transmission capability of power lines. In what follows, we will discuss these aspects of power transmission line performance. Wherever appropriate, we will consider a lossless line, as it offers considerable simplicity and a better insight into the performance characteristics of transmission lines.

6.1.7 Voltage and Current Profile under No-Load [3,10]

(a) Receiving end open-circuited

When the receiving end is open, I_R=0. Equations 6.8 and 6.9 then reduce to

$$\tilde{V} = \frac{\tilde{V}_R}{2} e^{\gamma x} + \frac{\tilde{V}_R}{2} e^{-\gamma x} \tag{6.29}$$

$$\tilde{I} = \frac{\tilde{V}_R}{2Z_C} e^{\gamma x} - \frac{\tilde{V}_R}{2Z_C} e^{-\gamma x} \tag{6.30}$$

For a lossless line, $\gamma=j\beta$, and the above two equations simplify to

$$\tilde{V} = \tilde{V}_R \cos(\beta x) \tag{6.31}$$

$$\tilde{I} = j(\tilde{V}_R/Z_C)\sin(\beta x) \tag{6.32}$$

The voltage[1] and current at the sending end are obtained by substituting line length l for x:

$$\begin{aligned} \tilde{E}_S &= \tilde{V}_R \cos\beta l \\ &= \tilde{V}_R \cos\theta \end{aligned} \tag{6.33}$$

and

$$\begin{aligned} \tilde{I}_S &= j(\tilde{V}_R/Z_C)\sin\theta \\ &= j(\tilde{E}_S/Z_C)\tan\theta \end{aligned} \tag{6.34}$$

where $\theta=\beta l$. The angle θ is referred to as the *electrical length* or the *line angle*, and is expressed in radians.

Based on Equations 6.31, 6.32 and 6.33, the line voltage and current can be expressed in terms of sending end voltage E_S as follows:

$$\tilde{V} = \tilde{E}_S \frac{\cos\beta x}{\cos\theta} \tag{6.35}$$

$$\tilde{I} = j\frac{\tilde{E}_S}{Z_C}\frac{\sin\beta x}{\cos\theta} \tag{6.36}$$

As an example, let us consider the voltage and current profiles for a 300 km, 500 kV line with the sending voltage at rated value and the receiving end open-circuited. The line is assumed to be lossless with $\beta=0.0013$ rad/km and $Z_C=250\ \Omega$.

The electrical length of the line is

$$\begin{aligned} \theta &= 300\times0.0013 = 0.39 \text{ rad} \\ &= 22.3^\circ \end{aligned}$$

---

[1] Since the sending end voltage in this case is a controlled voltage, it is denoted by the symbol E, instead of V.

From Equation 6.33,

$$V_R = \frac{1}{\cos 22.3^\circ} = 1.081 \text{ pu}$$

and from Equation 6.34

$$\tilde{I}_S = j(\tilde{E}_S/Z_C)\tan\theta$$

Expressing I_S in per unit with base current equal to that corresponding to the natural load, its magnitude is

$$\begin{aligned} I_S &= E_S \tan\theta \quad \text{pu} \\ &= 1.0 \tan 22.3^\circ \\ &= 0.411 \quad \text{pu} \end{aligned}$$

From Equations 6.35 and 6.36, the voltage and current magnitudes as functions of distance x from the receiving end are given by

$$\begin{aligned} V &= \frac{1.0\cos(0.0013x)}{\cos 22.3^\circ} \\ &= 1.0812\cos(0.0013x) \quad \text{pu} \end{aligned}$$

and

$$\begin{aligned} I &= \frac{1.0\sin(0.0013x)}{\cos 22.3^\circ} \\ &= 1.0812\sin(0.0013x) \quad \text{pu} \end{aligned}$$

The voltage and current profiles are shown in Figure 6.5. The current represents the capacitive charging current of the line, expressed in per unit of current at SIL.

The only line parameter, other than line length, that affects the results of Figure 6.5 is β. Since β is practically the same for overhead lines of all voltage levels (see Table 6.1), the results are universally applicable, not just for a 500 kV line.

The receiving end voltage V_R for the 300 km line is 1.081 pu, that is, 8.1% higher than the sending end voltage. For a 600 km line, the receiving-end open-circuit voltage would be 1.407 pu. A line of about 1,200 km (one quarter wavelength) would have infinitely high receiving end voltage on open-circuit.

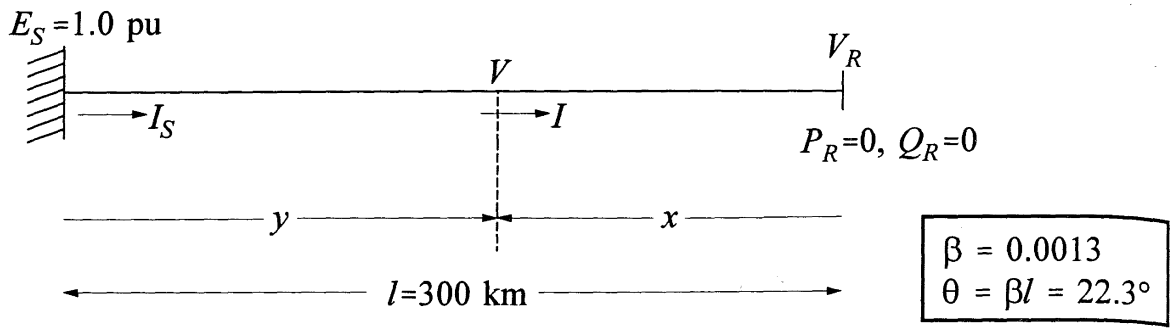

(a) Schematic diagram

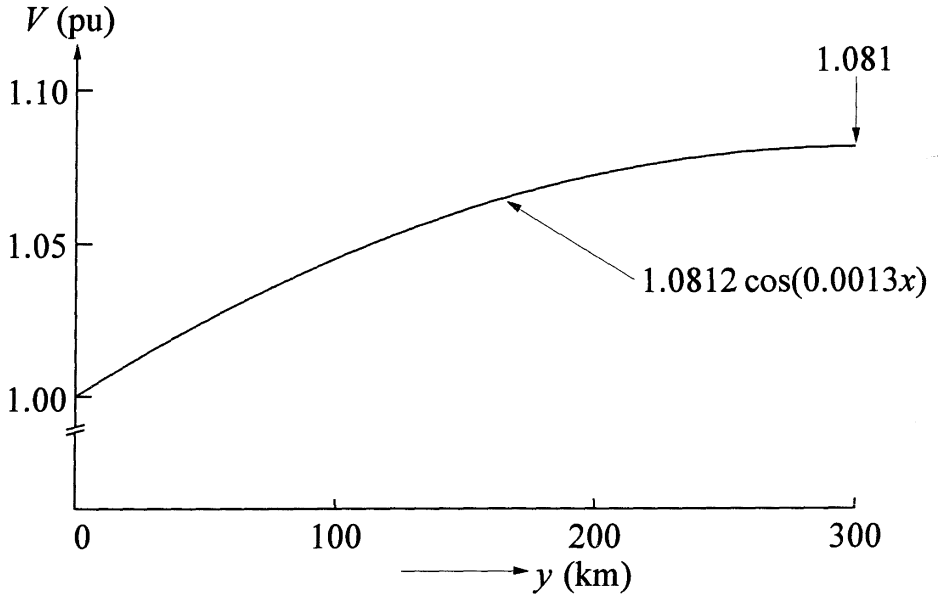

(b) Voltage profile

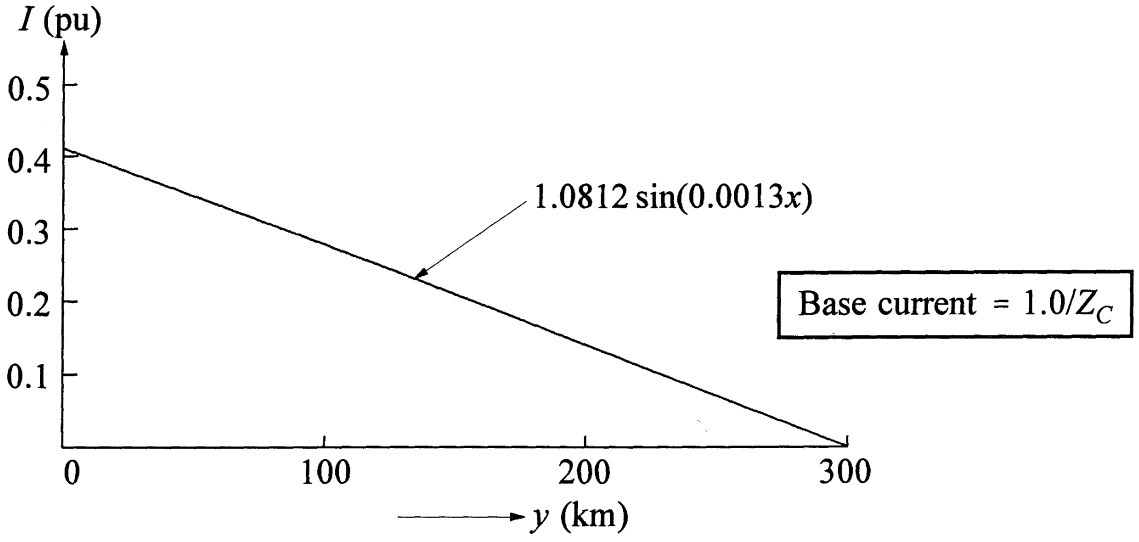

(c) Current profile

Figure 6.5 Voltage and current profiles for a 300 km lossless line with receiving end open-circuited

The rise in voltage at the receiving end on open-circuit is due to the flow of line charging (capacitive) current through line inductance. This phenomenon was first noticed by Ferranti on overhead lines supplying a lightly loaded (and hence highly capacitive) cable network; it is therefore referred to as the *Ferranti effect.*

In the above calculations, the sending end voltage has been assumed to be constant. In practice, following a sudden opening of the line at the receiving end, the sending end voltage will rise due to the capacitive current of the line flowing through the source impedance (mostly inductive reactance). Appropriate forms of reactive power compensation should be provided on long lines to keep the rise in voltage to acceptable levels. This is discussed in Chapter 11.

(b) Line connected to sources at both ends

For simplicity, let us assume that the line is symmetrical; i.e., it is connected to identical sources at the two ends. Let E_S and E_R denote the voltages at the sending end and receiving end, respectively. From Equations 6.8 and 6.9, with $x=l$ and $\theta=\beta l$, we have

$$\tilde{E}_S = \frac{\tilde{E}_R + Z_C \tilde{I}_R}{2} e^{\gamma l} + \frac{\tilde{E}_R - Z_C \tilde{I}_R}{2} e^{-\gamma l} \tag{6.37}$$

Hence,

$$\tilde{I}_R = \frac{2\tilde{E}_S - \tilde{E}_R (e^{\gamma l} + e^{-\gamma l})}{Z_C (e^{\gamma l} - e^{-\gamma l})} \tag{6.38}$$

Substituting the above expression for $\tilde{I}_R$ in Equations 6.8 and 6.9, we have

$$\tilde{V} = \frac{\tilde{E}_S - \tilde{E}_R e^{-\gamma l}}{e^{\gamma l} - e^{-\gamma l}} e^{\gamma x} + \frac{\tilde{E}_R e^{\gamma l} - \tilde{E}_S}{e^{\gamma l} - e^{-\gamma l}} e^{-\gamma x} \tag{6.39}$$

$$\tilde{I} = \frac{\tilde{E}_S - \tilde{E}_R e^{-\gamma l}}{Z_C (e^{\gamma l} - e^{-\gamma l})} e^{\gamma x} - \frac{\tilde{E}_R e^{\gamma l} - \tilde{E}_S}{Z_C (e^{\gamma l} - e^{-\gamma l})} e^{-\gamma x} \tag{6.40}$$

Since $\tilde{E}_S = \tilde{E}_R$, we have

$$\tilde{V} = \frac{\tilde{E}_S - \tilde{E}_S e^{-\gamma l}}{e^{\gamma l} - e^{-\gamma l}} e^{\gamma x} + \frac{\tilde{E}_S e^{\gamma l} - \tilde{E}_S}{e^{\gamma l} - e^{-\gamma l}} e^{-\gamma x} \tag{6.41}$$

$$\tilde{I} = \frac{\tilde{E}_S - \tilde{E}_S e^{-\gamma l}}{Z_C(e^{\gamma l} - e^{-\gamma l})} e^{\gamma x} - \frac{\tilde{E}_S e^{\gamma l} - \tilde{E}_S}{Z_C(e^{\gamma l} - e^{-\gamma l})} e^{-\gamma x} \tag{6.42}$$

For a lossless line, $\gamma = j\beta$. With $\theta = \beta l$, we have

$$\tilde{V} = \tilde{E}_S \frac{\cos\beta(l/2 - x)}{\cos(\theta/2)} \tag{6.43}$$

$$\tilde{I} = -j\frac{\tilde{E}_S}{Z_C} \frac{\sin\beta(l/2 - x)}{\cos(\theta/2)} \tag{6.44}$$

The voltage and current profiles are shown in Figure 6.6 for a 400 km line with $E_S = E_R = 1.0$ pu. The generators at the sending end and receiving end should be capable of absorbing the reactive power due to line charging. If this exceeds the underexcited reactive power capability of the connected generators, compensation may have to be provided.

If E_S and E_R are not equal, the voltage and current profiles are not symmetrical and the highest voltage is not at midpoint, but is nearer to the end with higher voltage.

6.1.8 Voltage-Power Characteristics [4,10]

(a) Radial line with fixed sending end voltage

Corresponding to a load of $P_R + jQ_R$ at the receiving end, we have

$$\tilde{I}_R = \frac{P_R - jQ_R}{\tilde{V}_R^*}$$

From Equation 6.8, with $x = l$, we have

$$\tilde{E}_S = \frac{\tilde{V}_R + Z_C(P_R - jQ_R)/\tilde{V}_R^*}{2} e^{\gamma l} + \frac{\tilde{V}_R - Z_C(P_R - jQ_R)/\tilde{V}_R^*}{2} e^{-\gamma l} \tag{6.45}$$

With $\gamma = j\beta$ (lossless line) and $\theta = \beta l$,

$$\tilde{E}_S = \tilde{V}_R \cos\theta + jZ_C \sin\theta \left(\frac{P_R - jQ_R}{\tilde{V}_R^*} \right) \tag{6.46}$$

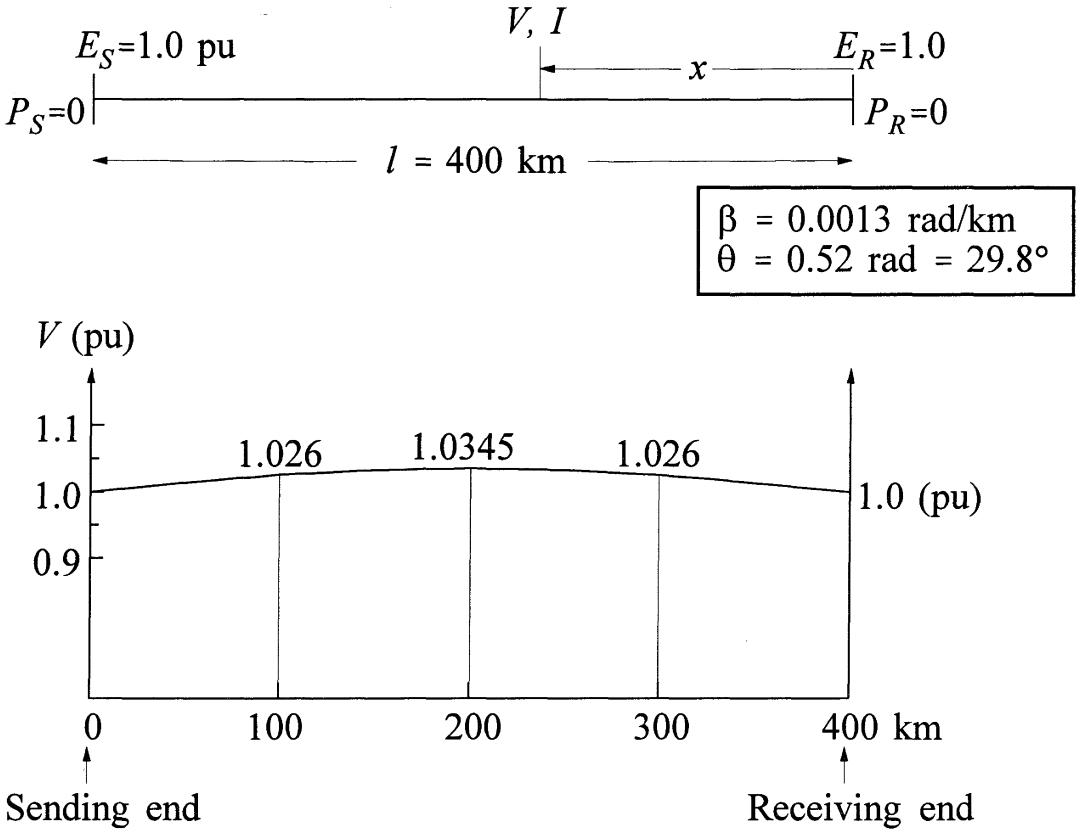

(a) Voltage profile

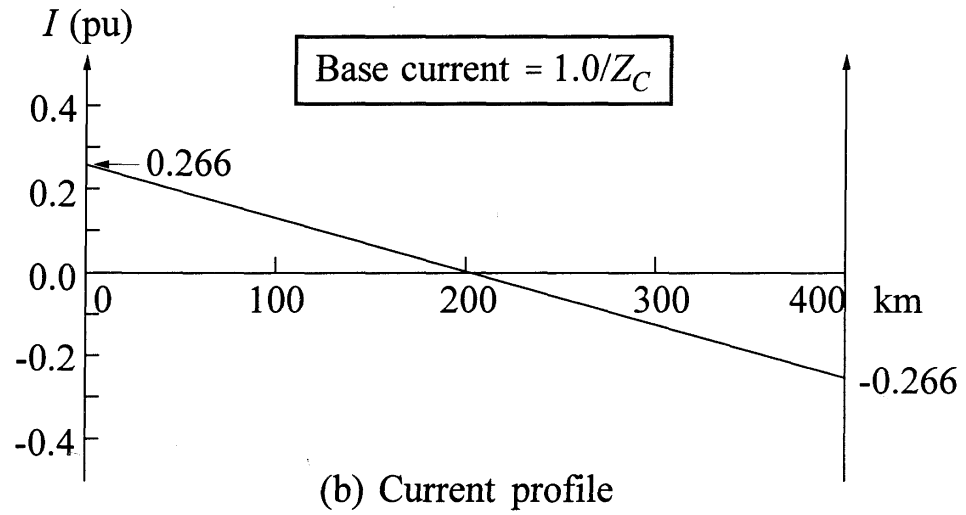

(b) Current profile

Figure 6.6 Voltage and current profile of a 400 km lossless line under no-load

The above equation can be solved for V_R for any given load and sending end voltage. Figure 6.7 shows a typical relationship between the receiving end voltage and load, for a fixed sending end voltage. The results shown are for a 300 km line with E_S=1.0 pu. The constant β for the line is assumed to be 0.0013 rad/km. The load is *normalized* by dividing P_R by P_o, the natural load (SIL), *so that the results are applicable to overhead lines of all voltage levels.* From Figure 6.7, several fundamental properties of ac transmission are evident:

- There is an inherent maximum limit of power that can be transmitted at any load power factor. Obviously, there has to be such a limit since, with E_S constant, the only way to increase power is by lowering the load impedance. This will result in increased current, but decreased V_R and large line losses. Up

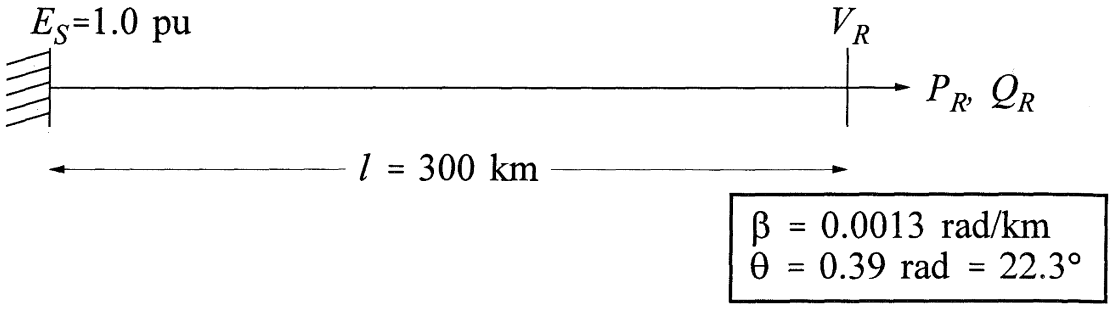

(a) System diagram

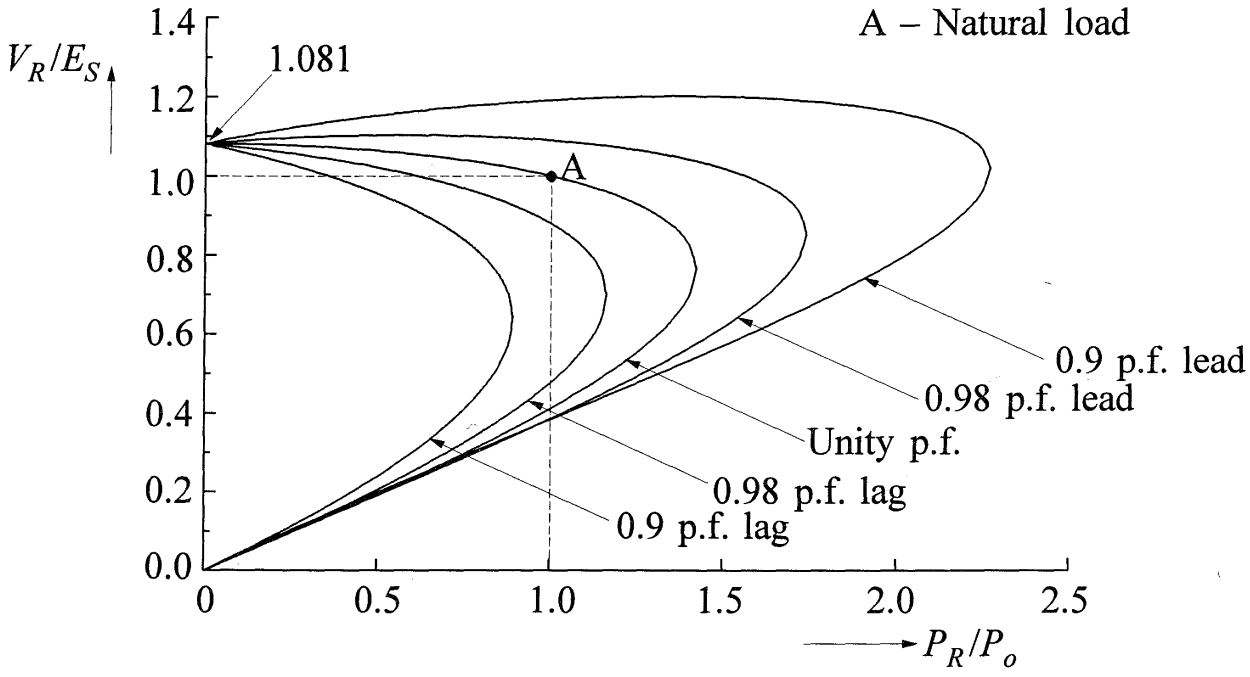

(b) Receiving end voltage versus power characteristic

Figure 6.7 Voltage-power characteristics of a 300 km lossless radial line

to a certain point the increase of current dominates the decrease of V_R, thereby resulting in an increased P_R. Finally, the decrease in V_R is such that the trend reverses.

- Any value of power below the maximum can be transmitted at two different values of V_R. The normal operation is at the upper value, within narrow limits around 1.0 pu. At the lower voltage, the current is higher and may exceed thermal limits. The feasibility of operation at the lower voltage also depends on load characteristics and may lead to voltage instability. This will be discussed in Chapter 14.

- The load power factor has a significant influence on V_R and the maximum power that can be transmitted. The power limit and V_R are lower with lagging power factors (inductive load, Q_R positive). With leading power factors (capacitive load, Q_R negative), the top portion of the voltage profile tends to be flatter and maximum power is higher. This means that the receiving end voltage can be regulated by the addition of shunt capacitive compensation.

The effect of line length is depicted in Figure 6.8, which shows the performance of lines with lengths of 200, 300, 400, 600 and 800 km with *unity power factor* load. The results show that, for longer lines, V_R is extremely sensitive to variations in P_R. For lines longer than 600 km (θ>45°), V_R at natural load is the lower of the two voltages which satisfy the Equation 6.46. Such operation is likely to be voltage unstable (see Chapter 14).

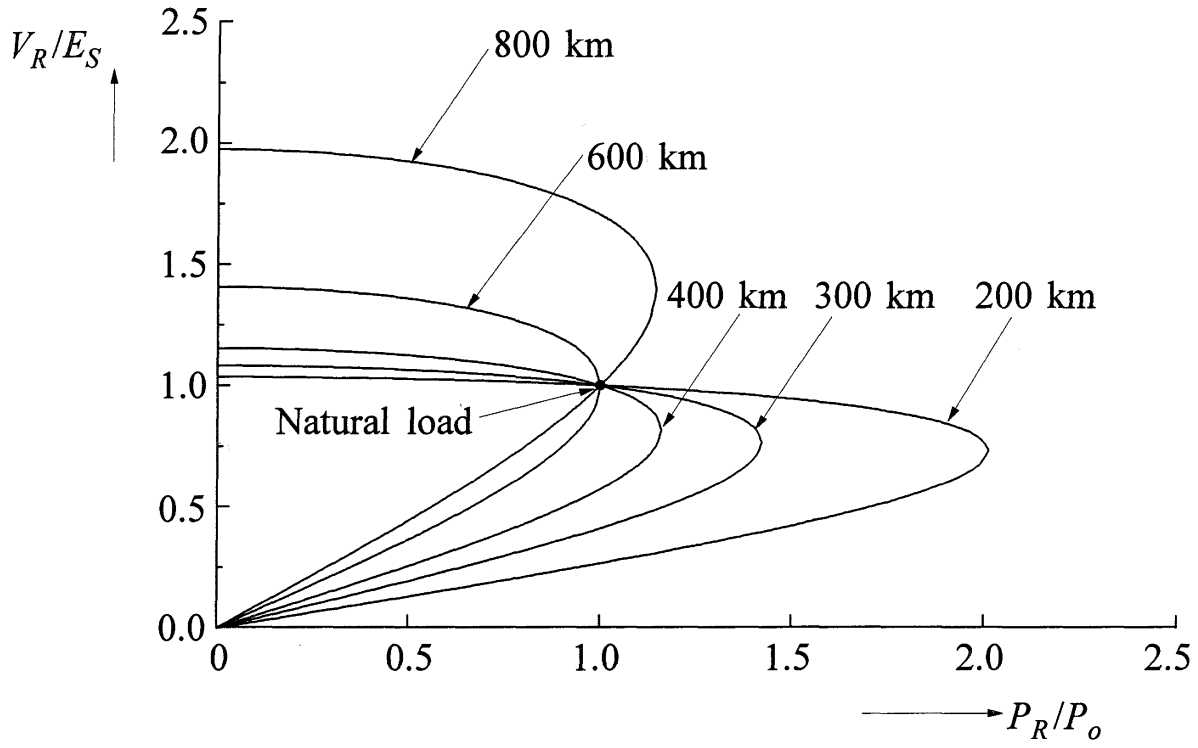

Figure 6.8 Relationship between receiving end voltage, line length, and load of a lossless radial line

(b) Line connected to sources at both ends

As in the no-load case (Section 6.1.7), we will assume the magnitudes of the source voltages at the two ends to be equal. Under load, E_S leads E_R in phase. Because the magnitudes of E_S and E_R are equal, the following conditions exist:

- The midpoint voltage is midway in phase between E_S and E_R.
- The power factor at midpoint is unity.
- With $P_R > P_o$, both ends supply reactive power to the line; with $P_R < P_o$, both ends absorb reactive power from the line.

The phasor diagram for $P_R < P_o$ is shown in Figure 6.9.

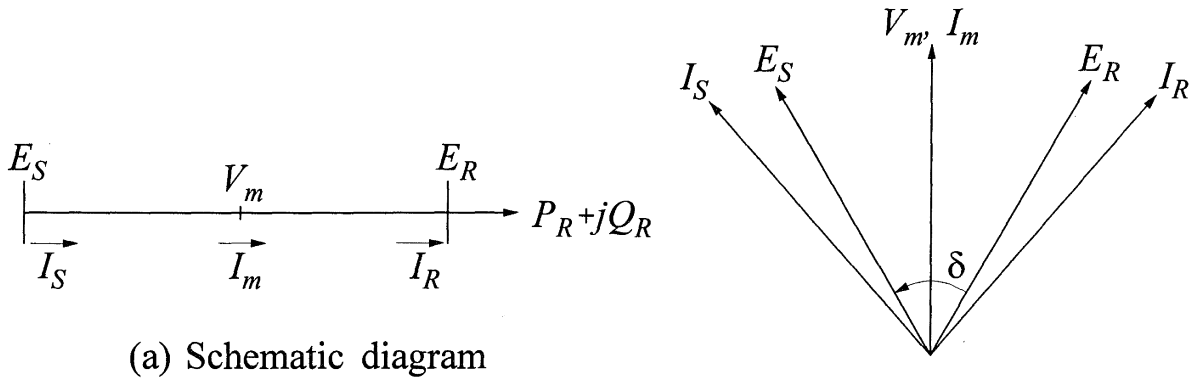

(a) Schematic diagram

(b) Phasor diagram

Figure 6.9 Voltage and current phase relationships with E_S equal to E_R, and P_R less than P_o

Figure 6.8 may be used to analyze how V_m varies with the power transmitted. With the magnitudes of E_S and E_R equal to 1.0 pu and the length equal to half that of the actual line, plots of V_R shown in Figure 6.8 give the values of V_m. For example, the variations in V_m with load of a 400 km line connected to sources at both ends are the same as the variations in V_R of a 200 km radial line.

At 400 km, the performance of the line is significantly improved by having sources at both ends. However, an 800 km symmetrical line would have unacceptably large voltage variations at midpoint.

Although we have considered a line connected to identical sources at the two ends, the observations made here are sufficiently general and provide a physical understanding helpful in dealing with more complex cases.

6.1.9 Power Transfer and Stability Considerations

Assuming a lossless line, from Equation 6.16, with $x=l$, and $\theta=\beta l$, we have

$$\tilde{E}_S = \tilde{E}_R\cos\theta + jZ_C\tilde{I}_R\sin\theta$$

Expressing I_R in terms of P_R and Q_R, we have

$$\tilde{E}_S = \tilde{E}_R\cos\theta + jZ_C\sin\theta\left(\frac{P_R - jQ_R}{\tilde{E}_R^*}\right) \tag{6.47}$$

As shown in Figure 6.9(b), let δ be the angle by which E_S leads E_R, i.e., the *load angle* or the *transmission angle*.

With E_R as reference phasor, E_S may be written as

$$\tilde{E}_S = E_S e^{j\delta} = E_S(\cos\delta + j\sin\delta) \tag{6.48}$$

Equating real and imaginary parts of Equations 6.47 and 6.48, we have

$$E_S\cos\delta = E_R\cos\theta + Z_C(Q_R/E_R)\sin\theta \tag{6.49}$$

$$E_S\sin\delta = Z_C(P_R/E_R)\sin\theta \tag{6.50}$$

Rearranging Equation 6.50 yields

$$P_R = \frac{E_S E_R}{Z_C\sin\theta}\sin\delta \tag{6.51}$$

The above equation gives a very important expression for power transferred across a line. It is valid for a synchronous as well as an asynchronous load at the receiving end. The only approximation is that line losses are neglected.

For a *short line*, $\sin\theta$ can be replaced by θ in radians. Hence,

$$Z_C\sin\theta = Z_C\theta = \sqrt{L/C}\,\omega\sqrt{LC}\,l = \omega Ll$$
$$= X_L \quad \text{the series inductive reactance}$$

Therefore, the expression for power transferred reduces to the more familiar form:

$$P_R \approx \frac{E_S E_R}{X_L} \sin\delta \tag{6.52}$$

If $E_S=E_R=V_o$, the rated voltage, then the natural load is

$$P_o = \frac{E_S E_R}{Z_C}$$

and Equation 6.51 becomes

$$P_R = \frac{P_o}{\sin\theta} \sin\delta \tag{6.53}$$

With the voltage magnitudes fixed, the power transmitted is a function of only the transmission angle δ. When P_R is equal to the natural load (P_o), $\delta=\theta$.

Figure 6.10(a) shows this relationship for a 400 km line, for which $\theta=0.52$ rads and $\sin\theta=0.497$. It is interesting to compare this with the voltage-power characteristic of Figure 6.8. The characteristic corresponding to the 400 km symmetrical line (equivalent to the 200 km radial line in Figure 6.8) is reproduced in Figure 6.10(b).

From Figures 6.10(a) and (b), we see that there is a maximum power that can be transmitted. As the load angle is increased (i.e., as the sending end synchronous system is advanced with respect to the receiving end synchronous system), the transmitted power increases according to Figure 6.10(a) and Equation 6.53. This is accompanied by a reduction in the midpoint voltage V_m [Figure 6.10(b)] and an increase in the midpoint current I_m so that there is an increase in power. Up to a certain point the increase in I_m dominates over the decrease of V_m. When the load angle reaches 90°, the transmitted power reaches its maximum value. Beyond this, the decrease in V_m is greater than the accompanying increase in I_m; hence, their product decreases with any further increase in transmission angle. The system, as explained below, is unstable when this condition is reached.

The sending end and receiving end systems may be considered in terms of equivalent synchronous machines. The load angle δ is then a measure of the relative position of the rotors of those two machines. Beyond the point of maximum power, an increase in the torque of the sending end machine results in an increase of δ, but the transmitted power decreases. This causes the sending end machine to accelerate and the receiving end machine to decelerate, resulting in a further increase of δ. This is a runaway situation, and the two machines (or the systems they represent) lose synchronism.

The maximum power that can be transmitted represents the small-signal or steady-state stability limit. For the 400 km line considered in Figures 6.10(a) and (b), this limit is equal to $P_o/0.497$ or 2.012 times the natural load.

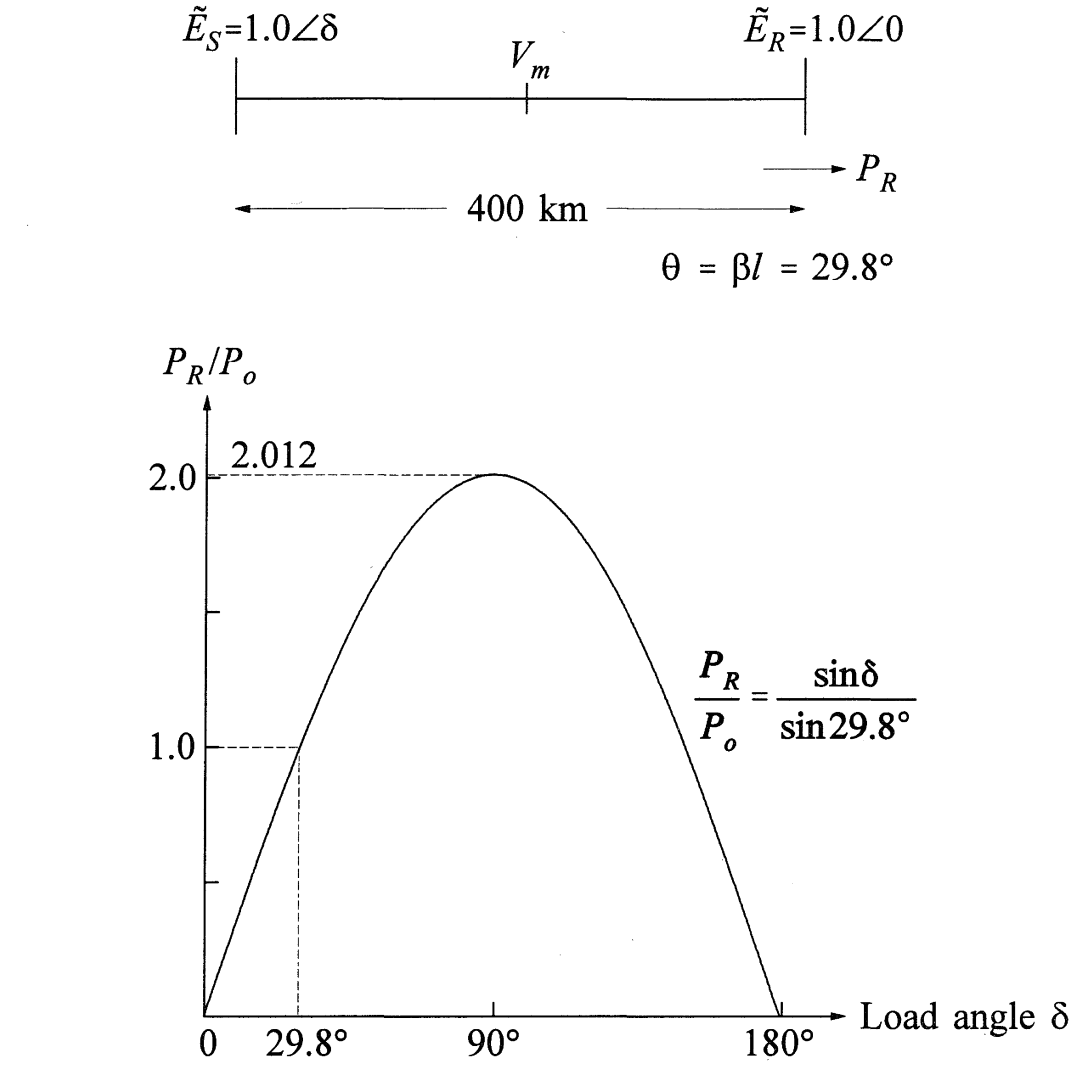

(a) Power/angle characteristics

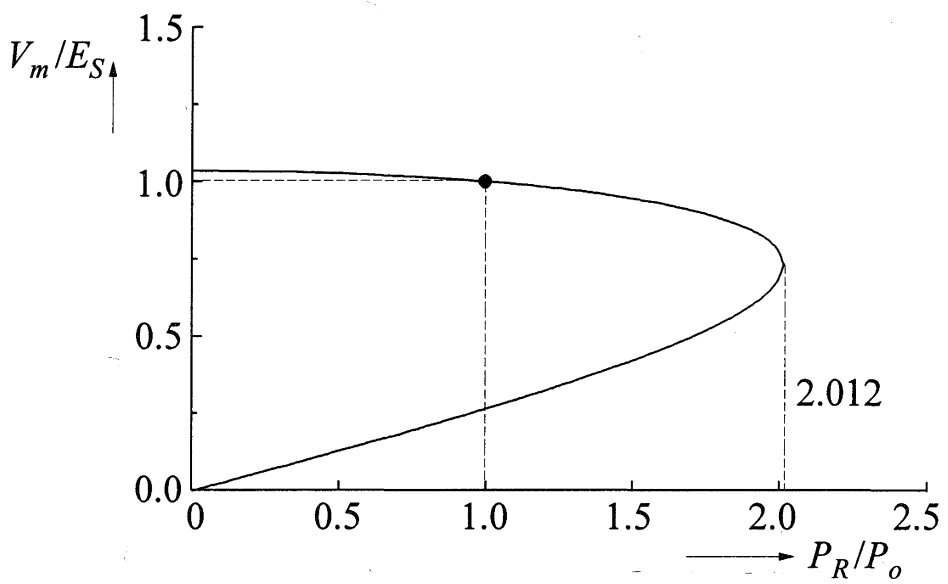

(b) Midpoint voltage as a function of power transmitted

Figure 6.10 The P_R-δ and V_m-P_R characteristics of 400 km lossless line transmitting power between two large systems

The stability analysis considered above represents a highly idealized situation. In particular, the assumption that E_S and E_R have constant magnitude is not realistic; the dynamic characteristics of the sending and receiving end systems need to be considered for accurate analysis. However, the analysis presented is useful for understanding the phenomenon and the performance characteristics of transmission lines. Chapter 12 provides a comprehensive description of the small-signal stability problem.

If the receiving end system is a nonsynchronous load, there is still a maximum value of power that can be transmitted, as illustrated in Figure 6.10(b), but maintenance of synchronism would not be an issue.

Reactive power requirements

The relationship between the receiving end reactive power and the voltages at the two ends is given by Equation 6.49 which is rewritten here for convenience.

$$E_S\cos\delta = E_R\cos\theta + Z_C(Q_R/E_R)\sin\theta$$

Rearranging, we get

$$Q_R = \frac{E_R(E_S\cos\delta - E_R\cos\theta)}{Z_C\sin\theta}$$

Similarly, the sending end reactive power is given by

$$Q_S = \frac{-E_S(E_R\cos\delta - E_S\cos\theta)}{Z_C\sin\theta}$$

If the magnitudes of E_S and E_R are equal, then

$$Q_R = -Q_S$$

$$= \frac{E_S^2(\cos\delta - \cos\theta)}{Z_C\sin\theta}$$

Figure 6.11 shows the terminal reactive power requirements of lines of different lengths as a function of active power transmitted. Both active power and reactive power have been normalized by dividing by the natural load P_o. When $P_R<P_o$, there is an excess of line charging; Q_S is negative and Q_R is positive, indicating reactive power absorption by the systems at both ends. When $P_R>P_o$, reactive power is supplied to the line from both ends.

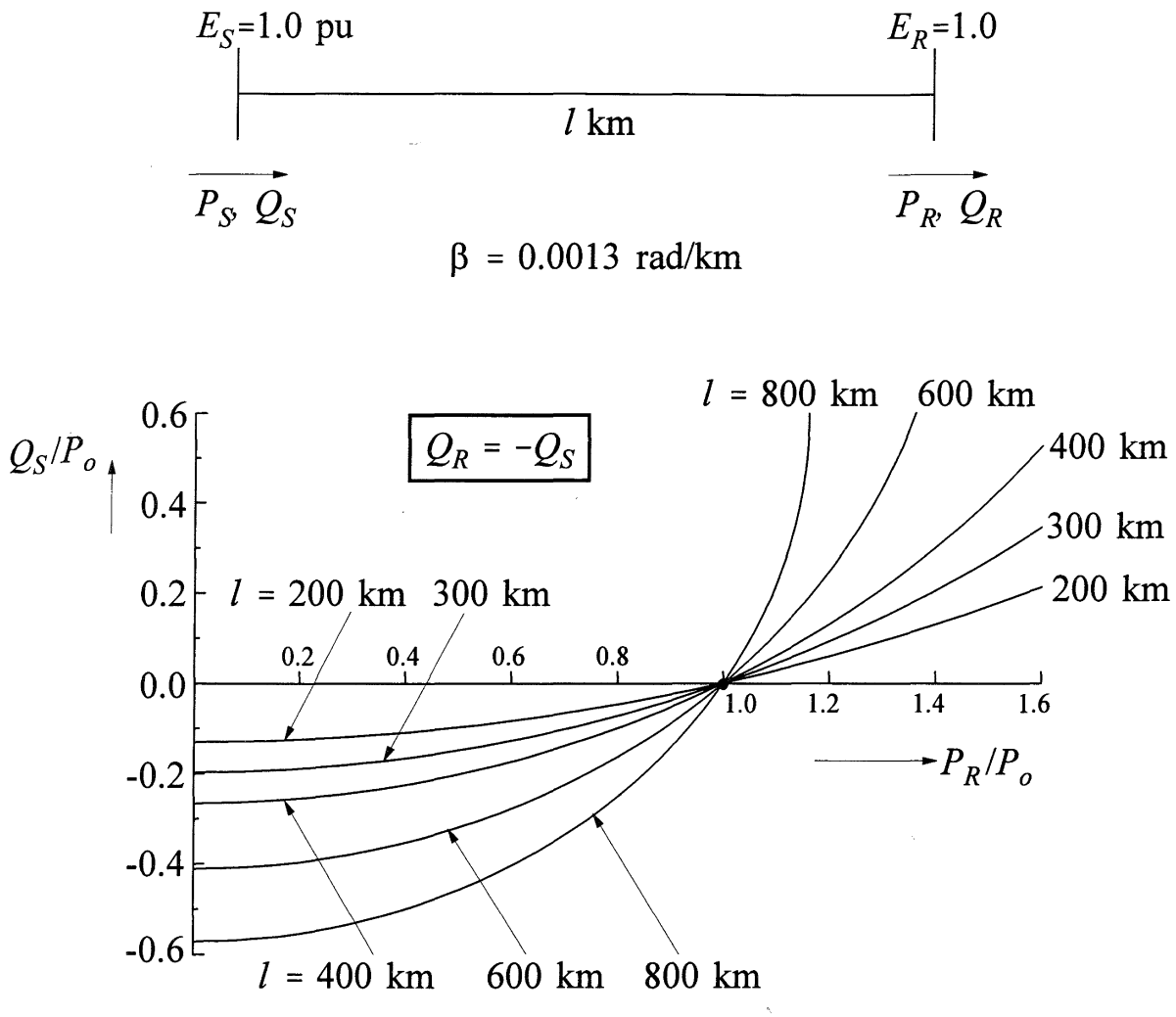

Figure 6.11 Terminal reactive power as a function of power transmitted for different line lengths

Transmission lines can be operated with varying load and nearly constant voltage at both ends, if adequate sources of reactive power are available at the two ends.

6.1.10 Effect of Line Loss on *V-P* and *Q-P* Characteristics

In the analysis of transmission line performance presented so far, we have neglected line losses. We will now examine the effect of line resistance on V_R-P_R and Q_S-P_R characteristics by considering a 300 km, 500 kV line having the following parameters:

R = 0.028 Ω/km x_L = 0.325 Ω/km b_C = 5.20 μs/km
α = 0.000057 nepers/km β = 0.0013 rad/km

The line is assumed to supply a radial load of *unity power factor*, with the sending end voltage E_S maintained constant at 1.0 pu.

The relationships between V_R and P_R and between Q_S and P_R are shown in Figure 6.12, with and without the line resistance included. The values of P_R and Q_S plotted are normalized values with 1.0 pu equal to P_o (1,008 MW).

We see from Figure 6.12(a) that the effect of the line resistance is to reduce the maximum power that can be transmitted by about 8.5%.

The lower portion of the Q_S-P_R curves shown in Figure 6.12(b) corresponds to the upper portion of the V_R-P_R characteristics, where the receiving end voltage V_R is closer to rated value. The high values of Q_S in the upper portion of the Q_S-P_R curve are due to the high values of line current (hence high XI^2 line loss) corresponding to the lower portion of the V_R-P_R curve. We see that the effect of line resistance on the computed value of Q_S in the normal lower portion is significant only when P_R exceeds P_o.

6.1.11 Thermal Limits

The heat produced by current flow in transmission lines has two undesirable effects:

- Annealing and gradual loss of mechanical strength of the aluminium conductor caused by continued exposure to temperature extremes

- Increased sag and decreased clearance to ground due to conductor expansion at higher temperatures

The second of the above two effects is generally the limiting factor in setting the maximum permissible operating temperature. At this limit, the resulting line sag approaches the statutory minimum ground clearance.

The maximum allowable conductor temperatures based on annealing considerations are 127°C for conductors with high aluminum content and 150°C for other conductors.

The allowable maximum current (i.e., the ampacity) depends on the ambient temperature and the wind velocity. The thermal time constant is on the order of 10 to 20 minutes. Therefore, distinction is usually made between continuous rating and limited time rating. Depending on the pre-contingency current, temperature and wind velocity, the limited time rating may be used during emergencies. As an example, the 230 kV line whose parameters are given in Table 6.1 has summer and winter emergency ratings of 1,880 A and 2,040 A, respectively. These are design values based on extreme values of ambient temperature, wind velocity, and solar radiation.

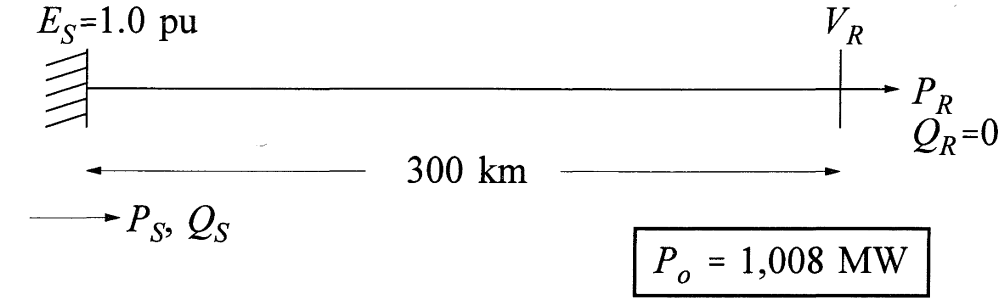

P_o = 1,008 MW

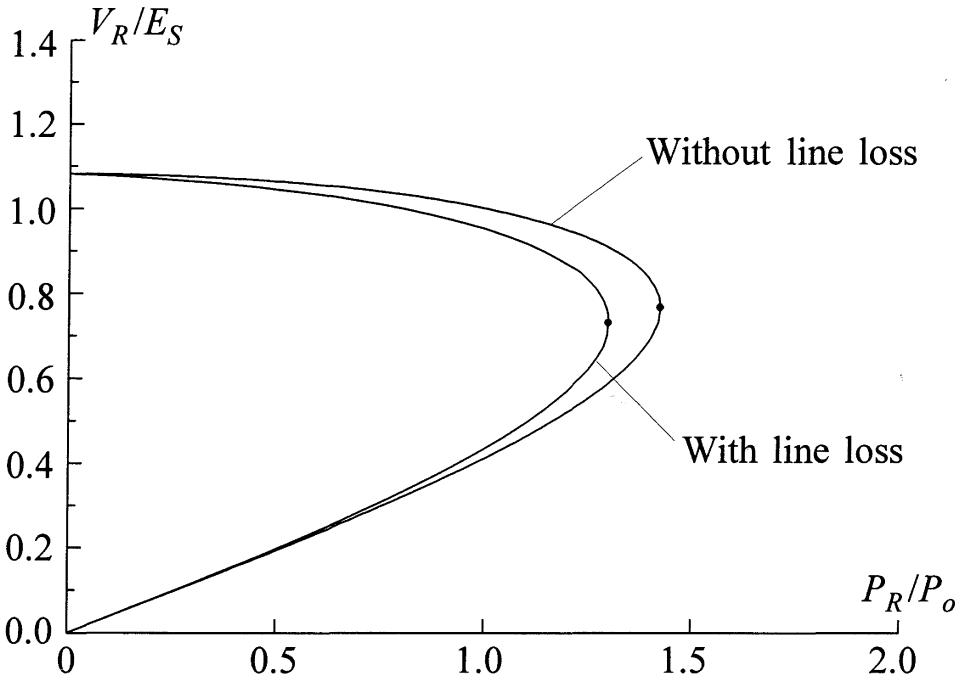

(a) V_R-P_R characteristic

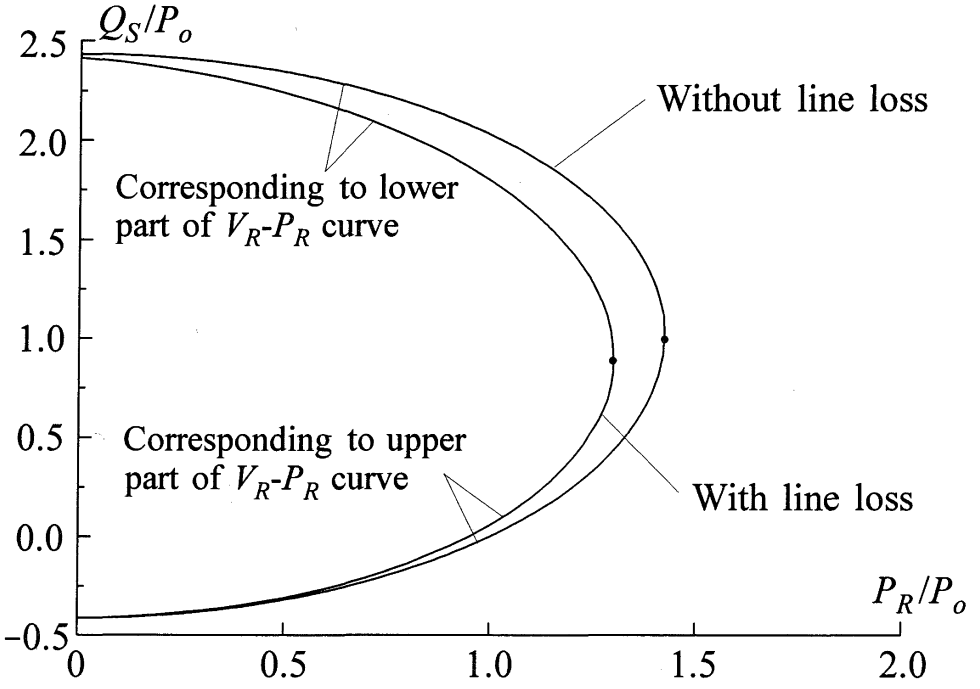

(b) Q_S-P_R characteristic

Figure 6.12 The V_R-P_R and Q_S-P_R characteristics of a 300 km, 500 kV line supplying a radial load

6.1.12 Loadability Characteristics

The concept of "line loadability" is useful in developing a fuller understanding of power transfer capability as influenced by voltage level and line length. Line loadability is defined as the degree of line loading (expressed in percent of SIL) permissible given the thermal, voltage drop, and stability limits. This concept was first introduced by H.P. St. Clair in 1953 [11]. Based on practical considerations and experience, St. Clair developed transmission line power-transfer capability curves covering voltage levels between 34.5 kV and 330 kV and line lengths up to 400 mi (approximately 645 km). These curves, known as *St. Clair curves*, have been a valuable tool for transmission planning engineers for quickly estimating the maximum line loading limits. This work was later extended in reference 12 by presenting an analytical basis for the St. Clair curves so as to be able to cover higher voltage levels (up to 1,500 kV) and longer line lengths (600 mi or 960 km).

Figure 6.13 shows the universal loadability curve for overhead *uncompensated* transmission lines applicable to all voltage levels. The curve, which is based on the results presented in reference 12, shows the limiting values of power that can be transmitted as a function of line length. Three factors influence the limiting values of power: thermal limit, voltage drop limit, and the small-signal or steady-state stability limit. In determining the loadability curve, it is assumed that the maximum allowable voltage drop along the line is 5% and that the minimum allowable steady-state stability margin is 30%. Referring to Figure 6.14, the percent steady-state stability margin is defined as

$$\text{Percent stability margin} = \frac{P_{max} - P_{limit}}{P_{max}} \times 100$$

As shown in Figure 6.14, for a 30% stability margin, the load angle δ is 44°. The calculation of stability limit includes the effects of the equivalent system reactances at the two ends of the line. In reference 12, the system strength at each end is taken to be that corresponding to 50 kA fault duty which represents a well-developed system.

Since the resistances of extra-high voltage (EHV) and ultra-high voltage (UHV) lines are very much smaller than their reactances, such lines closely approximate a lossless line. Since the parameter β is practically the same for all overhead lines, the loadabilities expressed in per unit of SIL are universally applicable to lines of all voltage classes.

As identified in Figure 6.13, the limits to line loading are governed by the following considerations:

- Thermal limits for lines up to 80 km (50 mi)
- Voltage drop limits for lines between 80 km and 320 km (200 mi) long
- Stability limits for lines longer than 320 km

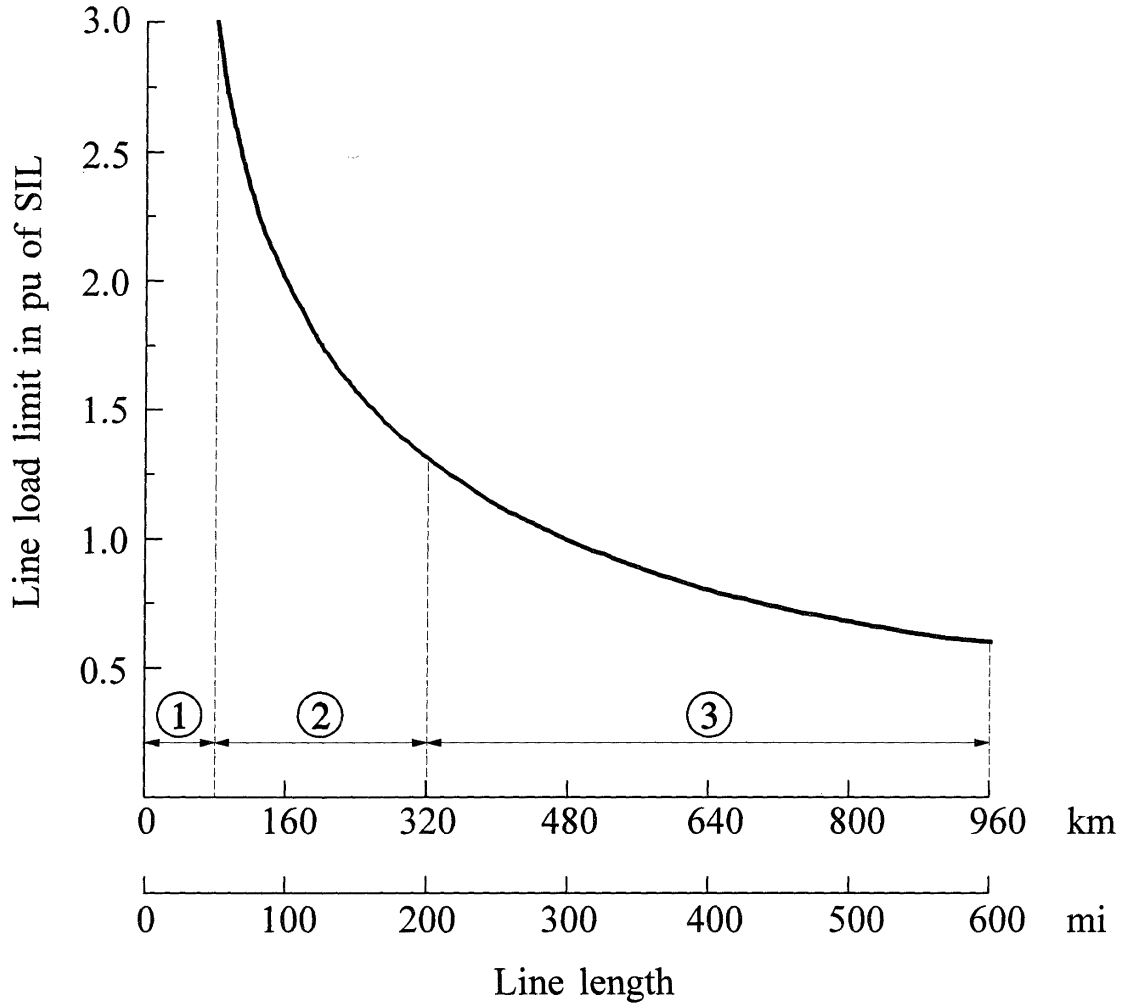

① 0–80 km: Region of thermal limitation
② 80–320 km: Region of voltage drop limitation
③ 320–960 km: Region of small-signal (steady-state) stability limitation

Figure 6.13 Transmission line loadability curve

For lines longer than 480 km (300 mi), the loadability is less than SIL. The loadability limits can be increased by "compensating" the lines.

Alternative forms of line compensation and consideration that influence their selection are discussed in Chapter 11.

The universal loadability curve discussed here provides a simple means of visualizing power-transfer capabilities of transmission lines. It is useful for developing conceptual guides to line loadability and preliminary planning of transmission systems. However, it must be used with some caution. Large complex power systems require detailed assessment of their performance and consideration of additional factors that influence their performance.

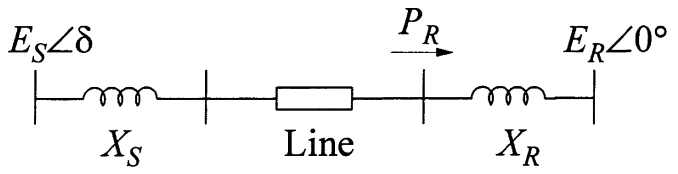

(a) System model

X_S = Sending end source reactance
X_R = Receiving end source reactance
Source short circuit current = 50 kA

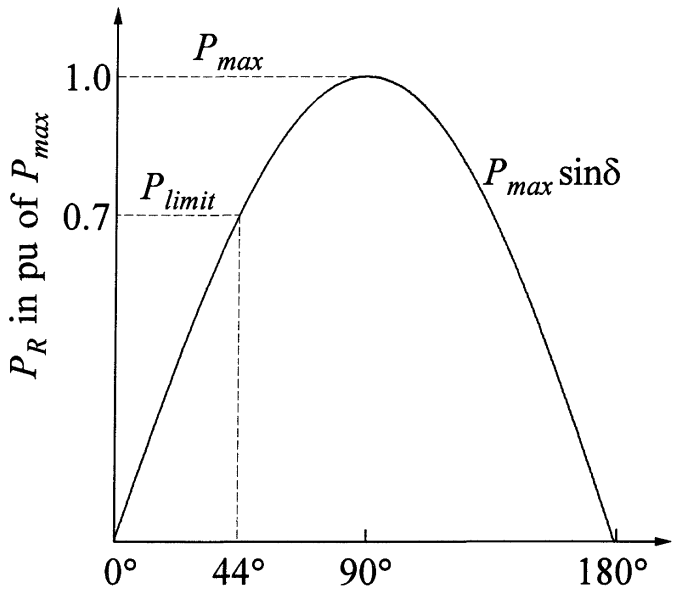

(b) Power-angle curve

For 30% stability margin:

$$P_{limit} = 0.7P_{max}$$
$$\delta = \sin^{-1}0.7$$
$$= 44°$$

Figure 6.14 Steady-state stability margin calculation

Effect of using bundled conductors

Bundled conductors are commonly used on EHV lines to control the voltage gradient at the surface of the conductors and thus avoid unacceptably high radio noise, audible noise, and corona loss.

The use of bundled conductors decreases the self geometric mean distance. Hence, it has an added advantage of reducing the characteristic impedance Z_C by decreasing the series inductance and increasing the shunt capacitance of the line. The reduction in Z_C is on the order of 10 to 20%. Consequently, SIL or natural load increases, thus contributing to the increase in loadability.

6.2 TRANSFORMERS

Transformers enable utilization of different voltage levels across the system. From the viewpoints of efficiency and power-transfer capability, the transmission voltages have to be high, but it is not practically feasible to generate and consume power at these voltages. In modern electric power systems, the transmitted power undergoes four to five voltage transformations between the generators and the ultimate consumers. Consequently, the total MVA rating of all the transformers in a power system is about five times the total MVA rating of all the generators.

In addition to voltage transformation, transformers are often used for control of voltage and reactive power flow. Therefore, practically all transformers used for bulk power transmission and many distribution transformers have taps in one or more windings for changing the turns ratio. From the power system viewpoint, changing the ratio of transformation is required to compensate for variations in system voltages. Two types of tap-changing facilities are provided: off-load tap changing and under-load tap changing (ULTC).[1] The off-load tap-changing facilities require the transformer to be de-energized for tap changing; they are used when the ratio will need to be changed only to meet long-term variations due to load growth, system expansion, or seasonal changes. The ULTC is used when the changes in ratio need to be frequent; for example, to take care of daily variations in system conditions. The taps normally allow the ratio to vary in the range of ±10% to ±15%.

Transformers may be either three-phase units or three single-phase units. The latter type of construction is normally used for large EHV transformers and for distribution transformers. Large EHV transformers are of single-phase design due to the cost of spare, insulation requirements, and shipping considerations. The distribution systems serve single-phase loads and are supplied by single-phase transformers.

When the voltage transformation ratio is small, *autotransformers* are normally used. The primary and secondary windings of autotransformers are interconnected so that the power to be transformed by magnetic coupling is only a portion of the total power transmitted through the transformer. There is thus inherent metallic connection between the primary side and secondary side circuits; this is unlike the conventional two-winding transformer which isolates the two circuits.

Autotransformers are usually Y connected, with neutrals solidly grounded to minimize the propagation of disturbances occurring on one side into the other side. It is a common practice to add a low-capacity delta-connected tertiary winding. The tertiary winding provides a path for third harmonic currents, thereby reducing their flow on the network. It also assists in stabilizing the neutral. Reactive compensation is often provided through use of switched reactors and capacitors on a tertiary bus

---

[1] Under-load tap changing is also referred to by other names such as on-load tap changing (OLTC) and load tap changing (LTC).

(see Chapter 11).

As compared to the *conventional two-winding transformer*, the autotransformer has advantages of lower cost, higher efficiency, and better regulation. These advantages become less significant as the transformation ratio increases; hence, autotransformers are used for low transformation ratios (for example, 500/230 kV).

In interconnected systems, it sometimes becomes necessary to make electrical connections that form loop circuits through one or more power systems. To control the circulation of power and prevent overloading certain lines, it is usually necessary in such situations to use *phase-angle transformers*. Often it is necessary to vary the extent of phase shift to suit changing system conditions; this requires provision of on-load phase-shifting capability. Voltage transformation may also be required in addition to phase shift.

The transformer is a well-known device. The basic principle of its operation is covered in standard textbooks [2,5,7]. References 2 and 8 provide information related to physical realization of various types of transformers and their performance characteristics. Here, we will focus on representation of transformers in stability and power-flow studies.

6.2.1 Representation of Two-Winding Transformers

Basic equivalent circuit in physical units:

The basic equivalent circuit of a two-winding transformer with all quantities in physical units is shown in Figure 6.15. The subscripts p and s refer to primary and secondary quantities, respectively.

The magnetizing reactance X_{mp} is very large and is usually neglected. For special studies requiring representation of transformer saturation, the magnetizing reactance representation may be approximated by moving it to the primary or the secondary terminals and treating it as a voltage-dependent variable shunt reactance.

Per unit equivalent circuit:

With appropriate choice of primary and secondary side base quantities, the equivalent circuit can be simplified by eliminating the ideal transformer. However, this is not always possible and the base quantities often have to be chosen independent of the actual turns ratio. It is therefore necessary to consider an off-nominal turns ratio.

From the equivalent circuit of Figure 6.15, with X_{mp} neglected, we have

$$\tilde{v}_p = Z_p \tilde{i}_p + \frac{n_p}{n_s}\tilde{v}_s - \frac{n_p}{n_s} Z_s \tilde{i}_s \tag{6.54}$$

$$\tilde{v}_s = \frac{n_s}{n_p}\tilde{v}_p - \frac{n_s}{n_p} Z_p \tilde{i}_p + Z_s \tilde{i}_s \tag{6.55}$$

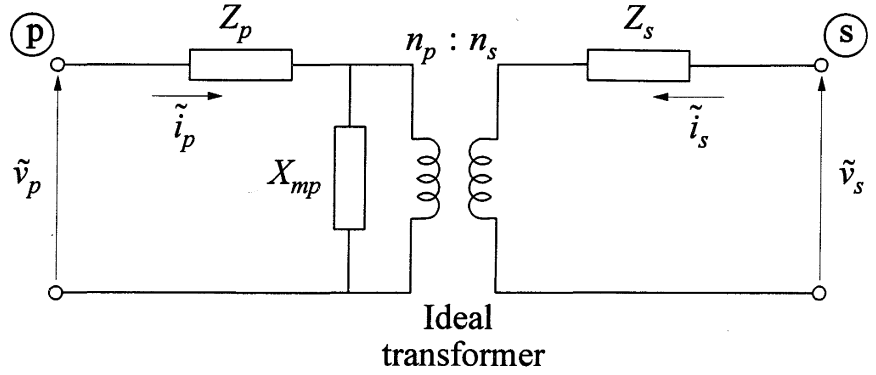

$Z_p = R_p + jX_p$; $Z_s = R_s + jX_s$
R_p, R_s = primary and secondary winding resistances
X_p, X_s = primary and secondary winding leakage reactances
n_p, n_s = number of turns of primary and secondary winding
X_{mp} = magnetizing reactance referred to the primary side

Figure 6.15 Basic equivalent circuit of a two-winding transformer

Let

Z_{p0} = Z_p at nominal primary side tap position
Z_{s0} = Z_s at nominal secondary side tap position
n_{p0} = primary side nominal number of turns
n_{s0} = secondary side nominal number of turns

Expressing Equations 6.54 and 6.55 in terms of the above nominal values,

$$\tilde{v}_p = \left(\frac{n_p}{n_{p0}}\right)^2 Z_{p0}\tilde{i}_p + \frac{n_P}{n_s}\tilde{v}_s - \frac{n_p}{n_s}\left(\frac{n_s}{n_{s0}}\right)^2 Z_{s0}\tilde{i}_s \tag{6.56}$$

$$\tilde{v}_s = \frac{n_s}{n_p}\tilde{v}_p - \frac{n_s}{n_p}\left(\frac{n_p}{n_{p0}}\right)^2 Z_{p0}\tilde{i}_p + \left(\frac{n_s}{n_{s0}}\right)^2 Z_{s0}\tilde{i}_s \tag{6.57}$$

Here, we have assumed that both leakage reactance and resistance of a transformer winding are proportional to the square of the number of turns. This assumption is generally valid for the leakage reactance, but not for the resistance. Since the resistance is much smaller than the leakage reactance and since the deviation of the actual turns ratio from the nominal turns ratio is not very large, the resulting approximation is acceptable. For convenience, we will assume that both primary and secondary windings are connected so as to form a Y-Y connected three-phase bank.

With the nominal number of turns related to the base voltages as follows:

$$\frac{n_{p0}}{n_{s0}} = \frac{v_{pbase}}{v_{sbase}}$$

and

$$v_{pbase} = Z_{pbase} i_{pbase}, \qquad v_{sbase} = Z_{sbase} i_{sbase}$$

Equations 6.56 and 6.57 in per unit form become

$$\bar{v}_p = \bar{n}_p^2 \bar{Z}_{p0} \bar{i}_p + \frac{\bar{n}_p}{\bar{n}_s} \bar{v}_s - \bar{n}_s^2 \frac{\bar{n}_p}{\bar{n}_s} \bar{Z}_{s0} \bar{i}_s \tag{6.58}$$

$$\bar{v}_s = \frac{\bar{n}_s}{\bar{n}_p} \bar{v}_p - \bar{n}_p^2 \frac{\bar{n}_s}{\bar{n}_p} \bar{Z}_{p0} \bar{i}_p + \bar{n}_s^2 \bar{Z}_{s0} \bar{i}_s \tag{6.59}$$

where the superbars denote per unit values, with $\bar{v}_p$, $\bar{v}_s$, $\bar{i}_p$, $\bar{i}_s$ equal to per unit values of *phasor* voltages and currents, and

$$\bar{n}_p = \frac{n_p}{n_{p0}} \tag{6.60}$$

$$\bar{n}_s = \frac{n_s}{n_{s0}} \tag{6.61}$$

The per unit equivalent circuit representing Equations 6.58 and 6.59 is shown in Figure 6.16.

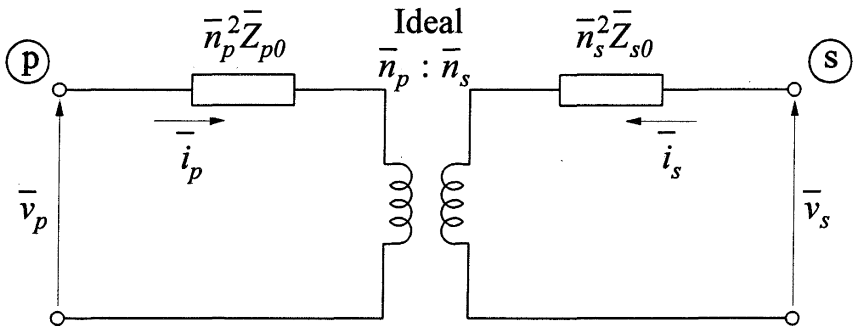

Figure 6.16 Per unit equivalent circuit

Standard equivalent circuit:

The equivalent circuit of Figure 6.16 can be reduced to the standard form shown in Figure 6.17, where $\bar{n}$ is the per unit turns ratio:

$$\bar{n} = \frac{\bar{n}_p}{\bar{n}_s} = \frac{n_p n_{s0}}{n_{p0} n_s} \tag{6.62}$$

and

$$\begin{aligned} \bar{Z}_e &= \bar{n}_s^2 (\bar{Z}_{p0} + \bar{Z}_{s0}) \\ &= \left(\frac{n_s}{n_{s0}} \right)^2 (\bar{Z}_{p0} + \bar{Z}_{s0}) \end{aligned} \tag{6.63}$$

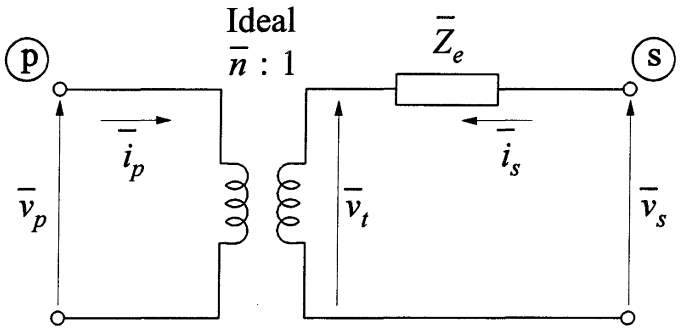

Figure 6.17 Standard equivalent circuit for a transformer

The equivalent circuit of Figure 6.17 is widely used for representation of two-winding transformers in power flow and stability studies. The IEEE common format for exchange of solved power flow cases uses this representation [13].

We see from Equation 6.63 that $\bar{Z}_e$ does not change with $\bar{n}_p$. Therefore, if the tap is on the primary side, only $\bar{n}$ changes.

If the actual turns ratio is equal to n_{p0}/n_{s0}, then $\bar{n}$=1.0, and the ideal transformer vanishes. When the actual turns ratio is not equal to the nominal turns ratio, $\bar{n}$ represents the off-nominal ratio (ONR).

The equivalent circuit of Figure 6.17 can be used to represent a transformer with a fixed (or off-load) tap on one side and an under-load tap changer (ULTC) on the other side. The off-nominal turns ratio is assigned to the side with ULTC and $\bar{Z}_e$ has a value corresponding to the fixed-tap position of the other side, as given by Equation 6.63.

Equivalent π circuit representation [14]:

In digital computer analysis of power flow, it is not convenient to represent an ideal transformer. We will therefore reduce the equivalent circuit of Figure 6.17 to the form of a π network of Figure 6.18(a).

From Figure 6.17, the terminal current at bus p is

$$\begin{aligned} \bar{i}_p &= (\bar{v}_t - \bar{v}_s)\frac{\bar{Y}_e}{\bar{n}} \\ &= (\frac{\bar{v}_P}{\bar{n}} - \bar{v}_s)\frac{\bar{Y}_e}{\bar{n}} \\ &= (\bar{v}_p - \bar{n}\bar{v}_s)\frac{\bar{Y}_e}{\bar{n}^2} \end{aligned} \tag{6.64}$$

where $\bar{Y}_e = 1/\bar{Z}_e$. Similarly, the terminal current at bus s is

$$\bar{i}_s = (\bar{n}\bar{v}_s - \bar{v}_p)\frac{\bar{Y}_e}{\bar{n}} \tag{6.65}$$

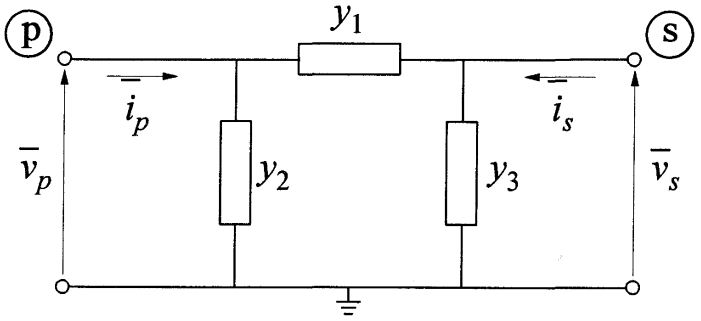

(a) General π network

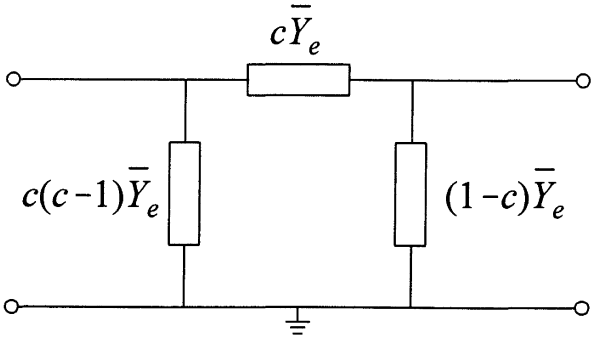

$\bar{Y}_e = 1/\bar{Z}_e$
$c = 1/\bar{n}$

(b) Equivalent π circuit

Figure 6.18 Transformer representation with ONR

The corresponding terminal currents for the π network shown in Figure 6.18(a) are

$$\bar{i}_p = y_1(\bar{v}_p - \bar{v}_s) + y_2\bar{v}_p \tag{6.66}$$

$$\bar{i}_s = y_1(\bar{v}_s - \bar{v}_p) + y_3\bar{v}_s \tag{6.67}$$

Equating the corresponding admittance terms in Equations 6.64 and 6.66, we have

$$y_1 = \frac{1}{\bar{n}}\bar{Y}_e = c\bar{Y}_e \tag{6.68}$$

and

$$y_2 = \left(\frac{1}{\bar{n}^2} - \frac{1}{\bar{n}}\right)\bar{Y}_e = (c^2 - c)\bar{Y}_e \tag{6.69}$$

where $c = \frac{1}{\bar{n}}$. Similarly, from Equations 6.65 and 6.67,

$$y_3 = (1-c)\bar{Y}_e \tag{6.70}$$

The equivalent π circuit with parameters expressed in terms of the ONR and transformer leakage impedance is shown in Figure 6.18(b).

Consideration of three-phase transformer connections

The standard equivalent circuit of Figure 6.17 represents the single-phase equivalent of a three-phase transformer. In establishing the ONR, the nominal turns ratio (n_{p0}/n_{s0}) is taken to be equal to the ratio of line-to-line base voltages on both sides of the transformer irrespective of the winding connections (Y-Y, Δ-Δ, or Y-Δ). For Y-Y and Δ-Δ connected transformers, this makes the ratios of the base voltages equal to the ratios of the nominal turns of the primary and secondary windings of each transformer phase. For a Y-Δ connected transformer, this in addition accounts for the factor $\sqrt{3}$ due to the winding connection.

In the case of a Y-Δ connected transformer, a 30° phase shift is introduced between line-to-line voltages on the two sides of the transformer. The line-to-neutral voltages and line currents are similarly shifted in phase due to the winding connections. As we will illustrate in Section 6.4, it is usually not necessary to take this phase shift into consideration in system studies. Thus, the single-phase equivalent circuit of a Y-Δ transformer does not account for the phase shift, except in so far as the phase shift of voltages due to the impedance of the transformer.

Example of modelling two-winding transformers

As an example, let us consider a 60 Hz, two-winding, three-phase transformer with the following data:

MVA rating	: 42.00 MVA
Primary (HV) nominal voltage	: 110.00 kV
Secondary (LV) nominal voltage	: 28.40 kV
Winding connections (HV/LV)	: Y/Δ
Resistance	: $\bar{R}_{p0}+\bar{R}_{s0}$=0.00411 pu on rating/phase
Leakage reactance	: $\bar{X}_{p0}+\bar{X}_{s0}$=0.1153 pu on rating/phase
Off-load tap changer on HV side	: 4 steps, 2.75 kV/step
Under-load tap changer on LV side	: ±2.84 kV in 16 steps

Let us examine the condition when the LV winding is initially at its nominal position, and the HV winding is manually set two steps above its nominal position, i.e., at 115.5 kV. The parameters of the standard equivalent circuit (Figure 6.17) with the ONR on the LV (ULTC) side and values expressed in per unit of the transformer rated values are as follows:

Initial off-nominal turns ratio:

$$\bar{n} = \frac{28.4}{28.4}\frac{110}{115.5} = 0.95238$$

Per unit equivalent impedance:

$$\bar{Z}_e = \left(\frac{115.5}{110}\right)^2 (0.00411+j0.1153)$$

$$= 0.00453+j0.12712 \quad \text{pu}$$

Maximum per unit turns ratio:

$$\bar{n}_{max} = \frac{31.24}{28.4}\frac{110}{115.5} = 1.04762$$

Minimum per unit turns ratio:

$$\bar{n}_{min} = \frac{25.56}{28.4}\frac{110}{115.5} = 0.85714$$

Per unit turns ratio step:

$$\Delta\bar{n} = \frac{2.84}{16\times28.4}\frac{110}{115.5} = 0.0059524$$

Now, if the common system voltage and MVA base values are

Primary system voltage base	: 115.0 kV
Secondary system voltage base	: 28.4 kV
System MVA base	: 100 MVA

the corresponding per unit parameters of the equivalent circuit are as follows:

Initial off-nominal turns ratio:

$$\bar{n} = 0.95238\frac{28.4}{28.4}\frac{115}{110} = 0.99567$$

Per unit equivalent impedance:

$$\bar{Z}_e = (0.00453+j0.12712)\left(\frac{110}{115}\right)^2\frac{100}{42}$$

$$= 0.009868+j0.27692$$

Maximum per unit turns ratio:

$$\bar{n}_{max} = 1.04762\frac{28.4}{28.4}\frac{115}{110} = 1.09524$$

Minimum per unit turns ratio:

$$\bar{n}_{min} = 0.85714\frac{28.4}{28.4}\frac{115}{110} = 0.89610$$

Per unit turns ratio step:

$$\Delta\bar{n} = 0.005924\frac{28.4}{28.4}\frac{115}{110} = 0.006193$$

The equivalent π circuit (Figure 6.18) parameters representing the initial tap position are as follows:

$$y_1 = \frac{1}{\bar{n}\bar{Z}_e} = \frac{1}{0.99567(0.009868+j0.27692)}$$

$$= 0.12908-j3.62226$$

$$y_2 = \left(\frac{1}{\bar{n}}-1\right)y_1 = \left(\frac{1}{0.99567}-1\right)\frac{1}{0.99567(0.009868+j0.27692)}$$

$$= 0.00056-j0.01575$$

$$y_3 = \left(1-\frac{1}{\bar{n}}\right)\frac{1}{Z_e} = \left(1-\frac{1}{0.99567}\right)\frac{1}{0.009868+j0.27692}$$

$$= -0.00056+j0.01568$$

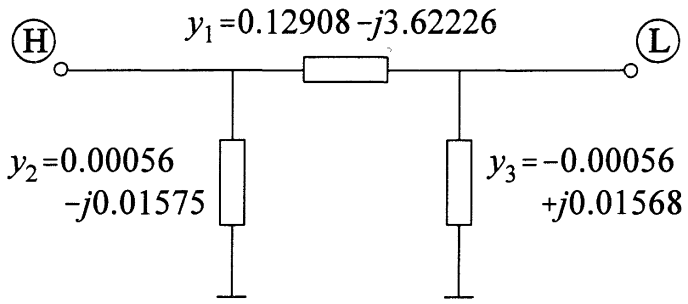

6.2.2 Representation of Three-Winding Transformers

Figure 6.19 shows the single-phase equivalent of a three-winding transformer under balanced conditions. The effect of the magnetizing reactance has been neglected, and the transformer is represented by three impedances connected to form a star. The common star point is fictitious and unrelated to the system neutral.

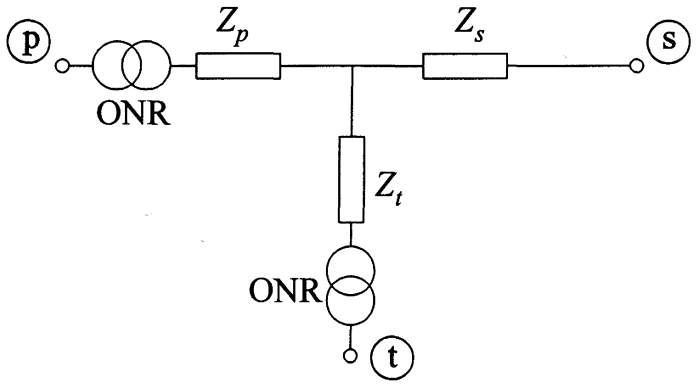

Figure 6.19 Equivalent circuit of a three-winding transformer

The three windings of the transformer may have different MVA ratings. However, the per unit impedances must be expressed on the same MVA base. As in the case of the two-winding transformer equivalent circuit developed in the previous section, off-nominal turns ratios are used to account for the differences between the ratios of actual turns and the base voltages. The values of the equivalent impedances Z_p, Z_s and Z_t may be obtained by standard short-circuit tests as follows [1]:

Z_{ps} = leakage impedance measured in primary with secondary shorted and tertiary open
Z_{pt} = leakage impedance measured in primary with tertiary shorted and secondary open
Z_{st} = leakage impedance measured in secondary with tertiary shorted and primary open

With the above impedances in ohms referred to the same voltage base, we have

$$\begin{aligned} Z_{ps} &= Z_p + Z_s \\ Z_{pt} &= Z_p + Z_t \\ Z_{st} &= Z_s + Z_t \end{aligned} \tag{6.71}$$

Hence,

$$\begin{aligned} Z_p &= \frac{1}{2}(Z_{ps} + Z_{pt} - Z_{st}) \\ Z_s &= \frac{1}{2}(Z_{ps} + Z_{st} - Z_{pt}) \\ Z_t &= \frac{1}{2}(Z_{pt} + Z_{st} - Z_{ps}) \end{aligned} \tag{6.72}$$

In large transformers, Z_s is small and may even be negative.

Example of modelling three-winding transformers

We will consider a 60 Hz, three-winding, three-phase transformer with the following data:

MVA rating	: 750 MVA
High/low/tertiary nominal voltages	: 500/240/28 kV
Winding connections (H/L/T)	: Y/Y/Δ

Measured positive-sequence impedances in pu on transformer MVA rating and nominal voltages at nominal tap position:

$Z_{H\text{-}L} = 0.0015 + j0.1339$
$Z_{L\text{-}T} = 0 + j0.1895$
$Z_{T\text{-}H} = 0 + j0.3335$

ULTC at high voltage side: 500±50 kV in 20 steps.

Neglecting the magnetizing reactance, the equivalent star circuit with ULTC at nominal tap position is

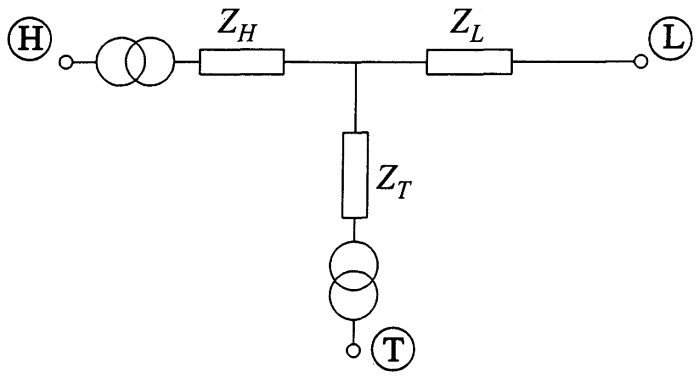

$$Z_H = \frac{Z_{H\text{-}L}+Z_{T\text{-}H}-Z_{L\text{-}T}}{2} = 0.00075+j0.13895$$

$$Z_L = \frac{Z_{H\text{-}L}+Z_{L\text{-}T}-Z_{T\text{-}H}}{2} = 0.00075-j0.00505$$

$$Z_T = \frac{Z_{L\text{-}T}+Z_{T\text{-}H}-Z_{H\text{-}L}}{2} = -0.00075+j0.19455$$

Equivalent delta circuit with parameters in pu on transformer MVA rating and nominal voltages:

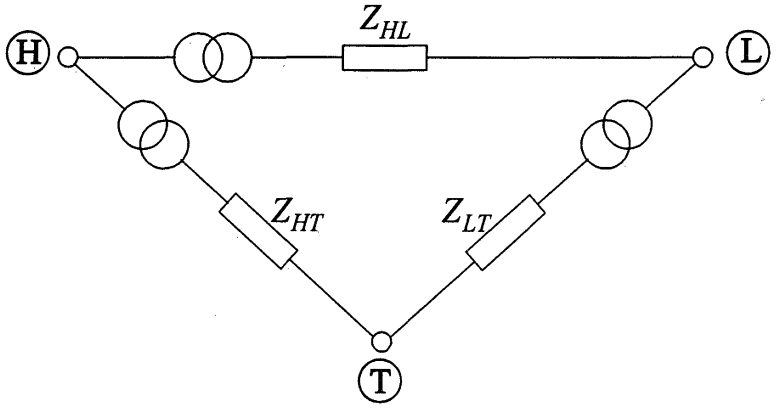

$$\Sigma = Z_H Z_L + Z_H Z_T + Z_L Z_T$$
$$= -0.02535+j0.0002914$$

$$Z_{HL} = \frac{\Sigma}{Z_T} = 0.0020+j0.1303$$

$$Z_{LT} = \frac{\Sigma}{Z_H} = 0.0011+j0.1824$$

$$Z_{HT} = \frac{\Sigma}{Z_L} = -0.7859-j4.9029$$

Equivalent delta circuit with parameters in pu on system MVA base of 100 MVA and voltage bases (H/L/T) of 500/220/27.6 kV:

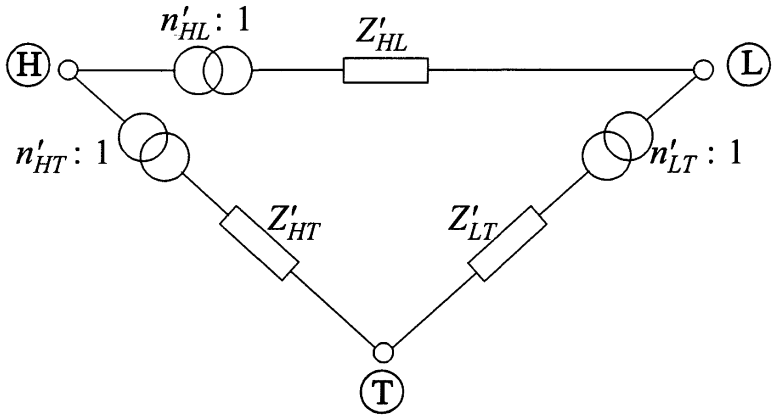

$$Z'_{HL} = Z_{HL}\frac{100}{750}\left(\frac{240}{220}\right)^2 = 0.00032+j0.02067$$

$$Z'_{LT} = Z_{LT}\frac{100}{750}\left(\frac{28.0}{27.6}\right)^2 = 0.00015+j0.02504$$

$$Z'_{TH} = Z_{TH}\frac{100}{750}\left(\frac{28.0}{27.6}\right)^2 = -0.10784-j0.6728$$

$$n'_{HL} = \frac{500}{500}\frac{220}{240} = 0.91667$$

$$n'_{LT} = \frac{240}{220}\frac{27.6}{28.0} = 1.07532$$

$$n'_{HT} = \frac{500}{500}\frac{27.6}{28.0} = 0.98571$$

ULTC data:

$$n'_{HLmax} = \frac{550}{500}\frac{500}{500}\frac{220}{240} = 1.00833$$

$$n'_{HLmin} = \frac{450}{500}\frac{500}{500}\frac{220}{240} = 0.8250$$

$$\Delta n'_{HL} = \frac{1.00833-0.825}{20} = 0.00917$$

$$n'_{HTmax} = \frac{550}{500}\frac{500}{500}\frac{27.6}{28.0} = 1.08429$$

$$n'_{HTmin} = \frac{450}{500}\frac{500}{500}\frac{27.6}{28.0} = 0.88714$$

$$\Delta n'_{HT} = \frac{1.08429-0.8814}{20} = 0.01014$$

We should recognize that the ULTC action at the high-voltage side changes the ONRs n'_{HL} and n'_{HT}; these two ONRs cannot be adjusted independently.

The three branches of the delta equivalent circuit can each be represented by an equivalent circuit as shown in Figure 6.18.

The equivalent π circuits representing the initial ULTC tap position are as follows.

H-L branch:

$$y_1 = \frac{1}{n'_{HL}Z'_{HL}} = \frac{1}{0.91667(0.00032+j0.02067)}$$

$$= 0.81687-j52.76457$$

$$y_2 = \left(\frac{1}{n'_{HL}}-1\right)y_1 = \left(\frac{1}{0.91667}-1\right)(0.81687-j52.26457)$$

$$= 0.074258-j4.79657$$

$$y_3 = \left(1-\frac{1}{n'_{HL}}\right)\frac{1}{Z'_{HL}} = \left(1-\frac{1}{0.91667}\right)\frac{1}{0.00032+j0.02067}$$

$$= -0.06807+j4.39687$$

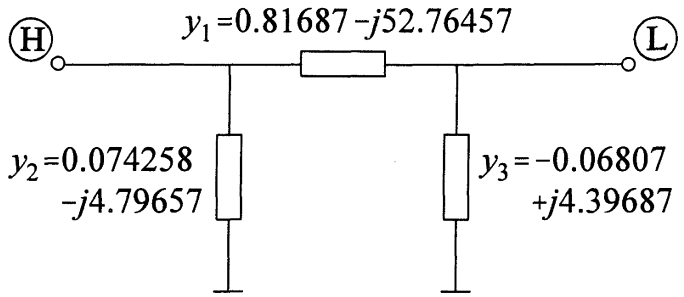

L-T branch:

$$y_1 = \frac{1}{n'_{LT}Z'_{LT}} = \frac{1}{1.07532(0.00015+j0.02504)}$$

$$= 0.22247-j37.13748$$

$$y_2 = \left(\frac{1}{n'_{LT}}-1\right)y_1 = \left(\frac{1}{1.07532}-1\right)(0.22247-j37.13748)$$

$$= -0.01558+j2.60127$$

$$y_3 = \left(1-\frac{1}{n'_{LT}}\right)\frac{1}{Z'_{LT}} = \left(1-\frac{1}{1.07532}\right)\frac{1}{0.00015+j0.02504}$$

$$= 0.01676-j2.79719$$

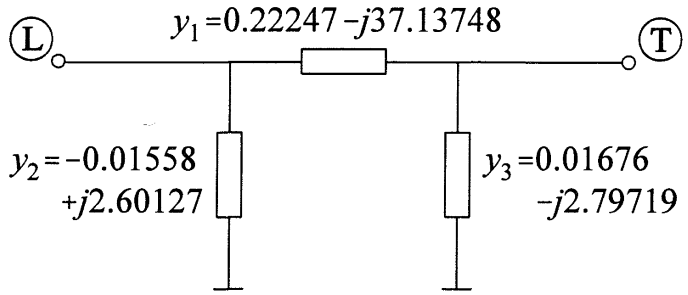

H-T branch:

$$y_1 = \frac{1}{n'_{HT}Z'_{HT}} = \frac{1}{0.98571(-0.10784-j0.67280)}$$

$$= -0.23564+j1.47010$$

$$y_2 = \left(\frac{1}{n'_{HT}}-1\right)y_1 = \left(\frac{1}{0.98571}-1\right)(-0.23564+j1.47010)$$

$$= -0.00342+j0.02131$$

$$y_3 = \left(1-\frac{1}{n'_{HT}}\right)\frac{1}{Z'_{HT}} = \left(1-\frac{1}{0.98571}\right)\frac{1}{-0.10784-j0.67280}$$

$$= 0.00337-j0.02101$$

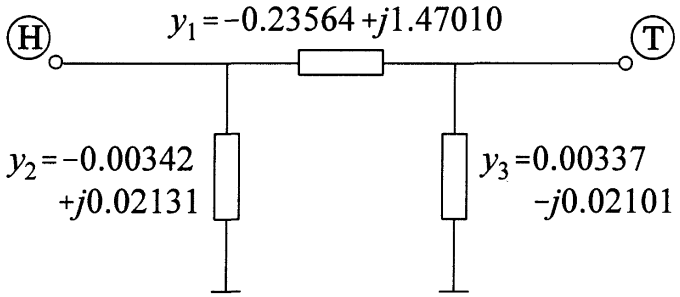

6.2.3 Phase-Shifting Transformers [14]

A phase-shifting transformer can be represented by the equivalent circuit shown in Figure 6.20. It consists of an admittance in series with an ideal transformer having a *complex turns ratio*, $\tilde{n}=n\angle\alpha$. The phase angle step size may not be equal at different tap positions. However, equal step size is usually used in power flow and transient stability programs.

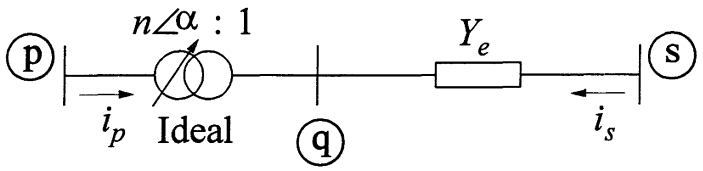

Figure 6.20 Phase-shifting transformer representation

By definition:

$$\frac{\tilde{v}_p}{\tilde{v}_q} = n\angle\alpha = n(\cos\alpha + j\sin\alpha) = a_s + jb_s \tag{6.73}$$

where α is the phase shift from bus p to bus q; it is positive when $\tilde{v}_p$ leads $\tilde{v}_q$. Since there is no power loss in an ideal transformer,

$$\tilde{v}_p \tilde{i}_p^* = -\tilde{v}_q \tilde{i}_s^* \tag{6.74}$$

Therefore, the transformer current at bus p is

$$\begin{aligned} \tilde{i}_p &= -\frac{1}{a_s - jb_s}\tilde{i}_s \\ &= \frac{Y_e}{a_s - jb_s}(\tilde{v}_q - \tilde{v}_s) \end{aligned} \tag{6.75}$$

Substituting for $\tilde{v}_q$ from Equation 6.73, we get

$$\begin{aligned} \tilde{i}_p &= \frac{Y_e}{a_s - jb_s}\left[\frac{1}{a_s + jb_s}\tilde{v}_p - \tilde{v}_s\right] \\ &= \frac{Y_e}{a_s^2 + b_s^2}[\tilde{v}_p - (a_s + jb_s)\tilde{v}_s] \end{aligned} \tag{6.76}$$

From Equation 6.75,

$$\tilde{i}_s = -(a_s - jb_s)\tilde{i}_p$$

Substituting for $\tilde{i}_p$ from Equation 6.76 gives

$$\tilde{i}_s = \frac{Y_e}{a_s+jb_s}[(a_s+jb_s)\tilde{v}_s-\tilde{v}_p] \tag{6.77}$$

Combining Equations 6.76 and 6.77, we obtain the following matrix equation relating the phase-shifter terminal voltages and currents

$$\begin{bmatrix}\tilde{i}_p\\ \tilde{i}_s\end{bmatrix} = \begin{bmatrix}\dfrac{Y_e}{a_s^2+b_s^2} & \dfrac{-Y_e}{a_s-jb_s}\\ \dfrac{-Y_e}{a_s+jb_s} & Y_e\end{bmatrix}\begin{bmatrix}\tilde{v}_p\\ \tilde{v}_s\end{bmatrix} \tag{6.78}$$

We see that the admittance matrix in the above equation is *not symmetrical*, that is, the transfer admittance from p to s is not equal to the transfer admittance from s to p. Therefore, a π equivalent circuit is not possible.

If the turns ratio is real (i.e., $a_s=\bar{n}$ and $b_s=0$), the model reduces to the equivalent π circuit shown in Figure 6.18(b).

Example of modelling a phase-shifting transformer

Let us consider a three-phase, two-winding phase shifter with the following data:

MVA rating	: 300 MVA
Primary/secondary base voltages	: 240/240 kV
Resistance per phase	: 0
Leakage reactance per phase	: 0.145 pu
Phase-shift range and steps	: ±40°, 36 steps
System voltage base (primary/secondary)	: 220/230 kV
System MVA base	: 100 MVA

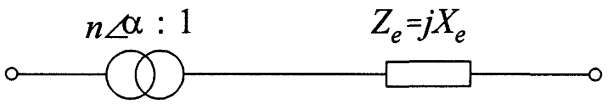

Leakage reactance in pu on system voltage and MVA base:

$$X_e = 0.145 \times \frac{100}{300} \times \left(\frac{240}{230}\right)^2$$

$$= 0.05263 \quad \text{pu}$$

Off-nominal turns ratio:

$$n = \frac{240}{220} \times \frac{230}{240} = 1.04545$$

Phase-shift angle limits:

$$\alpha_{max} = 40°$$

$$\alpha_{min} = -40°$$

The impedance of the transformer changes with the phase-shift angle. The following table (provided by the manufacturer) gives values of the impedance multiplier as a function of the angle.

Angle in degrees	±40	±29.5	±25.1	±20.6	0
Impedance multiplier	1.660	1.331	1.228	1.144	1.0

The admittance matrix of Equation 6.78 representing the phase shifter is

$$\mathbf{Y}_s = \begin{bmatrix} \dfrac{Y_e}{a_s^2+b_s^2} & \dfrac{-Y_e}{a_s-jb_s} \\ \dfrac{-Y_e}{a_s+jb_s} & Y_e \end{bmatrix}$$

As an illustration, we will determine the elements of the admittance matrix for two values of α.

(a) $\alpha=0$:

$$Y_e = \frac{1}{jX_e} = \frac{1}{j0.05263} = -j19.0006 \quad \text{pu}$$

The turns ratio of the ideal phase shifter is

$$a_s + jb_s = n(\cos\alpha + j\sin\alpha)$$

$$= 1.0455(\cos 0 + j\sin 0) = 1.0455 + j0$$

The corresponding admittance matrix $\mathbf{Y}_s$ is

$$\mathbf{Y}_s = \begin{bmatrix} -j17.3844 & j18.1745 \\ j18.1745 & -j19.0006 \end{bmatrix}$$

(b) α corresponding to the 10^{th} step:

$$\alpha = \frac{40}{36} \times 10 = 11.11°$$

The turns ratio is

$$a_s + jb_s = n(\cos 11.11° + j\sin 11.11°)$$

$$= 1.02585 + j0.20147$$

The phase-shifter leakage reactance at this value of α by interpolation is

$$X_e = \left[1.0 + \frac{11.11(1.144 - 1.0)}{20.6}\right] \times 0.05263$$

$$= 0.05672$$

Hence,

$$Y_e = \frac{1}{jX_e} = j17.6305$$

The admittance matrix $\mathbf{Y}_s$, with $a_s + jb_s = 1.02585 + j0.20147$ and $Y_e = j17.6305$, is

$$\mathbf{Y}_s = \begin{bmatrix} -j16.1310 & (-3.2499 + j16.5479) \\ (3.2499 + j16.5479) & -j17.6305 \end{bmatrix}$$

6.3 TRANSFER OF POWER BETWEEN ACTIVE SOURCES

We will now examine factors influencing transfer of active and reactive power between two sources connected by an inductive reactance as shown in Figure 6.21. Such a system is representative of two sections of a power system interconnected by a transmission system, with power transfer from one section to the other.

We have considered a purely inductive reactance interconnecting the two sources. This is because impedances representing transmission lines, transformers, and generators are predominantly inductive. When the full network is represented by an appropriate model for each of its elements and then reduced to a two-bus system, the resulting impedance will be essentially an inductive reactance. The shunt capacitances of transmission lines do not explicitly appear in the model shown in Figure 6.21; their effects are implicitly represented by the net reactive power transmitted. Analysis of transmission of active and reactive power through an inductive reactance thus gives useful insight into the characteristics of ac transmission systems.

Referring to Figure 6.21, the complex power at the receiving end is

$$\tilde{S}_R = P_R + jQ_R = \tilde{E}_R \tilde{I}^* = \tilde{E}_R \left[\frac{\tilde{E}_S - \tilde{E}_R}{jX} \right]^*$$

$$= E_R \left[\frac{E_S \cos\delta + jE_S \sin\delta - E_R}{jX} \right]^*$$

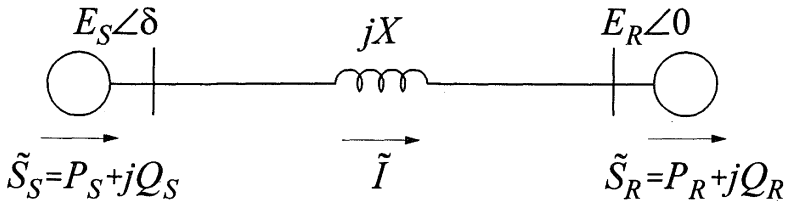

(a) Equivalent system diagram

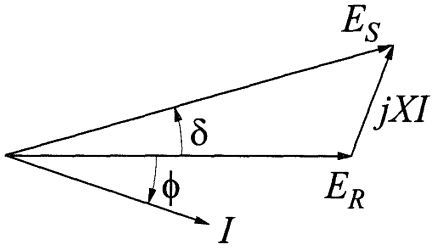

δ = load angle
ϕ = power factor angle

(b) Phasor diagram

Figure 6.21 Power transfer between two sources

Hence,

$$P_R = \frac{E_S E_R}{X}\sin\delta \tag{6.79}$$

$$Q_R = \frac{E_S E_R\cos\delta - E_R^2}{X} \tag{6.80}$$

Similarly,

$$P_S = \frac{E_S E_R}{X}\sin\delta \tag{6.81}$$

$$Q_S = \frac{E_S^2 - E_S E_R\cos\delta}{X} \tag{6.82}$$

Equations 6.79 to 6.82 describe the way in which active power and reactive power are transferred between active parts of a power network. Let us examine the dependence of active power and reactive power transfer on the source voltages by considering separately the effects of differences in voltage magnitudes and angles.

(a) We will look first at the condition with $\delta=0$. Equations 6.79 to 6.82 become

$$P_R = P_S = 0$$

and

$$Q_R = \frac{E_R(E_S - E_R)}{X}$$

$$Q_S = \frac{E_S(E_S - E_R)}{X}$$

The active power transfer is now zero. With $E_S > E_R$, Q_S and Q_R are positive, that is, reactive power is transferred from the sending end to the receiving end. The corresponding phasor diagram is shown in Figure 6.22(a). With $E_S < E_R$, Q_S and Q_R are negative, indicating that reactive power flows from the receiving end to the sending end. The phasor diagram is shown in Figure 6.22(b).

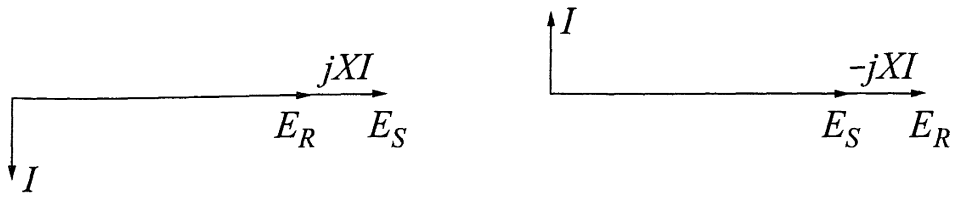

(a) $E_S > E_R$ (b) $E_R > E_S$

Figure 6.22 Phasor diagrams with $\delta = 0$

An alternative way of interpreting the above results is as follows:

- Transmission of lagging current through an inductive reactance causes a drop in receiving end voltage.
- Transmission of leading current through an inductive reactance causes a rise in receiving end voltage.

In each case,

$$Q_S - Q_R = \frac{(E_S - E_R)^2}{X} = XI^2$$

Therefore, the reactive power consumed by X is XI^2.

(b) We will next consider the condition with $E_S = E_R$, but with $\delta \neq 0$. From Equations 6.79 to 6.82, we now have

$$P_R = P_S = \frac{E^2}{X}\sin\delta$$

$$Q_S = -Q_R = \frac{E^2}{X}(1 - \cos\delta)$$

$$= \frac{1}{2}XI^2$$

With δ positive, P_S and P_R are positive, that is, active power flows from the sending end to the receiving end. With δ negative, the direction of active power flow reverses. In each case there is no reactive power transferred from one end to the other; instead, each end supplies half of the XI^2 consumed by X. The corresponding phasor diagrams are shown in Figure 6.23.

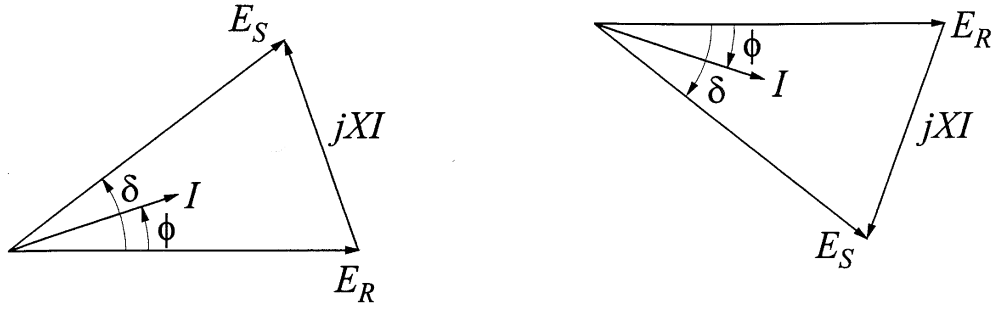

(a) δ>0 (b) δ<0

Figure 6.23 Phasor diagram with E_S=E_R

If the current I is in phase with E_R (i.e., the receiving end power factor is unity), the phasor diagram is as shown in Figure 6.24. In this case, the magnitude of E_S is only slightly larger than E_R. The sending end supplies all of the XI^2 consumed by X.

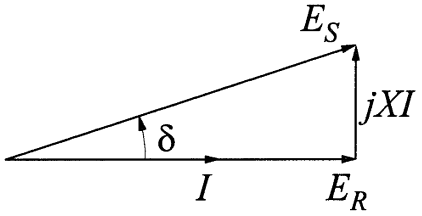

Figure 6.24 Phasor diagram with I in phase with E_R

We see that the active power transferred (P_R) is a function of voltage magnitudes and δ. However, for satisfactory operation of the power system, the voltage magnitude at any bus cannot deviate significantly from the nominal value. Therefore, control of active power transfer is achieved primarily through variations in angle δ.

(c) Finally, let us consider a general case applicable to any values of δ, E_S and E_R. The current I is

$$I = \frac{E_S\cos\delta + jE_S\sin\delta - E_R}{jX} \tag{6.83}$$

From Equations 6.80, 6.82, and 6.83, we have

$$Q_S - Q_R = \frac{E_S^2 + E_R^2 - 2E_S E_R \cos\delta}{X} = \frac{(XI)^2}{X} = XI^2 \tag{6.84}$$

If, in addition to inductive reactance X, we consider the series resistance R of the network, then

$$Q_{loss} = XI^2 = X\frac{P_R^2 + Q_R^2}{E_R^2} \tag{6.85}$$

$$P_{loss} = RI^2 = R\frac{P_R^2 + Q_R^2}{E_R^2} \tag{6.86}$$

We see from Equation 6.84 that the reactive power absorbed by X for all conditions is XI^2. This leads us to the concept of "reactive power loss," a companion term to active power loss RI^2 associated with resistive elements.

As seen from Equations 6.85 and 6.86, an increase of reactive power transmitted increases active as well as reactive power losses. This has an impact on efficiency of power transmission and voltage regulation.

From the above analysis, we can draw the following conclusions:

- Active power transfer depends mainly on the angle by which the sending end voltage leads the receiving end voltage.
- Reactive power transfer depends mainly on voltage magnitudes. It is transmitted from the side with higher voltage magnitude to the side with lower voltage magnitude.
- Reactive power cannot be transmitted over long distances since it would require a large voltage gradient to do so.
- An increase in reactive power transfer causes an increase in active as well as reactive power losses.

Although we have considered a simple system, the general conclusions are applicable to any practical system. In fact, the basic characteristics of ac transmission reflected in these conclusions have a dominant effect on the way in which we operate and control the power system.

6.4 POWER-FLOW ANALYSIS

So far in this chapter, we have considered simple system configurations and idealizing assumptions to gain an understanding of basic characteristics of ac transmission. In this section, we will describe analytical techniques for detailed analysis of power flow in large complex networks.

The power-flow (load-flow) analysis involves the calculation of power flows and voltages of a transmission network for specified terminal or bus conditions. Such calculations are required for the analysis of steady-state as well as dynamic performance of power systems.

The system is assumed to be balanced; this allows a single-phase representation of the system. For bulk power system studies, common practice is to represent the composite loads as seen from bulk power delivery points (see Chapter 7, Section 7.1). Therefore, the effects of distribution system voltage control devices on loads are represented implicitly.

In this section we will describe the power-flow analysis as it applies to the steady-state performance of the power system. The basic network equations presented here also apply to their representation in the analysis of system stability; however, as we will see in later chapters, some of the constraints vary depending on the type of stability problem being solved.

Bus classification

Associated with each bus are four quantities: active power P, reactive power Q, voltage magnitude V, and voltage angle θ.

The following types of buses (nodes) are represented, and at each bus two of the above four quantities are specified:

- Voltage-controlled (PV) bus: Active power and voltage magnitude are specified. In addition, limits to the reactive power are specified depending on the characteristics of the individual devices. Examples are buses with generators, synchronous condensers, and static var compensators.

- Load (PQ) bus: Active and reactive power are specified. Normally loads are assumed to have constant power. If the effect of distribution transformer ULTC operation is neglected, load P and Q are assumed to vary as a function of bus voltage.

- Device bus: Special boundary conditions associated with devices such as HVDC converters are recognized.

- Slack (swing) bus: Voltage magnitude and phase angle are specified. Because the power losses in the system are not known *a priori*, at least one bus must have unspecified P and Q. Thus the slack bus is the only bus with known voltage.

In some applications, it is desirable to keep the Q associated with the slack bus within reasonable limits; otherwise, the power-flow solution may become unrealistic. With Q at a limiting value, only the angle of the slack bus voltage is known.

Representation of network elements

Transmission lines are represented by equivalent π circuits with lumped parameters as described in Section 6.1.4. Shunt capacitors and reactors are represented as simple admittance elements connected to ground.

Transformers with off-nominal turns ratio are represented by equivalent π circuits as described in Section 6.2.2. Any phase shifts introduced due to transformer connections (such as Δ-Y connections) are not usually represented. In radial networks, such phase shifts do not affect power-flow analysis since currents and voltages are shifted by the same angle. In closed-loop networks, utilities take special care to connect transformer windings so that there is no net phase shift introduced in a common direction round a loop; otherwise, circulating current will flow, which is normally unacceptable. Figure 6.25 shows a scheme for connecting transformer windings with due regard to the resulting phase shifts.

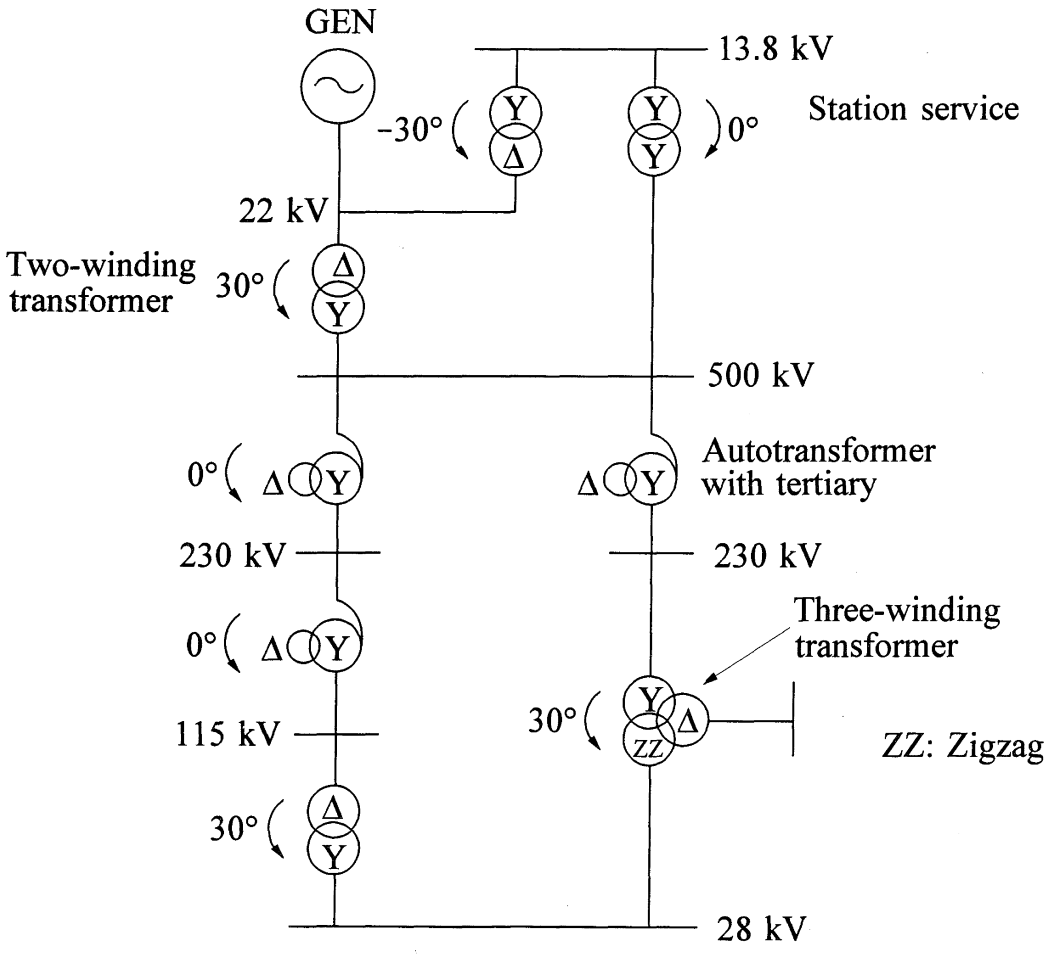

Figure 6.25 Illustration of a scheme for transformer-winding connections

Phase-shifting transformers, which are provided specifically for controlling power flow, are represented as illustrated in Section 6.2.3. This representation may also be used to account for phase shift introduced by the transformer-winding connection (Y-Δ, Y-Zigzag) in special situations where this is desired; the phase-shift angle in such cases, however, remains fixed.

As we are considering only the balanced operation of the power system, each element is modelled in terms of its single-phase equivalent (positive sequence).

6.4.1 Network Equations

The relationships between network bus (node) voltages and currents may be represented by either loop equations or node equations [1]. Node equations are normally preferred because the number of independent node equations is smaller than the number of independent loop equations.

The network equations in terms of the *node admittance matrix* can be written as follows:

$$\begin{bmatrix} \tilde{I}_1 \\ \tilde{I}_2 \\ \cdots \\ \tilde{I}_n \end{bmatrix} = \begin{bmatrix} Y_{11} & Y_{12} & \cdots & Y_{1n} \\ Y_{21} & Y_{22} & \cdots & Y_{2n} \\ \cdots & \cdots & \cdots & \cdots \\ Y_{n1} & Y_{n2} & \cdots & Y_{nn} \end{bmatrix} \begin{bmatrix} \tilde{V}_1 \\ \tilde{V}_2 \\ \cdots \\ \tilde{V}_n \end{bmatrix} \tag{6.87}$$

where

n is the total number of nodes
Y_{ii} is the self admittance of node i
= sum of all the admittances terminating at node i
Y_{ij} is mutual admittance between nodes i and j
= negative of the sum of all admittances between nodes i and j
$\tilde{V}_i$ is the phasor voltage to ground at node i
$\tilde{I}_i$ is the phasor current flowing into the network at node i

The effects of generators, nonlinear loads, and other devices (for example, dynamic reactive compensators, HVDC converters) connected to the network nodes are reflected in the node current. Constant impedance (linear) loads are, however, included in the node admittance matrix.

We will illustrate the formulation of the node equation by considering the simple three-bus system depicted in Figure 6.26.

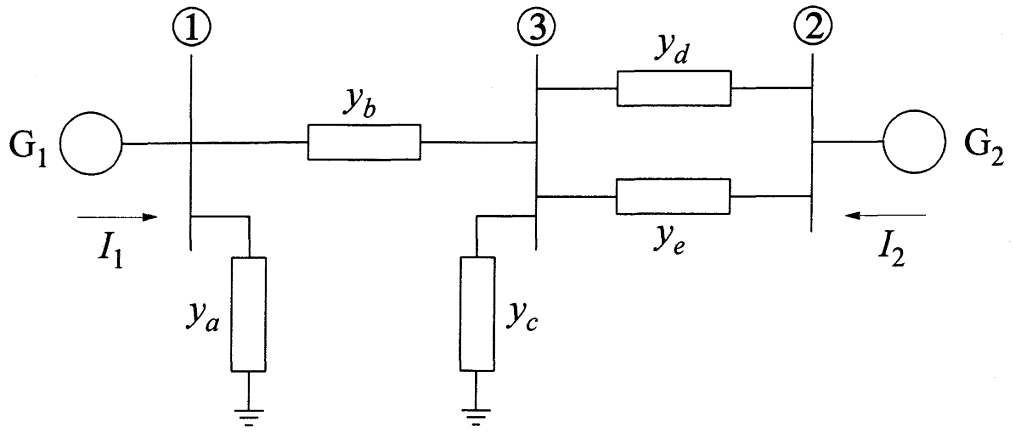

Figure 6.26 Single-line diagram of a three-bus system

The elements of the node admittance matrix are

$$Y_{11} = y_a + y_b \qquad Y_{12} = 0 \qquad Y_{13} = -y_b$$
$$Y_{21} = 0 \qquad Y_{22} = y_d + y_e \qquad Y_{23} = -(y_d + y_e)$$
$$Y_{31} = -y_b \qquad Y_{32} = -(y_d + y_e) \qquad Y_{33} = y_b + y_c + y_d + y_e$$

The node currents are

I_1 = current into node 1 from generator G_1
I_2 = current into node 2 from generator G_2
$I_3 = 0$

The node equation for the network of Figure 6.22 is

$$\begin{bmatrix} \tilde{I}_1 \\ \tilde{I}_2 \\ 0 \end{bmatrix} = \begin{bmatrix} Y_{11} & 0 & Y_{13} \\ 0 & Y_{22} & Y_{23} \\ Y_{31} & Y_{32} & Y_{33} \end{bmatrix} \begin{bmatrix} \tilde{V}_1 \\ \tilde{V}_2 \\ \tilde{V}_3 \end{bmatrix}$$

We can make the following general observations regarding the node admittance matrix:

(a) It is sparse with the degree of sparsity increasing with the network size.

(b) It is singular if floating (i.e., if there are no shunt branches to ground).

(c) It has weak diagonal dominance, i.e.,

$$|Y_{ii}| \geq \sum_{j \neq i} |Y_{ij}|$$

(d) It is symmetrical, if there are no phase-shifting transformers.

Nonlinear power-flow equations

Equations 6.87 would be *linear* if the current injections $\tilde{I}$ were known. However, in practice, the current injections are not known for most nodes. The current at any node k is related to P, Q and $\tilde{V}$ as follows:

$$\tilde{I}_k = \frac{P_k - jQ_k}{\tilde{V}_k^*} \tag{6.88}$$

For the PQ nodes, P and Q are specified; and for the PV nodes, P and the magnitude of $\tilde{V}$ are specified. For other types of nodes, the relationships between P, Q, $\tilde{V}$ and $\tilde{I}$ are defined by the characteristics of the devices connected to the nodes. Clearly the boundary conditions imposed by the different types of nodes make the problem *nonlinear* and therefore power-flow equations are solved iteratively using techniques such as the Gauss-Seidel or Newton-Raphson method. The principles of application of these methods are briefly described below. References 15 and 16 provide comprehensive reviews of numerical methods for power flow analysis.

6.4.2 Gauss-Seidel Method

This method is based on the iterative approach proposed by Seidel in 1874 (Academy of Science, Munich). For application to the power-flow problem, from Equations 6.87 and 6.88, for the k^{th} node we can write

$$\frac{P_k - jQ_k}{\tilde{V}_k^*} = Y_{kk}\tilde{V}_k + \sum_{\substack{i=1 \\ i \neq k}}^{n} Y_{ki}\tilde{V}_i \tag{6.89}$$

from which the voltage $\tilde{V}_k$ may be expressed as

$$\tilde{V}_k = \frac{P_k - jQ_k}{Y_{kk}\tilde{V}_k^*} - \frac{1}{Y_{kk}} \sum_{\substack{i=1 \\ i \neq k}}^{n} Y_{ki}\tilde{V}_i \tag{6.90}$$

Equation 6.89 is the heart of the iterative algorithm. The iterations begin with an informed guess of the magnitude and angle of the voltages at all load buses, and of the voltage angle at all generator buses.

For a load bus, P and Q are known, and Equation 6.90 is used to compute the voltage $\tilde{V}_k$ by using the best available voltages for all the buses. In other words, the upgraded values of bus voltages are used as soon as they are available. For example,

for the p^{th} iteration, the best values of bus voltages for computing the voltage V_k at bus k are $V_1^p, V_2^p, \cdots, V_{k-1}^p, V_k^{p-1}, V_{k+1}^{p-1}, \cdots, V_n^{p-1}$.

If the k^{th} bus is a generator bus, the following procedure is used:

(a) Rearranging Equation 6.89, we have

$$Q_k = -\text{Im}\left[\tilde{V}_k^* \sum_{i=1}^{n} Y_{ki} \tilde{V}_i\right] \tag{6.91}$$

where Q_k is calculated by using the best available values of bus voltages. If Q_k is within the limits $Q_{k\,max}$ and $Q_{k\,min}$, it is used in Equation 6.90 to compute the updated value of $\tilde{V}_k$. Its real and imaginary components are multiplied by the ratio of the *specified* value of the magnitude of the generator voltage to the magnitude of its updated value, thus complying with the magnitude constraint. In other words, the magnitude of the voltage is forced to be the specified value and Equations 6.90 and 6.91 are solved to compute the angle.

(b) If Q_k computed by Equation 6.91 exceeds either the maximum or minimum limit, it is set equal to the limit. The updated value of $\tilde{V}_k$ is computed by treating the generator bus as a PQ node.

The iterations are continued until the real and imaginary components of voltages at each bus computed by successive iterations converge to a specified tolerance.

The Gauss-Seidel method has slow convergence because of weak diagonal dominance of the node admittance matrix. Acceleration factors are often used to speed up the convergence:

$$\text{Accelerated } \tilde{V}_k^{\text{new}} = \tilde{V}_k^{\text{old}} + c(\tilde{V}_k^{\text{new}} - \tilde{V}_k^{\text{old}}) \tag{6.92}$$

where c is the acceleration factor, which is typically on the order of 1.4 to 1.7.

6.4.3 Newton-Raphson (N-R) Method

This is an iterative technique for solving a set of nonlinear equations. Let the following represent n such equations in n unknowns:

$$\begin{aligned} f_1(x_1, x_2, \cdots, x_n) &= b_1 \\ f_2(x_1, x_2, \cdots, x_n) &= b_2 \\ \cdots \quad \cdots \quad \cdots \quad \cdots \quad \cdots \quad \cdots \\ f_n(x_1, x_2, \cdots, x_n) &= b_n \end{aligned} \tag{6.93}$$

If the iterations start with an initial estimate of $x_1^0, x_2^0, \cdots, x_n^0$ for the n unknowns and if $\Delta x_1, \Delta x_2, \cdots, \Delta x_n$ are the corrections necessary to the estimates so that the equations are exactly satisfied, we have

$$\begin{aligned} f_1(x_1^0+\Delta x_1,\ x_2^0+\Delta x_2,\ \cdots,\ x_n^0+\Delta x_n) &= b_1 \\ f_2(x_1^0+\Delta x_1,\ x_2^0+\Delta x_2,\ \cdots,\ x_n^0+\Delta x_n) &= b_2 \\ \cdots\ \cdots\ \cdots\ \cdots\ \cdots\ \cdots\ \cdots\ \cdots\ \cdots\ \cdots\ \cdots & \\ f_n(x_1^0+\Delta x_1,\ x_2^0+\Delta x_2,\ \cdots,\ x_n^0+\Delta x_n) &= b_n \end{aligned} \tag{6.94}$$

Each of the above equations can be expanded using Taylor's theorem. The expanded form of the i^{th} equation is

$$\begin{aligned} & f_i(x_1^0+\Delta x_1, x_2^0+\Delta x_2, \cdots, x_n^0+\Delta x_n) \\ &= f_i(x_1^0, x_2^0, \cdots, x_n^0) + \left(\frac{\partial f_i}{\partial x_1}\right)_0 \Delta x_1 + \left(\frac{\partial f_i}{\partial x_2}\right)_0 \Delta x_2 + \cdots + \left(\frac{\partial f_i}{\partial x_n}\right)_0 \Delta x_n \\ &\quad + \text{terms with higher powers of } \Delta x_1, \Delta x_2, \cdots, \Delta x_n \\ &= b_i \end{aligned}$$

The terms of higher powers can be neglected, if our initial estimate is close to the true solution.

The resulting linear set of equations in matrix form is

$$\begin{bmatrix} b_1 - f_1(x_1^0, x_2^0, \cdots, x_n^0) \\ b_2 - f_2(x_1^0, x_2^0, \cdots, x_n^0) \\ \cdots\ \cdots\ \cdots\ \cdots\ \cdots\ \cdots\ \cdots\ \cdots \\ b_n - f_n(x_1^0, x_2^0, \cdots, x_n^0) \end{bmatrix} = \begin{bmatrix} \left(\frac{\partial f_1}{\partial x_1}\right)_0 & \left(\frac{\partial f_1}{\partial x_2}\right)_0 & \cdots & \left(\frac{\partial f_1}{\partial x_n}\right)_0 \\ \left(\frac{\partial f_2}{\partial x_1}\right)_0 & \left(\frac{\partial f_2}{\partial x_2}\right)_0 & \cdots & \left(\frac{\partial f_2}{\partial x_n}\right)_0 \\ \cdots & \cdots & \cdots & \cdots \\ \left(\frac{\partial f_n}{\partial x_1}\right)_0 & \left(\frac{\partial f_n}{\partial x_2}\right)_0 & \cdots & \left(\frac{\partial f_n}{\partial x_n}\right)_0 \end{bmatrix} \begin{bmatrix} \Delta x_1 \\ \Delta x_2 \\ \cdots \\ \Delta x_n \end{bmatrix} \tag{6.95}$$

or

$$\mathbf{\Delta f} = \mathbf{J}\Delta\mathbf{x} \tag{6.96}$$

where **J** is referred to as the *Jacobian.* If the estimates $x_1^0, \cdots, x_n^0$ were exact, then $\Delta\mathbf{f}$ and $\Delta\mathbf{x}$ would be zero. However, as $x_1^0, \cdots, x_n^0$ are only estimates, the errors $\Delta\mathbf{f}$ are finite. Equation 6.95 provides a linearized relationship between the errors $\Delta\mathbf{f}$ and the corrections $\Delta\mathbf{x}$ through the Jacobian of the simultaneous equations. A solution for $\Delta\mathbf{x}$ can be obtained by applying any suitable method for the solution of a set of linear equations. Updated values of x are calculated from

$$x_i^1 = x_i^0 + \Delta x_i$$

The process is repeated until the errors Δf_i are lower than a specified tolerance. The iterations have quadratic convergence. The Jacobian has to be recalculated at each step.

This method is sometimes referred to as *Newton's method.* However, it is more commonly called the *Newton-Raphson method* after J. Raphson (1648-1715) who wrote the iteration method in the form now commonly used.

Application of the N-R method to power-flow solution

To apply the Newton-Raphson method, each complex equation represented by Equation 6.89 has to be rewritten as two real equations in terms of two real variables instead of one complex variable. This is because Equation 6.89 is not an analytic function of the complex voltages due to the conjugate term $\tilde{V}_k^*$, and as a consequence the complex derivatives do not exist.

Most production-type power-flow programs use the power equation form with polar coordinates which we will use here. For any node k, we have

$$\tilde{S}_k = P_k + jQ_k = \tilde{V}_k \tilde{I}_k^* \tag{6.97}$$

From Equation 6.87,

$$\tilde{I}_k = \sum_{m=1}^{n} \tilde{Y}_{km} \tilde{V}_m \tag{6.98}$$

Substitution of $\tilde{I}_k$ given by Equation 6.98 in Equation 6.97 yields

$$P_k + jQ_k = \tilde{V}_k \sum_{m=1}^{n} (G_{km} - jB_{km}) \tilde{V}_m^* \tag{6.99}$$

The product of phasors $\tilde{V}_k$ and $\tilde{V}_m^*$ may be expressed as

$$\begin{aligned} \tilde{V}_k \tilde{V}_m^* &= (V_k e^{j\theta_k})(V_m e^{-j\theta_m}) = V_k V_m e^{j(\theta_k - \theta_m)} \\ &= V_k V_m (\cos\theta_{km} + j\sin\theta_{km}) \qquad (\theta_{km} = \theta_k - \theta_m) \end{aligned} \tag{6.100}$$

Therefore, the expressions for P_k and Q_k may be written in real form as follows:

$$\begin{aligned} P_k &= V_k \sum_{m=1}^{n} (G_{km}V_m\cos\theta_{km} + B_{km}V_m\sin\theta_{km}) \\ Q_k &= V_k \sum_{m=1}^{n} (G_{km}V_m\sin\theta_{km} - B_{km}V_m\cos\theta_{km}) \end{aligned} \tag{6.101}$$

Thus, P and Q at each bus are functions of voltage magnitude V and angle θ of *all buses*.

If the active power and reactive power at each bus are specified, using superscript *sp* to denote specified values, we may write the LF equation:

$$\begin{aligned} P_1(\theta_1, \cdots, \theta_n, V_1, \cdots, V_n) &= P_1^{sp} \\ \cdots \quad \cdots \quad \cdots \quad \cdots \quad \cdots \quad \cdots \quad \cdots \quad \cdots \quad \cdots \\ P_n(\theta_1, \cdots, \theta_n, V_1, \cdots, V_n) &= P_n^{sp} \\ Q_1(\theta_1, \cdots, \theta_n, V_1, \cdots, V_n) &= Q_1^{sp} \\ \cdots \quad \cdots \quad \cdots \quad \cdots \quad \cdots \quad \cdots \quad \cdots \quad \cdots \quad \cdots \\ Q_n(\theta_1, \cdots, \theta_n, V_1, \cdots, V_n) &= Q_n^{sp} \end{aligned} \tag{6.102}$$

Following the general procedure described earlier for the application of the N-R method (Equation 6.95), we have

$$\begin{bmatrix} P_1^{sp} - P_1(\theta_1^0, \cdots, \theta_n^0, V_1^0, \cdots, V_n^0) \\ \cdots \quad \cdots \quad \cdots \quad \cdots \quad \cdots \quad \cdots \quad \cdots \quad \cdots \\ P_n^{sp} - P_n(\theta_1^0, \cdots, \theta_n^0, V_1^0, \cdots, V_n^0) \\ Q_1^{sp} - Q_1(\theta_1^0, \cdots, \theta_n^0, V_1^0, \cdots, V_n^0) \\ \cdots \quad \cdots \quad \cdots \quad \cdots \quad \cdots \quad \cdots \quad \cdots \quad \cdots \\ Q_n^{sp} - Q_n(\theta_1^0, \cdots, \theta_n^0, V_1^0, \cdots, V_n^0) \end{bmatrix} = \begin{bmatrix} \frac{\partial P_1}{\partial \theta_1} & \cdots & \frac{\partial P_1}{\partial \theta_n} & \frac{\partial P_1}{\partial V_1} & \cdots & \frac{\partial P_1}{\partial V_n} \\ \cdots & \cdots & \cdots & \cdots & \cdots & \cdots \\ \frac{\partial P_n}{\partial \theta_1} & \cdots & \frac{\partial P_n}{\partial \theta_n} & \frac{\partial P_n}{\partial V_1} & \cdots & \frac{\partial P_n}{\partial V_n} \\ \frac{\partial Q_1}{\partial \theta_1} & \cdots & \frac{\partial Q_1}{\partial \theta_n} & \frac{\partial Q_1}{\partial V_1} & \cdots & \frac{\partial Q_1}{\partial V_n} \\ \cdots & \cdots & \cdots & \cdots & \cdots & \cdots \\ \frac{\partial Q_n}{\partial \theta_1} & \cdots & \frac{\partial Q_n}{\partial \theta_n} & \frac{\partial Q_n}{\partial V_1} & \cdots & \frac{\partial Q_n}{\partial V_n} \end{bmatrix} \begin{bmatrix} \Delta\theta_1 \\ \cdots \\ \Delta\theta_n \\ \Delta V_1 \\ \cdots \\ \Delta V_n \end{bmatrix}$$

or

$$\begin{bmatrix} \Delta \mathbf{P} \\ \Delta \mathbf{Q} \end{bmatrix} = \underbrace{\begin{bmatrix} \frac{\partial \mathbf{P}}{\partial \boldsymbol{\theta}} & \frac{\partial \mathbf{P}}{\partial \mathbf{V}} \\ \frac{\partial \mathbf{Q}}{\partial \boldsymbol{\theta}} & \frac{\partial \mathbf{Q}}{\partial \mathbf{V}} \end{bmatrix}}_{\text{Jacobian}} \begin{bmatrix} \Delta \boldsymbol{\theta} \\ \Delta \mathbf{V} \end{bmatrix} \tag{6.103}$$

The sparsity of each submatrix of the Jacobian is the same as that of the node admittance matrix. For efficient solution of the above equation, a suitable method, such as sparsity-oriented triangular factorization method (discussed in Section 6.4.6), must be used.

In formulating Equation 6.103, we have assumed that all buses are *PQ* buses. For a *PV* bus, only *P* is specified and the magnitude of *V* is fixed. Therefore, terms corresponding to ΔQ and ΔV would be absent for each of the *PV* buses. Thus the Jacobian would have only one row and one column for each *PV* bus.

Sensitivity analysis using the Jacobian

When we reach a solution with the N-R method, we have a linearized model around the given operating point:

$$\begin{bmatrix} \mathbf{J} \end{bmatrix} \begin{bmatrix} \Delta \boldsymbol{\theta} \\ \Delta \mathbf{V} \end{bmatrix} = \begin{bmatrix} \Delta \mathbf{P} \\ \Delta \mathbf{Q} \end{bmatrix} \tag{6.104}$$

We can, therefore, easily compute the expected small changes in θ and *V* for small changes in *P* and *Q*. This type of sensitivity information is useful for estimating expected voltage changes which result from the installation of reactive compensation.

As we will see in Chapter 14, the Jacobian also provides very useful information regarding voltage stability.

6.4.4 Fast Decoupled Load-Flow (FDLF) Methods [17,18]

These techniques take advantage of the physical weak coupling between *P* and *V*, and between *Q* and θ (see Section 6.3). They also make a number of approximations which simplify the power-flow problem.

The basic algorithm for FDLF may be derived as follows from Equation 6.103:

$$\begin{bmatrix} \Delta \mathbf{P} \\ \Delta \mathbf{Q} \end{bmatrix} = \begin{bmatrix} \frac{\partial \mathbf{P}}{\partial \boldsymbol{\theta}} & \frac{\partial \mathbf{P}}{\partial \mathbf{V}} \\ \frac{\partial \mathbf{Q}}{\partial \boldsymbol{\theta}} & \frac{\partial \mathbf{Q}}{\partial \mathbf{V}} \end{bmatrix} \begin{bmatrix} \Delta \boldsymbol{\theta} \\ \Delta \mathbf{V} \end{bmatrix}$$

The first step in applying the P-θ/Q-V decoupling is to neglect the coupling submatrices $\partial\mathbf{P}/\partial\mathbf{V}$ and $\partial\mathbf{Q}/\partial\boldsymbol{\theta}$ in Equation 6.103, giving two separate equations:

$$\begin{aligned}\Delta\mathbf{P} &= \frac{\partial\mathbf{P}}{\partial\boldsymbol{\theta}}\Delta\boldsymbol{\theta} \\ &= \mathbf{H}\Delta\boldsymbol{\theta}\end{aligned} \tag{6.105}$$

and

$$\begin{aligned}\Delta\mathbf{Q} &= \frac{\partial\mathbf{Q}}{\partial\mathbf{V}}\Delta\mathbf{V} \\ &= \mathbf{L}\Delta\mathbf{V}\end{aligned} \tag{6.106}$$

The elements of matrices **H** and **L** are derived from Equation 6.101 as follows [17]:

$$H_{km} = \frac{\partial P_k}{\partial\theta_m} = V_k V_m(G_{km}\sin\theta_{km} - B_{km}\cos\theta_{km}) \qquad \text{for } m \neq k$$

and

$$H_{kk} = \frac{\partial P_k}{\partial\theta_k} = -B_{kk}V_k^2 - Q_k$$

Similarly,

$$\begin{aligned}L_{km} &= \frac{\partial Q_k}{\partial V_m} = V_k(G_{km}\sin\theta_{km} - B_{km}\cos\theta_{km}) \\ &= H_{km}/V_m \qquad \text{for } m \neq k\end{aligned}$$

and

$$L_{kk} = -B_{kk}V_k + Q_k/V_k$$

Equations 6.105 and 6.106 may be solved alternately by the decoupled N-R method, re-evaluating and re-triangularizing matrices **H** and **L** at each iteration. However, further simplifications can be made by recognizing that in practical power systems the following approximations are valid:

$$\cos\theta_{km} \approx 1; \qquad G_{km}\sin\theta_{km} << B_{km}; \qquad Q_k << B_{kk}V_k^2$$

Therefore, Equations 6.105 and 6.106 simplify to

$$\Delta \mathbf{P} = (\mathbf{V}\mathbf{B}'\mathbf{V})\Delta\boldsymbol{\theta} \tag{6.107}$$

$$\Delta \mathbf{Q} = (\mathbf{V}\mathbf{B}'')\Delta\mathbf{V} \tag{6.108}$$

At this stage, matrices $\mathbf{B}'$ and $\mathbf{B}''$ are identical and equal to $-\mathbf{B}$, where $\mathbf{B}$ is the network susceptance matrix.

The following simplifications further improve the convergence rate of the iterative process [17]:

(a) The network elements that predominantly affect reactive power flows (i.e., shunt reactances and off-nominal ratio transformer taps) are omitted from $\mathbf{B}'$. Similarly, phase-shifter effects are omitted from $\mathbf{B}''$.

(b) The left-hand $\mathbf{V}$ terms in Equations 6.107 and 6.108 are moved to the left-hand sides of the equations, and the influence of reactive power flows on the calculation of $\Delta\boldsymbol{\theta}$ is removed by setting the right-hand $\mathbf{V}$ terms to 1.0 pu in Equation 6.107.

Equations 6.107 and 6.108 now simplify to

$$\Delta \mathbf{P}/\mathbf{V} = \mathbf{B}'\Delta\boldsymbol{\theta} \tag{6.109}$$

$$\Delta \mathbf{Q}/\mathbf{V} = \mathbf{B}''\Delta\mathbf{V} \tag{6.110}$$

The method originally proposed in reference 17, in addition to the approximations stated above, neglects the effects of series resistances in $\mathbf{B}'$; it is called the *XB scheme*. The method proposed later in reference 18 neglects the effects of series resistance in $\mathbf{B}''$ and is called the *BX scheme*.

The matrices $\mathbf{B}'$ and $\mathbf{B}''$ are both real and sparse. They contain only those network admittances that are constant. Therefore, they have to be triangularized only once at the beginning. Matrix $\mathbf{B}''$ is symmetrical so that only the upper triangular factor needs to be stored. If phase shifters are absent, $\mathbf{B}'$ is also symmetrical.

The advantage of using Equations 6.109 and 6.110 is that very fast repeat solutions of $\Delta\boldsymbol{\theta}$ and $\Delta\mathbf{V}$ can be obtained using constant triangular factors $\mathbf{B}'$ and $\mathbf{B}''$. These solutions may be iterated with each other in some defined manner toward the exact solution. The power-flow solution is reached when $\Delta\mathbf{P}/\mathbf{V}$ and $\Delta\mathbf{Q}/\mathbf{V}$ become less than the specified solution tolerance. At the i^{th} iteration $\Delta\mathbf{P}$ and $\Delta\mathbf{Q}$ are computed as follows by using Equations 6.101 and 6.102:

$$\Delta \mathbf{P} = \mathbf{P}^{sp} - \mathbf{P}(\boldsymbol{\theta}^{i-1}, \mathbf{V}^{i-1}) \tag{6.111}$$

$$\Delta \mathbf{Q} = \mathbf{Q}^{sp} - \mathbf{Q}(\boldsymbol{\theta}^{i-1}, \mathbf{V}^{i-1}) \tag{6.112}$$

This ensures that the full system equations are satisfied in the final solution. Equations 6.109 and 6.110 merely establish the corrections for $\Delta \mathbf{V}$ and $\Delta \boldsymbol{\theta}$ at each iteration step.

6.4.5 Comparison of the Power-Flow Solution Methods

The Gauss-Seidel method is the oldest of the power-flow solution methods. It is simple, reliable, and usually tolerant of poor voltage and reactive power conditions. In addition, it has low computer memory requirements. However, the computation time increases rapidly with system size. This method has a slow convergence rate and exhibits convergence problems when the system is stressed due to high levels of active power transfer.

The Newton-Raphson method has a very good convergence rate (quadratic). The computation time increases only linearly with system size. This method has convergence problems when the initial voltages are significantly different from their true values; it is therefore not suited for a "flat" voltage start.[1] Once the voltage solution is near the true solution, however, the convergence is very rapid. The Newton-Raphson method is therefore particularly suited for applications involving large systems requiring very accurate solutions.

The convergence properties of the Newton-Raphson method complement those of the Gauss-Seidel method. Therefore, many power-flow programs provide both solution techniques. The solution may be started with the Gauss-Seidel method and then switched to the Newton-Raphson method to obtain a rapid well-converged solution.

Fast decoupled load-flow (FDLF) methods are basically approximations to the Newton-Raphson (N-R) method. In the N-R method the Jacobian is required for computing $\Delta \boldsymbol{\theta}$ and $\Delta \mathbf{V}$. Therefore, the Jacobian has an impact on the convergence of the iterative solution but does not directly affect the final solution. The approximations made in the FDLF methods generally result in a small increase in the number of iterations. However, the computation effort is significantly reduced since the Jacobian does not have to be recalculated and refactorized in each iteration. In addition, the computer memory requirements are reduced. The convergence rate of the FDLF methods is linear as compared to the quadratic rate of the N-R method. The FDLF methods are less sensitive to the initial voltage and reactive power conditions than the N-R method. The fast decoupled *XB* method is not suited for systems with high *R/X* ratio; the *BX* method is better-suited for such systems. For most system conditions the FDLF methods provide rapid solution with good accuracy. However, for system conditions with very large angles across lines and with special control devices that strongly influence active and reactive power flows, full N-R formulation may be required.

---

[1] If a previously solved case for the same network with generally similar operating conditions is not available, a common practice is to start the solution with all load bus voltages at one per unit magnitude and zero angle, and all generator bus voltage magnitudes at specified magnitude and zero angle. This is known as a *flat* voltage start.

6.4.6 Sparsity-Oriented Triangular Factorization

Analysis of the power-flow problem using methods such as the N-R method and the FDLF method requires the solution of sparse linear matrix equations. Sparsity-oriented triangular factorization is commonly used for solving these equations.

A sparse linear matrix equation has the form

$$\mathbf{Ax} = \mathbf{b} \tag{6.113}$$

For any given **b**, the above equation can be solved for **x**, by triangular factorization of **A** as follows:

$$(\mathbf{LDU})\mathbf{x} = \mathbf{b} \tag{6.114}$$

where

L is lower triangular matrix
U is upper triangular matrix
D is diagonal matrix

The matrices **L** and **U** are also sparse. If **A** is symmetrical, **L** is the transpose of **U** and need not be computed or stored.

Equation 6.114 is solved for **x** in terms of **b** by forward and backward substitution. Forward substitution reduces Equation 6.114 to the form

$$\begin{bmatrix} \mathbf{U} \end{bmatrix} \begin{bmatrix} \mathbf{x} \end{bmatrix} = \begin{bmatrix} \mathbf{b}' \end{bmatrix} \tag{6.115}$$

This in effect is triangular factorization due to Gauss elimination. Solution of **x** is found by back substitution: the last equation gives x_n, inserted into $(n-1)^{\text{th}}$ equation gives x_{n-1}, and so on.

Sparsity techniques using optimal ordering are essential to this approach for the solution of large network equations [19]. The efficiency of sparse matrix methods can be enhanced by using sparse vector methods [20]. Reference 21 provides a detailed discussion of sparse matrix concepts and methods.

6.4.7 Network Reduction

The size of the network can be reduced by elimination of the passive nodes. If $I_k=0$, node k can be eliminated by replacing the elements of the remaining $n-1$ rows and columns with

$$y'_{ij} = y_{ij} - \frac{y_{ik}y_{kj}}{y_{kk}} \tag{6.116}$$

for $i=1, 2, \cdots, k-1, k+1, \cdots, n$ and $j=1, 2, \cdots, k-1, k+1, \cdots, n$.

By successive application of Equation 6.116, any desired number of passive nodes can be eliminated. Equation 6.116 is called *Kron's reduction formula.*

If sparsity techniques are used, it is not advisable to apply node elimination indiscriminately. In general, reduced systems become denser; therefore, the best compromise is to eliminate only those nodes that do not contribute to an increase in the number of branches when eliminated.

Reference 22 describes an efficient network reduction technique that takes advantage of certain special properties of sparse matrix factorization.

REFERENCES

[1] W.D. Stevenson, Jr., *Elements of Power System Analysis*, Third Edition, McGraw-Hill, 1975.

[2] O. Elgerd, *Electric Energy Systems Theory: An Introduction*, McGraw-Hill, 1971.

[3] J. Zaborszky and J.W. Rittenhouse, *Electric Power Transmission*, Vols. 1 and 2, 3rd reprint, The Rensselaer Book Store, Troy, N.Y., 1977.

[4] B.M. Weedy, *Electric Power Systems*, John Wiley & Sons, Third Edition, 1979.

[5] C.A. Gross, *Power System Analysis*, Second Edition, John Wiley & Sons, 1986.

[6] C.F. Wagner and R.D. Evans, *Symmetrical Components*, McGraw-Hill, 1933.

[7] M.E. El-Hawary, *Electrical Power Systems: Design and Analysis*, Reston Publishing Company, 1983.

[8] *Electrical Transmission and Distribution Reference Book*, Westinghouse Electric Corporation, East Pittsburgh, Pa., 1964.

[9] J.J. Leforest (editor), *Transmission Line Reference Book-345 kV and Above*, Second Edition, EPRI, 1982.

[10] T.J.E. Miller (editor), *Reactive Power Control in Electric Systems*, Wiley-Interscience, 1982.

[11] H.P. St. Clair, "Practical Concepts in Capability and Performance of Transmission Lines," *AIEE Trans.*, Vol. 72, pp. 1152-1157, December 1953.

[12] R.D. Dunlop, R. Gutman, and R.P. Marchenko, "Analytical Development of Loadability Characteristics for EHV and UHV Transmission Lines," *IEEE Trans.*, Vol. PAS-98, pp. 606-617, March/April 1979.

[13] IEEE Committee Report, "Common Format for the Exchange of Solved Load Flow Data," *IEEE Trans.*, Vol. PAS-92, pp. 1916-1925, November/December 1973.

[14] G.W. Stagg and A.H. El-Abiad, *Computer Methods in Power System Analysis*, McGraw-Hill, 1968.

[15] M.A. Laughton and M.W.H. Davies, "Numerical Techniques in Solution of Power System Load-Flow Problems," *Proceedings of IEE*, Vol. III, No. 9, 1964.

[16] B. Stott, "Review of Load-Flow Calculation Methods," *Proceedings of IEEE*, Vol. 62, pp. 916-929, July 1974.

[17] B. Stott and D. Alsac, "Fast Decoupled Load Flow," *IEEE Trans.*, Vol. PAS-93, pp. 859-869, May/June 1974.

[18] R.A.M. Van Amerongen, "A General-Purpose Version of the Fast Decoupled Load Flow," *IEEE Trans.*, Vol. PWRS-4, pp. 760-770, May 1989.

[19] W.F. Tinney and J.W. Walker, "Direct Solutions of Sparse Network Equations by Optimally Ordered Triangular Factorization," *Proceedings of IEEE*, Vol. 55, pp. 1801-1809, November 1967.

[20] W.F. Tinney, V. Brandwajn, and S.M. Chan, "Sparse Vector Methods," *IEEE Trans.*, Vol. PAS-104, pp. 295-301, February 1985.

[21] F.L. Alvarado, W.F. Tinney, and M.K. Enns, "Sparsity in Large-Scale Network Computation," *Control and Dynamic Systems*, Vol. 41: *Analysis and Control System Techniques for Electric Power Systems*, Part 1, pp. 207-271, Academic Press, Inc., 1991.

[22] W.F. Tinney and J.M. Bright, "Adaptive Reductions for Power Flow Equivalents," *IEEE Trans.*, Vol. PWRS-2, No. 2, pp. 351-360, May 1987.

Chapter 7

Power System Loads

Stable operation of a power system depends on the ability to continuously match the electrical output of generating units to the electrical load on the system. Consequently, load characteristics have an important influence on system stability.

The modelling of loads is complicated because a typical load bus represented in stability studies is composed of a large number of devices such as fluorescent and incandescent lamps, refrigerators, heaters, compressors, motors, furnaces, and so on. The exact composition of load is difficult to estimate. Also, the composition changes depending on many factors including time (hour, day, season), weather conditions, and state of the economy.

Even if the load composition were known exactly, it would be impractical to represent each individual component as there are usually millions of such components in the total load supplied by a power system. Therefore, load representation in system studies is based on a considerable amount of simplification.

This chapter will discuss basic load-modelling concepts, load composition and component characteristics, and acquisition of load model parameters. As induction motors constitute a major portion of the system loads, the characteristics and modelling of induction motors are discussed in detail.

7.1 BASIC LOAD-MODELLING CONCEPTS

In power system stability and power flow studies, the common practice is to represent the composite load characteristics as seen from bulk power delivery points. As illustrated in Figure 7.1, the aggregated load represented at a transmission

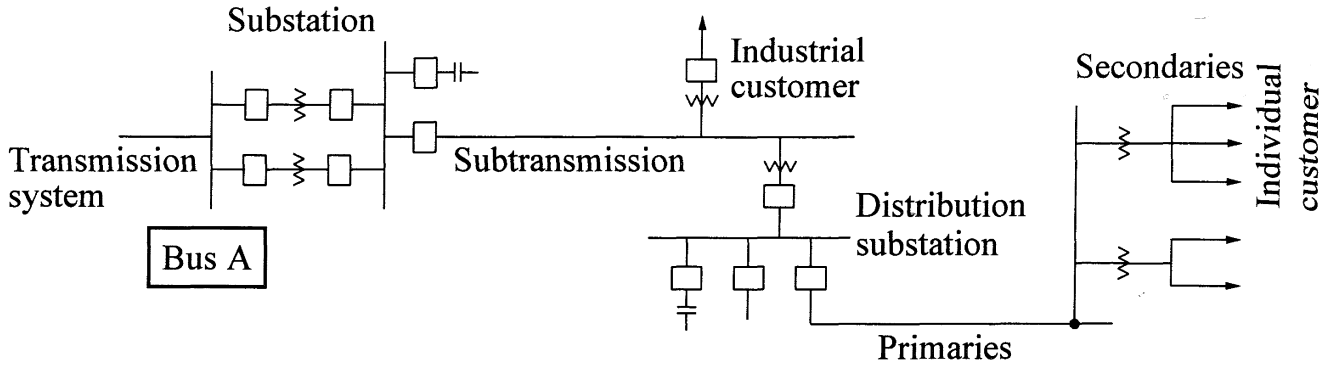

Figure 7.1 Power system configuration identifying parts of the system represented as load at a bulk power delivery point (bus A)

substation (bus A) usually includes, in addition to the connected load devices, the effects of substation step-down transformers, subtransmission feeders, distribution feeders, distribution transformers, voltage regulators, and reactive power compensation devices.

The load models are traditionally classified into two broad categories: static models and dynamic models.

7.1.1 Static Load Models

A static load model expresses the characteristics of the load at any instant of time as *algebraic functions* of the bus voltage magnitude and frequency at that instant [1]. The active power component P and the reactive power component Q are considered separately.

Traditionally, the voltage dependency of load characteristics has been represented by the *exponential model*:

$$P = P_0(\bar{V})^a$$
$$Q = Q_0(\bar{V})^b \tag{7.1}$$

In this and other load models described in this section,

$$\bar{V} = \frac{V}{V_0}$$

where P and Q are active and reactive components of the load when the bus voltage magnitude is V. The subscript 0 identifies the values of the respective variables at the initial operating condition.

The parameters of this model are the exponents a and b. With these exponents equal to 0, 1, or 2, the model represents constant power, constant current, or constant impedance characteristics, respectively. For composite loads, their values depend on the aggregate characteristics of load components.

The exponent a (or b) is nearly equal to the slope dP/dV (or dQ/dV) at $V=V_0$. For composite system loads, the exponent a usually ranges between 0.5 and 1.8; the exponent b is typically between 1.5 and 6. A significant characteristic of the exponent b is that it varies as a nonlinear function of voltage. This is caused by magnetic saturation in distribution transformers and motors. At higher voltages, Q tends to be significantly higher.

Reference 2 gives a summary of data available in the literature on voltage dependency of load. References 3 and 4 give results of measurements which provide information about the variation of the load characteristics with time of day, season, and/or temperature. In the absence of specific information, the most commonly accepted static load model is to represent active power as constant current (i.e., $a=1$) and reactive power as constant impedance (i.e., $b=2$) [2].

An alternative model which has been widely used to represent the voltage dependency of loads is the *polynomial model*:

$$\begin{aligned} P &= P_0\left[p_1\bar{V}^2+p_2\bar{V}+p_3\right] \\ Q &= Q_0\left[q_1\bar{V}^2+q_2\bar{V}+q_3\right] \end{aligned} \tag{7.2}$$

This model is commonly referred to as the *ZIP* model, as it is composed of constant impedance (Z), constant current (I), and constant power (P) components [1]. The parameters of the model are the coefficients p_1 to p_3 and q_1 to q_3, which define the proportion of each component.

The frequency dependency of load characteristics is usually represented by multiplying the exponential model or the polynomial model by a factor as follows:

$$\begin{aligned} P &= P_0(\bar{V})^a(1+K_{pf}\Delta f) \\ Q &= Q_0(\bar{V})^b(1+K_{qf}\Delta f) \end{aligned} \tag{7.3}$$

or

$$\begin{aligned} P &= P_0\left[p_1\bar{V}^2+p_2\bar{V}+p_3\right](1+K_{pf}\Delta f) \\ Q &= Q_0\left[q_1\bar{V}^2+q_2\bar{V}+q_3\right](1+K_{qf}\Delta f) \end{aligned} \tag{7.4}$$

where Δf is the frequency deviation ($f-f_0$). Typically, K_{pf} ranges from 0 to 3.0, and K_{qf} ranges from −2.0 to 0 [2]. The bus frequency f is usually not a state variable in the

system model used for stability analysis. Therefore, it is evaluated by computing the time derivative of the bus voltage angle.

A comprehensive static model which offers the flexibility of accommodating several forms of load representation is as follows [5]:

$$P = P_0[P_{ZIP}+P_{EX1}+P_{EX2}] \tag{7.5}$$

where

$$\begin{aligned} P_{ZIP} &= p_1\bar{V}^2+p_2\bar{V}+p_3 \\ P_{EX1} &= p_4(\bar{V})^{a1}(1+K_{pf1}\Delta f) \\ P_{EX2} &= p_5(\bar{V})^{a2}(1+K_{pf2}\Delta f) \end{aligned} \tag{7.6}$$

The expression for the reactive component of the load has a similar structure. The reactive power compensation associated with the load is represented separately.

The static models given by Equations 7.1 to 7.6 are not realistic at low voltages, and may lead to computational problems. Therefore, stability programs usually make provisions for switching the load characteristic to the constant impedance model when the bus voltage falls below a specified value. In the load model used in the EPRI Extended Transient/Midterm Stability Program (ETMSP) [5], the exponents a_1, a_2, b_1, and b_2 are varied as a function of voltage below a threshold value of bus voltage, and the constant power and constant current components are switched to constant impedance representation.

7.1.2 Dynamic Load Models

The response of most composite loads to voltage and frequency changes is fast, and the steady state of the response is reached very quickly. This is true at least for modest amplitudes of voltage/frequency change. The use of static models described in the previous sections is justified in such cases.

There are, however, many cases where it is necessary to account for the dynamics of load components. Studies of interarea oscillations, voltage stability, and long-term stability often require load dynamics to be modelled. Study of systems with large concentrations of motors also requires representation of load dynamics.

Typically, motors consume 60 to 70% of the total energy supplied by a power system. Therefore, the dynamics attributable to motors are usually the most significant aspects of dynamic characteristics of system loads. Modelling of motors is discussed in Section 7.2.

Other dynamic aspects of load components that require consideration in stability studies include the following [1,2,6]:

(a) Extinction of discharge lamps below a certain voltage and their restart when the voltage recovers. Discharge lamps include mercury vapour, sodium vapour, and fluorescent lamps. These extinguish at voltages in the range of 0.7 to 0.8 pu. When the voltage recovers, they restart after 1 or 2 seconds delay.

(b) Operation of protective relays, such as thermal and overcurrent relays. Many industrial motors have starters with electromagnetically held contactors. These drop open at voltages in the range of 0.55 to 0.75 pu; the dropout time is on the order of a few cycles. Small motors on refrigerators and air conditioners have only thermal overload protections, which typically trip in about 10 to 30 seconds.

(c) Thermostatic control of loads, such as space heaters/coolers, water heaters, and refrigerators. Such loads operate longer during low-voltage conditions. As a result, the total number of these devices connected to the system will increase in a few minutes after a drop in voltage. Air conditioners and refrigerators also exhibit such characteristics under sustained low-frequency conditions.

(d) Response of ULTCs on distribution transformers, voltage regulators, and voltage-controlled capacitor banks. These devices are not explicitly modelled in many studies. In such cases, their effects must be implicitly included in the equivalent load that is represented at the bulk power delivery point.

As these devices restore distribution voltages following a disturbance, the power supplied to voltage sensitive loads is restored to the pre-disturbance levels. The control action begins about 1 minute after the change in voltage, and the voltage restoration within the capability of these devices is completed in a total time of 2 to 3 minutes.

A composite load model which allows the representation of the wide range of characteristics exhibited by the various load components is shown in Figure 7.2. It is similar to the complex or aggregate load models described in references 6 and 7. The model has provision for representing aggregations of small induction motors, large induction motors, static load characteristics (Equations 7.5 and 7.6), discharge lighting, thermostatically controlled loads, transformer saturation effects, and shunt capacitors.

Thermostatically controlled loads:

Figure 7.3 shows a simple model of the aggregated thermostatically controlled (that is, constant energy) loads suggested in references 8 and 9. In this model, G is the load conductance, G_0 is the initial value of G, $K_L G_0$ is the maximum value of G which represents a condition with all such loads on, and T is a time constant.

A more realistic model of the thermostatically controlled loads used in the ETMSP [5] is shown in Figure 7.4. The basis for the model is as follows:

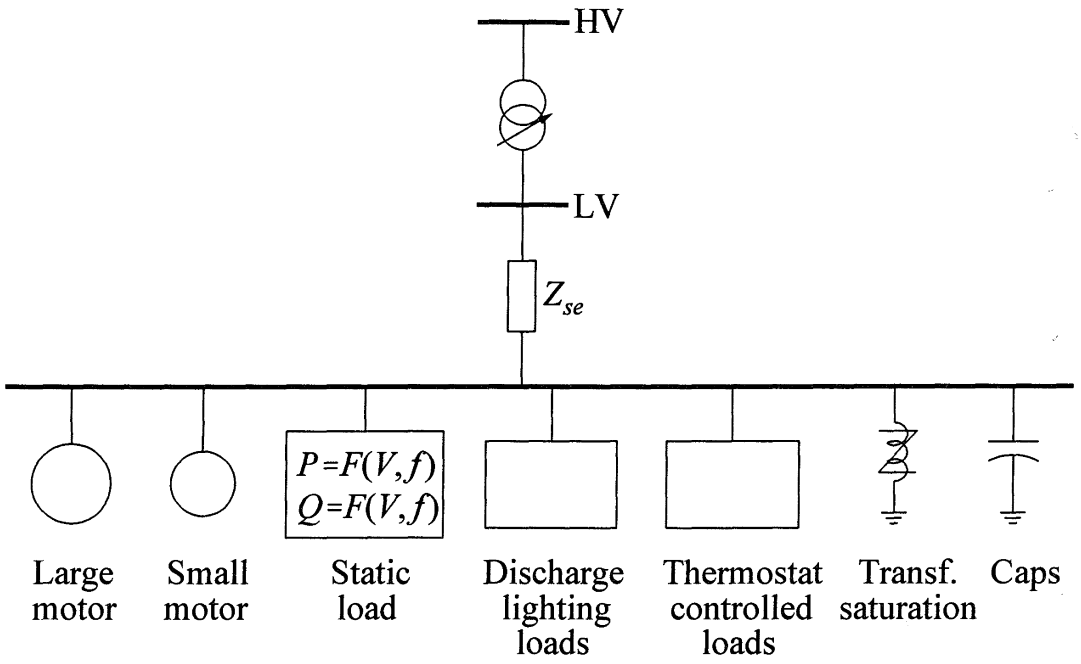

Figure 7.2 Composite static and dynamic load model

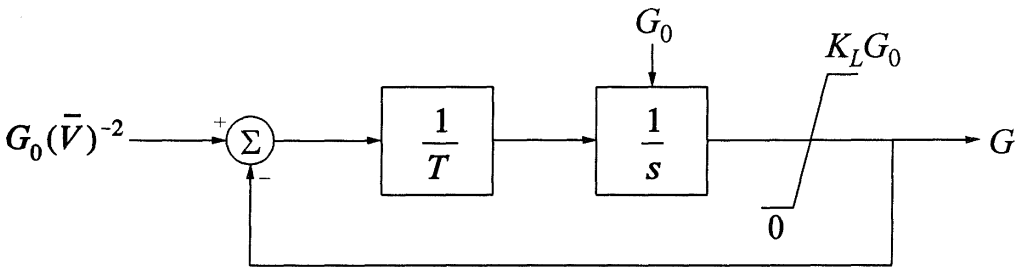

Figure 7.3 A simple model for thermostatically controlled loads

The dynamic equation of a heating device may be written as

$$K\frac{d\tau_H}{dt} = P_H - P_L \tag{7.7}$$

where

τ_H = temperature of heated area
τ_A = ambient temperature
P_H = power from the heater
$= K_H G V^2$
P_L = heat loss by escape to ambient area
$= K_A(\tau_H - \tau_A)$
G = load conductance

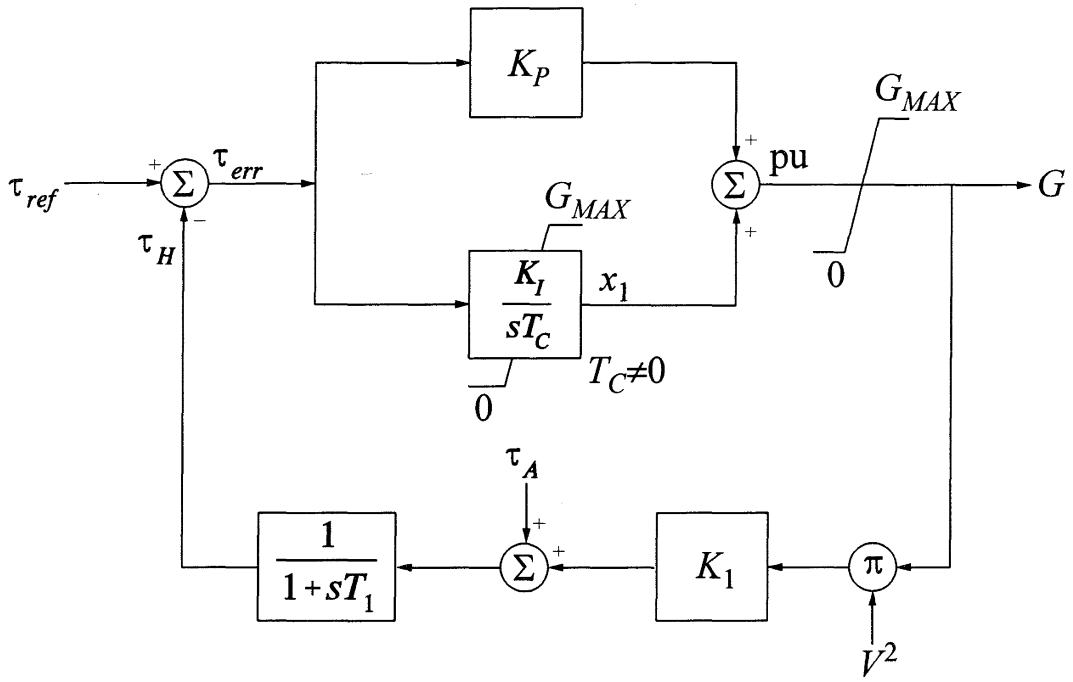

K_P = gain of proportional controller
K_I = gain of integral controller
T_C = time constant of integral controller, s
τ_{ref} = reference temperature
τ_A = ambient temperature
T_1 = load time constant, s
K_1 = gain associated with load model
G_0 = initial value of G
G_{MAX} = maximum value of G

Figure 7.4 A realistic model for thermostatically controlled loads

Substituting the expressions for P_H and P_L in Equation 7.7 gives

$$K\frac{d\tau_H}{dt} = K_H G V^2 - K_A(\tau_H - \tau_A) \tag{7.8}$$

Rearranging, we have

$$\frac{d\tau_H}{dt} = \frac{K_H}{K} G V^2 + \frac{K_A}{K}\tau_A - \frac{K_A}{K}\tau_H$$

or

$$\frac{d\tau_H}{dt} = \frac{K_1}{T_1} G V^2 + \frac{1}{T_1}\tau_A - \frac{1}{T_1}\tau_H \tag{7.9}$$

where

$$T_1 = \frac{K}{K_A}$$

and

$$K_1 = \frac{K_H}{K_A}$$

The temperature τ_H is compared with the reference temperature, and the error signal controls the load conductance through a proportional plus integral controller. When all the thermostatically controlled loads supplied by the load bus are on, G reaches its maximum value G_{MAX}.

From Figure 7.4, under pre-disturbance conditions τ_H is equal to τ_{ref}. Hence,

$$\tau_{ref} = K_1 V_0^2 G_0 + \tau_A$$

or

$$K_1 = \frac{\tau_{ref} - \tau_A}{V_0^2 G_0} \tag{7.10}$$

Discharge lighting loads:

Figure 7.5 shows a model suitable for representing the characteristics of discharge lighting loads in stability studies. At bus voltages less than V_1, the lamps extinguish. For voltages greater than V_1, P and Q vary as nonlinear functions of V.

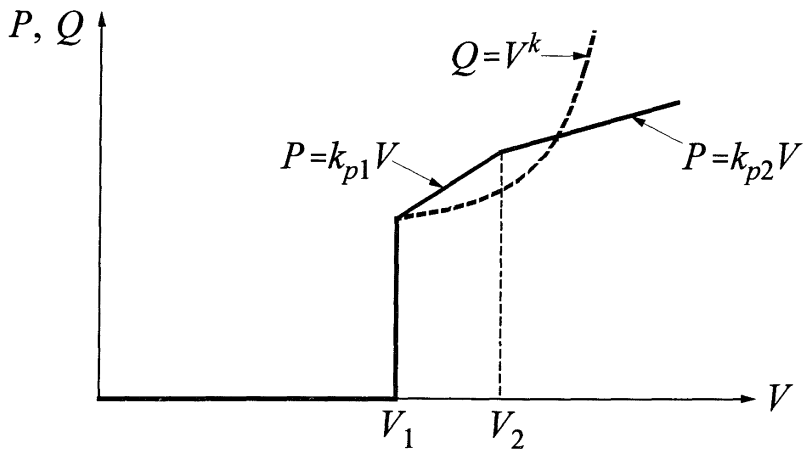

Figure 7.5 Discharge lighting characteristics

7.2 MODELLING OF INDUCTION MOTORS

As indicated in the previous section, motors form a major portion of the system loads. Induction motors in particular form the workhorse of the electric power industry; hence modelling of motors is important in system stability studies. In this section, we will develop in detail the mathematical model for an induction machine.

7.2.1 Equations of an Induction Machine

An induction machine carries alternating currents in both the stator and rotor windings. In a three-phase induction machine, the stator windings are connected to a balanced three-phase supply. The rotor windings are either short-circuited internally or connected through slip rings to a passive external circuit. The distinctive feature of the induction machine is that the rotor currents are induced by electromagnetic induction from the stator. This is the reason for the designation "induction machine."

The stator windings of a three-phase induction machine are similar to those of a synchronous machine (see Chapter 3, Section 3.1). When balanced three-phase currents of frequency f_s Hz are applied, the stator windings produce a field rotating at synchronous speed given by

$$n_s = \frac{120 f_s}{p_f} \tag{7.11}$$

where n_s is in r/min and p_f is the number of poles (2 per three-phase winding set).

When there is a relative motion between the stator field and the rotor, voltages are induced in the rotor windings. The frequency (f_r Hz) of the induced rotor voltages depends on the relative speeds of the stator field and the rotor. The current in each rotor winding is equal to the induced voltage divided by the rotor circuit impedance at the rotor frequency f_r. The rotor current reacting with the stator field produces a torque which accelerates the rotor in the direction of the stator field rotation. As the rotor speed n_r approaches the speed n_s of the stator field, the induced rotor voltages and currents approach zero. To develop a positive torque, n_r must be less than n_s. The rotor thus travels at a speed $n_s - n_r$ r/min in the backward direction with respect to the stator field. The *slip* speed of the rotor in per unit of the synchronous speed is

$$s = \frac{n_s - n_r}{n_s} \quad \text{per unit} \tag{7.12}$$

The frequency f_r of the induced rotor voltages is equal to the slip frequency sf_s.

At no load, the machine operates with negligible slip. If a mechanical load is applied, the slip increases (i.e., rotor speed decreases) such that the induced voltage and current produce the torque required by the load. The machine thus operates as a *motor*.

If the rotor is driven by a prime mover at a speed greater than that of the stator field, the slip is negative (i.e., rotor speed is greater than n_s). The polarities of the induced voltages are reversed so that the resulting torque is opposite in direction to that of rotation. The machine now operates as an induction *generator*.

We now develop a mathematical representation of induction machines appropriate for use in system studies. In the model, the effect of slots on the motor performance is ignored. In well-designed motors, their effect on motor performance is negligible. While our interest in this chapter is in the performance of induction machines as motors, the models we develop are sufficiently general to be applicable for generator as well as motor modes of operation. The general procedure followed here is similar to the approach used for modelling synchronous machines in Chapters 3 to 5. First we write the basic machine equations in terms of phase (a, b, c) variables; then, we transform the equations into the d-q reference frame; and finally, we make appropriate simplifications necessary to conform to the system equations in large-scale stability studies. In developing the model of an induction machine, it is worth noting the following aspects of its characteristics which differ from those of a synchronous machine:

- The rotor has a symmetrical structure. This makes the d- and q-axis equivalent circuits identical.
- The rotor speed is not fixed, but varies with load. This has an impact on the selection of the d–q reference frame.
- There is no excitation source applied to the rotor windings. Consequently, the dynamics of the rotor circuits are determined by slip, rather than by excitation control.
- The currents induced in the shorted rotor windings produce a field with the same number of poles as that produced by the stator winding. Rotor windings may therefore be modelled by an equivalent three-phase winding.

Basic equations of an induction machine

Figure 7.6 shows the circuits applicable to the analysis of an induction machine. The stator circuits consist of three-phase windings a, b, and c, distributed 120° apart in space. The rotor circuits have three distributed windings A, B, and C. The stator and rotor phases may be Y or Δ connected. In Figure 7.6, they are shown to be Y-connected.

There are two types of rotor structure. The *wound rotor* type has conventional three-phase windings brought out through three slip rings on the shaft so that they may be connected to an external circuit. The *squirrel-cage rotor* consists of a number of uninsulated bars in slots short-circuited by end rings at both ends. In the case of a squirrel-cage rotor, the rotor voltages v_A, v_B, and v_C are zero.

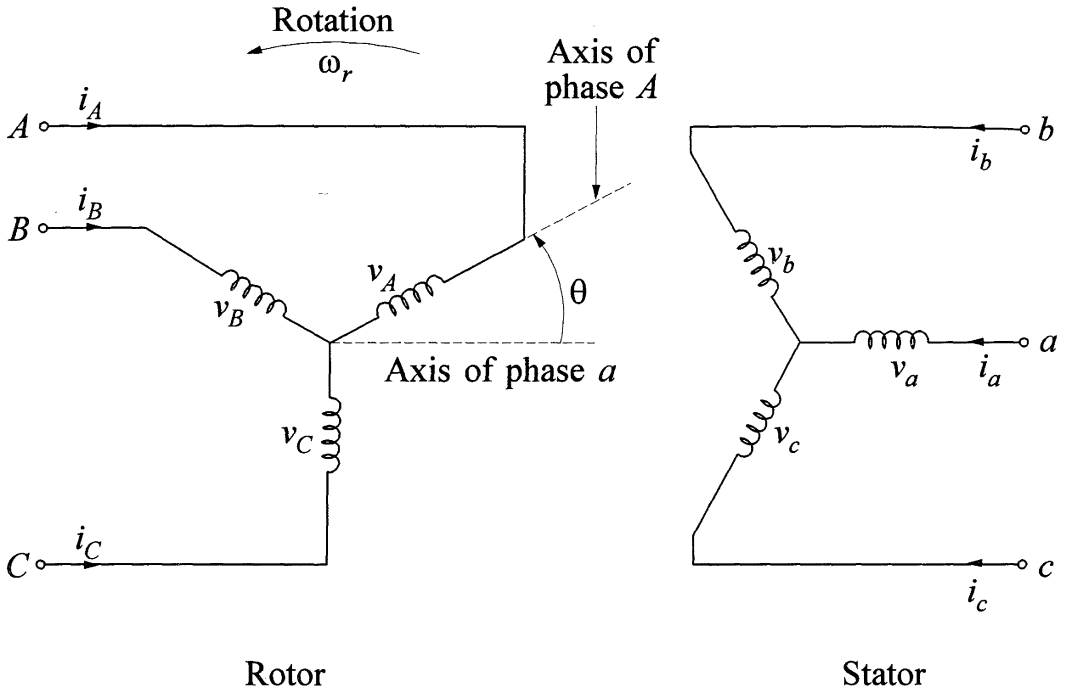

Figure 7.6 Stator and rotor circuits of an induction machine

For convenience in analysis, we consider only one pair of poles and measure all angles in electrical radians or degrees (see Section 3.1.2 of Chapter 3).

In Figure 7.6, θ is defined as the angle by which the axis of phase A rotor winding leads the axis of phase a stator winding in the direction of rotation. With a constant rotor angular velocity of ω_r in electrical rad/s,

$$\theta = \omega_r t \tag{7.13}$$

With a constant slip s,

$$\theta = (1-s)\omega_s t \tag{7.14}$$

where ω_s is the angular velocity of the stator field in electrical rad/s.

Neglecting saturation, hysteresis, and eddy currents, and assuming purely sinusoidal distribution of flux waves, the machine equations may be written as follows.

Stator voltage equations:

$$\begin{aligned} v_a &= p\psi_a + R_s i_a \\ v_b &= p\psi_b + R_s i_b \\ v_c &= p\psi_c + R_s i_c \end{aligned} \tag{7.15}$$

Rotor voltage equations:

$$\begin{aligned} v_A &= p\psi_A + R_r i_A \\ v_B &= p\psi_B + R_r i_B \\ v_C &= p\psi_C + R_r i_C \end{aligned} \tag{7.16}$$

In the above equations, ψ represents the flux linking the winding denoted by the subscript, R_s the stator phase resistance, R_r the rotor phase resistance, and p the differential operator d/dt. The positive directions of currents are into the windings.

For power system studies, the slot effects may be neglected and the rotor may be considered to have a symmetrical structure. Hence, only the mutual inductances between stator and rotor windings are functions of rotor position defined by angle θ.

The flux linkage in the stator phase a winding at any instant is given by

$$\psi_a = L_{aa} i_a + L_{ab}(i_b + i_c) + L_{aA}[i_A \cos\theta + i_B \cos(\theta + 120°) + i_C \cos(\theta - 120°)] \tag{7.17}$$

where L_{aa} is the self-inductance of the stator windings, L_{ab} the mutual inductance between stator windings, and L_{aA} is the maximum value of mutual inductance between stator and rotor windings. Similar expressions apply to flux linkages of windings b and c of the stator.

The flux linkage in the rotor phase A winding is

$$\psi_A = L_{AA} i_A + L_{AB}(i_B + i_C) + L_{aA}[i_a \cos\theta + i_b \cos(\theta - 120°) + i_c \cos(\theta + 120°)] \tag{7.18}$$

Similar expressions apply to ψ_B and ψ_C.

With no neutral currents due to winding connections or balanced conditions,

$$\begin{aligned} i_a + i_b + i_c &= 0 \\ i_A + i_B + i_C &= 0 \end{aligned} \tag{7.19}$$

Let

$$\begin{aligned} L_{ss} &= L_{aa} - L_{ab} \\ L_{rr} &= L_{AA} - L_{AB} \end{aligned} \tag{7.20}$$

Then the expressions for ψ_a and ψ_A may be written as

$$\psi_a = L_{ss} i_a + L_{aA}[i_A \cos\theta + i_B \cos(\theta + 120°) + i_C \cos(\theta - 120°)] \tag{7.21}$$

$$\psi_A = L_{rr} i_A + L_{aA}[i_a \cos\theta + i_b \cos(\theta - 120°) + i_c \cos(\theta + 120°)] \tag{7.22}$$

The d-q transformation

As for synchronous machine equations (see Section 3.3 of Chapter 3), the above equations for the induction machine can be simplified by appropriate transformation of phase variables into components along rotating axes. In the case of the synchronous machine, we chose axes rotating with the rotor. For an induction machine the preferred reference frame is one with the *axes rotating at synchronous speed* [10,11]. The q-axis is assumed to be 90° ahead of the d-axis in the direction of rotation. If the d-axis is so chosen that it coincides with the phase a axis at time t=0, its displacement from phase a axis at any time t is $\omega_s t$.

The transformation of the stator phase currents into d and q variables is as follows:

$$\begin{aligned} i_{ds} &= \frac{2}{3}[i_a \cos\omega_s t + i_b \cos(\omega_s t - 120°) + i_c \cos(\omega_s t + 120°)] \\ i_{qs} &= -\frac{2}{3}[i_a \sin\omega_s t + i_b \sin(\omega_s t - 120°) + i_c \sin(\omega_s t + 120°)] \end{aligned} \tag{7.23}$$

The inverse transformation is

$$\begin{aligned} i_a &= i_{ds} \cos\omega_s t - i_{qs} \sin\omega_s t \\ i_b &= i_{ds} \cos(\omega_s t - 120°) - i_{qs} \sin(\omega_s t - 120°) \\ i_c &= i_{ds} \cos(\omega_s t + 120°) - i_{qs} \sin(\omega_s t + 120°) \end{aligned} \tag{7.24}$$

Similar transformations apply to stator flux linkages and to stator voltages.

Let us now identify the corresponding transformations for rotor quantities in relation to the synchronously rotating d and q axes. Let θ_r be the angle by which d-axis leads phase A axis of the rotor. If the rotor slip is s, the d-axis is advancing with respect to a point on the rotor at the rate

$$\frac{d\theta_r}{dt} = p\theta_r = s\omega_s \tag{7.25}$$

The transformation of rotor currents into d and q components is as follows:

$$\begin{aligned} i_{dr} &= \frac{2}{3}[i_A\cos\theta_r + i_B\cos(\theta_r - 120°) + i_C\cos(\theta_r + 120°)] \\ i_{qr} &= -\frac{2}{3}[i_A\sin\theta_r + i_B\sin(\theta_r - 120°) + i_C\sin(\theta_r + 120°)] \end{aligned} \tag{7.26}$$

The inverse transformation is

$$\begin{aligned} i_A &= i_{dr}\cos\theta_r - i_{qr}\sin\theta_r \\ i_B &= i_{dr}\cos(\theta_r - 120°) - i_{qr}\sin(\theta_r - 120°) \\ i_C &= i_{dr}\cos(\theta_r + 120°) - i_{qr}\sin(\theta_r + 120°) \end{aligned} \tag{7.27}$$

Similar transformations apply to rotor flux linkages and voltages.

Basic machine equations in d-q reference frame

From Equations 7.14 and 7.25,

$$\theta = \omega_s t - \theta_r \tag{7.28}$$

From Equations 7.21 and 7.22, we can show that the stator and rotor flux linkages can be expressed in terms of the d and q components as follows.

Stator flux linkages:

$$\begin{aligned} \psi_{ds} &= L_{ss} i_{ds} + L_m i_{dr} \\ \psi_{qs} &= L_{ss} i_{qs} + L_m i_{qr} \end{aligned} \tag{7.29}$$

Rotor flux linkages:

$$\begin{aligned} \psi_{dr} &= L_{rr} i_{dr} + L_m i_{ds} \\ \psi_{qr} &= L_{rr} i_{qr} + L_m i_{qs} \end{aligned} \tag{7.30}$$

with $L_m = 3/2 L_{aA}$.

The stator voltages in terms of the d and q components are

$$\begin{aligned} v_{ds} &= R_s i_{ds} - \omega_s \psi_{qs} + p\psi_{ds} \\ v_{qs} &= R_s i_{qs} + \omega_s \psi_{ds} + p\psi_{qs} \end{aligned} \tag{7.31}$$

and the rotor voltages are

$$\begin{aligned} v_{dr} &= R_r i_{dr} - (p\theta_r)\psi_{qr} + p\psi_{dr} \\ v_{qr} &= R_r i_{qr} + (p\theta_r)\psi_{dr} + p\psi_{qr} \end{aligned} \tag{7.32}$$

The term $p\theta_r$ in Equation 7.32 is the slip angular velocity given by

$$p\theta_r = s\omega_s \tag{7.33}$$

This represents the relative angular velocity between the rotor and the reference *d-q* axes.

We have expressed the machine equations in a *synchronously rotating d-q reference frame*. For balanced synchronous operation, both stator and rotor mmf waves rotate at synchronous speed. The mmf waves due to stator windings are resolved into two sinusoidally distributed mmf waves rotating at synchronous speed so that one has its peak over the *d*-axis and the other has its peak over the *q*-axis. Therefore, i_{ds} and i_{qs} represent currents in fictitious windings rotating at synchronous speed and remaining in such positions that their axes always coincide with the *d*- and *q*-axis, respectively. A similar interpretation applies to the rotor currents i_{dr} and i_{qr}.

From Equations 7.31 and 7.32 we see that the expression for each voltage consists of three terms: The Ri drop term, the transient $p\psi$ term, and the speed voltage term. The first two are familiar terms associated with the voltage of any coil. The speed voltage terms, however, are peculiar to the specific situation at hand. The terms $\omega_s\psi_{qs}$ and $\omega_s\psi_{ds}$ in the stator voltage equations represent voltages created in the stationary windings by the synchronously rotating flux wave. Similarly, the terms $(p\theta_r)\psi_{qr}$ and $(p\theta_r)\psi_{dr}$ in the rotor voltage equations represent voltages created in the rotor windings which move at the slip speed $(p\theta_r = s\omega_s)$ with respect to the synchronously rotating flux waves. For motor action, s and $p\theta_r$ are positive. Conversely, for generator action, s and $p\theta_r$ are negative.

Electrical power and torque:

The instantaneous power input to the stator is

$$p_s = v_a i_a + v_b i_b + v_c i_c$$

In terms of the *d* and *q* components, the above expression becomes

$$p_s = \frac{3}{2}(v_{ds} i_{ds} + v_{qs} i_{qs}) \tag{7.34}$$

Similarly, the instantaneous power input to the rotor is

$$p_r = \frac{3}{2}(v_{dr}i_{dr}+v_{qr}i_{qr}) \tag{7.35}$$

The electromagnetic torque developed is obtained as the power associated with the speed voltages divided by the shaft speed in mechanical radians per second. From Equation 7.32, the speed voltage terms associated with v_{dr} and v_{qr} are $-\psi_{qr}(p\theta_r)$ and $\psi_{dr}(p\theta_r)$, respectively. Substituting in Equation 7.35, the power associated with the speed voltage is

$$\frac{3}{2}(\psi_{dr}i_{qr}-\psi_{qr}i_{dr})(p\theta_r)$$

The rotor speed with respect to the d, q axes is $-(p\theta_r)(2/p_f)$. Hence, the electromagnetic torque is

$$T_e = \frac{3}{2}(\psi_{qr}i_{dr}-\psi_{dr}i_{qr})\frac{p_f}{2} \tag{7.36}$$

Acceleration equation:

The electromagnetic torque developed by the motor drives the mechanical load. If there is a mismatch between the electromagnetic torque and the mechanical load torque (T_m), the differential torque accelerates the rotor mass. Consequently,

$$T_e - T_m = J\frac{d\omega_m}{dt} = J\frac{d^2\theta}{dt^2} \tag{7.37}$$

where ω_m is the angular velocity of the rotor in mechanical radians per second, and J is the polar moment of inertia of the rotor and the connected load. The load torque varies with speed. A commonly used expression for the load torque is

$$T_m = T_0(\bar{\omega}_r)^m \tag{7.38}$$

where $\bar{\omega}_r$ is the rotor speed expressed in per unit of synchronous speed. An alternative expression often used for the load torque is

$$T_m = T_0[A\bar{\omega}_r^2+B\bar{\omega}_r+C] \tag{7.39}$$

7.2.2 Steady-State Characteristics

For balanced steady-state operation, the stator currents may be written as

$$\begin{aligned} i_a &= I_m \cos(\omega_s t+\alpha) \\ i_b &= I_m \cos(\omega_s t+\alpha-120^\circ) \\ i_c &= I_m \cos(\omega_s t+\alpha+120^\circ) \end{aligned} \tag{7.40}$$

where α is the phase angle of i_a with respect to the time origin. Applying the *d-q* transformation (Equation 7.23), we have

$$\begin{aligned} i_{ds} &= I_m \cos\alpha \\ i_{qs} &= I_m \sin\alpha \end{aligned} \tag{7.41}$$

Thus, for balanced steady-state operation the stator currents appear as direct currents in the *d-q* reference frame. Similar expressions apply to stator voltages and rotor currents.

From Equation 7.24, the stator current may be written as

$$\begin{aligned} i_s = i_a &= i_{ds}\cos\omega_s t - i_{qs}\sin\omega_s t \\ &= i_{ds}\cos\omega_s t + i_{qs}\cos(\omega_s t+90^\circ) \end{aligned} \tag{7.42}$$

Using I_s to denote per unit RMS stator current, Equation 7.42 may be written in the phasor form:

$$\tilde{I}_s = I_{ds} + jI_{qs} \tag{7.43}$$

where $I_{ds} = i_{ds}/\sqrt{2}$ and $I_{qs} = i_{qs}/\sqrt{2}$. In a similar manner, the stator phase voltages and rotor phase currents can be expressed in the phasor form:

$$\tilde{V}_s = (v_{ds} + jv_{qs})/\sqrt{2} \tag{7.44}$$

$$\tilde{I}_r = (i_{dr} + ji_{qr})/\sqrt{2} \tag{7.45}$$

Under steady-state conditions, $p\psi$ terms in Equations 7.31 and 7.32 disappear. Substituting in Equation 7.31 the expressions for flux linkages given by Equation 7.29, we may write

$$\begin{aligned} v_{ds} &= R_s i_{ds} - \omega_s L_{ss} i_{qs} - \omega_s L_m i_{qr} \\ v_{qs} &= R_s i_{qs} + \omega_s L_{ss} i_{ds} + \omega_s L_m i_{dr} \end{aligned} \tag{7.46}$$

From Equations 7.43 to 7.46, we have

$$\begin{aligned} \tilde{V}_s &= R_s \tilde{I}_s + j\omega_s L_{ss} \tilde{I}_s + j\omega_s L_m \tilde{I}_r \\ &= R_s \tilde{I}_s + j\omega_s (L_{ss} - L_m) \tilde{I}_s + j\omega_s L_m (\tilde{I}_s + \tilde{I}_r) \\ &= R_s \tilde{I}_s + jX_s \tilde{I}_s + jX_m (\tilde{I}_s + \tilde{I}_r) \end{aligned} \tag{7.47}$$

where

$$X_s = \omega_s (L_{ss} - L_m) = \text{stator leakage reactance}$$

$$X_m = \omega_s L_m = \text{magnetizing reactance}$$

With the rotor circuits shorted, $v_{dr}=v_{qr}=0$. Hence, from Equations 7.30, 7.32, and 7.33, we have

$$\begin{aligned} v_{dr} &= 0 = R_r i_{dr} - s\omega_s (L_{rr} i_{qr} + L_m i_{qs}) \\ v_{qr} &= 0 = R_r i_{qr} + s\omega_s (L_{rr} i_{dr} + L_m i_{ds}) \end{aligned} \tag{7.48}$$

From Equations 7.43, 7.45, and 7.48, we may write

$$\begin{aligned} \tilde{V}_r = 0 &= \frac{R_r}{s} \tilde{I}_r + j\omega_s L_{rr} \tilde{I}_r + j\omega_s L_m \tilde{I}_s \\ &= \frac{R_r}{s} \tilde{I}_r + jX_r \tilde{I}_r + jX_m (\tilde{I}_s + \tilde{I}_r) \end{aligned} \tag{7.49}$$

where

$$X_r = \omega_s (L_{rr} - L_m) = \text{rotor leakage reactance}$$

Equivalent circuit

Equations 7.47 and 7.49 represent the steady-state performance of the induction machine. These equations can be represented by the equivalent circuit shown in Figure 7.7, which accounts for quantities in one phase.

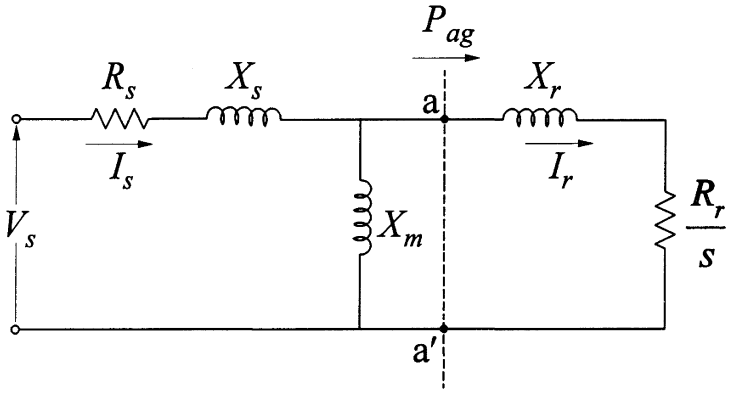

Figure 7.7 Equivalent circuit of a three-phase induction machine

In the equivalent circuit *all quantities have been referred to the stator side.* The directions of currents shown are positive when operating as a motor, in which case the slip s is positive.

The power transferred across the air-gap to the rotor is

$$P_{ag} = \frac{R_r}{s} I_r^2 \tag{7.50}$$

The rotor resistance loss is

$$P_{lr} = R_r I_r^2 \tag{7.51}$$

Therefore, the mechanical power transferred to the shaft is

$$\begin{aligned} P_{sh} &= P_{ag} - P_{lr} \\ &= \frac{R_r}{s} I_r^2 - R_r I_r^2 \\ &= R_r \frac{1-s}{s} I_r^2 \end{aligned} \tag{7.52}$$

This represents the mechanical power transferred to the shaft. An alternative form of induction machine equivalent circuit is shown in Figure 7.8 in which the rotor power is separated into resistance loss and shaft power.

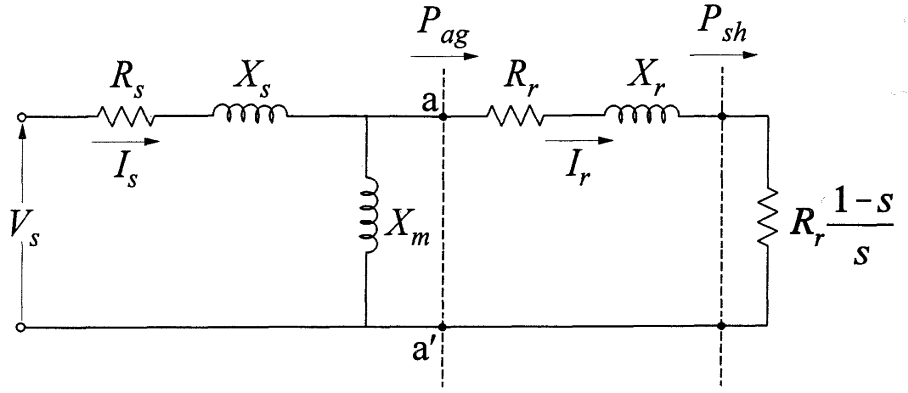

Figure 7.8 Alternative form of induction machine equivalent circuit

The above represent per phase values. For a three-phase motor, the electromagnetic torque developed by the motor is

$$T_e = \frac{3P_{sh}}{\omega_m}$$

where ω_m is the angular velocity of the rotor in mechanical rad/s given by

$$\omega_m = \omega_r \frac{2}{p_f}$$
$$= \omega_s(1-s)\frac{2}{p_f}$$

Hence,

$$T_e = 3\frac{p_f}{2}\frac{R_r}{s\omega_s}I_r^2 \tag{7.53}$$

where $\omega_s = 2\pi f$ and p_f is the number of poles.

Torque-slip characteristic

The torque is slip dependent. For analysis of torque-slip relationships, the equivalent circuit of Figure 7.7 may be simplified by replacing the part of the equivalent to the left of nodes a and a′ by its Thevenin's equivalent. Figure 7.9 shows the resulting simplified equivalent circuit.

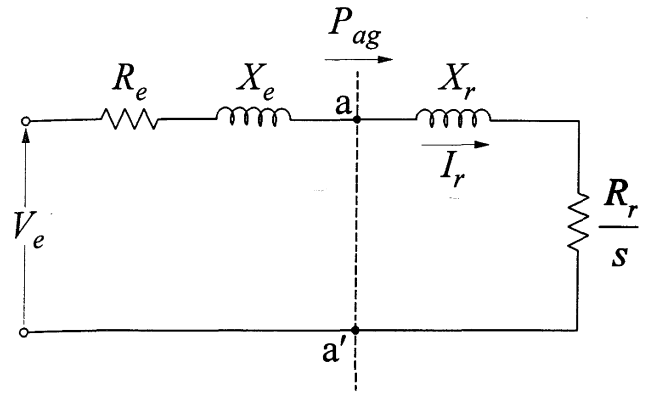

$$V_e = \frac{jX_m V_s}{R_s + j(X_s + X_m)}$$

$$R_e + jX_e = \frac{jX_m(R_s + jX_s)}{R_s + j(X_s + X_m)}$$

Figure 7.9 Equivalent circuit suitable for evaluating torque-slip relationships

From Figure 7.9, the rotor current is

$$\tilde{I}_r = \frac{\tilde{V}_e}{(R_e + R_r/s) + j(X_e + X_r)} \tag{7.54}$$

From Equation 7.53, the torque is

$$T_e = 3\frac{p_f}{2}\left(\frac{R_r}{s\omega_s}\right)\frac{V_e^2}{(R_e + R_r/s)^2 + (X_e + X_r)^2} \tag{7.55}$$

Figure 7.10 shows a typical relationship between torque and slip/speed. At standstill (i.e., at starting), speed is zero and slip s is equal to 1.0 pu. Between zero and synchronous speed, the machine performs as a motor. Beyond synchronous speed, slip is negative, representing generator operation.

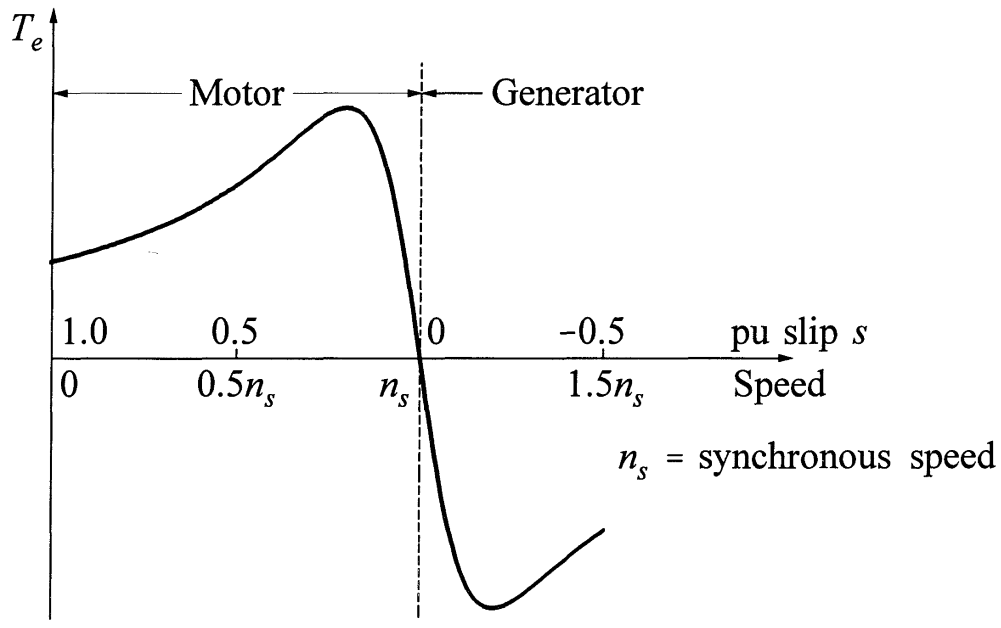

Figure 7.10 Typical torque-speed characteristic of an induction machine

The maximum torque occurs when

$$\frac{R_r}{s} = Z' \tag{7.56}$$

where

$$Z' = \sqrt{R_e^2 + (X_e + X_r)^2} \tag{7.57}$$

Therefore, per unit slip at maximum torque is

$$s_{Tmax} = \frac{R_r}{Z'} \tag{7.58}$$

From Equation 7.55, the maximum torque is

$$\begin{aligned} T_{max} &= 3\frac{p_f}{2\omega_s}\frac{0.5V_e^2}{R_e + Z'} \\ &= 3\frac{1}{\omega_{ms}}\frac{0.5V_e^2}{R_e + Z'} \end{aligned} \tag{7.59}$$

where $\omega_s = 2\pi f$ and ω_{ms} is the synchronous speed in mechanical radians per second.

From Equation 7.58, we see that the slip at maximum torque is directly proportional to the rotor resistance R_r. However, as seen from Equation 7.59, the value of maximum torque is independent of R_r and is affected principally by the stator and rotor leakage reactances.

Effect of rotor resistance on efficiency

The efficiency of an induction motor is highly dependent on the operating slip. If we neglect all losses except that due to rotor resistance loss, then the efficiency is given by the ratio of mechanical power transferred to the shaft to the air-gap power. Therefore, from Equations 7.50 and 7.52, the ideal efficiency is

$$\eta = \frac{P_{sh}}{P_{ag}} \times 100 = 1 - s \quad \text{per cent} \tag{7.60}$$

It is evident from the above relationship that, to achieve high efficiency, an induction motor must operate at low values of slip. Therefore, most three-phase induction motors are designed so that the per unit slip at normal full-load operation is less than 0.05. For large three-phase induction motors the actual maximum efficiency may be higher than 95%.

7.2.3 Alternative Rotor Constructions

The selection of an appropriate value of rotor resistance of an induction motor involves design compromises. High efficiency at normal operating conditions requires a low rotor resistance. On the other hand, a high rotor resistance is required to produce a high starting torque and to keep the magnitude of the starting current low and the power factor high.

The use of a *wound rotor* is one way of meeting the need for varying the rotor resistance at different operating conditions. At starting, resistors are connected in series with the rotor windings through slip rings. As the rotor speed picks up, the external resistance is reduced. For normal running, external resistance is made zero so that the full load slip is small. Figure 7.11 shows the effect of varying the rotor resistance on the shaft torque. Wound rotor motors are, however, more expensive than squirrel-cage motors.

Special squirrel-cage arrangements can also be used to obtain a high value of effective resistance at starting and a low value of the resistance at full-load operation. One such arrangement of rotor bars frequently used is the *double squirrel-cage* shown in Figure 7.12. It consists of two layers of bars, both short-circuited by end rings. The

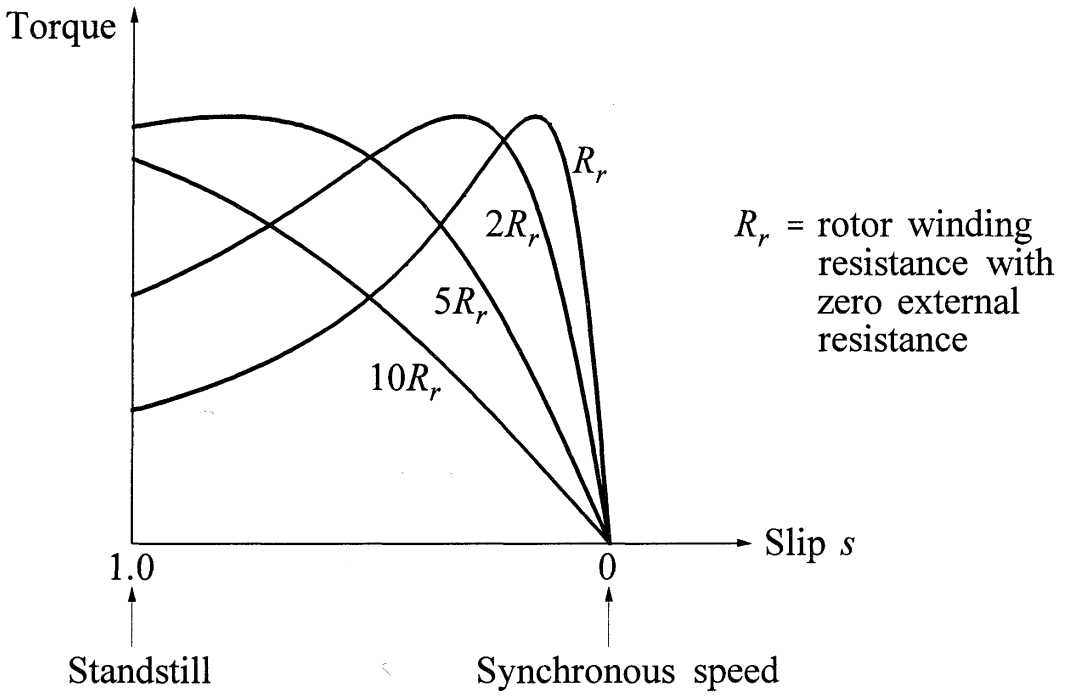

Figure 7.11 Torque-slip curves showing the effect of rotor circuit resistance

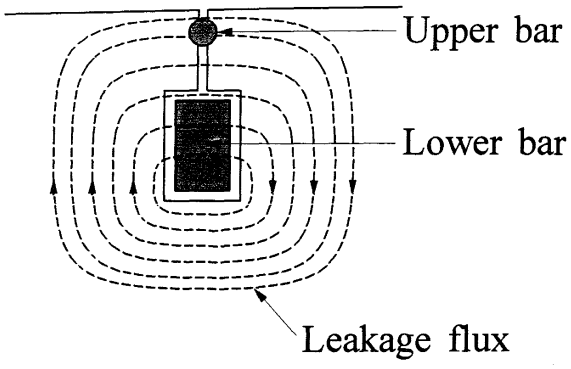

Figure 7.12 Double squirrel-cage rotor bars

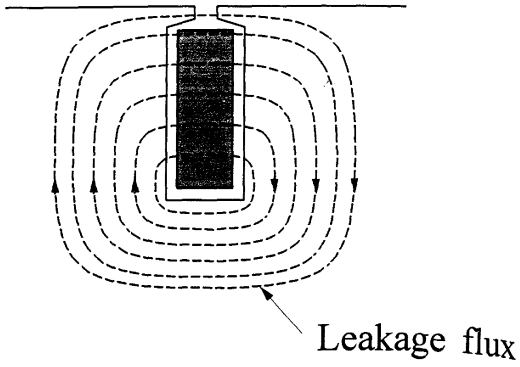

Figure 7.13 Deep-bar rotor construction

upper bars are small in cross section and have a high resistance. They are placed near the rotor surface so that the leakage flux sees a path of high reluctance; consequently, they have a low leakage inductance. The lower bars have a large cross section, a lower resistance, and a higher leakage inductance. At starting, rotor frequency is high and very little current flows through the lower bars; the effective resistance of the rotor then is that of the high-resistance upper bars. At normal low slip operation, leakage reactances are negligible, and the rotor current flows largely through the low-resistance lower bars; the effective rotor resistance is equal to that of the two sets of bars in parallel.

The use of *deep, narrow rotor bars* as shown in Figure 7.13 produces torque-speed characteristics similar to those of a double-cage rotor. As is evident from the flux paths shown in the figure, the leakage inductance of the top cross section of the rotor bar is relatively low; the lower cross sections have progressively higher leakage inductance. At starting, due to the high rotor frequency, the current is concentrated towards the top layers of the rotor bar. As the rotor accelerates and slip decreases, the current distribution becomes more uniform. At normal full-load operation, the current distribution is nearly uniform and the effective resistance is low.

The equivalent circuit of a single-cage induction motor (i.e., with one rotor winding) is shown in Figure 7.7. This is extended in Figure 7.14 to represent a motor with double-cage rotor. It may be represented by an equivalent single rotor circuit as shown in Figure 7.15, with slip-dependent rotor parameters:

$$R_r(s) = R_{r0}\frac{m^2+ms^2R_1/R_{r0}}{m^2+s^2} \tag{7.61}$$

$$X_r(s) = X_1+\frac{R_{r0}(mR_1/R_2)}{m^2+s^2} \tag{7.62}$$

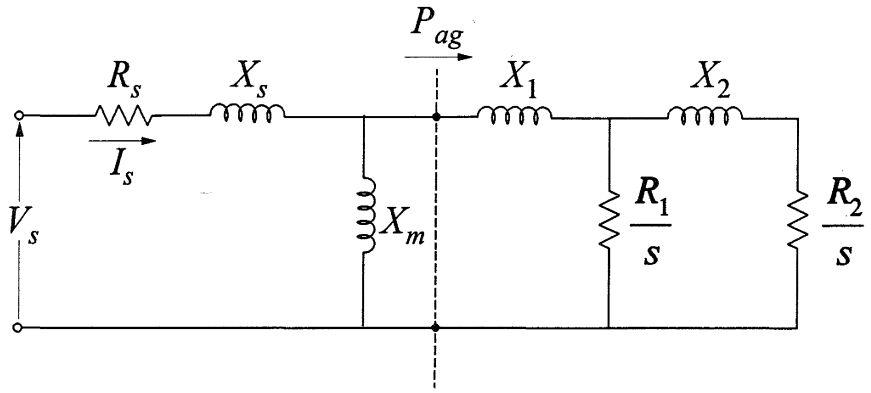

Figure 7.14 Equivalent circuit of an induction motor with a double-cage rotor

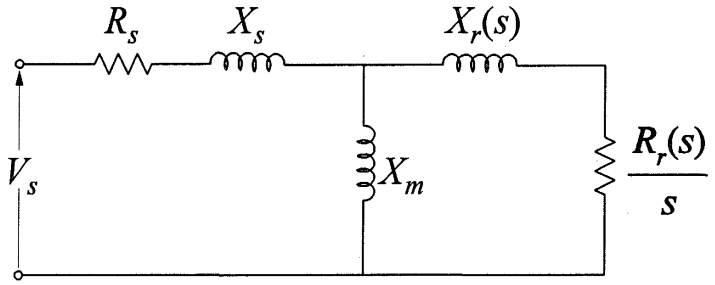

Figure 7.15 Equivalent single rotor circuit representation of a motor with a double-cage rotor or a deep-bar rotor

where

$$R_{r0} = \frac{R_1 R_2}{R_1 + R_2} \tag{7.63}$$

$$m = \frac{R_1 + R_2}{X_2} \tag{7.64}$$

The deep-bar effects may be represented by an equivalent in the form of a ladder network. For system studies, however, it is preferable to use a quasi steady-state approach, representing the rotor by a single rotor circuit whose parameters vary as a function of slip as shown in Figure 7.15.

The rotor parameters can be expressed as a function of slip based on the eddy current distribution within a rectangular bar [22]:

$$R_r(s) = \frac{R_{r0}}{2} \frac{\beta(\sinh\beta + \sin\beta)}{(\cosh\beta - \cos\beta)} \tag{7.65}$$

$$X_r(s) = X_{r0} + \frac{R_{r0}}{2}\frac{\beta(\sinh\beta - \sin\beta)}{(\cosh\beta - \cos\beta)} \tag{7.66}$$

$$\beta = \sqrt{|s|}B \tag{7.67}$$

where B is a deep-bar factor which determines the motor starting torque, X_{r0} is the rotor leakage reactance not associated with the rotor bar (for example, zigzag leakage reactance), and R_{r0} is the rotor bar running resistance.

The deep-bar factor is a function of the base frequency, the resistivity (ρ) and the depth (d) of the rotor bar, and the permeability of free space (μ_0):

$$B = 2d\sqrt{\mu_0\omega_0/(2\rho)}$$

In the limit, as s tends to zero, the deep-bar rotor resistance is equal to R_{r0}.

7.2.4 Representation of Saturation

The magnetizing reactance X_m varies with magnetic saturation. This is represented as a function of the air-gap voltage V_{ag}, in a manner similar to that used for synchronous machines.

Induction motors are normally designed so that their leakage reactances saturate at high-current levels. This assists in meeting the requirement for a high starting torque. For accurate analysis of conditions involving high-current levels, saturation representation should include variation of leakage reactance as shown in Figure 7.16.

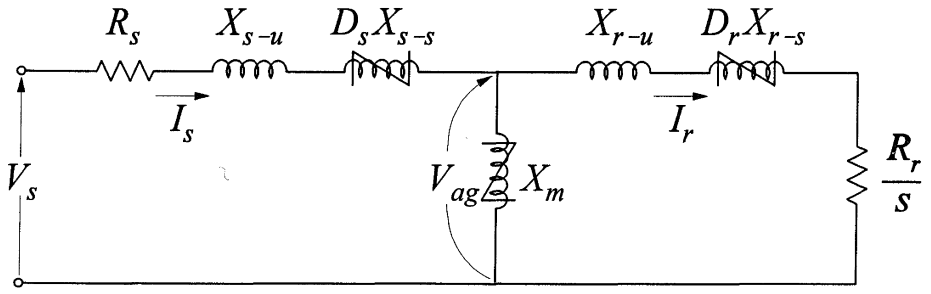

Figure 7.16 Induction motor equivalent circuit including effects of magnetic saturation

The stator and rotor leakage reactances are separated into saturating components (X_{s-s}, X_{r-s}) and unsaturated components (X_{s-u}, X_{r-u}). The saturating components of the reactances represent leakage flux that concentrate in the slot tooth tips which saturate and limit the magnetic field at the slot mouth [12]. The unsaturating portions of the reactances represent end leakage and peripheral leakage.

The leakage reactance saturation depends on the current. The limiting value of current (I_{sat}) at which saturation begins is typically in the range of 1.3 to 3.0 pu. The saturation of the leakage reactances due to current I can be represented by the describing function D [5,12] as follows:

$$\text{For } I \le I_{sat}, \quad D = 1.0$$

$$\text{For } I > I_{sat}, \quad D = \frac{2}{\pi}\left[\tan^{-1}\left(\frac{\gamma}{\sqrt{1-\gamma}}\right) + \gamma\sqrt{1-\gamma^2}\right] \tag{7.68}$$

where

$$\gamma = \frac{I_{sat}}{I} = \frac{\text{current at which saturation begins}}{\text{current through the leakage inductance}}$$

7.2.5 Per Unit Representation

As in the case of a synchronous machine (see Section 3.4 of Chapter 3), we choose the following base quantities for the stator:

$v_{s\,base}$ = peak value of rated phase voltage, V
$i_{s\,base}$ = peak value of rated phase current, A
f_{base} = rated frequency, Hz

The base values of the remaining quantities are automatically set:

$\omega_{base} = 2\pi f_{base}$, elec. rad/s
$\omega_{m\,base} = \omega_{base}(2/p_f)$, mech. rad/s
$Z_{s\,base} = v_{s\,base}/i_{s\,base}$, Ω
$L_{s\,base} = v_{s\,base}/(i_{s\,base}\omega_{base})$, H
$\psi_{s\,base} = v_{s\,base}/\omega_{base}$, Wb·turns
3-phase $VA_{base} = 3/2\,(v_{s\,base} i_{s\,base})$, VA
Torque base $= 3/2\,(p_f/2)\psi_{s\,base} i_{s\,base}$, N·m

With the rotor quantities referred to the stator side, the above base values also apply to the rotor.

From Equation 7.31,

$$v_{ds} = R_s i_{ds} - \omega_s \psi_{qs} + p\psi_{ds}$$

Dividing by $v_{s\,base}$, and noting that $v_{s\,base} = Z_{s\,base} i_{s\,base} = \omega_{base}\psi_{s\,base}$, we get

$$\frac{v_{ds}}{v_{sbase}} = \frac{R_s}{Z_{sbase}}\frac{i_{ds}}{i_{sbase}} - \frac{\omega_s}{\omega_{base}}\frac{\psi_{qs}}{\psi_{sbase}} + p\left(\frac{1}{\omega_{base}}\frac{\psi_{ds}}{\psi_{sbase}}\right)$$

In per unit notation,

$$\bar{v}_{ds} = \bar{R}_s\bar{i}_{ds} - \bar{\omega}_s\bar{\psi}_{qs} + \bar{p}\bar{\psi}_{ds} \tag{7.69}$$

Similarly,

$$\bar{v}_{qs} = \bar{R}_s\bar{i}_{qs} + \bar{\omega}_s\bar{\psi}_{ds} + \bar{p}\bar{\psi}_{qs} \tag{7.70}$$

Using the same approach to express Equation 7.32 in per unit form, we find

$$\bar{v}_{dr} = \bar{R}_r\bar{i}_{dr} - (\bar{p}\theta_r)\bar{\psi}_{qr} + \bar{p}\bar{\psi}_{dr} \tag{7.71}$$

$$\bar{v}_{qr} = \bar{R}_r\bar{i}_{qr} + (\bar{p}\theta_r)\bar{\psi}_{dr} + \bar{p}\bar{\psi}_{qr} \tag{7.72}$$

where

$$\bar{p}\theta_r = \frac{1}{\omega_{base}}(p\theta_r) = s\bar{\omega}_s = \frac{\omega_s - \omega_r}{\omega_s} \tag{7.73}$$

From Equations 7.29 and 7.30, by dividing throughout by $\psi_{s\,base} = L_{s\,base}\,i_{s\,base}$, the per unit flux linkage equations may be written as

$$\bar{\psi}_{ds} = \bar{L}_{ss}\bar{i}_{ds} + \bar{L}_m\bar{i}_{dr} \tag{7.74}$$

$$\bar{\psi}_{qs} = \bar{L}_{ss}\bar{i}_{qs} + \bar{L}_m\bar{i}_{qr} \tag{7.75}$$

$$\bar{\psi}_{dr} = \bar{L}_{rr}\bar{i}_{dr} + \bar{L}_m\bar{i}_{ds} \tag{7.76}$$

$$\bar{\psi}_{qr} = \bar{L}_{rr}\bar{i}_{qr} + \bar{L}_m\bar{i}_{qs} \tag{7.77}$$

From Equation 7.36, dividing by $T_{base} = 3/2(\psi_{s\,base}\,i_{s\,base})(p_f/2)$, we have

$$\frac{T_e}{T_{base}} = \frac{3/2(\psi_{qr}i_{dr} - \psi_{dr}i_{qr})(p_f/2)}{3/2(\psi_{sbase}i_{sbase})(p_f/2)}$$

or

$$\bar{T}_e = \bar{\psi}_{qr}\bar{i}_{dr} - \bar{\psi}_{dr}\bar{i}_{qr} \tag{7.78}$$

Dividing Equation 7.37 by $T_{base} = \mathrm{VA}_{base}/\omega_{m\,base}$ gives

$$\frac{T_e}{T_{base}} - \frac{T_m}{T_{base}} = J\left(\frac{\omega_{m\,base}}{\mathrm{VA}_{base}}\right)\omega_{m\,base}\,p\left(\frac{\omega_m}{\omega_{m\,base}}\right)$$

or

$$p(\bar{\omega}_r) = \frac{1}{2H}(\bar{T}_e - \bar{T}_m)$$

or

$$\bar{p}(\omega_r) = \frac{1}{2H\omega_{base}}(\bar{T}_e - \bar{T}_m) \tag{7.79}$$

where

$$H = \frac{1}{2}\frac{J\omega_{m\,base}^2}{\mathrm{VA}_{base}}$$

$$\bar{\omega}_r = \frac{\omega_m}{\omega_{m\,base}} = \frac{\omega_r/p_f}{\omega_{base}/p_f} = \frac{\omega_r}{\omega_{base}}$$

The parameter H is the combined inertia constant of the motor and the mechanical load.

Dividing Equation 7.38 by T_{base} to obtain an expression for the load torque in per unit, we have

$$\frac{T_m}{T_{base}} = \frac{T_0}{T_{base}}(\bar{\omega}_r)^m$$

or

$$\bar{T}_m = \bar{T}_0(\bar{\omega}_r)^m \tag{7.80}$$

Similarly, the per unit form of Equation 7.39, giving the alternative expression for load torque, is

$$\bar{T}_m = \bar{T}_0[A\bar{\omega}_r^2 + B\bar{\omega}_r + C] \tag{7.81}$$

Equations 7.69 to 7.81 represent the per unit dynamic equations of an induction motor.

The per unit time derivative $\bar{p}$ appearing in these equations is related to the derivative with time in seconds as follows:

$$\bar{p} = \frac{d}{d\bar{t}} = \frac{1}{\omega_{base}}\frac{d}{dt} = \frac{1}{\omega_{base}}p$$

For convenience in introducing the per unit equations, we have used superbars to denote per unit quantities. Further analysis of induction machines in this book will be solely in per unit form, and we will drop the superbar notation.

7.2.6 Representation in Stability Studies

For representation in power system stability studies, $p\psi_{ds}$ and $p\psi_{qs}$ are neglected in the stator voltage relations (Equations 7.69 and 7.70). These terms represent stator transients; their neglect corresponds to ignoring the dc component in the stator transient currents, permitting representation of only fundamental frequency components. As with synchronous machines, this simplification is essential to ensure compatibility with the models used for representing other system components, particularly the transmission network (see Chapter 5, Section 5.1.1).

With the stator transients neglected and the rotor windings shorted, the *per unit* induction motor electrical equations may be summarized as follows.

Stator voltages:

$$v_{ds} = R_s i_{ds} - \omega_s \psi_{qs} \tag{7.82}$$

$$v_{qs} = R_s i_{qs} + \omega_s \psi_{ds} \tag{7.83}$$

Rotor voltages:

$$v_{dr} = 0 = R_r i_{dr} - p\theta_r \psi_{qr} + p\psi_{dr} \tag{7.84}$$

$$v_{qr} = 0 = R_r i_{qr} + p\theta_r \psi_{dr} + p\psi_{qr} \tag{7.85}$$

Flux linkages:

$$\psi_{ds} = L_{ss} i_{ds} + L_m i_{dr} \tag{7.86}$$

$$\psi_{qs} = L_{ss} i_{qs} + L_m i_{qr} \tag{7.87}$$

$$\psi_{dr} = L_m i_{ds} + L_{rr} i_{dr} \tag{7.88}$$

$$\psi_{qr} = L_m i_{qs} + L_{rr} i_{qr} \tag{7.89}$$

with

$$L_{ss} = L_s + L_m \quad \text{and} \quad L_{rr} = L_r + L_m$$

where L_s and L_r are per unit stator and rotor leakage inductances.

The above equations assume a single rotor winding. As discussed earlier, the model for a machine with a *double-cage* rotor or a *deep-bar* rotor can be reduced to an equivalent single rotor circuit machine model whose parameters vary with slip.

To reduce Equations 7.82 to 7.89 to a form suitable for implementation in a stability program, we eliminate the rotor currents and express the relationship between stator current and voltage in terms of a voltage behind the transient reactance. Thus, from Equation 7.88,

$$i_{dr} = \frac{\psi_{dr} - L_m i_{ds}}{L_{rr}} \tag{7.90}$$

and, upon substitution in Equation 7.86,

$$\begin{aligned} \psi_{ds} &= L_{ss} i_{ds} + \frac{L_m(\psi_{dr} - L_m i_{ds})}{L_{rr}} \\ &= \frac{L_m}{L_{rr}} \psi_{dr} + \left(L_{ss} - \frac{L_m^2}{L_{rr}} \right) i_{ds} \end{aligned} \tag{7.91}$$

Similarly from Equations 7.87 and 7.89, we have

$$\psi_{qs} = \frac{L_m}{L_{rr}} \psi_{qr} + \left(L_{ss} - \frac{L_m^2}{L_{rr}} \right) i_{qs} \tag{7.92}$$

Substituting the above expression for ψ_{qs} in Equation 7.82, we may write

$$v_{ds} = R_s i_{ds} - X'_s i_{qs} + v'_d \tag{7.93}$$

and, similarly substituting the expression for ψ_{ds} in Equation 7.83,

$$v_{qs} = R_s i_{qs} + X'_s i_{ds} + v'_q \tag{7.94}$$

where

$$v'_d = -\frac{\omega_s L_m}{L_{rr}} \psi_{qr} \tag{7.95}$$

$$v'_q = \frac{\omega_s L_m}{L_{rr}} \psi_{dr} \tag{7.96}$$

$$X'_s = \omega_s \left(L_{ss} - \frac{L_m^2}{L_{rr}} \right) \tag{7.97}$$

The reactance X'_s is the *transient reactance* of the induction machine.

The stator voltage equations may be combined and expressed in the phasor form:

$$v_{ds} + jv_{qs} = (R_s + jX'_s)(i_{ds} + ji_{qs}) + (v'_d + jv'_q)$$

Noting that in per unit RMS and peak values are equal, we see that the above relationship may be expressed as

$$\tilde{V}_s = (R_s + jX'_s)\tilde{I}_s + \tilde{V}' \tag{7.98}$$

From the above equation, it is evident that the induction machine can be represented by the simple transient equivalent circuit of Figure 7.17.

By eliminating the rotor currents and expressing the rotor flux linkages in terms of v'_d and v'_q, Equations 7.84 and 7.85 can be written in the following form:

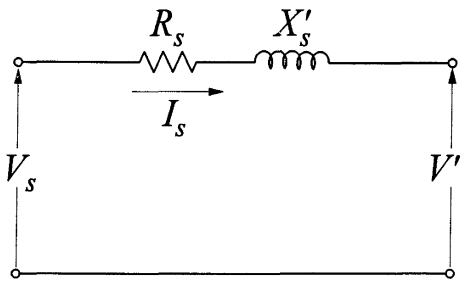

V_s = stator terminal voltage
V' = voltage behind transient impedance

Figure 7.17 Induction machine transient-equivalent circuit

$$p(v'_d) = -\frac{1}{T'_0}[v'_d + (X_s - X'_s) i_{qs}] + p\theta_r v'_q \tag{7.99}$$

$$p(v'_q) = -\frac{1}{T'_0}[v'_q - (X_s - X'_s) i_{ds}] - p\theta_r v'_d \tag{7.100}$$

where

$$T'_0 = \frac{L_r + L_m}{R_r} = \frac{L_{rr}}{R_r} \tag{7.101}$$

$$X_s = \omega_s(L_s + L_m) = \omega_s L_{ss} \tag{7.102}$$

$$p\theta_r = \frac{\omega_s - \omega_r}{\omega_s} \tag{7.103}$$

The constant T'_0 is the *transient open-circuit time constant* (expressed in radians) of the induction machine; it characterizes the decay of the rotor transients when the stator is open-circuited. In the above equations, p is the per unit time derivative; that is, time t is in radians.

In system studies, we normally prefer to express time in seconds. *The above equations are also applicable with time t and the time constant T'_0 expressed in seconds. In this case, $p\theta_r$ is the slip speed in radians per second.*

Equations 7.99 and 7.100 describe the rotor circuit dynamics. The rotor acceleration equation, with time expressed in seconds, is

$$p(\bar{\omega}_r) = \frac{1}{2H}(T_e - T_m) \tag{7.104}$$

From Equation 7.78, the per unit electromagnetic torque is

$$T_e = \psi_{qr} i_{dr} - \psi_{dr} i_{qr}$$

Eliminating the rotor currents by expressing them in terms of the stator currents and rotor flux linkages (see Equation 7.90), we find

$$T_e = \psi_{qr}\left(\frac{\psi_{dr}-L_m i_{ds}}{L_{rr}}\right) - \psi_{dr}\left(\frac{\psi_{qr}-L_m i_{qs}}{L_{rr}}\right)$$

$$= -\psi_{qr}\left(\frac{L_m}{L_{rr}}\right) i_{ds} + \psi_{dr}\left(\frac{L_m}{L_{rr}}\right) i_{qs}$$

$$= \frac{v'_d i_{ds} + v'_q i_{qs}}{\omega_s}$$

With ω_s=1.0 pu,

$$T_e = v'_d i_{ds} + v'_q i_{qs} \tag{7.105}$$

The load torque T_m (required for the solution of Equation 7.104) is given by Equation 7.80 or 7.81.

In Equations 7.99 and 7.100, the term $s\omega_s = p\theta_r$ represents the angular velocity between the rotor and the reference *d-q* axes rotating at synchronous speed ω_s. As ω_r changes, $s\omega_s$ is computed as being equal to $\omega_s - \omega_r$.

In the above induction machine equations, rotor slip with respect to the stator field does not appear explicitly. During system swings (electromechanical oscillations), the frequency of stator voltages and currents deviates from the synchronous frequency ω_s. This is reflected in the machine equations as oscillations in v_{ds}, v_{qs}, i_{ds} and i_{qs}. If the transient variation in slip were required, it would be necessary to compute the rate of change of stator voltage angle to establish the angular velocity of the stator field.

Simplified induction machine model

For many applications, particularly those involving small motors, it is not necessary to account for the dynamics of the rotor electrical circuits. In such cases, the rotor-circuit dynamics may be assumed to be very fast (i.e., T'_0 very small), and $p(v'_d)$ and $p(v'_q)$ are set to zero in Equations 7.99 and 7.100. With this simplification, the induction motor representation can be based on steady-state theory, including the equivalent circuit of Figure 7.9 and torque-slip relationship given by Equation 7.55.

Induction motor parameters

The equivalent-circuit parameters of an induction motor are given by design data. If the design data are not readily available, the parameters may be estimated from standard specifications as described in reference 13.

As an example of induction motor parameters, Figure 7.18 shows the data for a 150 HP double-cage induction motor and the corresponding torque and current characteristics.

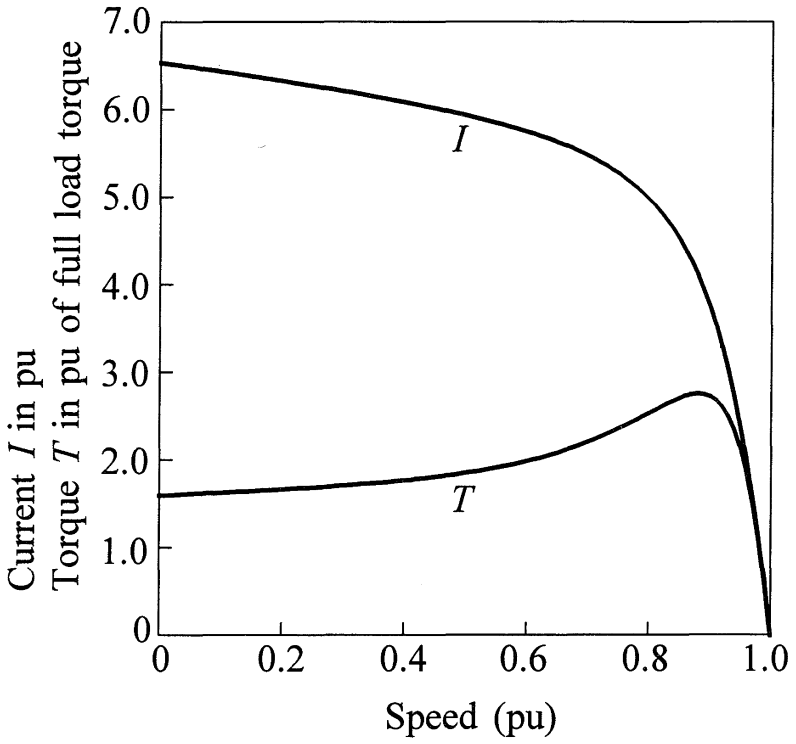

Motor specification data

Full-load efficiency	=	0.9151
Full-load power factor	=	0.8895
Full-load slip	=	0.0166
No-load loss (kW)	=	2.594
Starting current (pu)	=	6.4961
Starting torque ratio	=	1.5921
Pull-out torque	=	2.650
Pull-out slip	=	0.0914
kVA rating	=	137.0
Rated voltage (V)	=	400
Rated current (A)	=	198

Parameters of equivalent circuit in pu of 137 kVA and 400 V

$R_s = 0.0425$	$X_{s\text{-}u} = 0.0435$	$X_{s\text{-}s} = 0.0435$	$X_m = 2.9745$
$R_1 = 0.0739$	$X_{r\text{-}u} = 0.0329$	$X_{r\text{-}s} = 0.0329$	$R_2 = 0.0249$
$X_2 = 0.0739$	$H = 0.6$	$I_{sats} = 3.0$	$I_{satr} = 3.0$

Load torque exponent $m = 2.0$

(See Figures 7.14 and 7.16 for definition of parameters.)

Figure 7.18 Typical 150 HP double-cage induction motor data

7.3 SYNCHRONOUS MOTOR MODEL

A synchronous motor is modelled in the same manner as a synchronous generator (see Chapters 3 to 5). The only difference is that, instead of a prime mover providing mechanical torque input to the generator, the motor drives a mechanical load. As in the case of an induction motor, a commonly used expression for the load torque is

$$T_m = T_0 \omega_r^m \tag{7.106}$$

The rotor acceleration equation is given by

$$\frac{d\omega_r}{dt} = \frac{1}{2H}(T_e - T_m) \tag{7.107}$$

where H is the combined inertia constant of the motor and load.

The data to model the synchronous motor are identical to those of a synchronous generator, except for the exponent m associated with the load characteristic.

7.4 ACQUISITION OF LOAD-MODEL PARAMETERS

There are two basic approaches to the determination of system-load characteristics:

- Measurement-based approach
- Component-based approach

7.4.1 Measurement-Based Approach

In this approach, the load characteristics are measured at representative substations and feeders at selected times of the day and season. These are used to extrapolate the parameters of loads throughout the system. References 14 and 15 describe load models derived from staged tests, and reference 16 presents models derived from actual system transients. Reference 3 describes an alternative approach in which load characteristics are monitored continuously from naturally occurring system variations.

Steady-state load-voltage characteristics

Composite load characteristics are normally measured at the highest voltage level for which the voltage of radially connected load can be adjusted by transformer

tap changers. This is usually the highest distribution voltage level. The steady-state characteristics can be determined by adjusting the load voltage via the transformer tap changers over a range of voltage above and below the nominal value. Distribution tap changers and switched capacitors must be blocked to obtain meaningful results. The measured responses of voltage, active power, and reactive power are fitted to the polynomial and/or exponential expressions (Equation 7.1, 7.2, or 7.5).

Steady-state load-frequency characteristics

It is usually much more difficult to measure system load-frequency characteristics. To measure composite load-frequency characteristics, an isolated system must be formed and the frequency varied over the desired range. To obtain valid data, care must be taken to separate the effects of voltage changes and frequency changes. For many of the results reported in the literature this is not done, and the dP/df characteristic determined is a composite of the effects due to frequency change and the resulting voltage change.

Dynamic load-voltage characteristics

The small-signal dynamic characteristics of composite loads can be determined relatively easily from simple system tests. Figure 7.19 shows the testing configuration that may be employed when loads are supplied by two tap-changing transformers.

Initially, one tap changer is adjusted upward and the other downward by a few taps, keeping the load voltage constant. One of the transformers is then tripped; this produces not only a voltage magnitude change but also an instantaneous angle change at the load bus. By varying the initial tap positions, it is possible to obtain a range of voltage changes in both positive and negative directions. By selecting the tap positions appropriately, it is also possible to produce an angle change with only a very small

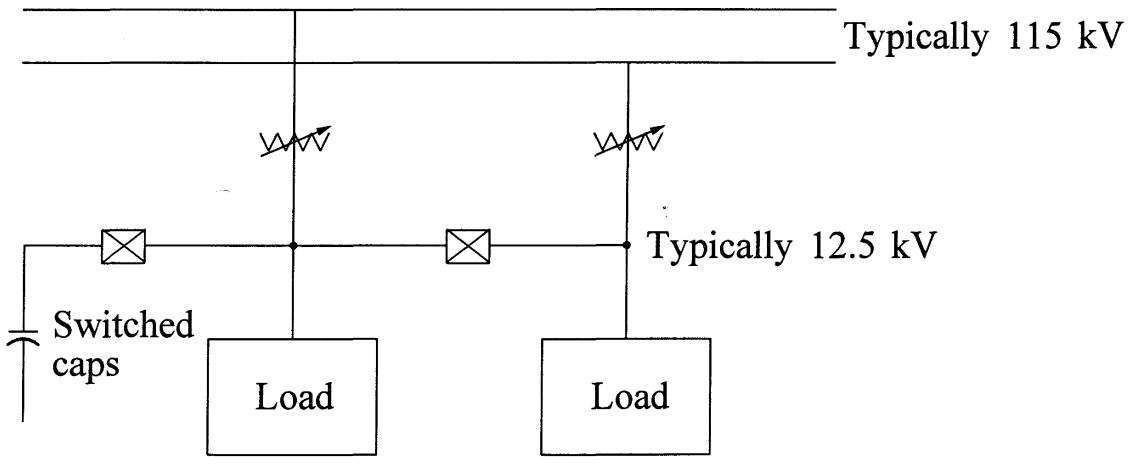

Figure 7.19 Typical station configuration for testing load characteristics

voltage change. This is useful in separating the effects of voltage magnitude and angle change.

If there is a switched capacitor bank at the load bus, it can be switched in and out to produce a voltage magnitude change at the load without an angle change.

The responses obtained in this fashion are essentially *small-signal*. Reference 14 describes load models derived from such tests at Ontario Hydro. Measured time responses of load-voltage magnitude, angle, active power, and reactive power are used to determine the parameters of a model with a structure as shown in Figure 7.20. The model structure assumes that the composite load appears as an induction motor and shunt static load.

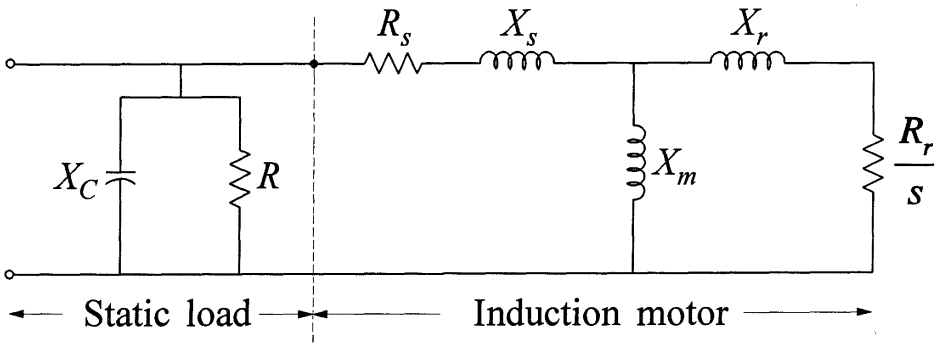

Figure 7.20 Composite induction motor/static load equivalent for representing an industrial load

A least square difference technique is used to optimize the match between the measured and model responses as the model parameters are adjusted. The result is a model whose parameters are chosen to match the small-signal response. However, because of the realistic model structure chosen, the model is likely to give reasonable results under large-disturbance conditions.

Reference 14 also describes *large-signal* models developed for industrial loads from responses monitored by transient monitoring systems during naturally occurring disturbances.

Reference 15 describes models derived from staged tests on generating station auxiliary systems and at bulk supply points supplying both industrial and residential loads in England. The resulting model consists of a constant impedance static load in parallel with a single rotor circuit induction motor. In addition, a nonlinear shunt reactance is included to account for magnetic saturation characteristics of motors and transformers.

7.4.2 Component-Based Approach

This approach was developed by EPRI under several research projects beginning in 1976 [16-19]. It involves building up the load model from information on its constituent parts as illustrated in Figure 7.21. The load supplied at a bulk power

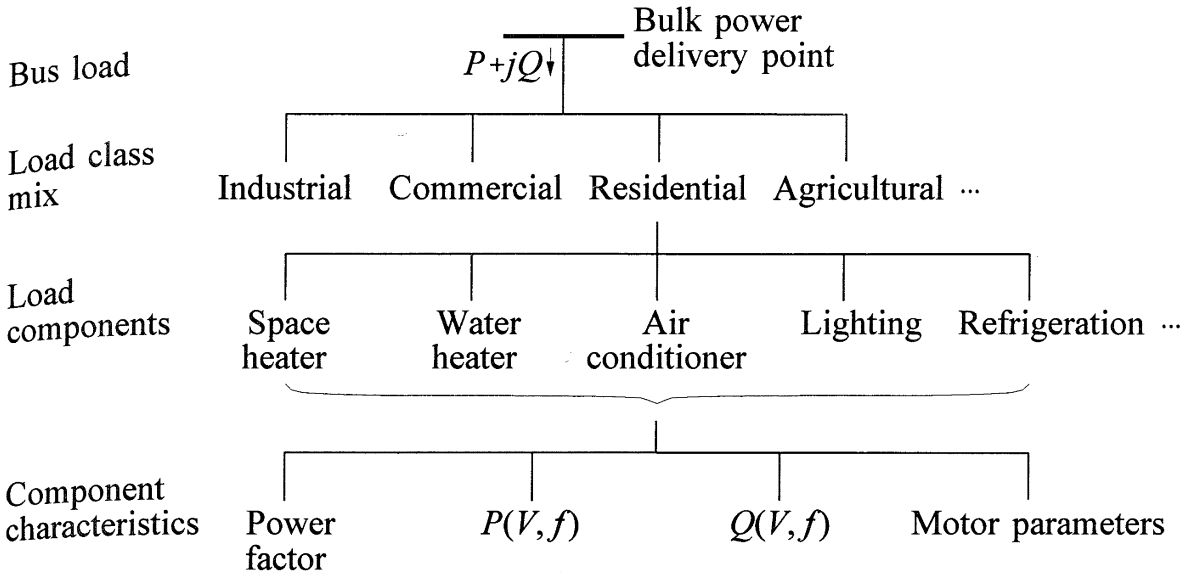

Figure 7.21 Component-based modelling approach

delivery point is categorized into *load classes* such as residential, commercial, industrial, agricultural, and mining. Each category of load class is represented in terms of *load components* such as lighting, air conditioning, space heating, water heating, and refrigeration.

The characteristics of individual appliances have been studied in detail and techniques have been developed to aggregate individual loads to produce a composite load model [16,17].

The EPRI LOADSYN program [18] converts data on the load class mix, components, and their characteristics into the form required for power flow and stability programs. Typical default data have been developed for load composition and characteristics for each class of load. A similar approach is used in reference 20, in which end-user energy consumption data are used to identify load mix data.

In reference 17, load characteristics determined by the component-based load-modelling approach are compared with measured load characteristics on the Long Island Lighting Company, Rochester Gas and Electric Company, and Montana-Dakota Utility systems. The load models correctly represented the steady-state active power versus voltage responses, but could not represent accurately the steady-state reactive power versus voltage responses. Also, the models could not represent accurately the transient responses of active and reactive power. These discrepancies between measured and model responses were subsequently resolved, as reported in reference 21, by using physically based models as opposed to the polynomial representation. Single-phase induction motor models were used to represent compressors and other rotating loads. Separate models were developed to represent compressor and non-compressor loads.

7.4.3 Sample Load Characteristics [2,14,16,20]

(a) Component static characteristics

Table 7.1 summarizes typical voltage and frequency-dependent characteristics of a number of load components.

Table 7.1 Static characteristics of load components

Component	Power factor	$\partial P/\partial V$	$\partial Q/\partial V$	$\partial P/\partial f$	$\partial Q/\partial f$
Air conditioner					
3-phase central	0.90	0.088	2.5	0.98	-1.3
1-phase central	0.96	0.202	2.3	0.90	-2.7
Window type	0.82	0.468	2.5	0.56	-2.8
Water heaters, Range top, oven, Deep fryer	1.0	2.0	0	0	0
Dishwasher	0.99	1.8	3.6	0	-1.4
Clothes washer	0.65	0.08	1.6	3.0	1.8
Clothes dryer	0.99	2.0	3.2	0	-2.5
Refrigerator	0.8	0.77	2.5	0.53	-1.5
Television	0.8	2.0	5.1	0	-4.5
Incandescent lights	1.0	1.55	0	0	0
Fluorescent lights	0.9	0.96	7.4	1.0	-2.8
Industrial motors	0.88	0.07	0.5	2.5	1.2
Fan motors	0.87	0.08	1.6	2.9	1.7
Agricultural pumps	0.85	1.4	1.4	5.0	4.0
Arc furnace	0.70	2.3	1.6	-1.0	-1.0
Transformer (unloaded)	0.64	3.4	11.5	0	-11.8

(b) Load class static characteristics

Table 7.2 summarizes the sample characteristics of different load classes.

Table 7.2

Load class	Power factor	$\partial P/\partial V$	$\partial Q/\partial V$	$\partial P/\partial f$	$\partial Q/\partial f$
Residential					
Summer	0.9	1.2	2.9	0.8	-2.2
Winter	0.99	1.5	3.2	1.0	-1.5
Commercial					
Summer	0.85	0.99	3.5	1.2	-1.6
Winter	0.9	1.3	3.1	1.5	-1.1
Industrial	0.85	0.18	6.0	2.6	1.6
Power plant auxiliaries	0.8	0.1	1.6	2.9	1.8

(c) Dynamic characteristics

The following are sample data for induction motor equivalents representing three different types of load (see Figure 7.7 for definition of parameters).

(i) The composite dynamic characteristics of a feeder supplying predominantly a commercial load:

$R_s = 0.001$ $X_s = 0.23$ $X_r = 0.23$
$X_m = 3.0$ $R_r = 0.02$ $H = 0.663$ $m = 5.0$

(ii) A large industrial motor:

$R_s = 0.007$ $X_{s\text{-}u} = 0.0409$ $X_{s\text{-}s} = 0.0409$ $X_{r\text{-}u} = 0.0267$
$X_{r\text{-}s} = 0.0267$ $X_m = 3.62$ $R_r = 0.0062$ $H = 1.6$
$m = 2.0$ $I_{sats} = 3.0$ $I_{satr} = 3.0$
Deep-bar factor = 6.59

(iii) A small industrial motor:

$R_s = 0.078$ $X_s = 0.065$ $X_r = 0.049$
$X_m = 2.67$ $R_r = 0.044$ $H = 0.5$ $m = 2.0$

REFERENCES

[1] IEEE Task Force Report, "Load Representation for Dynamic Performance Analysis," Paper 92WM126-3 PWRD, presented at the IEEE PES Winter Meeting, New York, January 26-30, 1992.

[2] C. Concordia and S. Ihara, "Load Representation in Power System Stability Studies," *IEEE Trans.*, Vol. PAS-101, pp. 969-977, April 1982.

[3] K. Srinivasan, C.T. Nguyen, Y. Robichaud, A. St. Jacques, and G.J. Rogers, "Load Response Coefficients Monitoring System: Theory and Field Experience," *IEEE Trans.*, Vol. PAS-100, pp. 3818-3827, August 1981.

[4] T. Ohyama, A. Watanabe, K. Nishimura, and S. Tsuruta, "Voltage Dependence of Composite Loads in Power Systems," *IEEE Trans.*, Vol. PAS-104, pp. 3064-3073, November 1985.

[5] EPRI Report of Project 1208-9, "Extended Transient-Midterm Stability Program," Final report, prepared by Ontario Hydro, December 1992.

[6] H.K. Clark, "Experience with Load Models in Simulation of Dynamic Phenomena," Paper presented at the Panel Discussion on Load Modelling Impact on System Dynamic Performance, IEEE PES Winter Meeting, New York, February 1, 1989.

[7] H.K. Clark and T.F. Laskowski, "Transient Stability Sensitivity to Detailed Load Models: A Parametric Study," Paper A78 559-7, IEEE PES Summer Meeting, Los Angeles, July 16-21, 1978.

[8] Klaus-Martin Graf, "Dynamic Simulation of Voltage Collapse Processes in EHV Power Systems," *Proceeding: Bulk Power System Voltage Phenomena-Voltage Stability and Security*, EPRI EL-6183, Section 6.3, January 1989.

[9] C.W. Taylor, *Power System Voltage Stability*, McGraw-Hill, 1993.

[10] D.S. Brereton, D.G. Lewis, and C.C. Young, "Representation of Induction-Motor Loads during Power System Stability Studies," *AIEE Trans.*, Vol. 76, Part III, pp. 451-460, August 1957.

[11] A.E. Fitzgerald and C. Kingsley, *Electric Machinery*, Second Edition, McGraw-Hill, 1961.

[12] G.J. Rogers and D.S. Benaragama, "An Induction Motor Model with Deep-Bar

Effect and Leakage Inductance Saturation," *Archiv Für Elektrotechnik*, Vol. 60, pp. 193-201, 1978.

[13] G.J. Rogers, J. Di Manno, and R.T.H. Alden, "An Aggregate Induction Motor Model for Industrial Plants," *IEEE Trans.*, Vol. PAS-103, pp. 683-690, 1984.

[14] S.A.Y. Sabir and D.C. Lee, "Dynamic Load Models Derived from Data Acquired during System Transients," *IEEE Trans.*, Vol. PAS-101, pp. 3365-3372, September 1982.

[15] G. Shackshaft, O.C. Symons, and J.G. Hadwick, "General Purpose Model of Power System Loads," *Proc IEE*, Vol. 124, No. 8, pp. 715-723, August 1977.

[16] EPRI Report of Project RP849-3, "Determining Load Characteristics for Transient Performance," EPRI EL-840, Vols. 1 to 3, prepared by the University of Texas at Arlington, May 1979.

[17] EPRI Report of Project RP849-1, "Determining Load Characteristics for Transient Performance," EPRI EL-850, prepared by General Electric Company, March 1981.

[18] EPRI Report of Project RP849-7, "Load Modelling for Power Flow and Transient Stability Studies," EPRI EL-5003, Prepared by General Electric Company, January 1987.

[19] T. Frantz, T. Gentile, S. Ihara, N. Simons, and M. Waldron, "Load Behaviour Observed in LILCO and RG&E Systems," *IEEE Trans.*, Vol. PAS-103, No. 4, pp. 819-831, April 1984.

[20] E. Vaahedi, M.A. El-Kady, J.A. Libaque-Esaine, and V.F. Carvalho, "Load Models for Large-Scale Stability Studies from End-User Consumption," *IEEE Trans.*, Vol. PWRS-2, pp. 864-872, November 1987.

[21] R.J. Frowd, R. Podmore, and M. Waldron, "Synthesis of Dynamic Load Models for Stability Studies," *IEEE Trans.*, Vol. PAS-101, pp. 127-135, January 1982.

[22] B. Adkins and R.G. Harley, *The General Theory of Alternating Current Machine*, Chapman and Hall, 1975.

Chapter 8

Excitation Systems

The basic function of an excitation system is to provide direct current to the synchronous machine field winding. In addition, the excitation system performs control and protective functions essential to the satisfactory performance of the power system by controlling the field voltage and thereby the field current.

The control functions include the control of voltage and reactive power flow, and the enhancement of system stability. The protective functions ensure that the capability limits of the synchronous machine, excitation system, and other equipment are not exceeded.

This chapter describes the characteristics and modelling of different types of synchronous generator excitation systems. In addition, it discusses dynamic performance criteria and provides definitions of related terms useful in the identification and specification of excitation system requirements. This subject has been covered in several IEEE reports [1-8]. These serve as useful references to utilities, manufacturers, and system analysts by establishing a common nomenclature, by standardizing models, and by providing guides for specifications and testing. Models and terminologies used in this chapter largely conform to these publications.

8.1 EXCITATION SYSTEM REQUIREMENTS

The performance requirements of the excitation system are determined by considerations of the synchronous generator as well as the power system [6,9].

Generator considerations

The basic requirement is that the excitation system supply and automatically adjust the field current of the synchronous generator to maintain the terminal voltage as the output varies within the *continuous capability* of the generator. This requirement can be visualized from the generator *V*-curves, such as those shown in Figure 5.19 of Chapter 5. Margins for temperature variations, component failures, emergency overrating, etc., must be factored in when the steady-state power rating is determined. Normally, the exciter rating varies from 2.0 to 3.5 kW/MVA generator rating.

In addition, the excitation system must be able to respond to transient disturbances with field forcing consistent with the generator instantaneous and short-term capabilities. The generator capabilities in this regard are limited by several factors: rotor insulation failure due to high field voltage, rotor heating due to high field current, stator heating due to high armature current loading, core end heating during underexcited operation, and heating due to excess flux (volts/Hz). The thermal limits have time-dependent characteristics, and the short-term overload capability of the generators may extend from 15 to 60 seconds. To ensure the best utilization of the excitation system, it should be capable of meeting the system needs by taking full advantage of the generator's short-term capabilities without exceeding their limits.

Power system considerations

From the power system viewpoint, the excitation system should contribute to effective control of voltage and enhancement of system stability. It should be capable of responding rapidly to a disturbance so as to enhance transient stability, and of modulating the generator field so as to enhance small-signal stability.

Historically, the role of the excitation system in enhancing power system performance has been growing continually. Early excitation systems were controlled manually to maintain the desired generator terminal voltage and reactive power loading. When the voltage control was first automated, it was very slow, basically filling the role of an alert operator. In the early 1920s, the potential for enhancing small-signal and transient stability through use of continuous and fast-acting regulators was recognized. Greater interest in the design of excitation systems developed, and exciters and voltage regulators with faster response were soon introduced to the industry. Excitation systems have since undergone continuous evolution. In the early 1960s, the role of the excitation system was expanded by using auxiliary stabilizing signals, in addition to the terminal voltage error signal, to control the field voltage to damp system oscillations. This part of excitation control is referred to as the *power system stabilizer*. Modern excitation systems are capable of providing practically instantaneous response with high ceiling voltages. The combination of high field-forcing capability and the use of auxiliary stabilizing signals contributes to substantial enhancement of the overall system dynamic performance. This will be discussed in detail in Chapters 12, 13, and 17.

To fulfill the above roles satisfactorily, the excitation system must satisfy the following requirements:

- Meet specified response criteria.
- Provide limiting and protective functions as required to prevent damage to itself, the generator, and other equipment.
- Meet specified requirements for operating flexibility.
- Meet the desired reliability and availability, by incorporating the necessary level of redundancy and internal fault detection and isolation capability.

8.2 ELEMENTS OF AN EXCITATION SYSTEM

Figure 8.1 shows the functional block diagram of a typical excitation control system for a large synchronous generator. The following is a brief description of the various subsystems identified in the figure.

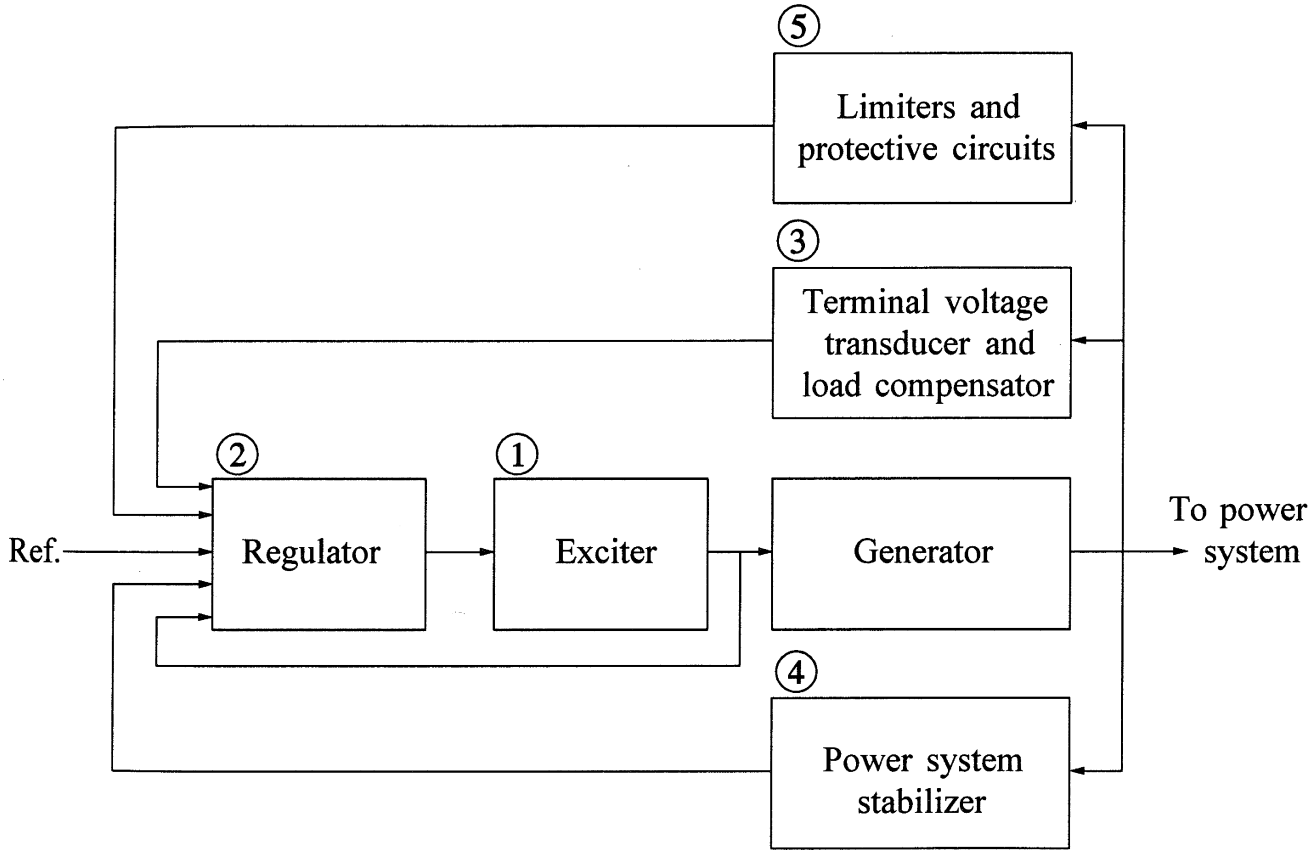

Figure 8.1 Functional block diagram of a synchronous generator excitation control system

(1) *Exciter.* Provides dc power to the synchronous machine field winding, constituting the power stage of the excitation system.

(2) *Regulator.* Processes and amplifies input control signals to a level and form appropriate for control of the exciter. This includes both regulating and excitation system stabilizing functions (rate feedback or lead-lag compensation).

(3) *Terminal voltage transducer and load compensator.* Senses generator terminal voltage, rectifies and filters it to dc quantity, and compares it with a reference which represents the desired terminal voltage. In addition, load (or line-drop, or reactive) compensation may be provided, if it is desired to hold constant voltage at some point electrically remote from the generator terminal (for example, partway through the step-up transformer).

(4) *Power system stabilizer.* Provides an additional input signal to the regulator to damp power system oscillations. Some commonly used input signals are rotor speed deviation, accelerating power, and frequency deviation.

(5) *Limiters and protective circuits.* These include a wide array of control and protective functions which ensure that the capability limits of the exciter and synchronous generator are not exceeded. Some of the commonly used functions are the field-current limiter, maximum excitation limiter, terminal voltage limiter, volts-per-Hertz regulator and protection, and underexcitation limiter. These are normally distinct circuits and their output signals may be applied to the excitation system at various locations as a summing input or a gated input. For convenience, they have been grouped and shown in Figure 8.1 as a single block.

8.3 TYPES OF EXCITATION SYSTEMS

Excitation systems have taken many forms over the years of their evolution. They may be classified into the following three broad categories based on the excitation power source used [4,8]:

- DC excitation systems
- AC excitation systems
- Static excitation systems

This section provides a description of the above classes of excitation systems, the different forms they take, and their general structure. Details regarding various regulating and protective functions often included with the excitation systems will be covered in Section 8.5.

8.3.1 DC Excitation Systems

The excitation systems of this category utilize dc generators as sources of excitation power and provide current to the rotor of the synchronous machine through slip rings. The exciter may be driven by a motor or the shaft of the generator. It may be either self-excited or separately excited. When separately excited, the exciter field is supplied by a pilot exciter comprising a permanent magnet generator.

DC excitation systems represent early systems, spanning the years from the 1920s to the 1960s. They lost favour in the mid-1960s and were superseded by ac exciters.

The voltage regulators for such systems range all the way from the early non-continuously acting rheostatic type to the later systems utilizing many stages of magnetic amplifiers and rotating amplifiers [10,11].

DC excitation systems are gradually disappearing, as many older systems are being replaced by ac or static type systems. In some cases, the voltage regulators alone have been replaced by modern solid-state electronic regulators. As many of the dc excitation systems are still in service, they still require modelling in stability studies.

Figure 8.2 shows a simplified schematic representation of a typical dc excitation system with an amplidyne voltage regulator. It consists of a dc commutator exciter which supplies direct current to the main generator field through slip rings. The exciter field is controlled by an amplidyne.

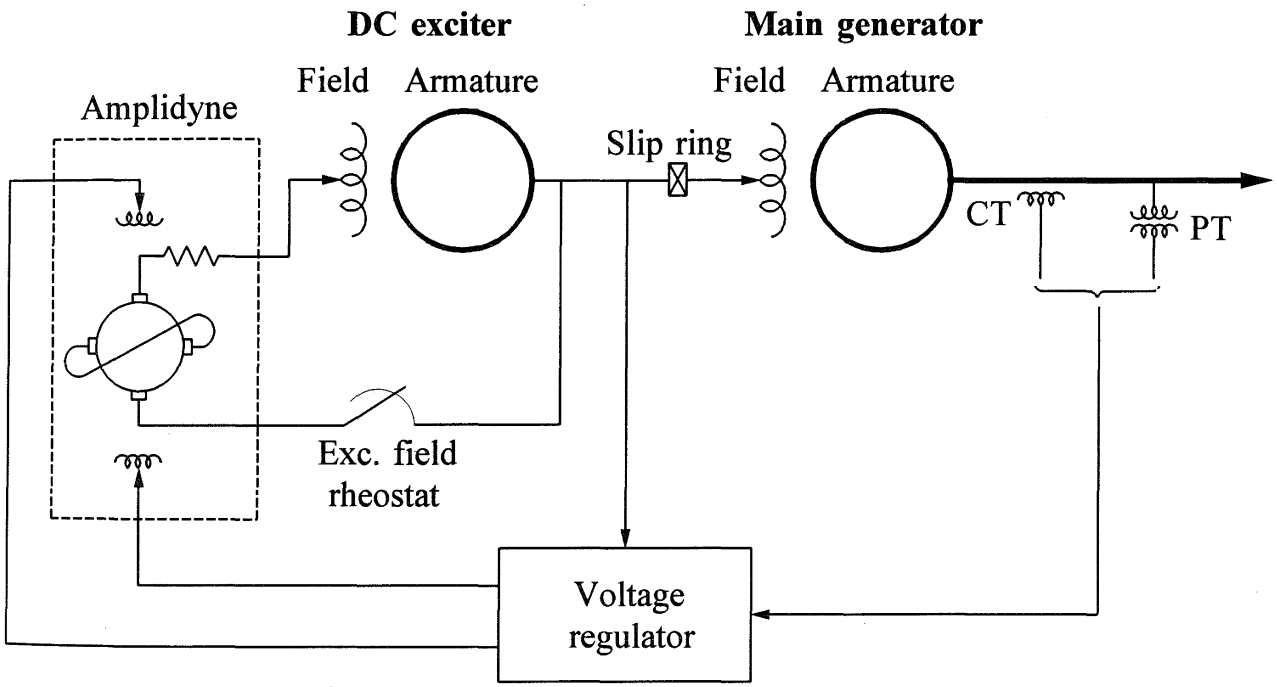

Figure 8.2 DC excitation system with amplidyne voltage regulator

An amplidyne is a special type of the general class of rotating amplifiers known as metadynes [11,12]. It is a dc machine of special construction having two sets of brushes 90 electrical degrees apart, one set on its direct (d) axis and the other set on its quadrature (q) axis. The control-field windings are located on the d-axis. A compensating winding in series with the d-axis load produces flux equal and opposite to the d-axis armature current, thereby cancelling negative feedback of the armature reaction. The brushes on the q-axis are shorted, and very little control-field power is required to produce a large current in the q-axis armature. The q-axis current produces the principal magnetic field, and the power required to sustain the q-axis current is supplied mechanically by the motor driving the amplidyne. The result is a device with power amplification on the order of 10,000 to 100,000 and a time constant in the range from 0.02 to 0.25 seconds.

In the excitation system of Figure 8.2, the amplidyne provides incremental changes to the exciter field in a "buck-boost" scheme. The exciter output provides the rest of its own field by self-excitation. If the amplidyne regulator is out of service, the exciter field is on "manual control" and is changed through adjustment of the field rheostat.

8.3.2 AC Excitation Systems

The excitation systems of this category utilize alternators (ac machines) as sources of the main generator excitation power. Usually, the exciter is on the same shaft as the turbine generator. The ac output of the exciter is rectified by either controlled or non-controlled rectifiers to produce the direct current needed for the generator field. The rectifiers may be stationary or rotating.

The early ac excitation systems used a combination of magnetic and rotating amplifiers as regulators [11]. Most new systems use electronic amplifier regulators.

AC excitation systems can thus take many forms depending on the rectifier arrangement, method of exciter output control, and source of excitation for the exciter [13-17]. The following is a description of different forms of ac excitation systems in use.

(a) Stationary rectifier systems

With stationary rectifiers, the dc output is fed to the field winding of the main generator through slip rings.

When non-controlled rectifiers are used, the regulator controls the field of the ac exciter, which in turn controls the exciter output voltage. A simplified one-line diagram of such a *field controlled alternator rectifier excitation system* is shown in Figure 8.3. In the system shown, which is representative of the General Electric ALTERREX[1] excitation system [14], the alternator exciter is driven from the main

[1] ALTERREX is a trademark of General Electric Co.

generator rotor. The exciter is self-excited with its field power derived through thyristor rectifiers. The voltage regulator derives its power from the exciter output voltage.

An alternative form of field-controlled alternator rectifier system uses a pilot exciter as the source of exciter field power.

When controlled rectifiers (thyristors) are used, the regulator directly controls the dc output voltage of the exciter. Figure 8.4 shows the schematic diagram of such an *alternator supplied controlled-rectifier system*, representative of the General Electric ALTHYREX[1] System [17]. The voltage regulator controls the firing of the thyristors. The exciter alternator is self-excited and uses an independent static voltage regulator to maintain its output voltage. Since the thyristors directly control the exciter output, this system inherently provides high initial response (small response time).

As shown in Figures 8.3 and 8.4, two independent modes of regulation are provided: (1) ac regulator to automatically maintain the main generator stator terminal voltage at a desired value corresponding to the ac reference; and (2) dc regulator to maintain constant generator field voltage as determined by the dc reference. The dc regulator or manual control mode caters to situations where the ac regulator is faulty or needs to be disabled. The input signals to the ac regulator include auxiliary inputs which provide additional control and protective functions which will be described in Section 8.5.

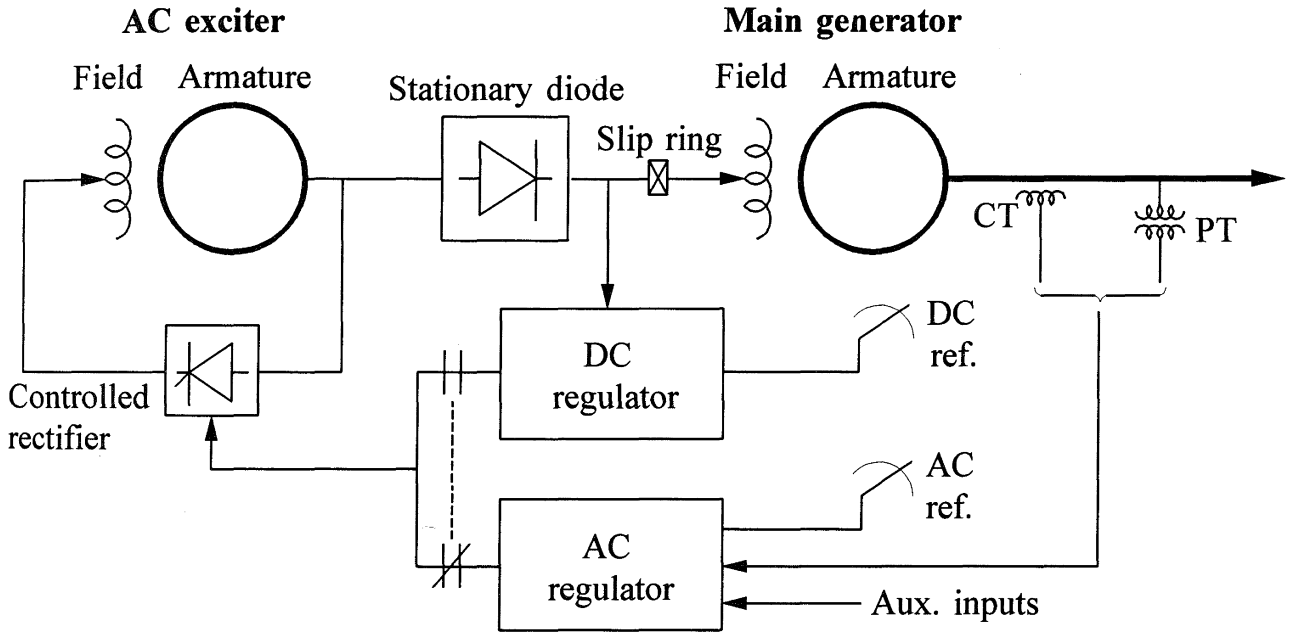

Figure 8.3 Field-controlled alternator rectifier excitation system

[1] ALTHYREX is a trademark of General Electric Co.

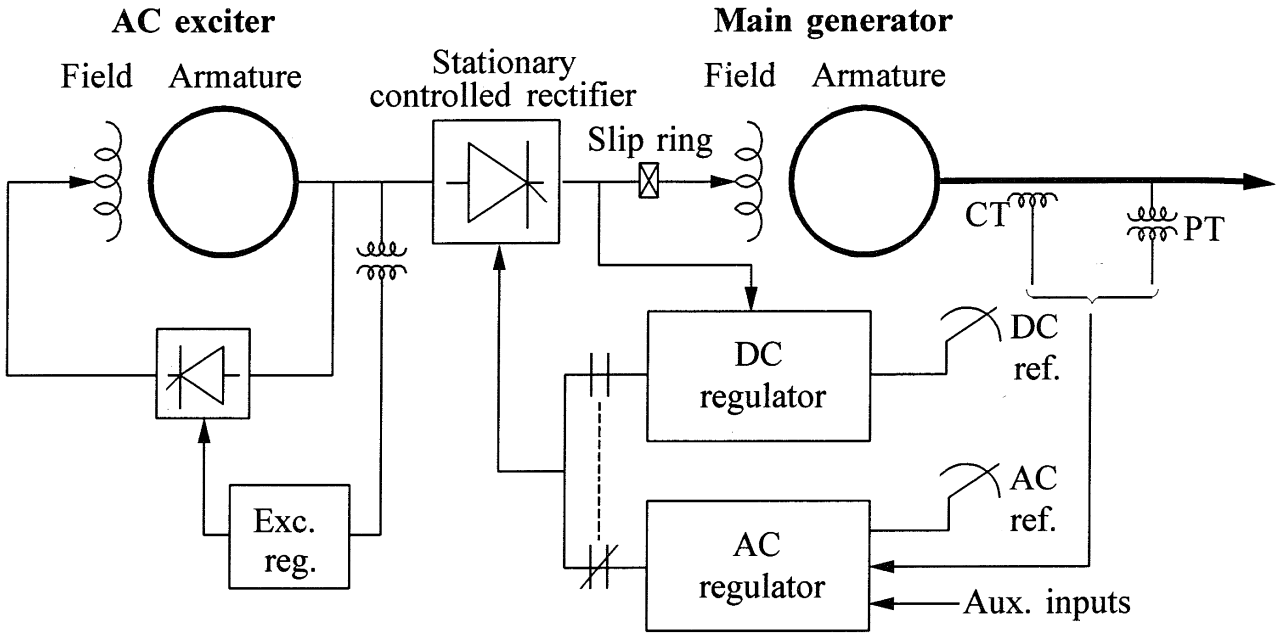

Figure 8.4 Alternator-supplied controlled-rectifier excitation system

(b) Rotating rectifier systems

With rotating rectifiers, the need for slip rings and brushes is eliminated, and the dc output is directly fed to the main generator field. As shown in Figure 8.5, the armature of the ac exciter and the diode rectifiers rotate with the main generator field. A small ac pilot exciter, with a permanent magnet rotor (shown as N S in the figure), rotates with the exciter armature and the diode rectifiers. The rectified output of the pilot exciter stator energizes the stationary field of the ac exciter. The voltage regulator controls the ac exciter field, which in turn controls the field of the main generator.

Such a system is referred to as a *brushless excitation system.* It was developed to avoid problems with the use of brushes that were perceived to exist when supplying the high field currents of very large generators; for example, the power supplied to the field of a 600 MW generator is on the order of 1 MW. However, with well-maintained brushes and slip rings, these perceived problems did not actually develop. AC excitation systems with and without brushes have performed equally well.

High initial-response performance of brushless excitation can be achieved by special design of the ac exciter and high voltage forcing of the exciter stationary field winding. An example of such a system is the Westinghouse high initial response brushless excitation system [13].

Brushless excitation systems do not allow direct measurement of generator field current or voltage. Manual control of main generator voltage is provided by an adjustable dc input setting to the thyristor gating circuits. For the sake of simplicity, the functions of the control circuitry are not shown in detail in Figure 8.5.

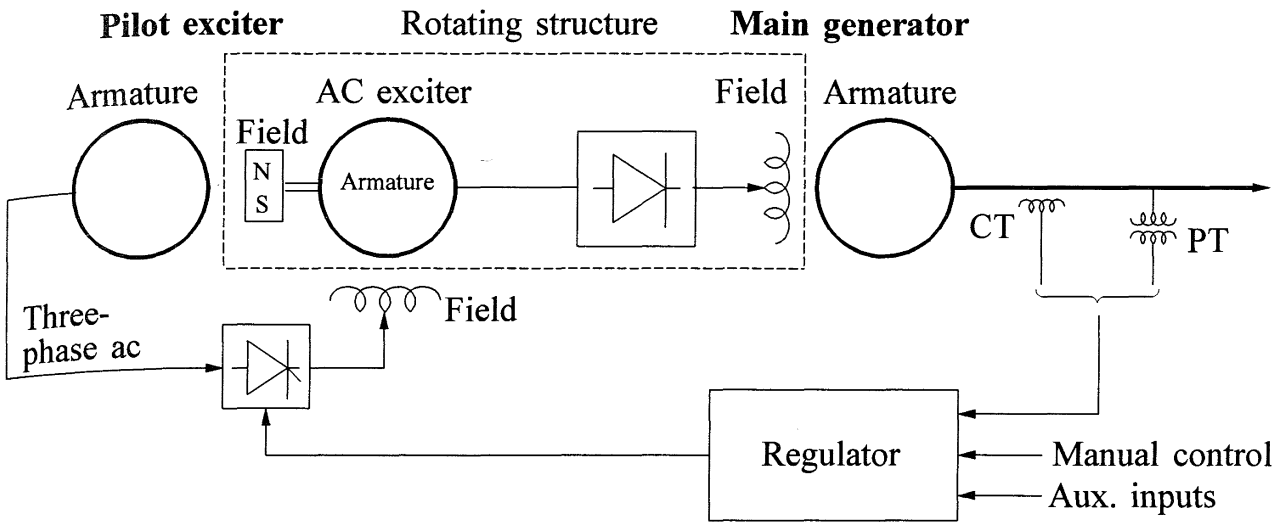

Figure 8.5 Brushless excitation system

8.3.3 Static Excitation Systems

All components in these systems are static or stationary. Static rectifiers, controlled or uncontrolled, supply the excitation current directly to the field of the main synchronous generator through slip rings. The supply of power to the rectifiers is from the main generator (or the station auxiliary bus) through a transformer to step down the voltage to an appropriate level, or in some cases from auxiliary windings in the generator.

The following is a description of three forms of static excitation systems that have been widely used.

(a) Potential-source controlled-rectifier systems

In this system, the excitation power is supplied through a transformer from the generator terminals or the station auxiliary bus, and is regulated by a controlled rectifier (see Figure 8.6). This type of excitation system is also commonly known as a *bus-fed* or *transformer-fed* static system.

This system has a very small inherent time constant. The maximum exciter output voltage (ceiling voltage) is, however, dependent on the input ac voltage. Hence, during system-fault conditions causing depressed generator terminal voltage, the available exciter ceiling voltage is reduced. This limitation of the excitation system is, to a large extent, offset by its virtually instantaneous response and high post-fault field-forcing capability [18,19]. In addition, it is inexpensive and easily maintainable. For generators connected to large power systems such excitation systems perform satisfactorily [18]. Compounding ancillaries, such as those described below, are not normally justified; they are likely important for generators feeding power directly into small industrial networks with slow fault-clearing.

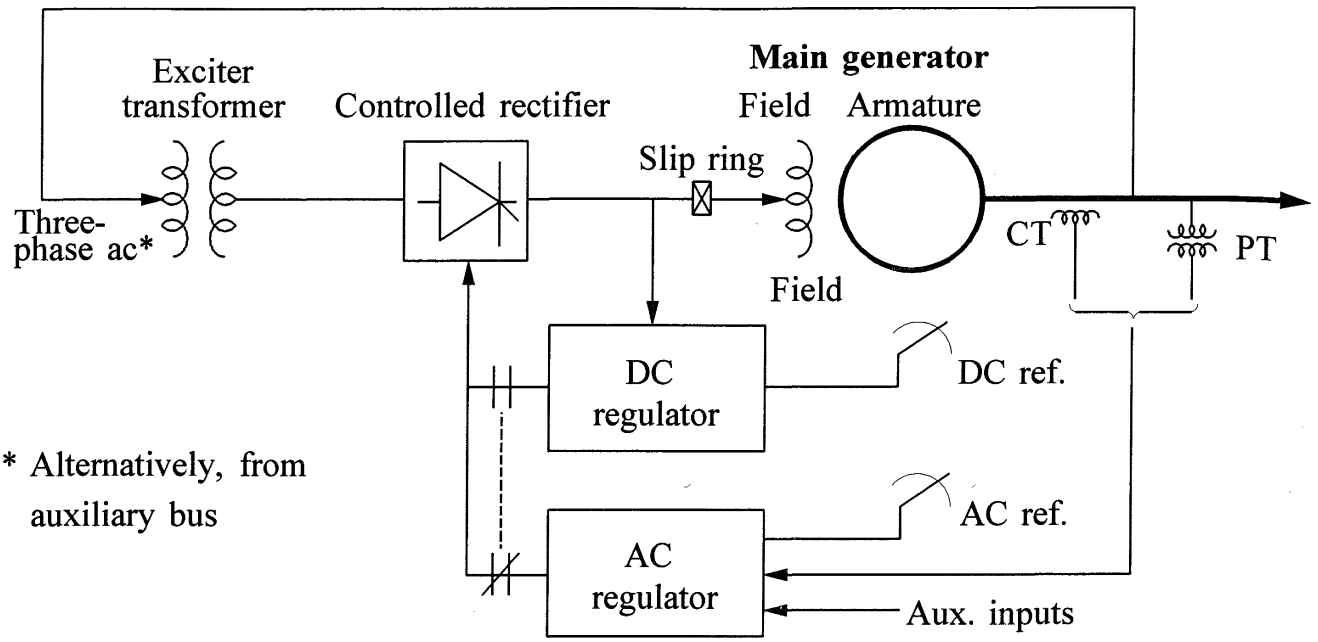

Figure 8.6 Potential-source controlled-rectifier excitation system

Examples of this type of excitation system are: Canadian General Electric Silicomatic excitation system, Westinghouse type PS excitation system, General Electric potential source static excitation system, and ABB, Reyrolle-Parsons, GEC-Eliott, Toshiba, Mitsubishi, and Hitachi static excitation systems.

(b) Compound-source rectifier systems

The power to the excitation system in this case is formed by utilizing the current as well as the voltage of the main generator. This may be achieved by means of a power potential transformer (PPT) and a saturable-current transformer (SCT) as illustrated in Figure 8.7. Alternatively, the voltage and current sources may be combined by utilizing a single excitation transformer, referred to as a saturable-current potential transformer (SCPT).

The regulator controls the exciter output through controlled saturation of the excitation transformer. When the generator is not supplying a load, the armature current is zero and the potential source supplies the entire excitation power. Under loaded conditions, part of the excitation power is derived from the generator current. During a system-fault condition, with severely depressed generator terminal voltage, the current input enables the exciter to provide high field-forcing capability.

Examples of this type of excitation system are General Electric SCT-PPT and SCPT static excitation systems.

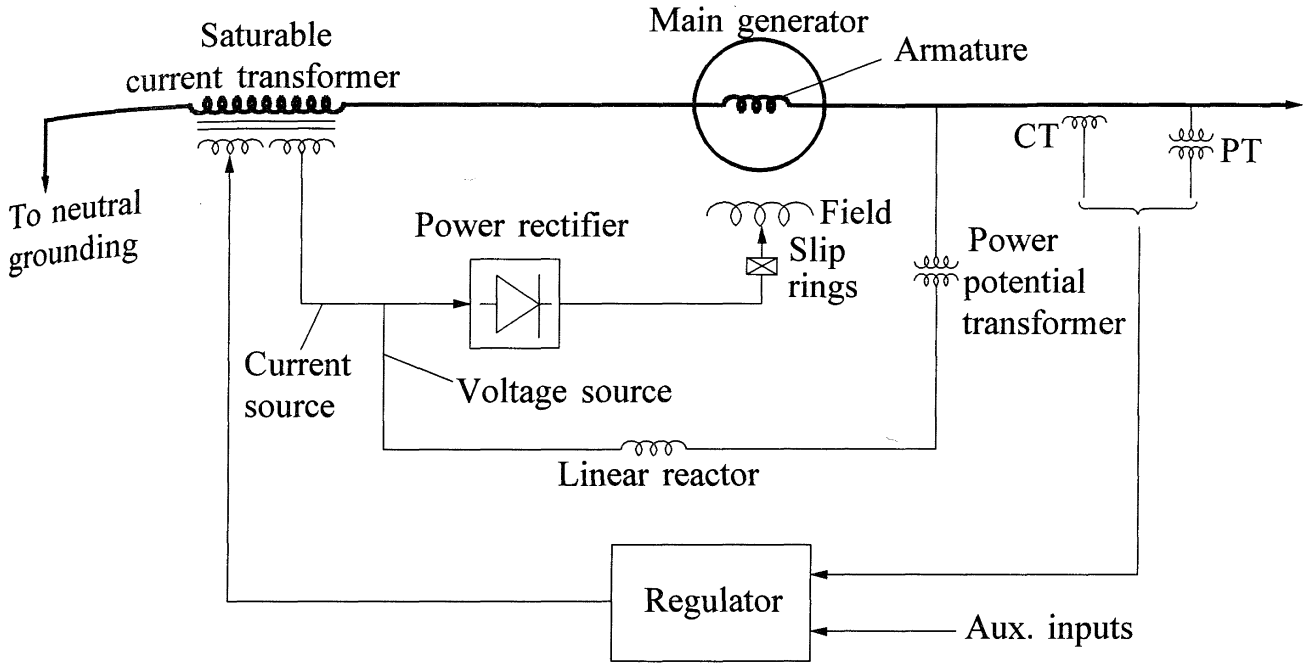

Figure 8.7 Compound-source rectifier excitation system

(c) Compound-controlled rectifier excitation systems

This system utilizes controlled rectifiers in the exciter output circuits and the compounding of voltage and current-derived sources within the generator stator to provide excitation power. The result is a high initial-response static excitation system with full "fault-on" forcing capability.

An example of this type of system is the compound power-source GENERREX[1] excitation system [15,16]. Figure 8.8 shows an elementary single-line diagram of the system. The voltage source is formed by a set of three-phase windings placed in three slots in the generator stator and a series linear reactor. The current source is obtained from current transformers mounted in the neutral end of the stator windings. These sources are combined through transformer action and the resultant ac output is rectified by stationary power semiconductors. The means of control is provided by a combination of diodes and thyristors connected to form a shunt bridge. A static ac voltage regulator controls the firing circuits of the thyristors and thus regulates the excitation to the generator field.

The excitation transformer consists of three single-phase units with three windings: current (C) and potential (P) primary windings, and a secondary output winding (F). Under fault conditions, the fault current flowing through the excitation transformer "C" windings provides the field-forcing capability when the generator voltage is depressed.

---

[1] GENERREX is a trademark of General Electric Co.

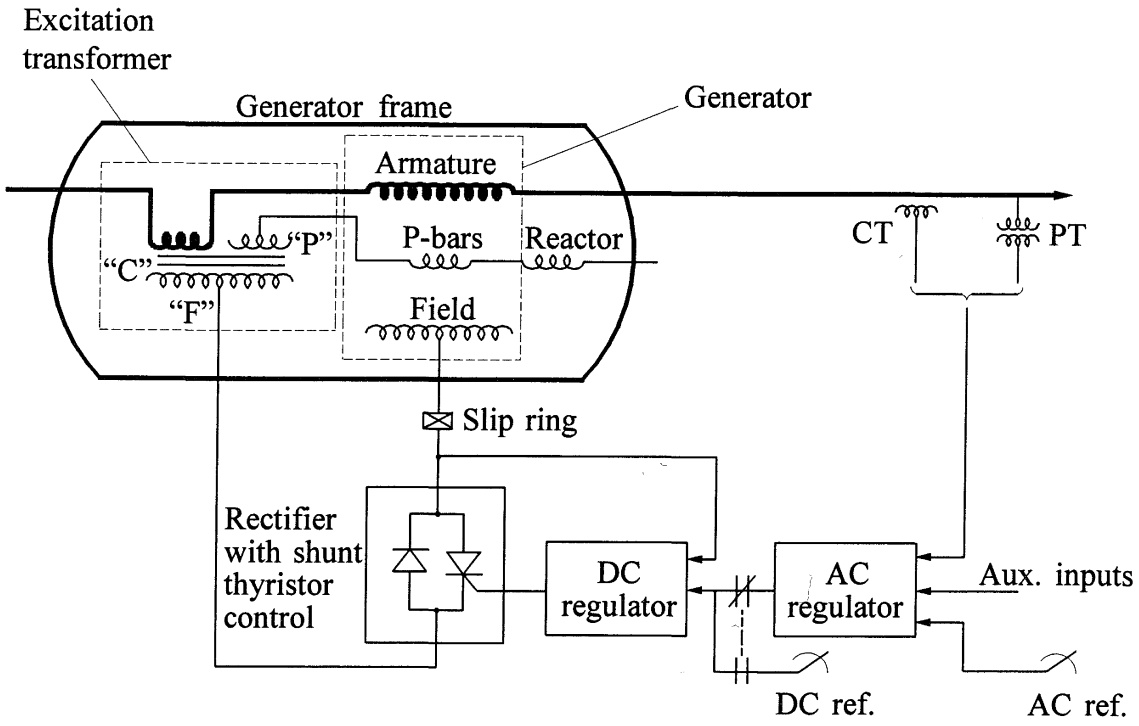

Figure 8.8 GENERREX compound-controlled rectifier excitation system ©IEEE1976 [16]

The reactor serves two functions: contribution to the desired compounding characteristic of the excitation system and reduction of fault currents for faults in the excitation system or the generator.

The excitation transformers and reactors are contained in an excitation dome that is bolted to the top of the generator frame, forming an integral part of the frame.

Field flashing for static exciters:

Since the source of power to a static excitation system is the main generator, it is in effect self-excited. The generator cannot produce any voltage until there is some field current. It is therefore necessary to have another source of power for a few seconds to initially provide the field current and energize the generator. This process of build-up of generator field flux is called *field flashing*. The usual field-flashing source is a station battery.

8.3.4 Recent Developments and Future Trends

The advances in excitation control systems over the last 20 years have been influenced by developments in solid-state electronics. Developments in analog-integrated circuitry have made it possible to easily implement complex control strategies.

The latest development in excitation systems has been the introduction of digital technology. Thyristors continue to be used for the power stage. The control, protection, and logic functions have been implemented digitally, essentially duplicating the functions previously provided by analog circuitry.

The digital controls are likely to be used extensively in the future as they provide a cheaper and possibly more reliable alternative to analog circuitry. They have the added advantage of being more flexible, allowing easy implementation of more complex control strategies, and interfacing with other generator control and protective functions.

8.4 DYNAMIC PERFORMANCE MEASURES

The effectiveness of an excitation system in enhancing power system stability is determined by some of its key characteristics. In this section, we identify and define performance measures which determine these characteristics and serve as a basis for evaluating and specifying the performance of the excitation control system. Figure 8.9 shows the representation of the overall excitation control system in the classical form used for describing feedback control systems.

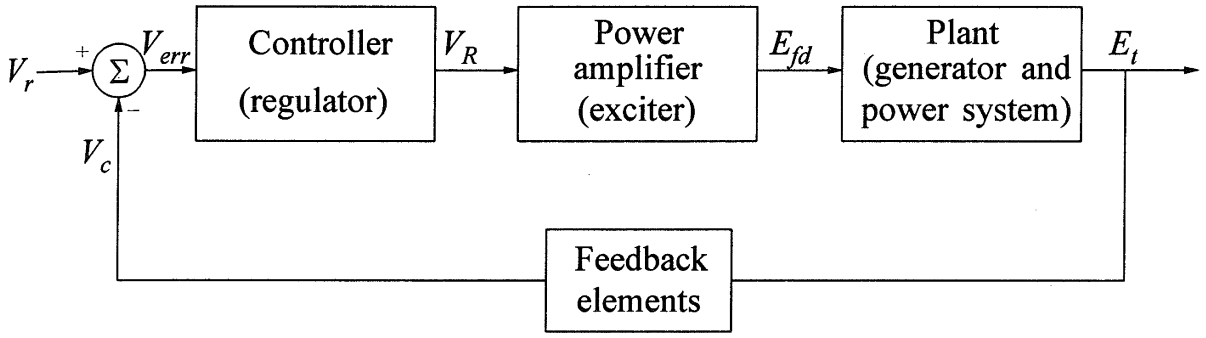

Figure 8.9 Excitation control system in the classical feedback control form

The performance of the excitation control system depends on the characteristics of excitation system, the generator, and the power system. Since the system is nonlinear, it is convenient to classify its dynamic performance into large-signal performance and small-signal performance. For large-signal performance, the nonlinearities are significant; for small-signal performance, the response is effectively linear.

8.4.1 Large-Signal Performance Measures [7]

Large-signal performance measures provide a means of assessing the excitation system performance for severe transients such as those encountered in the

consideration of transient, mid-term and long-term stability of the power system. Such measures are based on the quantities defined below. To permit maximum flexibility in the design, manufacture, and application of excitation equipment, some of the performance measures are defined "under specified conditions"; these conditions may be specified as appropriate for the specific situation.

(a) Excitation system ceiling voltage: The maximum direct voltage that the excitation system is able to supply from its terminals under specified conditions [7,20].

Ceiling voltage is indicative of the field-forcing capability of the excitation system; higher ceiling voltages tend to improve transient stability.

For potential source and compound source static excitation systems, whose supply depends on the generator voltage and current, the ceiling voltage is defined at specified supply voltage and current. For excitation systems with rotating exciters, the ceiling voltage is determined at rated speed.

(b) Excitation system ceiling current: The maximum direct current that the excitation system is able to supply from its terminals for a specified time [7,20].

When prolonged disturbances are a concern, the ceiling current may be based on the excitation system thermal duty.

(c) Excitation system voltage time response: The excitation system output voltage expressed as a function of time under specified conditions [7,20].

(d) Excitation system voltage response time: The time in seconds for the excitation voltage to attain 95% of the difference between the ceiling voltage and rated load-field voltage under specified conditions [7,20].

The *rated load field voltage* is the generator field voltage under rated continuous load conditions with the field winding at (i) 75°C for windings designed to operate at rating with a temperature rise of 60°C or less; or (ii) 100°C for windings designed to operate at rating with a temperature rise greater than 60°C.

(e) High initial-response excitation system: An excitation system having a voltage response time of 0.1 seconds or less [7]. It represents a high response and fast-acting system.

(f) Excitation system nominal response[1]: The rate of increase of the excitation system output voltage determined from the excitation system voltage response curve, divided by the rated field voltage. This rate, if maintained constant, would develop the same voltage-time area as obtained from the actual curve over the first half-second interval (unless a different time interval is specified) [7,20].

---

[1] Historically, the excitation system nominal response has been referred to as the *excitation system response ratio* (see 1978 version of [7], and [20]).

The nominal response is determined by initially operating the excitation system at the rated load field voltage (and field current) and then suddenly creating the three-phase terminal voltage input signal conditions necessary to drive the excitation system voltage to ceiling. It should include any delay time that may be present before the excitation system responds to the initiating disturbance.

Referring to Figure 8.10, the excitation response is illustrated by line ac. This line is determined by establishing area acd equal to area abd:

$$\text{Nominal response} = \frac{cd}{(ao)(oe)}$$

where

oe = 0.5 s

ao = rated load field voltage

The basis for considering a nominal time span of 0.5 s in the above definition is that, following a severe disturbance, the generator rotor angle swing normally peaks between 0.4 s and 0.75 s. The excitation system must act within this time period to be effective in enhancing transient stability. Accordingly, 0.5 s was chosen for the definition time period of nominal response.

In the past, the nominal response has been a well-established and useful criterion for evaluating the large-signal performance of excitation systems. With older and slower excitation systems, this was an acceptable performance measure, but it is

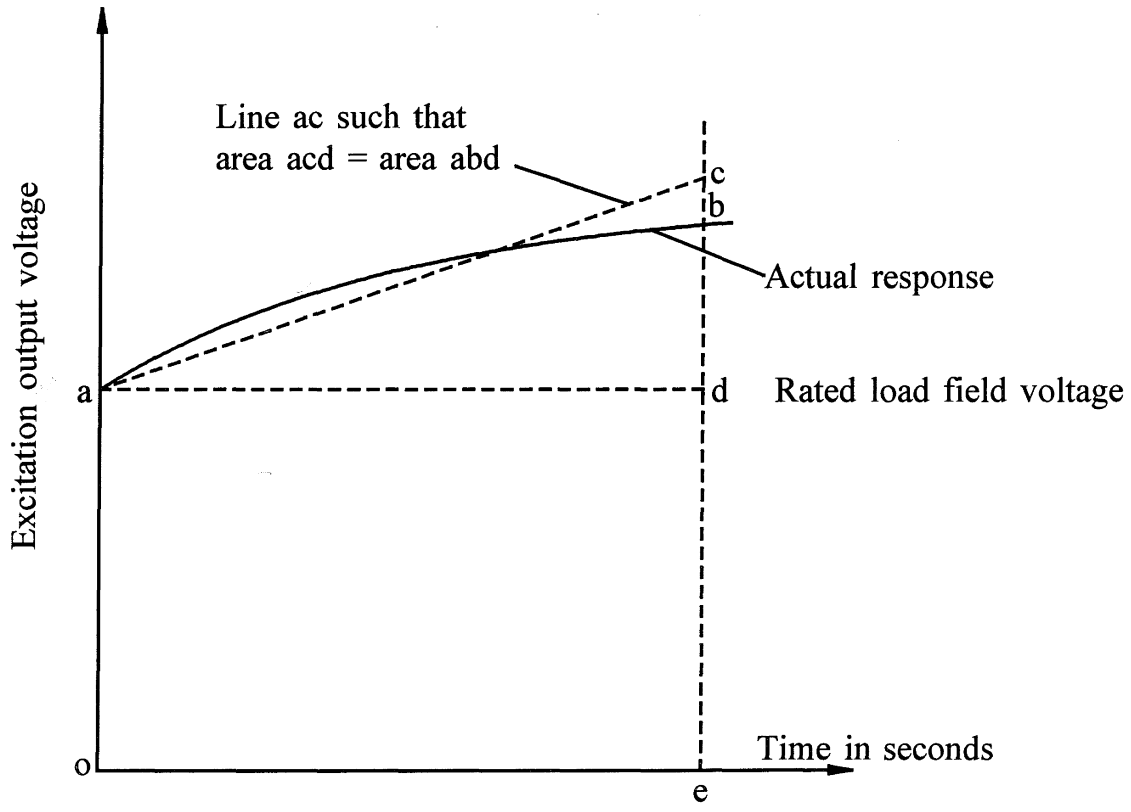

Figure 8.10 Excitation system nominal response

not adequate to cover many of the modern excitation systems. In particular, it is not a good figure of merit for excitation systems supplied from the generator or the power system, due to the reduced capability of such systems during a system fault.

For high initial-response excitation systems, the nominal response merely establishes the required ceiling voltage. The ceiling voltage and voltage response time are more meaningful parameters for such systems.

8.4.2 Small-Signal Performance Measures [3,7]

Small-signal performance measures provide a means of evaluating the response of the closed-loop excitation control systems to incremental changes in system conditions. In addition, small-signal performance characteristics provide a convenient means for determining or verifying excitation system model parameters for system studies.

Small-signal performance may be expressed in terms of performance indices used in feedback control system theory:

- Indices associated with time response; and
- Indices associated with frequency response

The typical time response of a feedback control system to a step change in input is shown in Figure 8.11. The associated indices are rise time, overshoot, and settling time.

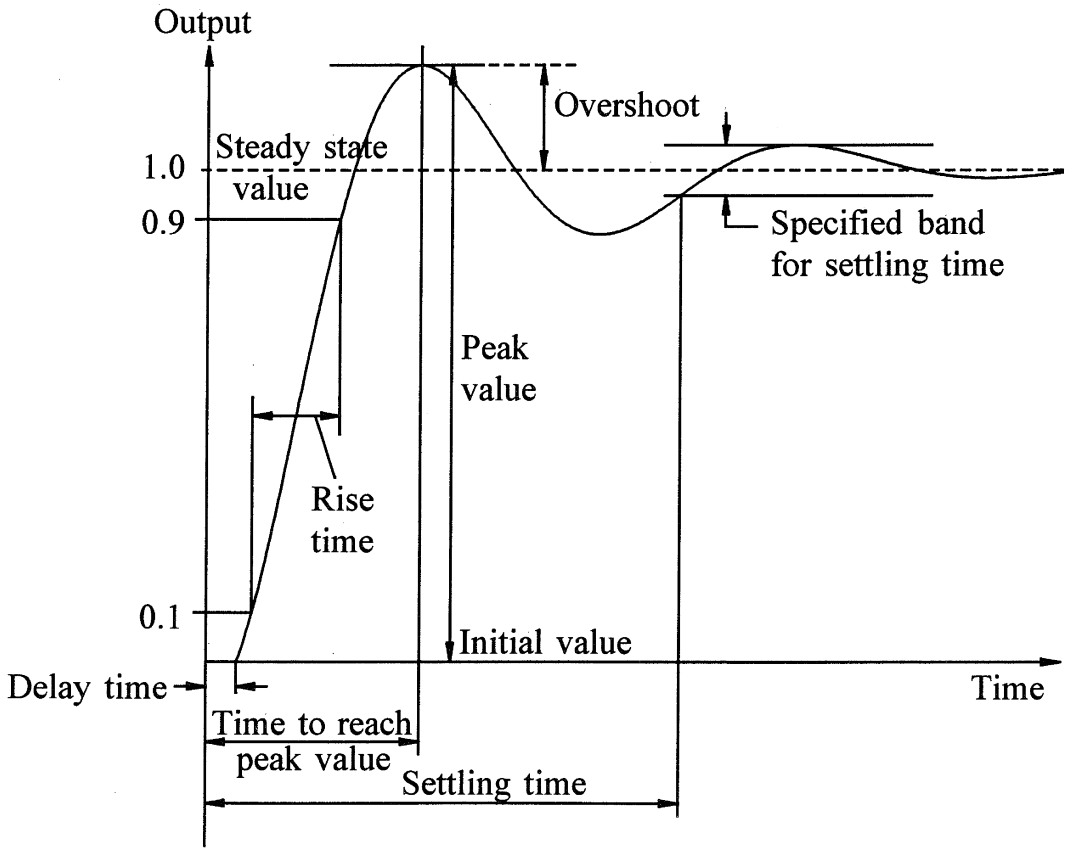

Figure 8.11 Typical time response to step input. © IEEE 1990 [7]

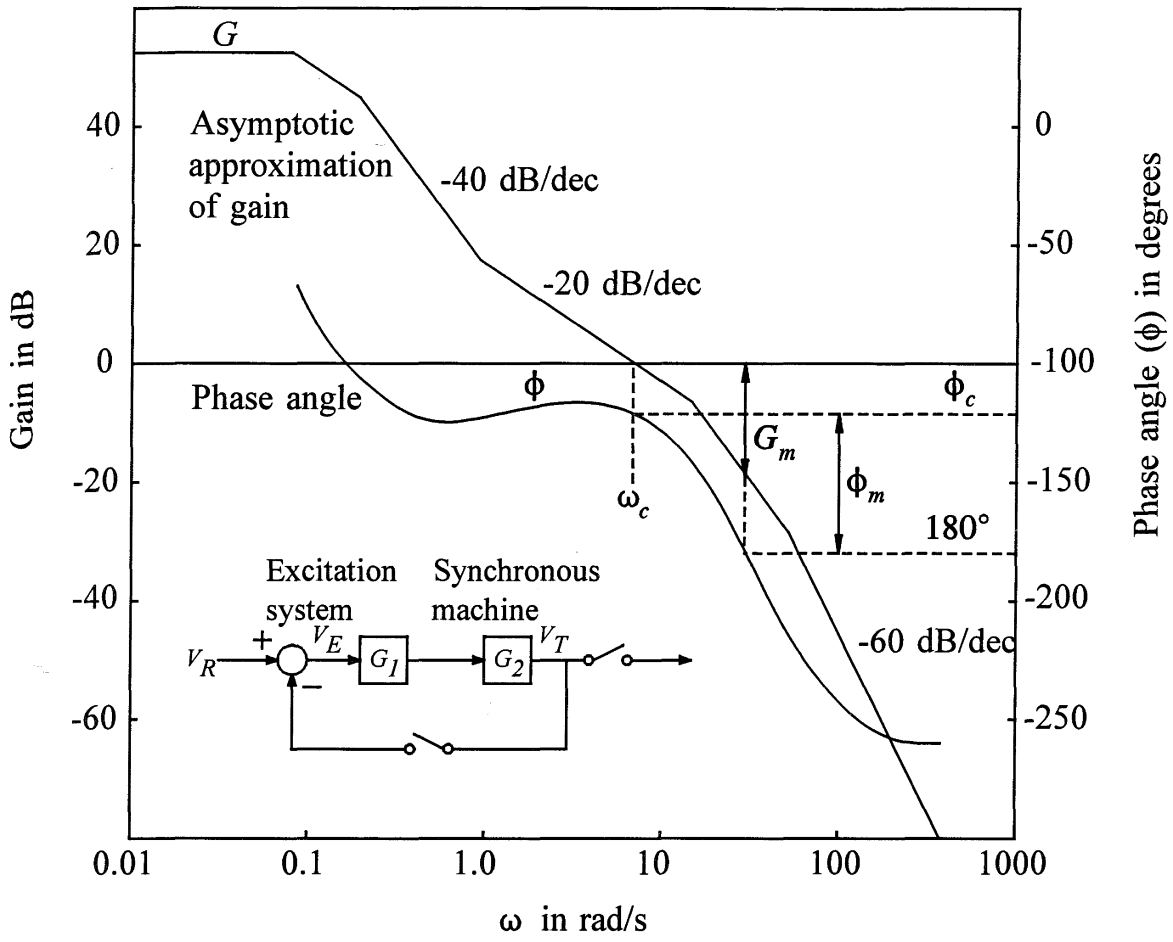

Figure 8.12 Typical open-loop frequency response of an excitation control system with generator open-circuited. © IEEE 1990 [7]

A typical open-loop frequency response characteristic of an excitation control system with the generator open-circuited is shown in Figure 8.12.

The performance indices associated with the open-loop frequency response are the low frequency gain G, crossover frequency ω_c, phase margin ϕ_m, and gain margin G_m. Larger values of G provide better steady-state voltage regulation, and larger crossover frequency ω_c indicates faster response. Larger values of phase margin ϕ_m and gain margin G_m provide a more stable excitation control loop. (The reference here is to excitation control system stability and not power system synchronous stability.)

In tuning the voltage regulator, an improvement to one index will most likely be to the detriment of other indices. For example, an increase in regulator gain will shift the gain curve in Figure 8.12 upward. This has the beneficial effect of increasing the low-frequency gain and crossover frequency, but has the undesirable effect of decreasing the gain and phase margins. In general, a phase margin of 40° or more and a gain margin of 6 dB or more are considered a good design practice for obtaining a stable, non-oscillatory voltage regulator system.

Figure 8.13 shows the corresponding closed-loop frequency response with the generator open-circuited.

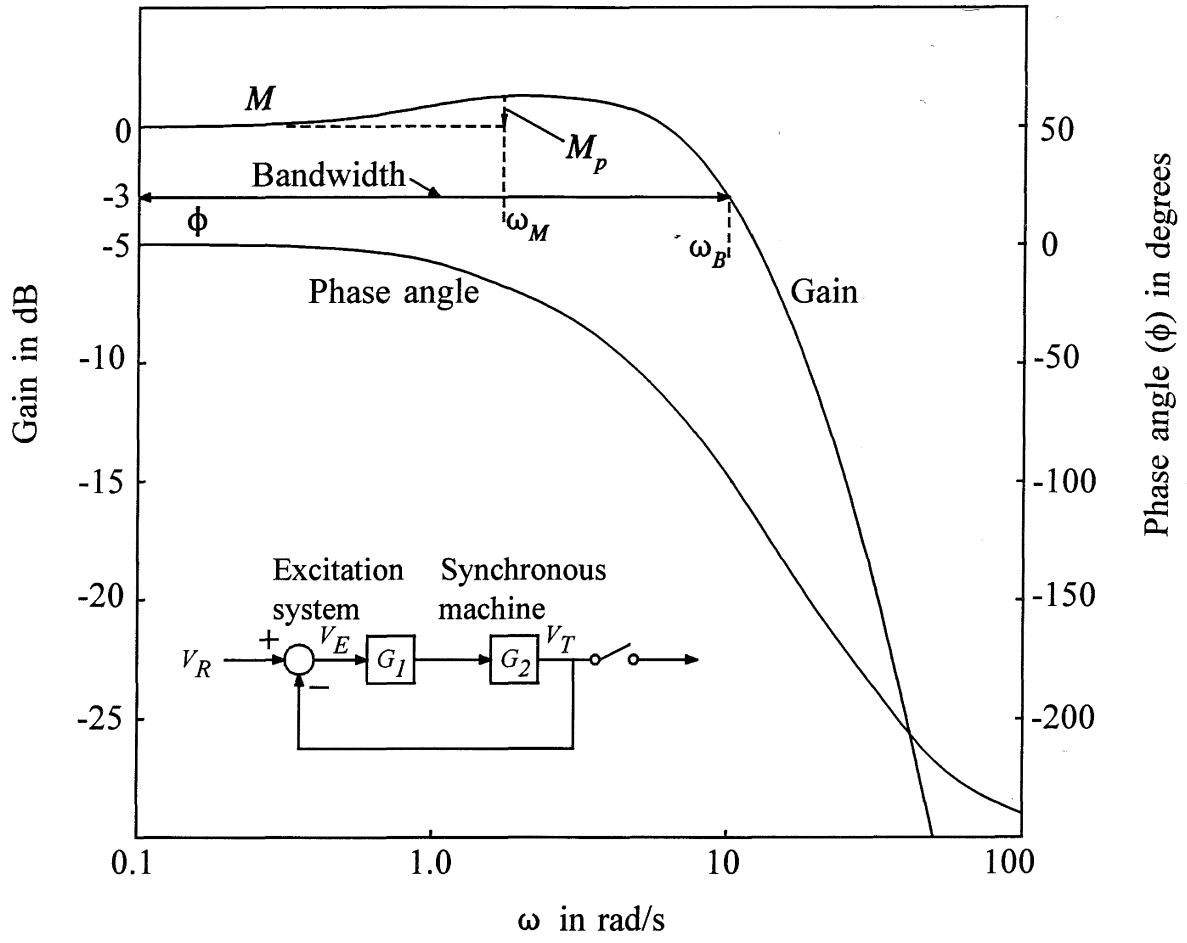

Figure 8.13 Typical closed-loop frequency response with generator open-circuited. © IEEE 1990 [7]

The indices of interest associated with the closed-loop frequency response are the bandwidth ω_B and peak value M_p.

A high value of M_p (>1.6) is indicative of an oscillatory system exhibiting large overshoot in its transient response. In general, a value of M_p between 1.1 and 1.5 is considered a good design practice.

Bandwidth is an important closed-loop frequency response index. Larger values indicate faster response. It approximately describes filtering or noise-rejection characteristics of the system.

Generally accepted values of performance indices characterizing good feedback control system performance are:

Gain margin ≥ 6 dB
Phase margin ≥ 40°
Overshoot = 5-15%
M_p = 1.1-1.6

It is not possible to define such generally acceptable ranges of values for other small-signal performance indices: rise time, settling time, and bandwidth. These indices are a measure of the relative speed of the control action. They are primarily determined by the synchronous machine dynamic characteristics.

The performance indices given above are applicable to any feedback control system having a single major feedback loop, i.e., a single controlled-output variable. Therefore, they are applicable to an excitation control system with the synchronous machine on open circuit or feeding an isolated load. Stable operation of the excitation control system with the generator off-line is ensured based on these performance indices and associated analytical techniques [3]. On the other hand, synchronous machines connected to a power system form a complex multiloop, multivariable, high-order control system. For such a system, the performance indices identified above are not applicable. The state-space approach using eigenvalue techniques is an effective method of assessing the performance of such complex systems. This is covered in detail in Chapter 12.

8.5 CONTROL AND PROTECTIVE FUNCTIONS

A modern excitation control system is much more than a simple voltage regulator. It includes a number of control, limiting, and protective functions which assist in fulfilling the performance requirements identified in Section 8.1. The extensive nature of these functions and the manner in which they interface with each other are illustrated in Figure 8.14. Any given excitation system may include only some or all of these functions, depending on the requirements of the specific application and on the type of exciter. The philosophy is to have the control functions regulate specific quantities at the desired level, and the limiting functions prevent certain quantities from exceeding set limits. If any of the limiters fail, then the protective functions remove appropriate components or the unit from service.

The following is a brief description of the various control and protective functions, and the associated elements identified in Figure 8.14.

8.5.1 AC and DC Regulators

The basic function of the ac regulator is to maintain the generator stator voltage. In addition, other auxiliary control and protection functions act through the ac regulator to control the generator field voltage as shown in Figure 8.14.

The dc regulator holds constant generator field voltage and is commonly referred to as *manual control*. It is used primarily for testing and start-up, and to cater to situations where the ac regulator is faulty. In this mode of operation, it is the field voltage that is regulated; only operator intervention by adjusting the setpoint will modify the field voltage. In some excitation systems, facilities for automatic setpoint tracking are provided. This will cause the manual setpoint to continually track the generator excitation variation due to the ac regulator and thus minimize the voltage

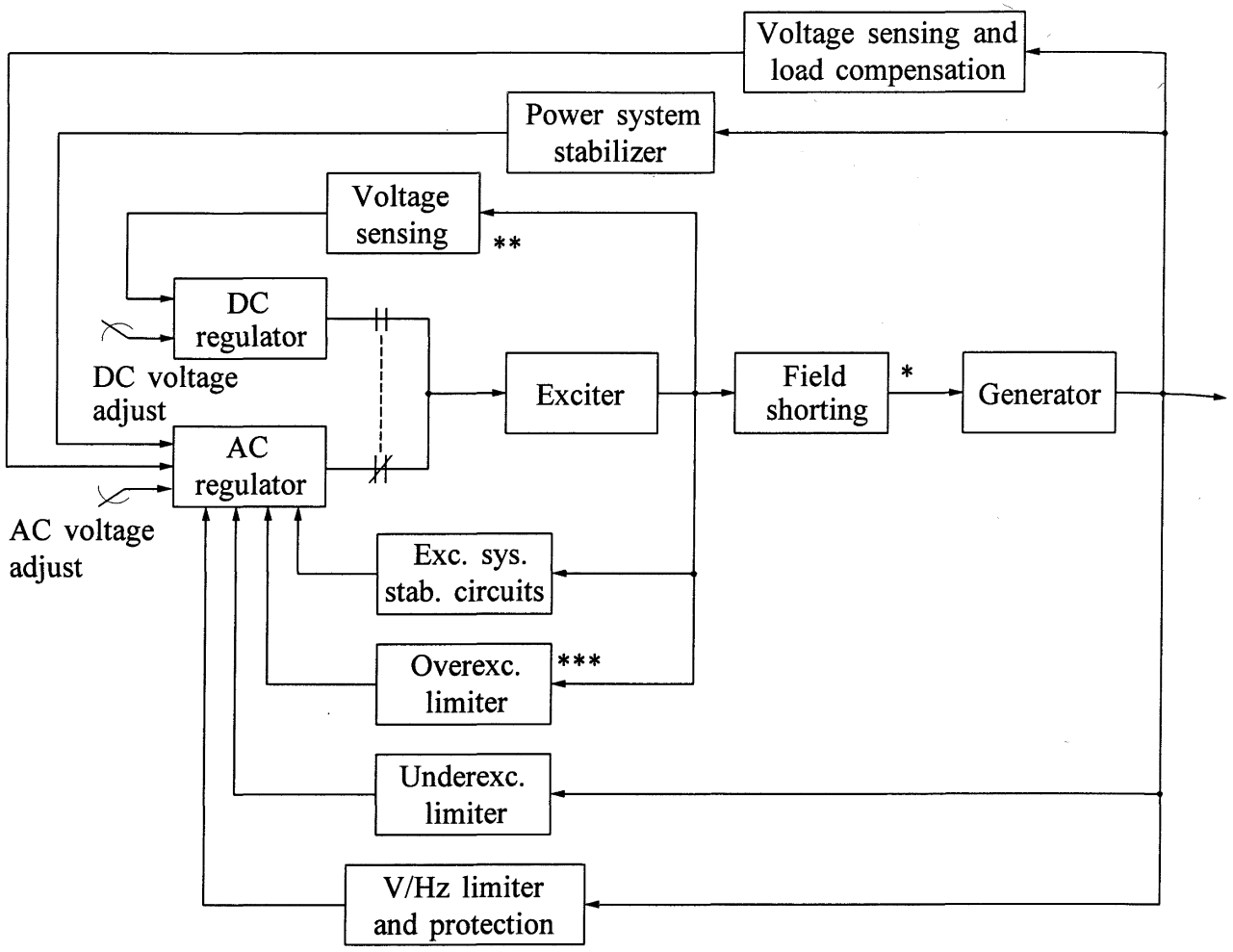

* Field-shorting circuits are applicable to ac and static exciters only.
** Some systems have open-loop dc regulator.
*** Overexcitation limiter may also be used with dc regulator

Figure 8.14 Excitation system control and protective circuits

and reactive power excursions in the event the ac regulator is removed from service abruptly. Care must be taken to ensure that a trip of the unit operating on manual control does not leave the generator in an overexcited condition.

8.5.2 Excitation System Stabilizing Circuits

Excitation systems comprised of elements with significant time delays have poor inherent dynamic performance. This is particularly true of dc and ac type excitation systems. Unless a very low steady-state regulator gain is used, the excitation control (through feedback of generator stator voltage) is unstable when the generator is on open circuit. Therefore, excitation control system stabilization, comprising either series or feedback compensation, is used to improve the dynamic performance of the control system. The most commonly used form of compensation is a derivative feedback as shown in Figure 8.15. The effect of the compensation is

to minimize the phase shift introduced by the time delays over a selected frequency range [3]. This results in a stable off-line performance of the generator, such as that existing just prior to synchronization or following a load rejection. The feedback parameters can also be adjusted to improve the on-line performance of the generating unit. Depending on the type of excitation system, there may be many levels of excitation control system stabilization involving the major outer loop and minor inner loops. Static excitation systems have negligible inherent time delays and do not require excitation control-system stabilization to ensure stable operation with the generator off-line (see closure of reference 21).

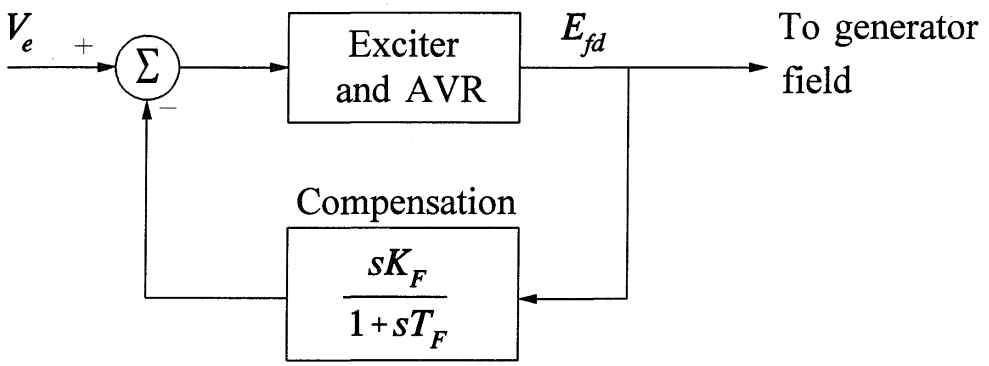

Figure 8.15 Derivative feedback excitation control system stabilization

8.5.3 Power System Stabilizer (PSS)

The power system stabilizer uses auxiliary stabilizing signals to control the excitation system so as to improve power system dynamic performance. Commonly used input signals to the power system stabilizer are shaft speed, terminal frequency and power. Power system dynamic performance is improved by the damping of system oscillations. This is a very effective method of enhancing small-signal stability performance.

The principle of operation of power system stabilizers and their structure and tuning are discussed in detail in Chapters 12 and 17.

8.5.4 Load Compensation

The automatic voltage regulator (AVR) normally controls the generator stator terminal voltage. Sometimes, load compensation is used to control a voltage which is representative of the voltage at a point either within or external to the generator. This is achieved by building additional circuitry into the AVR loop as shown in Figure 8.16. The compensator has adjustable resistance (R_c) and inductive reactance (X_c) that simulate the impedance between the generator terminals and the point at which the voltage is being effectively controlled. Using this impedance and the measured armature current, a voltage drop is computed and added to or subtracted

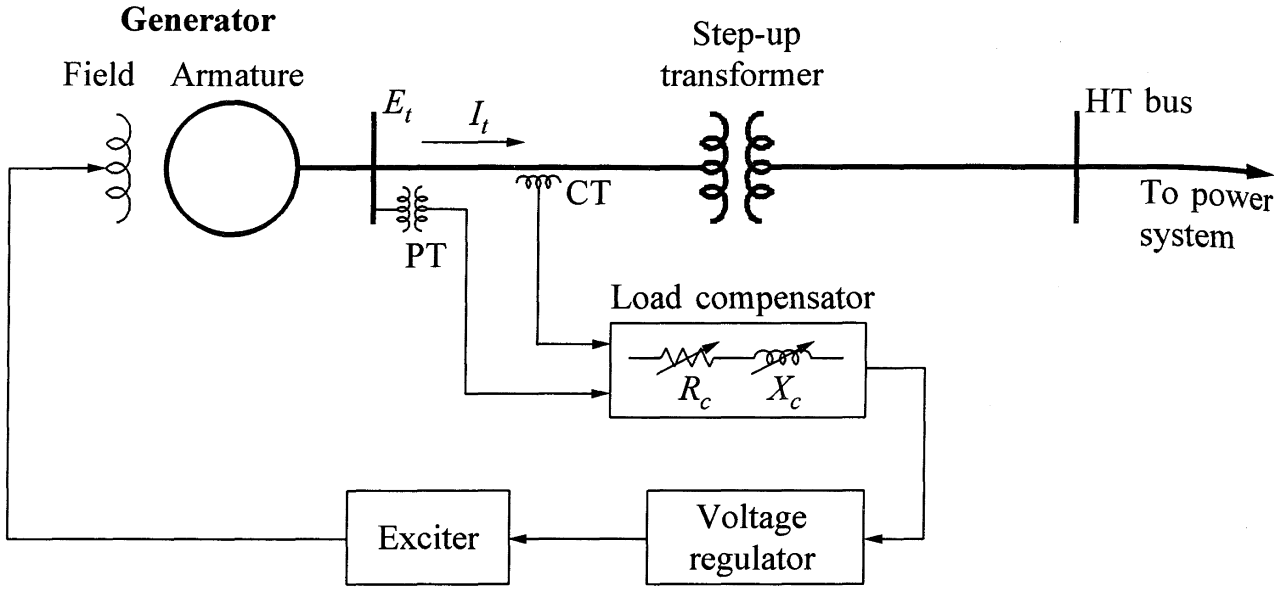

Figure 8.16 Schematic diagram of a load compensator

from the terminal voltage. The magnitude of the resulting compensated voltage (V_c), which is fed to the AVR, is given by

$$V_c = |\tilde{E}_t + (R_c + jX_c)\tilde{I}_t| \tag{8.1}$$

With R_c and X_c positive in Equation 8.1, the voltage drop across the compensator is added to the terminal voltage. The compensator regulates the voltage at a point within the generator and thus provides voltage droop. This is used to ensure proper sharing of reactive power between generators bussed together at their terminals, sharing a common step-up transformer. Such an arrangement is commonly used with hydro electric generating units and cross-compound thermal units. The compensator functions as a *reactive-current compensator* by creating an artificial coupling between the generators. Without this provision, one of the generators would try to control the terminal voltage slightly higher than the other; hence, one generator would tend to supply all of the required reactive power while the other would absorb reactive power to the extent allowed by underexcited limits.

With R_c and X_c negative, the compensator regulates the voltage at a point beyond the machine terminals. This form of compensation is used to compensate for the voltage drop across the step-up transformer, when two or more units are connected through individual transformers. Typically, 50% to 80% of the transformer impedance is compensated, ensuring voltage droop at the paralleling point so that generators can operate in parallel satisfactorily. This device is commonly referred to as a *line-drop compensator* although it is practically always used to compensate only for transformer drop. The nomenclature appears to have been derived from a similar compensator used on distribution system voltage regulators (see Chapter 11, Section 11.2).

In most cases, the resistance component of the impedance to be compensated is negligible and R_c may be set to zero.

Alternative forms of reactive-current and line-drop compensators are described in references 8 and 22.

8.5.5 Underexcitation Limiter [23-26]

The underexcitation limiter (UEL) is intended to prevent reduction of generator excitation to a level where the small-signal (steady-state) stability limit or the stator core end-region heating limit (see Chapter 5, Figure 5.16) is exceeded. This limiter is also referred to by other names such as underexcitation reactive-ampere limiter (URAL) and minimum excitation limiter (MEL).

The control signal of the UEL is derived from a combination of either voltage and current or active and reactive power of the generator. The limits are determined by the signal exceeding a reference level. There are a wide variety of implementations of the UEL function. Some UEL applications act on the voltage error signal of the AVR; when the UEL set limit is reached, a nonlinear element (such as a diode) begins to conduct and the limiter output signal is combined with other signals controlling the excitation system. In a more widely used form of UEL application, the limiter output signal is fed into an auctioneering circuit (high-value gate) which gives control to the larger of the voltage regulator and UEL signals; when the UEL set limit is reached, the limiter is given full control of the excitation system until the limiter signal is below the set limit.

Methods of setting the UEL characteristics are described in references 23 to 25. The settings should be based on the needed protection, i.e., system instability or stator core heating. In addition, the limiter performance should be coordinated with the generator loss-of-excitation protection (see Chapter 13). Figure 8.17 indicates the way in which the UEL characteristic (represented on a P-Q plane) is usually coordinated with the calculated small-signal stability limit and the loss-of-excitation (LOE) relay characteristic [28]. If the UEL is used to protect against stator end-region heating, the coordination is done in a similar manner, except that the stability limit is replaced by the heating limit.

If the input signals to the UEL are the generator stator voltage and current, the limiting characteristic appears circular on a P-Q plane as shown in Figure 8.17. With active and reactive power as input signals, the limiting characteristic would be a straight line.

Care should be taken to ensure that the UEL performance during a transient disturbance is not to the detriment of the power system performance [26,27].

8.5.6 Overexcitation Limiter

The purpose of the overexcitation limiter (OXL) is to protect the generator from overheating due to prolonged field overcurrent. This limiter is also commonly referred to as the maximum excitation limiter (MXL).

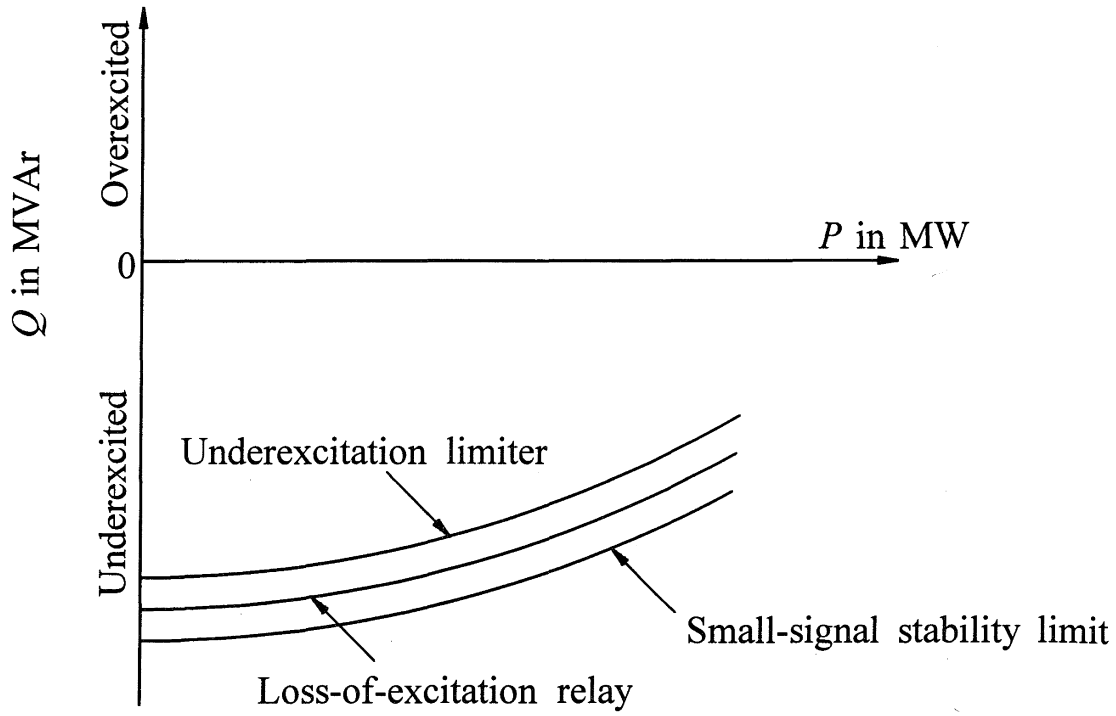

Figure 8.17 Coordination between UEL, LOE relay and stability limit

The generator field winding is designed to operate continuously at a value corresponding to rated load conditions. The permissible thermal overload of the field winding of round rotor generators, as specified by ANSI Standard C50.13-1977, is given by the solid curve of Figure 8.18. The curve passes through the following points:

Time (seconds)	10	30	60	120
Field voltage/current (Percent of rated)	208	146	125	112

The actual implementation of overexcitation limiting function varies depending on the manufacturer and vintage of the unit. Limiters supplied by two manufacturers are described in references 28 and 29.

The overexcitation limiting function typically detects the high field current condition and, after a time delay, acts through the ac regulator to ramp down the excitation to a preset value (typically 100% to 110% of rated field current). If this is unsuccessful, it trips the ac regulator, transfers control to the dc regulator, and repositions the setpoint to a value corresponding to the rated value. If this also does not reduce the excitation to a safe value, the limiter will initiate an exciter field breaker trip and a unit trip.

Two types of time delays are used: (a) fixed time and (b) inverse time. The fixed time limiters operate when the field current exceeds the pickup value for a fixed set time, irrespective of the degree of overexcitation. The inverse time limiters operate with the time delay matching the field thermal capability, as shown in Figure 8.18.

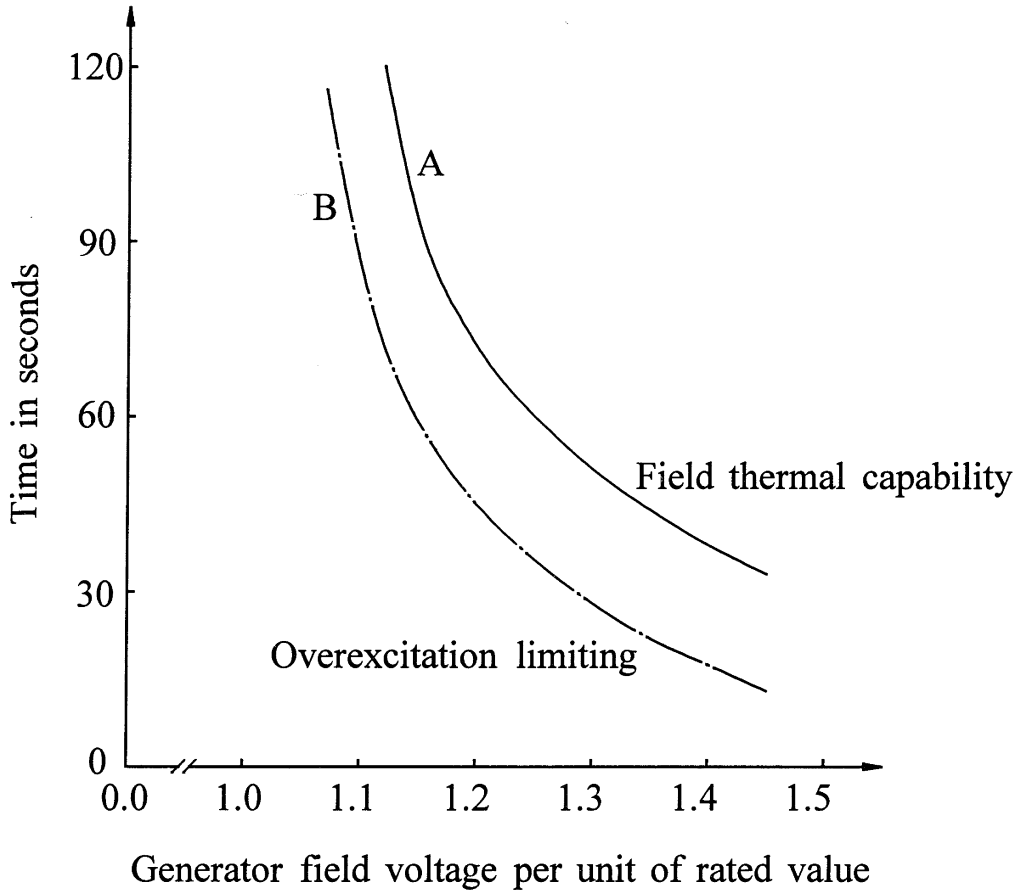

Figure 8.18 Coordination of overexcitation limiting with field thermal capability

Exciters with very high ceiling voltages may be provided with an additional *field current limiter*, which acts instantaneously through the ac regulator and limits the field current to the short time limit (typically 160% of rated value).

8.5.7 Volts-per-Hertz Limiter and Protection

These are used to protect the generator and step-up transformer from damage due to excessive magnetic flux resulting from low frequency and/or overvoltage. Excessive magnetic flux, if sustained, can cause serious overheating and may result in damage to the unit transformer and to the generator core.

The ratio of per unit voltage to per unit frequency, referred to as volts per hertz (V/Hz), is a readily measurable quantity that is proportional to magnetic flux. Typical V/Hz limitations for generators (GEN) and step-up transformers (XFMR) are shown in the following table.

V/Hz (pu)		1.25	1.2	1.15	1.10	1.05
Damage Time in Minutes	GEN	0.2	1.0	6.0	20.0	∞
	XFMR	1.0	5.0	20.0	∞	

The unit step-up transformer low voltage rating is frequently 5% below the generator voltage rating; therefore, V/Hz limiting and protection requirements are usually determined by the transformer limitation. If, however, the generator and transformer voltage ratings are the same, the generator limitation would be more restrictive.

The *V/Hz limiter* (or regulator, as it is sometimes called) controls the field voltage so as to limit the generator voltage when the V/Hz value exceeds a preset value.

The *V/Hz protection* trips the generator, when the V/Hz value exceeds a preset value for a specified time. Usually, a dual-level protection is provided, one with a higher V/Hz setting and a shorter time setting, and the other with a lower V/Hz setting and a longer time setting. When used in conjunction with a V/Hz limiter, it serves as a backup.

For many units, the V/Hz protection becomes overvoltage protection above 60 Hz.

8.5.8 Field-Shorting Circuits

Since rectifiers cannot conduct in the reverse direction, the exciter current cannot be negative in the case of ac and static exciters. Under conditions of pole slipping and system short circuits, the induced current in the generator field winding may be negative. If a path is not provided for this negative current to flow, very high voltages may result across the field circuit. Therefore, special circuitry is usually provided to bypass the exciter to allow negative field current to flow. This takes the form of either a field-shorting circuit, commonly referred to as *crowbar*, or a varistor [8,30].

A crowbar consists of a thyristor and a field discharge resistor (FDR) connected across the generator field as shown in Figure 8.19. The thyristor is gated in response to an overvoltage condition that is created by the induced current not initially having a path in which to flow. The thyristor so gated conducts induced field current through the field discharge resistor.

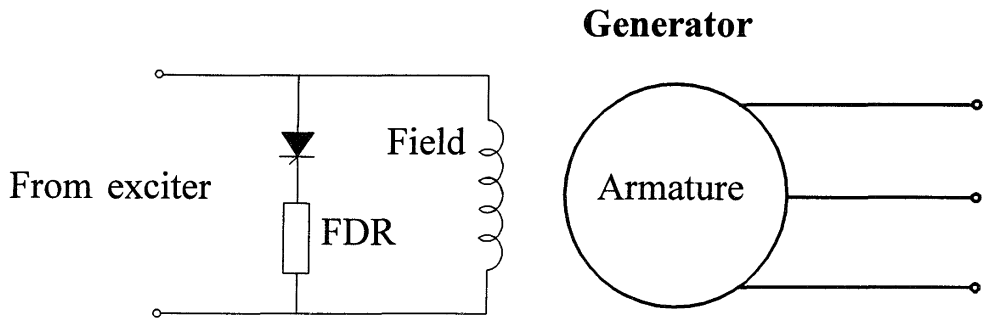

Figure 8.19 Field bypass circuit using a crowbar

A varistor is a nonlinear resistor. When connected across the generator field winding, as shown in Figure 8.20, it provides an effective means of bypassing the exciter under conditions of high induced voltage. With normal exciter voltage across the varistor, it has very high resistance and hence carries negligible current. As the voltage across the varistor increases beyond a threshold value, its resistance decreases and current through it increases very rapidly. Thus the varistor provides a low resistance path to induced negative field current and limits the voltage across the field and exciter.

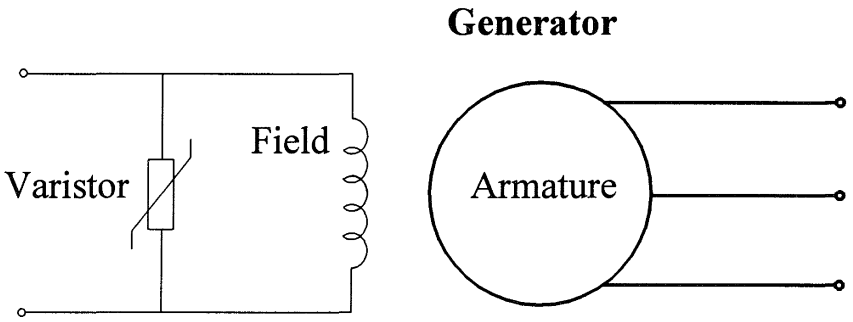

Figure 8.20 Field bypass circuit using a varistor

In some cases, no special field shorting circuits are provided. The amortisseurs associated with the solid rotor iron provide paths for the induced rotor currents. This is sufficient to limit the induced voltage to a level that is below the withstand capabilities of the generator field and the exciter. Since the field is not shorted, it carries no current in the negative direction.

8.6 MODELLING OF EXCITATION SYSTEMS

Mathematical models of excitation systems are essential for the assessment of desired performance requirements, for the design and coordination of supplementary control and protective circuits, and for system stability studies related to the planning and operation of power systems. The detail of the model required depends on the purpose of the study. Referring to Figure 8.14, the control and protective features that impact on transient and small-signal stability studies are the voltage regulator, power system stabilizer, and excitation control stabilization. The limiter and protective circuits identified in the figure normally need to be considered only for mid-term, long-term, and voltage stability studies. Some excitation systems are provided with fast-acting terminal voltage limiters in conjunction with power system stabilizers; these have to be modelled in transient stability simulations.

In this section, modelling of excitation systems is described. We begin with consideration of an appropriate per unit system, then describe models for the various components, and finally present complete models for selected types of excitation systems.

The material presented in this section conforms to the IEEE committee reports on excitation system modelling. The IEEE work on standardization of these models began in the 1960s, and the first set of models was published in 1968 [1]. This work was extended, and improved models to reflect advances in equipment and better modelling practices were published in 1981 [4]. These were updated and refined in 1992 [8].

8.6.1 Per Unit System

In choosing the per unit system for exciter output voltage and current, there are several options.

First, the per unit system used for the main synchronous machine field circuit would appear to be the obvious choice. While this system was chosen to simplify the synchronous machine equations (see Chapter 3, Section 3.4), it is not considered suitable for expressing the exciter output quantities. This is because, for normal operating conditions, the per unit exciter output voltage would be very small, being on the order of 0.001.

Second, for excitation system specification purposes it has become standard practice to use the rated-load field voltage as 1.0 per unit. However, this is not convenient for use in the formulation of synchronous machine and excitation system equations for system studies.

The third choice is to have 1.0 per unit exciter output voltage equal to the field voltage required to produce rated synchronous machine armature terminal voltage on the air-gap line; 1.0 per unit exciter output current is the corresponding synchronous machine field current. This per unit system is universally used in power system stability studies as it offers considerable simplicity. Here, we refer to this system as the *non-reciprocal per unit system* to distinguish it from the reciprocal per unit system used for modelling synchronous machines.

Excitation system models must interface with the synchronous machine model at both the field terminals and armature terminals. The input control signals to the excitation system are the synchronous machine stator quantities and rotor speed. The per unit systems used for expressing these input variables are the same as those used for modelling the synchronous machine. Thus, a change of per unit system is required only for those related to the field circuit.

We now develop the relationship between the per unit values of the exciter output voltage/current expressed in the non-reciprocal system and the synchronous machine field voltage/current expressed in the L_{ad}-base reciprocal system (see Section 3.4). For the synchronous machine, under open-circuit conditions, $i_d=i_q=0$. Substituting in Equations 3.139, 3.140, 3.142 and 3.143 yields

$$e_d = -\psi_q = -L_q i_q = 0 \tag{8.2}$$

$$e_q = \psi_d = L_{ad} i_{fd} \tag{8.3}$$

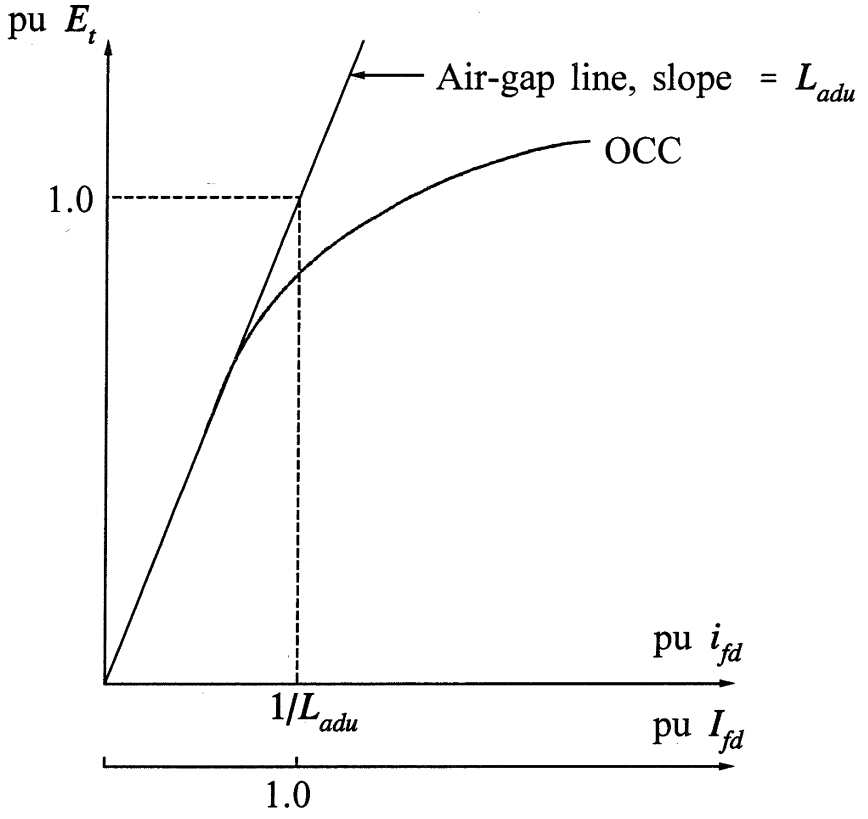

Figure 8.21 Synchronous machine open circuit characteristics

Referring to Figure 8.21, the field current required to produce 1.0 per unit stator terminal voltage on the air-gap line (slope = L_{adu}) is determined by

$$E_t = e_q = L_{adu} i_{fd} = 1.0 \quad \text{pu} \tag{8.4}$$

Therefore, in the reciprocal per unit system, the field current i_{fd} required to generate rated stator terminal voltage on the air-gap line is given by

$$i_{fd} = \frac{1}{L_{adu}} \quad \text{pu}$$

The corresponding field voltage is

$$e_{fd} = R_{fd} i_{fd} = \frac{R_{fd}}{L_{adu}} \quad \text{pu}$$

By definition, the corresponding value of exciter output current I_{fd} is equal to 1.0 per unit. Therefore,

$$I_{fd} = L_{adu} i_{fd} \tag{8.5}$$

and the corresponding exciter output voltage is

$$E_{fd} = \frac{L_{adu}}{R_{fd}} e_{fd} \tag{8.6}$$

Physically, exciter output voltage/current and generator field voltage/current are the same; distinction is made only in their per unit values to allow independent selection of the per unit systems for modelling excitation systems and synchronous machines. This is illustrated in Figure 8.22.

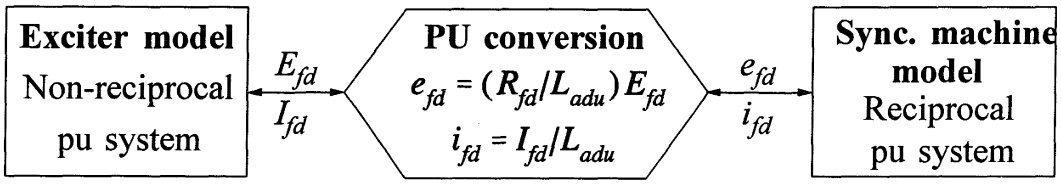

Figure 8.22 Per unit conversion at the interface between excitation system and synchronous machine field circuit

Under steady-state conditions, the per unit values of E_{fd} and I_{fd} are equal. During a transient condition, however, E_{fd} and I_{fd} differ; E_{fd} is determined by the excitation system and I_{fd} is determined by the dynamics of the field circuits.

A few interesting observations regarding the above per unit conversion are appropriate at this time:

1. The factor L_{adu}/R_{fd} in Equation 8.6 is the steady-state value of $G(s)$ (see Chapter 4, Equations 4.14 and 4.17), in the absence of saturation.

2. Equation 4.24 in terms of ΔE_{fd} becomes

$$\begin{aligned} \Delta\psi_d(s) &= \frac{1+sT_{kd}}{(1+sT'_{d0})(1+sT''_{d0})}\Delta E_{fd} \\ &= \bar{G}(s)\Delta E_{fd} \end{aligned} \tag{8.7A}$$

The steady-state value of $\bar{G}(s)$ is equal to 1.0. There is thus a one to one relationship between ψ_d and E_{fd}.

With amortisseurs neglected, Equation 8.7A becomes

$$\Delta\psi_d(s) = \frac{1}{1+sT'_{d0}}\Delta E_{fd} \tag{8.7B}$$

3. From the steady equations developed in Section 3.6.3, with the generator on open circuit, we have

$$\Delta\psi_d = \Delta e_q = \Delta E_t$$

Substitution in Equation 8.7B yields the following *open-circuit transfer function* of the generator:

$$\frac{\Delta E_t(s)}{\Delta E_{fd}(s)} = \frac{1}{1+sT'_{d0}} \tag{8.7C}$$

Example 8.1

The following are the parameters in per unit on machine rating of the 555 MVA, 0.9 p.f., 24 kV turbine generator considered in Examples 3.1, 3.2 and 3.3 of Chapter 3:

$L_{adu} = 1.66$	$L_{aqu} = 1.61$	$L_l = 0.15$
$L_{fd} = 0.165$	$R_{fd} = 0.0006$	$R_a = 0.003$

(a) The field current required to generate rated stator voltage E_t on the air-gap line is 1300 A and the corresponding field voltage is 92.95 V. Determine the base values of E_{fd} and I_{fd} in the non-reciprocal per unit system and the base values of e_{fd} and i_{fd} in the reciprocal per unit system.

(b) Compute the per unit values of E_{fd} and I_{fd}, when the generator is delivering rated MVA at rated power factor and terminal voltage. Assume that the corresponding values of the saturation factors K_{sd} and K_{sq} are equal to 0.835.

Solution

(a) By definition, the base values of E_{fd} and I_{fd} are respectively equal to the field voltage and field current required to produce rated air-gap line voltage. Hence,

$$E_{fd\ base} = 92.95 \text{ V}$$
$$I_{fd\ base} = 1300 \text{ A}$$

From Equations 8.5 and 8.6, the base values of e_{fd} and i_{fd} are

$$i_{fd\ base} = L_{adu} I_{fd\ base}$$
$$= 1.66 \times 1300 = 2158 \text{ A}$$

$$e_{fd\ base} = (L_{adu}/R_{fd})E_{fd\ base}$$
$$= (1.66/0.0006)92.95 = 257.2 \text{ kV}$$

The above base values of e_{fd} and i_{fd}, as expected, agree with the values computed in Example 3.1.

(b) From the results of Example 3.2, at the rated output conditions,

$$e_{fd} = 0.000939 \text{ pu}$$
$$i_{fd} = 1.565 \text{ pu}$$

The corresponding per unit values of E_{fd} and I_{fd} are

$$E_{fd} = (L_{adu}/R_{fd})e_{fd}$$
$$= (1.66/0.0006)0.000939 = 2.598 \text{ pu}$$
$$I_{fd} = L_{adu}i_{fd}$$
$$= 1.66\times1.565 = 2.598 \text{ pu}$$ ■

Specification of temperature

The base exciter output voltage depends on the synchronous machine field resistance, which in turn depends on the field temperature. The standard temperatures used for calculating the base exciter output voltage are 100°C for thermal units (operating temperature rise greater than 60°C) and 75°C for hydraulic units (operating temperature rise 60°C or less) [5]. However, care should be exercised in using these temperatures for modelling of excitation systems.

The value of the field resistance used should correspond to the resistance under the actual operating conditions being simulated, as closely as possible. The value of T'_{d0} should be consistent with this value of field resistance.

The field resistance corrected to a specified operating temperature may be calculated as follows [31]:

$$R_s = R_t\left(\frac{t_s + k}{t_t + k}\right) \tag{8.8}$$

where

t_s = specified operating temperature, °C
t_t = temperature corresponding to known or measured value of winding resistance, °C
R_s = winding resistance at temperature t_s
R_t = winding resistance at temperature t_t

The characteristic constant k depends on winding material. It is equal to 234.5 for pure copper and 225 for aluminium based on a volume conductivity of 62% pure copper [31].

Example 8.2

The per unit R_{fd} of a steam-turbine-driven generator is 0.00063 at 75°C and the corresponding value of T'_{d0} is 7.6125 s. The base exciter output voltage at the standard temperature of 100°C is 105.575 V. If the generator is operating at a temperature of 60°C, find consistent values of R_{fd}, T'_{d0}, and base E_{fd} at this temperature. Assume that the constant k of the field winding material is 234.5.

Solution

The field resistance at 60°C is

$$R_{fd\,60} = 0.00063\frac{234.5+60}{234.5+75}$$
$$= 0.0006 \text{ pu}$$

The time constant T'_{d0} is inversely proportional to R_{fd}. Hence at 60°C it is

$$T'_{d0} = T'_{d0}\frac{R_{fd\,75}}{R_{fd\,60}}$$

$$= 7.6125\times\frac{0.00063}{0.0006} = 8.0 \text{ s}$$

The base E_{fd} is directly proportional to R_{fd}. Hence at 60°C,

$$\text{Base } E_{fd\,60} = \text{base } E_{fd\,100}\left(\frac{234.5+60}{234.5+100}\right)$$

$$= 105.575\times 0.8804 = 92.95 \text{ V}$$ ■

8.6.2 Modelling of Excitation System Components

The basic elements which form different types of excitation systems are the dc exciters (self or separately excited); ac exciters; rectifiers (controlled or non-controlled); magnetic, rotating, or electronic amplifiers; excitation system stabilizing feedback circuits; signal sensing and processing circuits. We describe here models for these individual elements. In the next section we will consider modelling of complete excitation systems.

(a) Separately excited dc exciter

The circuit model of the exciter is shown in Figure 8.23.

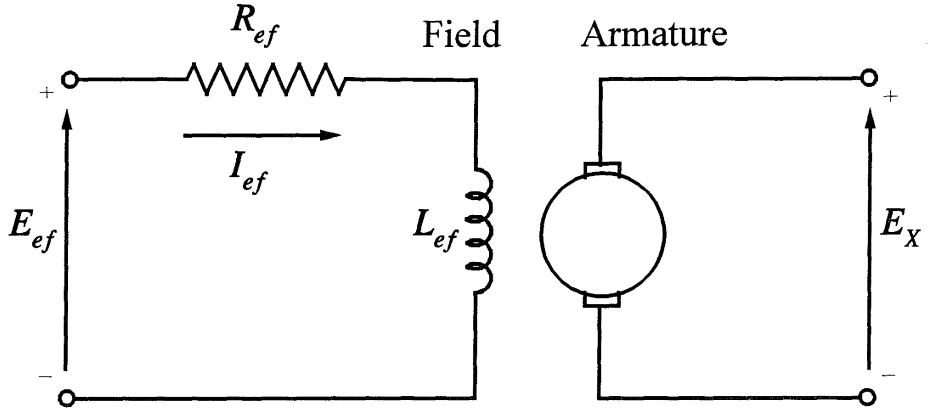

Figure 8.23 Separately excited dc exciter

For the exciter field circuit, we write

$$E_{ef} = R_{ef}I_{ef} + \frac{d\psi}{dt} \tag{8.9}$$

with

$$\psi = L_{ef}I_{ef}$$

Neglecting field leakage, the exciter output voltage E_X is given by

$$E_X = K_X\psi \tag{8.10}$$

where K_X depends on the speed and winding configuration of the exciter armature.

The output voltage E_X is a nonlinear function of the exciter field current I_{ef} due to magnetic saturation. The voltage E_X is also affected by the load on the exciter. The common practice [1,4] in dc exciter modelling is to account for saturation and load regulation approximately by combining the two effects and using the constant-resistance load-saturation curve, as shown in Figure 8.24.

The air-gap line is tangent to the lower linear portion of the open circuit saturation curve. Let R_g be the slope of the air-gap line and ΔI_{ef} denote the departure of the load saturation curve from the air-gap line. From Figure 8.24, we write

$$I_{ef} = \frac{E_X}{R_g} + \Delta I_{ef} \tag{8.11}$$

where ΔI_{ef} is a nonlinear function of E_X and may be expressed as

$$\Delta I_{ef} = E_X S_e(E_X) \tag{8.12}$$

where $S_e(E_X)$ is the *saturation function* dependent on E_X.

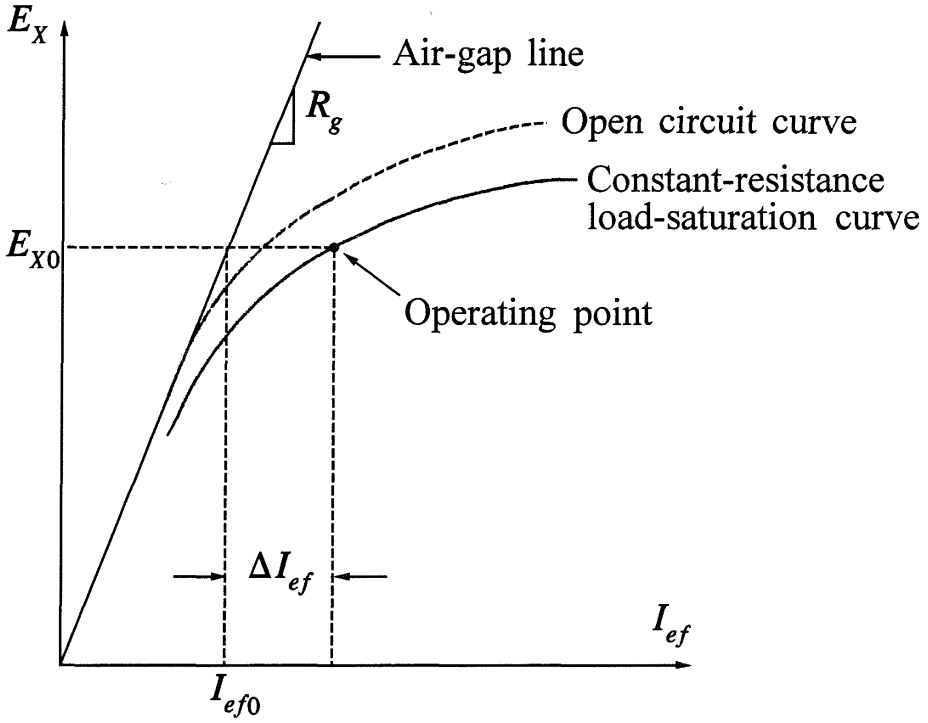

Figure 8.24 Exciter load-saturation curve

From Equations 8.9 to 8.12, we have

$$E_{ef} = \frac{R_{ef}}{R_g}E_X + R_{ef}S_e(E_X)E_X + \frac{1}{K_X}\frac{dE_X}{dt} \tag{8.13}$$

The above equation gives the relationship between the output E_X and the input voltage E_{ef}. A convenient per unit system for this equation is one with base values of E_X and I_{ef} chosen to be equal to those values required to give rated synchronous machine voltage on the air-gap line. Thus,

$$\begin{aligned} E_{Xbase} &= E_{fdbase} \\ I_{efbase} &= E_{fdbase}/R_g \\ R_{gbase} &= R_g \end{aligned} \tag{8.14}$$

Dividing Equation 8.13 by E_{Xbase}, we have

$$\frac{E_{ef}}{E_{Xbase}} = \frac{R_{ef}}{R_g}\frac{E_X}{E_{Xbase}} + R_{ef}S_e(E_X)\frac{E_X}{E_{Xbase}} + \frac{1}{K_X}\frac{d}{dt}\left(\frac{E_X}{E_{Xbase}}\right)$$

In per unit form, we have

$$\bar{E}_{ef} = \frac{R_{ef}}{R_g}\bar{E}_X[1+\bar{S}_e(\bar{E}_X)]+\frac{1}{K_X}\frac{d\bar{E}_X}{dt} \tag{8.15}$$

In the above equation, $\bar{S}_e(\bar{E}_X)$ is the per unit saturation function defined as follows:

$$\bar{S}_e(\bar{E}_X) = \frac{\Delta\bar{I}_{ef}}{\bar{E}_X} = R_g S_e(E_X) \tag{8.16}$$

From Figure 8.25, with E_X and I_{ef} expressed in per unit, the per unit saturation function is given by [4]

$$\bar{S}_e(\bar{E}_X) = \frac{A-B}{B} \tag{8.17}$$

The parameter K_X defined by Equation 8.10 may be written as

$$K_X = \frac{E_X}{\psi} = \frac{E_X}{L_{ef}I_{ef}} = \frac{R_g}{L_{ef}}\frac{\bar{E}_X}{\bar{I}_{ef}}$$

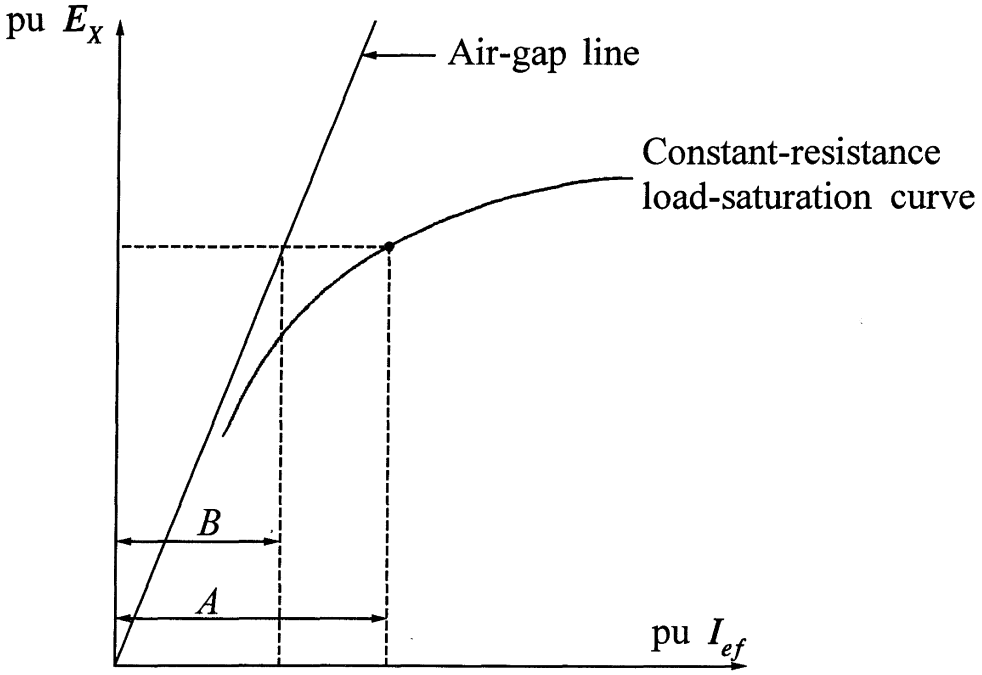

Figure 8.25 Exciter saturation characteristic

Corresponding to any given operating point (I_{efo}, E_{XO}), let

$$L_{fu} = L_{ef}\frac{\bar{I}_{efo}}{\bar{E}_{XO}} \tag{8.18}$$

Therefore, $K_X=R_g/L_{fu}$. Substituting in Equation 8.15, we get

$$\bar{E}_{ef} = K_E\bar{E}_X+S_E(\bar{E}_X)\bar{E}_X+T_E\frac{d\bar{E}_X}{dt} \tag{8.19}$$

where

$$\begin{aligned} K_E &= \frac{R_{ef}}{R_g} \\ T_E &= \frac{L_{fu}}{R_g} \\ S_E(\bar{E}_X) &= \bar{S}_e(\bar{E}_X)\frac{R_{ef}}{R_g} \end{aligned} \tag{8.20}$$

Equation 8.19 represents the input-output relationship of the exciter. For a separately excited exciter, the input voltage E_{ef} is the regulator output V_R. The output voltage E_X of a dc exciter is directly applied to the field of the synchronous machine. Therefore, the exciter may be represented in block diagram form as shown in Figure 8.26. *In the diagram, all variables are in per unit; however, the superbar notation denoting this has been dropped.*

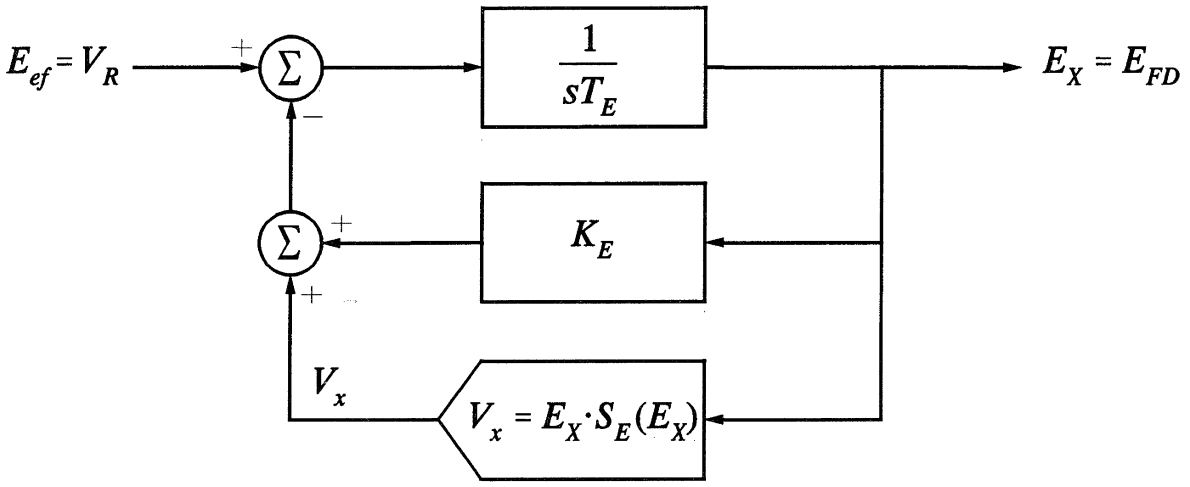

Commonly used representation: $V_X = A_{EX}e^{B_{EX}E_X}$

Figure 8.26 Block diagram of a dc exciter

The adjustment of field-circuit resistance R_{ef} affects K_E as well as the saturation function $S_E(E_X)$, but not the integration time T_E of the forward loop.

There are several convenient mathematical expressions that may be used to approximate the effect of exciter saturation. A commonly used expression is the exponential function

$$V_X = E_X S_E(E_X) = A_{EX} e^{B_{EX} E_X} \tag{8.21}$$

The block diagram of Figure 8.26 provides a convenient means of representing the dc exciter in stability studies. However, the effective gain and time constant of the exciter are not readily apparent from it. These are more evident when the block diagram is reduced to the standard form by considering small-signal response:

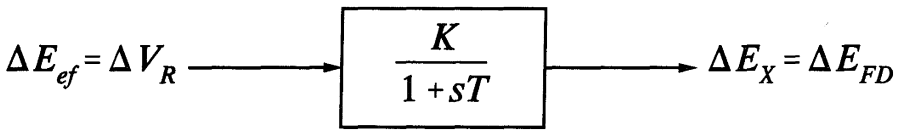

For any operating point with $E_X = E_{FD} = E_{FD0}$, the effective gain K and time constant of the exciter for small perturbations are

$$K = \frac{1}{B_{EX} S_E(E_{FD0}) + K_E} \tag{8.22}$$

$$T = \frac{T_E}{B_{EX} S_E(E_{FD0}) + K_E} \tag{8.23}$$

where $S_E(E_{X0}) = A_{EX} e^{B_{EX} E_{FD0}}$.

(b) Self-excited dc exciter

Figure 8.27 shows a circuit model of a self-excited dc exciter.

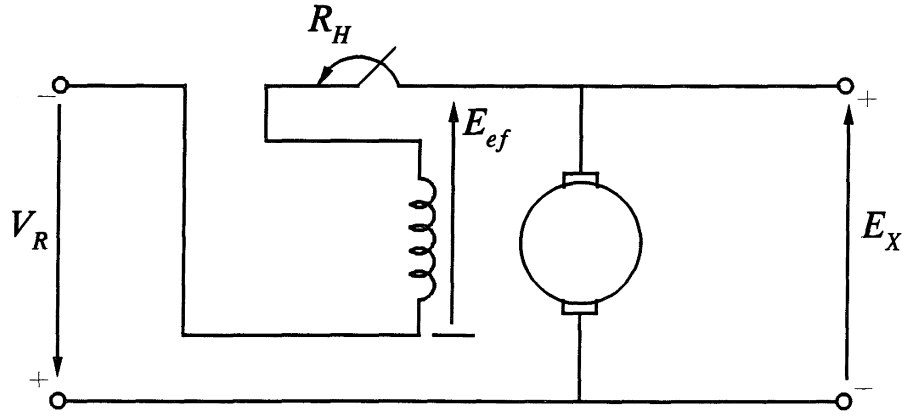

Figure 8.27 Self-excited dc exciter

For this exciter, the regulator output V_R is in series with the exciter shunt field. Therefore, the per unit voltage across the exciter field (without the explicit per unit notation) is

$$E_{ef} = V_R + E_X \tag{8.24}$$

The relationship between the per unit values of E_{ef} and E_X developed for the separately excited exciter also applies in this case. Substituting for E_{ef} given by Equation 8.24 in Equation 8.15, we have

$$V_R + E_X = \frac{R_{ef}}{R_g} E_X[1 + S_e(E_X)] + \frac{1}{K_X}\frac{dE_X}{dt}$$

This reduces to

$$V_R = K_E E_X + S_E(E_X) E_X + T_E \frac{dE_X}{dt} \tag{8.25}$$

where

$$\begin{aligned} K_E &= \frac{R_{ef}}{R_g} - 1 \\ T_E &= \frac{L_{fu}}{R_g} \\ S_E &= S_e(E_X)\frac{R_{ef}}{R_g} \end{aligned} \tag{8.26}$$

The block diagram of Figure 8.26 also applies to the self-excited dc exciter. The value of K_E, however, is now equal to $R_{ef}/R_g - 1$ as compared to R_{ef}/R_g for the separately excited case.

The station operators usually track the voltage regulator by periodically adjusting the rheostat setpoint so as to make the voltage regulator output zero. This is accounted for by selecting the value of K_E so that the initial value of V_R is equal to zero. *The parameter K_E is therefore not fixed, but varies with the operating condition.*

(c) AC exciters and rectifiers

The ac exciter representation (excluding rectification) recommended in reference 8 for use in large-scale stability studies is shown in Figure 8.28.

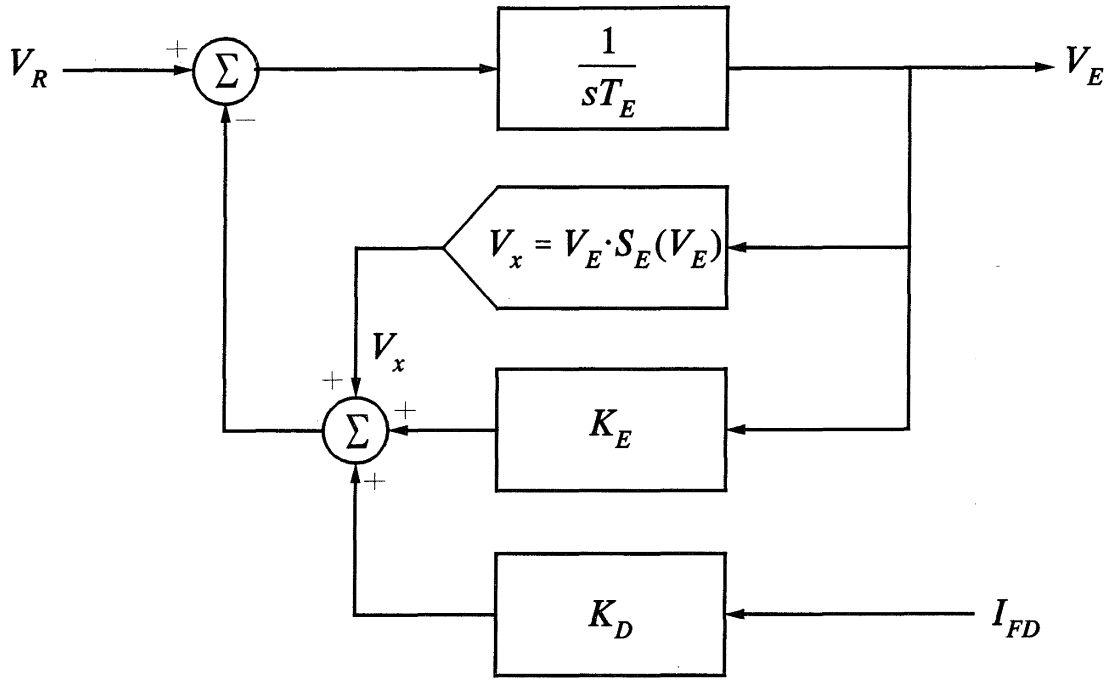

Figure 8.28 Block diagram of an ac exciter

The general structure of the model is similar to that of the dc exciter. However, in this case the load regulation due to the armature reaction effect is accounted for distinctly, and the no-load saturation curve is used to define the saturation function S_E. The exciter internal voltage V_E is the no-load voltage as determined by the saturation function. The main generator field current I_{FD} represents the exciter load current, and the negative feedback of $K_D I_{FD}$ accounts for the armature reaction demagnetizing effect. The constant K_D depends on the ac exciter synchronous and transient reactances [32]. Figure 8.29 illustrates the calculation of the saturation function S_E for a specified value of V_E.

The per unit saturation function is

$$S_E(V_E) = \frac{A-B}{B} \tag{8.27}$$

Any convenient mathematical expression can be used to represent the saturation function. As in the case of dc exciters, a commonly used expression for $V_X = V_E S_E(V_E)$ is the exponential function given by Equation 8.21.

Three-phase full-wave bridge rectifier circuits are commonly used to rectify the ac exciter output voltage. The effective ac source impedance seen by the rectifier is predominantly an inductive reactance. As described in Chapter 10, the effect of this inductive reactance (referred to as the *commutating reactance*) is to delay the process of commutation, i.e., transfer of current from one valve to another. This produces a

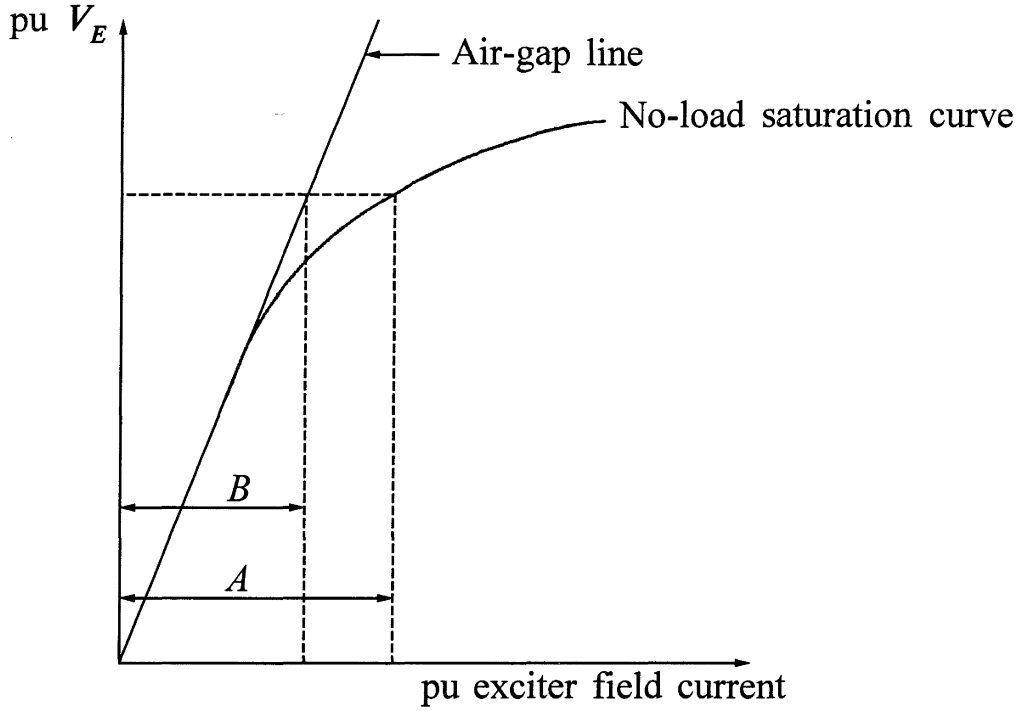

Figure 8.29 AC exciter saturation characteristic

decrease in the average output voltage of the rectifier as its load current increases. Reference 33 shows that a three-phase full-wave bridge rectifier circuit operates in one of three distinct modes as the rectifier load current varies from no load to the short circuit level. The mode of operation depends on the commutating voltage drop (equal to the product of commutating reactance and load current).

The equations defining the rectifier regulation as a function of commutation voltage drop may be expressed as follows [8,34]:

$$E_{FD} = F_{EX}V_E \tag{8.28}$$

where

$$F_{EX} = f(I_N) \tag{8.29}$$

and

$$I_N = \frac{K_C I_{FD}}{V_E} \tag{8.30}$$

The constant K_C depends on the commutating reactance. The expressions for the function $f(I_N)$ characterizing the three modes of rectifier circuit operation are

$$\begin{aligned} &\text{Mode 1:} && f(I_N) = 1.0 - 0.577 I_N, && \text{if } I_N \le 0.433 \\ &\text{Mode 2:} && f(I_N) = \sqrt{0.75 - I_N^2}, && \text{if } 0.433 < I_N < 0.75 \\ &\text{Mode 3:} && f(I_N) = 1.732(1.0 - I_N), && \text{if } 0.75 \le I_N \le 1.0 \end{aligned} \tag{8.31}$$

Now I_N should not be greater than 1.0, but if for some reason it is, F_{EX} should be set to zero [8].

The rectifier regulation effects identified above may be depicted in the block diagram form as shown in Figure 8.30.

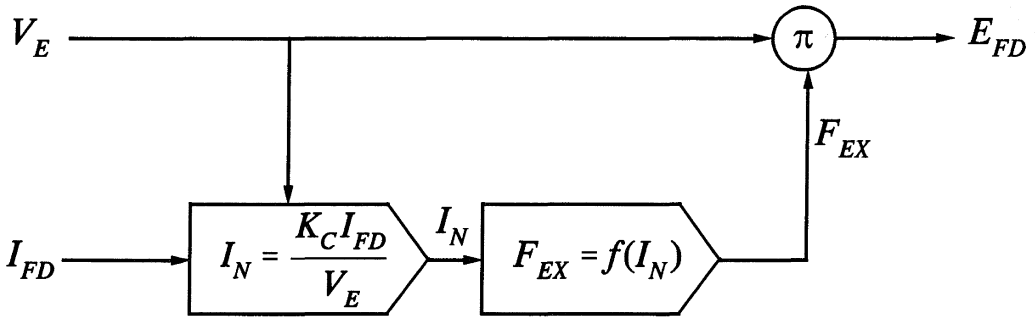

Figure 8.30 Rectifier regulation model

Referring to Figures 8.28 and 8.29, the exciter output voltage E_{FD} is simulated as the ac exciter internal voltage V_E reduced by the armature reaction ($I_{FD}K_D$) and rectifier regulation (F_{EX}).

(d) Amplifiers

Amplifiers may be the magnetic, rotating, or electronic type. Magnetic and electronic amplifiers are characterized by a gain and may also include a time constant. As such they may be represented by the block diagram of Figure 8.31.

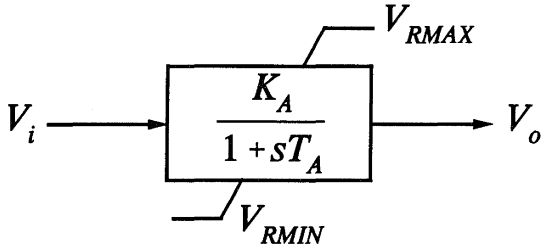

Figure 8.31 Amplifier model

The amplifier output is limited by saturation or power-supply limitations; this is represented by "non-windup" limits V_{RMAX} and V_{RMIN} in Figure 8.31. A description of such limits is provided later in this section.

The output limits of some amplifiers having power supplies from generator or auxiliary bus voltage vary with generator terminal voltage. In such cases, V_{RMAX} and V_{RMIN} vary directly with generator terminal voltage E_t.

The transfer function of an amplidyne is derived in reference 12 and has the general form shown in Figure 8.32.

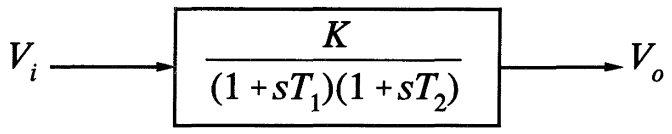

Figure 8.32 Amplidyne model

(e) Excitation system stabilizing circuit

There are several ways of physically realizing the stabilizing function identified in Figure 8.15. Some excitation systems use series transformers as shown in Figure 8.33.

The transformer equations in Laplace notation are

$$\begin{aligned} V_1 &= R_1 i_1 + sL_1 i_1 + sMi_2 \\ V_2 &= R_2 i_2 + sL_2 i_2 + sMi_1 \end{aligned} \tag{8.32}$$

where subscripts 1 and 2 denote primary and secondary quantities; R, L, and M denote resistance, leakage inductance and mutual inductance, respectively.

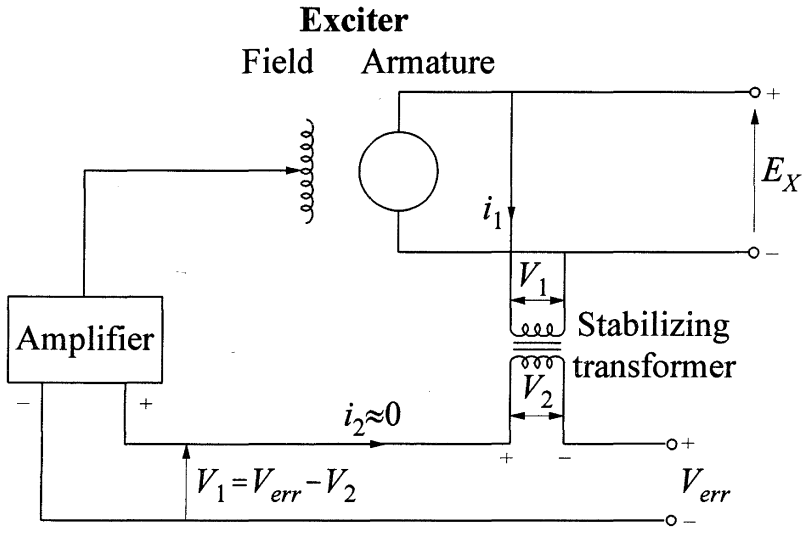

Figure 8.33 Excitation system stabilizing transformer

The secondary of the transformer is connected to a high impedance circuit. Therefore, neglecting i_2, we have

$$\begin{aligned} V_1 &= (R_1 + sL_1) i_1 \\ V_2 &= sMi_1 \end{aligned} \tag{8.33}$$

Thus

$$\begin{aligned} \frac{V_1}{V_2} &= \frac{sM}{R_1 + sL_1} \\ &= \frac{sK_F}{1 + sT_F} \end{aligned} \tag{8.34}$$

where $K_F = M/R$ and $T_F = L_1/R$.

(f) Windup and non-windup limits

In the modelling of excitation systems, it is necessary to distinguish between windup and non-windup limits. Such limits are encountered with integrator blocks, single time constant blocks, and lead-lag blocks.

Figures 8.34(a) and (b) show the differences between the two types of limits when applied to an integrator block.

Representation:

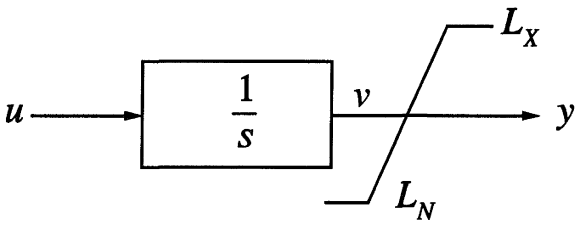

System equation:

$$\frac{dv}{dt} = u$$

Limiting action:

If $L_N < v < L_X$, then $y = v$
If $v \geq L_X$, then $y = L_X$
If $v \leq L_N$, then $y = L_N$

Figure 8.34 (a) Integrator with windup limits

Representation:

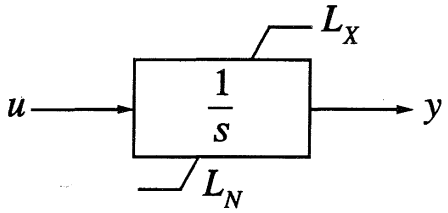

System equation:

$$\frac{dy}{dt} = u$$

Limiting action:

If $L_N < y < L_X$, then $\frac{dy}{dt} = u$

If $y \geq L_X$ and $\frac{dy}{dt} > 0$, then set $\frac{dy}{dt} = 0$, $y = L_X$

If $y \leq L_N$ and $\frac{dy}{dt} < 0$, then set $\frac{dy}{dt} = 0$, $y = L_N$

Figure 8.34 (b) Integrator with non-windup limits

With windup limits the variable v is not limited. Therefore, the output variable y cannot come off a limit until v comes within the limit. With non-windup limits, the output variable y is limited; it comes off the limit as soon as the input u changes sign.

Figures 8.35(a) and (b) show the difference between the two types of limits when applied to a single time constant block. The significance of the two types of limits is similar to that for an integrator. With a windup limit, the output y cannot come off a limit until v comes within the limit. With a non-windup limit, however, the output y comes off the limit as soon as the input u re-enters the range within limits.

Representation:

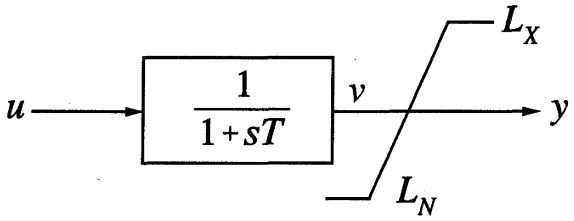

System equation:

$$\frac{dv}{dt} = \frac{u - v}{T}$$

Limiting action:

If $L_N < v < L_X$, then $y = v$

If $v \geq L_X$, then $y = L_X$

If $v \leq L_N$, then $y = L_N$

Figure 8.35 (a) Single time constant block with windup limits

Representation:

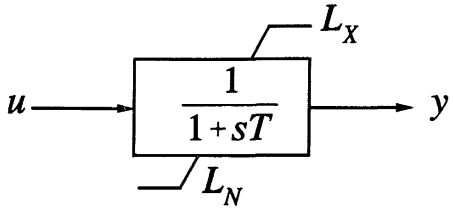

System equation: $f = \dfrac{u-y}{T}$

Limiting action:

If $L_N < y < L_X$, then $\dfrac{dy}{dt} = f$

If $y \geq L_X$ and $f > 0$, then set $\dfrac{dy}{dt} = 0$, $y = L_X$

If $y \leq L_N$ and $f < 0$, then set $\dfrac{dy}{dt} = 0$, $y = L_N$

Figure 8.35 (b) Single time constant block with non-windup limits

Representation:

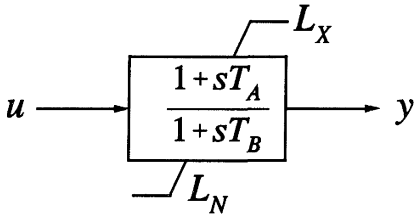

$T_A < T_B$

Physical realization:

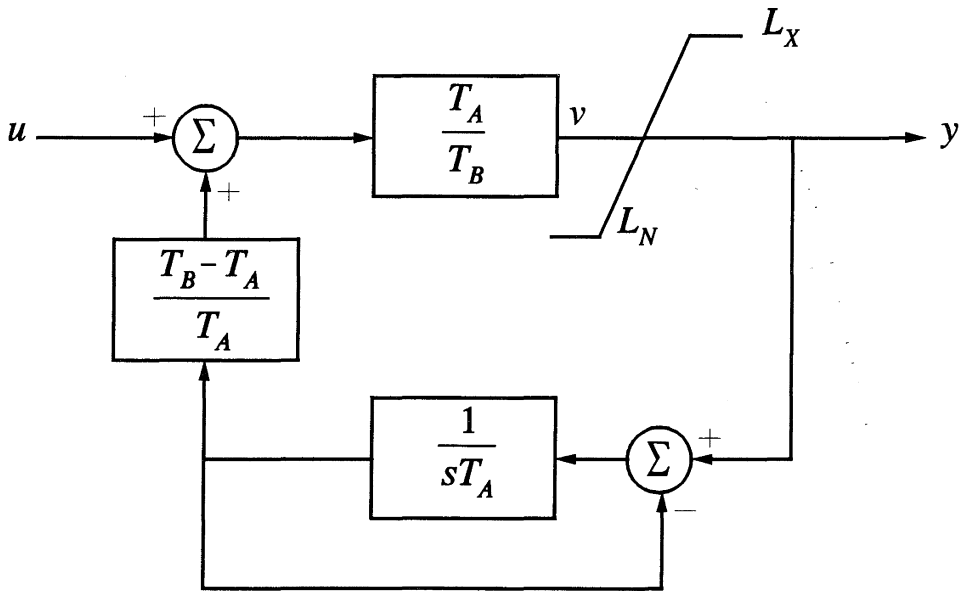

Figure 8.36 Lead-lag function with non-windup limits
(Continued on next page)

Limiting action:

If $L_N \le v \le L_X$, then $y = v$
If $v > L_X$, then $y = L_X$
If $v < L_N$, then $y = L_N$

Figure 8.36 (*Continued*) Lead-lag function with non-windup limits

With a lead-lag block, the interpretation of the action of a windup limit is straightforward and is similar to that of a single time constant block. However, the way in which a non-windup limit can be realized is not unique; the interpretation of the limiting action should therefore be based on the physical device represented by the block. Figure 8.36 illustrates such limiting action associated with electronic implementation of lead-lag functions.

(g) Gating functions

Gating or auctioneering circuits are used when it is required to give control to one of two input signals, depending on their relative size with respect to each other. Figure 8.37 illustrates the functions of a low value (LV) gate and a high value (HV) gate, and the symbols used to represent them in block diagrams.

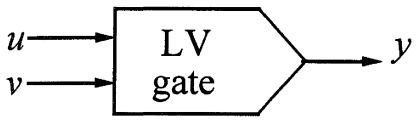

If $u \le v$, $y = u$
If $u > v$, $y = v$

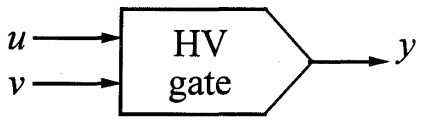

If $u \ge v$, $y = u$
If $u < v$, $y = v$

Figure 8.37 Low- and high-value gating functions

(h) Terminal voltage transducer and load compensator [8]

The block diagram representation of these elements is shown in Figure 8.38. The time constant T_R represents rectification and filtering of the synchronous machine terminal voltage. The parameters of the load compensator (described in Section 8.5.4) are R_C and X_C. The input variables E_t and I_t are in phasor form. When load compensation is not used, R_C and X_C are set to zero.

The voltage transducer output V_C forms the principal control signal to the excitation system. If a load compensator is not used and T_R is negligible, $V_C = E_t$.

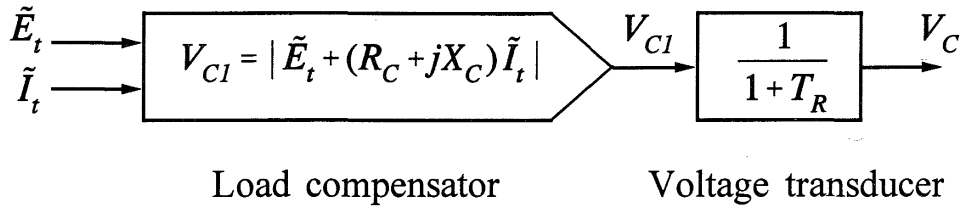

Figure 8.38 Terminal voltage transducer and load compensator model

8.6.3 Modelling of Complete Excitation Systems

Figure 8.39 depicts the general structure of a detailed excitation system model having a one-to-one correspondence with the physical equipment. While this model structure has the advantage of retaining a direct relationship between model parameters and physical parameters, such detail is considered too great for general system studies. Therefore, model reduction techniques are used to simplify and obtain a practical model appropriate for the type of study for which it is intended.

The parameters of the reduced model are selected such that the gain and phase characteristics of the reduced model match those of the detailed model over the frequency range of 0 to 3 Hz. In addition, all significant nonlinearities that impact on system stability are accounted for. With a reduced model, however, direct correspondence between the model parameters and the actual system parameters is generally lost.

The appropriate structure for the reduced model depends on the type of excitation system. The IEEE has standardized 12 model structures in block diagram form for representing the wide variety of excitation systems currently in use [8].

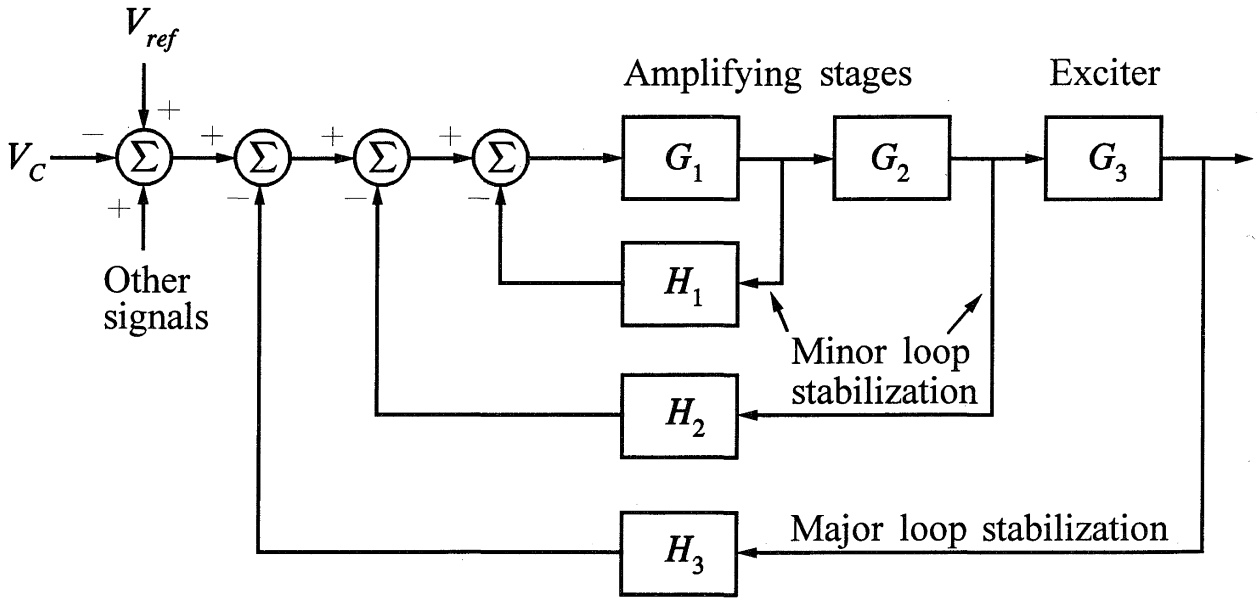

Figure 8.39 Structure of a detailed excitation system model

These are intended for use in *transient stability and small-signal stability studies*. For purposes of illustration, we will consider five of these models. These are shown in Figures 8.40 to 8.44, with slight modification of the block diagram conventions to conform to the recommendations made in reference 35. The figures include a brief description of the key features and sample data. The suffix "A" accompanying the designations is for the purpose of differentiating these models developed in 1992 from similar models developed previously in 1981 [4].

The principal input signal to each of the excitation systems is the output V_C of the voltage transducer shown in Figure 8.38. At the first summing point, the signal V_C is subtracted from the voltage regulator reference V_{ref} and the output V_S of the power system stabilizer, if used, is added to produce the actuating signal which controls the excitation system. Additional signals, such as the underexcitation limiter output (V_{UEL}), come into play only during extreme or unusual conditions. Under steady state, V_S=0 and V_{ref} takes on a value unique to the synchronous machine loading condition so that the error signal results in the required field voltage E_{fd}. This is illustrated in Example 8.3.

1. Type DC1A exciter model

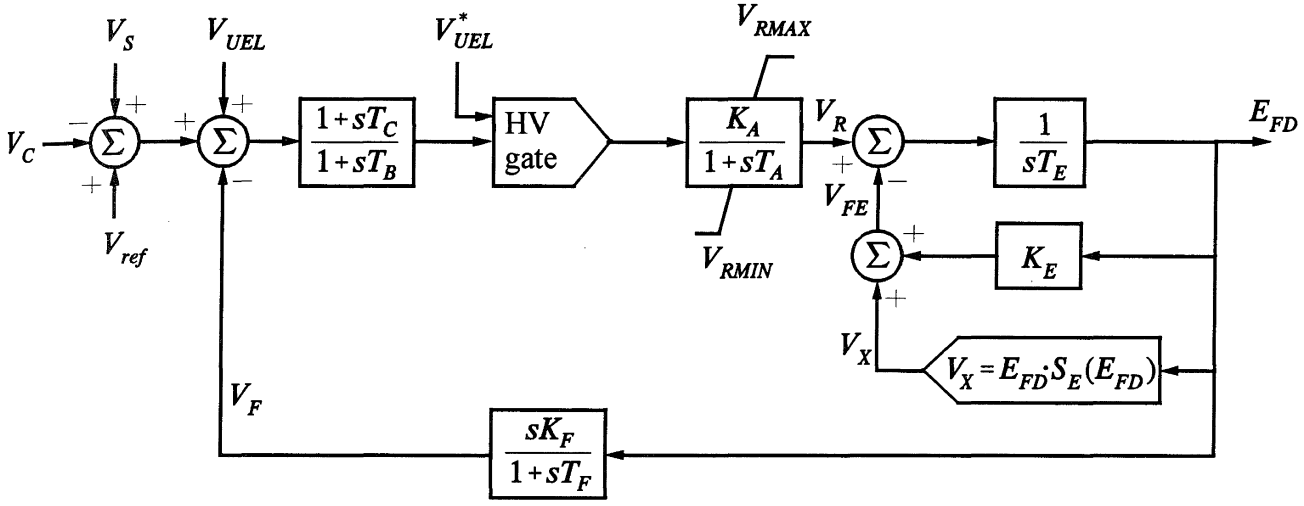

* Alternate input point

Figure 8.40 IEEE type DC1A excitation system model. © IEEE 1992 [8]

The type DC1A exciter model represents field-controlled dc commutator exciters, with continuously acting voltage regulators. The exciter may be separately excited or self-excited, the latter type being more common. When self-excited, K_E is selected so that initially V_R=0, representing operator action of tracking the voltage regulator by periodically trimming the shunt field rheostat setpoint.

Sample data

Self-excited dc exciter:

K_A=187	T_A=0.89	T_E=1.15	A_{EX}=0.014	B_{EX}=1.55
K_F=0.058	T_F=0.62	T_B=0.06	T_C=0.173	T_R=0.05
V_{RMAX}=1.7	V_{RMIN}=−1.7			

K_E is computed so that initially V_R=0, and the load compensator is not used.

2. *Type AC1A exciter model*

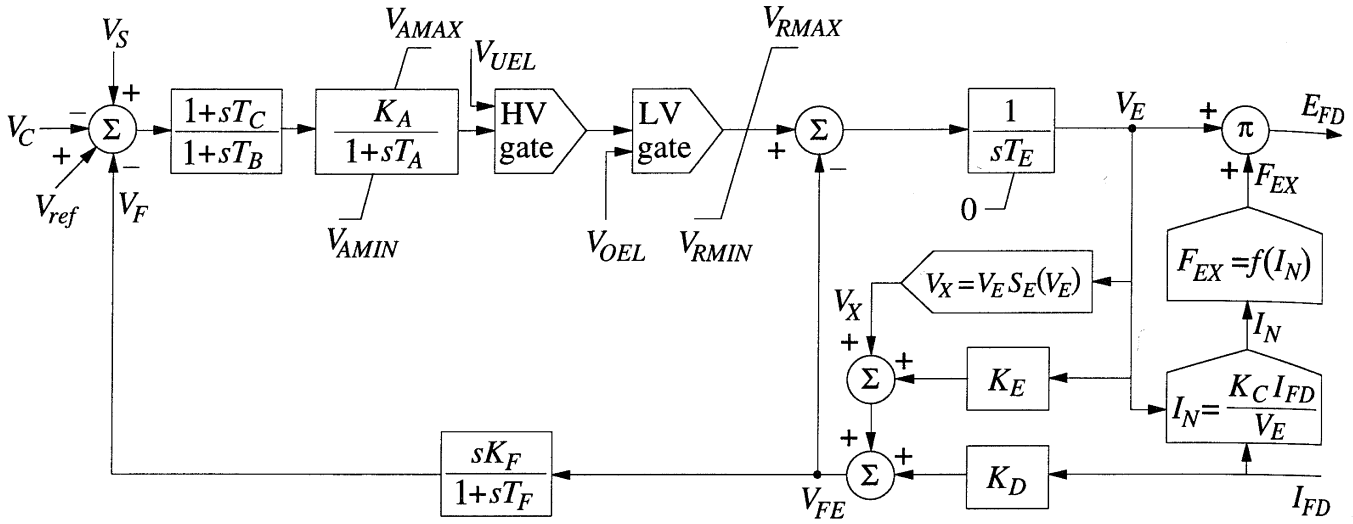

Figure 8.41 IEEE type AC1A excitation system model. © IEEE 1992 [8]

The type AC1A exciter model represents a field-controlled alternator excitation system with non-controlled rectifiers, and is applicable to brushless excitation systems. The diode rectifier characteristic imposes a lower limit of zero on the exciter output voltage. The exciter field is supplied by a pilot exciter, and the voltage regulator power supply is not affected by external transients.

Sample data

Exciter and regulator:

K_A=400.0	T_A=0.02	T_B=0	T_C=0	K_F=0.03
T_F=1.0	K_E=1.0	T_E=0.8	K_D=0.38	K_C=0.2
V_{RMAX}=7.3	V_{RMIN}=−6.6	V_{AMAX}=15.0	V_{AMIN}=−15.0	A_{EX}=0.1
B_{EX}=0.03				

The load compensator is not used, and T_R is negligible.

3. Type AC4A exciter model

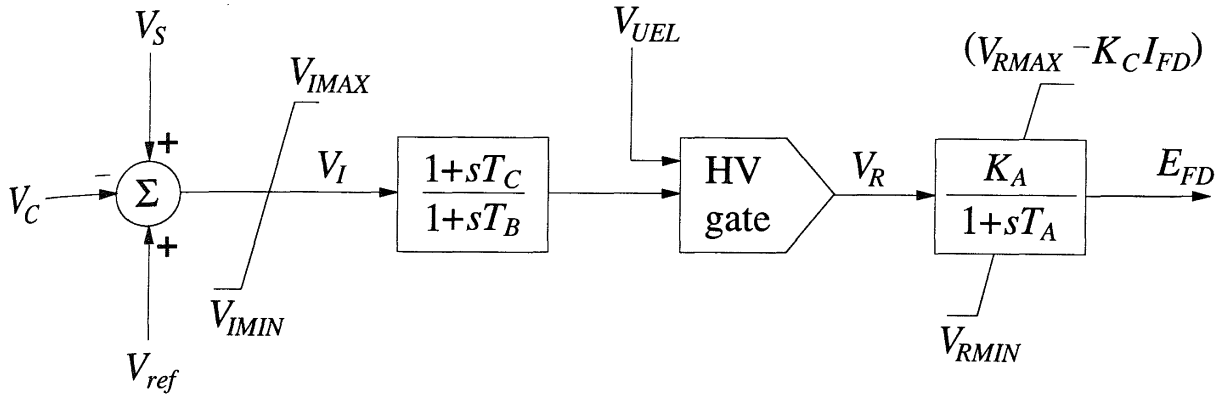

Figure 8.42 IEEE type AC4A excitation system model. © IEEE 1992 [8]

The type AC4A exciter model represents an alternator-supplied controlled-rectifier excitation system – a high initial-response excitation system utilizing a full-wave thyristor bridge circuit. Excitation system stabilization is usually provided in the form of a series lag-lead network (transient gain reduction). The time constant associated with the regulator and firing of thyristors is represented by T_A. The overall gain is represented by K_A. The rectifier operation is confined to mode 1 region. Rectifier regulation effects on exciter output limits are accounted for by constant K_C.

Sample data

Exciter and regulator:

K_A=200.0	T_A=0.04	T_C=1.0	T_B=12.0	V_{RMAX}=5.64
V_{RMIN}=-4.53	K_C=0	V_{IMAX}=1.0	V_{IMIN}=-1.0	

4. Type ST1A exciter model

The type ST1A exciter model represents a potential-source controlled-rectifier system. The excitation power is supplied through a transformer from generator terminals; therefore, the exciter ceiling voltage is directly proportional to the generator terminal voltage. The effect of rectifier regulation on ceiling voltage is represented by K_C. The model provides flexibility to represent series lag-lead or rate feedback stabilization. Because of the very high field-forcing capability of the system, a field-current limiter is sometimes employed; the limit is defined by I_{LR} and the gain by K_{LR}.

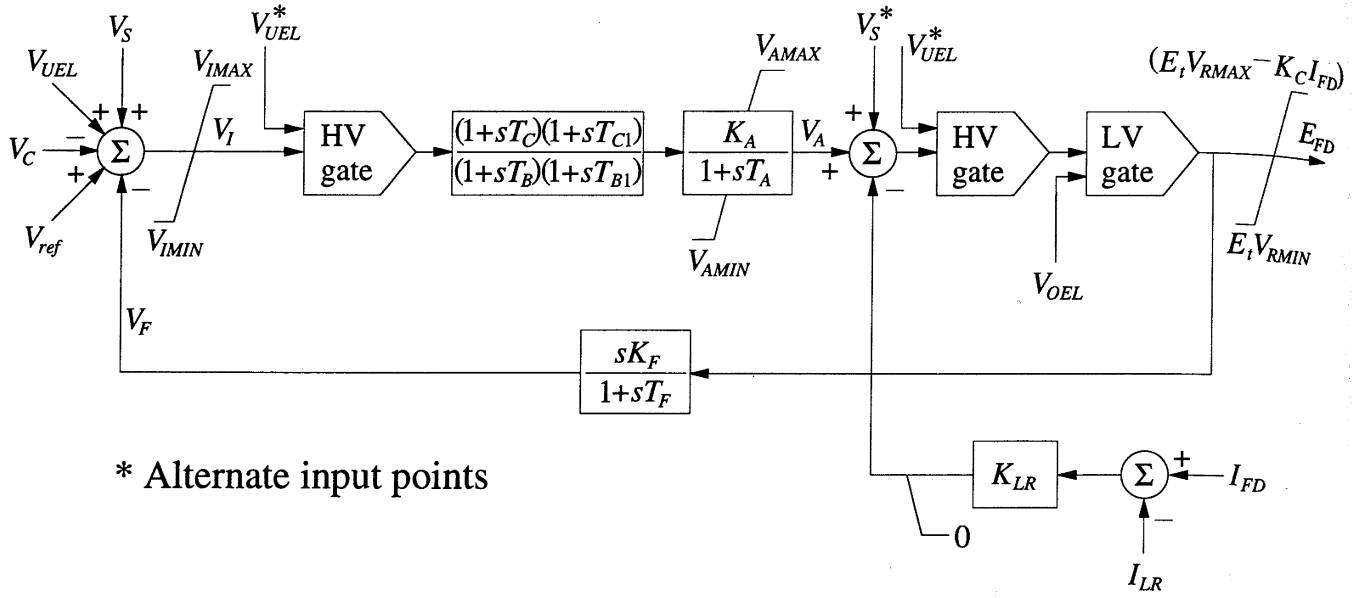

Figure 8.43 IEEE type ST1A excitation system model. © IEEE 1992 [8]

Sample data

Exciter and regulator:

K_A=200.0	T_A=0	V_{RMAX}=7.0	V_{RMIN}=−6.4	K_C=0.04
K_{LR}=4.54	I_{LR}=4.4	T_B, T_C, T_{B1}, T_{C1}, K_F, T_F not used		
V_{IMAX}, V_{IMIN}, V_{AMAX}, V_{AMIN} are not represented.				

Voltage transducer and load compensator:

T_R=0.015	R_C=0	X_C=0

5. Type ST2A exciter model

The type ST2A exciter model represents a compound-source rectifier excitation system. The exciter power source is formed by phasor combination of main generator armature voltage and current. The regulator controls the exciter output through controlled saturation of the power transformer. The parameter T_E represents the integration rate associated with the control windings; E_{FDMAX} represents the limit on exciter output due to magnetic saturation.

Sample data

K_A=120.0	T_A=0.15	K_E=1.0	T_E=0.5	K_C=0.65
K_F=0.02	T_F=0.56	V_{RMAX}=1.2	V_{RMIN}=−1.2	E_{FDMAX}=3.55
K_P=1.19	K_I=1.62			

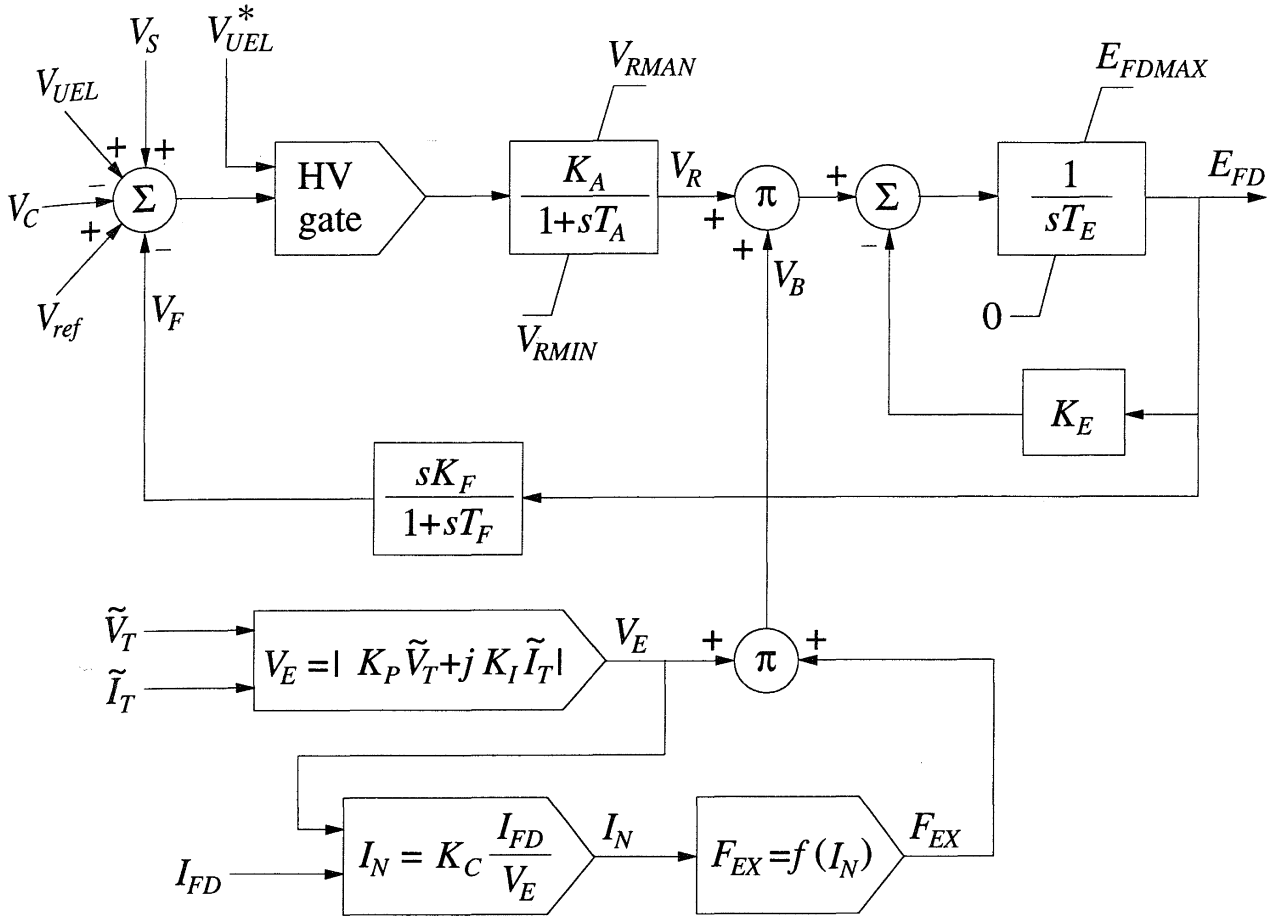

Figure 8.44 IEEE type ST2A excitation system model. © IEEE 1992 [8]

Example 8.3

A generator is operating under steady-state conditions with an E_{fd} of 2.598 pu and E_t=1.0 pu.

(a) If it is equipped with a type AC4A excitation system represented by the block diagram of Figure 8.42, determine the value of V_{ref}.

(b) If it is equipped with a self-excited dc excitation system represented by the block diagram of Figure 8.40, determine the values of K_E and V_{ref}.

The parameters of the excitation systems are the same as for the sample data provided with the figures.

Solution

(a) *Type AC4A excitation system of Figure 8.42*

When E_{fd} is 2.598 pu, we have

$$V_R = E_{fd}/K_A$$

$$= \frac{2.598}{200.0} = 0.013 \quad \text{pu}$$

Since a load compensator is not used,

$$V_C = E_t = 1.0 \text{ pu}$$

Under steady-state operation, $V_I = V_R$ and $V_S = 0$. Since the generator is operating under normal conditions, $V_{UEL} = 0$. Therefore, from Figure 8.42 we see that

$$V_{ref} = V_C + V_I$$

$$= 1.0 + 0.013 = 1.013 \quad \text{pu}$$

(b) *Self-excited dc exciter of Figure 8.40*

In this case, K_E takes a value such that $V_R = 0$. With E_{fd} at a steady-state value and $V_R = 0$, $V_{FE} = 0$. Hence,

$$K_E E_{fd} = -V_X$$

$$= -A_{EX} e^{B_{EX} E_{fd}} = -0.014 e^{1.55 \times 2.598}$$

$$= -0.7852$$

Therefore,

$$K_E = -\frac{0.7852}{2.598}$$

$$= -0.3022$$

Under steady-state normal operation, $V_F = 0$ and $V_S = 0$. With $V_R = 0$,

$$V_{ref} = V_C = E_t = 1.0 \text{ pu}$$ ■

Modelling of limiters

The standard models shown in Figures 8.40 to 8.44 do not include representation of limiting circuits, namely, the underexcitation limiter, V/Hz limiter, and maximum excitation limiter. These circuits do not come into play under normal conditions and are not usually modelled in transient and small-signal stability studies. They may, however, be important for long-term stability and voltage stability studies.

The actual implementation of these limiting functions varies widely depending on the manufacturer, the vintage of the equipment, and the requirements specified by the utility. Therefore, models for these circuits have to be established on a case by case basis. Here we will illustrate how such devices are modelled by considering specific examples.

(a) Underexcitation limiter:

Figure 8.45 shows the model of an underexcitation limiter used in conjunction with a type ST1A (static) exciter. The parameters K_C and K_R determine the characteristics of the limiter on the P-Q plane. The output V_{UEL} of the limiter is applied to the HV gate of the exciter model of Figure 8.43.

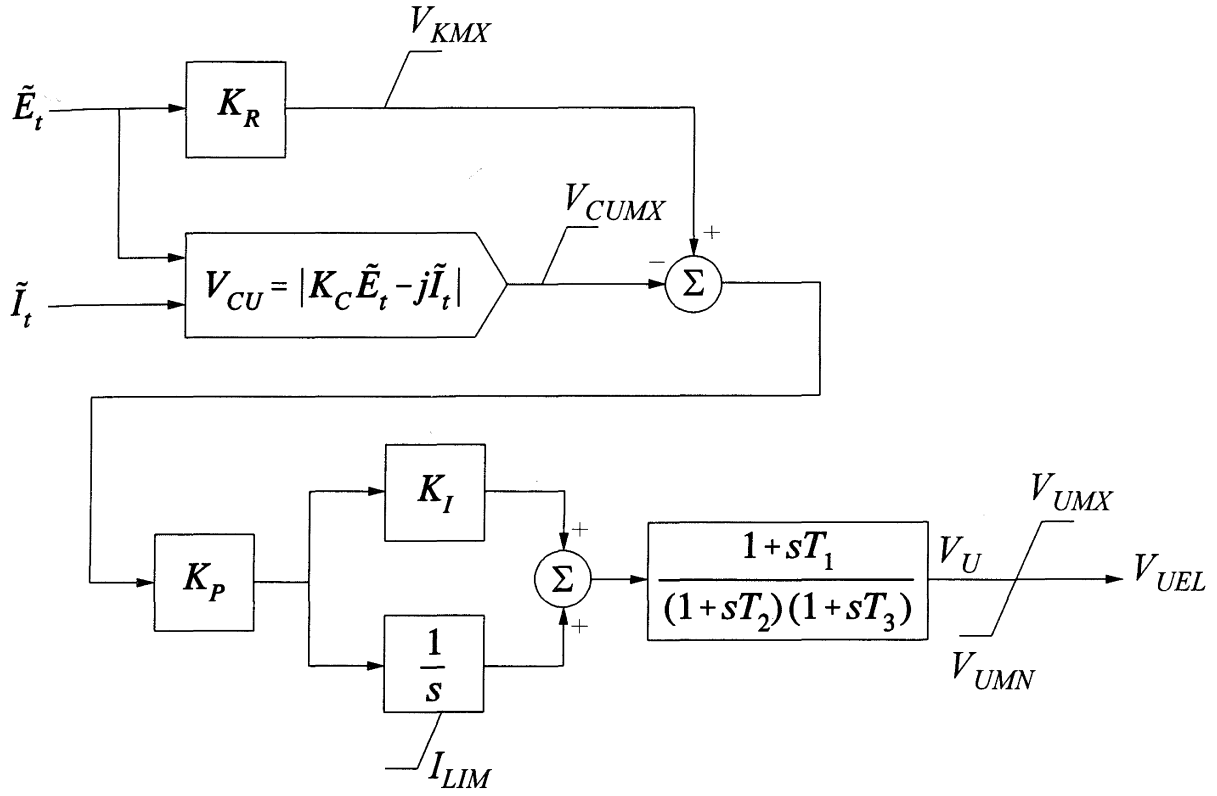

Sample data:

K_P = 0.015 K_I = 10.0 T_1 = 6.4 s T_2 = 0.8 s
T_3 = 0.64 s V_{KMX} = 4.0 V_{CUMX} = 4.0
V_{UMX} = 0.2 V_{UMN} = −0.2 I_{LIM} = −0.012
K_R = Radius of UEL characteristic
K_C = Centre of UEL characteristic

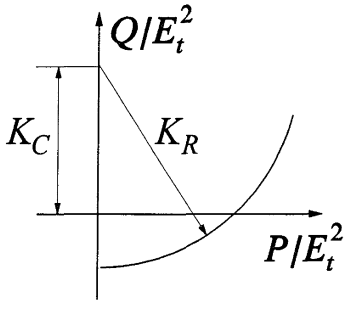

Figure 8.45 An example of UEL model [26]

(b) V/Hz limiter:

An example of the V/Hz limiter model is shown in Figure 8.46. The operation of the limiter is quite straightforward. When the per unit V/Hz value exceeds the limiting value of V_{ZLM}, a strong negative signal drives the excitation down. The V_{ZLM} limit is set typically at 1.07 to 1.09 pu.

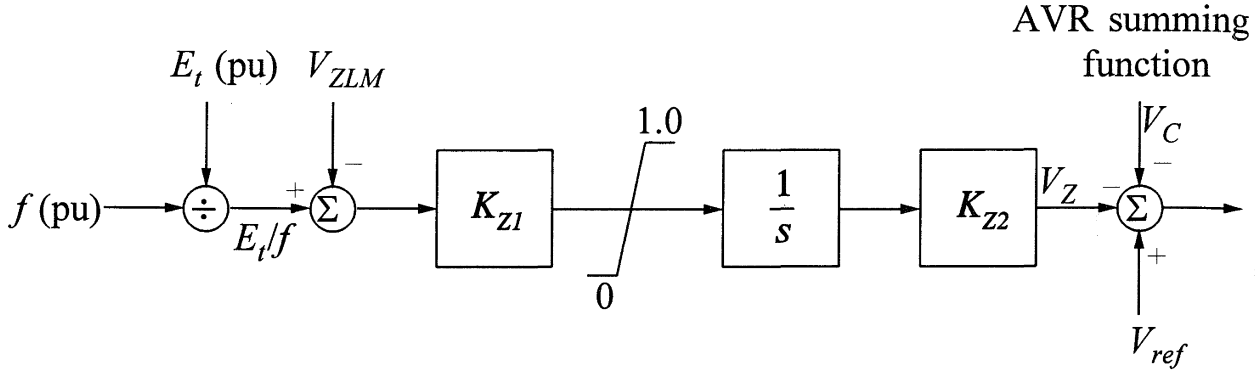

Sample data:

V_{ZLM} = 1.07 K_{Z1} = 1000 K_{Z2} = 0.007

Figure 8.46 V/Hz limiter model

(c) Field-current or overexcitation limiter:

Figure 8.47 shows the model of a field-current limiter circuit. It is designed to have a limiting action as shown in Figure 8.47(b). A high setting provides almost instantaneous limiting at 1.6 times full-load current (FLC). A low setting of 1.05×FLC in conjunction with a ramp timing function provides a limiting action with time delay dependent on the level of field current. For example, a field current level of 1.325×FLC will be allowed for 15 s, followed by a reduction in current level to 1.05×FLC over the next 15 s.

Referring to the block diagram of Figure 8.47(a), when I_{fd} exceeds the high setting I_{FLM1}, signal V_{F1} of control loop ① acts to reduce excitation instantaneously. When the field current is below I_{FLM1}, the limiting action is through the control loop ②. The magnitude of the control signal V_{F2} and the value of gain K_2 determine the time delay and ramping action. Once the field current reaches the low setting I_{FLM2}, the select switch changes to the low select position; this ensures that the field current, in the event of a second disturbance, does not exceed the low setting for a minimum period to allow cooling of the machine. When the field current is below I_{FLM2}, the signal V_{F4} helps to reset rapidly the integrator output to zero.

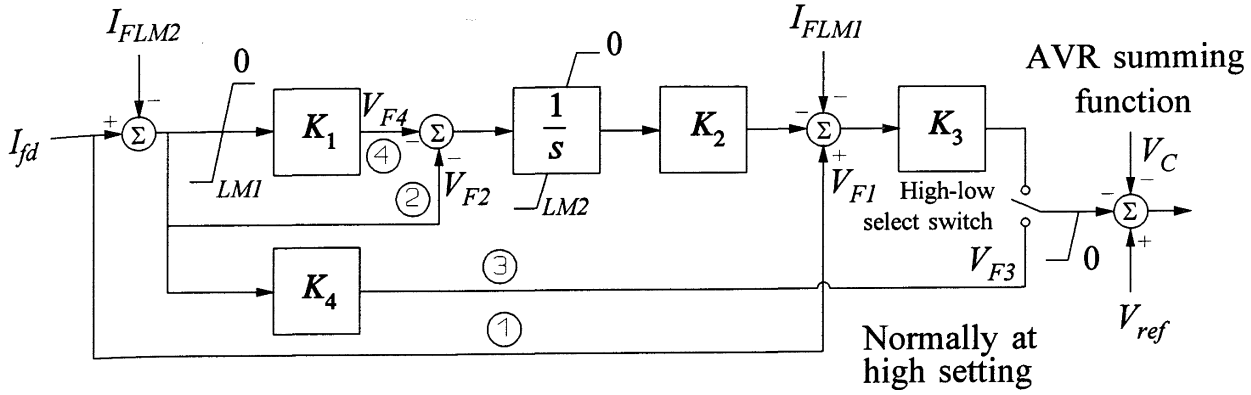

(a) Block diagram representation

Sample data:

I_{FLM1} = 1.6×full load I_{fd} I_{FLM2} = 1.05×full load I_{fd}
K_1 = 150 K_2 = 0.248 K_3 = 12.6
K_4 = 140 $LM1$ = -0.085 $LM2$ = -3.85

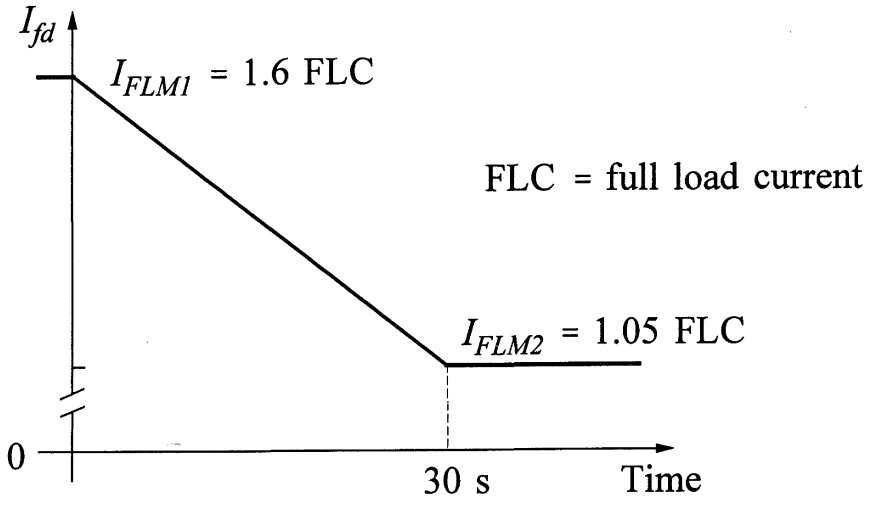

(b) Limiting characteristics

Figure 8.47 Field-current limiter model

8.6.4 Field Testing for Model Development and Verification

Although most of the data related to excitation system models can be obtained from factory tests, such data can only be considered as typical. The actual settings are usually determined on site during installation and commissioning of the equipment. It is therefore desirable to determine the model parameters by performing tests on the actual equipment on site.

The nature of the tests required will depend on the type of excitation system being tested. A general procedure for model verification and development is as follows:

1. Obtain circuit diagrams, block diagrams, nominal settings and setting ranges. Construct a detailed block diagram of the complete excitation system, identifying gains, time constants, and non-linearities.

2. With the generator (synchronous machine) shut down, perform frequency response tests and/or transient response tests on the individual elements comprising the excitation system. Identify their transfer functions, non-linearities, saturation characteristics, and ceiling limits. Using these data, validate as much of the detailed block diagram of the excitation system as possible and modify the diagram as necessary.

3. Perform frequency response and time-response tests with the generator running at rated speed and producing rated voltage on open-circuit. Measure the overall linear response and responses at various points of the system to a step change in terminal voltage. Perform additional tests with the generator operating near rated load. Validate the detailed model of the complete system by comparison with the measured responses.

4. Reduce the detailed model to fit the standard model applicable to the specific type of excitation system using techniques of classical control theory. Validate the responses of the reduced model against the measured responses.

The above procedure is quite involved and time-consuming for the older slow-response exciter. For a high-response excitation system, frequency response tests are usually not required as the number of time constants within the major feedback loop is small. For static excitation systems, model parameters can usually be obtained from design data; field tests are required only for verification.

Techniques for field testing, performance verification and model development of excitation systems are described in references 3, 7, and 36.

REFERENCES

[1] IEEE Committee Report, "Computer Representation of Excitation Systems," *IEEE Trans.*, Vol. PAS-87, pp. 1460-1464, June 1968.

[2] IEEE Committee Report, "Proposed Excitation System Definitions for Synchronous Machines," *IEEE Trans.*, Vol. PAS-88, pp. 1248-1258, August 1969.

[3] IEEE Committee Report, "Excitation System Dynamic Characteristics," *IEEE Trans.*, Vol. PAS-92, pp. 64-75, January/February 1973.

[4] IEEE Committee Report, "Excitation System Models for Power System Stability Studies," *IEEE Trans.*, Vol. PAS-100, pp. 494-509, February 1981.

[5] *IEEE Standard Definitions for Excitation Systems for Synchronous Machines*, IEEE Standard 421.1-1986.

[6] *IEEE Guide for the Preparation of Excitation System Specifications*, IEEE Standard 421.4-1987.

[7] *IEEE Guide for Identification, Testing and Evaluation of the Dynamic Performance of Excitation Control Systems*, IEEE Standard 421.2-1990 (revision to IEEE Standard 421A-1978).

[8] *IEEE Recommended Practice for Excitation System Models for Power System Stability Studies*, IEEE Standard 421.5-1992.

[9] *Guide to the Characteristics, Performance, and Hardware Requirements in the Specification of Excitation Systems*, Report of the Governor and Excitation Control System Committee of the Canadian Electrical Association, 1982.

[10] Westinghouse Electric Corporation, *Electric Transmission and Distribution Reference Book,* East Pittsburgh, Pa., 1964.

[11] E.W. Kimbark, *Power System Stability, Vol. III: Synchronous Machines,* John Wiley & Sons, 1956.

[12] A.E. Fitzgerald and C. Kingsley, *Electric Machinery,* Second Edition, McGraw-Hill, 1961.

[13] T.L. Dillman, J.W. Skooglund, F.W. Keay, W.H. South, and C. Raczkowski, "A High Initial Response Brushless Excitation System," *IEEE Trans.*, Vol.

PAS-90, pp. 2089-2094, September/October 1971.

[14] J.S. Bishop, D.H. Miller, and A.C. Shartrand, "Experience with ALTERREX Excitation for Large Turbine-Generators," Paper presented at the Joint IEEE/ASME Power Conference, Miami Beach, September 15-19, 1974.

[15] R.K. Gerlitz, R.E. Gorman, and M. Temoshok, "The GENERREX Excitation System for Large Steam Turbine-Generators," Paper GE3-3003, Pacific Coast Electric Association Engineering and Operation Conference, Culver City, Calif., March 20-21, 1975.

[16] P.H. Beagles, K. Carlsen, M.L. Crenshaw, and M. Temoshok, "Generator and Power System Performance with the GENERREX Excitation System," *IEEE Trans.,* Vol. PAS-95, pp. 489-493, March/April 1976.

[17] H.M. Rustebakke (editor), *Electric Utility Systems and Practices,* John Wiley & Sons, 1983.

[18] F. Peneder and R. Bertschi, "Static Excitation Systems with and without a Compounding Ancillary," *Brown Boveri Review* 7-85, pp. 343-348.

[19] D.C. Lee and P. Kundur, "Advanced Excitation Controls for Power System Stability Enhancement," CIGRE Paper 38-01, Paris, France, 1986.

[20] *IEEE Standard Dictionary of Electrical and Electronics Terms* (ANSI), IEEE Standard 100-1988.

[21] P. Kundur, M. Klein, G.J. Rogers, and M.S. Zywno, "Application of Power System Stabilizers for Enhancement of Overall System Stability," *IEEE Trans.*, Vol. PWRS-4, No. 2, pp. 614-626, May 1989.

[22] A.S. Rubenstein and W.W. Walkley, "Control of Reactive kVA with Modern Amplidyne Voltage Regulators," *AIEE Trans.,* Part III, pp. 961-970, December 1957.

[23] A.S. Rubenstein and M. Temoshok, "Underexcited Reactive Ampere Limit for Modern Amplidyne Voltage Regulator," *AIEE Trans.,* Vol. PAS-73, pp. 1433-1438, December 1954.

[24] J.T. Carleton, P.O. Bobo, and D.A. Burt, "Minimum Excitation Limit for Magnetic Amplifier Regulating System," *AIEE Trans.,* Vol. PAS-73, pp. 869-874, August 1954.

[25] I. Nagy, "Analysis of Minimum Excitation Limits of Synchronous Machines,"

IEEE Trans., Vol. PAS-89, No. 6, pp. 1001-1008, July/August 1970.

[26] J.R. Ribeiro, "Minimum Excitation Limiter Effects on Generator Response to System Disturbances," *IEEE Trans. on Energy Conversion*, Vol. 6, No. 1, pp. 29-38, March 1991.

[27] Discussion of reference 26 by D.C. Lee, R.E. Beaulieu, P. Kundur, and G.J. Rogers.

[28] M.S. Baldwin and D.P. McFadden, "Power Systems Performance as Affected by Turbine-Generator Controls Response during Frequency Disturbances," *IEEE Trans.,* Vol. PAS-100, pp. 2486-2494, May 1981.

[29] General Electric Instructions GEK-15014C, *Inverse Time Maximum Excitation Limit.*

[30] P. Kundur and P.L. Dandeno, "Implementation of Synchronous Machine Models into Power System Stability Programs," *IEEE Trans.,* Vol. PAS-102, pp. 2047-2054, July 1983.

[31] *IEEE Guide: Test Procedures for Synchronous Machines*, IEEE Standard 115-1983.

[32] R.W. Ferguson, H. Herbst, and R.W. Miller, "Analytical Studies of the Brushless Excitation System," *AIEE Trans.,* Part III, pp. 961-970, 1957.

[33] R.L. Witzke, J.V. Kresser, and J.K. Dillard, "Influence of AC Reactance on Voltage Regulation of 6-Phase Rectifiers," *AIEE Trans.,* Vol. 72, pp. 244-253, July 1953.

[34] L.L. Freris, "Analysis of a Hybrid Bridge Rectifier," *Direct Current*, pp. 22-23, February 1966.

[35] IEEE Task Force, "Conventions for Block Diagram Representations," *IEEE Trans.,* Vol. PWRS-1, No. 3, pp. 95-100, August 1986.

[36] IEEE Tutorial Course Text, "Power System Stabilization via Excitation Control - Chapter IV: Field Testing Techniques," Publication 81 EHO 175-0 PWR.

Chapter 9

Prime Movers and Energy Supply Systems

The prime sources of electrical energy supplied by utilities are the kinetic energy of water and the thermal energy derived from fossil fuels and nuclear fission. The prime movers convert these sources of energy into mechanical energy that is, in turn, converted to electrical energy by synchronous generators. The prime mover governing systems provide a means of controlling power and frequency, a function commonly referred to as load-frequency control or automatic generation control (AGC). Figure 9.1 portrays the functional relationship between the basic elements associated with power generation and control.

This chapter examines the characteristics of prime movers and energy supply systems and develops appropriate models suitable for their representation in power system dynamic studies. The principles and implementation of automatic generation control are described in Chapter 11.

The focus here is on those characteristics of the power plants that impact on the overall performance of the power system, and not on a detailed study of the associated processes.

9.1 HYDRAULIC TURBINES AND GOVERNING SYSTEMS

Hydraulic turbines are of two basic types: impulse turbines and reaction turbines. They are briefly described here; the reader may refer to reference 1 for a more detailed description.

The *impulse-type turbine* (also known as Pelton wheel) is used for high heads - 300 metres or more. The runner is at atmospheric pressure, and the whole of the

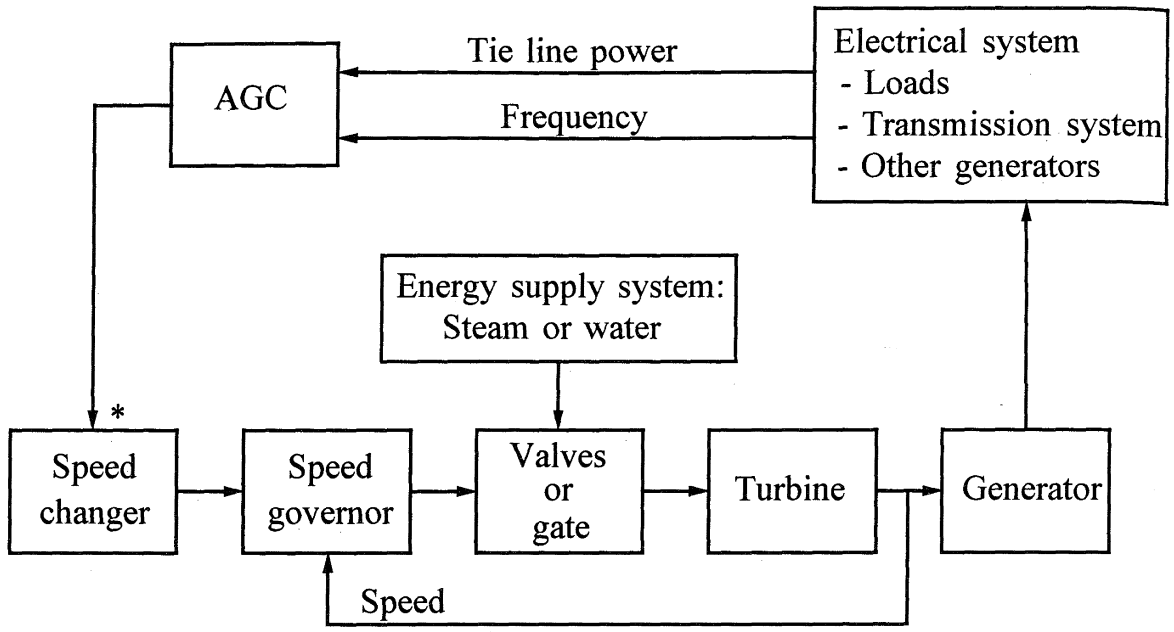

* AGC applied only to selected units

Figure 9.1 Functional block diagram of power generation and control system

pressure drop takes place in stationary nozzles that convert potential energy to kinetic energy. The high-velocity jets of water impinge on spoon-shaped buckets on the runner, which deflect the water axially through about 160°; the change in momentum provides the torque to drive the runner, the energy supplied being entirely kinetic.

In a *reaction turbine* the pressure within the turbine is above atmospheric; the energy is supplied by the water in both kinetic and potential (pressure head) forms. The water first passes from a spiral casing through stationary radial guide vanes and gates around its entire periphery. The gates control water flow. There are two subcategories of reaction turbines: Francis and propeller.

The *Francis turbine* is used for heads up to 360 metres. In this type of turbine, water flows through guide vanes impacting on the runner tangentially and exiting axially.

The *propeller turbine*, as the name implies, uses propeller-type wheels. It is for use on low heads - up to 45 metres. Either fixed blades or variable-pitch blades may be used. The variable-pitch blade propeller turbine, commonly known as the *Kaplan wheel*, has high efficiency at all loads.

The performance of a hydraulic turbine is influenced by the characteristics of the water column feeding the turbine; these include the effects of water inertia, water compressibility, and pipe wall elasticity in the penstock. The effect of water inertia is to cause changes in turbine flow to lag behind changes in turbine gate opening. The effect of elasticity is to cause travelling waves of pressure and flow in the pipe; this phenomenon is commonly referred to as "water hammer." For a detailed analysis of hydraulic transients the reader may refer to references 2 and 3.

Precise modelling of hydraulic turbines requires inclusion of transmission-line-like reflections which occur in the elastic-walled pipe carrying compressible fluid. Typically, the speed of propagation of such travelling waves is about 1200 metres per second. Therefore, travelling wave models may be required only if penstocks are long.

In what follows, we will first develop models of the hydraulic turbine and penstock system without travelling wave effects and assuming that there is no surge tank. We will then identify special governing requirements of hydraulic turbines. Finally, we will extend the model to include the effects of water hammer and surge tank.

9.1.1 Hydraulic Turbine Transfer Function [4-9]

The representation of the hydraulic turbine and water column in stability studies is usually based on the following assumptions:

1. The hydraulic resistance is negligible.
2. The penstock pipe is inelastic and the water is incompressible.
3. The velocity of the water varies directly with the gate opening and with the square root of the net head.
4. The turbine output power is proportional to the product of head and volume flow.

The essential elements of the hydraulic plant are depicted in Figure 9.2.

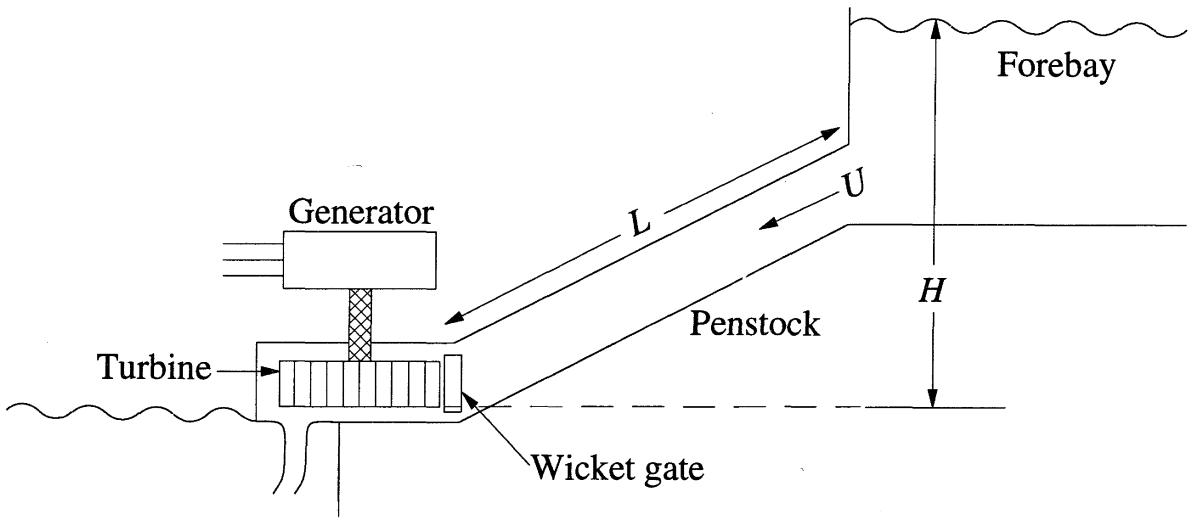

Figure 9.2 Schematic of a hydroelectric plant

The turbine and penstock characteristics are determined by three basic equations relating to the following:

(a) Velocity of water in the penstock
(b) Turbine mechanical power
(c) Acceleration of water column

The *velocity of the water* in the penstock is given by

$$U = K_u G\sqrt{H} \tag{9.1}$$

where

U = water velocity
G = gate position
H = hydraulic head at gate
K_u = a constant of proportionality

For small displacements about an operating point,

$$\Delta U = \frac{\partial U}{\partial H}\Delta H + \frac{\partial U}{\partial G}\Delta G$$

Substituting the appropriate expressions for the partial derivatives and dividing through by $U_0 = K_u G_0\sqrt{H_0}$ yields

$$\frac{\Delta U}{U_0} = \frac{\Delta H}{2H_0} + \frac{\Delta G}{G_0}$$

or

$$\Delta \bar{U} = \frac{1}{2}\Delta \bar{H} + \Delta \bar{G} \tag{9.2}$$

where the subscript 0 denotes initial steady-state values, the prefix Δ denotes small deviations, and the superbar "–" indicates normalized values based on *steady-state operating values.*

The *turbine mechanical power* is proportional to the product of pressure and flow; hence,

$$P_m = K_p HU \tag{9.3}$$

Linearizing by considering small displacements, and normalizing by dividing both sides by $P_{m0}=K_pH_0U_0$, we have

$$\frac{\Delta P_m}{P_{m0}} = \frac{\Delta H}{H_0} + \frac{\Delta U}{U_0}$$

or

$$\Delta \bar{P}_m = \Delta \bar{H} + \Delta \bar{U} \tag{9.4}$$

Substituting for $\Delta \bar{U}$ from Equation 9.2 yields

$$\Delta \bar{P}_m = 1.5\Delta \bar{H} + \Delta \bar{G} \tag{9.5A}$$

Alternatively, by substituting for ΔH from Equation 9.2, we may write

$$\Delta \bar{P}_m = 3\Delta \bar{U} - 2\Delta \bar{G} \tag{9.5B}$$

The *acceleration of water column* due to a change in head at the turbine, characterized by Newton's second law of motion, may be expressed as

$$(\rho LA)\frac{d\Delta U}{dt} = -A(\rho a_g)\Delta H \tag{9.6}$$

where

L = length of conduit
A = pipe area
ρ = mass density
a_g = acceleration due to gravity
ρLA = mass of water in the conduit
$\rho a_g \Delta H$ = incremental change in pressure at turbine gate
t = time in seconds

By dividing both sides by $A\rho a_g H_0 U_0$, the acceleration equation in normalized form becomes

$$\frac{LU_0}{a_g H_0}\frac{d}{dt}\left(\frac{\Delta U}{U_0}\right) = -\frac{\Delta H}{H_0}$$

or

$$T_w \frac{d\Delta\bar{U}}{dt} = -\Delta\bar{H} \tag{9.7}$$

where by definition,

$$T_w = \frac{LU_0}{a_g H_0} \tag{9.8}$$

Here T_w is referred to as the *water starting time.* It represents the time required for a head H_0 to accelerate the water in the penstock from standstill to the velocity U_0. It should be noted that T_w varies with load. Typically, T_w at full load lies between 0.5 s and 4.0 s.

Equation 9.7 represents an important characteristic of the hydraulic plant. A descriptive explanation of the equation is that if back pressure is applied at the end of the penstock by closing the gate, then the water in the penstock will decelerate. That is, if there is a positive pressure change, there will be a negative acceleration change.

From Equations 9.2 and 9.7, we can express the relationship between change in velocity and change in gate position as

$$T_w \frac{d\Delta\bar{U}}{dt} = 2(\Delta\bar{G} - \Delta\bar{U}) \tag{9.9}$$

Replacing d/dt with the Laplace operator s, we may write

$$T_w s\Delta\bar{U} = 2(\Delta\bar{G} - \Delta\bar{U})$$

or

$$\Delta\bar{U} = \frac{1}{1+\frac{1}{2}T_w s}\Delta\bar{G} \tag{9.10}$$

Substituting for $\Delta\bar{U}$ from Equation 9.5B and rearranging, we obtain

$$\frac{\Delta \bar{P}_m}{\Delta \bar{G}} = \frac{1 - T_w s}{1 + \frac{1}{2} T_w s} \tag{9.11}$$

Equation 9.11 represents the "classical" transfer function of a hydraulic turbine. It shows how the turbine power output changes in response to a change in gate opening for an *ideal lossless* turbine.

Non-ideal turbine

The transfer function of a non-ideal turbine may be obtained by considering the following general expression for perturbed values of water velocity (flow) and turbine power:

$$\Delta \bar{U} = a_{11} \Delta \bar{H} + a_{12} \Delta \bar{\omega} + a_{13} \Delta \bar{G} \tag{9.12}$$

$$\Delta \bar{P}_m = a_{21} \Delta \bar{H} + a_{22} \Delta \bar{\omega} + a_{23} \Delta \bar{G} \tag{9.13}$$

where $\Delta \bar{\omega}$ is the per unit speed deviation. The speed deviations are small, especially when the unit is synchronized to a large system; therefore, the terms related to $\Delta \bar{\omega}$ may be neglected. Consequently,

$$\Delta \bar{U} = a_{11} \Delta \bar{H} + a_{13} \Delta \bar{G} \tag{9.14}$$

$$\Delta \bar{P}_m = a_{21} \Delta \bar{H} + a_{23} \Delta \bar{G} \tag{9.15}$$

The coefficients a_{11} and a_{13} are partial derivatives of flow with respect to head and gate opening, and the coefficients a_{21} and a_{23} are partial derivatives of turbine power output with respect to head and gate opening. These a coefficients depend on machine loading and may be evaluated from the turbine characteristics at the operating point.

With Equations 9.14 and 9.15 replacing Equations 9.2 and 9.5A, the transfer function between $\Delta \bar{P}_m$ and $\Delta \bar{G}$ becomes

$$\frac{\Delta \bar{P}_m}{\Delta \bar{G}} = a_{23} \frac{1 + (a_{11} - a_{13} a_{21} / a_{23}) T_w s}{1 + a_{11} T_w s} \tag{9.16}$$

The a coefficients vary considerably from one turbine type to another. For an ideal lossless Francis type turbine:

$$a_{11} = 0.5, \qquad a_{13} = 1.0, \qquad a_{21} = 1.5, \qquad a_{23} = 1.0$$

Typical measured values of the a coefficients for a 40 MW unit with Francis turbine are as follows [6]:

Load level	a_{11}	a_{13}	a_{21}	a_{23}
100% of rated	0.58	1.1	1.40	1.5
No load	0.57	1.1	1.18	1.5

Special characteristics of hydraulic turbine

The transfer function given by Equation 9.11 or 9.16 represents a "non-minimum phase" system.[1] The special characteristic of the transfer function may be illustrated by considering the response to a step change in gate position.

For a step change in $\bar{G}$, for the ideal turbine, the initial value theorem gives

$$\Delta \bar{P}_m(0) = \lim_{s \to \infty} s \frac{1}{s} \frac{1 - T_w s}{1 + 0.5 T_w s}$$

$$= -2.0$$

and the final value theorem gives

$$\Delta \bar{P}_m(\infty) = \lim_{s \to 0} s \frac{1}{s} \frac{1 - T_w s}{1 + 0.5 T_w s}$$

$$= 1.0$$

---

[1] Systems with poles or zeros in the right half of the s-plane are referred to as non-minimum phase systems; they do not have the minimum amount of phase shift for a given magnitude plot. Such systems cannot be uniquely identified by a knowledge of magnitude versus frequency plot alone.

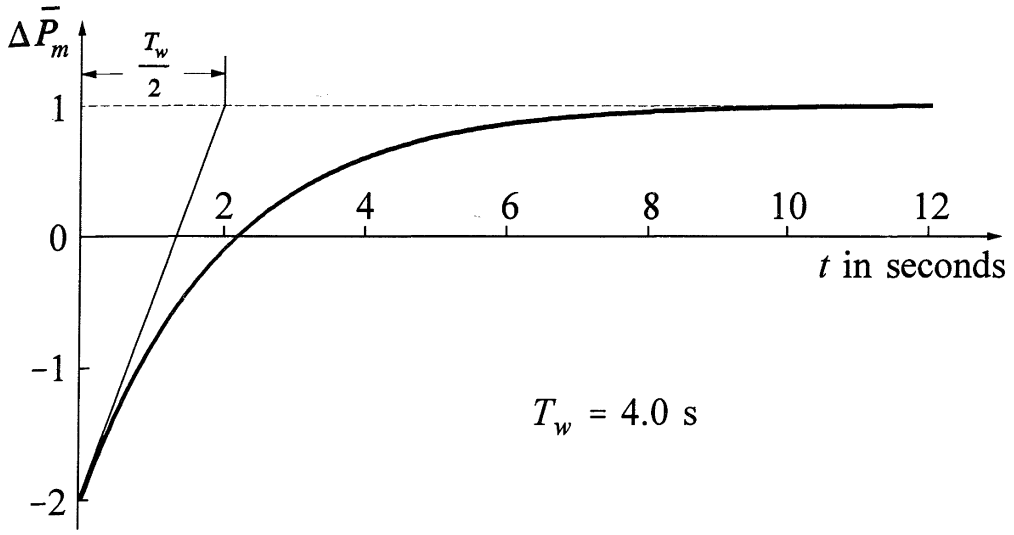

Figure 9.3 Change in turbine mechanical power following a unit step change in gate position

The complete time response is given by

$$\Delta \bar{P}_m(t) = \left[1 - 3e^{-(2/T_w)t}\right] \Delta \bar{G}$$

Figure 9.3 shows a plot of the response of an ideal turbine model with $T_w = 4.0$. Immediately following a unit increase in gate position, the mechanical power actually decreases by 2.0 per unit. It then increases exponentially with a time constant of $T_w/2$ to a steady-state value of 1.0 per unit above the initial steady-state value.

The initial power surge is opposite to that of the direction of change in gate position. This is because, when the gate is suddenly opened, the flow does not change immediately due to water inertia; however, the pressure across the turbine is reduced, causing the power to reduce. With a response determined by T_w, the water accelerates until the flow reaches the new steady value which establishes the new steady-power output.

Figure 9.4 shows the responses of power, head, and water velocity of a hydraulic turbine with $T_w = 1.0$ s when the gate opening is reduced by 0.1 pu by

(a) A step change

(b) A 1-second ramp.

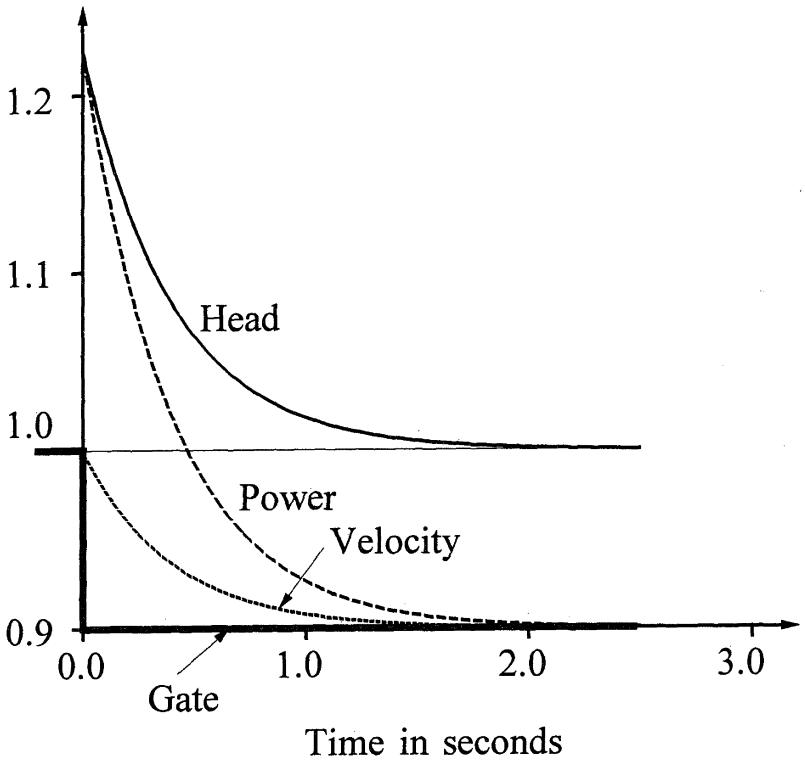

(a) Step reduction in gate opening

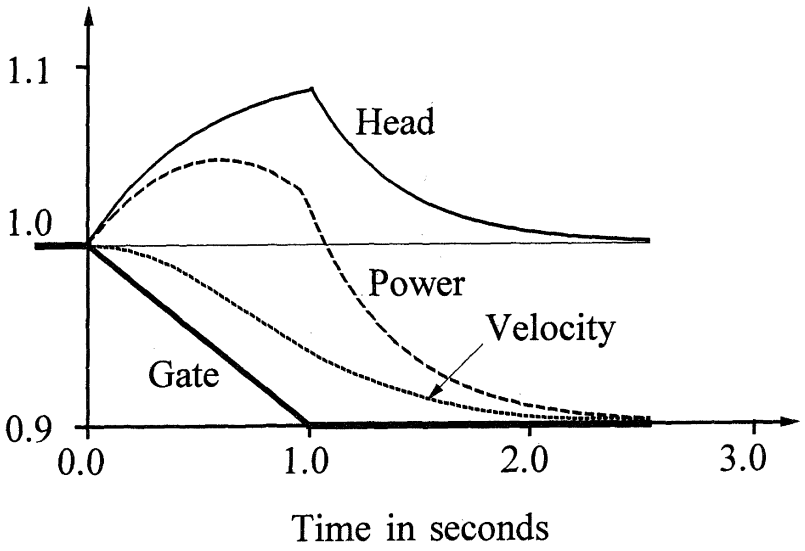

(b) 1-second ramp reduction in gate opening

Figure 9.4 Hydraulic turbine response to a step change and a ramp change in gate position, with initial values of head power, velocity, and gate position equal to 1.0 pu

Electrical analog

In understanding the performance of a hydraulic turbine system, it is useful to visualize a lumped-parameter electrical analog as shown in Figure 9.5. The hydraulic and electrical systems are nearly equivalent, with the water velocity u, gate opening G, and head H, corresponding to the current I, load conductance G, and voltage V, respectively.

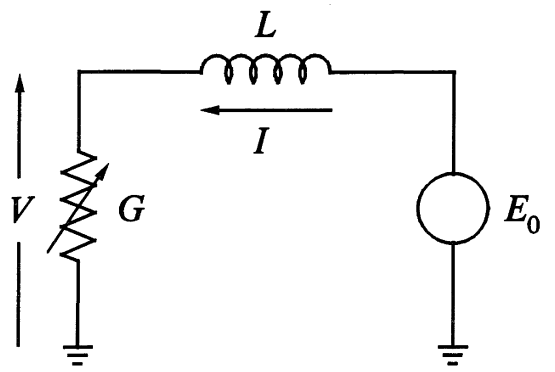

$$I = GV$$

$$\frac{dI}{dt} = \frac{1}{L}(E_0 - V)$$

$$P = VI$$

Figure 9.5 Electrical analog of a hydraulic turbine

When the load is suddenly decreased by a step reduction in conductance G, the current I does not change instantly; however, the voltage across the load suddenly increases because of the reduction in conductance (or increase in resistance). This causes the output power to suddenly increase initially. With a rate determined by the inductance L, the current I decreases exponentially until a new steady value is reached establishing the new steady output power. The responses of I, V, and P are very similar to those of velocity, head, and power shown in Figure 9.4(a) for a step reduction in gate position.

9.1.2 Nonlinear Turbine Model Assuming Inelastic Water Column

The linear model given by Equation 9.16 represents the small-signal performance of the turbine. It is useful for control system tuning using linear analysis techniques (frequency response, root locus, etc.). Because of the simplicity of its structure, this model provides insight into the basic characteristics of the hydraulic system.

In the past, the hydraulic turbine representation in system stability studies was largely based on the transfer function of Equation 9.11 or Equation 9.16 [10]. However, such a model is inadequate for studies involving large variations in power output and frequency [11]. In this section, we describe a nonlinear model which is more appropriate for large-signal time-domain simulations.

Once again we consider a simple hydraulic system configuration with unrestricted head and tail race, and with either a very large or no surge tank.

Assuming a rigid conduit and incompressible fluid, the basic hydrodynamic equations are

$$U = K_u G\sqrt{H} \tag{9.17}$$

$$P = K_P HU \tag{9.18}$$

$$\frac{dU}{dt} = -\frac{a_g}{L}(H-H_0) \tag{9.19}$$

$$Q = AU \tag{9.20}$$

where

U = water velocity
G = ideal gate opening
H = hydraulic head at gate
H_0 = initial steady-state value of H
P = turbine power
Q = water-flow rate
A = pipe area
L = length of conduit
a_g = acceleration due to gravity
t = time in seconds

Since we are interested in the large-signal performance, we normalize the above equations based on *rated values*. Equations 9.17 and 9.18 in normalized form become

$$\frac{U}{U_r} = \frac{G}{G_r}\left(\frac{H}{H_r}\right)^{\frac{1}{2}} \tag{9.21}$$

$$\frac{P}{P_r} = \frac{U}{U_r}\frac{H}{H_r} \tag{9.22}$$

where the subscript r denotes rated values. In per unit notation, the above equations may be written as

$$\bar{U} = \bar{G}(\bar{H})^{1/2} \tag{9.23}$$

$$\bar{P} = \bar{U}\bar{H} \tag{9.24}$$

From Equation 9.23,

$$\bar{H} = \left(\frac{\bar{U}}{\bar{G}}\right)^2 \tag{9.25}$$

Similarly, the per unit form of Equation 9.19 is

$$\frac{d}{dt}\left(\frac{U}{U_r}\right) = -\frac{a_g}{L}\frac{H_r}{U_r}\left(\frac{H}{H_r} - \frac{H_0}{H_r}\right)$$

or

$$\frac{d\bar{U}}{dt} = -\frac{1}{T_W}(\bar{H} - \bar{H}_0) \tag{9.26A}$$

or in Laplace notation

$$\frac{\bar{U}}{\bar{H} - \bar{H}_0} = \frac{-1}{T_W s} \tag{9.26B}$$

where T_W is the *water starting time at rated load.*[1] It has a fixed value for a given turbine-penstock unit and is given by

$$T_W = \frac{LU_r}{a_g H_r} = \frac{LQ_r}{a_g A H_r} \tag{9.27}$$

The mechanical power output P_m is

$$P_m = P - P_L \tag{9.28}$$

where P_L represents the fixed power loss of the turbine given by

$$P_L = U_{NL} H \tag{9.29}$$

---

[1] From Equations 9.8 and 9.27, the water starting time T_w at any load is related to its value T_W at rated load by

$$T_w = \frac{U_0}{U_r}\frac{H_r}{H_0} T_W$$

with U_{NL} representing the no-load water velocity. In normalized form, we have

$$\frac{P_m}{P_r} = \frac{P}{P_r} - \frac{P_L}{P_r} = \left(\frac{U}{U_r} - \frac{U_{NL}}{U_r}\right)\frac{H}{H_r}$$

or

$$\bar{P}_m = (\bar{U} - \bar{U}_{NL})\bar{H} \tag{9.30}$$

The above equation gives the per unit value of the turbine power output on a base equal to the turbine MW rating. In system stability studies, solution of the machine swing equation requires turbine mechanical torque on a base equal to either the generator MVA rating or a common MVA base. Hence,

$$\bar{T}_m = \left(\frac{\omega_0}{\omega}\right)\bar{P}_m\left(\frac{P_r}{\text{MVA}_{base}}\right) = \frac{1}{\bar{\omega}}(\bar{U} - \bar{U}_{NL})\bar{H}\bar{P}_r \tag{9.31}$$

where

$\bar{\omega}$ = per unit speed

MVA_{base} = base MVA on which turbine torque is to be made per unit

$\bar{P}_r$ = per unit turbine rating = $\dfrac{\text{turbine MW rating}}{\text{MVA}_{base}}$

In the above equations, G is the *ideal gate opening* based on the change from no load to full load being equal to 1 per unit. This is related to the real gate opening g as shown in Figure 9.6. The *real gate opening* is based on the change from the fully closed to the fully open position being equal to 1 per unit [12].

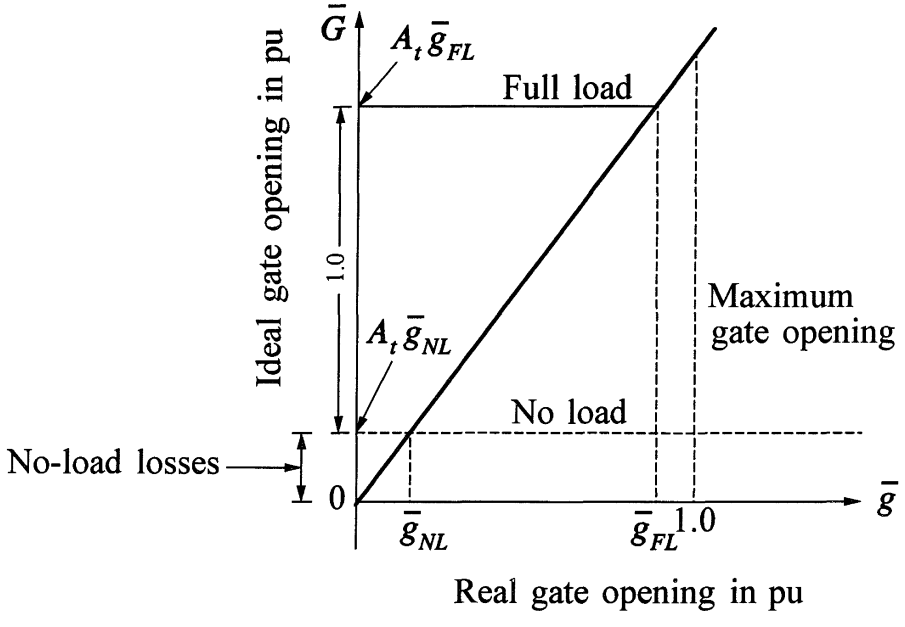

Figure 9.6 Relationship between ideal and real gate openings

The ideal gate opening is related to real gate opening as follows

$$\bar{G} = A_t \bar{g} \tag{9.32}$$

where A_t is the turbine gain given by

$$A_t = \frac{1}{\bar{g}_{FL} - \bar{g}_{NL}} \tag{9.33}$$

Equations 9.25 to 9.27 and 9.31 to 9.33 completely describe the water column and turbine characteristics. These may be represented in block diagram form as shown in Figure 9.7.

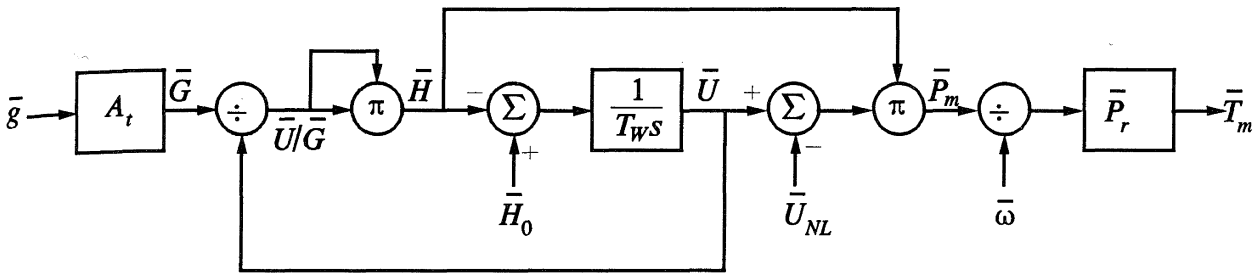

$$A_t = \frac{1}{\bar{g}_{FL} - \bar{g}_{NL}} \qquad \bar{P}_r = \frac{\text{turbine MW rating}}{\text{base MVA}}$$

$$T_W = \frac{L U_r}{a_g H_r} \qquad \bar{U}_{NL} = A_t \bar{g}_{NL} (\bar{H}_0)^{1/2}$$

Sample data:

$$\bar{g}_{FL} = 0.96 \text{ pu} \qquad \bar{g}_{NL} = 0.16 \text{ pu} \qquad T_W = 1.0 \text{ s}$$

Figure 9.7 Hydraulic turbine block diagram assuming inelastic water column

The turbine and penstock model may be rearranged and expressed in terms of two equations, one representing the water column and the other the turbine.

Water column equation:

$$\frac{d\bar{U}}{dt} = -\frac{1}{T_W}(\bar{H} - \bar{H}_0) = -\frac{1}{T_W}\left[\left(\frac{\bar{U}}{A_t \bar{g}}\right)^2 - \bar{H}_0\right] \tag{9.34}$$

Turbine equation:

$$\bar{T}_m = \frac{\bar{U}-\bar{U}_{NL}}{\bar{\omega}}\left(\frac{\bar{U}}{A_t \bar{g}}\right)^2 \bar{P}_r \tag{9.35}$$

From Equation 9.34, by considering the steady-state condition corresponding to no load, we have

$$\bar{U}_{NL} = A_t \bar{g}_{NL}(\bar{H}_0)^{1/2} \tag{9.36}$$

Usually $\bar{H}_0$=1.0.

Example 9.1

The data related to the turbine, penstock, and generator of a hydraulic power plant are as follows:

Generator rating = 140 MVA	Turbine rating = 127.4 MW
Penstock length = 300 m	Piping area = 11.15 m^2
Rated hydraulic head = 165 m	Water-flow rate at rated load = 85 m^3/s
Gate opening at rated load = 0.94 pu	Gate opening at no load = 0.06 pu

(a) Calculate (i) the velocity of water in the penstock, and (ii) water starting time, at full load.

(b) Determine the classical transfer function of the turbine relating the change in power output to change in gate position at rated load.

(c) Determine the nonlinear model of the turbine, assuming an inelastic water column. Identify the values of the parameters and variables of the model at rated output. The turbine mechanical power/torque is to be expressed on a common MVA base of 100.

Solution

(a) (i) Velocity of water in the penstock at rated load is

U_r = flow rate at rated load/piping area

$$= \frac{85 \text{ m}^3/\text{s}}{11.15 \text{ m}^2}$$

$$= 7.62 \text{ m/s}$$

(ii) Water starting time T_W at full load, from Equation 9.27, is

$$T_W = \frac{LU_r}{a_g H_r}$$

$$= \frac{300 \times 7.62}{9.81 \times 165} = 1.41 \text{ s}$$

(b) From Equation 9.11, the classical transfer function of the turbine at rated load is

$$\frac{\text{pu } \Delta P_m}{\text{pu } \Delta G} = \frac{1 - T_W s}{1 + 0.5 T_W s}$$

$$= \frac{1 - 1.41s}{1 + 0.705s}$$

(c) Referring to Figure 9.7, the parameters of the nonlinear turbine model are as follows:

Turbine gain

$$A_t = \frac{1}{\bar{g}_{FL} - \bar{g}_{NL}}$$

$$= \frac{1}{0.94 - 0.06} = 1.136$$

No-load velocity

$$\bar{U}_{NL} = A_t \bar{g}_{NL} \sqrt{\bar{H}_0}$$

$$= 1.136 \times 0.06 \times 1.0$$

$$= 0.068 \text{ pu}$$

The per unit conversion factor is

$$\bar{P}_r = \frac{\text{turbine MW rating}}{\text{MVA}_{base}}$$

$$= \frac{127.4}{100} = 1.274$$

Figure E9.1 shows the turbine model. The values of the variables corresponding to rated output are identified on the model.

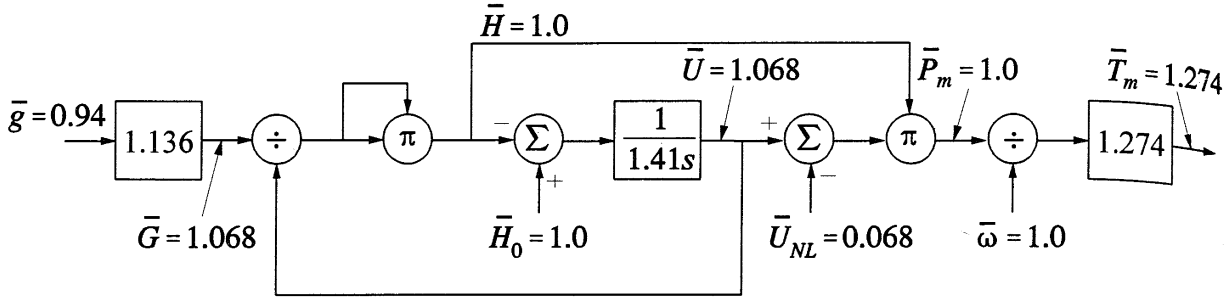

Figure E9.1

9.1.3 Governors for Hydraulic Turbines

The basic function of a governor is to control speed and/or load. The general principles of load/frequency control will be described in Chapter 11. Here, we discuss the special requirements of governing hydraulic turbines, their physical realization and modelling in system studies.

The primary speed/load control function involves feeding back speed error to control the gate position. In order to ensure satisfactory and stable parallel operation of multiple units, the speed governor is provided with a droop characteristic. The purpose of the droop is to ensure equitable load sharing between generating units (see Chapter 11, Section 11.1.1). Typically, the steady-state droop is set at about 5%, such that a speed deviation of 5% causes 100% change in gate position or power output; this corresponds to a gain of 20. For a hydro turbine, however, such a governor with a simple steady-state droop characteristic would be unsatisfactory. This is illustrated in the following example.

Example 9.2

A simplified block diagram representation of the speed control of a hydraulic generating unit feeding an isolated load is shown in Figure E9.2. The turbine is represented by the classical model and the speed governor by pure gain $K_G=1/R$. The generator is represented in terms of the combined inertia of the generator and turbine rotors. (For derivation of the transfer function used see Chapter 3, Section 3.9.)

If T_W=2.0 s, T_M=10.0 s, and K_D=0.0, determine (i) the lowest value of the droop R for which the speed governing is stable, and (ii) the value of R for which the speed control action is critically damped.

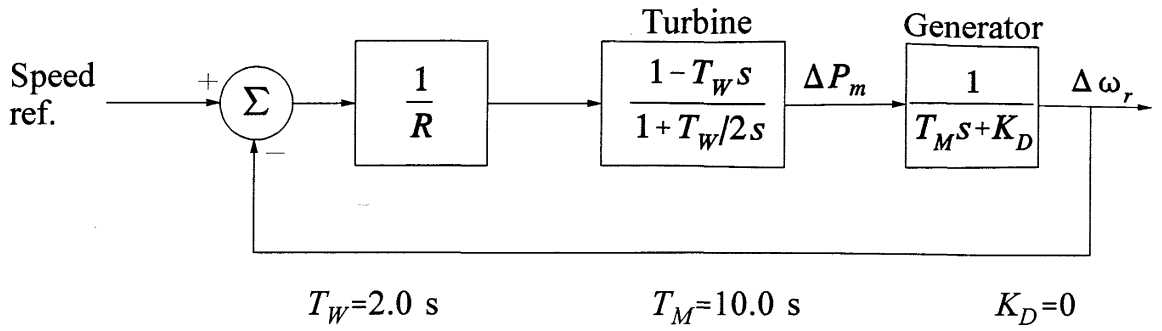

Figure E9.2

Solution

The characteristic equation (of the form $1+GH=0$) of the closed-loop system is

$$1+\frac{1-2s}{1+s}\frac{1}{10s}\frac{1}{R} = 0$$

or

$$10Rs^2+(10R-2)s+1 = 0$$

(i) For stability, the roots of the characteristic equation have to be in the left side of the complex s-plane. In case of a quadratic, a sufficient and necessary condition is that all quadratic coefficients are positive. Hence,

$$10R>0, \quad \text{i.e.,} \quad R>0$$

and

$$10R-2>0, \quad \text{i.e.,} \quad R>0.2$$

The smallest value of R resulting in stable response is thus 0.2 or 20%. In other words, the speed governor gain K_G has to be less than 5. With the standard 5% droop (or gain of 20), the speed control would be unstable.

(ii) For critical damping

$$(10R-2)^2-4(10R) = 0$$

Solving yields

$$R_1 = 0.746 \qquad R_2 = 0.0536$$

with $R_1=0.746$ corresponding to the critical damping (damping ratio $\zeta=1$) and stable response. And $R_2=0.0536$ is less than the limiting value of 0.2; it corresponds to $\zeta=-1.0$ and represents unstable operation. Therefore, $R=0.746$ or gain $K_G=1.34$ is required for critical damping. ■

Requirement for a transient droop

As discussed in Section 9.1.1, hydro turbines have a peculiar response due to water inertia: a change in gate position produces an initial turbine power change which is opposite to that sought. For stable control performance, a large transient (temporary) droop with a long resetting time is therefore required. This is accomplished by the provision of a rate feedback or transient gain reduction compensation as shown in Figure 9.8. The rate feedback retards or limits the gate movement until the water flow and power output have time to catch up. The result is a governor which exhibits a high droop (low gain) for fast speed deviations, and the normal low droop (high gain) in the steady state. Example 9.3 illustrates the effect of the transient droop compensation on the stability characteristics of the governing system.

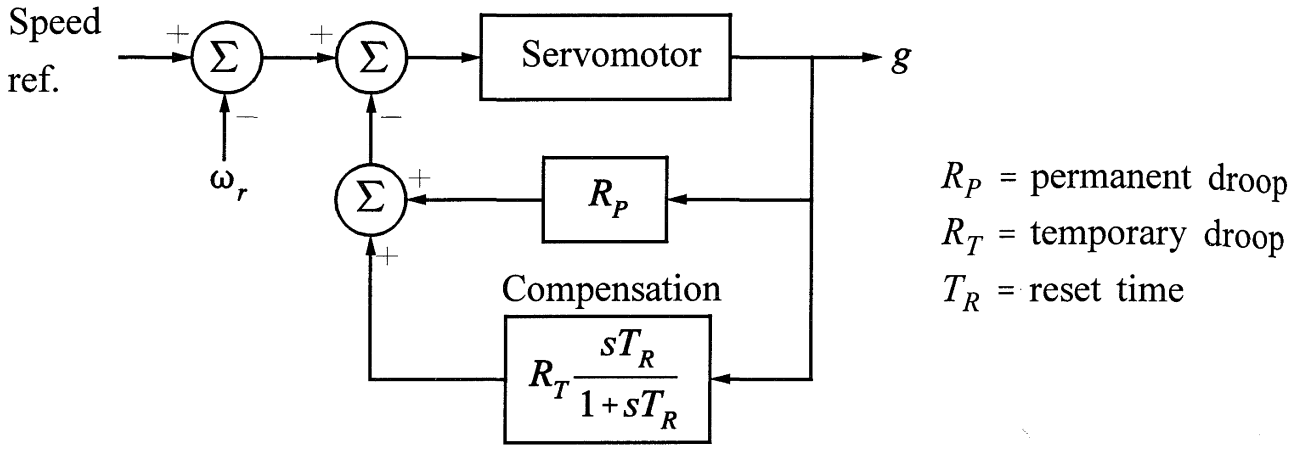

Figure 9.8 Governor with transient droop compensation

Mechanical-hydraulic governor

On older units the governing function is realized using mechanical and hydraulic components. Figure 9.9 shows a simplified schematic of a mechanical-hydraulic governor. Speed sensing, permanent droop feedback, and computing functions are achieved through mechanical components; functions involving higher power are achieved through hydraulic components. A dashpot is used to provide transient droop compensation. A bypass arrangement is usually provided to disable the dashpot if so desired.

The transfer function of the relay valve and gate servomotor is

$$\frac{g}{a} = \frac{K_1}{s} \tag{9.37}$$

The transfer function of the pilot valve and pilot servo is

$$\frac{a}{b} = \frac{K_2}{1+sT_P} \tag{9.38}$$

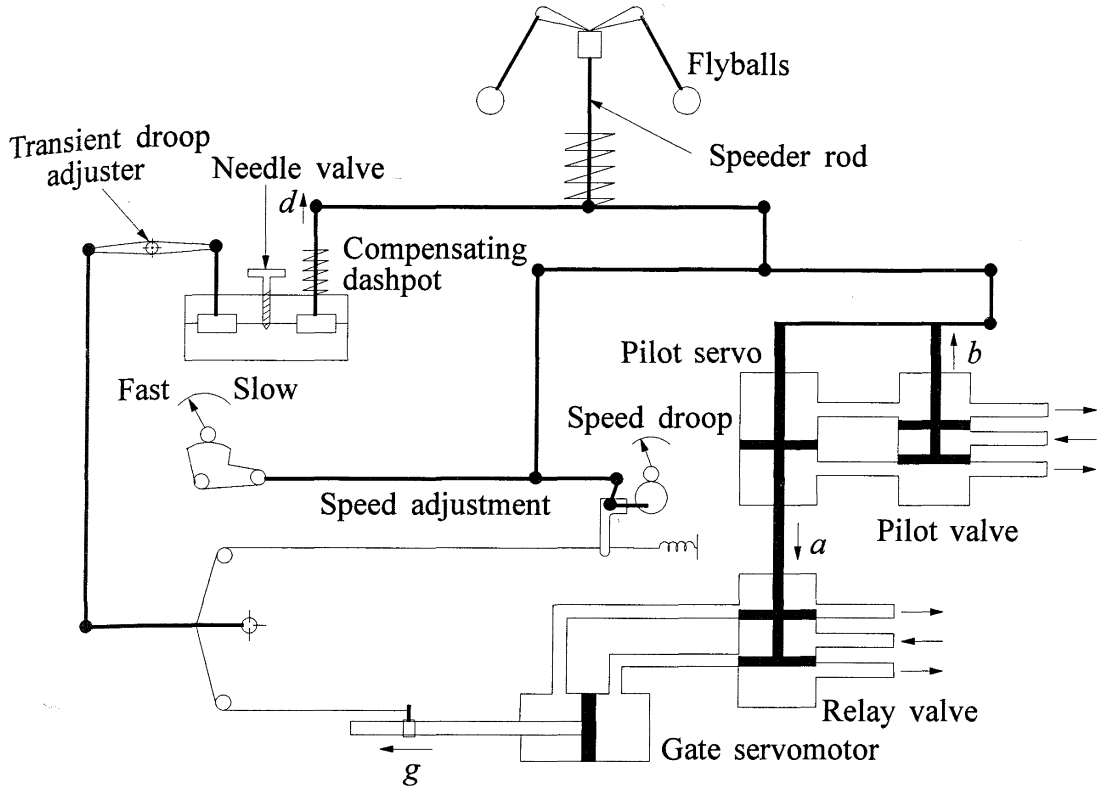

Figure 9.9 Schematic of a mechanical-hydraulic governor for a hydro turbine

where K_2 is determined by the feedback lever ratio, and T_P by port areas of the pilot valve and K_2 [9]. Combining Equations 9.37 and 9.38 yields

$$\frac{g}{b} = \frac{K_1 K_2}{s(1+sT_P)} = \frac{K_s}{s(1+sT_P)} \tag{9.39}$$

where K_s is the servo gain and T_P is the pilot valve/servomotor time constant. The servo gain K_s is determined by the pilot valve feedback lever ratio.

Assuming that the dashpot fluid flow through the needle valve is proportional to the dashpot pressure, the dashpot transfer function is

$$\frac{d}{g} = R_T \frac{sT_R}{1+sT_R} \tag{9.40}$$

The temporary droop R_T is determined by the lever ratio, and the reset or washout time T_R is determined by the needle valve setting.

Water is not a very compressible fluid; if the gate is closed too rapidly, the resulting pressure could burst the penstock. Consequently, the gate movement is rate limited. Often, the rate of gate movement is limited even further in the buffer region near full closure to provide cushioning.

A block diagram representation of the governing system suitable for system stability studies is shown in Figure 9.10. This diagram together with the diagram of

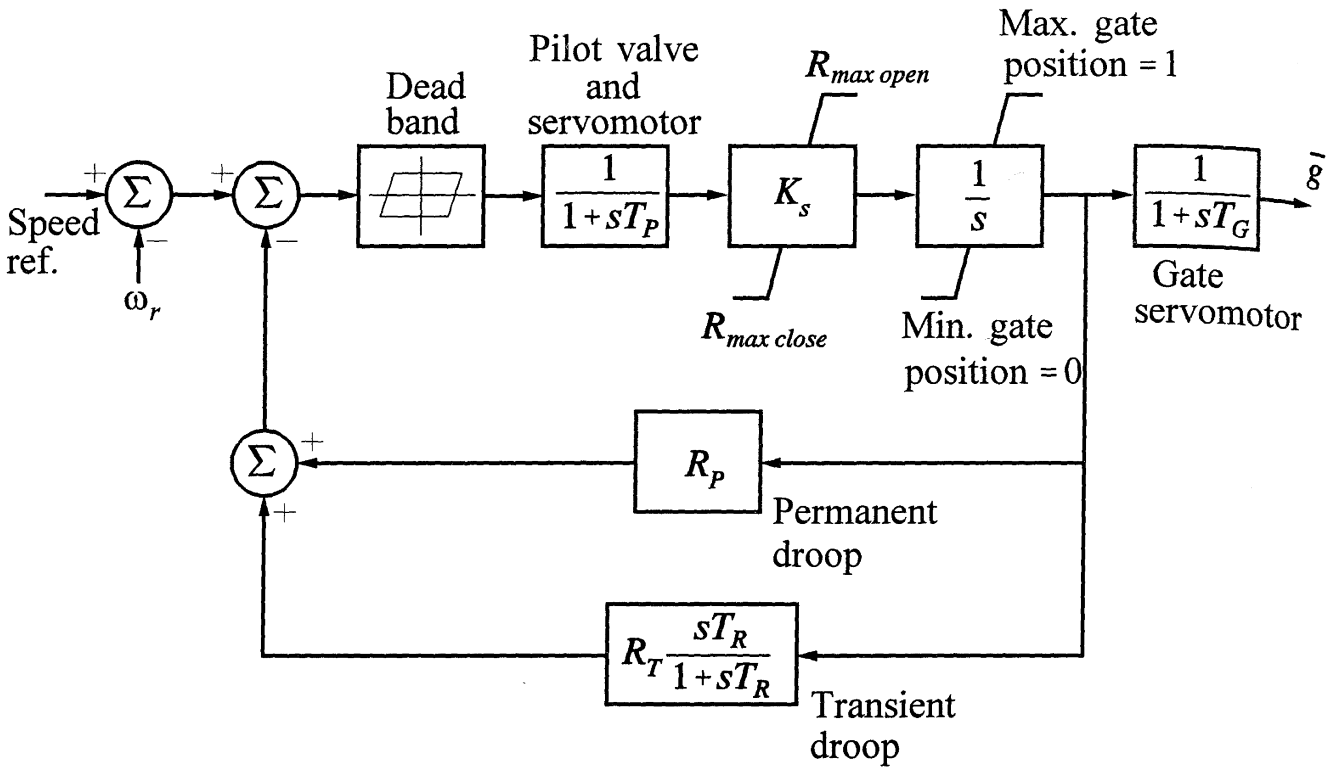

Parameters:		Sample data
T_P	= pilot valve and servomotor time constant	0.05 s
K_s	= servo gain	5.0
T_G	= main servo time constant	0.2 s
R_P	= permanent droop	0.04
R_T	= temporary droop	0.4
T_R	= reset time	5.0 s

Constraints:

Maximum gate position limit = 1.0		
Minimum gate position limit = 0		
$R_{max\ open}$	= maximum gate opening rate	0.16 pu/s
$R_{max\ close}$	= maximum gate closing rate	0.16 pu/s
$R_{max\ buff}$	= maximum gate closing rate in buffered region	0.04 pu/s
g_{buff}	= buffered region in pu of servomotor stroke	0.08 pu

Figure 9.10 Model of governors for hydraulic turbines

Figure 9.7 provides a complete model of the hydraulic turbine and speed-governing system.

The governor model shown in Figure 9.10 has provision for representing the effects of dead bands. However, it is usually difficult to get data that identify their magnitudes and locations. Consequently, dead-band effects are not usually modelled in system studies.

Electrohydraulic governor

Modern speed governors for hydraulic turbines use electrohydraulic systems. Functionally, their operation is very similar to that of mechanical-hydraulic governors. Speed sensing, permanent droop, temporary droop, and other measuring and computing functions are performed electrically. The electric components provide greater flexibility and improved performance with regard to dead bands and time lags. The dynamic characteristics of electric governors are usually adjusted to be essentially similar to those of the mechanical-hydraulic governors.

Tuning of speed-governing systems

The basis for selection of hydraulic turbine governor settings is covered in references 7, 13, and 14. We will review this briefly here and discuss it in detail in Chapter 16.

There are two important considerations in the selection of governor settings:

1. Stable operation during system-islanding conditions or isolated operation; and
2. Acceptable speed of response for loading and unloading under normal synchronous operation.

For stable operation under islanding conditions, the optimum choice of the temporary droop R_T and reset time T_R is related to the water starting time T_W and mechanical starting time $T_M=2H$ (see Chapter 3, Section 3.9.3) as follows [14]:

$$R_T = [2.3-(T_W-1.0)0.15]\frac{T_W}{T_M} \tag{9.41}$$

$$T_R = [5.0-(T_W-1.0)0.5]T_W \tag{9.42}$$

In addition, the servosystem gain K_s should be set as high as is practically possible. The above settings ensure good stable performance when the unit is at full load supplying an isolated load. This represents the most severe requirement and ensures stable operation for all situations involving system islanding.

For loading and unloading during normal interconnected system operation, the above settings result in too slow a response. For satisfactory loading rates, the reset time T_R should be less than 1.0 s, preferably close to 0.5 s.

The above conflicting requirements may be met by using the dashpot bypass arrangement as follows:

- With the dashpot not bypassed, the settings satisfy the requirements for system-islanding conditions or isolated operation.
- With the dashpot bypassed, the reset time T_R has a reduced value, resulting in acceptable loading rates.

The dashpot is normally not bypassed, so that in the event of a disturbance leading to an islanding operation, the speed control would be stable. The dashpot is bypassed for brief periods during loading and unloading.

Example 9.3

Figure E9.3 shows the block diagram of the speed-governing system of a hydraulic unit supplying an isolated load. The speed governor representation includes a transient droop compensation $G_c(s)$ and a governor time constant T_G of 0.5 s. (Such a representation may be readily shown to be a linear approximation to the governor model shown in Figure 9.10, with T_P=0.) The generator is represented by its equation of motion with a mechanical starting time T_M of 10.0 s and a system-damping coefficient of 1.0 per unit.

Examine the stability of the speed-governing system, by considering its open-loop frequency response with

(a) No transient droop compensation, i.e., $G_c(s)=1$
(b) A transient droop compensation having the transfer function

$$G_c(s) = \frac{1+T_R s}{1+(R_T/R_P)T_R s}$$

where T_R and R_T are determined by Equations 9.41 and 9.42.

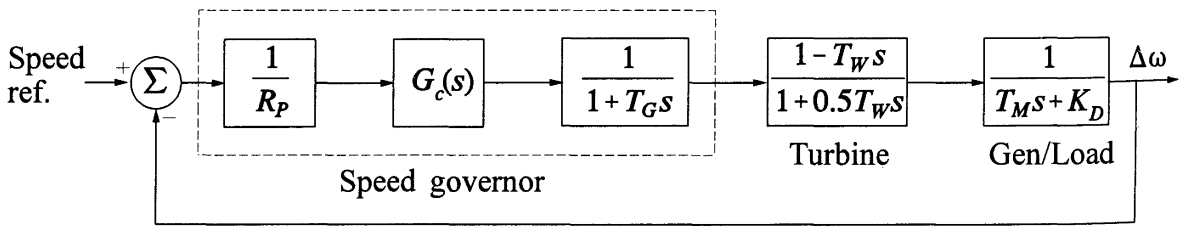

R_P=0.05 T_G=0.5 s T_W=2.0 s T_M=10.0 s K_D=1.0

Figure E9.3 Block diagram of speed-governing system

Solution

(a) *Without transient droop compensation [$G_c(s)$ =1.0]*

The feedback control system of Figure E9.3 has the standard form

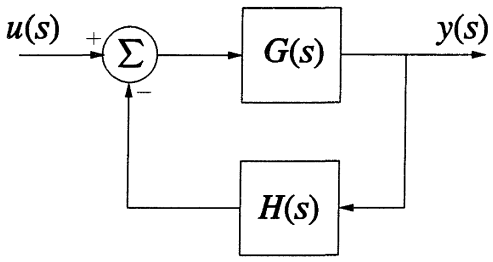

The open-loop transfer function of the system is

$$GH(s) = \frac{20(1-2s)}{(1+0.5s)(1+s)(1+10s)} \tag{E9.1}$$

This system has a zero corresponding to

$$s = 0.5$$

and three poles corresponding to

$$s = -0.1,\ -1.0,\ -2.0$$

The frequency response function for the system is obtained by setting $s=j\omega$ so that

$$GH(j\omega) = \frac{20(1-j2\omega)}{(1+j0.5\omega)(1+j\omega)(1+j10\omega)} \tag{E9.2}$$

The frequency response may be computed using the linear approximation (Bode plot). The corresponding corner frequencies are

$$\omega = 0.1,\ 0.5,\ 1.0,\ 2.0 \quad \text{rad/s}$$

The linear approximation, particularly for the phase plot, tends to be very approximate in this case. We will therefore compute the frequency response accurately, with the magnitude characteristic given by

$$M(\omega) = \frac{20\sqrt{1+4\omega^2}}{\sqrt{1+0.25\omega^2}\sqrt{1+\omega^2}\sqrt{1+100\omega^2}}$$

and the phase characteristic given by

$$\phi(\omega) = -\tan^{-1}2\omega - \tan^{-1}0.5\omega - \tan^{-1}\omega - \tan^{-1}10\omega$$

The magnitude and phase as a function of frequency are plotted in Figure E9.4. We see from the figure that the crossover frequency ω_{c1}, which is the value of ω for which the magnitude is unity (0 dB), is 2.5 rad/s (0.4 Hz). The phase angle at crossover is −290°. The gain and phase margins are

$$G_{m1} = -12 \text{ dB}$$

$$\phi_{m1} = -110°$$

The uncompensated system is hence unstable.

(b) *With transient droop compensation*

From Equations 9.41 and 9.42

$$T_R = [5.0-(2.0-1.0)0.5]2.0 = 9.0 \text{ s}$$

and

$$R_T = [2.3-(2.0-1.0)0.15](2.0/10.0) = 0.43$$

Hence the transfer function of the compensation is

$$G_c(s) = \frac{1+9.0s}{1+(0.43/0.05)9.0s}$$

$$= \frac{1+9.0s}{1+77.4s}$$

This adds a pole at $s=-0.0129$ and a zero at $s=-0.111$. The open-loop frequency response function of the overall system is

$$GH(j\omega) = \frac{20(1-j2\omega)(1+j9\omega)}{(1+j0.5\omega)(1+j\omega)(1+j10\omega)(1+j77.4\omega)}$$

The corresponding magnitude and phase plots are shown in Figure E9.4. The crossover frequency ω_{c2} is 0.25 rad/s and the phase at crossover is −138°. The gain and phase margins are

$$G_{m2} = 6 \text{ dB}$$

$$\phi_{m2} = 42°$$

The compensated system is thus stable and the above values of gain and phase margins are considered good values from the viewpoint of compensator design. A lower value of reset time T_R would increase the crossover frequency, and decrease the gain and phase margins. The net effect would be a more oscillatory but faster control system.

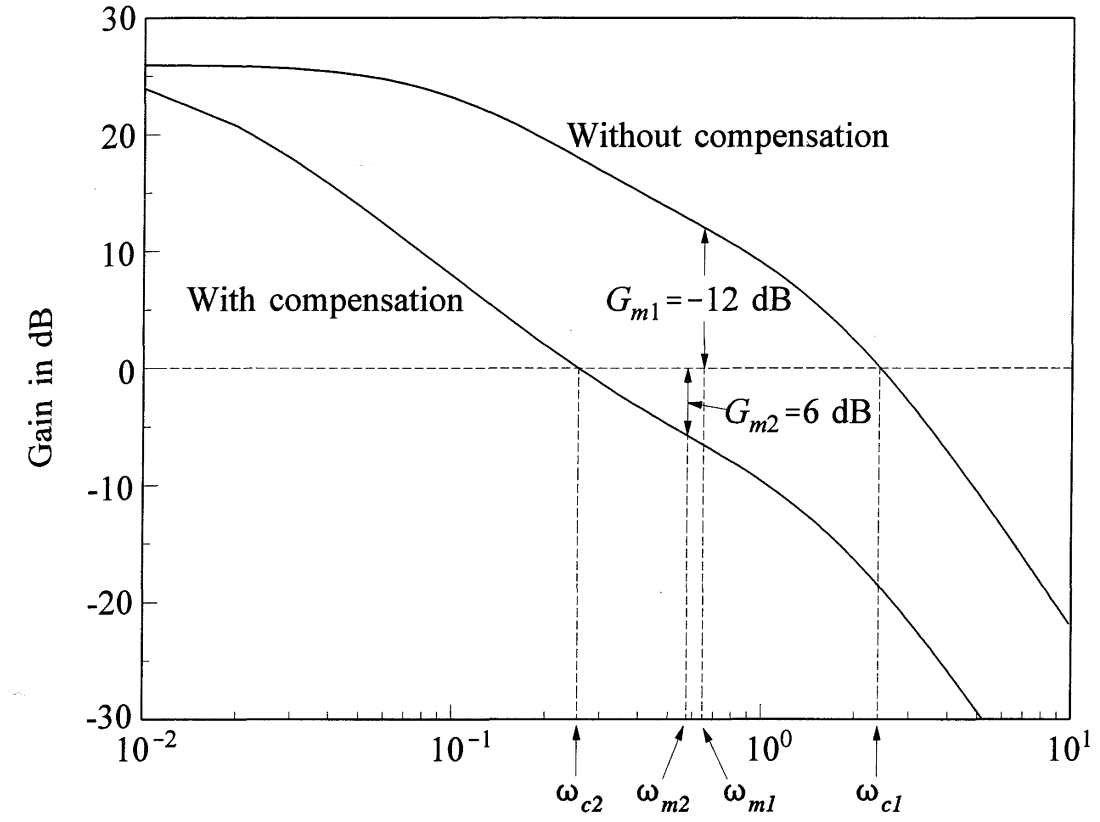

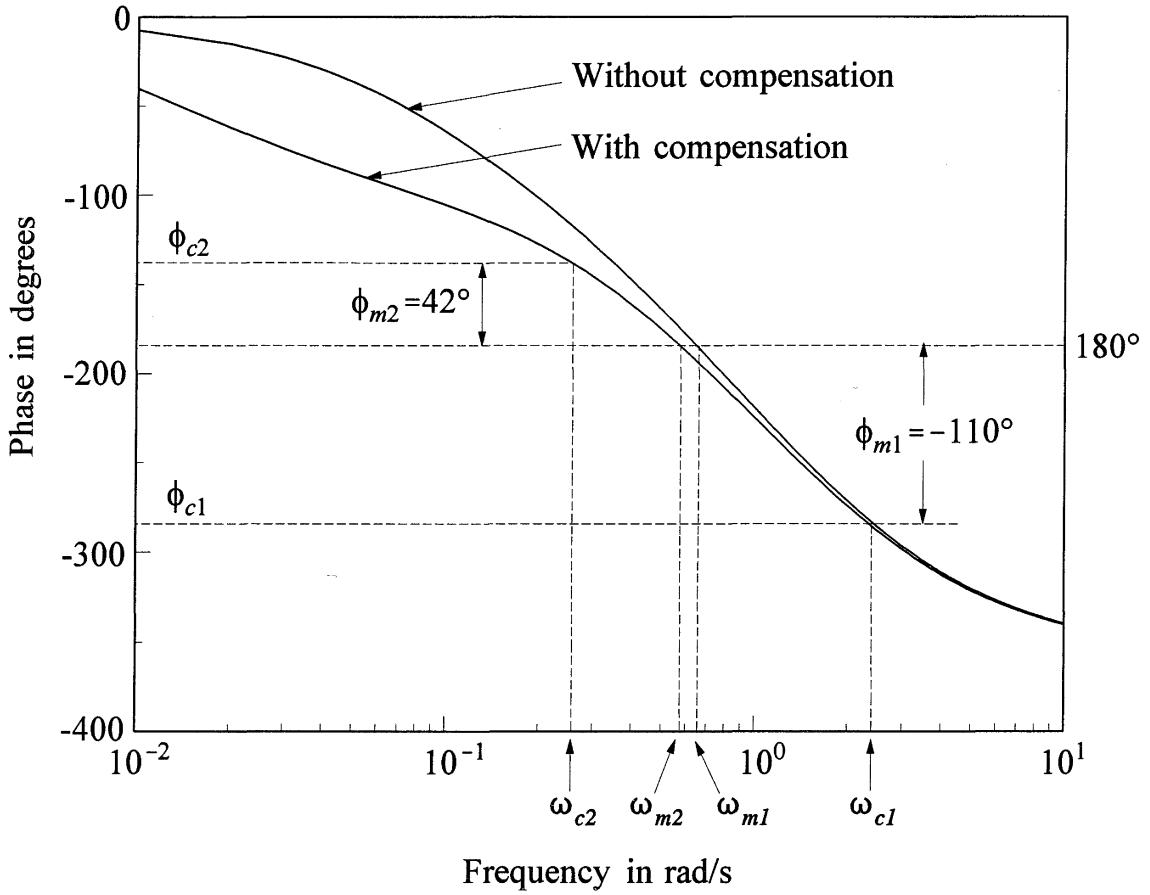

Figure E9.4 Open-loop frequency response characteristics with and without transient droop compensation ■

PID governor [11,15]

Some electrohydraulic governors are provided with three-term controllers with proportional-integral-derivative (PID) action, as shown in Figure 9.11. These allow the possibility of higher response speeds by providing both transient gain reduction and transient gain increase. The derivative action is beneficial for isolated operation, particularly for plants with large water starting time (T_W=3 s or more). Typical values are K_P=3.0, K_I=0.7, and K_D=0.5. However, the use of a high derivative gain or transient gain increase will result in excessive oscillations and possibly instability when the generating unit is strongly connected to an interconnected system. Therefore, the derivative gain is usually set to zero; without the derivative action, the transfer function of a PID (now PI) governor is equivalent to that of the mechanical-hydraulic governor. The proportional and integral gains may be selected to result in the desired temporary droop and reset time.

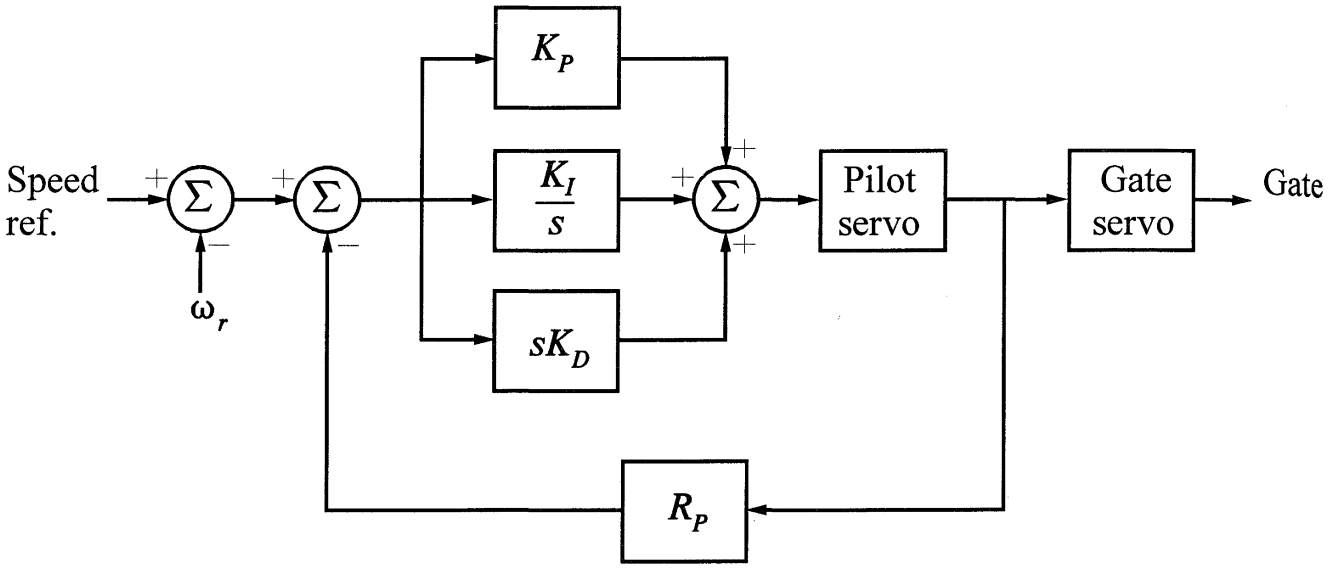

Figure 9.11 PID governor

9.1.4 Detailed Hydraulic System Model

The conventional hydraulic system models developed in Sections 9.1.1 and 9.1.2 neglect the effects of water compressibility and pipe elasticity. In addition, the surge tank, if present, was assumed to be ideal and to isolate the tunnel from the penstock. While these assumptions are valid for a wide range of system studies, there are many applications where a detailed hydraulic system model is necessary to accurately account for the dynamic interaction between the hydraulic system and the power system.

We will first develop the pressure-flow wave equations in a closed conduit and then apply them to derive a detailed model of a hydraulic plant.

Wave equation of flow in a conduit [2,6]

Consider the flow of water through the conduit shown in Figure 9.12(a). When the gate is partially closed suddenly, a pressure wave is set up which moves upstream. A short section of the conduit illustrating the effect of the pressure wave in stretching the conduit walls is shown in Figure 9.12(b). The relationships identified in the figure correspond to the instant when the wave front is at a section of the conduit distance x from the reservoir.

Let the pressure p in the slice Δx increase by Δp. The equation of motion (Newton's second law) of the water in the pipe section is

$$(A\Delta x\,\rho)\frac{dU}{dt} = -A\Delta p \tag{9.43}$$

where ρ = mass density. The change in pressure in terms of change in head is given by

$$\Delta p = \rho a_g \Delta H$$

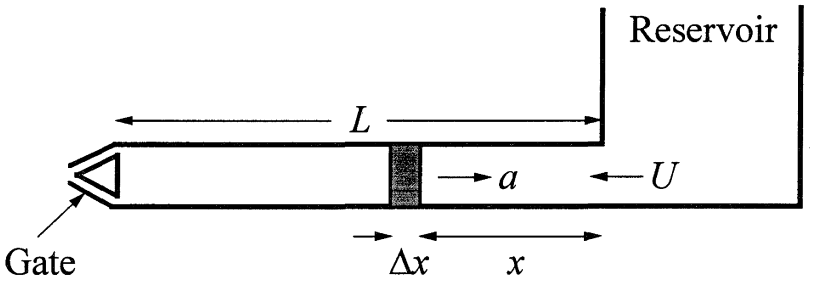

(a) Hydraulic system configuration

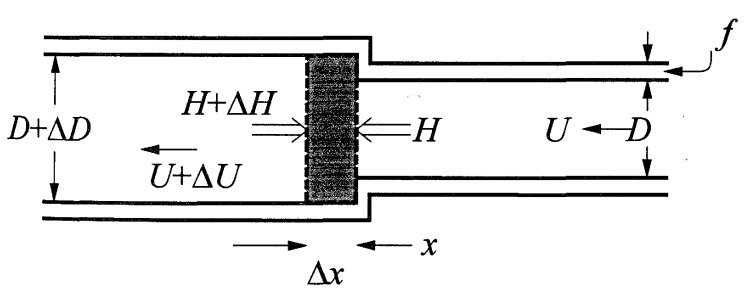

H = total head (static plus water hammer)
U = water velocity
A = area of conduit $= \pi D^2/4$
f = thickness of conduit wall
a = wave velocity

(b) Stretching of the conduit wall at the wave front

Figure 9.12 Water flow through an elastic conduit

where a_g=acceleration due to gravity. By taking infinitesimally small values of Δx, ΔU, and Δt, Equation 9.43 may be written as

$$\boxed{\frac{\partial U}{\partial t} = -a_g \frac{\partial H}{\partial x}} \tag{9.44}$$

The increase in volume due to stretching of the conduit walls is

$$\Delta V_E = \frac{AD\Delta x}{Ef}\Delta p \tag{9.45}$$

where

E = Young's modulus of elasticity of pipe material
f = thickness of pipe wall

The change in volume of water in the section due to compressibility of water is

$$\Delta V_C = \frac{A\Delta x}{K}\Delta p \tag{9.46}$$

where

K = bulk modulus of compression of water

The increase in mass of water in the pipe section due to the combined effects of pipe elasticity and water compressibility is

$$\begin{aligned} \Delta m &= \rho(\Delta V_E + \Delta V_C) \\ &= \rho A \Delta x \left[\frac{1}{K} + \frac{D}{Ef}\right]\Delta p \end{aligned} \tag{9.47}$$

This should be equal to the change in mass of water within the pipe section during the period Δt given by the difference in flow into the section and out of the section as follows:

$$\begin{aligned} \Delta m &= \rho AU\Delta t - \rho(U + \Delta U)A\Delta t \\ &= -\rho A \Delta U \Delta t \end{aligned} \tag{9.48}$$

Equating the expressions for Δm given by Equations 9.47 and 9.48, we have

$$\frac{\Delta U}{\Delta x} = -\left(\frac{1}{K}+\frac{D}{Ef}\right)\frac{\Delta p}{\Delta t} = -\left(\frac{1}{K}+\frac{D}{Ef}\right)\rho a_g \frac{\Delta H}{\Delta t} \tag{9.49}$$

By taking infinitesimally small incremental values, the above equation may be written as

$$\boxed{\frac{\partial U}{\partial x} = -\alpha\frac{\partial H}{\partial t}} \tag{9.50}$$

where

$$\alpha = \rho a_g\left(\frac{1}{K}+\frac{D}{Ef}\right) \tag{9.51}$$

Equations 9.44 and 9.50 are the basic hydraulic equations which determine the flow of a compressible fluid through a uniform elastic pipe, with friction neglected. These equations are similar to the electrical transmission line equations; the fluid velocity U and head H are analogous to the transmission line current and voltage, respectively. These equations may be conveniently solved using Laplace transforms. As shown in reference 6, the solution is given by

$$H_2 = H_1\,\mathrm{sech}(T_e s) - Z_0 Q_2 \tanh(T_e s) \tag{9.52}$$

$$Q_1 = Q_2\cosh(T_e s) + \frac{1}{Z_0}H_2\sinh(T_e s) \tag{9.53}$$

where

T_e = elastic time

$$= \frac{\text{conduit length } L}{\text{wave velocity } a} = \frac{L}{\sqrt{a_g/\alpha}} \tag{9.54}$$

Z_0 = hydraulic surge impedance of the conduit

$$= \frac{\text{wave velocity } a}{Aa_g} = \frac{1}{A\sqrt{a_g\alpha}} \tag{9.55}$$

Q = water flow = AU

and the subscripts 1 and 2 refer to the conditions at the upstream and downstream ends of the conduit, respectively.

Typical values of wave velocity ($a = \sqrt{a_g/\alpha}$) for water are 1220 m/s for steel conduit and 1420 m/s for rock tunnels.

Expressing Equations 9.52 and 9.53 in per unit form with rated head H_r and rated flow Q_r as base values, we obtain

$$\bar{H}_2 = \bar{H}_1 \operatorname{sech}(T_e s) - Z_n \bar{Q}_2 \tanh(T_e s) \tag{9.56}$$

$$\bar{Q}_1 = \bar{Q}_2 \cosh(T_e s) + \frac{1}{Z_n} \bar{H}_2 \sinh(T_e s) \tag{9.57}$$

where Z_n is the normalized value of the hydraulic surge impedance of the conduit given by

$$Z_n = Z_0 \left(\frac{Q_r}{H_r} \right) \tag{9.58}$$

In per unit, water flow is equal to velocity, since

$$\frac{Q}{Q_r} = \frac{AU}{AU_r}$$

Therefore, Equation 9.57 is valid with the per unit flow $\bar{Q}$ replaced by per unit velocity $\bar{U}$.

In the above formulation, friction has been assumed to be negligible. Following the approach used in reference 6, the effect of head loss due to friction may be approximated by modifying Equation 9.56 as follows:

$$\bar{H}_2 = \bar{H}_1 \operatorname{sech}(T_e s) - Z_n \bar{U}_2 \tanh(T_e s) - k_f \bar{U}_2 |\bar{U}_2| \tag{9.59}$$

where k_f is the head loss constant due to friction.

Writing Equations 9.57 and 9.59 in terms of *deviations* of head and velocity from steady-state values, we obtain

$$h_2 = h_1 \operatorname{sech}(T_e s) - Z_n u_2 \tanh(T_e s) - \phi u_2 \tag{9.60}$$

$$u_1 = u_2 \cosh(T_e s) + \frac{1}{Z_n} h_2 \sinh(T_e s) \tag{9.61}$$

where

h = deviation of head $(H - H_0)$ in pu

u = deviation of velocity $(U-U_0)$ in pu
ϕ = friction coefficient $= 2k_f|U_{20}|$
U_{20} = initial steady-state value of downstream velocity U_2

Model of hydraulic plant with no surge tank

Referring to Figure 9.13, for a large reservoir, the deviation in head at the upstream end of the penstock is zero; that is, $h_w = 0$. Therefore, based on Equation 9.60, the expression for turbine head deviation is

$$h_t = -Z_p u_t \tanh(T_{ep}s) - \phi_p u_t \tag{9.62}$$

Consequently the transfer function relating head and flow at the turbine end of the penstock may be written as

$$F(s) = \frac{u_t}{h_t} = \frac{-1}{\phi_p + Z_p \tanh(T_{ep}s)} \tag{9.63}$$

where

Z_p = normalized hydraulic impedance of penstock
ϕ_p = friction coefficient of the penstock
$= 2k_p|U_{t0}|$
T_{ep} = elastic time of penstock

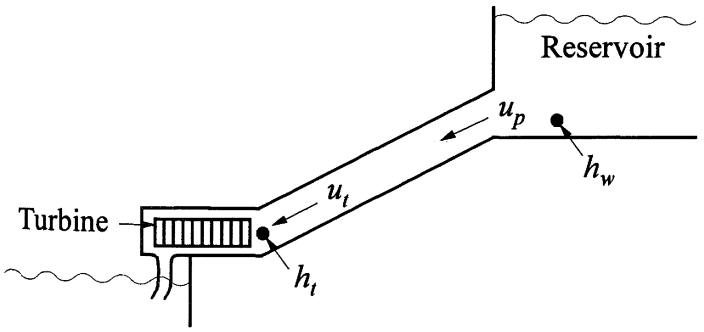

h_t = turbine head deviation
h_w = reservoir head deviation
u_t = turbine velocity deviation
u_p = upper penstock velocity deviation

Figure 9.13 Hydraulic plant with no surge tank

The transfer function $F(s)$ of Equation 9.63 represents a *distributed-parameter system*, with

$$\tanh(T_{ep}s) = \frac{1-e^{-2T_{ep}s}}{1+e^{-2T_{ep}s}} = \frac{sT_{ep}\prod_{n=1}^{n=\infty}\left[1+\left(\frac{sT_{ep}}{n\pi}\right)^2\right]}{\prod_{n=1}^{n=\infty}\left[1+\left(\frac{2sT_{ep}}{(2n-1)\pi}\right)^2\right]} \tag{9.64}$$

The infinite product expansions of Equation 9.64 are required to preserve all the characteristic roots of $F(s)$. However, the transfer function may be approximated by a *lumped-parameter equivalent* by retaining an appropriate number of terms of the expansions, depending on the purpose of the study and the accuracy required [16].

Lumped-parameter approximations

With $n=0$, $\tanh(T_{ep}s)=T_{ep}s$ and

$$F(s) = \frac{-1}{\phi_p + Z_p T_{ep} s} \tag{9.65}$$

From Equations 9.54, 9.55, 9.58, and 9.27, we see that

$$Z_p T_{ep} = \frac{Q_r}{H_r}\frac{L}{Aa_g} = T_{Wp} \tag{9.66}$$

Thus, Z_pT_{ep} is equal to the water starting time T_{Wp} of the penstock at rated load. With friction neglected, $F(s)$ given by Equation 9.65 is the same as Equation 9.26B for u/h derived in Section 9.1.2. The approximation $n=0$ is therefore equivalent to assuming the water column to be inelastic.

With $n=1$, the first pole and zero of the tanh function (representing the fundamental harmonic of the water column) are preserved. The corresponding expression for the transfer function $F(s)$ is

$$F(s) = \frac{-1}{\phi_p + F_2(s)} \tag{9.67}$$

where

$$F_2(s) = Z_p \tanh(T_{ep}s) \approx \frac{sT_{Wp}\left[1+s^2\left(\frac{T_{ep}}{\pi}\right)^2\right]}{\left[1+s^2\left(\frac{2T_{ep}}{\pi}\right)^2\right]} \tag{9.68}$$

For most power system stability studies the above approximation should be adequate.

Example 9.4

The parameters of a penstock are as follows:

Water starting time T_{Wp} = 1.0 s (at full load)
Elastic time T_{ep} = 0.5 s

The head loss due to friction may be neglected. Examine the accuracy of lumped-parameter approximations to the water hammer effects by considering the frequency response characteristics of the $\Delta P_m/\Delta G$ transfer function at full load.

Solution

The normalized hydraulic impedance of the penstock is

$$Z_p = \frac{T_{Wp}}{T_{ep}} = \frac{1.0}{0.5} = 2.0$$

From Equation 9.63, with ϕ_p=0, the water column transfer function is

$$\frac{h_t(s)}{u_t(s)} = -Z_p \tanh(T_{ep}s) = -2.0\tanh(0.5s) \tag{E9.3}$$

Combining the above with Equations 9.2 and 9.5B gives

$$\frac{\Delta P_m(s)}{\Delta G(s)} = \frac{1-Z_p\tanh(T_{ep}s)}{1+\frac{1}{2}Z_p\tanh(T_{ep}s)} = \frac{1.0-2.0\tanh(0.5s)}{1+\tanh(0.5s)} \tag{E9.4}$$

where

$$\tanh(0.5s) = \frac{1-e^{-s}}{1+e^{-s}} = \frac{0.5s\prod_{n=1}^{n=\infty}\left[1+\left(\frac{0.5s}{n\pi}\right)^2\right]}{\prod_{n=1}^{n=\infty}\left[1+\left(\frac{s}{(2n-1)\pi}\right)^2\right]}$$

With $n=0$ (inelastic water column)

$$\frac{\Delta P_m(s)}{\Delta G(s)} = \frac{1.0-s}{1.0+0.5s}$$

This represents the classical transfer function.

Figure E9.5(a) shows the magnitude versus frequency plots of the transfer function $\Delta P_m/\Delta G$ given by Equation E9.4, when $\tanh(0.5s)$ is represented exactly and by approximations corresponding to $n=0$, $n=1$, and $n=2$. The corresponding phase characteristics are shown in Figure E9.5(b). It is seen that the classical model is valid up to about 0.1 Hz. With $n=1$ (i.e., with the fundamental component of the water column represented), the lumped-parameter approximation is valid up to about 1.0 Hz.

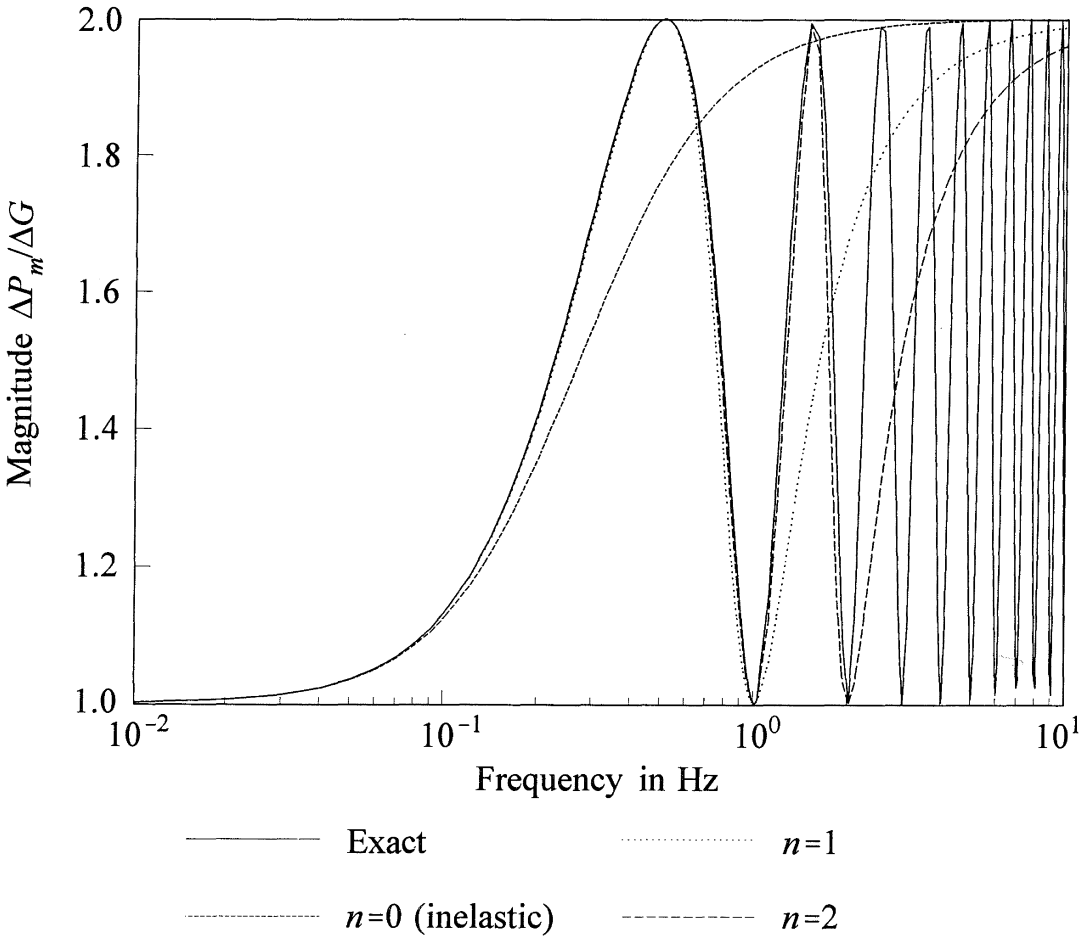

Figure E9.5(a)

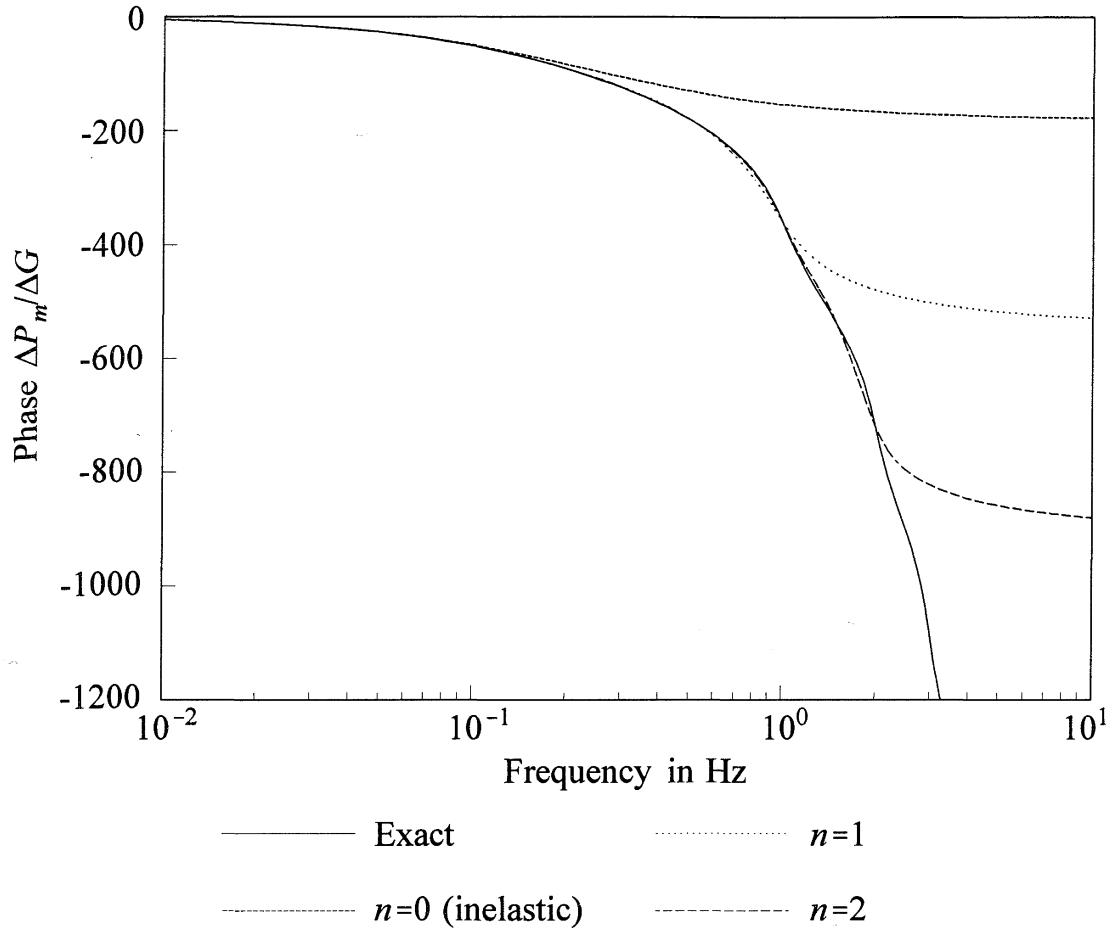

Figure E9.5(b) ■

Model of hydraulic plant with surge tank

A surge tank is sometimes installed near the turbine to reduce the pressure increase which accompanies rapid closure of turbine gates. The kinetic energy of the flowing water in the penstock is converted to potential energy in the surge tank, thus relieving the pressure. A differential surge tank, shown in Figure 9.14, has two compartments: a small area riser connected by orifices to a large area tank. The riser helps suppress water hammer and the tank provides the water storage/supply function.

The following are the equations of the various components of the hydraulic system: tunnel, surge tank, penstock, and the reservoir. All equations are in per unit form. Water velocities and heads are in terms of deviations from steady-state values.

Equation 9.60 applied to the tunnel yields

$$h_r = h_w \text{sech}(T_{ec}s) - Z_c u_c \tanh(T_{ec}s) - \phi_c u_c \tag{9.69}$$

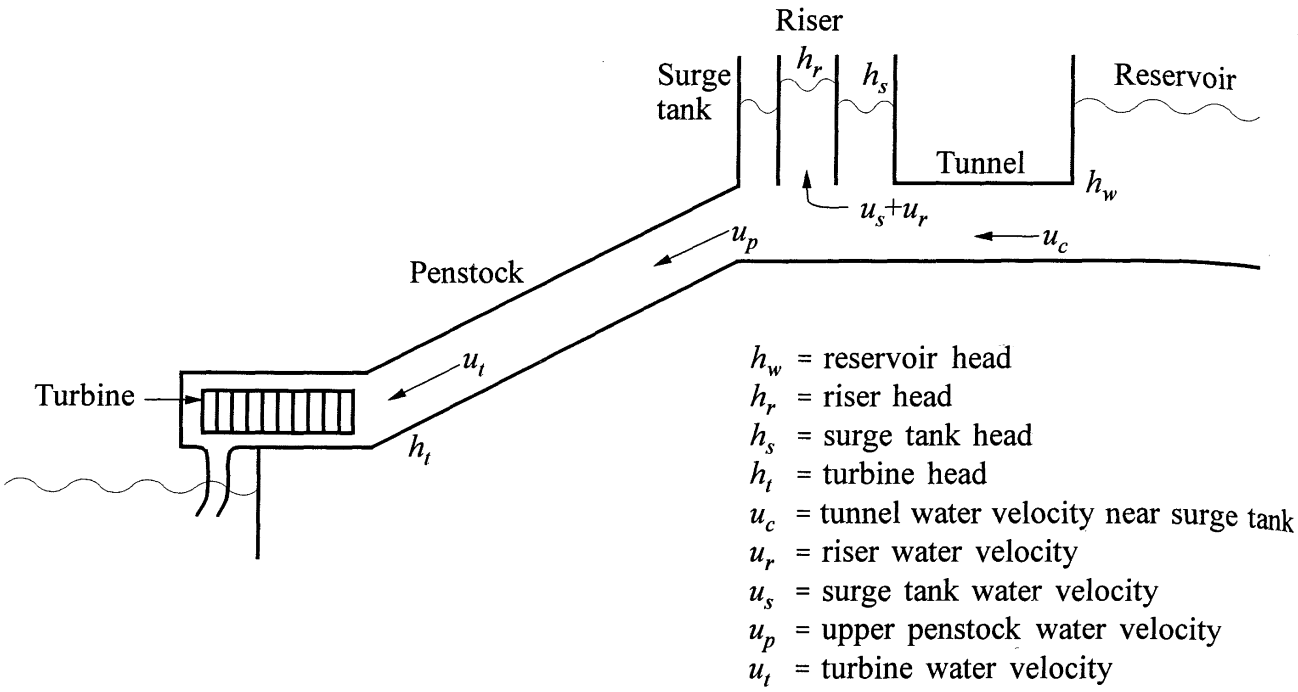

Figure 9.14 Hydraulic plant with surge tank

For a large reservoir, the deviation in head at the upstream end of the tunnel is zero; hence, h_w=0. In addition, the wave effects in the tunnel are insignificant and the $T_{ec}s$ term may be approximated by setting n=0 in the infinite product expansion form of Equation 9.64. Therefore, Equation 9.69 simplifies to

$$h_r = -sT_{Wc}u_c - \phi_c u_c \tag{9.70}$$

where

T_{Wc} = water starting time of the tunnel = $Z_c T_{ec}$
ϕ_c = friction coefficient of the tunnel = $2k_c|U_{c0}|$

The flow rates and velocities at the surge tank are related by the continuity equation

$$u_c = (u_s+u_r)+u_p \tag{9.71}$$

The water velocities in the surge tank and the riser are related to the riser head by the equation

$$u_s+u_r = sT_s h_r \tag{9.72}$$

where T_s is the surge tank riser time.

The surge tank and riser heads are related by the equation

$$h_r = h_s + \phi_s(u_s + u_r) \tag{9.73}$$

where

ϕ_s = surge tank friction coefficient = $2k_f|U_{s0} + U_{r0}|$

Under steady-state conditions, the time derivatives of all variables are zero. Hence, from Equation 9.72, using total values rather than incremental values, we have

$$U_{s0} + U_{r0} = T_s \frac{dH_r}{dt} = 0$$

Therefore, $\phi_s = 0$ and Equation 9.73 reduces to

$$h_r = h_s \tag{9.74}$$

Application of Equations 9.60 and 9.61 to the penstock yields

$$h_t = h_r \text{sech}(T_{ep}s) - Z_p u_t \tanh(T_{ep}s) - \phi_p u_t \tag{9.75}$$

$$u_p = u_t \cosh(T_{ep}s) + \frac{1}{Z_p} h_t \sinh(T_{ep}s) \tag{9.76}$$

where

Z_p = hydraulic impedance of penstock
ϕ_p = friction coefficient of penstock = $2k_p|U_{t0}|$
T_{ep} = penstock elastic time

From Equations 9.70 to 9.74, the tunnel and surge tank transfer function may be written as

$$F_1(s) = -\frac{h_s}{u_p} = \frac{\phi_c + sT_{Wc}}{1 + sT_s\phi_c + s^2 T_{Wc} T_s} \tag{9.77}$$

The overall transfer function relating the water velocity to head at the turbine, formed by using Equations 9.74 to 9.77, is

$$F(s) = \frac{u_t}{h_t} = -\frac{1+[F_1(s)/Z_p]\tanh(T_{ep}s)}{\phi_p + F_1(s) + Z_p\tanh(T_{ep}s)} \tag{9.78}$$

$$= -\frac{1+[F_1(s)/Z_p^2]F_2(s)}{\phi_p + F_1(s) + F_2(s)}$$

where

$$F_2(s) = Z_p\tanh(T_{ep}s) \tag{9.79}$$

As noted earlier, $F(s)$ represents a distributed-parameter system and an infinite product expansion is required to accurately represent the function $F_2(s)$. A lumped-parameter approximation to $F_2(s)$, with $n = 1$ in the expression for $\tanh(T_{ep}s)$, is given by Equation 9.68.

The complete hydraulic system is represented by the transfer function $F(s)$ relating turbine velocity (flow) to the turbine head. Figure 9.15 shows the block diagram of the hydraulic turbine with $F(s)$ representing the hydraulic system. The diagram is based on Figure 9.7 and has been modified to allow representation of water hammer and surge tank effects.

The following are sample values of parameters associated with the representation of $F(s)$ [6]:

$T_{ec} = 13$ s	$Z_c = 4$	$\phi_c = 0.009$	$T_s = 900$ s
$T_{ep} = 0.25$ s	$Z_p = 4$	$\phi_p = 0.001$	

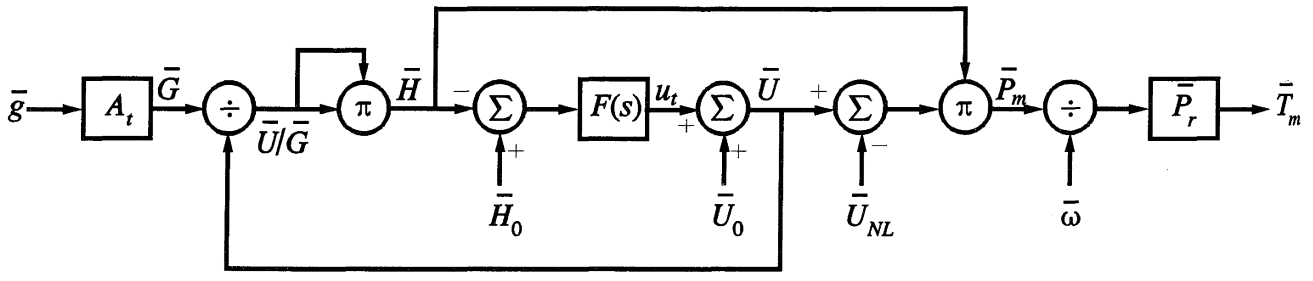

Figure 9.15 Hydraulic turbine block diagram including water hammer and surge tank effects

If there is no surge tank, T_{Wc} and ϕ_c are zero, and the transfer function $F_1(s)$ vanishes in Equation 9.78. The transfer function $F(s)$ reduces to that given by Equation 9.67. If in addition the water hammer and friction effects in the penstock are neglected, $F(s)$ simplifies to the conventional form

$$F(s) = -\frac{1}{sT_{Wp}} \tag{9.80}$$

If water hammer effects in the penstock are to be neglected and surge tank is to be modelled, $F_2(s)$ in Equation 9.78 is set equal to sT_{Wp}.

9.1.5 Guidelines for Modelling Hydraulic Turbines

The modelling detail required for any given study depends on the scope of the study and the system characteristics. The following are general guidelines for the selection of appropriate models.

Governor tuning studies

From the results of Example 9.4, we see that there could be significant differences between frequency response characteristics of the exact elastic model and the simplified inelastic model of the water column, beyond 0.1 Hz. These differences have negligible effect on the conventional governor with transient droop compensation or the equivalent PI controller. The larger bandwidth of PID controllers requires a more accurate representation of the penstock water column. Usually a lumped-parameter approximation (with n=1 or 2) should be acceptable.

The surge tank natural period is on the order of several minutes. Its representation in governor tuning studies is usually not necessary.

Transient stability studies

The hydraulic turbine governors have a very slow response from the viewpoint of transient stability. Their effects are likely to be more significant in studies of small isolated systems. A nonlinear turbine model assuming inelastic water column (Figure 9.7) would be adequate for such studies. The speed governor model should account for gate position and rate limits (Figure 9.10).

Small-signal stability studies

The speed governors have negligible effect on local plant mode oscillations of frequencies on the order of 1.0 Hz. However, the effect on low frequency interarea oscillations of frequencies below 0.5 Hz may be significant. These effects can be modelled adequately by linearizing the nonlinear turbine-penstock model of Figure 9.7

and the governor model of Figure 9.10. For plants with long penstocks, it may be prudent to consider the water hammer effects.

Small-signal studies are also ideally suited for investigating interactions between the hydraulic system dynamics and the network power oscillations.

Long-term dynamic studies

Depending on the nature of the problem, a very detailed nonlinear representation of the turbine and water column dynamics may be required. This includes travelling wave effects and surge tank dynamics. Such studies are invaluable for studying problems associated with special plant layouts and establishing appropriate operating procedures.

9.2 STEAM TURBINES AND GOVERNING SYSTEMS

A steam turbine converts stored energy of high pressure and high temperature steam into rotating energy, which is in turn converted into electrical energy by the generator. The heat source for the boiler supplying the steam may be a nuclear reactor or a furnace fired by fossil fuel (coal, oil, or gas).

Steam turbines with a variety of configurations have been built depending on unit size and steam conditions. They normally consist of two or more turbine sections or cylinders coupled in series. Each turbine section consists of a set of moving blades attached to rotor and a set of stationary vanes. The moving blades are called buckets. The stationary vanes, referred to as nozzle sections, form nozzles or passages in which steam is accelerated to high velocity. The kinetic energy of this high velocity steam is converted into shaft torque by the buckets.

A turbine with multiple sections may be either *tandem-compound or cross-compound.* In a tandem-compound turbine, the sections are all on one shaft, with a single generator. In contrast, a cross-compound turbine consists of two shafts, each connected to a generator and driven by one or more turbine sections; however, it is designed and operated as a single unit with one set of controls. The cross-compounding results in greater capacity and improved efficiency, but is more expensive. It is seldom used now; most new units placed in service in recent years have been of the tandem-compound design.

Fossil-fuelled units can be of tandem-compound or cross-compound design. Typical configurations of tandem-compound turbines and cross-compound turbines for fossil-fuelled units are shown in Figures 9.16 and 9.17, respectively. Tandem-compound units run at 3600 r/min. Cross-compound units may have both shafts rotating at 3600 r/min, or more commonly, one shaft at 3600 r/min and the other at 1800 r/min.[1]

---

[1] Turbine speeds given here correspond to 60 Hz systems. For 50 Hz systems, the corresponding speeds are 3000 r/min and 1500 r/min.

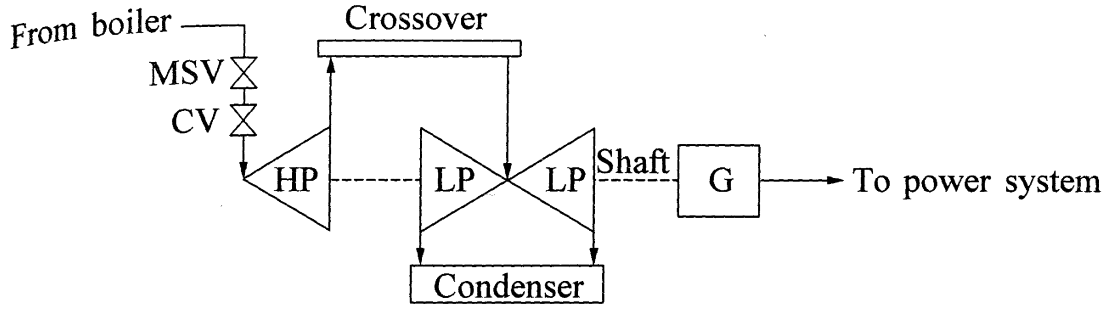

(a) Non-reheat

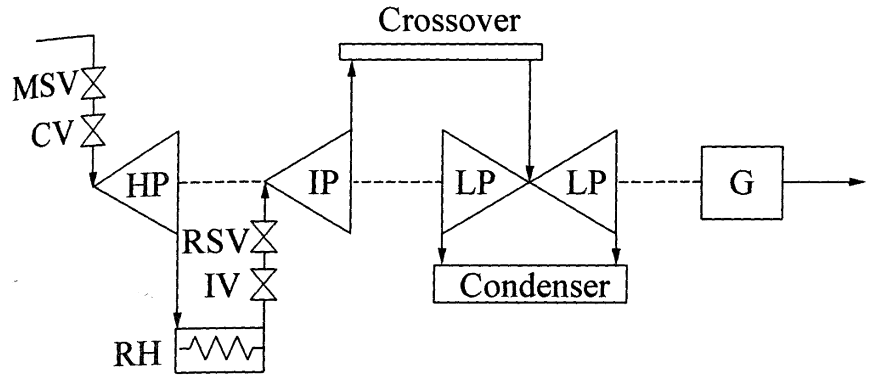

(b) Single reheat

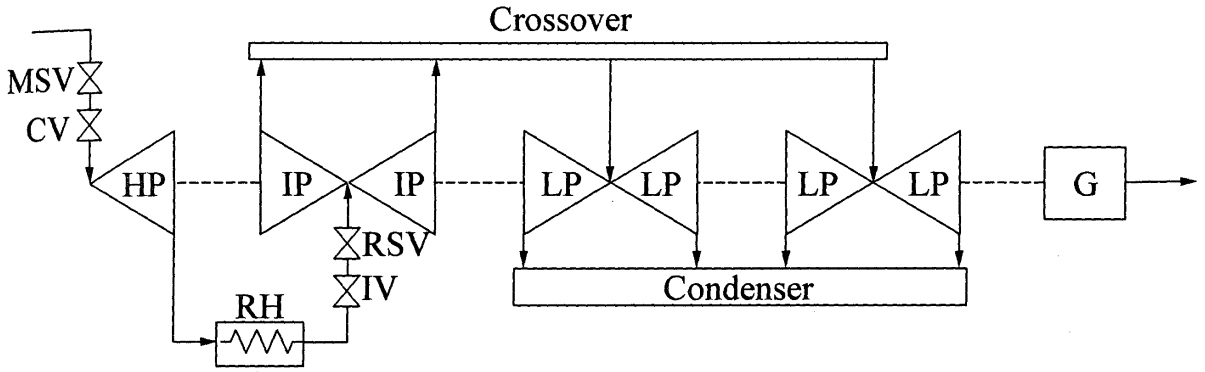

(c) Single reheat

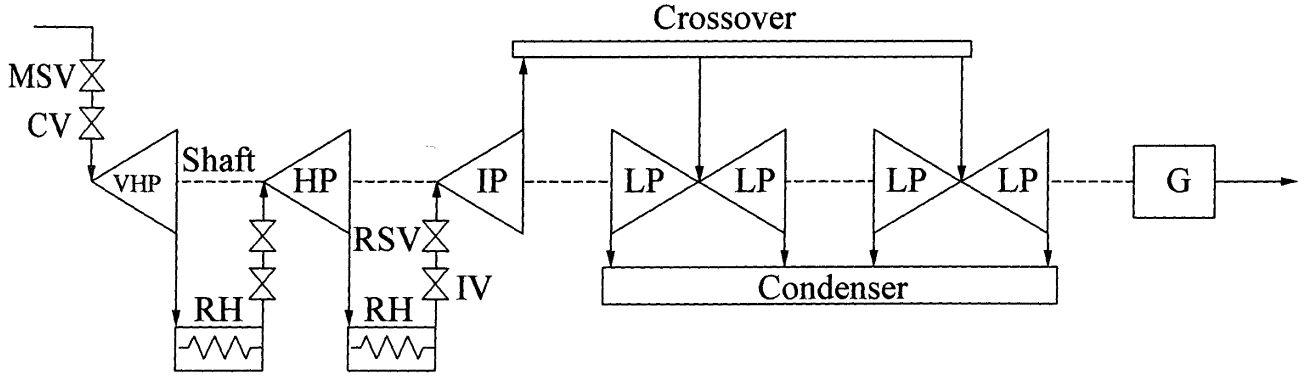

(d) Double reheat

Figure 9.16 Common configurations of tandem-compound steam turbine of fossil-fuelled units

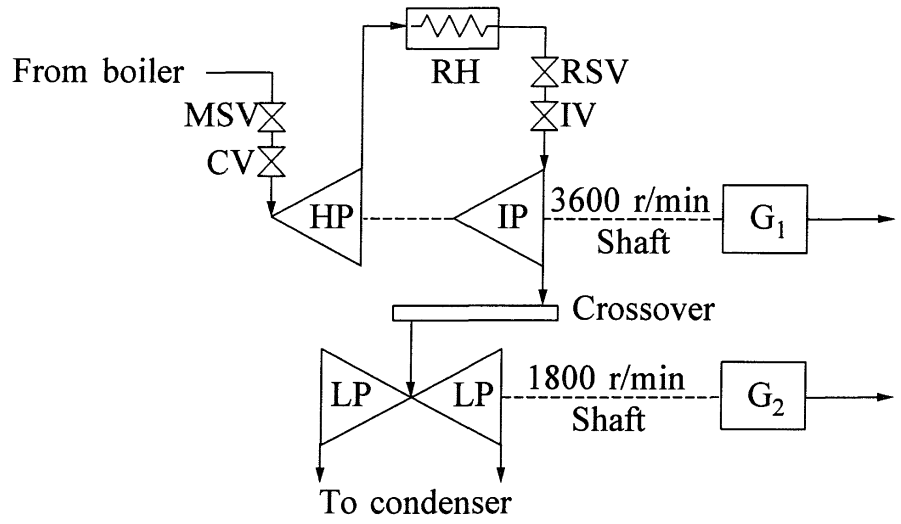

(a) Single reheat, 3600/1800 r/min shaft speeds

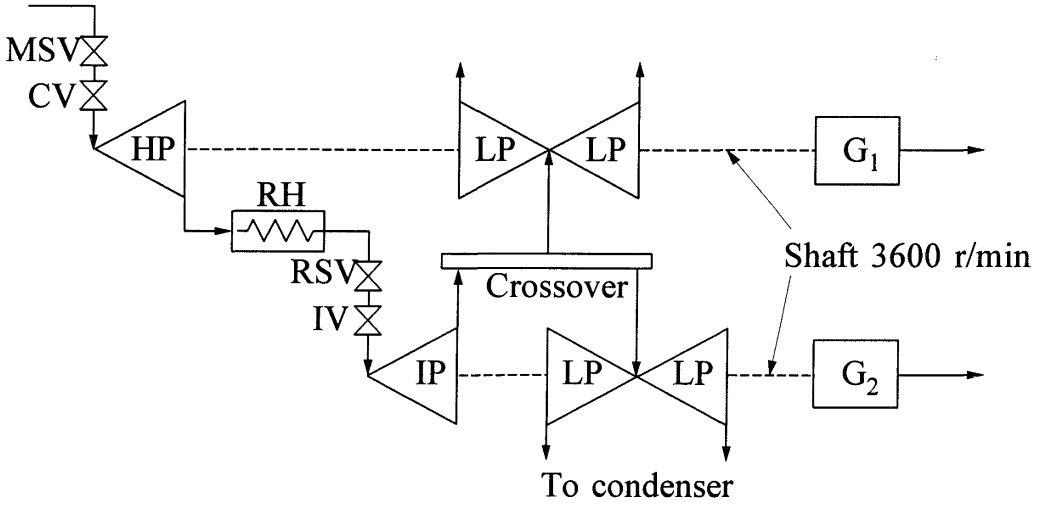

(b) Single reheat, 3600/3600 r/min shaft speeds

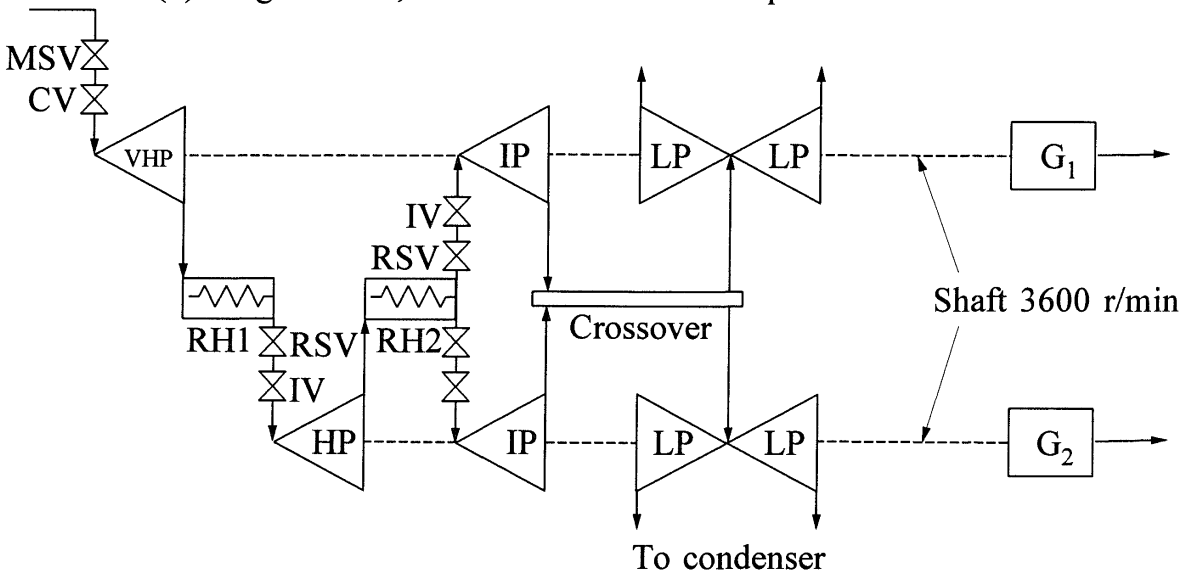

(c) Double reheat, 3600/3600 r/min shaft speeds

Figure 9.17 Examples of cross-compound steam turbine configurations

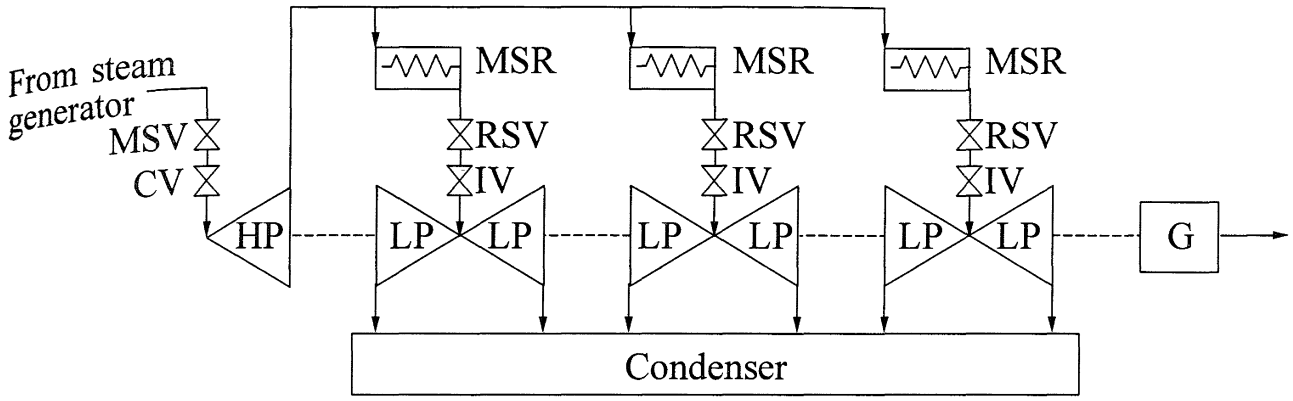

Figure 9.18 An example of nuclear unit turbine configuration

Depending on the turbine configuration, fossil-fuelled units consist of high pressure (HP), intermediate pressure (IP), and low pressure (LP) turbine sections. They may be of either *reheat* type or *non-reheat* type. In a reheat type turbine, the steam upon leaving the HP section returns to the boiler, where it is passed through a reheater (RH) before returning to the IP section. Reheating improves efficiency.

Some units have neither an IP turbine section nor a reheater, in which case the steam passes directly to the LP section. On the other hand, some units have two reheater sections.

The steam exhausted from the turbine is expanded to subatmospheric pressure and condensed in a condenser before returning to the boiler to repeat the cycle.

Nuclear units usually have tandem-compound turbines and run at 1800 r/min. A typical configuration of the turbine is shown in Figure 9.18. It consists of one HP section and three LP sections. The HP exhaust steam passes through the moisture-separator-reheater (MSR) before entering the LP turbines. The moisture separator reduces moisture content of the steam entering the LP section, thereby reducing moisture losses and erosion rates. High-pressure steam is used to reheat the HP exhaust (not shown in figure).

As shown in Figures 9.16, 9.17 and 9.18, large steam turbines for fossil-fuelled and nuclear units are equipped with four sets of valves: main inlet stop valves (MSVs) and control valves (CVs), and the reheater stop valves (RSVs) and intercept valves (IVs). Normally, there are at least two of each of these valves in parallel. Many turbines actually have four or more control valves, operating either in parallel or sequentially. The stop valves are primarily emergency trip valves and are not normally used for control of speed and load. The main inlet control (governor) valves modulate the steam flow through the turbine during normal operation. Control valves as well as intercept valves are responsive to overspeed following a sudden loss of electrical load.

The control valves are usually of the plug diffuser type whereas the intercept valves may be either plug type or butterfly type (used normally for nuclear units). The steam flow area versus valve position characteristics of the two types of valves are shown in Figure 9.19.

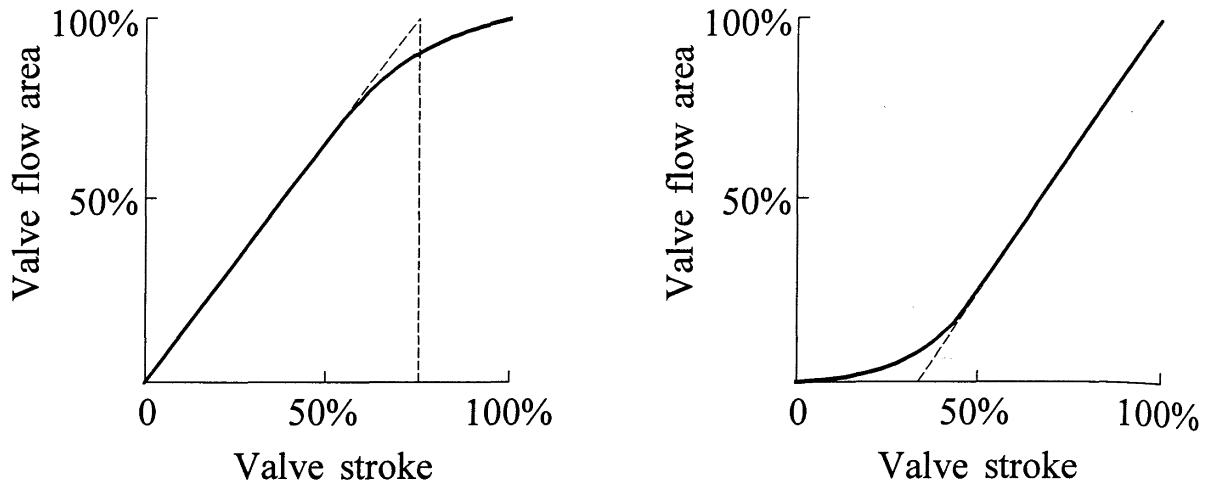

(a) Plug-type valve (b) Butterfly-type valve

Figure 9.19 Steam valve flow area versus position characteristics

In the following sections we describe the characteristics and modelling of steam turbines and the associated governing systems. In addition, we discuss the requirements for protecting steam turbines during abnormal frequency conditions.

Torsional characteristics of the turbine-generator shaft system and their impact on the performance of the power system are considered in Chapter 15.

9.2.1 Modelling of Steam Turbines

Before we develop the model of a complete turbine, let us first derive the transfer function of a steam vessel and the expression for power developed by a turbine stage.

Time constant of a steam vessel

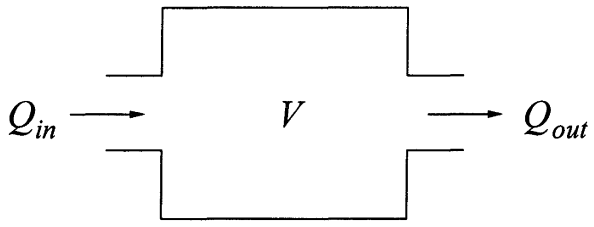

Figure 9.20 Steam vessel

The continuity equation for the vessel is

$$\frac{dW}{dt} = V\frac{d\rho}{dt} = Q_{in} - Q_{out} \tag{9.81}$$

where

W = weight of steam in the vessel (kg)
= $V\rho$
V = volume of vessel (m^3)
ρ = density of steam (kg/m^3)
Q = steam mass flow rate (kg/s)
t = time (s)

Assuming the flow out of the vessel to be proportional to pressure in the vessel,

$$Q_{out} = \frac{Q_0}{P_0} P \tag{9.82}$$

where

P = pressure of steam in the vessel (kPa)
P_0 = rated pressure
Q_0 = rated flow out of vessel

With *constant temperature* in the vessel,

$$\frac{d\rho}{dt} = \frac{dP}{dt}\frac{\partial\rho}{\partial P} \tag{9.83}$$

The change in density of steam with respect to pressure ($\partial\rho/\partial P$) at a given temperature may be determined from steam tables.

From Equations 9.81, 9.82, and 9.83, we have

$$\begin{aligned} Q_{in} - Q_{out} &= V\frac{\partial\rho}{\partial P}\frac{dP}{dt} \\ &= V\frac{\partial\rho}{\partial P}\frac{P_0}{Q_0}\frac{dQ_{out}}{dt} \\ &= T_V\frac{dQ_{out}}{dt} \end{aligned} \tag{9.84}$$

where

$$T_V = \frac{P_0}{Q_0} V\frac{\partial\rho}{\partial P} \tag{9.85}$$

In Laplace form, Equation 9.84 may be written as

$$Q_{in} - Q_{out} = T_V s Q_{out}$$

or

$$\frac{Q_{out}}{Q_{in}} = \frac{1}{1 + T_V s} \tag{9.86}$$

Equation 9.86 represents the transfer function of the steam vessel, and T_V is its time constant.

Torque developed by a steam turbine stage

In modern steam turbines the force on each rotor blade, and hence the turbine torque, is proportional to the steam flow rate. Thus

$$T_m = kQ \tag{9.87}$$

where k is a proportional constant.

Example 9.5

The following data relate to a reheater steam volume:

Q_0 = 230 kg/s $\qquad$ V = 115 m^3

P_0 = 4140 kPa $\qquad$ $\frac{\partial \rho}{\partial P}$ = 0.0035

Calculate the reheater time constant.

Solution

From Equation 9.85, the reheater time constant is

$$T_R = \frac{P_0}{Q_0} V \frac{\partial \rho}{\partial P}$$

$$= \frac{4140}{230} \times 115 \times 0.0035 = 7.25 \text{ s}$$

■

Complete turbine model

To illustrate the modelling of steam turbines, let us consider a fossil-fuelled single reheat tandem-compound turbine, a type in common use. The basic configuration identifying the turbine elements that need to be considered for purposes

of modelling is shown in Figure 9.21(a).

Steam enters the HP section through the control valve and the inlet piping. The housing for the control valves is called the steam chest. A substantial amount of steam is stored in the chest and the inlet piping to the HP section. The HP exhaust steam is passed through the reheater. The reheat steam flows into the IP turbine section through the reheat intercept valve (IV) and the inlet piping. The crossover piping provides a path for the steam from IP section exhaust to the LP inlet. Since the stop valves merely provide a backup means of stopping steam flow, they need not be modelled in system studies and are not shown in Figure 9.21(a).

As indicated earlier, the control valves modulate the steam flow through the turbine for load/frequency control during normal operation. The response of steam flow to a change in control valve opening exhibits a time constant T_{CH} due to the charging time of the steam chest and the inlet piping to the HP section. This time constant is on the order of 0.2 s to 0.3 s.

The intercept valve is normally used only for rapid control of turbine mechanical power in the event of an overspeed. It is very effective for this purpose, since it is ahead of the reheater and controls steam flow to IP and LP sections, which generate nearly 70% of the total turbine power. The steam flow in the IP and LP sections can change only with the buildup of pressure in the reheater volume. The reheater holds a substantial amount of steam and the time constant T_{RH} associated with it is in the range of 5 s to 10 s. The steam flow into the LP sections experiences an additional time constant T_{CO} associated with the crossover piping; this is on the order of 0.5 s.

Figure 9.21(b) shows the block diagram representation of the tandem-compound reheat turbine. The model accounts for the effects of inlet steam chest, reheater, and the nonlinear characteristics of the control and intercept valves. The representation of the reheater differs from those of steam chest and LP inlet crossover piping. This is to allow computation of reheater pressure to account for the effects of intercept valve actuation. Care must be taken in selecting a per unit system for specifying the turbine parameters and variables. A convenient per unit system is one with base power equal to the *maximum turbine power* at rated main steam pressure with the control valves fully open. In this system, CV position is 1.0 pu when fully open. The sum of the power fractions of the various turbine sections ($F_{HP}+F_{IP}+F_{LP}$) is equal to 1.0.

The per unit turbine power P_{mech} so computed is multiplied by the ratio of P_{MAX} in MW to MVA base to obtain the turbine mechanical power in per unit of a common MVA base used for representing the complete power system. In this system per unit torque is defined as

$$\bar{T}_m = \frac{\omega_{\text{base}}}{P_{\text{base}}} T_m \tag{9.88}$$

Thus, at steady state, per unit mechanical torque is equal to per unit mechanical power.

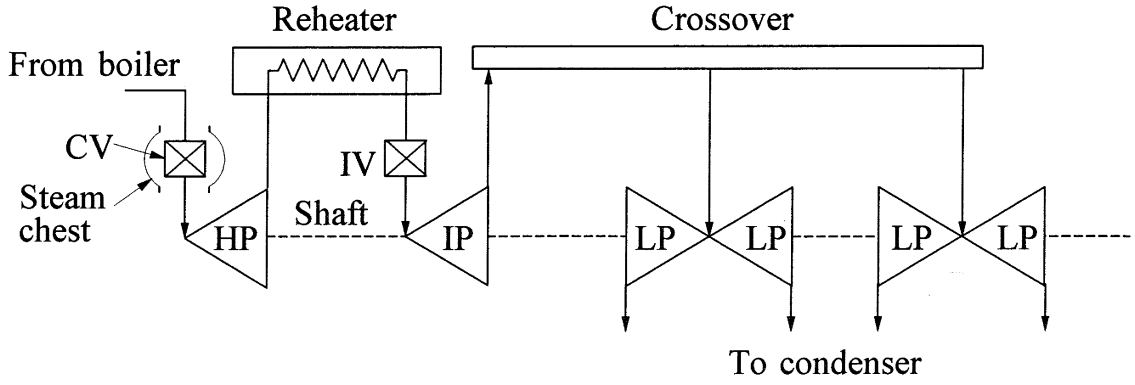

(a) Turbine configuration

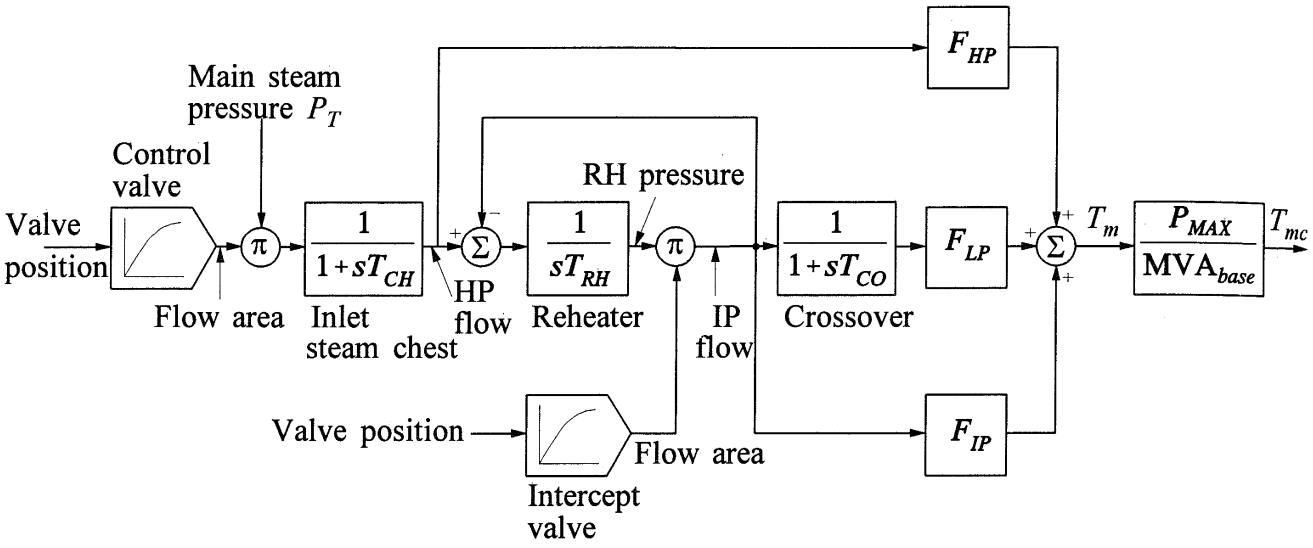

(b) Block diagram representation

Parameters

T_{CH} = time constant of main inlet volumes and steam chest
T_{RH} = time constant of reheater
T_{CO} = time constant of crossover piping and LP inlet volumes
T_m = total turbine torque in per unit of maximum turbine power
T_{mc} = total turbine mechanical torque in per unit of common MVA base
P_{MAX} = maximum turbine power in MW
F_{HP}, F_{IP}, F_{LP} = fraction of total turbine power generated by HP, IP, LP sections, respectively
MVA_{base} = common MVA base

Figure 9.21 Single reheat tandem-compound steam turbine model

Typical values of parameters of the model shown in Figure 9.21 applicable to a tandem-compound single reheat turbine of fossil-fuelled units are

$F_{HP} = 0.3$ $F_{IP} = 0.3$ $F_{LP} = 0.4$
$T_{CH} = 0.3$ s $T_{RH} = 7.0$ s $T_{CO} = 0.5$ s

The model of Figure 9.21 can also be used to represent a nuclear unit turbine having the configuration shown in Figure 9.19. In this case, there is no IP section and $F_{IP}=0$. Typical values of the parameters are

$F_{HP} = 0.3$ $F_{IP} = 0.0$ $F_{LP} = 0.7$
$T_{CH} = 0.3$ s $T_{RH} = 5.0$ s $T_{CO} = 0.2$ s

This model neglects main steam flow used for reheating the HP exhaust.

The most significant time constant encountered in controlling steam flow and the turbine power is that associated with the reheater. Therefore, the responses of the reheat turbines are significantly slower than those of the non-reheat turbine.

Simplified transfer function

From Figure 9.21(b), a simplified transfer function of the turbine relating perturbed values of the turbine torque (ΔT_m) and control valve position (ΔV_{CV}) may be written as follows:

$$\frac{\Delta T_m}{\Delta V_{CV}} = \frac{F_{HP}}{1+sT_{CH}} + \frac{1-F_{HP}}{(1+sT_{CH})(1+sT_{RH})} = \frac{1+sF_{HP}T_{RH}}{(1+sT_{CH})(1+sT_{RH})} \tag{9.89}$$

In writing the above transfer function, it is assumed that T_{CO} is negligible in comparison with T_{RH}. In addition, the control valve characteristic is assumed to be linear.

Figure 9.22 shows the response of a tandem-compound turbine with $T_{RH}=7$ s, for a ramp down of control valve opening by 0.1 pu in 1 second. It is interesting to compare these results with those of the hydraulic turbine shown in Figure 9.4. It is clear that the response of a steam turbine has no peculiarity such as that exhibited by a hydraulic turbine due to water inertia. The governing requirements of steam turbines, in this respect, are more straightforward. The control action, as shown in Example 9.6, is stable with the normal speed regulation of about 5%, and there is no need for transient droop compensation.

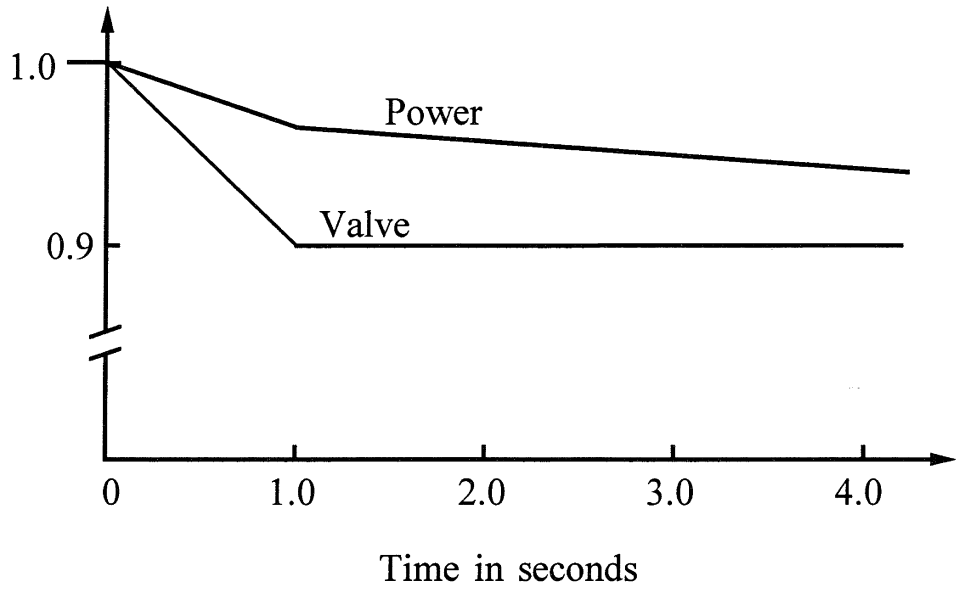

Figure 9.22 Steam turbine response to a 1-second ramp change in CV opening $T_{RH}=7.0$ s, $F_{HP}=0.3$; T_{CH} and T_{CO} negligible

Example 9.6

Figure E9.6 shows a simplified block diagram of speed control of a thermal-generating unit feeding an isolated load. The steam turbine is of the tandem-compound single reheat type whose transfer function may be approximated by

$$\frac{\Delta T_m}{\Delta V_{cv}} = \frac{1+F_{HP}T_{RH}s}{1+T_{RH}s}$$

where $T_{RH}=6.0$ s and $F_{HP}=0.333$. The mechanical starting time T_M of the generator is 12.0 s.

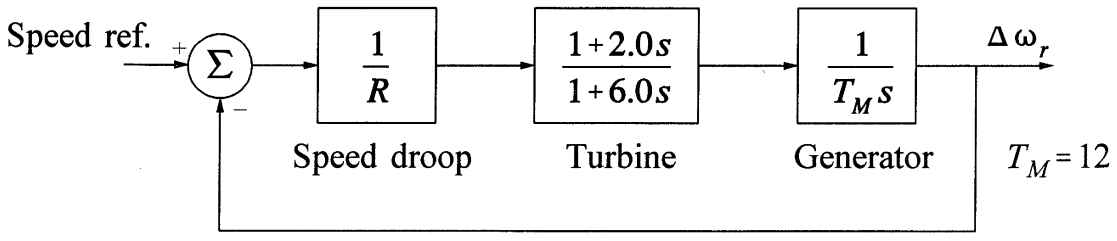

Figure E9.6

Determine (i) the lowest value of R for which the speed control is stable, and (ii) the value of R for which the speed control action is critically damped.

Solution

(i) The characteristic equation ($1+GH=0$) of the closed-loop system is

$$1+\left(\frac{1+2.0s}{1+6.0s}\frac{1}{12s}\frac{1}{R}\right) = 0$$

This simplifies to

$$s^2+\frac{12R+2}{72R}s+\frac{1}{72R} = 0$$

This is in the standard form

$$s^2+2\zeta\omega_n s+\omega_n^2 = 0$$

For stability the following conditions must be satisfied

$$\frac{1}{72R}>0 \quad \text{or} \quad R>0$$

and

$$\frac{12R+2}{72R}>0 \quad \text{or} \quad R>-\frac{1}{6}$$

Therefore, any positive value of R will result in a stable response.

With the standard 4 to 5% droop, the speed control is quite stable. Unlike a hydraulic turbine, the steam turbine does not require transient droop compensation.

(ii) For critical damping, $\zeta=1.0$. Therefore,

$$2\zeta\omega_n = 2\times 1.0\times\frac{1}{\sqrt{72R}} = \frac{12R+2}{72R}$$

Hence,

$$288R = (12R+2)^2$$

Simplifying, we find

$$R^2-1.667R+0.0278 = 0$$

Solving for R, we have

$$R = 0.017 \quad \text{or} \quad 1.65$$

From practical considerations, the lower of the above two values is of significance. Thus, critical damping can be obtained with R=1.7%, i.e., a gain of 59. ■

Detailed generic model

A generic model structure applicable to all commonly encountered steam turbine configurations is shown in Figure 9.23. By neglecting appropriate time constants and setting some of the power fractions to zero, this model can be used to represent any of the turbine configurations shown in Figures 9.16 and 9.17.

The time constant T_1 represents the main inlet volume and steam chest time constant. The time constants T_2 and T_3 represent reheater time constants. For a single reheat turbine, T_2 is neglected and K_2 and K_3 are set to zero. For example, a single reheat cross-compound turbine of Figure 9.17(b) may be represented by setting the parameters as follows:

$K_1 = F_{HP}$ $K_2 = 0$ $K_3 = 0$ $K_4 = 0$ $K_5 = F_{IP}$
$K_6 = F_{LP1}$ $K_7 = 0$ $K_8 = 0$ $K_9 = F_{LP2}$
$T_1 = T_{CH}$ $T_3 = T_{RH}$ $T_4 = T_{CO1}$ $T_5 = T_{CO2}$
T_2 is neglected

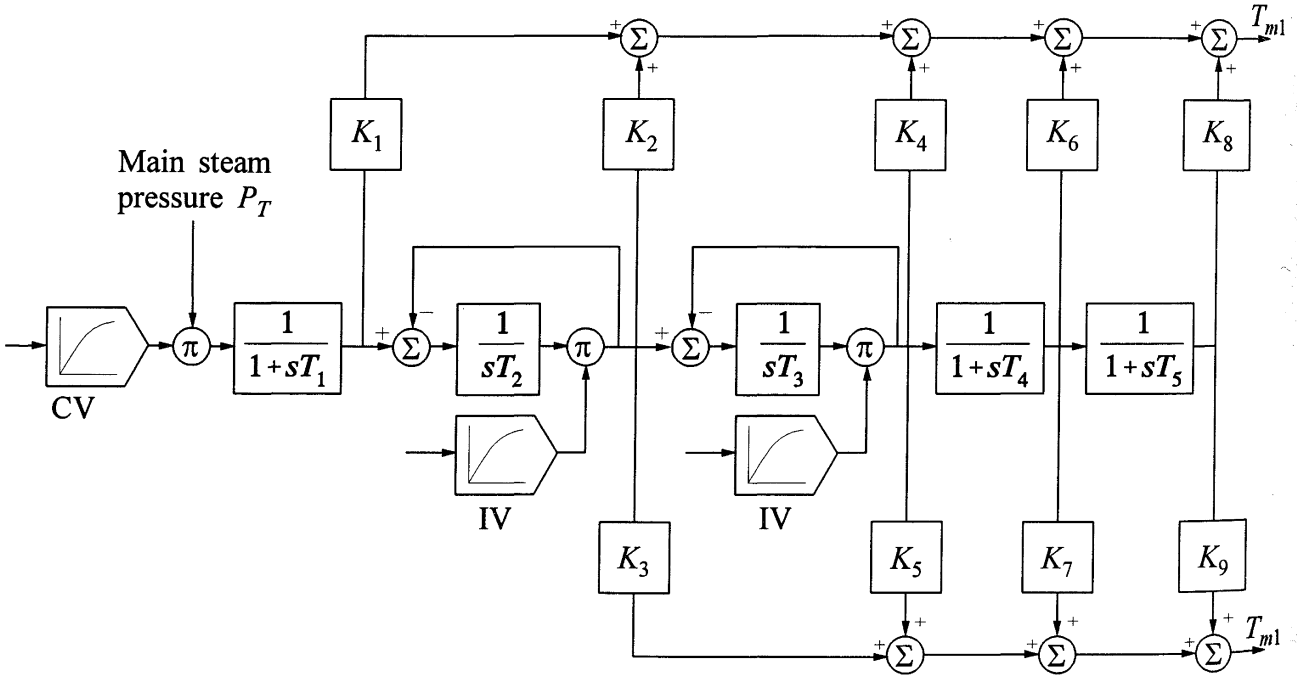

Figure 9.23 Generic model for steam turbines

Enhanced model for significant IV control

For simulations involving closing of IVs for significant periods causing high reheater pressure (for example, fast valving for enhancement of transient stability) a more rigorous representation of the turbine may be necessary [17,18]. An enhancement of the model of Figure 9.21 to account for the effects of reheater pressure is shown in Figure 9.24. The negative feedback of reheat pressure to the HP section accounts for the reduction in pressure difference across the section when the reheater pressure is high. The non-windup limit associated with the reheat pressure accounts for safety valve action.

The multiplier A accounts for the increase in flow through the intercept valves due to the pressure difference across the valve. As the valve opens, after being closed for some time, the flow is limited by the critical pressure ratio. Based on the equation for compressible flow of an ideal gas, assuming an isentropic expansion [19], the expression for the multiplier A is given by

$$A = A_k\sqrt{r^{2/k} - r^{(k+1)/k}} \tag{9.90}$$

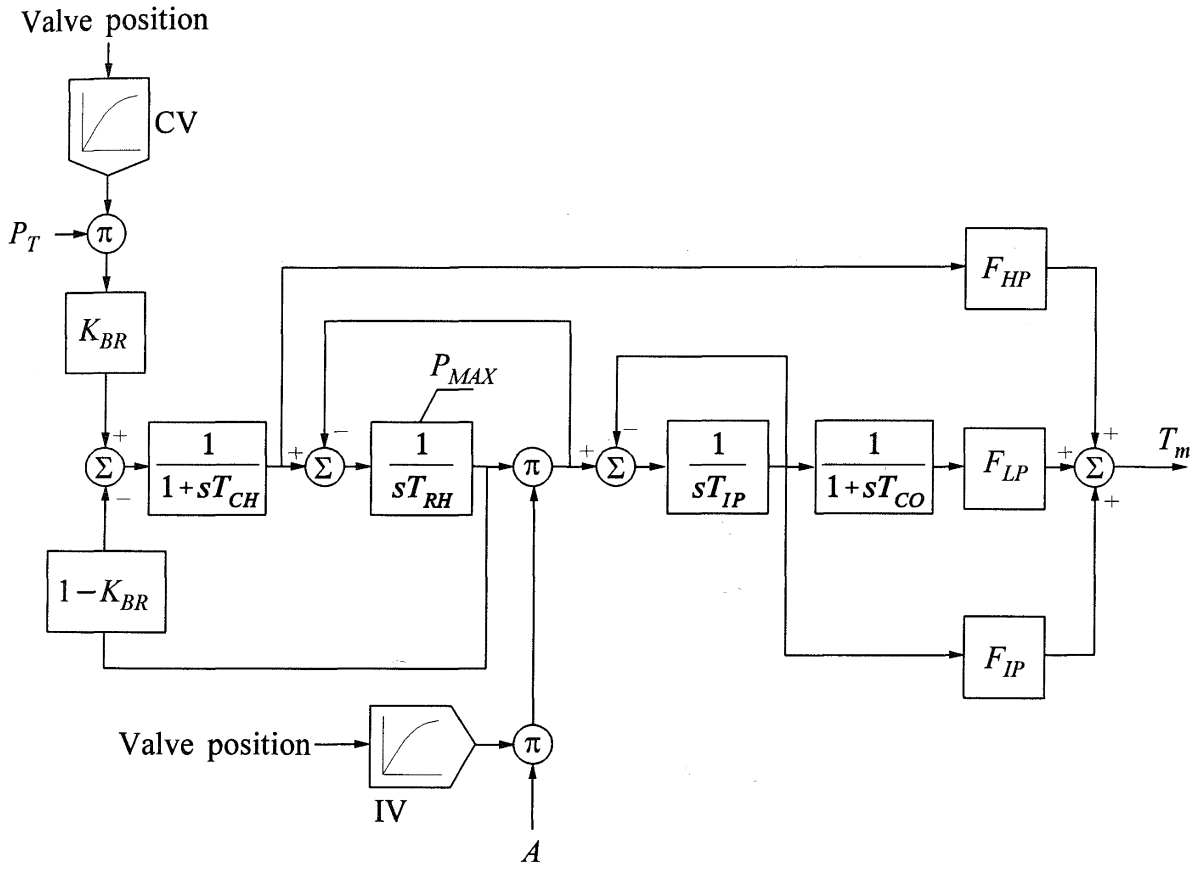

Figure 9.24 Enhanced steam turbine model

where

$$r = \frac{\text{downstream pressure}}{\text{upstream pressure}}$$

$$= \frac{\text{IP turbine pressure}}{\text{RH pressure}}(1 - P_{drop}) \qquad \text{with } r \geq r_{critical}$$

P_{drop} = pressure drop across the valve

For superheated steam (fossil-fuelled units),

$$k = 1.3 \quad \text{and} \quad r_{critical} = 0.547$$

and for wet or saturated steam (nuclear unit),

$$k = 1.135 \quad \text{and} \quad r_{critical} = 0.577$$

Typically P_{drop} is 2% (i.e., 0.02 pu) at full load with valves wide open. In the model, a block has been added, accounting for time constant T_{IP} of IP inlet piping and allowing for computation of IV downstream pressure. IP turbine pressure is required for the calculation of the multiplier A. The critical flow condition that exists as the IVs open is in fact largely caused by the low pressure in IP turbine.

Sample data for the parameters of the model of Figure 9.24 are

T_{CH} = 0.42 s	T_{RH} = 4.2 s	T_{IP} = 0.1 s	T_{CO} = 0.7 s
K_{BR} = 1.073	F_{HP} = 0.25	F_{IP} = 0.25	F_{LP} = 0.5

For a nuclear unit turbine, as noted earlier, there is no IP section; T_{IP} represents the time constant of the inlet piping.

9.2.2 Steam Turbine Controls

The governing systems for steam turbines have three basic functions: normal speed/load control, overspeed control, and overspeed trip. In addition, the turbine controls include a number of other functions such as start-up/shutdown controls and auxiliary pressure control.

The *speed/load control* function is similar to that for hydraulic units. It is a fundamental requirement for any generating unit. In the case of steam turbines, it is achieved through control of the CVs. The speed control function provides the governor with a 4 to 5% speed droop. This enables the generating unit to operate satisfactorily in parallel with other units with proper division of load. The load control function is achieved by adjusting the speed/load reference. The principles of speed/load control are discussed in detail in Chapter 11. The net effect of this control is to adjust the position of the CVs to control admission of steam to the turbine.

The overspeed control and protection requirements are peculiar to steam turbines, and are of critical importance for their safe operation. The integrity of the turbine depends on the ability of the turbine controls to limit the speed of the rotor, following a reduction of electrical load, to well below the typical design maximum speed of 120%. Steam turbines of the reheat type have two separate valving systems that can be used for rapidly controlling the steam energy supplied to the turbine, one system involving the CVs and the other involving the IVs.

The *overspeed control* is the first line of defense against excessive speed. Its function is to limit the overspeed that occurs on partial or full load rejection and to return the turbine to a steady-state condition such that the turbine is ready for reloading. The objective is to prevent overspeed tripping following a load rejection. Typically, the overspeed trip is set at 110 to 115% of rated speed; the overspeed control attempts to limit overspeed to about 0.5 to 1% below the overspeed trip level. The overspeed control involves fast control of the CVs as well as the IVs. The use of the IVs is very effective in this regard, since they control steam flow to IP and LP turbine sections, which together develop 60 to 80% of the total turbine power. Because of the large amount of stored steam in the reheater, the rapid closure of the CVs alone would not be effective in limiting overspeed.

The *overspeed* or *emergency* trip is a backup protection in the event of failure of normal and overspeed control to limit the rotor speed to a safe level. The overspeed trip is designed to be independent of the overspeed control. The trip function, in addition to fast closing the main and reheat stop valves, trips the boiler.

The characteristics of steam valves, as shown in Figure 9.19, are highly nonlinear. Therefore, compensation is often used to linearize the steam flow response with respect to the control signal. The following are the alternative forms of compensation used:

- A forward loop series compensation comprising a function generator having a characteristic reciprocal to that of the steam valve
- A minor loop feedback compensation comprising a function generator with a characteristic similar to that of the valve
- A major loop feedback compensation in the form of a proportional feedback around the steam valve

Typically, four or more parallel operated CVs are used. Each of these valves admits steam through a nozzle section. The different nozzle sections are distributed around the periphery of the first stage turbine section. The CVs may be controlled in unison (full arc) or in sequence (partial arc).

Under normal operation, the CVs are opened sequentially; with only some of the CVs open, the steam admission is along only a partial arc, rather than uniformly along the circumference. This is referred to as "partial-arc admission" mode of operation [21]. The advantage of this mode of operation is that it ensures higher efficiency at partial load.

During start-up, however, the steam is admitted symmetrically through all nozzle sections to reduce thermal stresses. The CVs are maintained fully open, and stop valves are used to control steam flow. This mode of operation, referred to as "full-arc admission" operation, is used until the load reaches a specified level. Depending on the type of turbine governing system, the control of the stop valves is achieved through either auxiliary speed control equipment or the main speed control. Additional measures to minimize thermal stresses in the turbine include limiting the rate of speed increase and the rate of load increase. The speed ramping during start-up is handled by an acceleration control.

Systems used for the above turbine control functions and other auxiliary functions have continually evolved over the years. Older turbine governor designs used mechanical-hydraulic control. Electrohydraulic control was introduced in the 1960s, and its use has been gradually growing. Most governors supplied today are electrohydraulic or digital electrohydraulic. References 21, 22, and 23 provide descriptions of the elements of the control systems. The following are brief descriptions of the functional characteristics of these elements and their models.

Mechanical-hydraulic control (MHC)

The functional block diagram of an MHC system used for governing a steam turbine is shown in Figure 9.25. The basic elements of the governing system are a speed governor, speed relays, and hydraulic servomotors.

The *speed governor* is essentially a mechanical transducer which transforms the shaft speed into a position output, as shown schematically in Figure 9.26. While mechanical speed governors come in different forms, they all operate on the same basic principle of the classical flyball governor: rotor speed signal (ω_r) is converted

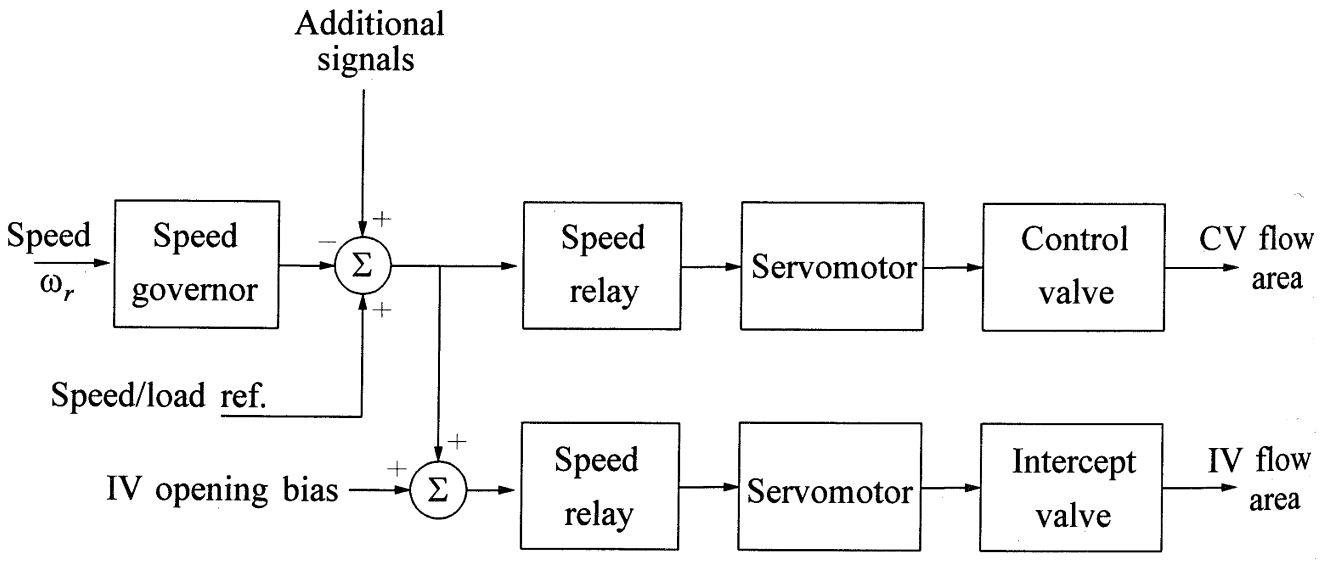

Figure 9.25 Functional block diagram of MHC turbine-governing system

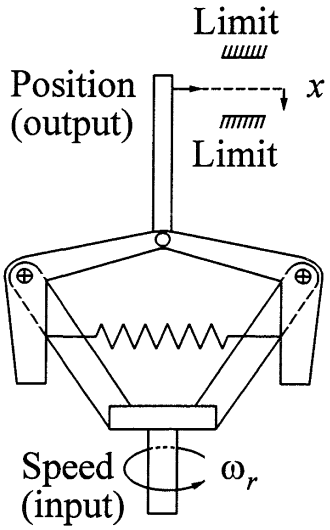

Figure 9.26 Mechanical speed governor [22]

to linear displacement by means of centrifugal forces opposed by a spring. Their performance equation is

$$x = K_G \omega_r \tag{9.91}$$

The speed governor output is compared with a speed/load reference determined by the speed changer position. The resulting error signal is used to control the CVs as well as the IVs. However, for normal speed/load control only the CVs respond. The IVs are held fully open by a bias (IV opening bias) signal. On overspeed, due to the resulting large speed error signal, the bias is overcome and IVs are closed rapidly. When the control signal is restored to a value less than the bias, IVs are again fully opened. Additional signals may be used, as described later, to provide special control and protection functions. The speed governor speeder rod cannot develop the forces necessary to control the steam valves. Therefore, a pilot valve and a spring-loaded servomotor (commonly referred to as *speed relay*) are used to amplify the speed governor signal. Figure 9.27 shows the basics of speed relay-pilot valve combination. A downward displacement of the speeder rod from the speed governor lowers the pilot valve. The oil supply system then forces the servomotor piston upward, allowing increased steam flow to the turbine. The transfer function of the speed relay has the forms shown in Figure 9.28.

On very large turbines, additional amplification to the energy levels necessary to move the steam valves is obtained using *hydraulic servomotors*. They use a high-pressure fire resistant fluid for auxiliary power. A schematic diagram of the servomotor is shown in Figure 9.29(a) and the block diagram representation is shown in Figure 9.29(b). The position limits may correspond to either the fully open valve position or the setting of a load limiter.

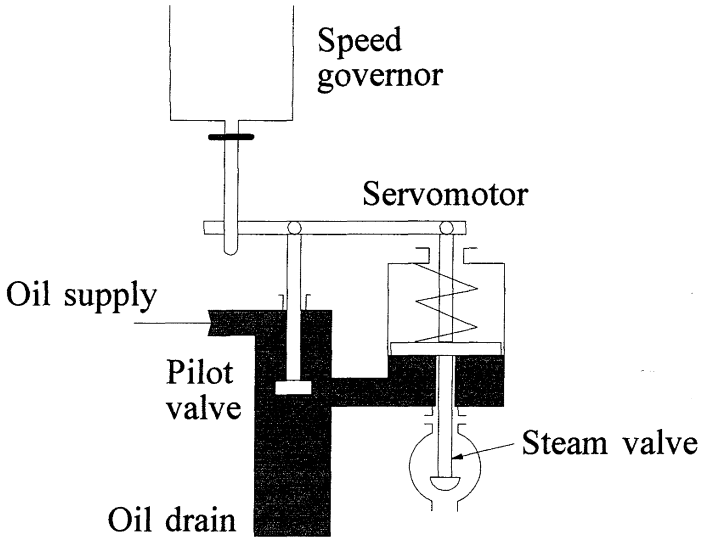

Figure 9.27 Speed relay pilot valve

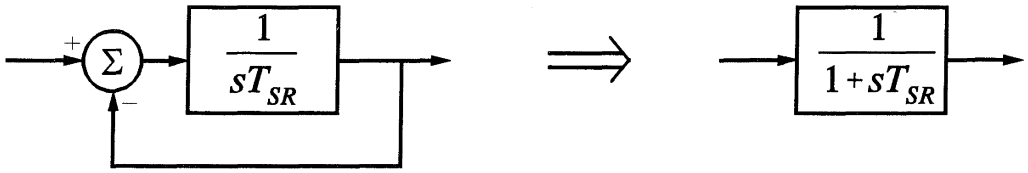

Figure 9.28 Alternative forms of speed relay representation

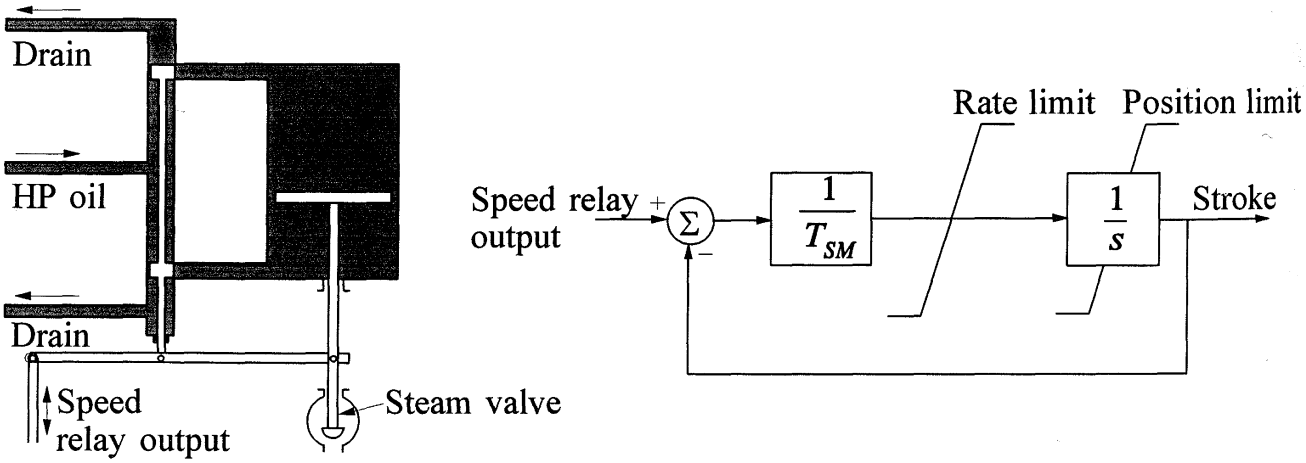

(a) Schematic diagram (b) Block diagram model

Figure 9.29 Hydraulic servomotor

The basic elements and the general principle of operation of all MHC governing systems are similar. However, the details of the control logic used vary widely depending on the make and vintage of the turbine.

Modelling of MHC governors

For studies involving small deviations in speed (frequency), only normal speed regulation or primary speed control needs to be considered. Such studies include transient and small-signal stability studies. For normal-speed regulation, it is standard practice to use the CVs with proportional control on speed error. A generic model shown in Figure 9.30 can be used to model this turbine control function.

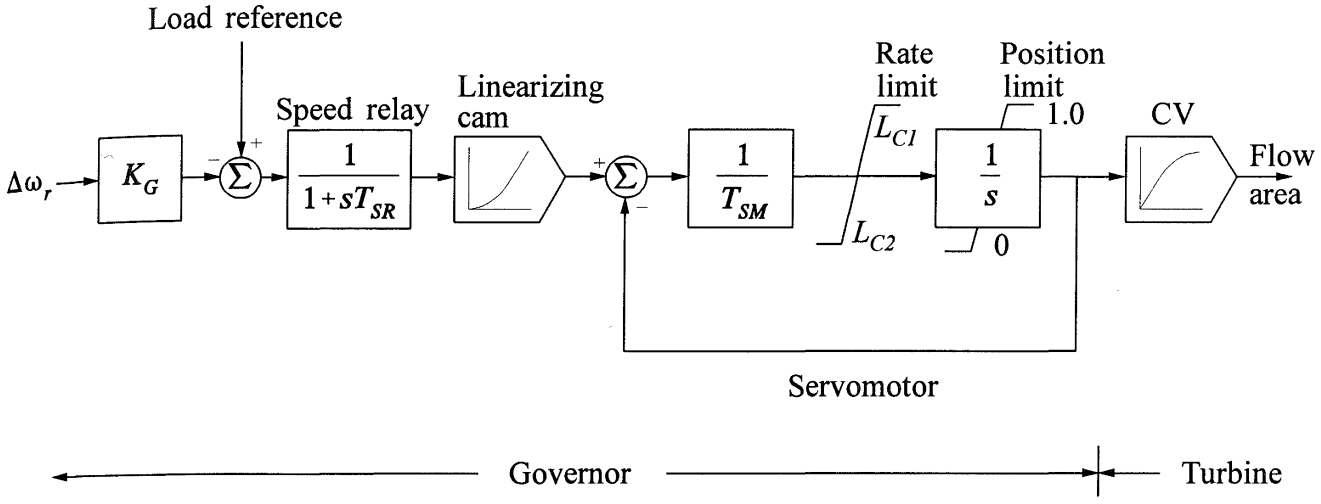

Figure 9.30 Generic speed-governing system model representing normal speed/load control function

As an approximation, the valve characteristic may be assumed to be perfectly compensated, and the valve and cam nonlinearities may be neglected.

Sample values of the parameters are:

K_G = 20 (5% droop) T_{SR} = 0.1 s T_{SM} = 0.3 s

Rate limits: L_{C1} = 0.1 pu/s (opening)
L_{C2} = −1.0 pu/s (closing)

For studies involving significant turbine control action, the performance of overspeed controls and other related auxiliary devices needs to be modelled [18,24]. These controls have nonlinear and discrete characteristics, and the control logic is very specific to the make and vintage of the turbine. Their input signals could be rotor speed, acceleration, electrical power, generator current, or circuit-breaker opening. Although there are many variations of control logic used, the general principles of these controls are similar. We will illustrate this by providing several examples.

Figure 9.31 shows the block diagram representation of an MHC speed-governing system, including the overspeed control function, applicable to one make [24]. The model shown accounts for CV and IV controls, valve nonlinearities, linearizing cams, and an "auxiliary governor" for limiting overspeed. Under steady-state conditions and during speed deviations, the IVs are kept fully open by the opening bias (IVOB); only the CVs provide speed regulation. The auxiliary governor, when speed exceeds its setting V_1 (ranging from 1% to 3% over the rated speed), acts in parallel with the main governor so as to effectively increase the gain of the speed control loop by a factor of about 8. This causes the CVs as well as the IVs to close rapidly and thus limit overspeed.

Figure 9.32 shows another example of the MHC speed-governing system described in references 18 and 20. The CV position is determined by the speed relay output signal S_1. The IVs respond to the lower of the two signals applied to the *low-*

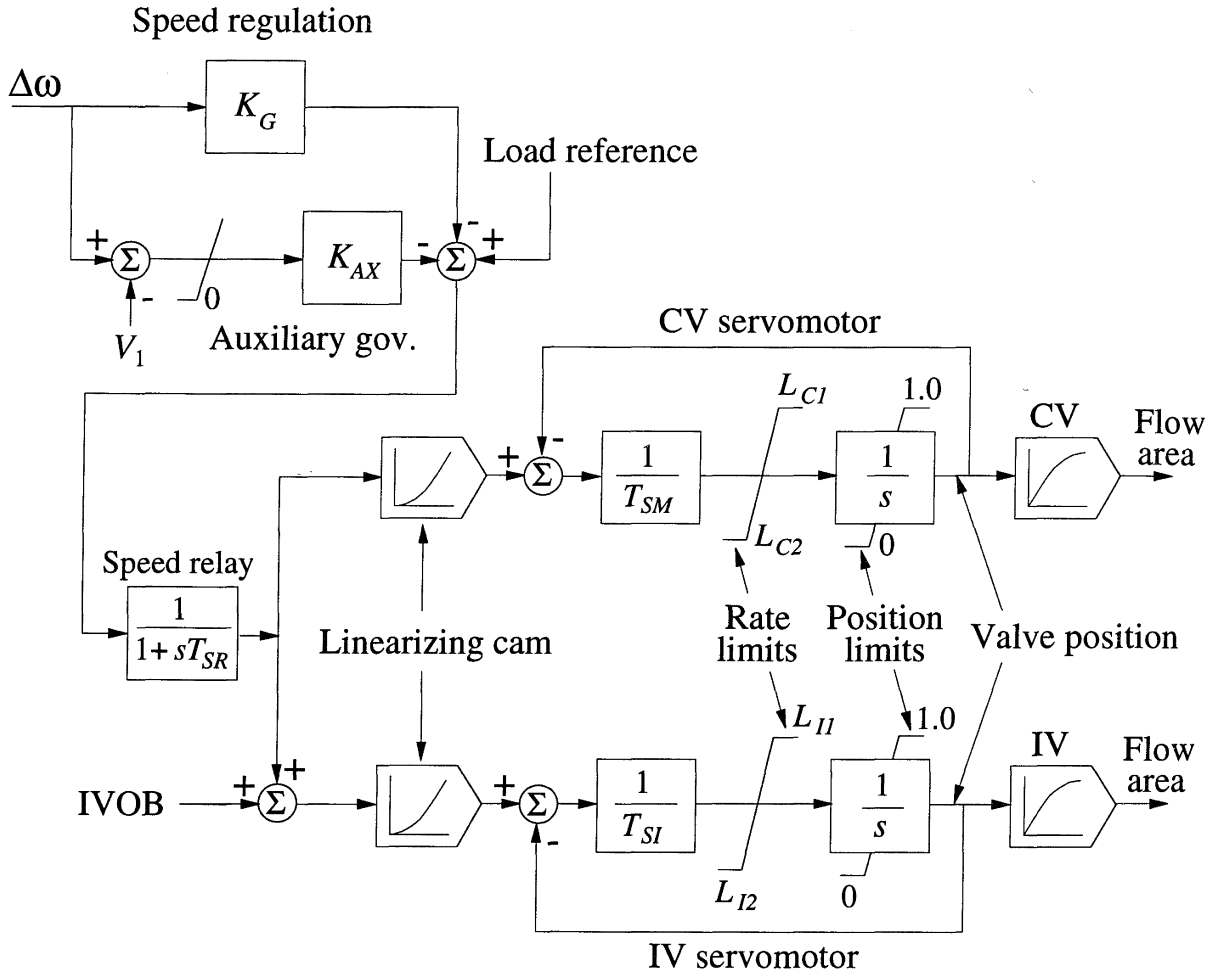

Typical values of parameters:

$K_G = 20$	$V_1 = 0.02$	$K_{AX} = 149$	$T_{SR} = 0.7$	IVOB = 1.17
$T_{SM} = 0.23$	$L_{C1} = 1.0$	$L_{C2} = -3.0$		
$T_{SI} = 0.23$	$L_{I1} = 1.0$	$L_{I2} = -2.5$		

Figure 9.31 MHC turbine-governing system with auxiliary governor

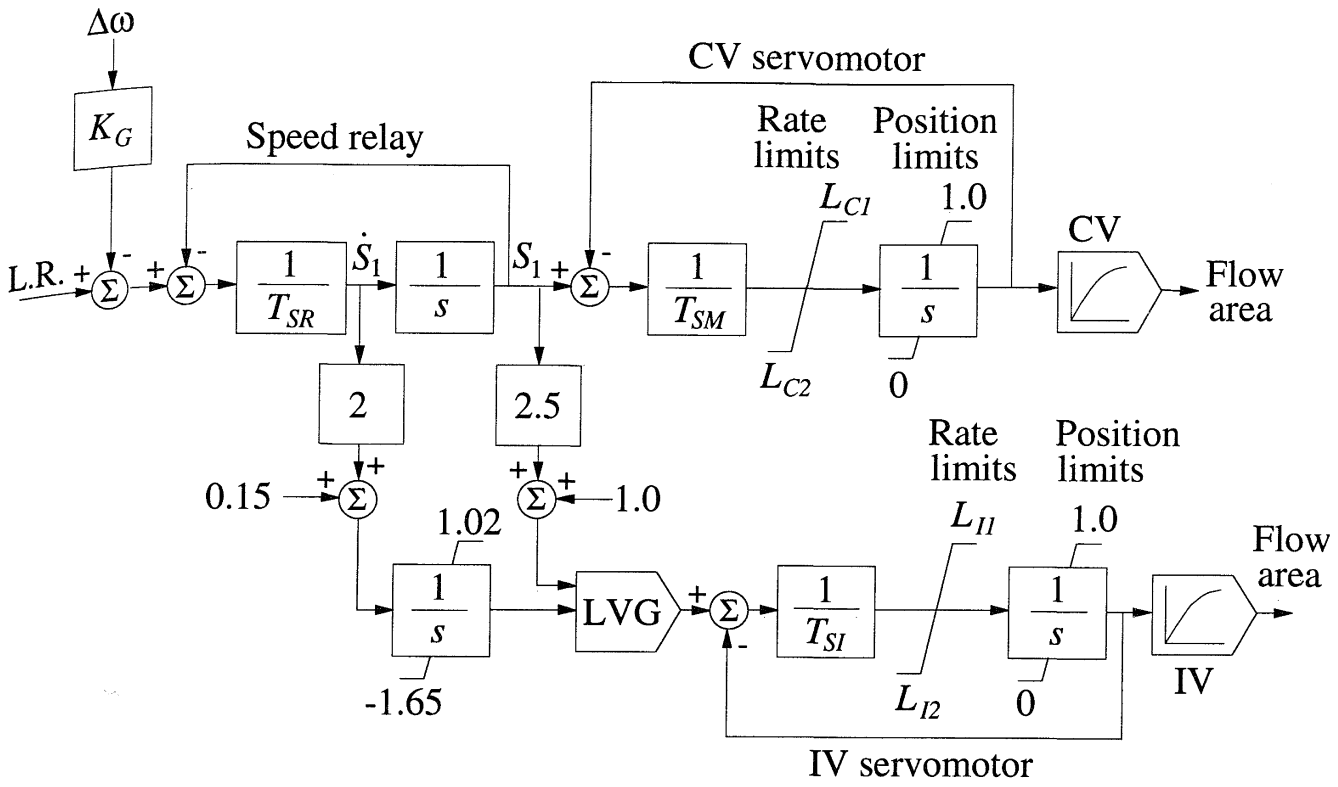

Typical values of parameters:

K_G = 20	T_{SR} = 0.1 s	T_{SM} = 0.2 s	T_{SI} = 0.2 s
L_{C1} = 0.2	L_{C2} = −0.5	L_{I1} = 0.2	L_{I2} = −0.5

Figure 9.32 MHC turbine governing system. ©IEEE 1990 [18]

value gate (LVG); these signals are derived from S_1 and the derivative of S_1 (proportional to negative of rotor acceleration). For small speed deviations, the CVs respond to the normal speed/load control command which determines S_1, and the IVs remain fully open due to the opening bias (LVG input is at 1.02). During an overspeed condition, the IVs transiently respond by closing rapidly, driven by the lower of the two signals $\dot{S}_1$ and S_1 which depend on rotor acceleration and speed respectively. The control of IV through signal S_1 has a gain of 2.5 and a bias of 1.0. With K_G=20 (5% droop) and load reference at 100%, the signal S_1 becomes effective in controlling IV when $\Delta\omega \geq 5\%$ and the effective speed control gain is 50 (2% droop).

Electrohydraulic control (EHC)

The EHC systems use electronic circuits in place of mechanical components associated with the MHC in the low-power portions. EHC systems offer more flexibility and adaptability, allowing incorporation of a number of features that cannot be obtained on mechanical systems. This contributes to faster response and improved linearity. However, the overall functional requirements of the EHC systems are essentially very similar to those of the MHC system.

Figures 9.33 and 9.34 show two examples of EHC speed-governing systems.

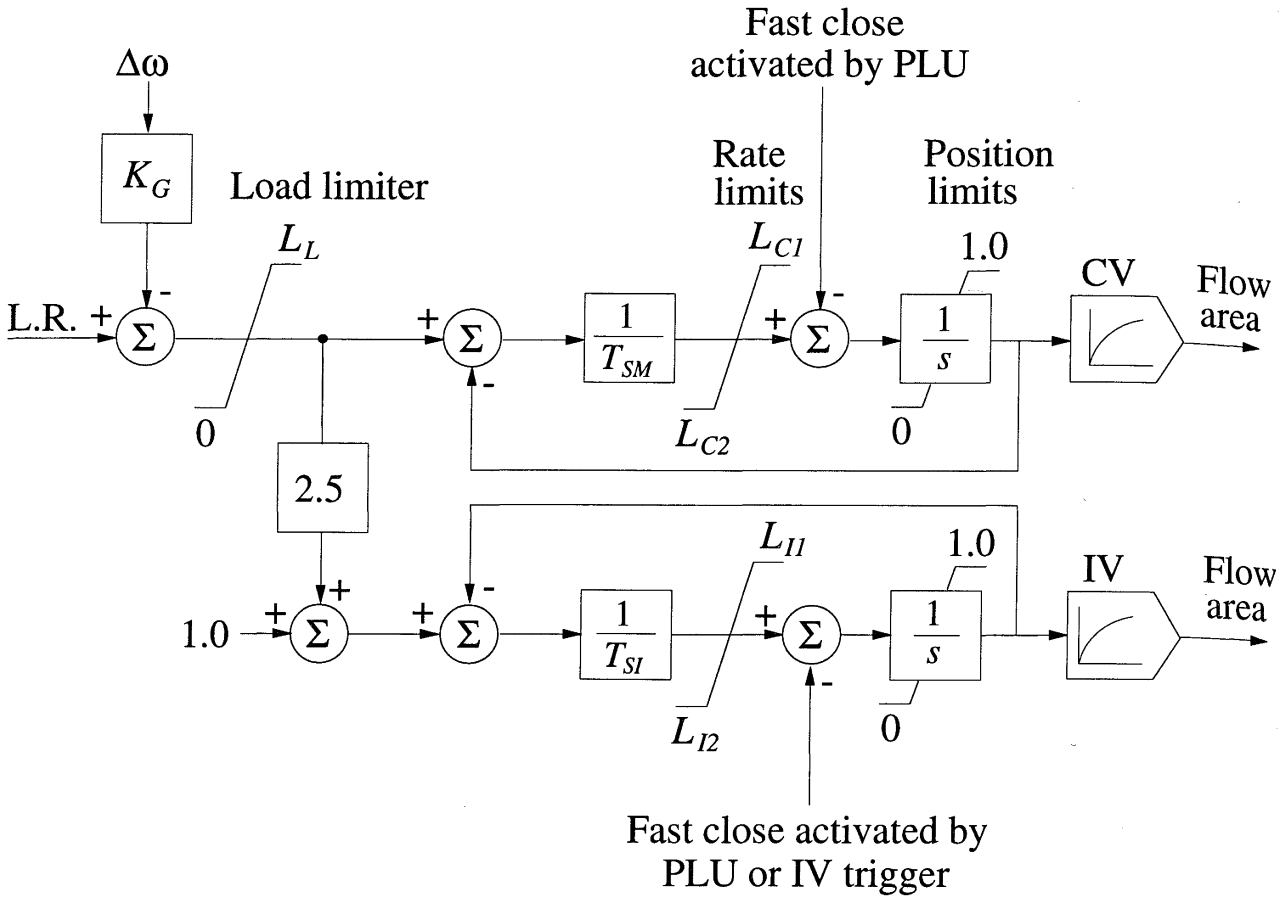

Typical values of parameters:

$K_G = 20$ $T_{SM} = 0.1$ $T_{SI} = 0.1$
$L_{C1} = 0.1$ $L_{C2} = -0.2$ $L_{I1} = 0.1$ $L_{I2} = -0.2$

(a) Block diagram of governing system

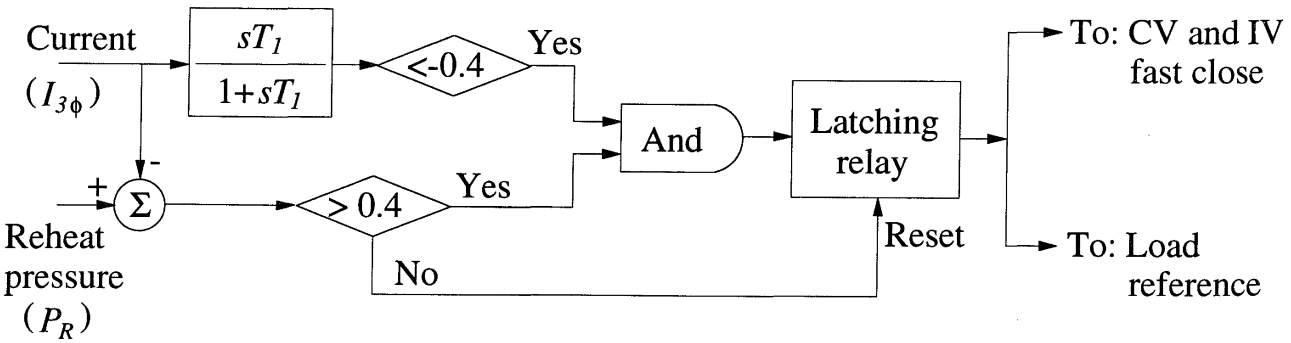

(b) Power load unbalance relay logic

Figure 9.33 EHC governing system with PLU relay and IV trigger

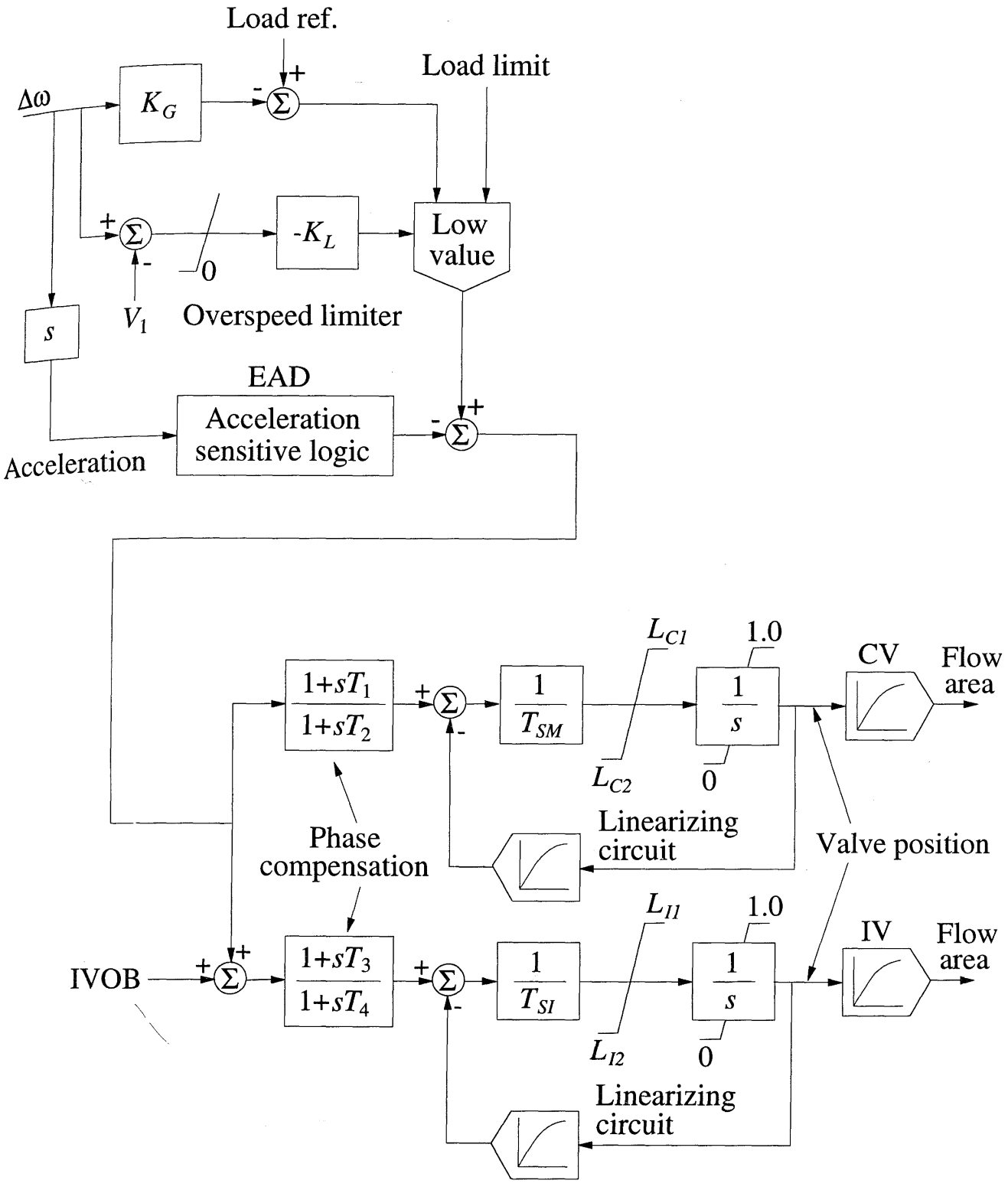

Figure 9.34 EHC governing system with electronic overspeed limiter and acceleration detection

The speed governor of Figure 9.33 has a similar steady-state IV speed versus flow characteristic to the MHC governor of Figure 9.32. In addition, it has two special features for limiting overspeed: IV trigger and power load unbalance relay [18,20].

The *IV trigger* is armed when the load (measured by reheat pressure) is greater than 0.1 per unit. It fast closes the IVs when the control error signal to the IV servovalve is less than −0.1 per unit. This represents a condition where per unit speed deviation $\Delta\omega$ is greater than $0.05LR+0.002$. Following an IV trip, the IV control is blocked for 1 second to permit hydraulic transients to decay, after which it is free to respond to speed control. The opening rate of the IV is limited to 0.1 pu/s by limiting the input signal to the servovalve.

The *power load unbalance* (PLU) *relay* is designed to fast close CVs and IVs under load rejection conditions that might lead to excessive overspeed. It is provided with selectivity to distinguish such conditions from stable system fault conditions. The PLU relay logic is shown in Figure 9.33(b). The relay circuit trips when the difference between turbine power and generator load exceeds a preset amount (0.4 pu) and the load decreases faster than a preset rate (equivalent to going from rated to zero load in about 35 ms). The turbine power is measured by a signal from the cold reheat pressure and the generator load by a signal derived from the three-phase currents. The use of current rather than electrical power helps discriminate between load loss and temporary system faults; under fault conditions current increases whereas power decreases. The tripping of the PLU relay causes the following actions:

- The CVs and IVs close completely.
- The load reference signal is removed from the CV and IV control signals.
- The load reference runs back to a minimum value at a rate of about 2.5% per second.

About 1 second after tripping, the CVs and IVs respond to their control signals. However, the load reference positions of these signals are not restored until the PLU relay resets, at which point the load reference runback stops. The load reference is not restored to the value prior to the disturbance, but remains at the value attained at the time the PLU relay resets.

The EHC speed-governing system shown in Figure 9.34 represents a fast-acting and highly responsive system [24]. Two forms of overspeed controls are provided: an electronic acceleration detection (EAD) function and an electronic overspeed limiting function. The EAD uses the governor end-of-shaft speed (with shaft torsional signals suitably filtered out) which it differentiates electronically to obtain acceleration. If acceleration exceeds the preset rate for a specified time, a prescribed valve opening and closing sequence is initiated, thereby limiting overspeed to an acceptable level. The overspeed limiter consists of a circuit which increases the governor gain by a factor of about 4 if speed exceeds a preset level of about 2%. Phase compensation circuits are provided as shown so that the phase characteristics of the control loops may be adjusted to ensure stable control performance.

Digital electrohydraulic (DEH) control system

A DEH system uses a digital controller, which is interfaced with the turbine valve actuators through an analog hybrid section [25]. The digital control system offers considerable flexibility since the control functions can be implemented through software.

The normal speed control function is set to provide the standard 4 to 5% regulation. The response of the governor is very fast, the time constant being on the order of 0.03 s. Filtering is normally provided to the speed signal to eliminate small variations in measured frequency. Additionally, programmable dead band may be provided to prevent governor response to small frequency variations.

In the DEH system described in reference 25, overspeed protection has two components: load overspeed anticipator (LOA) and overspeed sensing. The LOA function closes the CVs and the IVs rapidly when the main generator breaker opens, if the initial turbine power (determined by measuring IP section steam pressure) is greater than 30% of rated. The overspeed sensing function closes the CVs and IVs when speed exceeds 103% of rated; it is a discontinuous control causing the valves to close rapidly and then reopen. The LOA function does not affect the unit performance when connected to the power system. The overspeed sensing, however, could be triggered during severe system swings and should be designed so that it does not have an adverse effect on system performance. The modelling of the overall DEH turbine control is similar to that of Figures 9.33 and 9.34.

Initial pressure regulator

Often an auxiliary pressure control referred to as the *initial pressure regulator* (also known as *throttle pressure control*) is used to maintain the main steam pressure above a minimum value (usually 90% of rated pressure) [18,25]. When the pressure drops below the setpoint, the initial pressure regulator will introduce a closing signal, as shown in Figure 9.35. This effectively reduces the load reference at a rate of about 100% load/min, until the throttle pressure is restored above the setpoint or a minimum valve position (typically, corresponding to 20% flow) is reached.

The purpose of the initial pressure regulator is to protect the turbine against water induction from the boiler due to uncontrolled throttle pressure reduction during a boiler disturbance. However, the regulator may be triggered during a system transient, causing a rapid decrease in frequency. This in turn may result in a rapid load-pickup by the generators with the possibility of the throttle pressure dropping below the setpoint [25].

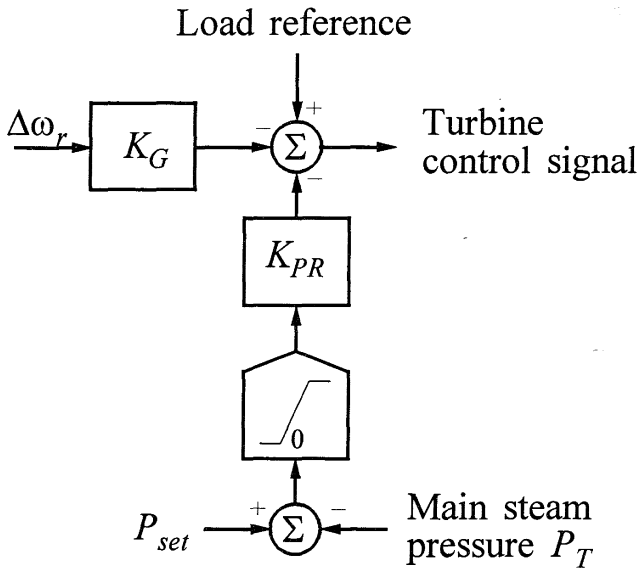

Figure 9.35 Initial pressure regulator

Generic model of steam turbine controls

A general model which can accommodate essentially all significant features of the different forms of steam turbine controls is shown in Figure 9.36. It allows representation of special control logic such as the power load unbalance (PLU) relay, IV trigger, fast valving (see Chapter 17, Section 17.1.8), acceleration and speed sensitive overspeed limit controls. It also includes facilities for representing feedback as well as series linearity compensation for valve nonlinearities, and phase compensation. The CV and IV controls have facilities for representing time constants associated with additional power amplification stages, and the speed governor model can account for transducer and filter time constant. Dead-band effects can be represented at five different locations.

9.2.3 Steam Turbine Off-Frequency Capability

Both the turbine and generator can tolerate only limited off-frequency operation; the turbine, however, is the more restrictive.

The principal risk in off-frequency operation of a steam turbine is the vibration and resonance of long low-pressure turbine blades. The blade vibration stresses are dependent on the excitation forces and the natural vibratory response characteristics of the blade's structural system. The predominant source of excitation is the stimulus produced by natural variations in steam flow. The magnitude of the excitation increases with increased steam flow.

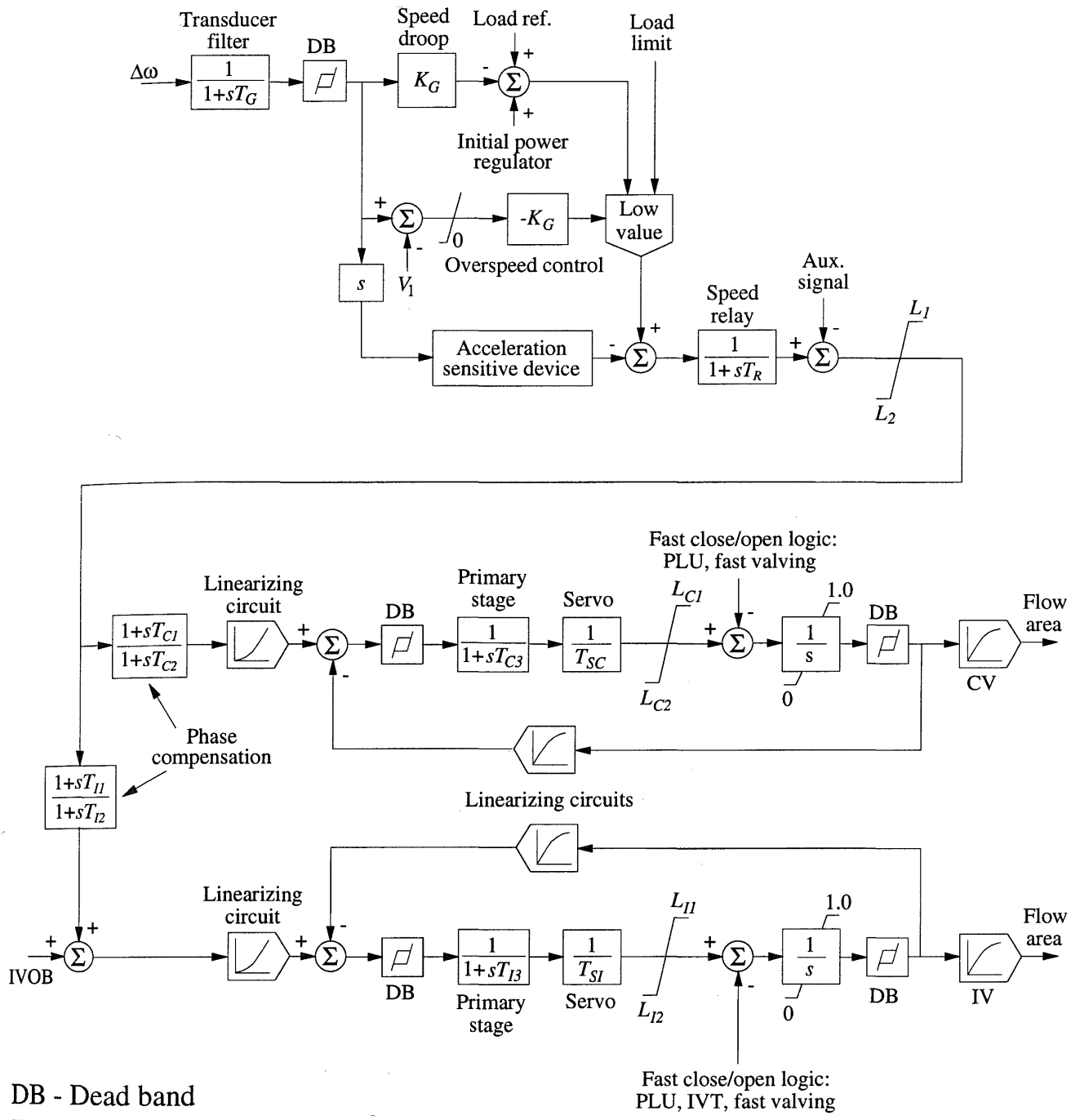

DB - Dead band
IVOB - IV opening bias

Figure 9.36 Generic steam turbine controls model

The vibratory response of a blade depends on the nearness of the excitation frequency to the blade natural frequency and on blade damping. For a resonant condition, the vibratory stress can be several hundred times greater than the stress during nonresonant operating conditions. The most critical blades are the ones in the last three rows in the LP turbine and, in some cases, the last row in the IP turbine. These blades have their natural frequencies controlled or tuned so that their vibration modes will not resonate at normal frequency operation.

There are three principal natural vibration modes associated with steam turbine blades [26]. The first is a tangential mode with blades vibrating in phase in the plane of maximum blade flexibility, perpendicular to the axis of the unit. The second mode is also an in-phase vibration, but with deflection essentially in an axial direction. The third is a torsional mode with the vibration of the blade group in approximately an axial direction.

The diagram shown in Figure 9.37, known as the Campbell diagram, illustrates how a change in turbine speed can provide steam excitation frequencies that coincide with the natural frequencies of a blade. The three nearly horizontal bands represent the characteristics of the three natural vibration modes of a long slender blade of an LP turbine section. The width of these bands indicates the scatter band and variations in natural frequencies due to manufacturing tolerances. The diagonal lines drawn at integral multiples (1 through 7) of turbine operating speed represent the stimulus frequencies inherent in the steam flow. An intersection of a blade natural vibration mode band and a steam stimulus frequency line represents a condition of resonance. Turbines are designed so that such resonant conditions are avoided at rated speed. However, departure from rated speed will bring the stimulus frequencies closer to one or more of the blade natural frequencies with the resulting higher vibrational stresses.

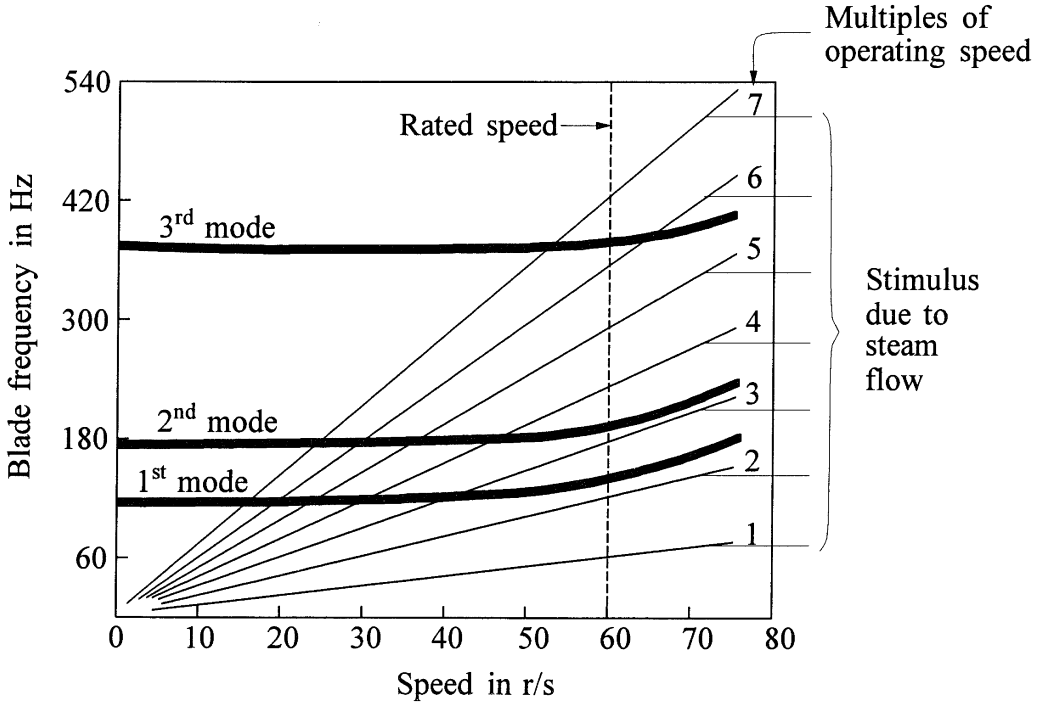

Figure 9.37 Typical Campbell diagram showing blade vibration characteristics

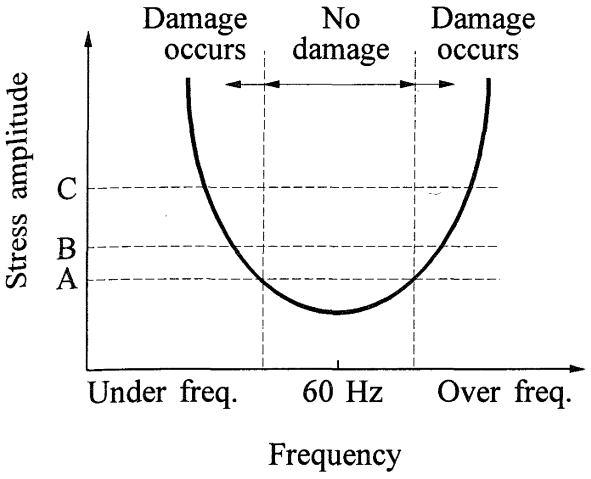

Figure 9.38 Increase in vibration amplitude with off-frequency operation

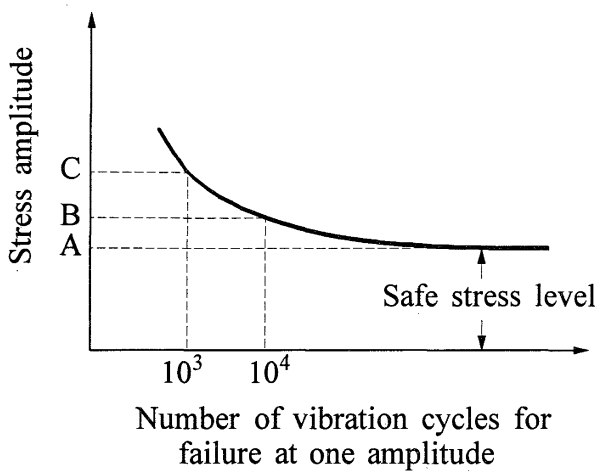

Figure 9.39 Stress versus number of cycles to failure

Figures 9.38 and 9.39 illustrate the relationship between blade failure due to fatigue and off-frequency operation. Below stress level A, the vibration stress amplitude is low enough that no damage results. Operation at stress level B would produce a failure at 10,000 cycles, and at level C failure would occur at 1000 cycles.

Operation at off-nominal frequencies is time-restricted depending on specific blade designs. Figure 9.40 is a composite representation of steam turbine off-nominal-frequency limitations of a large sample of turbines built by five different manufacturers [27]. The figure shows that sustained operation within the band 59.5 Hz to 60.5 Hz would not have any effect on blade life, while the dotted areas above 60.5 Hz and below 59.5 Hz are areas of restricted time operating frequency limits. Operation outside these areas is not recommended.

The characteristics shown in Figure 9.40 represent the composite operating limits of a large number of units and are useful for evaluating the requirements for protective relaying schemes. The applicable limit for a specific turbine may be less restrictive.

The effect of off-frequency operation in a given frequency band is cumulative, but independent of the time accumulated in any other band. The abnormal frequency capability curves are applicable whenever the unit is connected to the system. These curves also apply when the unit is not connected to the system, if it is operated at abnormal frequency while supplying its auxiliary load. During the period when the unit is being brought up to speed, is being tested at no-load for operation of overspeed trip device, or is being shut down, blade life will not be significantly affected if proper procedures are followed.

The most frequently encountered *overfrequency* condition is that of a sudden reduction of generator power resulting from a generator breaker trip. Under these conditions, the governor droop characteristic may result in a steady-state speed as high as 105% following the transient speed rise, and therefore speed reduction to near rated speed should be initiated promptly. For such sudden power reduction, units equipped with modern electrohydraulic turbine-governing systems provide this speed reduction automatically.

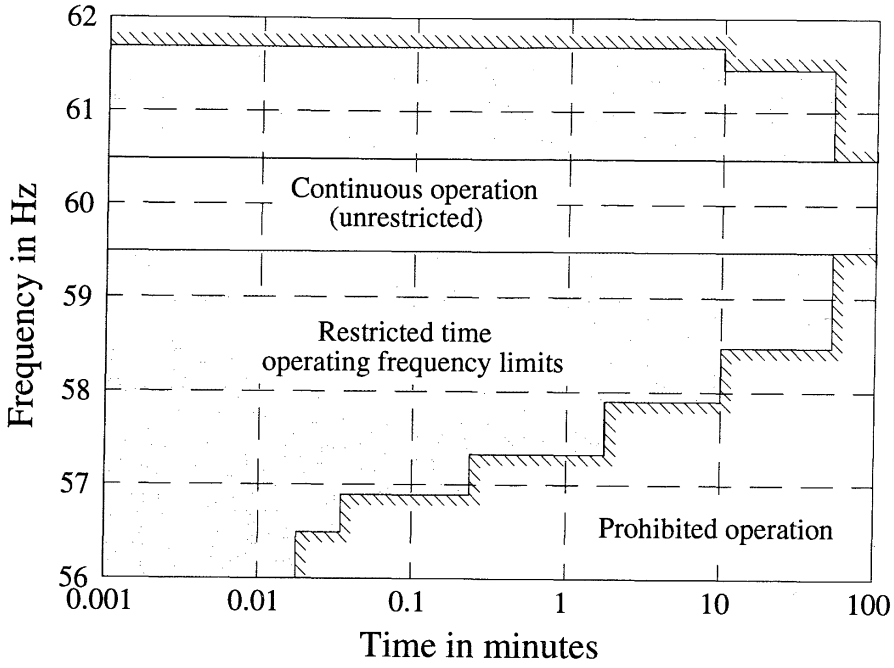

Figure 9.40 Steam turbine partial or full-load operating limitations during abnormal frequency, representing composite worst-case limitations of five manufacturers. ©ANSI/IEEE - 1987 [27]

For partial load reduction or system-islanding conditions, the system frequency will depend on the composite droop characteristic. Assuming a 5% droop characteristic, a generator-load mismatch of 50% would cause approximately a 2.5% (1.5 Hz) rise in frequency. Referring to Figure 9.40, the operating time-limit at this frequency is 35 minutes which is within the practical range of operator action to reduce speed settings. For higher frequencies, automatic control action such as use of overfrequency relay to initiate runback of the governor load reference is often employed.

Underfrequency operation of a steam turbine poses a more critical problem since generation cannot be increased more than full output. Underfrequency protective relays are normally employed to protect the unit. As an example, such relays may be set to trip the unit in 10 s if frequency remains below 57.5 Hz, or instantaneously if frequency drops below 56.0 Hz.

In order to prevent extended operation at lower than normal frequencies during system disturbances, load-shedding schemes are commonly employed to reduce the connected load to a level that can be supplied by the available generation. This is discussed in Chapter 11 (Section 11.1.7). If system load shedding is provided, then it is considered as the primary turbine underfrequency protection. Appropriate load shedding can cause the system frequency to return to normal before the turbine abnormal frequency limit is reached. Turbine underfrequency tripping should be considered as the last line of defense, as it may cause an area blackout.

9.3 THERMAL ENERGY SYSTEMS

9.3.1 Fossil-Fuelled Energy Systems [28]

In a fossil-fuelled power plant, fossil fuels such as coal, oil, or gas are used as the primary energy source to produce heat by combustion which, in turn, is transferred to the cold feed-water to generate (superheated) steam. Turbines convert the steam energy to mechanical energy which eventually produces electrical energy via the generators. The steam exhausting from the high pressure turbine is cycled back through the furnace for reheating (superheating) before it is admitted back to the lower pressure turbines. The exhaust steam, at close to saturation condition, is cooled in condensers (which are maintained at a very high vacuum - about 5 kPa) and converted back into liquid form. Large cooling water pumps provide the necessary heat removal capacity in the condensers. The condensate is then cycled back to the furnace as feed-water at high pressure, after various stages of pumping, feed-heating (to improve the energy conversion efficiency), and de-aerating.

Figure 9.41 illustrates the interrelationships among the various subsystems of a fossil-fuelled power plant.

Primary fuel system

The primary fuel system converts the primary fossil fuel into thermal energy. The raw fuel is transformed into thermal energy in the *furnace*. Fuel enters the furnace as controlled flow of oil, gas, or coal in the form of fine particles suspended in an airstream. A controlled amount of air is also injected to ensure complete combustion. This results in extremely high temperatures within the flame volume and the surrounding furnace. Energy is transferred to waterwall tubes carrying colder liquid from the drum or to the superheaters and reheaters carrying steam. The heat transfer is both radiative and convective.

The by-products of the combustion process are in both gaseous (flue gas) and solid (ash) forms (in coal fired plants). The solid by-products are removed in the furnace and only the gaseous by-products (flue gas) leave the furnace. Energy is extracted from the flue gases by various heat exchange systems. After passage through these heat exchanger banks (superheaters, reheaters, economizer, air heater, etc.) and ductworks, these gases are exhausted into the atmosphere via the induced draft (ID) fans through the chimneys or stacks.

The fuel flow enters the furnace through burner nozzles which, in some furnace designs, can be tilted upward or downward to position the flame in the furnace. The position of the flame affects the radiative heat transfer and is utilized in controlling superheat/reheat temperatures.

Both fuel and air entering the furnace are controlled to provide desired heat generation, while the ID fans are controlled to maintain the furnace at a suitable sub-atmospheric pressure. If a furnace (or pulverizer) trip occurs, it must be purged by air

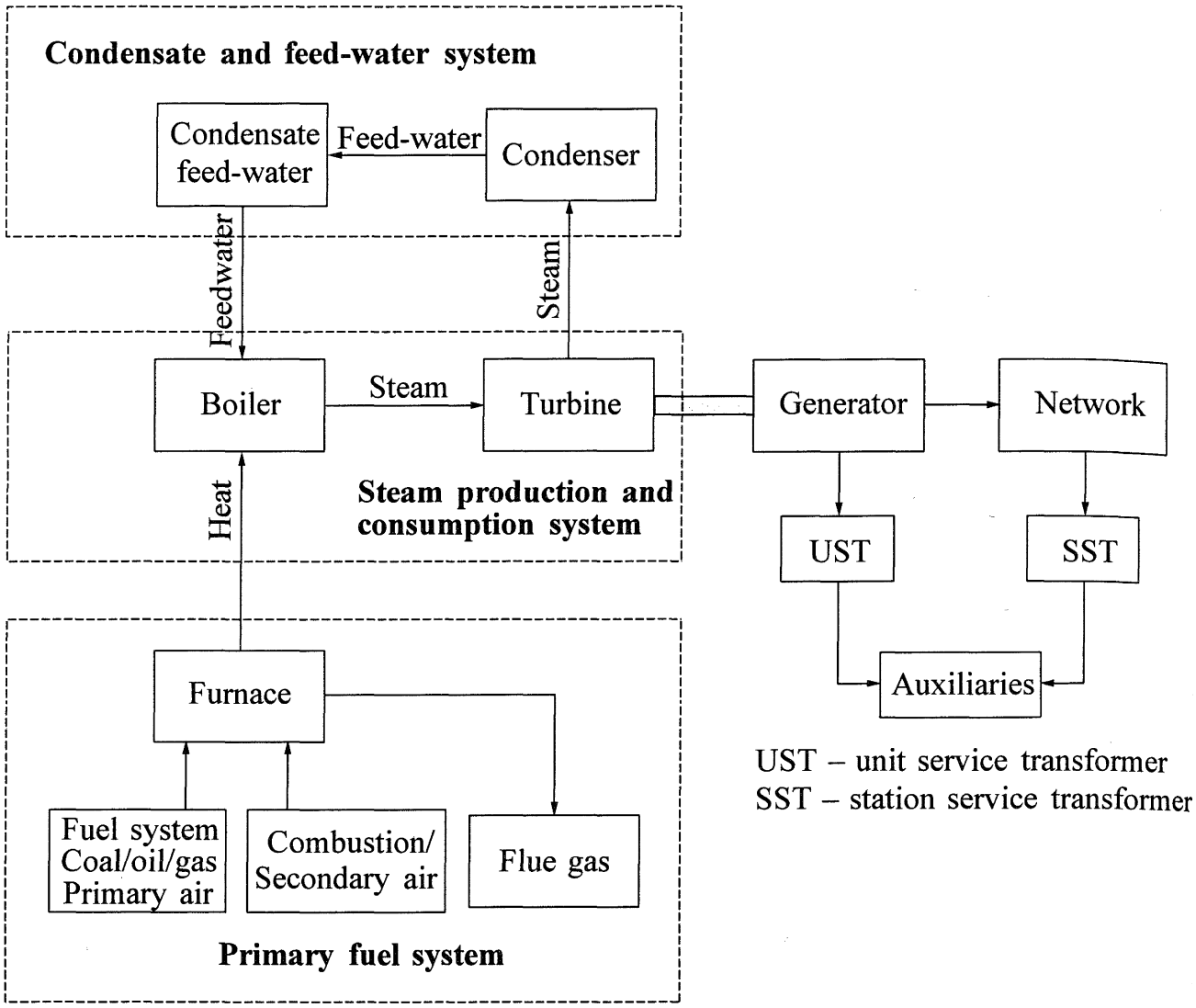

Figure 9.41 Subsystems of a fossil-fuelled power plant

for a preset minimum time before being placed in service again, to prevent duct explosions.

The *fuel system* supplies the fuel (coal, oil or gas) to the furnace. Oil- and gas-fired units can respond to load demand changes more quickly than coal-fired units. This is because solid fuels such as coal require additional processing, such as pulverizing and drying, before they can be used for combustion. Furthermore, pulverized coal systems make use of several pulverizers in parallel, each with a limited capacity and requiring an additional warm-up period when started. In the case of a rapid decrease in firing demand, the burner management controls may automatically trip a number of pulverizers. When pulverizers are tripped, the firing rate is limited to a level corresponding to the number of pulverizers remaining in service. Therefore, the re-loading rate is dictated by the time required for bringing the tripped or shutdown pulverizers back into service.

The *secondary air system* provides the supply of combustion air to the furnace windbox, whence it enters the furnace via fuel air and auxiliary air dampers. The source of the air is the forced draft (FD) fan. The demand for the flow rate is received from the fuel and air controller in the form of a desired flow rate to maintain adequate and complete combustion in the furnace. The air controller logic monitors the actual (measured) flow rate and manipulates inlet vanes of the FD fans to control the air flow rate. The air flow passes through secondary air heaters where it is preheated by extracting heat from exhaust flue gases before it enters the windbox. Usually, the windbox pressure is controlled by manipulation of a number of fuel and auxiliary air dampers so that a required differential pressure exists between the windbox and the furnace.

The *flue gas system* includes the flue gas path from furnace exit to the chimney stacks via the induced draft (ID) fans. The flow rate of the flue gas is controlled by manipulating the variable inlet vanes for the ID fans by the furnace pressure controller. The heating zones in the flue gas path include the primary and secondary superheaters, reheater, economizer, and primary and secondary air heaters. Each section in the flue gas path acts as a heat exchanger, transferring heat from hot gases to colder steam, feed-water, or air. The first two levels of heat exchangers (secondary superheater and reheater sections) receive radiative heat directly from the furnace in addition to convective heat transfer from the gases.

Steam production and utilization system

The steam is produced in the *boiler* and superheated in the superheater and reheater. The thermal energy of the steam is converted to mechanical energy in the various sections of the turbine. Boiler designs fall into two categories: (a) drum type boilers, and (b) once-through boilers. Figure 9.42 shows schematics of the two types of boilers.

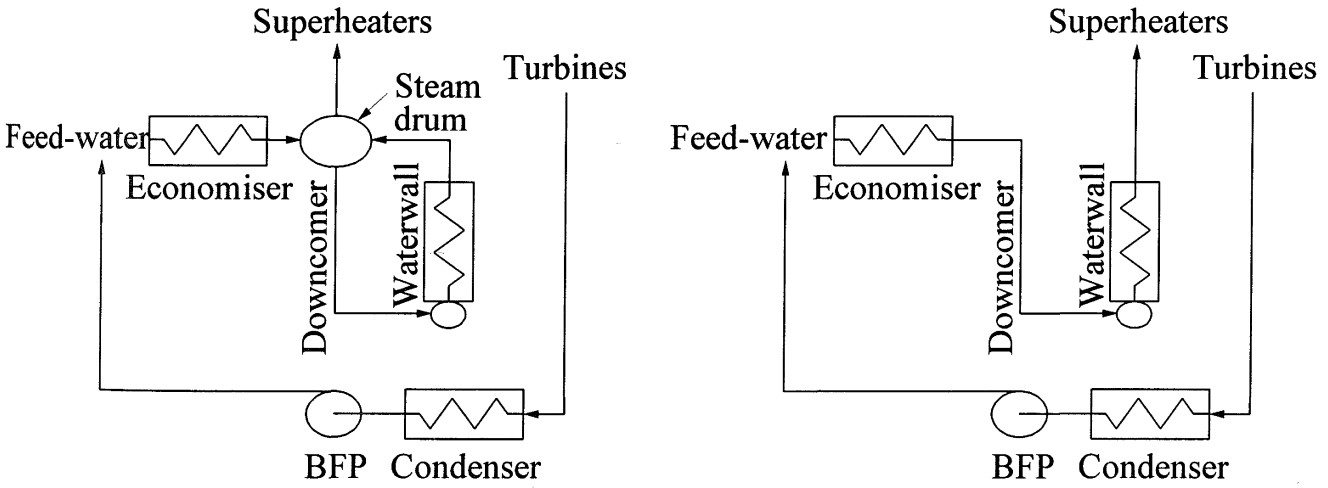

(a) Drum-type boiler (b) Once-through boiler

Figure 9.42 Fossil-fuelled unit boiler types

Drum-type boilers:

Drum-type or recirculation boilers rely on natural or forced circulation of drum liquid to absorb energy from the hot furnace walls, called waterwalls, for generating steam. The boiler receives feed-water which has been preheated in the economiser and provides saturated steam outflow. The circulation loop consists of almost saturated water being carried from the drum via downcomer tube banks which is then passed through waterwall tubes (which, in effect, form the walls of the furnace - hence the nomenclature) where they absorb radiant and convective heat from the flame and hot flue gases. This system operates at subcritical pressures as long as there is some finite density difference between the steam and water phases. Low pressure subcritical boilers depend totally on the natural recirculation phenomena resulting from the static thermal head difference between the water in the downcomers and the steam-water mixture in the heated steam generating tubes. Higher pressure (but still subcritical) boilers usually make use of the circulating pump to supplement the thermal head. Recirculation boilers make use of a drum to separate steam from the recirculation water so that it can proceed to the superheaters as a heatable vapour; hence, recirculation boilers are referred to as drum type boilers.

The steaming rate is predominantly a function of heat absorbed in the furnace waterwalls. Any discrepancy from the steam utilization rate (in turbines) results in boiler pressure variation. To protect against overpressurization, relief valves are used.

Once-through boilers:

In a once-through boiler, there is no recirculation of water within the furnace. Instead, feed-water, at high pressure, flows straight through the waterwalls where it receives furnace heat and is converted to steam which then passes through the superheaters and eventually enters the HP turbine. The operation of the feed-water system, including the *boiler feed pump* (BFP), is needed to produce the through flow, and a suitable means must be provided to dispose of the circulated flow without incurring loss of heat or working fluid. This is normally done with a steam-turbine bypass system.

The once-through design has been used for both the high subcritical and the supercritical pressure ranges. In the supercritical range (i.e., above 22,120 kPa), the fluid's physical properties change continuously from those of a liquid (water) to those of a vapour (steam). There is no saturation temperature or two-phase mixture. Instead, the temperature rises steadily, and the specific heat and its rate of rise vary considerably during the process. Therefore, the nature of supercritical steam generation rules out the use of a boiler drum to separate steam from water.

Unlike in a drum type boiler, there is no drum level to be controlled in a once-through boiler. There are three major control loops involving megawatt, throttle pressure, and steam temperature. These are controlled by manipulating the governor valve, feed-water valve, and firing rates either individually or in a coordinated mode by manipulating all three loops simultaneously.

A once-through boiler has less stored energy than a drum-type boiler. Therefore, a generating unit with a once-through boiler is more responsive to changes in boiler firing rate. On the other hand, a drum-type boiler unit can deliver power without any fuel flow for a longer time. Neither type of boiler can supply full load steam flow for more than 1 or 2 minutes; however, both types can supply sufficient steam to support unit service load at normal throttle pressure for at least 30 minutes [29].

Control systems

The control systems associated with fossil-fuelled plants vary with the manufacturer and vintage of the unit. Nevertheless, some generalizations about the plant controls are possible. Most boilers have several controlled outputs and several manipulated variables which affect these outputs. Usually the firing rate, pumping rate, and throttle valve settings are the controlled variables. The controlled output variables of interest are temperature, pressure, electrical power, and speed. If, in the process, the plant variables exceed safe limits, the protection systems are designed to reduce the plant output or trip the unit.

The control systems associated with a thermal plant can be classified into two broad categories:

- Overall unit control
- Process parameter controls

There are four *overall unit control* strategies or modes of operation: boiler following (turbine leading), turbine following (boiler leading), integrated or coordinated boiler-turbine control, and sliding pressure control.

Under the *boiler-following* or *turbine-leading* mode of control, changes in generation are initiated by turbine control valves. The boiler controls respond to the resulting changes in steam flow and pressure by changing steam production. A difference between steam production and steam demand results in a change in boiler pressure. The throttle pressure deviation from its setpoint value is used as an error signal by the combustion controls to regulate fuel and air input to the furnace. Usually, a proportional-plus-integral (reset) controller is used to maintain appropriate firing rate at different load levels. In some cases, the turbine first-stage pressure is incorporated as a feedforward signal to the combustion controls to improve initial response.

Under the *turbine-following* or *boiler-leading* mode of control, changes in generation are initiated by changing input to the boiler. The MW demand signal is applied to the combustion controls. The turbine control valves regulate boiler pressure; fast action of the valves maintains essentially constant pressure.

Figure 9.43 shows the relative responses of the boiler-following and the turbine-following modes of control to a large change in load. With the boiler-following mode of operation, the boiler's stored energy is initially used to meet the

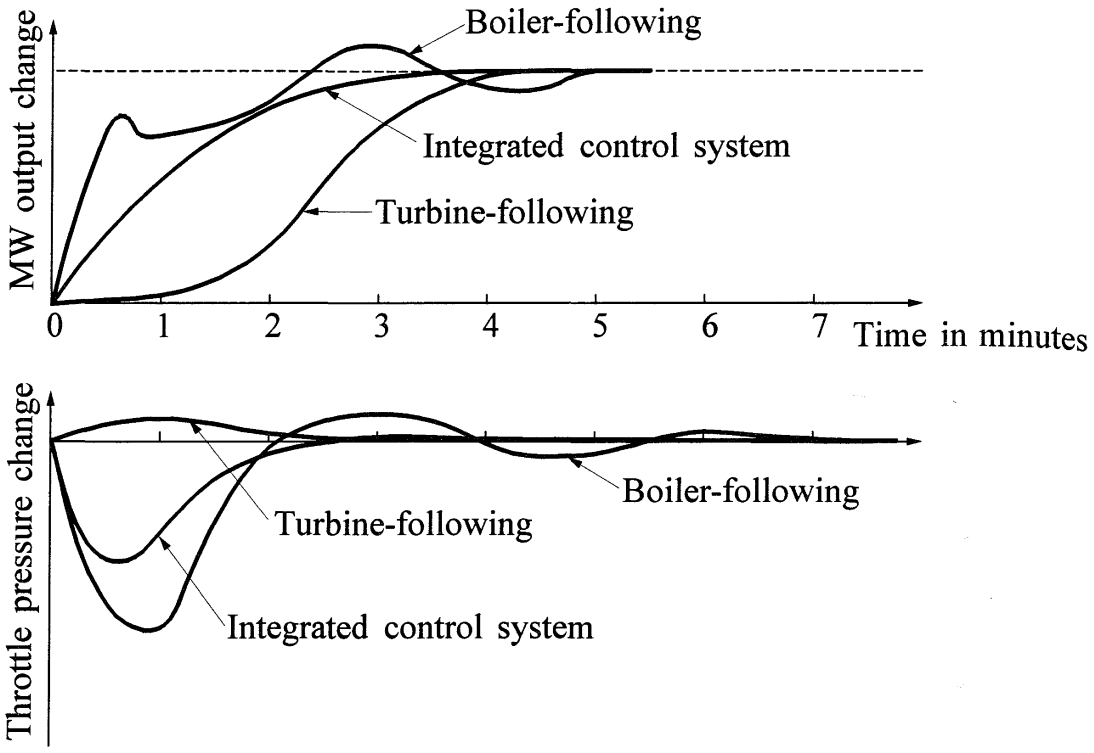

Figure 9.43 Comparison of boiler-turbine control system response to a large load change

steam demand and the initial response of MW output is rapid. The coupling between throttle pressure and MW output results in a "dip" in the MW output when the boiler pressure is at a minimum. This coupling, along with the boiler time lag, produces an oscillatory response. For large changes, the deviations in boiler variables may be excessive. In contrast, with the turbine-following mode, no use is made of stored energy in the boiler; hence, steam flow and MW output closely follow steam production in the boiler. While the unit can be manoeuvred in a well-controlled manner, the response rate is limited by the slow response of the boiler.

The *integrated* or *coordinated boiler-turbine* control provides an adjustable blend of both boiler-following and turbine-following modes of control. The improvement in unit response achieved through integrated control is demonstrated in Figure 9.43. It is evident that the integrated control strikes a compromise between fast response and boiler safety.

In the *sliding pressure mode* of control, the throttle pressure setpoint is made a function of unit load rather than a constant value. The control valves are left wide open (provided the drum pressure is above a minimum level) and the turbine power output is controlled by controlling the throttle pressure through manipulation of the boiler controls. It is thus essentially a turbine-following mode of operation. A major advantage of this mode of control is that no change in throttling action occurs during load manoeuvring; therefore, temperature in the HP turbine can remain nearly constant.

The *process parameter controls* include systems that regulate unit MW output, main steam pressure, feed-water, and air/fuel.

Protection systems

The function of the protection system is to monitor important plant process parameters and initiate a trip and/or derating of processes (such as furnace and turbine) or auxiliary equipment (such as ID/FD fans) under adverse conditions.

A typical boiler protection monitors the following in determining if the furnace is to be tripped: furnace pressure, status of ID/FD fans, air flow, drum level, feed-water flow, black furnace (loss of flame), and main steam pressure. Each protection is usually time-conditioned.

The protection of auxiliary motors is generally based on voltage, frequency, or current supplied to the motor.

9.3.2 Nuclear-Based Energy Systems [28]

Two basic types of nuclear power plant reactors are in common use in North America: the *pressurized water reactor* (PWR) and the *boiling water reactor* (BWR). A variation of the PWR type is the *Canadian deuterium uranium* (CANDU) reactor.

The pressurized water reactor (PWR)

Figure 9.44 shows a simplified representation of a PWR unit. It uses water under pressure as a heat transport medium which absorbs heat from the reactor core and exchanges it with the shell-side feed-water in a *steam generator* which produces the steam used to drive the turbine. The steam produced is saturated, requiring wet-steam turbines.

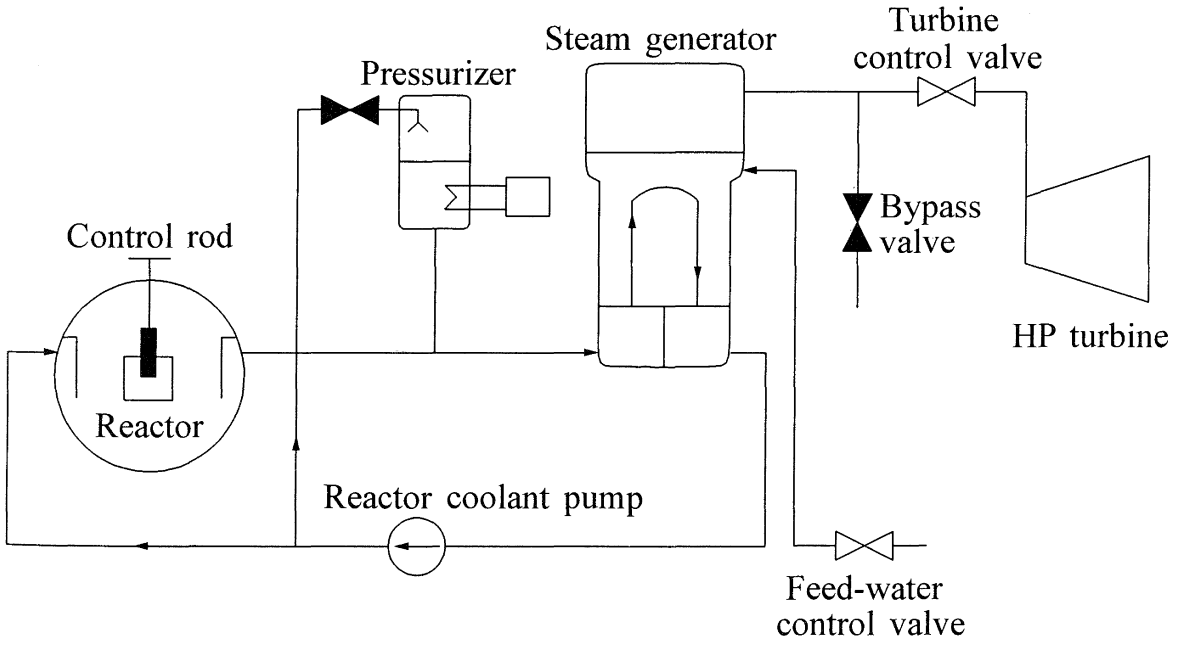

Figure 9.44 Schematic diagram of a PWR

The coolant circuit in a PWR acts as a heat transport medium as well as a nuclear reaction moderating medium. As a moderator, the coolant is used to slow down high energy neutrons to thermal energy levels, thus facilitating the nuclear fission reaction. This function provides a mechanism for self-regulation of the reactor process. An increase of reactor power results in an increase of the coolant temperature and a corresponding decrease of the fluid density. This lowers the nuclear fission reaction rate, thereby acting as a negative feedback in the reactor process dynamics. The coolant pressure control is facilitated by the use of a *pressurizer*, which comprises a liquid-filled tank feeding the coolant circuit. A steam space at the top of the tank is used to maintain the pressure at setpoint by means of electric water heaters and water sprays. The liquid level in the tank is controlled by using a make-up and let-down system of valves. The fluid flow in the reactor is sustained by means of large electrically driven *reactor coolant pumps*. The control of the reactor power is achieved by means of neutron-absorbing *control rods* which are inserted to a variable depth in the reactor core. The controller directs the movement of preselected groups of control rod clusters to increase or decrease reactor power as required to maintain the average coolant temperature at a programmed setpoint. A neutron flux signal and a turbine power signal are used to enhance the controller's response to load variations. Long-term regulation of core reactivity is accomplished by adjusting the concentration of neutron-absorbing boric acid in the reactor coolant.

The most critical pumps in a nuclear power plant are those associated with the reactor systems. Low-frequency operation has been cited as a cause of low reactor coolant flow in PWR units. If reactor power remains constant as coolant flow decreases, the heat content per unit of coolant-flowing increases. Steam bubbles can no longer be swept from the surface of the fuel cladding sufficiently quickly, and a blanketing of the hot surfaces with a steam film results. This condition is termed *departure from nucleate boiling* (DNB). At DNB the heat transfer rate is drastically reduced, and the resultant fuel and cladding temperature increases, leading to cladding failure and the release of radioactive fission products to the coolant. To prevent this condition from occurring, minimum reactor coolant pump-flow limits and motor undervoltage and underfrequency limits are established. Should these limits be violated, the reactor is automatically tripped.

In the conventional PWR design, the coolant temperature is a very important variable - it is used for both reactor control and steam dump operations.

The operation of the PWR is best visualized by considering its response to an increase in load demand. The control valves open to let more steam into the turbine to meet the increased demand. This in turn causes the water level in the steam generator to drop. The feed-water flow then increases to restore the water level. The mismatch between the reactor power level and the steam generator load results in a decrease of the reactor's coolant temperature and pressure, and a corresponding decrease in the moderating fluid's density. This change in density results in an increase of the neutron multiplication rate which provides the initial rise in the reactor power level. In response to the decreased coolant temperature, the reactor control system initiates a control absorber rod withdrawal to raise reactor power. The coolant

pressure control system responds to the pressure change by operating the pressurizer heaters. Finally, the pressurizer water level is restored by the make-up and let-down system. A new steady-state condition is established when the equilibrium between the generator electrical power output and the reactor power level is reached.

The response to a decrease in load demand is similar to the above but in reverse. Typically, a PWR is capable of a load manoeuvring rate of ±5% reactor full power (RFP) per minute, and a step change of ±10% RFP.

Canadian deuterium uranium (CANDU) reactors

A CANDU reactor is a variation on the PWR design which uses heavy water in the coolant circuit for the heat transport function but assigns the moderating function to another independently controlled circuit - the moderator system. The moderator temperature is controlled by regulating the service-water flow through cooling heat exchangers. While the conventional PWR design relies on the thermal feedback of the moderating fluid to provide the initial load-following reactor response and steady-state reactor power level fine-tuning, the CANDU design utilizes a separate mechanism to directly control reactivity by means of a series of light water-filled tubes (zones) distributed in the reactor core. This design offers a faster response to reactor power demand change and a decoupling of the reactor controls from the steam generator dynamics. The steam generator pressure is also directly controlled to be maintained at a pressure setpoint. Feedforward action is also added to improve response and maintain the balance between reactor power and turbine load. The coolant circuit of some CANDU plants is not equipped with a pressurizer and relies solely on a make-up and let-down system to control coolant pressure. In these cases, the pressure setpoint is made a function of reactor power level in an effort to minimize swell and shrink in the coolant circuit. Despite this effort, the pressure swings in response to system electrical disturbances are still more pronounced than in a pressurizer-equipped system and may determine the outcome of the reactor protection system's reaction to the disturbance.

CANDU plants can be operated in two basic control modes: *reactor-following-turbine* (RFT) and *turbine-following-reactor* (TFR). Steam generator pressure control plays a pivotal role in these schemes. In TFR mode the reactor power is held constant at a level set by the operator and the turbine governor control valves are used to regulate steam pressure. This mode is suitable for unit operation within a large system network where it is used to supply the base loads while other units are used to supply peak loads. Since reactor conditions remain constant, this mode also constitutes a safer state of operation from the nuclear plant perspective. The control system reverts to this mode of operation during plant upsets. In RFT mode, the turbine load is set by the operator and the reactor is used to regulate steam pressure. In both TFR and RFT modes, the turbine is also used to regulate speed and assist the system in meeting short-term changes in electrical load demand. In RFT mode, the governor control valves also attempt to maintain a constant generator output.

In CANDU units, the steam dump valves are modulated in proportion to the amount of pressure error in excess of a preset value (the pressure error offset) with a power mismatch feedforward term added. Some CANDU units permit a small amount of steam dump (5%) into the condenser without initiating a reactor power reduction. Beyond that, the reactor power is set back at the rate of 0.05%/s until no more than 5% steam dump is admitted. In the case of large load rejections (greater than 40%) the pressure offset term is removed from the bypass valve control equation, and the reactor is stepped back to 60% RFP by a free-fall drop of the control rods into the reactor core. In addition, a fast-action scheme is put in effect whereby the bypass valves are opened fully for a short period of time and the control program sampling rate is increased.

In CANDU reactor design, the coolant temperature is less critical than in the conventional PWR design except for its heat transfer implication. The reactor is controlled based on flux measurements, with thermal measurements serving as correction factors only. The CANDU reactor power level is so tightly controlled that it is virtually decoupled from the turbine side of the plant. Therefore, the steam generator pressure control is more critical than the reactor control in the simulation of CANDU units.

The boiling water reactor (BWR)

Figure 9.45 shows a schematic diagram of a BWR. The feed-water enters directly into the reactor core and heat is transferred to the boiling water. The efficiency of heat removal is thus improved by use of the latent heat of evaporation. The steam produced at the reactor outlet header is used to drive the turbine. As in the case of a PWR, saturated steam is produced, requiring wet-steam turbines.

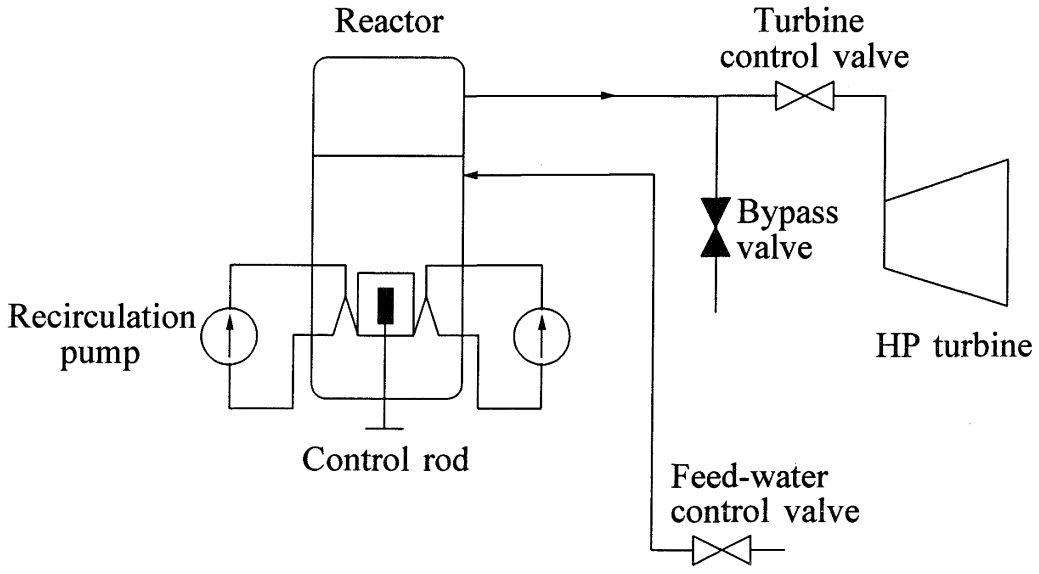

Figure 9.45 Schematic diagram of a BWR

The BWR relies on the moderating effect of the steam generated in the reactor to adjust the neutron multiplication rate. The power level is determined by the balance established between the amount of fuel in the core, the amount of neutron-absorbing material within the control rods in the core, and the core steam/water volume ratio (void content). In addition to the feed-water circuit, which acts as the main source of water into the reactor, a recirculation circuit also contributes to the water flow through the reactor core. Increasing either the feed-water or recirculation flow decreases the reactor steam void and thus raises reactor power. The control rod position establishes the relationship between reactor power level and core flow. Control rod withdrawal/insertion is used for quick manoeuvring of the reactor. The recirculation flow is sustained by using variable-speed electrically driven pumps and the flow is directed into the reactor core by means of an array of jet pumps. Feed-water flow is also sustained by using electrically driven pumps and adjusted by means of control valves to maintain the reactor water level at setpoint. Steam pressure is maintained by means of the turbine governor control valves.

To illustrate the dynamics and control of a BWR, let us consider its response to an increase in load demand. The governing system responds by opening the control valve to increase the steam flow and, in anticipation of this increase, the master controller increases recirculation flow. The steam pressure setpoint is momentarily decreased to permit the governor control valves to open. The steam pressure drops as the steam outflow is increased. An increase in recirculation flow decreases the steam void in the reactor core (i.e., moderator density increases) and the reactor power level rises. With the increase in reactor power, steam pressure is restored and the steam pressure setpoint is returned to its original value. The reactor water level decreases following the increased steam outflow, but the water inventory is soon restored by an increase in feed-water flow. The BWR maximum load manoeuvring rate is dictated by the recirculation controller response and by limits set on changes to reactor water level and steam pressure.

A BWR is capable of load following over the entire reactor operating range. Newer units, such as the BWR 6 design, are capable of step changes of up to ±25% RFP.

A BWR unit can withstand a decrease in load of up to almost 100% without tripping. For decreases in load of more than 25%, the turbine bypass valves operate to temporarily relieve excess steam which is supplied by the reactor but not delivered to the turbine. The bypass valves close automatically as reactor power is reduced by a combination of flow control and control rod insertion.

9.3.3 Modelling of Thermal Energy Systems

Dynamics of thermal energy systems play an important role in the long-term dynamic response of power systems. In addition to the process physics of the individual elements of these systems, the associated auxiliaries, protections, and controls need to be appropriately represented in the study of long-term stability.

Models for representation of thermal energy systems in system studies are still evolving, and standard models for common use by the utility industry have not yet been developed. Reference 30 presents detailed nuclear and thermal power plant models recently developed by Ontario Hydro and CRIEPI (Japan) under a joint EPRI/CRIEPI study.

REFERENCES

[1] H.M. Rustebakke (editor), *Electric Utility Systems and Practices*, John Wiley & Sons, 1983.

[2] G.R. Rich, *Hydraulic Transients*, Dover Publications, Inc., 1963.

[3] V.L. Streeter and E.B. Wylie, *Fluid Mechanics,* McGraw-Hill, 1975.

[4] C. Concordia and L.K. Kirchmayer, "Tie-Line Power and Frequency Control of Electric Power Systems," *AIEE Trans.,* Vol. PAS-73, pp. 131-146, 1954.

[5] Discussion of reference 4 by H.M. Paynter.

[6] R. Oldenburger and J. Donelson, Jr., "Dynamic Response of a Hydroelectric Plant," *AIEE Trans.,* Vol. PAS-81, Part III, pp. 403-419, October 1962.

[7] L.M. Hovey, "Optimum Adjustment of Hydro Governors on Manitoba Hydro System," *AIEE Trans.,* Vol. PAS-81, Part III, pp. 581-587, December 1962.

[8] J.L. Woodward, "Hydraulic-Turbine Transfer Function for Use in Governing Studies," *Proc. IEE,* Vol. 115, No. 3, pp. 424-426, March 1968.

[9] D.G. Ramey and J.W. Skooglund, "Detailed Hydrogovernor Representation for System Stability Studies," *IEEE Trans.,* Vol. PAS-89, pp. 106-112, January 1970.

[10] IEEE Committee Report, "Dynamic Models for Steam and Hydro Turbines in Power System Studies," *IEEE Trans.,* Vol. PAS-92, pp. 1904-1915, November/December 1973.

[11] IEEE Working Group Report, "Hydraulic Turbine and Turbine Control Models for System Dynamic Studies," *IEEE Trans.,* Vol. PWRS-7, No. 1, pp. 167-179, February 1992.

[12] J.M. Undrill and J.L. Woodward, "Nonlinear Hydro Governing Model and Improved Calculation for Determining Temporary Droop," *IEEE Trans.,* Vol.

PAS-86, pp. 443-453, April 1967.

[13] F.R. Schleif and A.B. Wilbor, "The Coordination of Hydraulic Turbine Governors for Power System Operation," *IEEE Trans.,* Vol. PAS-85, pp. 750-758, July 1966.

[14] P.L. Dandeno, P. Kundur, and J.P. Bayne, "Hydraulic Unit Dynamic Performance under Normal and Islanding Conditions - Analysis and Validation," *IEEE Trans.,* Vol. PAS-97, pp. 2134-2143, November/December 1978.

[15] M. Leum, "The Development and Field Experience of a Transistor Electric Governor for Hydro Turbines," *IEEE Trans.,* Vol. PAS-85, pp. 393-400, April 1966.

[16] R.E. Goodson, "Distributed System Simulation Using Infinite Product Expansions," *Simulation,* Vol. 15, No. 6, pp. 255-263, December 1970.

[17] P. Kundur and J.P. Bayne, "A Study of Early Valve Actuation Using Detailed Prime Mover and Power System Simulation," *IEEE Trans.,* Vol. PAS-94, pp. 1275-1287, July/August 1975.

[18] IEEE Working Group Report, "Dynamic Models for Fossil Fueled Steam Units in Power System Studies," *IEEE Trans.,* Vol. PWRS-6, No. 2, pp. 753-761, May 1991.

[19] E.F. Church, *Steam Turbines,* McGraw Hill, pp. 70-74, 1950.

[20] T.D. Younkins and L.H. Johnson, "Steam Turbine Overspeed Control and Behaviour during System Disturbances," *IEEE Trans.,* Vol. PAS-100, pp. 2504-2511, May 1981.

[21] M.A. Eggenberger, "An Advanced Electrohydraulic Control System for Reheat Steam Turbines," American Power Conference, Chicago, April 1965.

[22] M.A. Eggenberger, "A Simplified Analysis of the No-Load Stability of Mechanical-Hydraulic Speed Control Systems for Steam Turbines," ASME Paper 60-WA-34, December 1960.

[23] M. Birnbaum and E.G. Noyes, "Electro Hydraulic Control for Improved Availability and Operation of Large Steam Turbines," ASME-IEEE National Power Conference, Albany, September 1965.

[24] P. Kundur, D.C. Lee, and J.P. Bayne, "Impact of Turbine Generator Overspeed

Controls on Unit Performance under System Disturbance Conditions," *IEEE Trans.*, Vol. PAS-104, pp. 1262-1267, June 1985.

[25] M.S. Baldwin and D.P. McFadden, "Power Systems Performance as Affected by Turbine-Generator Controls Response during Frequency Disturbances," *IEEE Trans.*, Vol. PAS-100, pp. 2486-2494, May 1981.

[26] H.T. Akers, J.D. Dickinson, and J.W. Skooglund, "Operation and Protection of Large Steam Turbine Generators under Abnormal Conditions," *IEEE Trans.*, Vol. PAS-87, pp. 1180-1188, April 1968.

[27] ANSI/IEEE Standard C37.106-1987, *IEEE Guide for Abnormal Frequency Protection for Power Generating Plants.*

[28] EPRI Report EL-6627, "Long-Term Dynamics Simulation: Modelling Requirements," Final Report of Project 2473-22, Prepared by Ontario Hydro, December 1989.

[29] O.W. Durrant and R.P. Siegfried, "Operation of Drum and Once-Through Boilers during Electrical Power System Emergencies," Paper presented at the ASME-IEEE Joint Power Generation Conference, Detroit, Mich., September 1967.

[30] EPRI Report EL-6627, "Long-Term Dynamic Simulation: Nuclear and Thermal Power Plant Models," Final Report of Project 3144-01, Prepared by Ontario Hydro and CRIEPI (Japan), September 1992.

Chapter 10

High-Voltage Direct-Current Transmission

High-voltage direct-current (HVDC) transmission has advantages over ac transmission in special situations. The first commercial application of HVDC transmission was between the Swedish mainland and the island of Gotland in 1954. This system used mercury-arc valves and provided a 20 MW underwater link of 90 km. Since then, there has been a steady increase in the application of HVDC transmission.

With the advent of thyristor valve converters, HVDC transmission became even more attractive. The first HVDC system using thyristor valves was the Eel River scheme commissioned in 1972, forming a 320 MW back-to-back dc interconnection between the power systems of the Canadian provinces of New Brunswick and Quebec. Thyristor valves have now become standard equipment for dc converter stations. Recent developments in conversion equipment have reduced their size and cost, and improved their reliability. These developments have resulted in a more widespread use of HVDC transmission. In North America, the total capacity of HVDC links in 1987 was over 14,000 MW [1]. There are more links under construction.

The following are the types of applications for which HVDC transmission has been used:

1. Underwater cables longer than about 30 km. AC transmission is impractical for such distances because of the high capacitance of the cable requiring intermediate compensation stations.

2. Asynchronous link between two ac systems where ac ties would not be feasible because of system stability problems or a difference in nominal frequencies of the two systems.

3. Transmission of large amounts of power over long distances by overhead lines. HVDC transmission is a competitive alternative to ac transmission for distances in excess of about 600 km.

HVDC systems have the ability to rapidly control the transmitted power. Therefore, they have a significant impact on the stability of the associated ac power systems. An understanding of the characteristics of the HVDC systems is essential for the study of the stability of the power system. More importantly, proper design of the HVDC controls is essential to ensure satisfactory performance of the overall ac/dc system.

This chapter will provide a general introduction to the basic principles of operation and control of HVDC systems and describe their modelling for power-flow and stability studies. Two terminal systems will be considered in detail, followed by a brief discussion of multiterminal systems.

For additional general information on HVDC transmission, the reader may refer to references 2 to 8. Reference 9 provides information related to specification of HVDC systems.

10.1 HVDC SYSTEM CONFIGURATIONS AND COMPONENTS

10.1.1 Classification of HVDC Links

HVDC links may be broadly classified into the following categories:

- Monopolar links
- Bipolar links
- Homopolar links

The basic configuration of a *monopolar link* is shown in Figure 10.1. It uses one conductor, usually of negative polarity. The return path is provided by ground or water. Cost considerations often lead to the use of such systems, particularly for cable transmission. This type of configuration may also be the first stage in the development of a bipolar system.

Instead of ground return, a metallic return may be used in situations where the earth resistivity is too high or possible interference with underground/underwater metallic structures is objectionable. The conductor forming the metallic return is at low voltage.

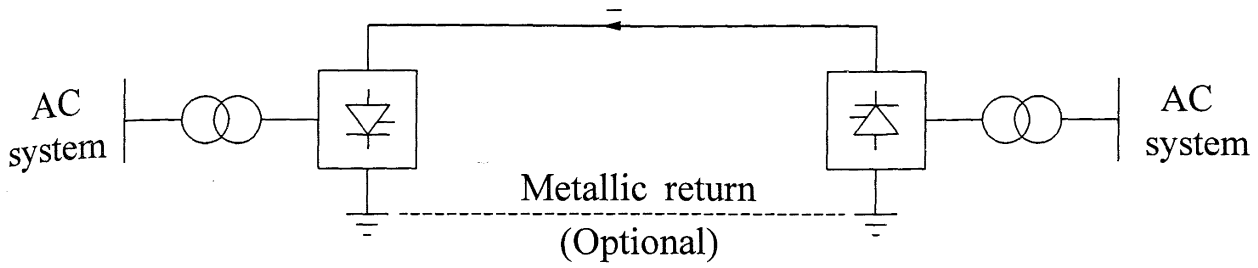

Figure 10.1 Monopolar HVDC link

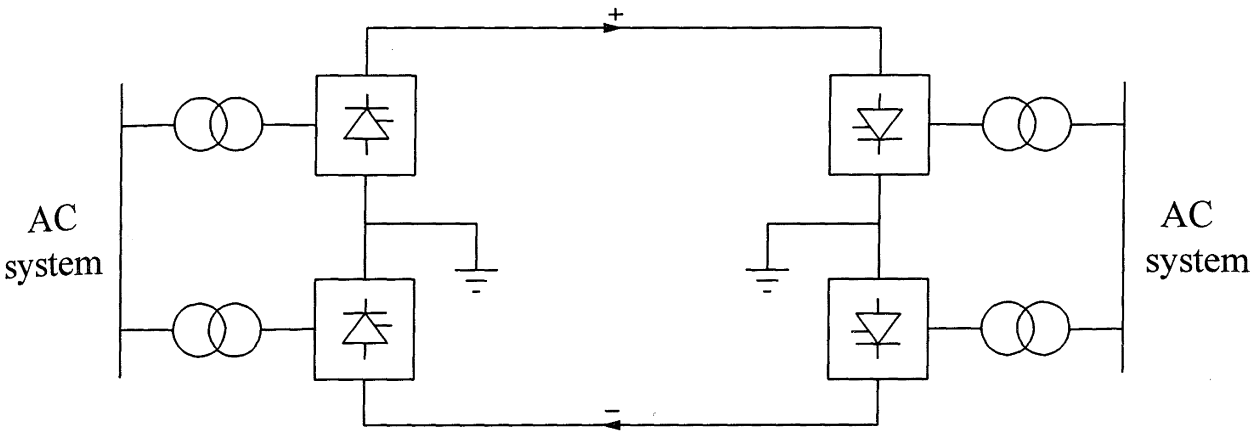

Figure 10.2 Bipolar HVDC link

The *bipolar link* configuration is shown in Figure 10.2. It has two conductors, one positive and the other negative. Each terminal has two converters of equal rated voltage, connected in series on the dc side. The junctions between the converters is grounded. Normally, the currents in the two poles are equal, and there is no ground current. The two poles can operate independently. If one pole is isolated due to a fault on its conductor, the other pole can operate with ground and thus carry half the rated load or more by using the overload capabilities of its converters and line.

From the viewpoint of lightning performance, a bipolar HVDC line is considered to be effectively equivalent to a double-circuit ac transmission line. Under normal operation, it will cause considerably less harmonic interference on nearby facilities than the monopolar system. Reversal of power-flow direction is achieved by changing the polarities of the two poles through controls (no mechanical switching is required).

In situations where ground currents are not tolerable or when a ground electrode is not feasible for reasons such as high earth resistivity, a third conductor is used as a metallic neutral. It serves as the return path when one pole is out of service or when there is imbalance during bipolar operation. The third conductor requires low insulation and may also serve as a shield wire for overhead lines. If it is fully insulated, it can serve as a spare.

The *homopolar link*, whose configuration is shown in Figure 10.3, has two or more conductors, all having the same polarity. Usually a negative polarity is preferred because it causes less radio interference due to corona. The return path for such a system is through ground. When there is a fault on one conductor, the entire converter is available for feeding the remaining conductor(s) which, having some overload capability, can carry more than the normal power. In contrast, for a bipolar scheme reconnection of the whole converter to one pole of the line is more complicated and usually not feasible. Homopolar configuration offers an advantage in this regard in situations where continuous ground current is acceptable.

The ground current can have side effects on gas or oil pipe lines that lie within a few miles of the system electrodes. Pipelines act as conductors for the ground current which can cause corrosion of the metal. Therefore, configurations using ground return may not always be acceptable.

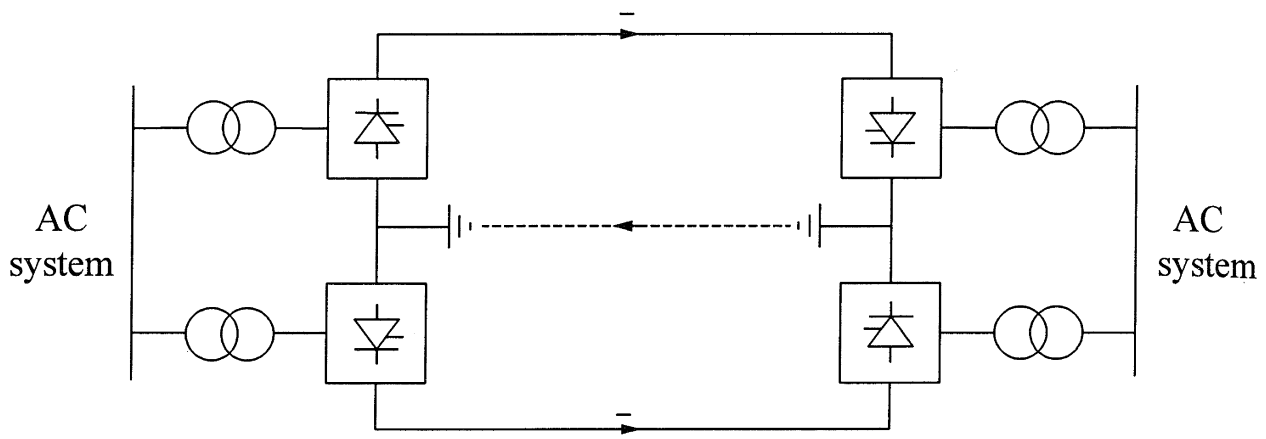

Figure 10.3 Homopolar HVDC link

Each of the above HVDC system configurations usually has cascaded groups of several converters, each having a transformer bank and a group of valves. The converters are connected in parallel on the ac side (transformer) and in series on the dc side (valve) to give the desired level of voltage from pole to ground.

Back-to-back HVDC systems (used for asynchronous ties) may be designed for monopolar or bipolar operation with a different number of valve groups per pole, depending on the purpose of the interconnection and the desired reliability.

Most point-to-point (two-terminal) HVDC links involving lines are bipolar, with monopolar operation used only during contingencies. They are normally designed to provide maximum independence between poles to avoid bipolar shutdowns.

A multiterminal HVDC system is formed when the dc system is to be connected to more than two nodes on the ac network. The possible configurations of multiterminal systems will be discussed in Section 10.8.

10.1.2 Components of HVDC Transmission System

The main components associated with an HVDC system are shown in Figure 10.4, using a bipolar system as an example. The components for other configurations are essentially the same as those shown in the figure. The following is a brief description of each component.

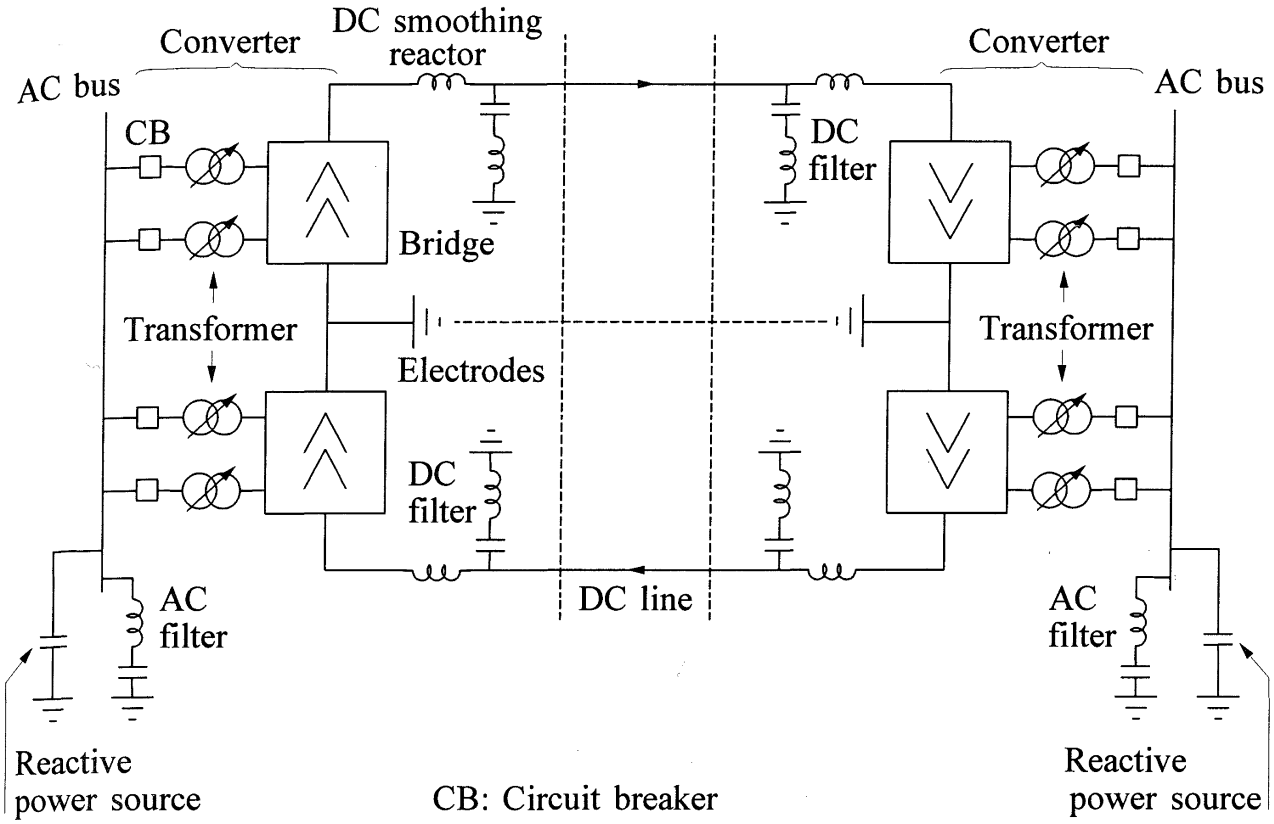

Figure 10.4 A schematic of a bipolar HVDC system identifying main components

Converters. They perform ac/dc and dc/ac conversion, and consist of valve bridges and transformers with tap changers. The valve bridges consist of high-voltage valves connected in a 6-pulse or 12-pulse arrangement as described in Section 10.2. The converter transformers provide ungrounded three-phase voltage source of appropriate level to the valve bridge. With the valve side of the transformer ungrounded, the dc system will be able to establish its own reference to ground, usually by grounding the positive or negative end of the valve converter.

Smoothing Reactors. These are large reactors having inductance as high as 1.0 H connected in series with each pole of each converter station. They serve the following purposes:

- Decrease harmonic voltages and currents in the dc line.
- Prevent commutation failure in inverters.
- Prevent current from being discontinuous at light load.
- Limit the crest current in the rectifier during short-circuit on the dc line.

Harmonic Filters. Converters generate harmonic voltages and currents on both ac and dc sides. These harmonics may cause overheating of capacitors and nearby generators, and interference with telecommunication systems. Filters are therefore used on both ac and dc sides.

Reactive Power Supplies. As we will see in Section 10.2, dc converters inherently absorb reactive power. Under steady-state conditions, the reactive power consumed is about 50% of active power transferred. Under transient conditions, the consumption of reactive power may be much higher. Reactive power sources are therefore provided near the converters. For strong ac systems, these are usually in the form of shunt capacitors. Depending on the demands placed on the dc link and on the ac system, part of the reactive power source may be in the form of synchronous condensers or static var compensators. The capacitors associated with the ac filters also provide part of the reactive power required.

Electrodes. Most dc links are designed to use earth as a neutral conductor for at least brief periods of time. The connection to the earth requires a large-surface-area conductor to minimize current densities and surface voltage gradients. This conductor is referred to as an electrode. As discussed earlier, if it is necessary to restrict the current flow through the earth, a metallic return conductor may be provided as part of the dc line.

DC Lines. They may be overhead lines or cables. Except for the number of conductors and spacing required, dc lines are very similar to ac lines.

AC Circuit Breakers. For clearing faults in the transformer and for taking the dc link out of service, circuit-breakers are used on the ac side. They are not used for clearing dc faults, since these faults can be cleared more rapidly by converter control.

10.2 CONVERTER THEORY AND PERFORMANCE EQUATIONS

A converter performs ac/dc conversion and provides a means of controlling the power flow through the HVDC link. The major elements of the converter are the valve bridge and converter transformer. The valve bridge is an array of high-voltage switches or valves that sequentially connect the three-phase alternating voltage to the dc terminals so that the desired conversion and control of power are achieved. The converter transformer provides the appropriate interface between the ac and dc systems.

In this section, we will describe the structure and operation of practical converter circuits. In addition, we will develop equations relating dc quantities and

fundamental frequency ac quantities.

10.2.1 Valve Characteristics

The valve in an HVDC converter is a controlled electronic switch. It normally conducts in only one direction, the forward direction, from anode to cathode. When it is conducting, there is only a small voltage drop across it. In the reverse direction, when the voltage applied across the valve is such that the cathode is positive relative to the anode, the valve blocks the current.

The early HVDC systems used mercury-arc valves. Mercury-arc valves with rated currents of the order of 1,000 to 2,000 A and rated peak inverse voltage of 50 to 150 kV have been built and used. Among the disadvantages of mercury-arc valves are their large size and tendency to conduct in the reverse direction.

All HVDC systems built since the mid-1970s have used thyristor valves. Thyristor valves rated at 2,500 to 3,000 A and 3 to 5 kV have been developed. The thyristors are connected in series to achieve the desired system voltage. They are available in various designs: air cooled, air insulated; oil cooled, oil insulated; water cooled, air insulated; and freon cooled, SF_6 insulated. The valves can be designed for indoor or outdoor installation.

For the valve to conduct, it is necessary for the anode to be positive relative to the cathode. In a mercury-arc valve, with the control grid at sufficiently negative voltage with respect to the cathode, the valve is prevented from conducting, although the anode may be positive. The instant of firing can be controlled by the grid.

Similarly, a thyristor valve will conduct only when the anode is positive with respect to the cathode and when there is a positive voltage applied to the gate. Conduction may be initiated by applying a momentary or sustained current pulse of proper polarity to the gate.

Once conduction is initiated, the current through the valve continues until current drops to zero and a reverse voltage bias appears across the valve. In the forward direction, the current is blocked until a control pulse is applied to the gate. When not conducting, the valve should be capable of withstanding the forward or reverse bias voltages appearing between its cathode and anode.

Figure 10.5 shows the symbol used to represent a controlled valve (mercury-arc or thyristor).

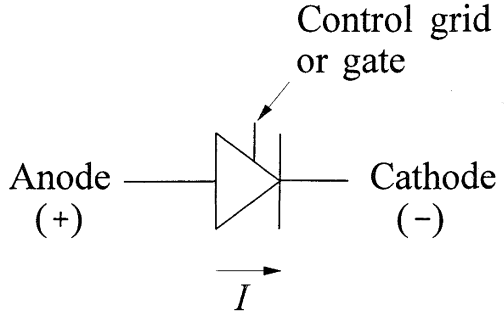

Figure 10.5 Symbol for controlled valve

10.2.2 Converter Circuits

The basic module of an HVDC converter is the three-phase, full-wave bridge circuit shown in Figure 10.6. This circuit is also known as a Graetz bridge. Although there are several alternative configurations possible, the Graetz bridge has been universally used for HVDC converters as it provides better utilization of the converter transformer and a lower voltage across the valve when not conducting [2,6]. The latter is referred to as the peak inverse voltage and is an important factor that determines the rating of the valves.

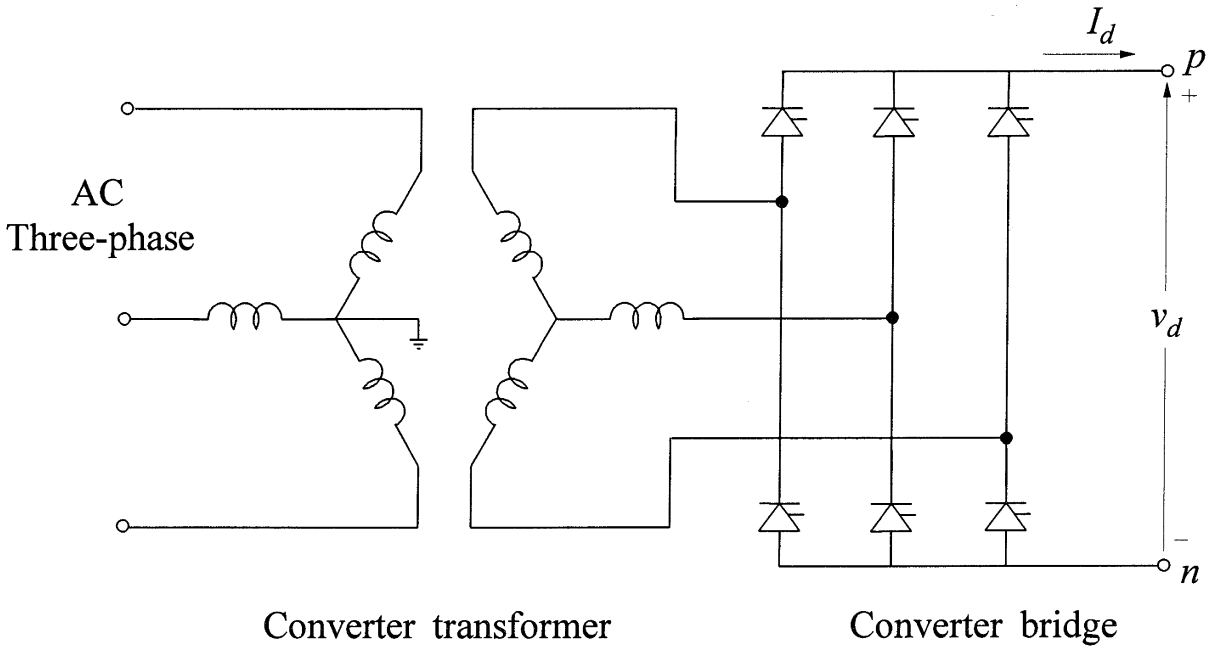

Figure 10.6 Three-phase, full-wave bridge circuit

The converter transformer has on-load taps on the ac side for voltage control. The ac side windings of the transformer are usually star-connected with grounded neutral; the valve side-windings are delta-connected or star-connected with ungrounded neutral.

Analysis of three-phase, full-wave bridge circuit

For purposes of analysis, we will make the following assumptions:

(a) The ac system, including the converter transformer, may be represented by an ideal source of constant voltage and frequency in series with a lossless inductance (representing primarily the transformer leakage inductance).

(b) The direct current (I_d) is constant and ripple-free; this is justified because of the large smoothing reactor (L_d) used on the dc side.

(c) The valves are ideal switches with zero resistance when conducting, and infinite resistance when not conducting.

Based on the above assumptions, the bridge converter of Figure 10.6 may be represented by the equivalent circuit shown in Figure 10.7.

Let the instantaneous line-to-neutral source voltages be

$$\begin{aligned} e_a &= E_m\cos(\omega t+60°) \\ e_b &= E_m\cos(\omega t-60°) \\ e_c &= E_m\cos(\omega t-180°) \end{aligned} \tag{10.1}$$

The line-to-line voltages are then

$$\begin{aligned} e_{ac} &= e_a-e_c = \sqrt{3}E_m\cos(\omega t+30°) \\ e_{ba} &= e_b-e_a = \sqrt{3}E_m\cos(\omega t-90°) \\ e_{cb} &= e_c-e_b = \sqrt{3}E_m\cos(\omega t+150°) \end{aligned} \tag{10.2}$$

Figure 10.8(a) shows the voltage waveforms corresponding to Equations 10.1 and 10.2.

To simplify analysis and help understand the operation of the bridge converter, we will first consider the case with negligible source inductance (i.e., L_c=0) and no ignition delay. After developing a basic understanding of the converter performance, we will extend the analysis to include the effect of delaying the valve ignition through gate/grid control and then the effect of source inductance.

Analysis assuming negligible source inductance

(a) With no ignition delay

In Figure 10.7, the cathodes of valves 1, 3, and 5 of the upper row are connected together. Therefore, when the phase-to-neutral voltage of phase *a* is more positive than the voltages of the other two phases, valve 1 conducts. The common potential of the cathodes of the three valves is then equal to that of the anode of valve 1. Since the cathodes of valves 3 and 5 are at a higher potential than their anodes, these valves do not conduct.

In the lower row, the anodes of valves 2, 4 and 6 are connected together. Therefore, valve 2 conducts when phase *c* voltage is more negative than the other two phases.

From the waveforms shown in Figure 10.8(a) we see that valve 1 conducts when ωt is between −120° and 0°, since e_a is greater than e_b or e_c. Valve 2 conducts when ωt is between −60° and 60°, since e_c is more negative than e_a or e_b during this

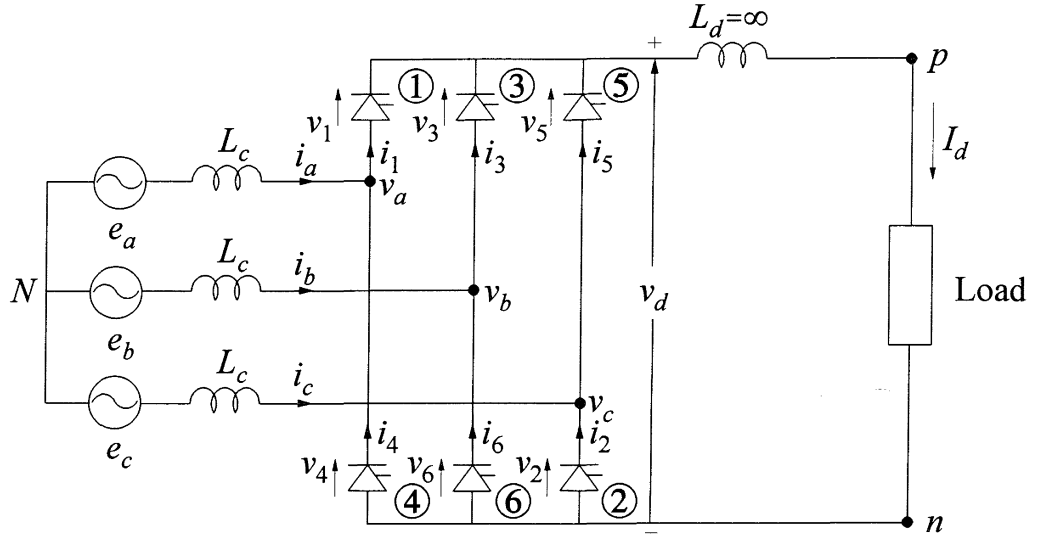

Note: Valves are numbered in order of firing.

Figure 10.7 Equivalent circuit for three-phase full-wave bridge converter

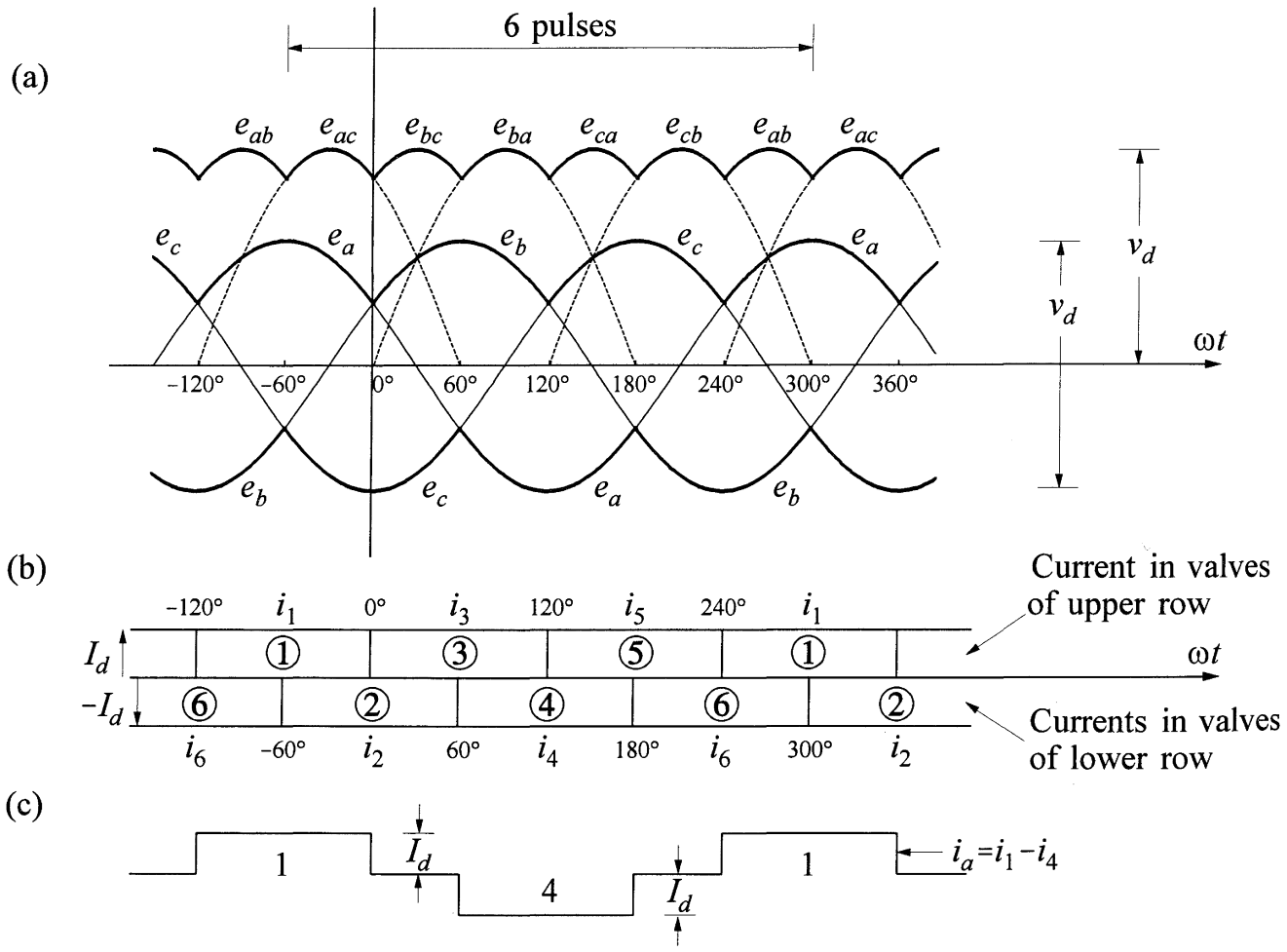

Figure 10.8 Waveforms of voltages and currents of bridge circuit of Figure 10.7
(a) Source line-to-neutral and line-to-line voltages
(b) Valve currents and periods of conduction
(c) Phase current i_a

period. This is shown in Figure 10.8(b), which identifies the period of conduction of each valve, and the magnitude and duration of current in it. Since, by assumption, the direct current I_d is assumed constant, the current in each valve is I_d when conducting and zero when not conducting.

Let us now examine the period when ωt is between 0° and 120°. Just before ωt=0, valves 1 and 2 are conducting. Just after ωt=0°, e_b becomes more positive than e_a and valve 3 ignites; valve 1 is extinguished because its cathode is now at a higher potential than its anode. For the next 60°, valves 2 and 3 conduct. At ωt=60°, e_a is more negative than e_c, causing valve 4 to ignite and valve 2 to extinguish.

At ωt=120°, e_c is more positive than e_b, resulting in the ignition of valve 5 and extinction of valve 3. Similarly, at ωt=180° conduction switches from valve 4 to 6 in the lower row; at ωt=240° conduction switches from valve 5 to valve 1 in the upper row. This completes one cycle, and the sequence continues.

The valve-switching sequence is illustrated in Figure 10.9, which shows only the conducting valves during the six distinct periods of a complete cycle.

Each valve thus conducts for a period of 120°. When it is conducting, the magnitude of valve current is I_d; the valves in the upper row carry positive current and the valves in the lower row carry negative (or return) current.

The current in each phase of the ac source is composed of currents in the two valves connected to that phase. For example, the current in phase *a*, as shown in Figure 10.8(c), is equal to $i_1 - i_4$. This represents the current in the secondary (valve side) winding of the converter transformer of Figure 10.6.

The transfer of current from one valve to another in the same row is called "commutation." In the above analysis, we have assumed that the source inductance L_c is negligible. Therefore, commutation occurs instantaneously, i.e., without "overlap." The result is that no more than two valves (one from the top row and the other from the bottom row) conduct at any time.

From Figure 10.8(a), we see that the number of pulsations (cycles of ripple) of v_d per cycle of alternating voltage is six. Hence, the bridge circuit of Figure 10.6 is referred to as a "6-pulse bridge circuit."

Average direct voltage:

The instantaneous direct voltage v_d across the bridge (between the cathodes of the upper-row valves and anodes of lower-row valves) is composed of 60° segments of the line-to-line voltages. Therefore, the average direct voltage can be found by integrating the instantaneous values over any 60° period.

Denoting ωt by θ, and considering the period between ωt=−60° and 0°, the average direct voltage with no ignition delay is given by

$$V_{d0} = \frac{3}{\pi} \int_{-60°}^{0} e_{ac} \, d\theta$$

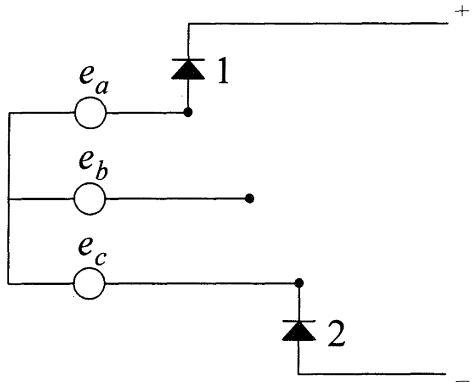

(a) $\omega t = -60°$ to $0°$

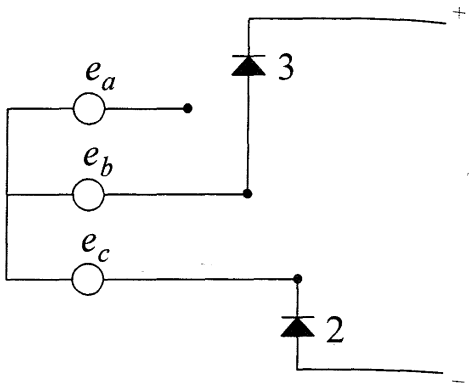

(b) $\omega t = 0°$ to $60°$

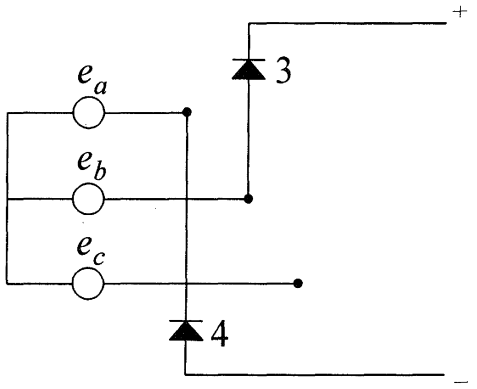

(c) $\omega t = 60°$ to $120°$

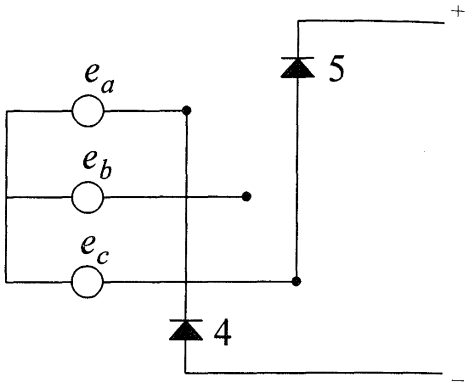

(d) $\omega t = 120°$ to $180°$

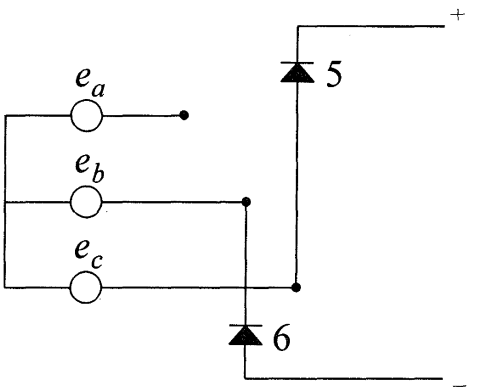

(e) $\omega t = 180°$ to $240°$

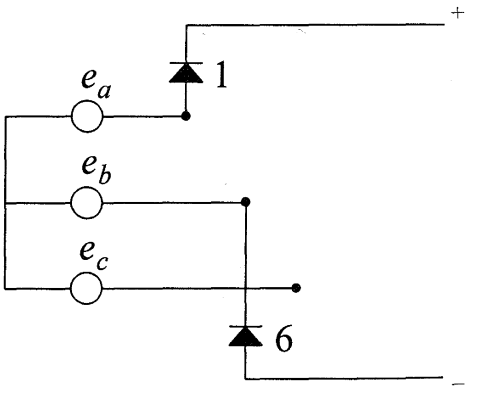

(f) $\omega t = 240°$ to $300°$

Figure 10.9 Valve-switching sequence with no ignition delay and no overlap

Substituting for e_{ac} from Equation 10.2, we get

$$V_{d0} = \frac{3}{\pi}\int_{-60°}^{0}\sqrt{3}E_m\cos(\theta+30°)\,d\theta$$

$$= \frac{3\sqrt{3}}{\pi}E_m\sin(\theta+30°)\Big|_{-60°}^{0} \qquad (10.3A)$$

$$= \frac{3\sqrt{3}}{\pi}E_m 2\sin 30° = \frac{3\sqrt{3}}{\pi}E_m = 1.65E_m$$

where E_m is the peak value of the line-to-neutral voltage.

In terms of RMS line-to-neutral (E_{LN}) and line-to-line (E_{LL}) voltages, the expression for V_{d0} becomes

$$V_{d0} = \frac{3\sqrt{6}}{\pi}E_{LN} = 2.34E_{LN} \qquad (10.3B)$$

$$= \frac{3\sqrt{2}}{\pi}E_{LL} = 1.35E_{LL} \qquad (10.3C)$$

and V_{d0} is called the "ideal no-load direct voltage."

(b) With ignition delay

The grid or gate control can be used to delay the ignition of the valves. The "delay angle" is denoted by α; it corresponds to time delay of α/ω seconds.

With delay, valve 3 ignites when $\omega t=\alpha$ (instead of $\omega t=0$), valve 4 when $\omega t=\alpha+60°$, valve 5 when $\omega t=\alpha+120°$, and so on. This is illustrated in Figure 10.10.

The delay angle is limited to 180°. If α exceeds 180°, the valve fails to ignite. For example, consider the ignition of valve 3. With $\alpha=0$, valve 3 ignites at $\omega t=0$. The ignition can be delayed up to $\omega t=180°$. Beyond this, e_b is no longer greater than e_a, and hence valve 3 will not ignite.

Average direct voltage:

Referring to Figure 10.10, the average direct voltage V_d when the delay angle is equal to α is given by

$$V_d = \frac{3}{\pi}\int_{-(60°-\alpha)}^{\alpha} e_{ac}\,d\theta = \frac{3}{\pi}\int_{\alpha-60°}^{\alpha}\sqrt{3}E_m\cos(\theta+30°)\,d\theta$$

$$= V_{d0}\int_{\alpha-60°}^{\alpha}\cos(\theta+30°)\,d\theta = V_{d0}\sin(\theta+30°)\Big|_{\alpha-60°}^{\alpha} \qquad (10.4)$$

$$= V_{d0}[\sin(\alpha+30°)-\sin(\alpha-30°)]$$

$$= V_{d0}(2\sin 30°)\cos\alpha = V_{d0}\cos\alpha$$

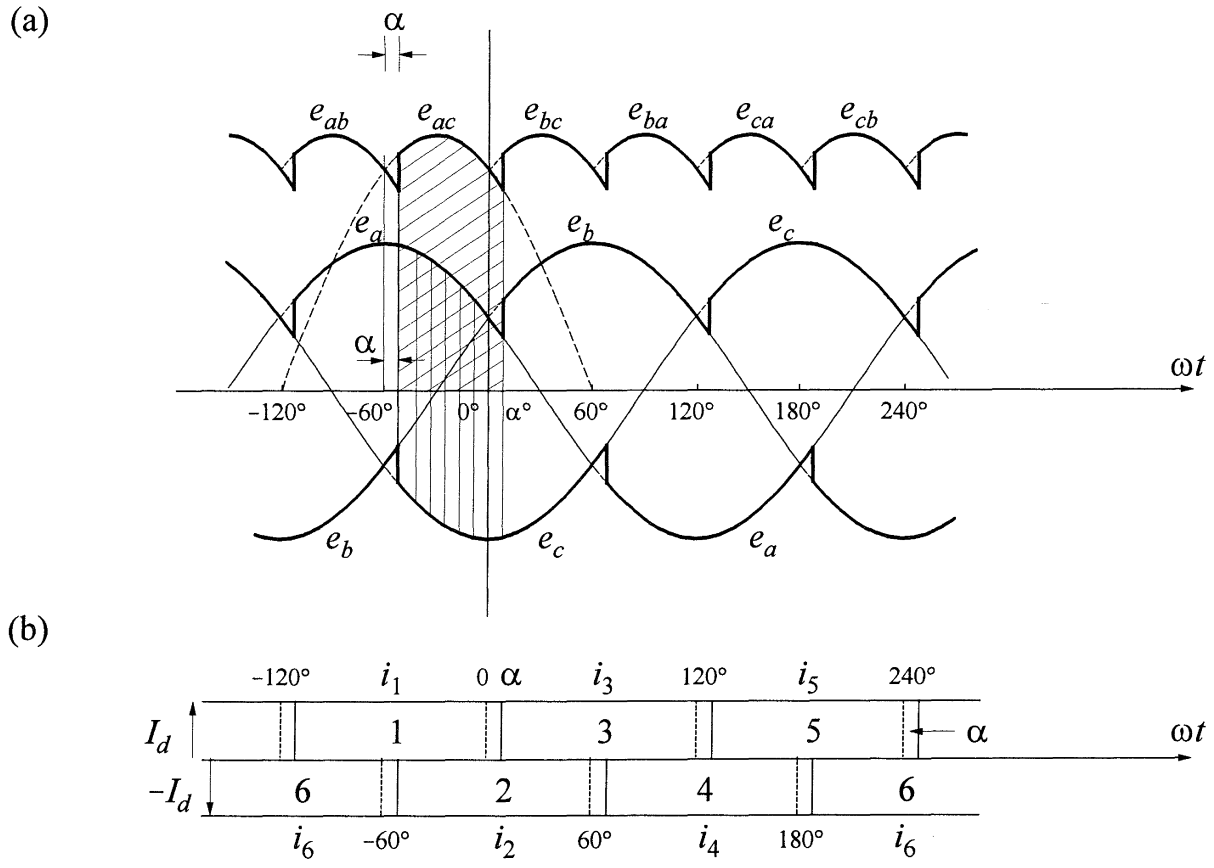

Figure 10.10 Voltage waveforms and valve currents, with ignition delay

The effect of the delayed ignition is thus to reduce the average direct voltage by the factor $\cos\alpha$.

Since α can range from 0° to 180°, $\cos\alpha$ can range from 1 to −1. Therefore, V_d can range from V_{d0} to $-V_{d0}$. Negative V_d, as discussed later in this section, represents inversion as opposed to rectification.

Current and phase relations:

As the ignition delay angle α is increased, the phase displacement between alternating voltage and alternating current in a supply phase also changes. This is illustrated in Figure 10.11 for phase *a*. The current wave shape, as shown in Figure 10.8(c), is composed of rectangular segments associated with currents in valves 1 and 4.

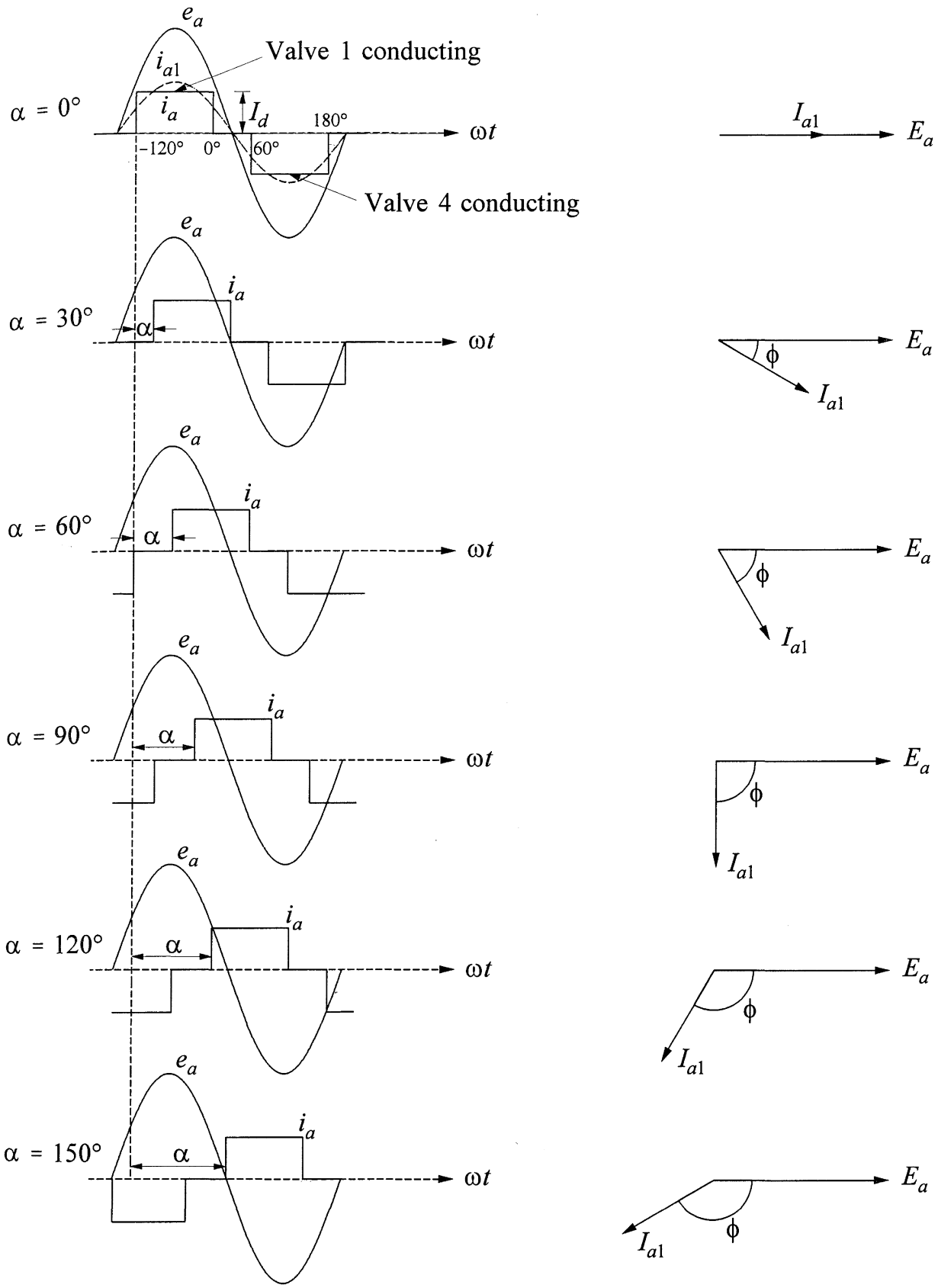

e_a = phase a line-neutral voltage
i_a = phase a line current
E_a = voltage phasor
I_{a1} = fundamental current phasor

Figure 10.11 Variation of phase displacement between voltage and current of phase a with delay angle

The direct current I_d is constant by assumption (L_d in Figure 10.7 prevents I_d from changing). Since each valve conducts for a period of 120°, the alternating line currents appear as rectangular pulses of magnitude I_d and duration of 120° or $2\pi/3$ rad. With the assumption that there is no overlap, the shape of the alternating line currents is independent of α. Only the phase displacement changes with α.

The fundamental frequency component of the alternating line current can be determined by Fourier analysis of the current wave shape shown in Figure 10.12.

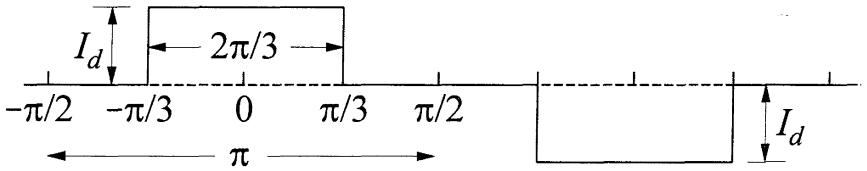

Figure 10.12 Line current waveform

The peak value of the fundamental frequency component of the alternating line current is

$$\begin{aligned} I_{LM} &= \frac{2}{\pi}\int_{-\pi/3}^{\pi/3} I_d \cos x\,dx = \frac{2}{\pi} I_d \sin x \Big|_{-60°}^{60°} \\ &= \frac{2}{\pi} I_d [\sin 60° - \sin(-60°)] \\ &= \frac{2}{\pi}\sqrt{3} I_d = 1.11 I_d \end{aligned} \tag{10.5A}$$

The RMS value of the fundamental frequency component of the alternating line current is

$$\begin{aligned} I_{L1} &= \frac{I_{LM}}{\sqrt{2}} = \frac{2\sqrt{3}}{\pi\sqrt{2}} I_d \\ &= \frac{\sqrt{6}}{\pi} I_d = 0.78 I_d \end{aligned} \tag{10.5B}$$

With losses in the converter neglected, the ac power must equal the dc power. Therefore,

$$\begin{aligned} 3 E_{LN} I_{L1} \cos\phi &= V_d I_d \\ &= (V_{d0} \cos\alpha) I_d \end{aligned}$$

where

E_{LN} = RMS value of the line-to-neutral voltage
ϕ = angle by which fundamental line current lags the line-to-neutral source voltage as shown in Figure 10.11

Substituting for V_{d0} from Equation 10.3B and for I_{L1} from Equation 10.5B, we have

$$\left(3E_{LN}\frac{\sqrt{6}}{\pi}I_d\right)\cos\phi = \left(\frac{3\sqrt{6}}{\pi}E_{LN}I_d\right)\cos\alpha$$

Hence, the power factor of the fundamental wave is

$$\cos\phi = \cos\alpha \tag{10.6}$$

The term $\cos\phi$ is referred to by some authors as the "vector power factor" or "displacement factor" [2].

The converter thus operates as a device that converts alternating to direct current (or direct to alternating current) so that the current ratio is fixed but the voltage ratio varies with the ignition delay caused by grid or gate control.

The ignition delay α shifts the current wave and its fundamental component by an angle $\phi=\alpha$, as shown in Figure 10.11. With $\alpha=0°$, the fundamental current component (i_{a1}) is in phase with the phase voltage e_a; the active power ($P_a=E_aI_{a1}\cos\phi$) is positive and the reactive power ($Q_a=E_aI_{a1}\sin\phi$) is zero. As α increases from 0° to 90°, P_a decreases and Q_a increases. At $\alpha=90°$, P_a is zero and Q_a is maximum. As α increases from 90° to 180°, P_a becomes negative and increases in magnitude; Q_a remains positive and decreases in magnitude. At $\alpha=180°$, P_a is negative maximum and Q_a is zero. We see that the converter, whether it is acting as a rectifier or as an inverter, draws reactive power from the ac system.

Analysis including commutation overlap

Due to the inductance L_c of the ac source (see Figure 10.7), the phase currents cannot change instantly. Therefore, the transfer of current from one phase to another requires a finite time, called the commutation time or overlap time. The corresponding *overlap* or *commutation angle* is denoted by μ.

In normal operation, the overlap angle is less than 60°; typical full-load values are in the range of 15° to 25°. With $0°<\mu<60°$, during commutation three valves conduct simultaneously. However, between commutations only two valves conduct. A new commutation begins every 60° and lasts for an angular period of μ. Therefore, the angular period when two valves conduct with no ignition delay (i.e., $\alpha=0$) is $60°-\mu$, as shown in Figure 10.13. During each commutation period, the current in the incoming valve increases from 0 to I_d, and the current in the outgoing valve reduces from I_d to 0. For simplicity, in Figure 10.13 we have identified only the valve conduction periods, but not the valve currents.

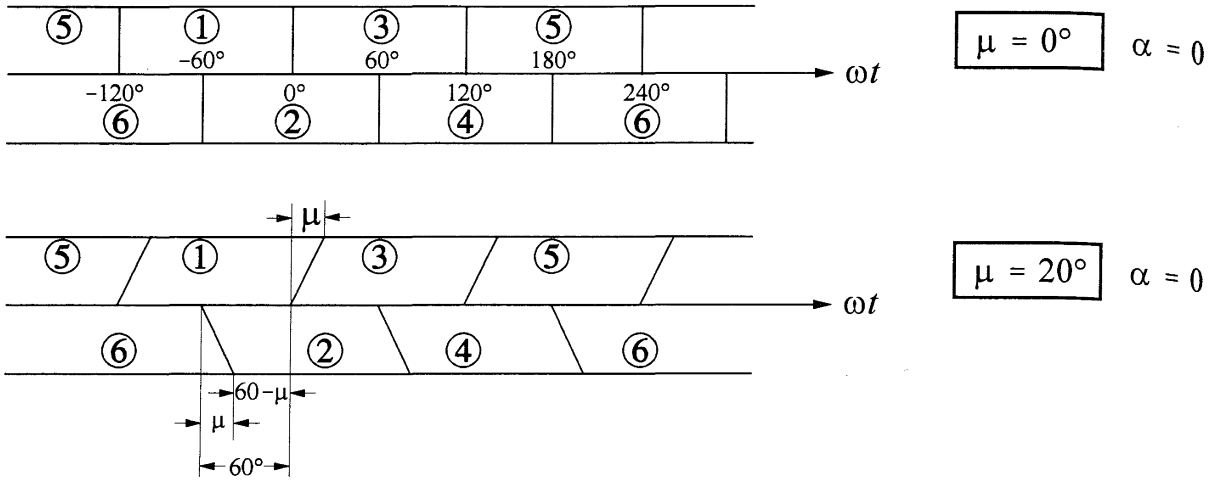

Figure 10.13 Effect of overlap angle on periods of conduction of valves

If $60° \le \mu < 120°$, an abnormal mode of operation occurs in which alternately three and four valves conduct [2]. Here we will consider only the normal operation when μ is less than 60°.

Let us analyze the effect of overlap by considering the commutation from valve 1 to valve 3. Figure 10.14 shows the periods of valve conduction, when ignition delay is included. The commutation begins when $\omega t = \alpha$ (delay angle) and ends when $\omega t = \alpha + \mu = \delta$, where δ is *extinction angle* (equal to the sum of the delay angle α and commutation angle μ).

At the beginning of commutation ($\omega t = \alpha$): $i_1 = I_d$ and $i_3 = 0$

At the end of commutation ($\omega t = \alpha + \mu = \delta$): $i_1 = 0$ and $i_3 = I_d$

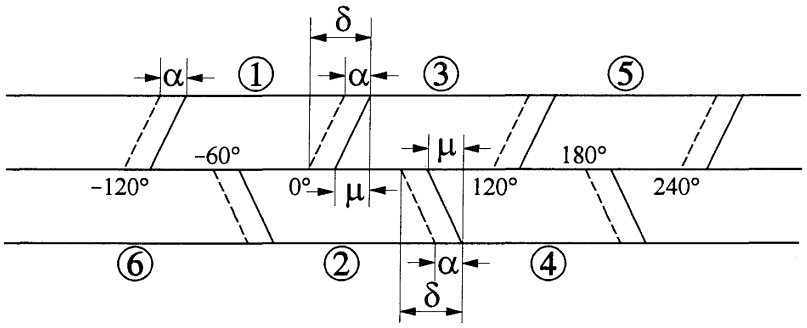

Figure 10.14 Periods of valve conduction with ignition delay

During the period of commutation, valves 1, 2 and 3 are conducting and the effective converter circuit is as shown in Figure 10.15. From the figure, for the loop containing valves 1 and 3, we have

$$e_b - e_a = L_c \frac{di_3}{dt} - L_c \frac{di_1}{dt}$$

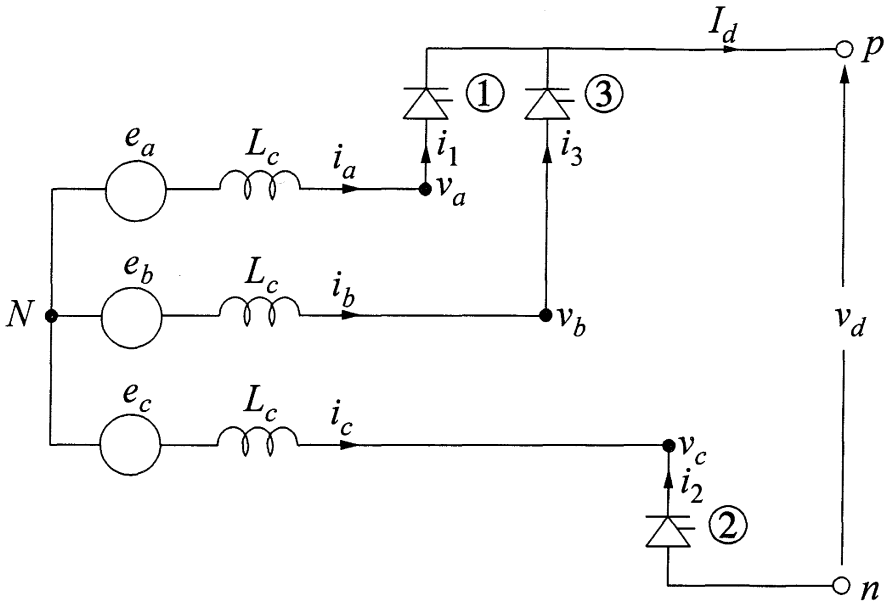

Note: Non-conducting valves not shown.

Figure 10.15 Equivalent circuit during commutation

The voltage $e_b - e_a$ is called the "commutating voltage." From Equation 10.2, it is equal to $\sqrt{3}E_m \sin\omega t$. Therefore,

$$\sqrt{3}E_m \sin\omega t = L_c \frac{di_3}{dt} - L_c \frac{di_1}{dt}$$

Since $i_1 = I_d - i_3$,

$$\frac{di_1}{dt} = 0 - \frac{di_3}{dt}$$

Hence,

$$e_b - e_a = \sqrt{3}E_m \sin\omega t = 2L_c \frac{di_3}{dt} \tag{10.7A}$$

or

$$\frac{di_3}{dt} = \frac{\sqrt{3}E_m}{2L_c} \sin\omega t \tag{10.7B}$$

Taking a definite integral with respect to t, with the lower limit corresponding to the beginning of commutation ($\omega t = \alpha$ or $t = \alpha/\omega$) and a running upper limit, we have

$$\int_0^{i_3} di_3 = \frac{\sqrt{3}E_m}{2L_c} \int_{\alpha/\omega}^{t} \sin\omega t dt$$

Integration of the above equation yields

$$\begin{aligned} i_3 &= \frac{\sqrt{3}E_m}{2\omega L_c}(\cos\alpha - \cos\omega t) \\ &= I_{S2}(\cos\alpha - \cos\omega t) \end{aligned} \tag{10.8A}$$

where

$$I_{S2} = \frac{\sqrt{3}E_m}{2\omega L_c} \tag{10.8B}$$

The current i_3 of the incoming valve during commutation consists of a constant term ($I_{S2}\cos\alpha$) and a sinusoidal term ($-I_{S2}\cos\omega t$) lagging the commutating voltage by 90°. This is to be expected because what we have here is a line-to-line short-circuit through an inductance of $2L_c$. The constant component of i_3 depends on α; it serves to make $i_3=0$ at the beginning of commutation.

As shown in Figure 10.16, the current during commutation is a segment of a sinusoidal current with a peak value of $I_{S2}=\sqrt{3}E_m/(2\omega L_c)$. The shape of the segment is a function of the control angle α. Therefore, the overlap angle depends on I_d, L_c and α.

During commutation, the shape of i_1 satisfies $i_1=I_d-i_3$. For α nearly equal to 0° (or 180°), the commutation period or the overlap is the greatest. The overlap is the shortest when $\alpha=90°$, since i_3 is associated with the segment of the sine wave which is nearly linear. Also, if the source voltage E_m is lowered or if I_d is increased, the overlap increases.

Voltage reduction due to commutation overlap:

During commutation,

$$v_a = v_b = e_b - L_c\frac{di_3}{dt}$$

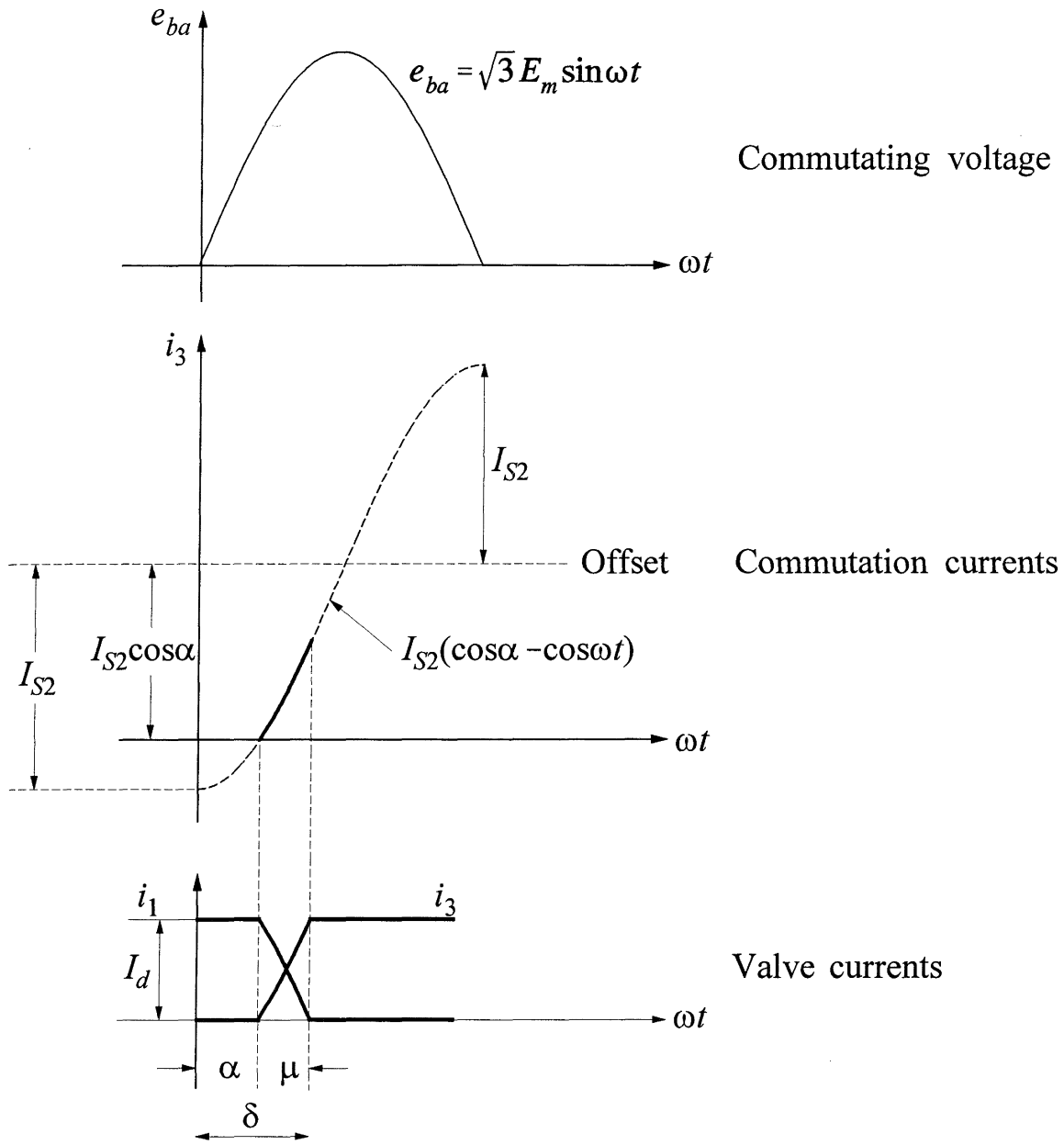

Figure 10.16 Valve currents during commutation in relation to commutating voltage

From Equation 10.7A,

$$L_c \frac{di_3}{dt} = \frac{e_b - e_a}{2}$$

Hence,

$$v_a = v_b = e_b - \frac{e_b - e_a}{2}$$

$$= \frac{e_a + e_b}{2}$$

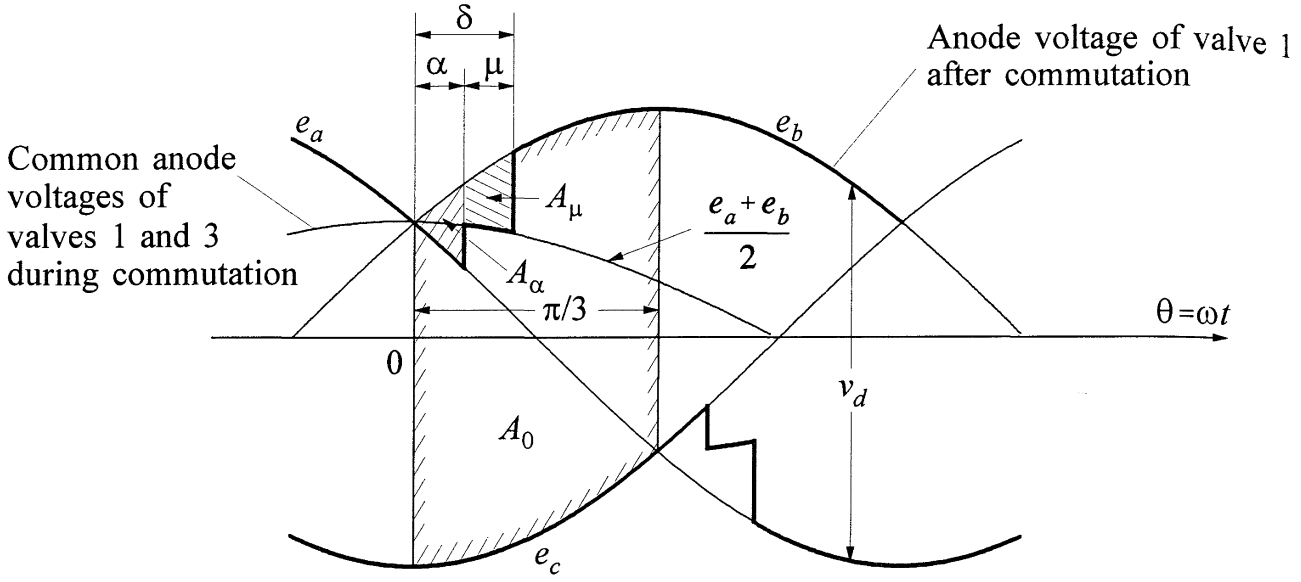

Figure 10.17 Voltage waveforms showing the effect of overlap during commutation from valve 1 to valve 3

Because of the overlap, the voltage of the terminal p (see Figure 10.15) immediately after $\omega t=\alpha$ recovers to $(e_a+e_b)/2$, instead of e_b. Therefore, as shown in Figure 10.17, the effect of the overlap is measured by subtracting an area A_μ from the area A_0, once every 60° (π/3 rad).

$$A_\mu = \int_\alpha^\delta \left(e_b - \frac{e_a+e_b}{2}\right) d\theta = \int_\alpha^\delta \frac{e_b-e_a}{2} d\theta$$

$$= \frac{\sqrt{3}E_m}{2}\int_\alpha^\delta \sin\theta\, d\theta = \frac{\sqrt{3}E_m}{2}(\cos\alpha - \cos\delta)$$

The corresponding average voltage drop (due to overlap) is given by

$$\Delta V_d = \frac{A_\mu}{\pi/3} = \frac{3}{\pi}\frac{\sqrt{3}}{2}E_m(\cos\alpha - \cos\delta) \qquad (10.9)$$

$$= \frac{V_{d0}}{2}(\cos\alpha - \cos\delta)$$

where V_{d0} is the ideal no-load voltage given by Equation 10.3.

From Equation 10.8A, the current i_3 during commutation is

$$i_3 = \frac{\sqrt{3}E_m}{2\omega L_c}(\cos\alpha - \cos\omega t)$$

Since at the end of the commutation $\omega t=\delta$ and $i_3=I_d$,

$$I_d = \frac{\sqrt{3}E_m}{2\omega L_c}(\cos\alpha - \cos\delta) = I_{S2}(\cos\alpha - \cos\delta) \tag{10.10}$$

Hence,

$$\frac{\sqrt{3}E_m}{2}(\cos\alpha - \cos\delta) = I_d\omega L_c$$

Substituting in Equation 10.9 gives

$$\Delta V_d = \frac{3}{\pi}I_d\omega L_c$$

With commutation overlap and ignition delay, the reduction in direct voltage is represented by areas A_α and A_μ; the direct voltage is given by

$$V_d = V_{d0}\cos\alpha - \Delta V_d = V_{d0}\cos\alpha - R_c I_d \tag{10.11}$$

where

$$R_c = \frac{3}{\pi}\omega L_c = \frac{3}{\pi}X_c \tag{10.12}$$

and R_c is called the "equivalent commutating resistance." It accounts for the voltage drop due to commutation overlap. It does not, however, represent a real resistance and consumes no power.

Rectifier operation

The equivalent circuit of the bridge rectifier based on the above analysis is given in Figure 10.18. The direct voltage and current in the equivalent circuit are the average values. The internal voltage is a function of the ignition angle α. The overlap angle μ does not explicitly appear in the equivalent circuit; the effect of commutation overlap is represented by R_{cr}. The voltage wave shapes and periods of valve conduction for rectifier mode of operation, including commutation overlap, are shown in Figure 10.19(a).

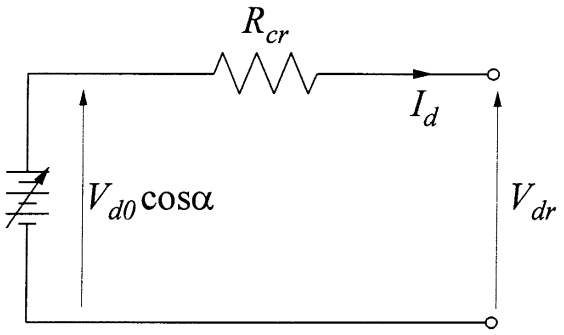

$$R_{cr} = \frac{3}{\pi} X_{cr}$$

$$V_{d0} = \frac{3\sqrt{3}}{\pi} E_m$$

Figure 10.18 Bridge rectifier equivalent circuit

Inverter operation

If there is no commutation overlap, $V_d = V_{d0}\cos\alpha$. Therefore, V_d reverses when $\alpha = 90°$.

With overlap,

$$V_d = V_{d0}\cos\alpha - \Delta V_d$$

Substituting for ΔV_d from Equation 10.9, we have

$$\begin{aligned} V_d &= V_{d0}\cos\alpha - \frac{V_{d0}}{2}(\cos\alpha - \cos\delta) \\ &= \frac{V_{d0}}{2}(\cos\alpha + \cos\delta) \end{aligned} \tag{10.13}$$

The transitional value of the ignition delay angle, α_t, beyond which inversion takes place is given by

$$\cos\alpha_t + \cos\delta_t = 0$$

or

$$\begin{aligned} \alpha_t &= \pi - \delta_t = \pi - \alpha_t - \mu \\ &= \frac{\pi - \mu}{2} \end{aligned} \tag{10.14}$$

The effect of the overlap is thus to reduce α_t from 90° to $90° - \mu/2$.

At first sight, it may seem strange to delay the firing pulse until the actual anode voltage becomes negative. We should, however, realize that commutation is always possible as long as the commutating voltage ($e_{ba} = e_b - e_a$) is positive and as long as the outgoing valve will have reversed voltage applied to it after it extinguishes.

Since valves conduct in only one direction, the current in a converter cannot be reversed. A reversal of V_d results in a reversal of power. An alternating voltage must exist on the primary side of the transformer for inverter operation. The direct voltage of the inverter opposes the current, as in a dc motor, and is called a countervoltage or back voltage. The applied direct voltage from the rectifier forces current through the inverter valves against this back voltage.

Figure 10.19(b) shows the voltage wave shapes and periods of valve conduction for inverter mode of operation. For successful commutation, the changeover from the outgoing valve to the incoming valve must be complete before the commutating voltage becomes negative. For example, commutation from valve 1 to valve 3 is possible only when e_b is more positive than e_a; the current changeover from valve 1 to valve 3 must be complete before e_a becomes more positive than e_b with sufficient margin to allow for valve de-ionization.

For description of rectifier operation, we use the following angles:

α = ignition delay angle
μ = overlap angle
δ = extinction delay angle = $\alpha+\mu$

As illustrated in Figure 10.20, α is the angle by which ignition is delayed from the instant at which the commutating voltage (e_{ba} for valve 3) is zero and increasing.

The inverter operation may also be described in terms of α and δ defined in the same way as for the rectifier, but having values between 90° and 180°. However, the common practice is to use *ignition advance angle* β and *extinction advance angle* γ for describing inverter performance. These angles are defined by their advance with respect to the instant (ωt=180° for ignition of valve 3 and extinction of valve 1) when the commutating voltage is zero and decreasing, as shown in Figure 10.20. From the figure, we see that

$\beta = \pi-\alpha$ = ignition advance angle
$\gamma = \pi-\delta$ = extinction advance angle
$\mu = \delta-\alpha = \beta-\gamma$ = overlap

Since $\cos\alpha = -\cos\beta$ and $\cos\delta = -\cos\gamma$, Equations 10.10 and 10.13 may be written in terms of γ and β as follows:

$$I_d = I_{S2}(\cos\gamma - \cos\beta) \tag{10.15}$$

$$V_d = V_{d0}\frac{\cos\gamma + \cos\beta}{2} \tag{10.16}$$

or

$$V_d = V_{d0}\cos\beta + R_c I_d \tag{10.17A}$$

(a) Rectifier mode:

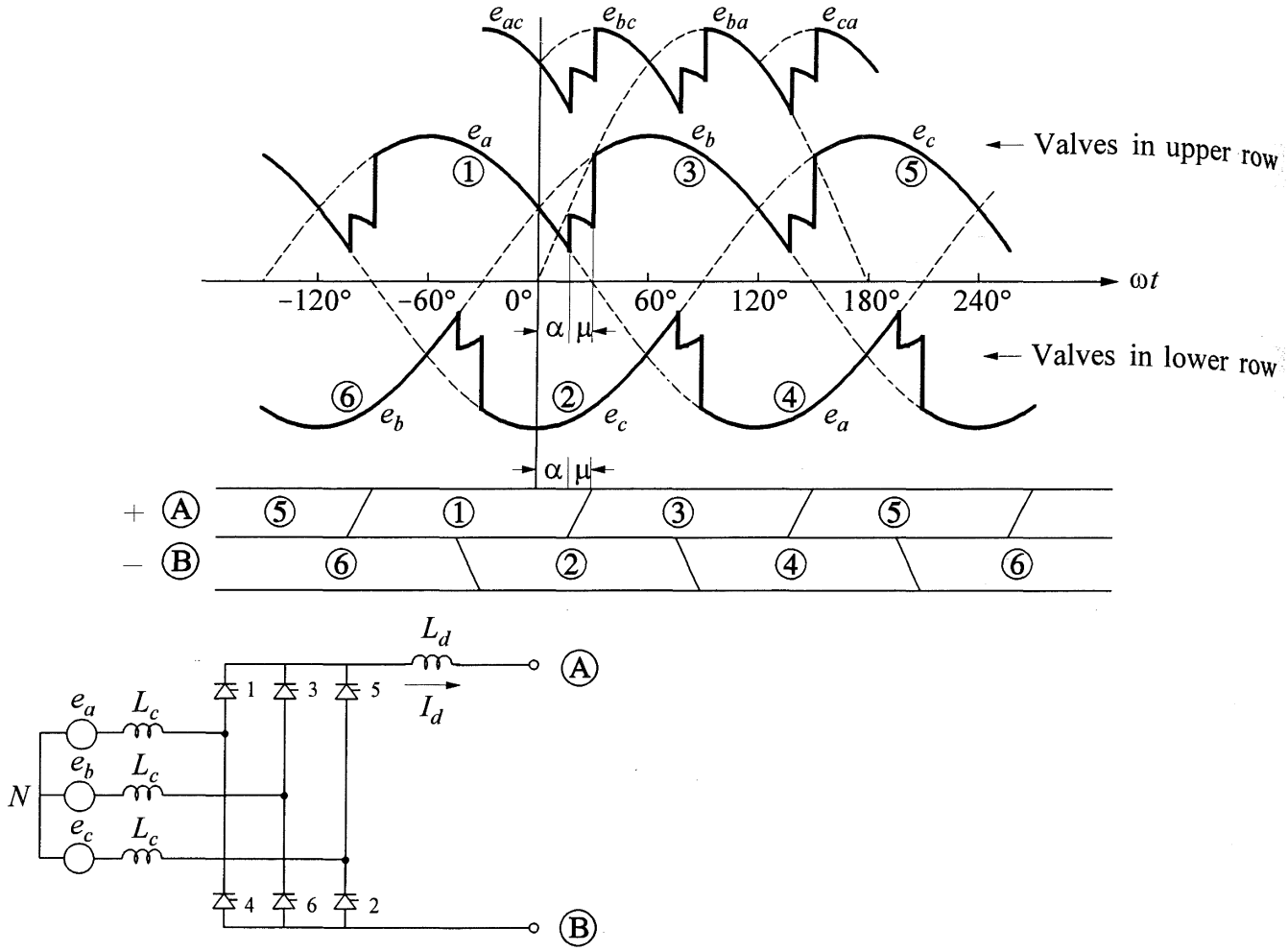

(b) Inverter mode:

α > 120°

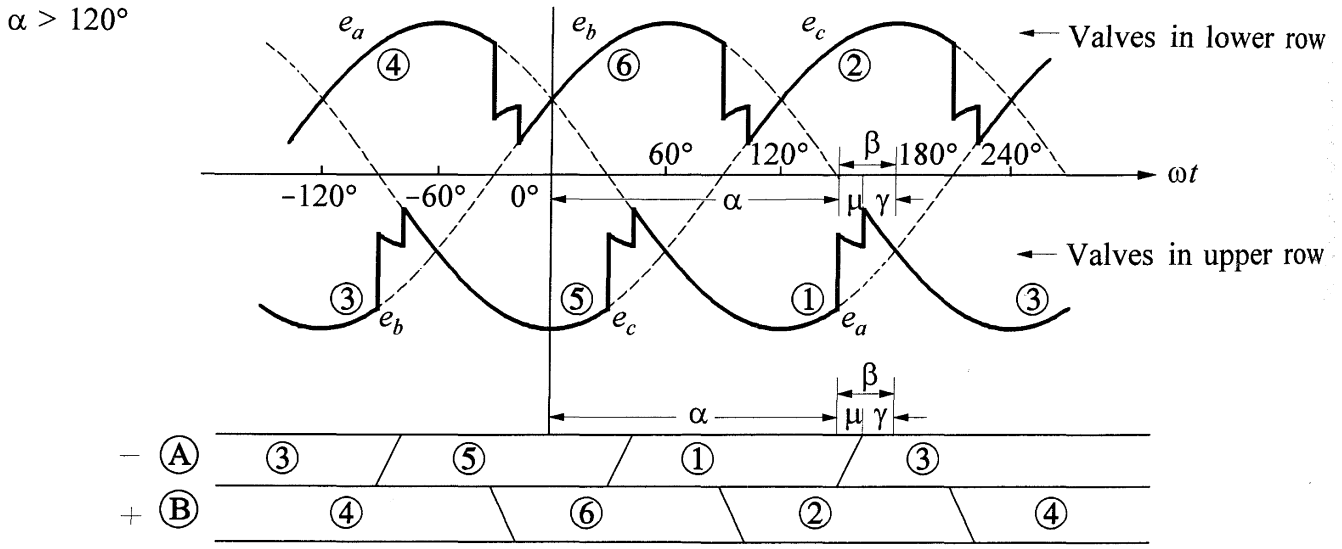

Figure 10.19 Voltage wave shapes and valve conduction periods

Converter Angle Definitions

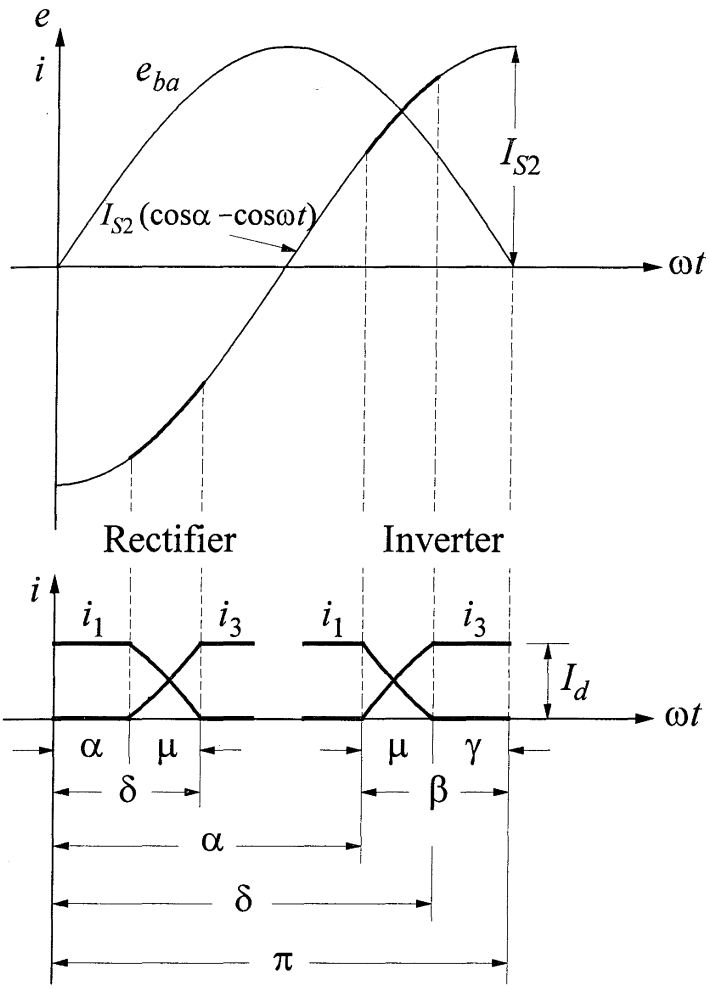

e_{ba} = commutating voltage
$I_{S2}(\cos\alpha - \cos\omega t)$ = current during commutating period

i_1 = current in valve 1
i_3 = current in valve 3

Figure 10.20 Angles used in the description of rectifier and inverter operations

or

$$V_d = V_{d0}\cos\gamma - R_c I_d \tag{10.17B}$$

The inverter voltage, considered negative in general converter equations, is usually taken as positive when written specifically for an inverter.

Based on the above equations, the inverter may be represented by the two alternative equivalent circuits shown in Figure 10.21.

Relationship between ac and dc quantities

From Equation 10.13, the average direct voltage V_d is given by

$$V_d = V_{d0}\cos\alpha - \Delta V_d = V_{d0}\frac{\cos\alpha + \cos\delta}{2} \tag{10.18A}$$

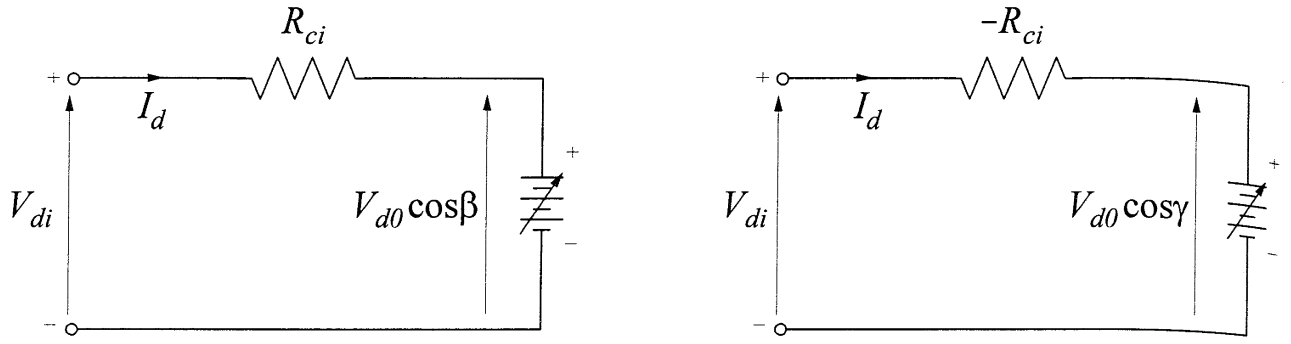

(a) In terms of β (b) In terms of γ

Figure 10.21 Inverter equivalent circuits (with V_{di} positive)

Substituting for V_{d0} from Equation 10.3B in terms of RMS line-to-neutral voltage E_{LN}, we get

$$V_d = \frac{3\sqrt{6}}{\pi}\frac{\cos\alpha + \cos\delta}{2}E_{LN} \tag{10.18B}$$

With losses neglected, ac power is equal to the dc power:

$$P_{ac} = P_{dc}$$

Hence,

$$3E_{LN}I_{L1}\cos\phi = V_d I_d$$

where

E_{LN} = RMS line-to-neutral voltage
I_{L1} = RMS fundamental frequency current

From Equation 10.18,

$$3E_{LN}I_{L1}\cos\phi = \frac{3\sqrt{6}}{\pi}\frac{\cos\alpha + \cos\delta}{2}E_{LN}I_d$$

Hence,

$$I_{L1}\cos\phi = \left(\frac{\sqrt{6}}{\pi}I_d\right)\left(\frac{\cos\alpha + \cos\delta}{2}\right) \tag{10.19}$$

From Equation 10.5B, with $\mu=0$

$$I_{L1} = \frac{\sqrt{6}}{\pi} I_d$$

Denoting this value of I_{L1} (when $\mu=0$) by I_{L10}, Equation 10.19 can be written as

$$I_{L1}\cos\phi = I_{L10}\left(\frac{\cos\alpha + \cos\delta}{2}\right) \tag{10.20}$$

where

$$I_{L10} = \frac{\sqrt{6}}{\pi} I_d \tag{10.21}$$

Approximate expressions

As an approximation I_{L1} may be considered equal to I_{L10}:

$$I_{L1} \approx I_{L10} = \frac{\sqrt{6}}{\pi} I_d \tag{10.22}$$

The above relationship is exact if $\mu=0°$; with $\mu=60°$ the error is 4.3%, and with $\mu<30°$ (normal value) the error is less than 1.1% [2].

It follows that the power factor is given by

$$\cos\phi \approx \frac{\cos\alpha + \cos\delta}{2} \tag{10.23}$$

As a result of the approximation, from Equation 10.18A,

$$V_d \approx V_{d0}\cos\phi \tag{10.24A}$$

Hence,

$$\cos\phi \approx \frac{V_d}{V_{d0}} \tag{10.24B}$$

From Equation 10.11, $V_d = V_{d0}\cos\alpha - R_c I_d$. Hence,

$$\cos\phi \approx \cos\alpha - \frac{R_c I_d}{V_{d0}} \tag{10.25}$$

Substituting for V_{d0} from Equation 10.3A in Equation 10.24A, we get

$$V_d \approx \frac{3\sqrt{6}}{\pi} E_{LN}\cos\phi \tag{10.26}$$

We see from Equation 10.22 that the converter has essentially fixed current ratio I_d/I_{L1}, the variation with load being only a few percent. The power factor $\cos\phi$, as seen from Equation 10.25, depends on load in addition to ignition delay angle α.

10.2.3 Converter Transformer Rating

The RMS value of the transformer secondary current (total and not just the fundamental frequency component) I_{TRMS} is given by

$$I_{TRMS}^2 = \frac{1}{T}\int_0^T i^2(t)\,dt$$

The alternating line-current wave consists of rectangular pulses of amplitude I_d and width $2\pi/3$ rad as shown in Figure 10.12. Therefore,

$$\begin{aligned} I_{TRMS}^2 &= \frac{1}{\pi}\int_{-\pi/2}^{\pi/2} i^2(t)\,dt \\ &= \frac{1}{\pi}\int_{-\pi/3}^{\pi/3} I_d^2\,dt \\ &= \frac{2}{3} I_d^2 \end{aligned}$$

and hence,

$$I_{TRMS} = \sqrt{2/3}\, I_d \tag{10.27}$$

The RMS value of the line-to-neutral transformer secondary voltage is given by

$$E_{LN} = \frac{\pi}{3\sqrt{6}} V_{d0}$$

Transformer volt-ampere rating is given by

$$\begin{aligned} \text{3-phase rating} &= 3E_{LN}I_{TRMS} \\ &= 3\left(\frac{\pi}{3\sqrt{6}}\right)V_{d0}\sqrt{\frac{2}{3}}I_d \\ &= \frac{\pi}{3}V_{d0}I_d \\ &= 1.0472\,(\text{ideal no-load direct voltage})\,(\text{rated direct current}) \end{aligned} \tag{10.28}$$

10.2.4 Multiple-Bridge Converters

Two or more bridges are connected in series to obtain as high a direct voltage as required. The bridges are in series on the dc side and parallel on the ac side. A bank of transformers is connected between the ac source and bridge-connected valves. The ratios of the transformers are adjustable under load.

In practice, multiple-bridge converters have an even number of bridges arranged in pairs so as to result in a 12-pulse arrangement. As shown in Figure 10.22,

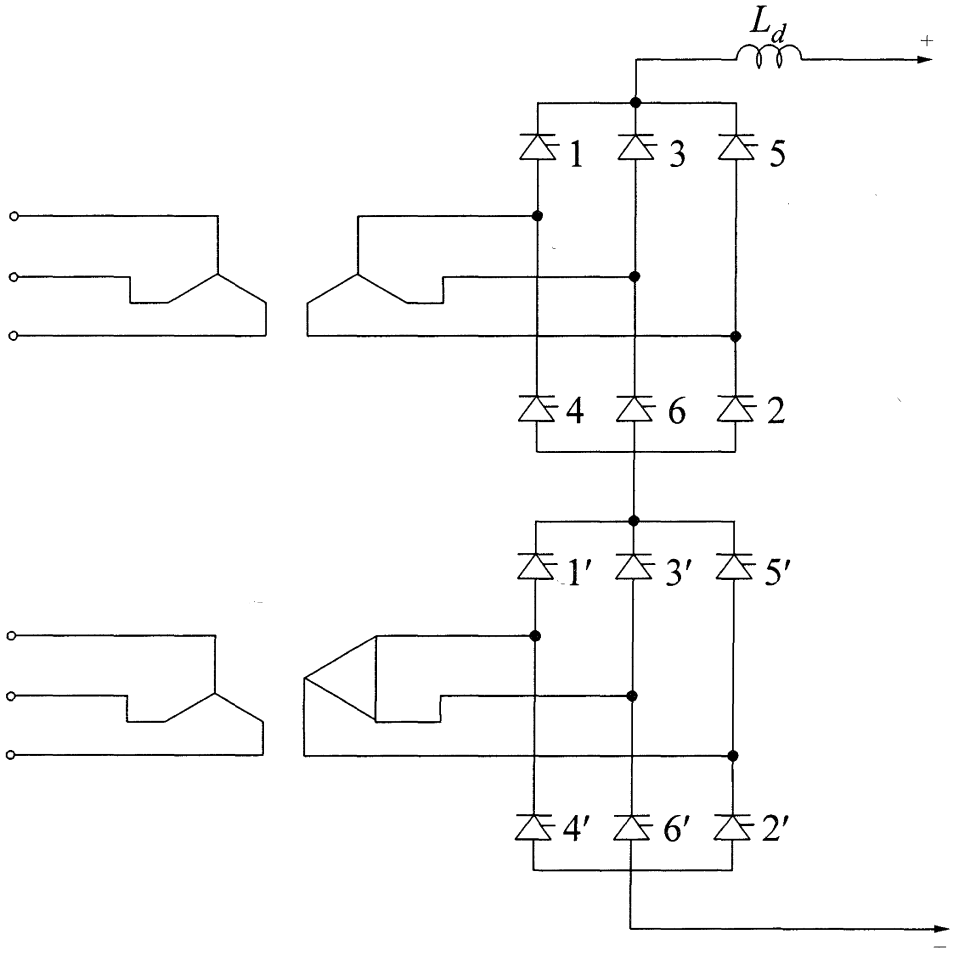

Figure 10.22 12-pulse bridge converter

two banks of transformers, one connected Y-Y and the other Y-Δ, are used to supply each pair of bridges. The three-phase voltages supplied at one bridge are displaced by 30° from those supplied at the other bridge. The ac wave shapes for the two bridges, as illustrated in Figure 10.23, add up so as to produce a wave shape which is more sinusoidal than the current waves for each of the 6-pulse bridges. As we will see in Section 10.6, with a 12-pulse arrangement, *fifth and seventh harmonics are effectively eliminated* on the ac side. This reduces the cost of harmonic filters significantly.

In addition, with a 12-pulse bridge arrangement, the dc voltage ripple is reduced; sixth and eighteenth harmonics are eliminated (6-pulse bridges have multiples of sixth harmonics on the dc side whereas 12-pulse bridges have only multiples of the twelfth harmonic).

For converters having more than two bridges, higher pulse numbers are possible: 18-pulse, three-bridge converter; 24-pulse, four-bridge converters. The transformer connections required are more complex than those for 12-pulse converters. Therefore, it is more practical to use 12-pulse converters and provide the necessary filtering.

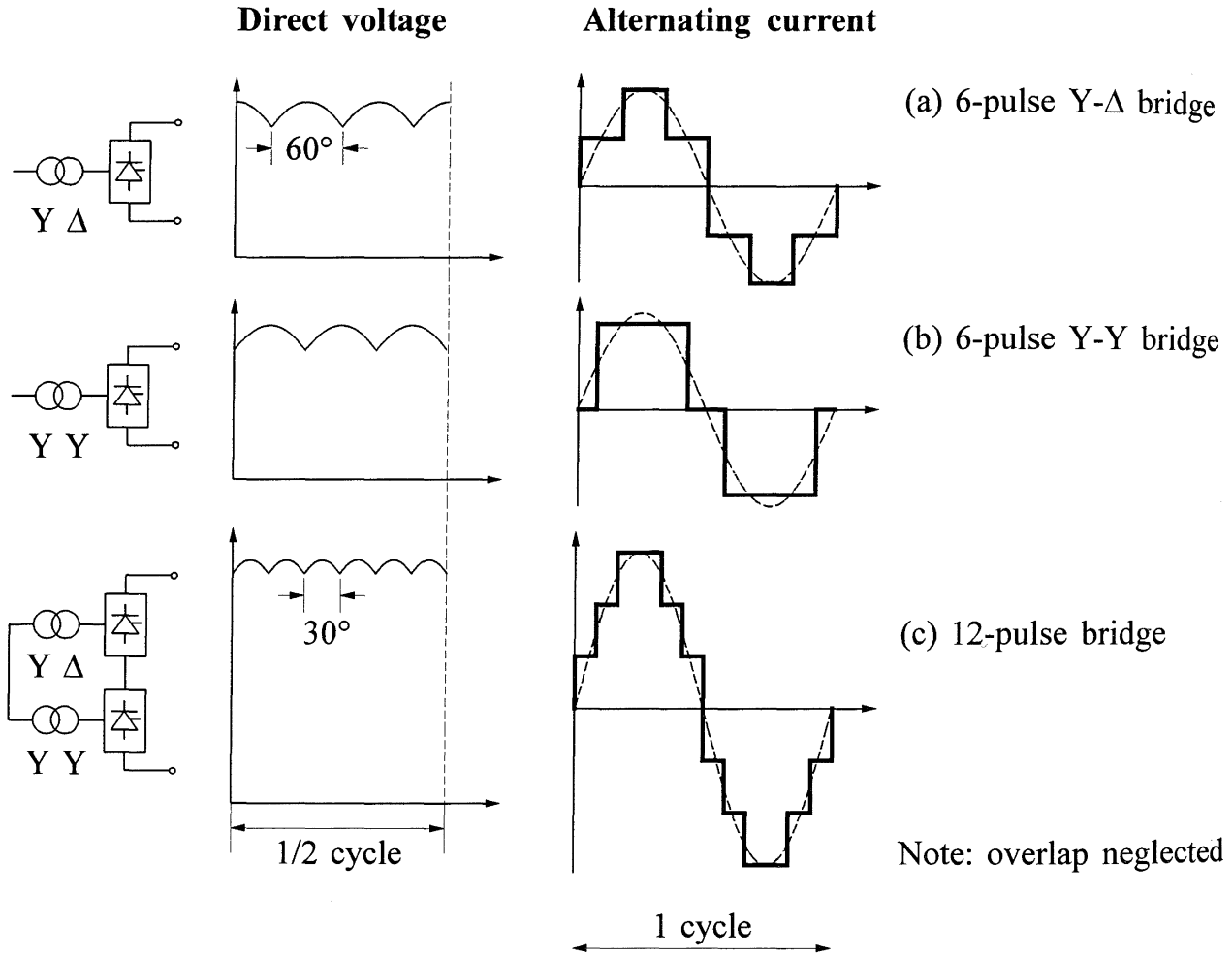

Figure 10.23 Direct voltage and alternating current wave shapes

Relationships between ac and dc quantities, with multiple bridges

Let

B = no. of bridges in series
T = transformer ratio

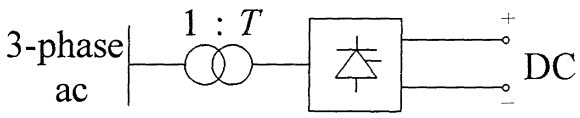

The ideal no-load voltage (corresponding to Equation 10.3C) is

$$V_{d0} = \frac{3\sqrt{2}}{\pi} BTE_{LL} = 1.3505BTE_{LL} \tag{10.29}$$

Since voltage drop per bridge is $I_d(3X_c/\pi)$ and there are B bridges in series, the dc voltage (corresponding to Equations 10.11) is given by

$$V_d = V_{d0}\cos\alpha - I_d B\left(\frac{3}{\pi}X_c\right) \tag{10.30A}$$

or

$$V_d = V_{d0}\cos\gamma - I_d B\left(\frac{3}{\pi}X_c\right) \tag{10.30B}$$

The dc voltage in terms of the power factor per Equation 10.24A is given by

$$V_d \approx V_{d0}\cos\phi \tag{10.31}$$

However, with multiple bridges, V_{d0} is given by Equation 10.29. The average dc output voltage of a 12-pulse bridge is, therefore, twice that of a 6-pulse bridge converter. The RMS value of the fundamental frequency component of the total alternating current (corresponding to Equation 10.22) is given by

$$I_{L1} \approx \frac{\sqrt{6}}{\pi} BTI_d = 0.78BTI_d \tag{10.32}$$

Example 10.1

A three-phase, 12-pulse rectifier is fed from a transformer with nominal voltage ratings of 220 kV/110 kV.

(a) If the primary voltage is 230 kV and the effective turns ratio T is 0.48, determine the dc output voltage when the ignition delay angle α is 20° and the commutation angle μ is 18°.

(b) If the direct current delivered by the rectifier is 2,000 A, calculate the effective commutating reactance X_c, RMS fundamental component of alternating current, power factor cosϕ, and reactive power at the primary side of the transformer.

Solution

(a) A 12-pulse bridge circuit comprises two 6-pulse bridges. Hence B=2.

The no-load direct voltage is

$$V_{d0} = \frac{3\sqrt{2}}{\pi} BTE_{LL}$$

$$= 1.3505 \times 2 \times 0.48 \times 230$$

$$= 298.18 \quad \text{kV}$$

The extinction angle is

$$\delta = \alpha + \mu = 20° + 18° = 38°$$

Hence, the reduction in average direct voltage due to commutation overlap is

$$\Delta V_d = V_{d0} \frac{\cos\alpha - \cos\delta}{2}$$

$$= 298.18 \times \frac{\cos 20° - \cos 38°}{2}$$

$$= 22.61 \quad \text{kV}$$

The dc output voltage is

$$V_d = V_{d0}\cos\alpha - \Delta V_d$$

$$= 298.18 \cos 20° - 22.61$$

$$= 257.58 \quad \text{kV}$$

Alternatively,

$$V_d = V_{d0} \frac{\cos\alpha + \cos\delta}{2}$$

$$= 298.18 \times \frac{\cos 20° + \cos 38°}{2}$$

$$= 257.58 \quad \text{kV}$$

(b) $\Delta V_d = BR_cI_d$. Hence,

$$R_c = \frac{\Delta V_d}{BI_d} = \frac{22.61}{2\times2} = 5.65 \quad \Omega$$

$$X_c = \frac{\pi R_c}{3} = \frac{\pi\times5.65}{3} = 5.92 \quad \Omega/\text{phase}$$

Fundamental component of alternating current on the primary side is

$$I_{L1} = \frac{\sqrt{6}}{\pi}BTI_d$$

$$= 0.7797\times2\times0.48\times2$$

$$= 1.497 \quad \text{kA}$$

Power factor at the HT bus is

$$\cos\phi \approx \frac{V_d}{V_{d0}} = \frac{257.58}{298.18} = 0.8638$$

Hence, $\phi = \cos^{-1}(0.8638) = 30.25°$

$$P_{ac} = P_{dc} = V_dI_d = 257.58\times2 = 515.16 \quad \text{MW}$$

$$Q_{HT} = P_{ac}\tan\phi = 515.16\times\tan30.25° = 300.43 \quad \text{MVAr}$$

The solution is shown in Figure E10.1.

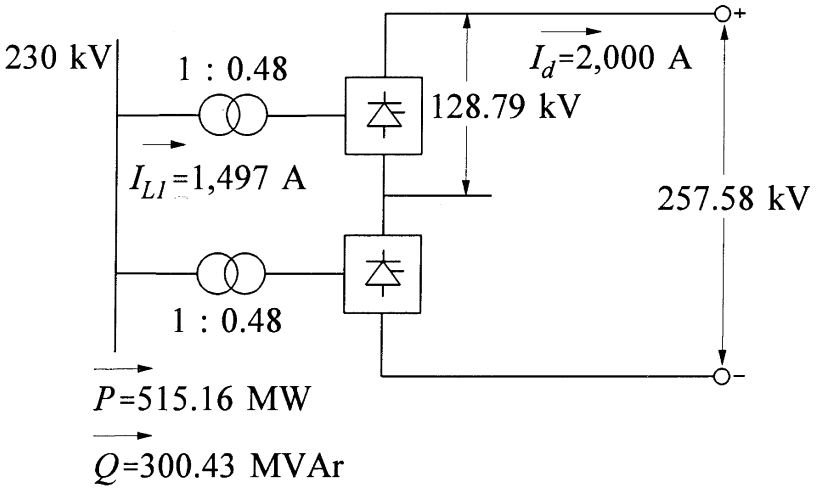

Figure E10.1

■

10.3 ABNORMAL OPERATION

10.3.1 Arc-back (Backfire)

Arc-back refers to conduction in the reverse direction and is one of the serious problems associated with mercury-arc valves. Since arc-back is reverse conduction, it can occur only when there is inverse voltage across a valve. In rectification each valve is exposed to inverse voltage during approximately two-thirds of each cycle. Therefore, arc-backs are more common during rectification than during inversion.

Arc-back is a random phenomenon. Among the factors that tend to increase its occurrence are high-peak inverse voltage, overcurrent, high rate of change of current at the end of conduction, condensation of mercury vapour on anodes, and high rate of increase of inverse voltage. The effect of the arc-back is to place a short-circuit across two phases of the secondary of the converter transformers. These short-circuit currents subject the transformers and valves to much greater current than in normal operation. The transformer windings must be firmly braced to withstand more numerous short-circuits than ordinary power transformers; this adds to the cost. The valves require increased maintenance.

To remove an arc-back, current is diverted into a bypass valve. The bypass valve is a separate valve connected across a 6-pulse valve group. This valve has a higher current rating than other valves and is capable of carrying 1 pu direct current for about 60 seconds. The control grid of the bypass valve is normally blocked. When a bridge is to be bypassed, its bypass valve is unblocked and the main valves are simultaneously blocked by discontinuing the transmission of positive pulses to their grids. The direct current shifts from the main valves to the bypass valve in a few milliseconds. By simultaneously unblocking the main valve and blocking the bypass valve, the direct current can be transferred back to the main valves.

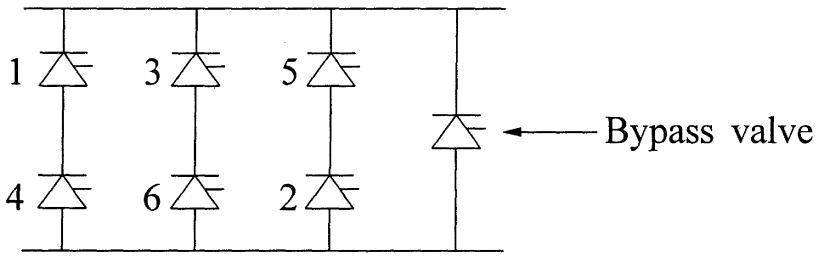

Figure 10.24

Arc-back does not occur in thyristor valves. Thyristors can individually fail in a shorted condition. However, thyristors arrayed into converter valves utilize redundancy and protection to prevent reverse conduction.

10.3.2 Commutation Failure

Failure to complete commutation before the commutating voltage reverses (with sufficient margin for de-ionization) is referred to as commutation failure. It is not due to any misoperation of the valve but to conditions in the circuits outside the valve. Commutation failures are more common with inverters and occur during disturbances such as high direct current or low alternating voltage. A rectifier can have a commutation failure only if the firing circuit fails.

Figure 10.25 illustrates how commutation failure occurs in an inverter. A failure of commutation from valve 1 to valve 3 is considered.

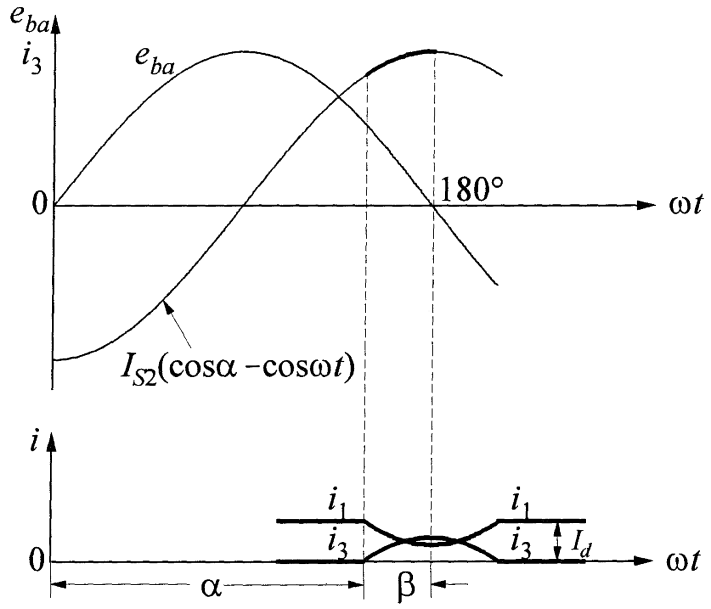

Figure 10.25 Commutation failure in inverters

Because of increased direct current, low alternating voltage (possibly caused by an ac system short-circuit), late ignition, or a combination of these, valve 1 is not extinguished before e_{ba} reverses. Current in valve 3 will decrease to zero and the valve will extinguish. Valve 1 current will return to I_d, and thus valve 1 will continue to conduct.

As shown in Figure 10.26, when valve 4 fires next, because valve 1 is still conducting, a short is placed across the dc side of the bridge. The zero dc voltage keeps the voltage across valve 5 negative so that valve 5 cannot conduct. Valve 4 is extinguished and valve 6 is ignited in the normal fashion.

Valve 1 thus conducts for one full cycle (3 times normal duration) and extinguishes when valve 3 ignites during the next cycle.

For the period when valves 1 and 4 are both conducting (i.e., for 120°), the inverter dc voltage is zero and hence there is no power flow on the dc system.

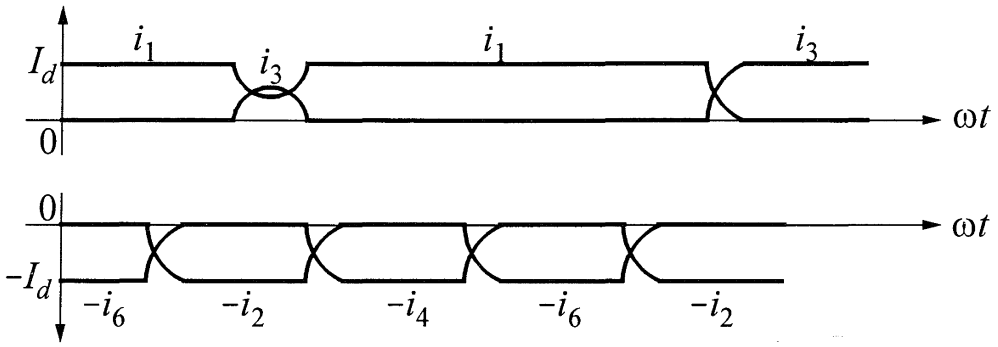

Figure 10.26 Valve currents during commutation failure

Double commutation failure is the failure of two successive commutations in the same cycle. If the unsuccessful commutation from valve 1 to valve 3 were followed by a failure in the commutation from valve 2 to valve 4, valves 1 and 2 would be left conducting until the next cycle when they would be normally conducting again. During the time that only valves 1 and 2 are conducting, the alternating voltages of terminals *a* and *c* appear across the dc terminals.

Double commutation failures are very rare. Usually, after one commutation failure, either the firing angle initiating the next commutation is advanced sufficiently by the inverter control, or "double overlap" during the period when valves 1 and 3 as well as valves 2 and 4 are conducting hastens the commutation. Double commutation failure, like the single failure, is self-curing.

10.4 CONTROL OF HVDC SYSTEMS

An HVDC transmission system is highly controllable. Its effective use depends on appropriate utilization of this controllability to ensure desired performance of the power system. With the objectives of providing efficient and stable operation and maximizing flexibility of power control without compromising the safety of equipment, various levels of control are used in a hierarchical manner. In this section, we will describe the principles of operation of these controls, their implementation and their performance during normal and abnormal system conditions.

10.4.1 Basic Principles of Control

Consider the HVDC link shown in Figure 10.27(a). It represents a monopolar link or one pole of a bipolar link. The corresponding equivalent circuit and voltage profile are shown in Figures 10.27(b) and (c), respectively.

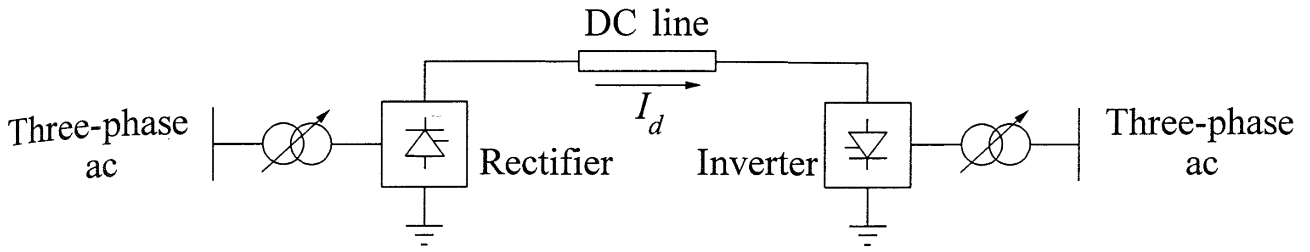

(a) Schematic diagram

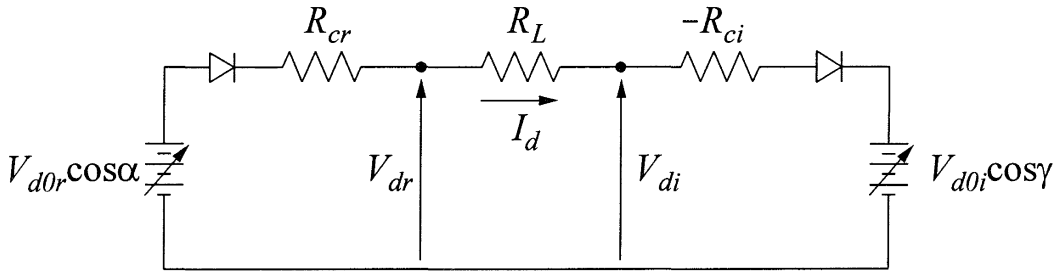

(b) Equivalent circuit

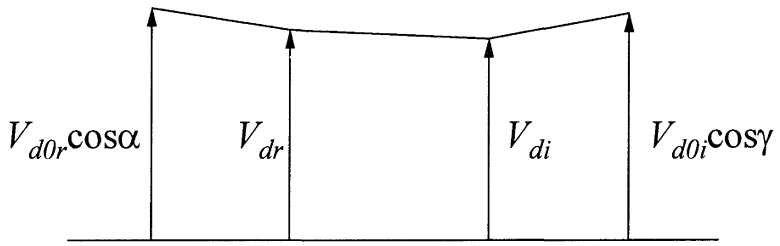

(c) Voltage profile

Figure 10.27 HVDC transmission link

The direct current flowing from the rectifier to the inverter is

$$I_d = \frac{V_{dor}\cos\alpha - V_{doi}\cos\gamma}{R_{cr}+R_L-R_{ci}} \tag{10.33}$$

The power at the rectifier terminals is

$$P_{dr} = V_{dr}I_d \tag{10.34}$$

and at the inverter terminal is

$$P_{di} = V_{di}I_d = P_{dr}-R_L I_d^2 \tag{10.35}$$

Basic means of control

The direct voltage at any point on the line and the current (or power) can be controlled by controlling the internal voltages ($V_{dor}\cos\alpha$) and ($V_{doi}\cos\gamma$). This is accomplished by grid/gate control of the valve ignition angle or control of the ac voltage through tap changing of the converter transformer.

Grid/gate control, which is rapid (1 to 10 ms), and tap changing, which is slow (5 to 6 s per step), are used in a complementary manner. Grid/gate control is used initially for rapid action, followed by tap changing to restore the converter quantities (α for rectifier and γ for inverter) to their normal range.

Power reversal is obtained by reversal of polarity of direct voltages at both ends.

Basis for selection of controls

The following considerations influence the selection of control characteristics:

1. Prevention of large fluctuations in direct current due to variations in ac system voltage.

2. Maintaining direct voltage near rated value.

3. Maintaining power factors at the sending and receiving end that are as high as possible.

4. Prevention of commutation failure in inverters and arc-back in rectifiers using mercury-arc valves.

Rapid control of the converters to prevent large fluctuations in direct current is an important requirement for satisfactory operation of the HVDC link. Referring to Equation 10.33, the line and converter resistances are small; hence, a small change in V_{dor} or V_{doi} causes a large change in I_d. For example, a 25% change in the voltage at either the rectifier or the inverter could cause direct current to change by as much as 100%. This implies that, if both α_r and γ_i are kept constant, the direct current can vary over a wide range for small changes in the alternating voltage magnitude at either end. Such variations are generally unacceptable for satisfactory performance of the power system. In addition, the resulting current may be high enough to damage the valves and other equipment. Therefore, rapid converter control to prevent fluctuations of direct current is essential for proper operation of the system; without such a control, the HVDC system would be impractical.

For a given power transmitted, the direct voltage profile along the line should be close to the rated value. This minimizes the direct current and thereby the line losses.

There are several reasons for maintaining the power factor high:

(a) To keep the rated power of the converter as high as possible for given current and voltage ratings of transformer and valve;

(b) To reduce stresses in the valves;

(c) To minimize losses and current rating of equipment in the ac system to which the converter is connected;

(d) To minimize voltage drops at the ac terminals as loading increases; and

(e) To minimize cost of reactive power supply to the converters.

From Equation 10.23,

$$\begin{aligned}\cos\phi &\approx 0.5[\cos\alpha+\cos(\alpha+\mu)]\\ &\approx 0.5[\cos\gamma+\cos(\gamma+\mu)]\end{aligned}$$

Therefore, to achieve high power factor, α for a rectifier and γ for an inverter should be kept as low as possible.

The rectifier, however, has a *minimum α limit* of about 5° to ensure adequate voltage across the valve before firing. For example, in the case of thyristors, the positive voltage appearing across each thyristor before firing is used to charge the supply circuit providing the firing pulse energy to the thyristor. Therefore, firing cannot occur earlier than about α=5° [10]. Consequently, the rectifier normally operates at a value of α within the range of 15° to 20° so as to leave some room for increasing rectifier voltage to control dc power flow.

In the case of an inverter, it is necessary to maintain a certain minimum extinction angle to avoid commutation failure. It is important to ensure that commutation is completed with sufficient margin to allow for de-ionization before commutating voltage reverses at α=180° or γ=0°. The extinction angle γ is equal to $\beta-\mu$, with the overlap μ depending on I_d and the commutating voltage. Because of the possibility of changes in direct current and alternating voltage even after commutation has begun, sufficient *commutation margin above the minimum γ limit* must be maintained. Typically, the value of γ with acceptable margin is 15° for 50 Hz systems and 18° for 60 Hz systems.

Control characteristics

Ideal characteristics:

In satisfying the basic requirements identified above, the responsibilities for voltage regulation and current regulation are kept distinct and are assigned to separate

terminals. Under normal operation, the rectifier maintains constant current (CC), and the inverter operates with *constant extinction angle*[1] (CEA), maintaining adequate commutation margin. The basis for this control philosophy is best explained by using the steady-state voltage-current (*V-I*) characteristics, shown in Figure 10.28. The voltage V_d and the current I_d forming the coordinates may be measured at some common point on the dc line. In Figure 10.28, we have chosen this to be at the rectifier terminal. The rectifier and inverter characteristics are both measured at the rectifier; the inverter characteristic thus includes the voltage drop across the line.

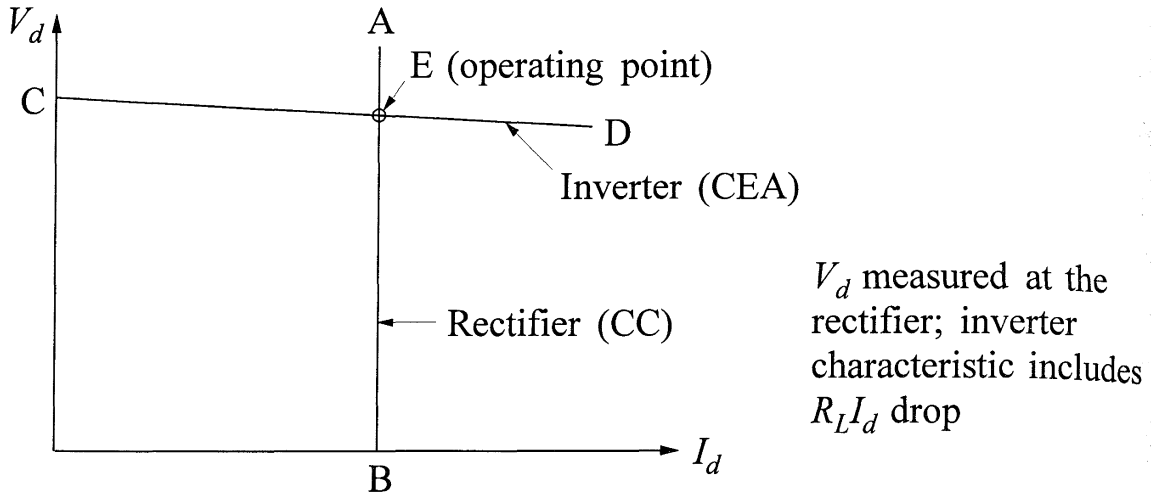

Figure 10.28 Ideal steady-state *V-I* characteristics

With the rectifier maintaining constant current, its *V-I* characteristic, shown as line AB in Figure 10.28, is a vertical line. From Figure 10.27(b),

$$V_d = V_{d0i}\cos\gamma + (R_L - R_{ci})I_d \tag{10.36}$$

This gives the inverter characteristic, with γ maintained at a fixed value. If the commutating resistance R_{ci} is slightly larger than the line resistance R_L, the characteristic of the inverter, shown as line CD in Figure 10.28, has a small negative slope.

---

[1] Constant extinction angle control mode is essentially the same as constant margin angle control. Under normal operation, the commutation margin angle and the extinction angles are equal. The distinction arises during conditions such as operation with a large overlap angle; the valve voltage may become positive earlier than when the sinusoidal portion of the voltage would have crossed zero under normal conditions. Under these conditions the concept of maintaining minimum extinction angle is not meaningful. Therefore, the commutation margin angle (representing the interval between the end of conduction and the instant when the actual voltage across the valve becomes positive) is maintained for safe inverter operation.

Since an operating condition has to satisfy both rectifier and inverter characteristics, it is defined by the intersection of the two characteristics (E).

The rectifier characteristic can be shifted horizontally by adjusting the "current command" or "current order." If measured current is less than the command, the regulator advances the firing by decreasing α.

The inverter characteristic can be raised or lowered by means of its transformer tap changer. When the tap changer is moved, the CEA regulator quickly restores the desired γ. As a result, the direct current changes, which is then quickly restored by the current regulator of the rectifier. The rectifier tap changer acts to bring α into the desired range between 10° and 20° to ensure a high power factor and adequate room for control.

To operate the inverter at a constant γ, the valve firing is controlled by a computer which takes into consideration variations in the instantaneous values of voltage and current. The computer controls the firing times so that the extinction angle γ is larger than the de-ionization angle of the valve.

Actual characteristics:

The rectifier maintains constant current by changing α. However, α cannot be less than its minimum value (α_{min}). Once α_{min} is reached, no further voltage increase is possible, and the rectifier will operate at *constant ignition angle* (CIA). Therefore, the rectifier characteristic has really two segments (AB and FA) as shown in Figure 10.29. The segment FA corresponds to minimum ignition angle and represents the CIA control mode; the segment AB represents the normal constant current (CC) control mode.

In practice, the constant current characteristic may not be truly vertical, depending on the current regulator. With a proportional controller, it has a high negative slope due to the finite gain of the current regulator, as shown below.

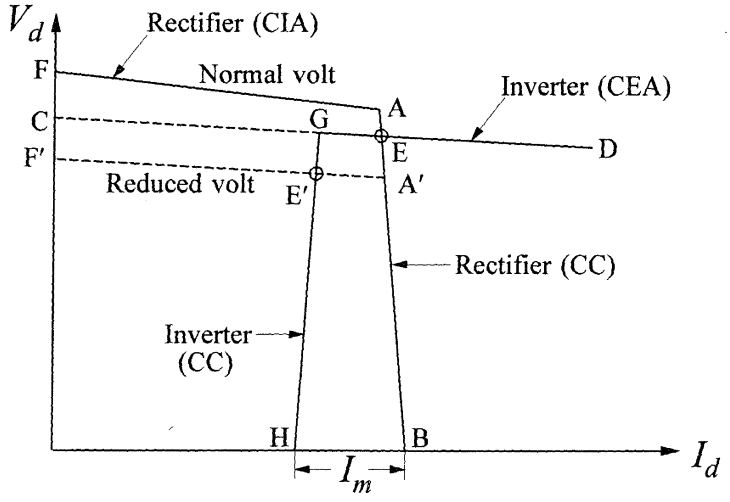

Figure 10.29 Actual converter control steady-state characteristics

With a regulator gain of K, we have

$$V_{d0}\cos\alpha = K(I_{ord} - I_d)$$
$$= V_d + R_{cr} I_d$$

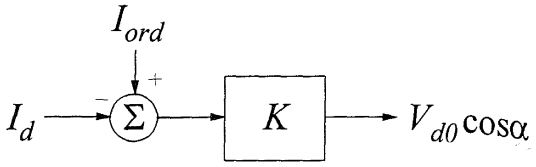

I_{ord} = current order

Figure 10.30 Current regulator

Therefore,

$$V_d = KI_{ord} - (K + R_{cr}) I_d$$

In terms of perturbed values,

$$\Delta V_d = -(K + R_{cr})\,\Delta I_d$$

or

$$\Delta V_d / \Delta I_d = -(K + R_{cr}) \tag{10.37}$$

With a proportional plus integral regulator, the CC characteristic is quite vertical. The complete rectifier characteristic at normal voltage is defined by FAB. At a reduced voltage it shifts, as indicated by F′A′B.

The CEA characteristic of the inverter intersects the rectifier characteristic at E for normal voltage. However, the inverter CEA characteristic (CD) does not intersect the rectifier characteristic at a reduced voltage represented by F′A′B. Therefore, a big reduction in rectifier voltage would cause the current and power to be reduced to zero after a short time depending on the dc reactors. The system would thus run down.

In order to avoid the above problem, the inverter is also provided with a current controller, which is set at a lower value than the current setting for the rectifier. The complete inverter characteristic is given by DGH, consisting of two segments: one of CEA and one of constant current.

The difference between the rectifier current order and the inverter current order is called the *current margin*, denoted by I_m in Figure 10.29. It is usually set at 10 to 15% of the rated current so as to ensure that the two constant current characteristics do not cross each other due to errors in measurement or other causes.

Under normal operating conditions (represented by the intersection point E), the rectifier controls the direct current and the inverter the direct voltage. With a reduced rectifier voltage (possibly caused by a nearby fault), the operating condition is represented by the intersection point E′. The inverter takes over current control and the rectifier establishes the voltage. In this operating mode, the roles of the rectifier and inverter are reversed. The change from one mode to another is referred to as a *mode shift*.

Combined rectifier and inverter characteristics

In most HVDC systems, each converter is required to function as a rectifier

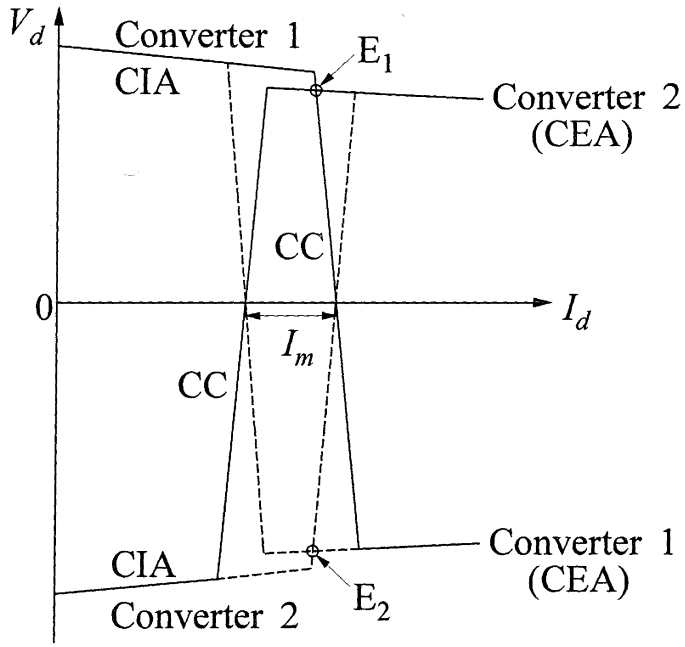

Figure 10.31 Operation with each converter having combined inverter and converter characteristics

as well as an inverter. Consequently, each converter is provided with a combined characteristic as shown in Figure 10.31.

The characteristic of each converter consists of three segments: constant ignition angle (CIA) corresponding to α_{min}, constant current (CC), and constant extinction angle (CEA).

The power transfer is from converter 1 to converter 2, when the characteristics are as shown in Figure 10.31 by solid lines. The operating condition in this mode of operation is represented by point E_1.

The power flow is reversed when the characteristics are as shown by the dotted lines. This is achieved by reversing the "margin setting," i.e., by making the current order setting of converter 2 exceed that of converter 1. The operating condition is now represented by E_2 in the figure; the current I_d is the same as before, but the voltage polarity has changed.

Alternative inverter control modes

The following are variations to the CEA control mode described above for the inverter. These variations offer some advantages in special cases.

DC voltage control mode:

Instead of regulating to a fixed γ value (CEA), a closed-loop voltage control may be used so as to maintain a constant voltage at a desired point on the dc line,

usually the sending end (rectifier). The necessary inverter voltage to maintain the desired dc voltage is estimated by computing the line *RI* drop. As compared to constant γ control (which has drooping voltage characteristic), the voltage control mode has the advantage that the inverter *V-I* characteristic is flat as shown in Figure 10.32(a). In addition, the voltage control mode has a slightly higher value of γ and is thus less prone to commutation failure. Normally the voltage control mode maintains a γ of about 18° in conjunction with the tap changers.

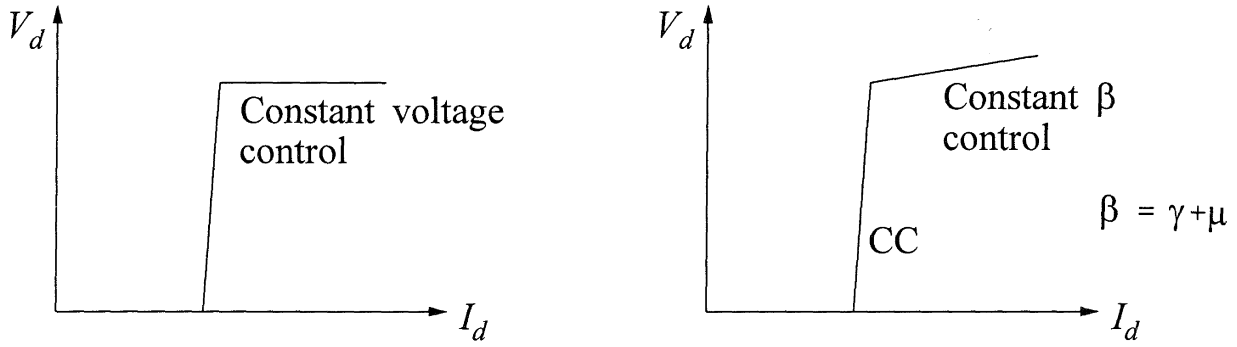

(a) Constant voltage mode (b) Constant β mode

Figure 10.32 Alternative inverter control modes

Beta (β) control:

The inverter equivalent circuit in terms of ignition advance angle β is as shown in Figure 10.21(a). With constant β, the *V-I* characteristic of the inverter therefore has a positive slope as shown in Figure 10.32(b). At low loads, constant β gives additional security against commutation failure. However, at higher currents (larger overlap), the minimum γ may be encountered. Constant β control mode is not used for normal operation. It is viewed as a backup type of control mode useful for acting directly upon the firing angle during transient conditions.

Mode stabilization

As shown in Figure 10.33, the intersection of rectifier α_{min} characteristic and the inverter CEA may not be well defined at certain voltage levels near the transition between the inverter CEA and CC characteristics. In this region, a small change in ac voltage will cause a large (10%) change in direct current. There will also be a tendency to "hunt" between modes and tap changing. In order to avoid this problem, a characteristic with positive slope (constant β) at the transition between CEA and CC control characteristic of the inverter is often provided as shown in Figure 10.34(a). Another variation, shown in Figure 10.34(b), controls the direct voltage with a voltage feedback loop.

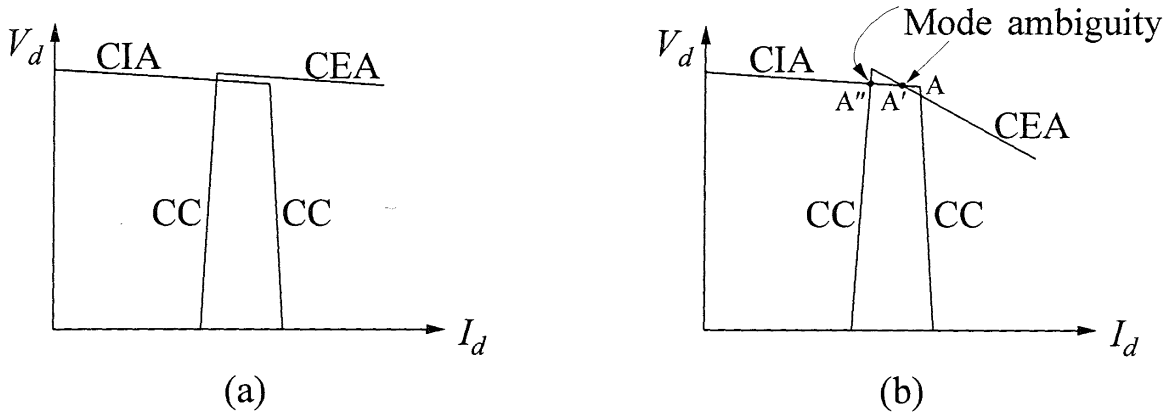

Figure 10.33 Regions of mode ambiguity

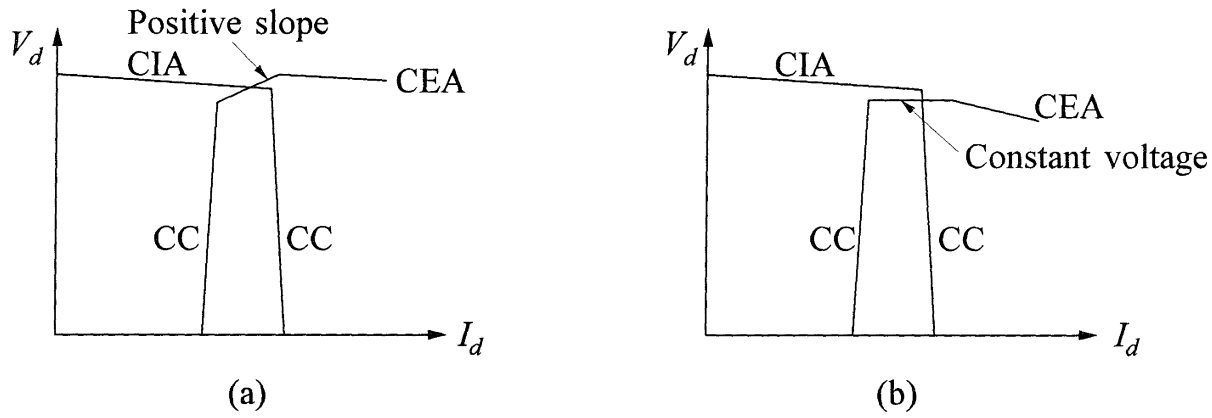

Figure 10.34 Modification of *V-I* characteristic for mode stabilization

Tap changer control

Tap changer control is used to keep the converter firing angles within the desired range, whenever α (for rectifier) or γ (for inverter) exceeds this range for more than a few seconds.

Normally, the inverter operates at constant extinction angle, thus fixing the line voltage with superimposed voltage control by the tap changer. The rectifier operates in current control mode with superimposed $\alpha=\alpha_{nominal}$ control by the tap changer.

Tap changers are usually sized to allow for minimum and maximum steady-state voltage variations, and for minimum to maximum power flow under worst-case steady-state voltage conditions. Unnecessary tap movements during transient conditions are prevented by using time delays. Hunting of the tap changer is avoided by having a dead band wider than the tap-step size.

Current limits

The following limits have to be recognized in establishing the current order.

(a) Maximum current limit:

The maximum short-time current is usually limited to 1.2 to 1.3 times normal

full-load current, to avoid thermal damage to valves.

(b) Minimum current limit:

At low values of current, the ripple in the current may cause it to be discontinuous or intermittent. In a 12-pulse operation, the current is then interrupted 12 times per cycle. This is objectionable because of the high voltages (Ldi/dt) induced in the transformer windings and the dc reactor by the high rate of change of current at the instants of interruption.

At low values of direct current, the overlap is small. Operation is objectionable even with continuous current if the overlap is too small. With a very small overlap, the two jumps in direct voltage at the beginning and end of commutation merge to form one jump twice as large, resulting in an increased stress on the valves. It may also cause flashover of protective gaps placed across the terminals of each bridge [2].

(c) Voltage-dependent current-order limit[1] *(VDCOL):*

Under low voltage conditions, it may not be desirable or possible to maintain rated direct current or power for the following reasons:

(a) When voltage at one converter drops by more than about 30%, the reactive power demand of the remote converter increases, and this may have an adverse effect on the ac system. A higher α or γ at the remote converter necessary to control the current causes the increase in reactive power. The reduced ac system voltage levels also significantly decrease the reactive power supplied by the filters and capacitors, which often supply much of the reactive power absorbed by the converters.

(b) At reduced voltages, there are also risks of commutation failure and voltage instability.

These problems associated with operation under low-voltage conditions may be prevented by using a "voltage-dependent current-order limit" (VDCOL). This limit reduces the maximum allowable direct current when the voltage drops below a predetermined value. The VDCOL characteristics may be a function of the ac commutating voltage or the dc voltage. The two types of VDCOLs are illustrated in Figure 10.35.

The rectifier inverter static *V-I* characteristics, including VDCOL, are shown in Figure 10.36. The inverter characteristic matches the rectifier VDCOL to preserve the current margin. The general practice is to transiently reduce the current order through voltage-dependent current limit. For VDCOL operation, the measured direct

---

[1] This is also referred to as *voltage dependent current limit* (VDCL).

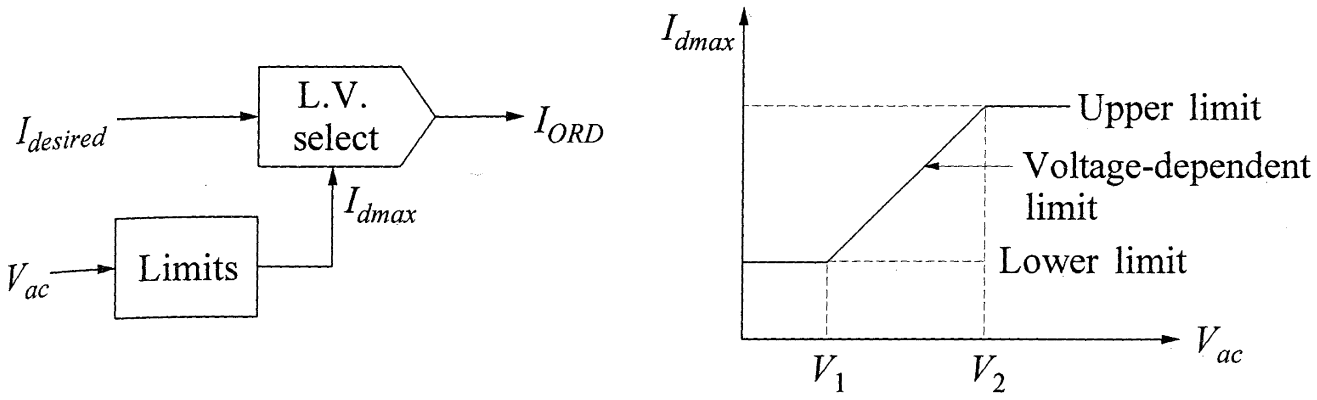

(a) Current limit as a function of alternating voltage

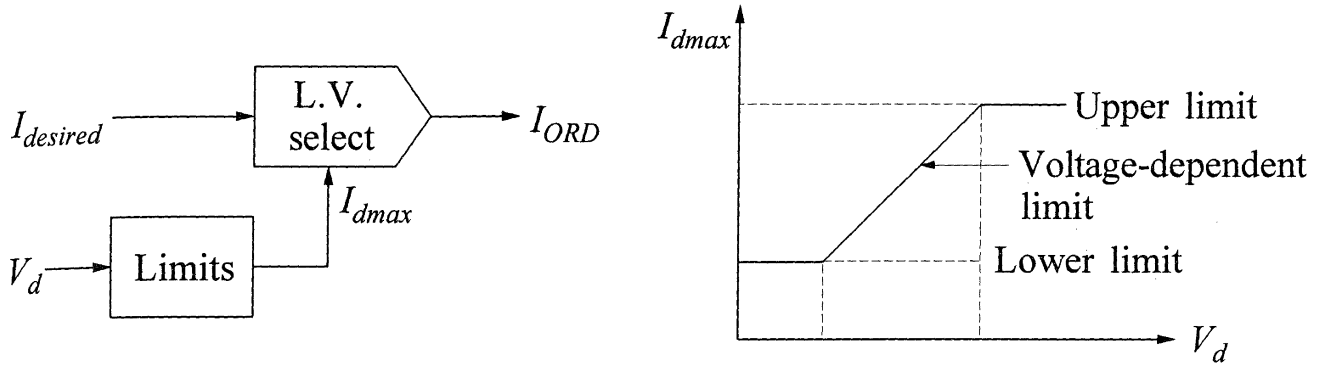

(b) Current limit as a function of direct voltage

Figure 10.35 Voltage-dependent current limits

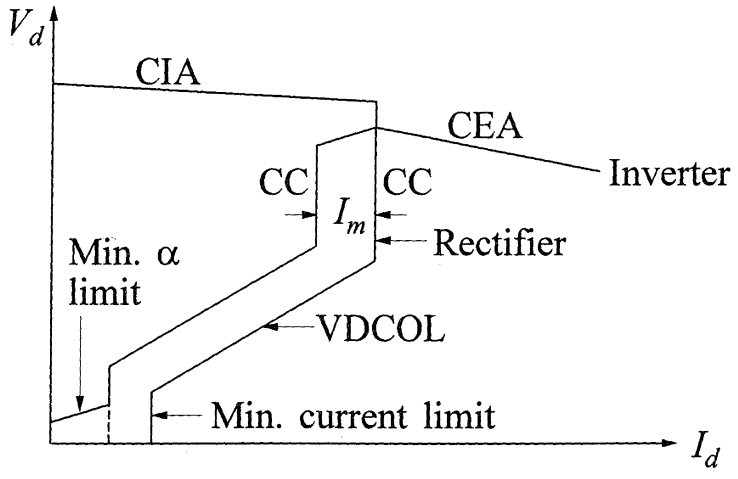

Figure 10.36 Steady-state *V-I* characteristic with VDCOL, minimum current limit and firing angle limits

voltage is passed through a first-order time lag element. Generally, this time lag is different for increasing and decreasing voltage conditions. While the voltage is going down, fast VDCOL action is required; hence, the time lag is small. If the same short time lag is used during voltage recovery, it may lead to oscillations and possibly instability. To prevent this, the larger time lag is used when the direct voltage is recovering.

Minimum firing angle limit

As shown in Figure 10.31, power transfer over the dc line can be controlled by manipulation of current order and current margin. These signals are transmitted to the converter stations through a telecommunication link. In the event that the communication fails or in case of a dc line fault, there is a possibility that the inverter station may switch to the rectification mode. This would result in a reversal of power flow. To prevent this from occurring, the inverter control is provided with a minimum-α limit, as indicated by the lowest portion of the inverter *V-I* characteristic in Figure 10.36. This restricts the firing angle of the inverter to a value greater than 90°, typically in the range of 95° to 110°. The rectifier is, however, allowed to operate in the inverter region to assist the system under certain fault conditions. As a consequence, the maximum limit imposed on the rectifier firing angle is typically between 90° and 140°.

Power control

Usually, an HVDC link is required to transmit a scheduled power. In such an application, the corresponding current order is determined as being equal to the power order (P_0) divided by the measured direct voltage:

$$I_{ord} = P_0/V_d$$

The current order so computed is used as input signal to the current control. However, high-speed constant power control may have an adverse effect on ac system stability. From the viewpoint of system stability, high-speed constant current control with a superimposed slow power control is preferable. This is acceptable since the dispatcher is not interested in a very high speed power control. Thus, from the stability viewpoint, the HVDC system control performs as a constant current control, but for the dispatcher it appears as constant power control.

Auxiliary controls for ac system

To enhance ac system performance, auxiliary signals derived from the ac system quantities may be used to control the converters. The control strategy could include modulation of either direct current or direct voltage, or both. In addition, special control measures may be used to assist recovery of dc systems from faults. These higher-level controls will be discussed in more detail later in this chapter.

Summary of basic control principles

The HVDC system is basically constant-current controlled for the following two important reasons:

- To limit overcurrent and minimize damage due to faults
- To prevent the system from running down due to fluctuations of the ac voltages

It is because of the high-speed constant current control characteristic that the HVDC system operation is very stable.

The following are the significant aspects of the basic control system:

(a) The rectifier is provided with a *current control* and an *α-limit control.* The minimum α reference is set at about 5° so that sufficient positive voltage across the valve exists at the time of firing, to ensure successful commutation. In the current control mode, a closed-loop regulator controls the firing angle and hence the dc voltage to maintain the direct current equal to the current order. Tap changer control of the converter transformer brings α within the range of 10° to 20°. A time delay is used to prevent unnecessary tap movements during transient excursions of α.

(b) The inverter is provided with a *constant extinction angle* (CEA) control and a *current control.* In the CEA control mode, γ is regulated to a value of about 15°. This value represents a trade-off between acceptable var consumption and a low risk of commutation failure. While CEA control is the norm, there are variations which include *voltage control* and *β control.* Tap changer control is used to bring the value of γ close to the desired range of 15° to 20°.

(c) Under normal conditions, the rectifier is on current control mode and the inverter is on CEA control mode. If there is a reduction in ac voltage at the rectifier end, the rectifier firing angle decreases until it hits the α_{min} limit. At this point, the rectifier switches to α_{min} control and the inverter will assume current control.

(d) To ensure satisfactory operation and equipment safety, several limits are recognized in establishing the current order: maximum current limit, minimum current limit, and voltage-dependent current limit.

(e) Higher-level controls may be used, in addition to the above basic controls, to improve ac/dc system interaction and enhance ac system performance.

All schemes used to date have used the above modes of operation for the rectifier and the inverter. However, there are some situations that may warrant serious

investigation of a control scheme in which the inverter is operated continuously in current control mode and the rectifier in α-minimum control mode. Enhanced performance into weak systems may be one case.

10.4.2 Control Implementation

In Section 10.4.1, we considered the basic principles of control of one pole. Figure 10.37 illustrates a general scheme for implementing the controls. In many cases there are two to four converter bridges per pole connected in series. Usually, two bridges with Y-Y and Y-Δ connected transformers are considered as one 12-pulse unit. Thus, the smallest unit to be controlled is a 6-pulse or a 12-pulse bridge unit.

The control hierarchy varies from one dc system to another, but the general concepts are common. Figure 10.38 illustrates the control hierarchy of a typical bipolar HVDC system. The control scheme is divided into four levels: bridge or converter unit control, pole control, master control and overall control.

The *bridge* or *converter unit control* determines the firing instants of the valves within a bridge and defines α_{min} and γ_{min} limits. This has the fastest response within the control hierarchy.

The *pole control* coordinates the control of bridges in a pole. The conversion of current order to a firing angle order, tap changer control, and certain protection sequences are handled by the pole control. This includes coordination of starting up, deblocking, and balancing of bridge controls.

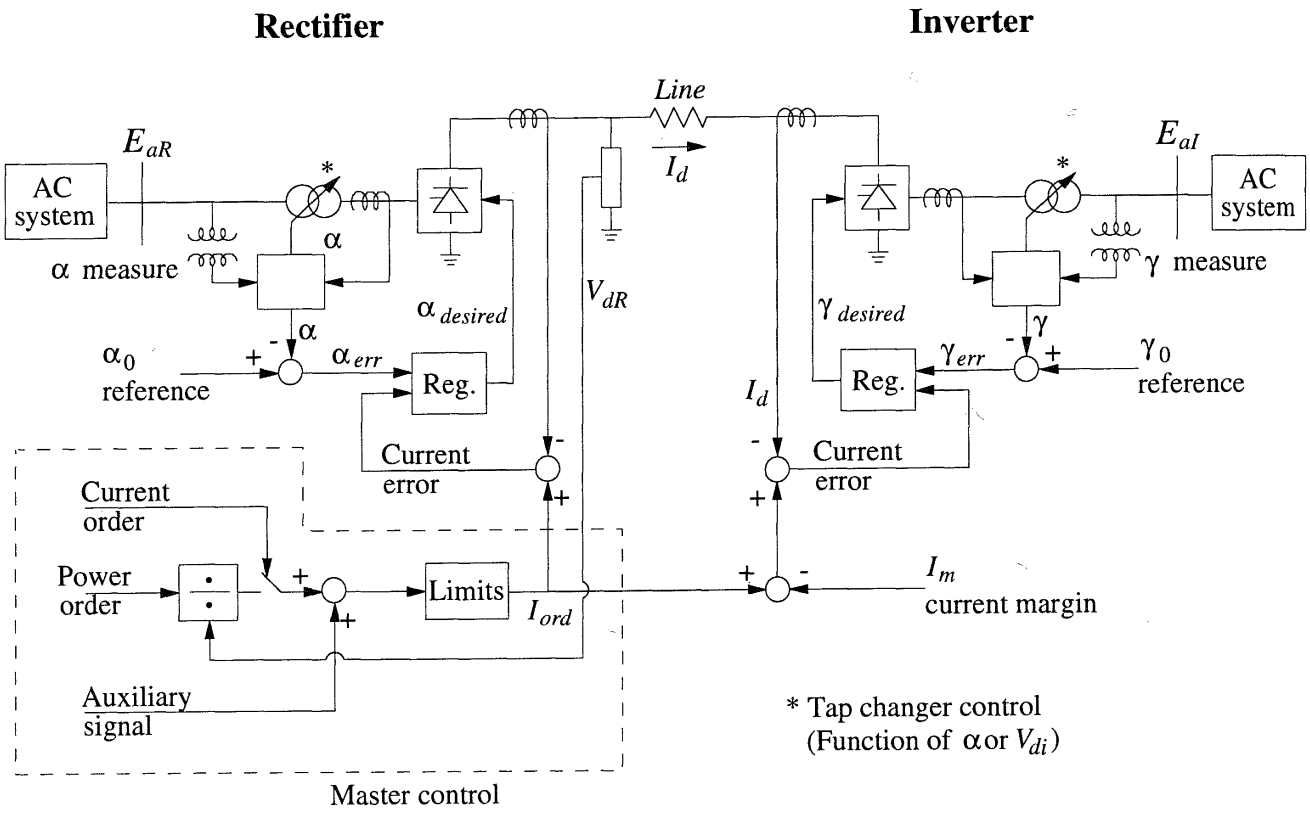

Figure 10.37 Basic control scheme

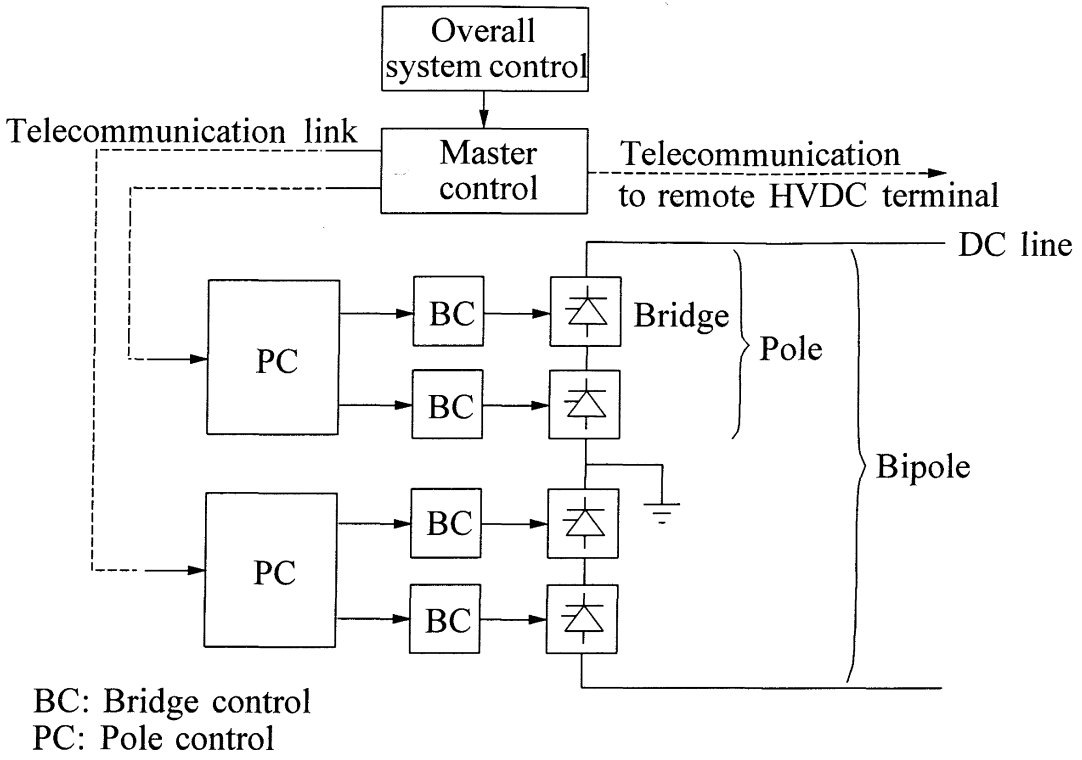

Figure 10.38 Hierarchy of different levels of HVDC system controls

The *master control* determines the current order and provides coordinated current order signals to all the poles. It interprets the broader demands for controlling the HVDC system by providing an interface between pole controls and the *overall system control*. This includes power-flow scheduling determined by the control centre and ac system stabilization.

The basic control functions are similar for most applications. However, higher-level control functions are determined by the specific performance objectives of individual systems. For reliable operation of the HVDC system, each pole should function as independently as possible. The control and protection functions should be segregated and implemented at the lowest possible level of hierarchy.

The control of HVDC systems clearly requires communication between terminals for proper operation. In the case of rapid changes in power level, high-speed communication is required to maintain consistent current settings at the two terminals. Change of power direction requires communication to transfer the current margin setting from one terminal to the other. The starting and stopping of the terminals require coordination of the operations at the two terminals. Communication is also required for transmittal of general status information needed by the operators. Protection may also require communication between the terminals for detection of some faults.

There are several alternative transmission media available for the telecommunications: direct wires via private lines or telephone networks, power-line carrier, microwave systems, and fibre optics. The choice of the telecommunication medium will depend on the amount of information to be transmitted and the required speed of response, degree of security, and noise immunity.

10.4.3 Converter Firing-Control Systems

The converter firing-control system establishes the firing instants for the converter valves so that the converter operates in the required mode of control: constant current (CC), constant ignition angle (CIA), or constant extinction angle (CEA).

Two basic types of controls have been used for the generation of converter firing pulses:

- Individual phase control (IPC)
- Equidistant pulse control (EPC)

The implementation of the above basic forms of converter firing control has evolved over the years. There are several different versions in existence depending on the manufacturer and the vintage of equipment. Their detailed description is beyond the scope of this book. The following descriptions illustrate the principles of operation of the two forms of converter firing-control systems.

Individual phase control system [11,12]

This system was widely used in the early HVDC installations. Its main feature is that the firing pulses are generated individually for each valve, determined by the zero crossing of its commutation voltage.

The commutation process in a three-phase bridge circuit was analyzed in Section 10.2. Referring to Figure 10.15 and Equation 10.7A, the commutation voltage is given by

$$\begin{aligned} e_{ba} &= e_b - e_a \\ &= \sqrt{3}E_m \sin\omega t = 2L_c \frac{di_3}{dt} \end{aligned}$$

As depicted in Figure 10.39, commutation begins when ωt equals the ignition angle (α) and ends when ωt equals the normal extinction angle ($\pi-\gamma$).

If $t=t_1$ at the beginning of commutation, and $t=t_2$ at the end of commutation, we may write

$$\int_{t_1}^{t_2} \sqrt{3}E_m \sin\omega t\, dt = 2L_c \int_0^{I_d} di_3$$

or

$$-\sqrt{3}\frac{E_m}{\omega}(\cos\omega t_2 - \cos\omega t_1) = 2L_c I_d$$

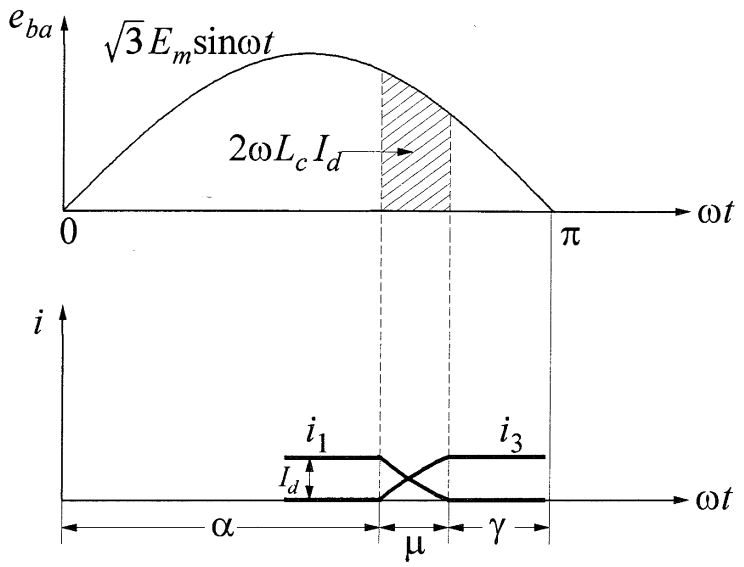

Figure 10.39 Commutation voltage and valve currents

or

$$-\sqrt{3}E_m[\cos(\pi-\gamma)-\cos\omega t_1] = 2\omega L_c I_d$$

Thus the control has to satisfy the condition that the voltage integral $2\omega L_c I_d$ is available between $\omega t=\omega t_1=\alpha$ and $\omega t=\omega t_2=\pi-\gamma$. The equation to be satisfied may be written as

$$-\sqrt{3}E_m\cos\omega t_1-\sqrt{3}E_m\cos\gamma+2X_c I_d = 0 \qquad (10.38)$$

CEA control with IPC:

In Equation 10.38, the direct current (I_d) and the commutating voltage vary with changes in operating conditions. The grid control, therefore, senses these two quantities to determine the instant of firing ($t=t_1$) so as to satisfy Equation 10.38. With extinction angle equal to a set value γ_c, and $X_c=\omega L_c$, we have

$$-\sqrt{3}E_m\cos\omega t_1-\sqrt{3}E_m\cos\gamma_c+2X_c I_d = 0 \qquad (10.39)$$

The required ignition time t_1 can be found from the solution of Equation 10.39. This is accomplished by using analog circuits in the early converter control applications. The control system consists of three units: the first unit giving a dc output proportional to the direct current I_d; the second giving an output proportional to $E_m\cos\gamma_c$; and the third giving an alternating voltage proportional to the commutating voltage but with a phase lag of 90° (i.e., $E_m\cos\omega t$).

The three outputs are added, and a firing pulse is generated when the sum passes through zero. Under steady-state conditions, such a system controls each valve with constant commutation margin, irrespective of load and voltage variations or unbalance.

Constant current control with IPC:

In this case, an additional signal V_{cc} is added to Equation 10.39 as follows:

$$-\sqrt{3}E_m\cos\omega t_1 - \sqrt{3}E_m\cos\gamma_c + 2X_cI_d + V_{cc} = 0 \tag{10.40}$$

where

$V_{cc} = K(I_o - I_d)$
I_o = current order
I_d = actual direct line current
K = gain of CC control

The same circuit may be used for both CEA and CC control operations [12]. The error $(I_o - I_d)$ is amplified only when I_d is less than I_o. When I_d is greater than I_o, the amplifier output is clamped to zero, and the converter operates on CEA control. When $(I_o - I_d) > 0$, it operates on constant-current control.

The converter characteristics for the full range of inverter and rectifier operation is shown in Figure 10.40. The realization of CIA control ($\alpha = \alpha_c$) is similar to that of CEA control.

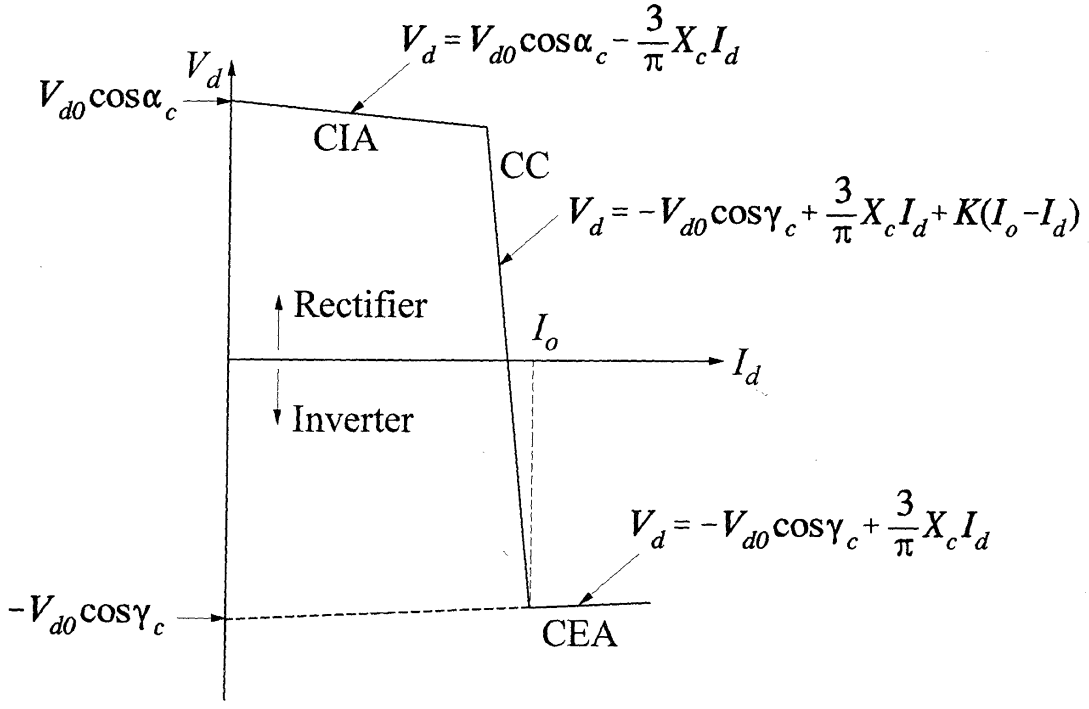

Figure 10.40 Converter characteristics with IPC

The IPC system has the advantage of being able to achieve the highest possible direct voltage under unsymmetrical or distorted supply waveforms since the firing instant for each valve is determined independently. However, the IPC system in effect has a voltage feedback, since the control signal is derived from the alternating line voltage. Any deviation from the ideal voltage waveforms will disturb the symmetry of the current waveforms. This will in turn cause additional waveform distortions, thus introducing non-characteristic harmonics (see Section 10.5). If the ac network to which the converter is connected is weak (i.e., has high impedance), the feedback effect may further distort the altering voltage and thereby lead to harmonic instability.

The harmonic instability problem can be reduced by altering the harmonic characteristics of the ac network (for example, by using additional filters) or adding filters in the control circuit. Alternatively, a firing control system independent of the ac system quantities may be used. This leads to the EPC system described next.

Equidistant pulse control system [10,13]

In this system, valves are ignited at equal time intervals, and the ignition angles of all valves are retarded or advanced equally so as to obtain the desired control mode. There is only indirect synchronization to the ac system voltage.

An EPC system using a phase-locked oscillator to generate the firing pulses was first suggested in reference 13. Since the late 1960s, all manufacturers of HVDC equipment have used this system for converter firing control.

Figure 10.41 shows an EPC-based constant-current control system. The basic components of the system are a voltage-controlled oscillator (VCO) and a ring counter. The VCO delivers pulses at a frequency directly proportional to the input control voltage. The train of pulses is fed to the ring counter, which has six or twelve stages (depending on the pulse number of the converter). Only one stage is on at any time, with the pulse train output of the VCO changing the on stage of the ring counter in cyclic manner. As each stage turns on, it produces a short output pulse once per

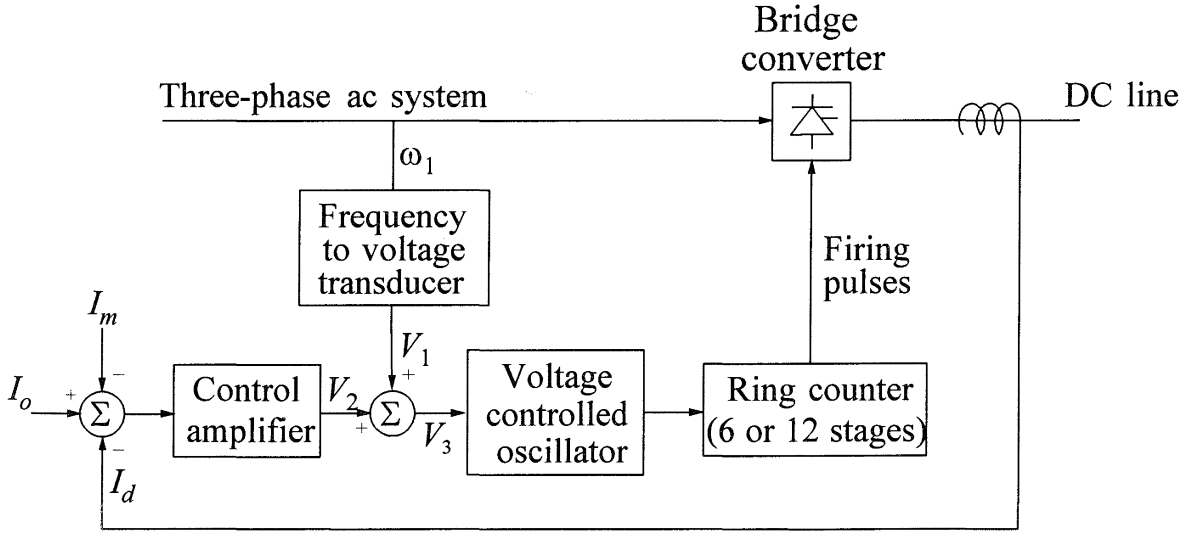

Figure 10.41 Current control system with equidistant pulse control

cycle. Over one full cycle, a complete set of 6 (or 12) output pulses is produced by the ring counter at equal intervals. These pulses are transferred by the firing-pulse generator to the appropriate valves of the converter bridge.

Under steady-state conditions, V_2 is zero and the voltage V_1 is proportional to the ac line frequency ω_1. This generates pulses at line frequency, and maintains a constant firing delay angle α. If there is a change in current order I_o, margin setting I_m, or line frequency ω_1, a change in V_3 occurs which in turn results in a change in the frequency of the firing pulses. A change in firing delay angle ($\Delta\alpha$) results from the *time integral* of the differences between line and firing pulse frequencies. It is apparent that this equidistant pulse control firing scheme is based on pulse frequency control.

An alternative equidistant pulse control firing scheme based on pulse phase control is proposed in reference 14. In this scheme, a step change in control signal causes the spacing of only one pulse to change; this results in a shift of phase only.

For CEA control, the basic circuits of Figure 10.41, illustrated for CC control, must be supplemented by additional circuitry. Since the extinction angle ($\gamma=\pi-\alpha-\mu$) cannot be controlled directly, either a predictive or a feedback control has to be used. In the scheme described in reference 10, a predictive method is used to ensure that adequate commutation voltage-time area (see Figure 10.39) is available at the instant of firing for successful commutation. The firing angle is based on calculation of the overlap angle (μ) from measured values of current and voltage. Reference 13 uses a feedback method to achieve this.

These schemes provide equal pulse spacing in the steady state. Symmetry is maintained relative to the most vulnerable control angle. For example, the smallest γ becomes the set angle in the presence of finite ac voltage unbalance.

The equidistant firing control results in a lower level of non-characteristic harmonics and stable control performance when used with weak ac systems. However, when the ac network asymmetry is large, it results in a lower direct voltage and power than the individual phase control.

Firing system

In modern converters, the valve firing and valve monitoring are provided through an *optical* interface. Light guides are used to carry the firing pulse to each thyristor. Each thyristor is provided with a special control unit that changes a light pulse to an electrical pulse to the gate input on the thyristor. Information about the condition of thyristors, required for protection and supervision of valves, is also transmitted by a light guide system from each thyristor.

At present many manufacturers are developing thyristors that are triggered directly by fibre optics.

10.4.4 Valve Blocking and Bypassing

Valve blocking (stopping) is achieved by interruption of positive pulses to the gates of all the valves in a bridge. However, this may result in overvoltages due to

current extinction. In some instances, blocking of the valves at the inverter can lead to continuous conduction through previously conducting phases placing the ac voltage on the dc line and direct current on the converter transformer.

It is, therefore, necessary to bypass the bridge when the valves are blocked. This is achieved by using a bypass valve and bypass switch, as shown in Figure 10.42.

The valve currents are commutated into the bypass valve and then the bypass switch is closed to relieve the bypass valve from carrying current continuously.

Bypass pair operation

In converters using thyristors, the use of a separate bypass valve per bridge has been discontinued. Instead, as shown in Figure 10.43, bypass is implemented by firing a valve to establish a series pair on the same phase as an already conducting valve. A bypass switch closes to relieve the valves during a sustained blocking.

The logic for bypass operation is made part of the converter control.

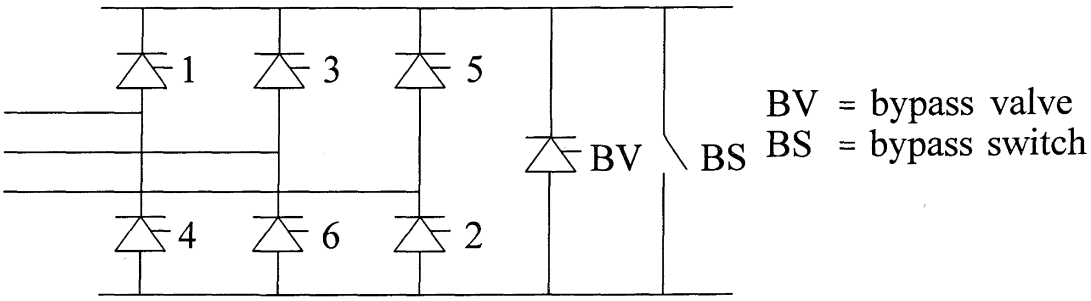

Figure 10.42

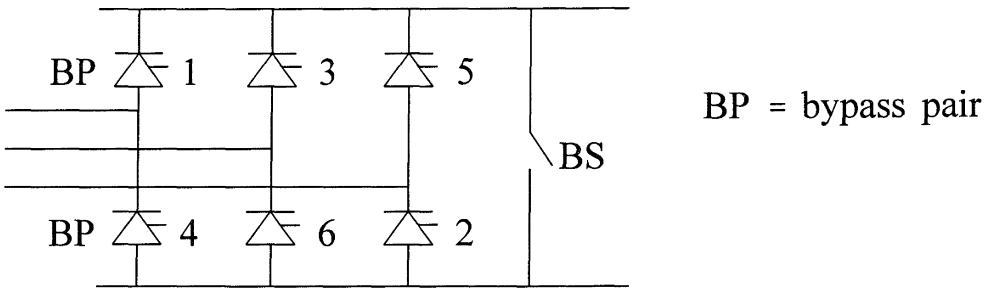

Figure 10.43

10.4.5 Starting, Stopping, and Power-Flow Reversal

The sequences that are used for starting and stopping HVDC systems vary depending on the manufacturer and equipment capability. The rate of rise of voltage, current, and power is tailored to the individual application. The following are typical steps and procedures involved [15].

Normal starting (deblocking) sequence

1. Either the inverter or the rectifier may start first. The converter that is started first establishes valve firing and conduction. Voltage is held low with the deblocking firing angle being in the range of 60° to 70°.

2. Following a communication delay, the other converter also establishes firing. A fairly low voltage is maintained with a firing angle of 60° to 70° and a starting current on the order of 0.2 to 0.3 pu (optimized to equipment or system conditions) is circulated.

3. After a successful start has been established, voltages are increased according to the relaxation rate on firing angle (α or β). The initial current order of 0.2 to 0.3 pu is maintained until the voltage has reached a setpoint of 40% to 80%. The current order is then released to the desired value.

4. When the current is established and can be maintained by the rectifier, the inverter goes into voltage/margin angle control mode.

The entire procedure can take as short a time as a fraction of a second or as long as several minutes, depending on the power order and limitations imposed by the ac system. The load may be increased exponentially or in small steps.

Normal stopping (blocking) sequence

Unlike in ac systems where a circuit-breaker is operated to isolate a line, the dc link is shut down gradually through controls. The blocking of a pole is achieved by reducing the voltage and current to zero as follows:

1. The current and voltage are ramped down within 100 to 300 ms. Then the rectifier is operated in or near the inverter region. This removes any stored energy from the dc system.

2 Bypass switches, if provided, are closed.

If one of two valve groups is to be blocked, it cannot involve reduction of current flow to zero. Therefore, the firing angle of the valve group is ramped to 90°, a bypass is formed with a bypass switch, and the valves are blocked. The ramp rate may be limited to avoid regulator mode changes.

Reversal of power flow

HVDC systems are inherently capable of power flow in either direction. Most schemes have full control features that permit bidirectional power flow.

Power reversal can be smoothly executed by following a prescribed series of ramps or it can be very fast with or without blocking of the firing of the valves. Control techniques for power reversal may include the following [15]:

1. Reduction of current to 0.1 to 0.5 pu via a step or ramp.

2. Decrease/increase of voltage via ramp or exponential function followed by a current ramp to reach the required level.

The basis for deciding the sequence to be followed is normally the ability of the ac system to survive the resulting disturbance and the need for power reversal within a specified time. Typically, fast power reversal times would be on the order of 20 to 30 ms, although ac system limitations, dc cable design constraints, or power dispatch conditions may increase it to several seconds. HVDC controls can meet this entire range of requirements.

10.4.6 Controls for Enhancement of AC System Performance

In a dc transmission system, the basic controlled quantity is the direct current, controlled by the action of the rectifier with the direct voltage maintained by the inverter. A dc link controlled in this manner buffers one ac system from disturbances on the other. However, it does not allow the flow of synchronizing power which assists in maintaining stability of the ac systems. The converters in effect appear to the ac systems as frequency-insensitive loads and this may contribute to negative damping of system swings. Further, the dc links may contribute to voltage collapse during swings by drawing excessive reactive power.

Supplementary controls are therefore often required to exploit the controllability of dc links for enhancing the ac system dynamic performance. There are a variety of such higher level controls used in practice. Their performance objectives vary depending on the characteristics of the associated ac systems. The following are the major reasons for using supplementary control of dc links:

- Improvement of damping of ac system electromechanical oscillations.
- Improvement of transient stability.
- Isolation of system disturbance.
- Frequency control of small isolated systems.
- Reactive power regulation and dynamic voltage support.

References 18 to 21 provide descriptions of supplementary controls used in a number of HVDC transmission systems for enhancement of ac system performance. The controls used tend to be unique to each system. To date, no attempt has been made to develop generalized control schemes applicable to all systems.

The supplementary controls use signals derived from the ac systems to modulate the dc quantities. The modulating signals can be frequency, voltage magnitude and angle, and line flows. The particular choice depends on the system characteristics and the desired results.

The principles of dc modulation schemes and details of their application for enhancement of ac system performance are discussed further in Chapter 17.

10.5 HARMONICS AND FILTERS

Converters generate harmonic voltages and currents on both ac and dc sides. In this section we will briefly describe the types of harmonics produced by the converters and the characteristics of filters used to minimize their adverse effects.

10.5.1 AC Side Harmonics

Figure 10.12 shows the wave shape of the alternating current under the "ideal" condition with no commutation overlap, ripple-free direct current, balanced purely sinusoidal commutating voltages, and equally-spaced converter firing pulses. The current may be expressed as a Fourier series.

For a 6-pulse bridge with Y-Y transformer connection, the Fourier series expansion for the alternating current is

$$i = \frac{2\sqrt{3}}{\pi} I_d \left(\sin\omega t - \frac{1}{5}\sin 5\omega t - \frac{1}{7}\sin 7\omega t + \frac{1}{11}\sin 11\omega t + \frac{1}{13}\sin 13\omega t - \cdots\right) \tag{10.41}$$

For a Δ-Y transformer connection, the current is

$$i = \frac{2\sqrt{3}}{\pi} I_d \left(\sin\omega t + \frac{1}{5}\sin 5\omega t + \frac{1}{7}\sin 7\omega t + \frac{1}{11}\sin 11\omega t + \frac{1}{13}\sin 13\omega t + \cdots\right) \tag{10.42}$$

The second harmonic and all even harmonics are absent in the above because there are two current pulses of equal size and opposite polarity per cycle. Since the current pulse width is one-third of a cycle, third and all triple-n harmonics are also absent. The remaining harmonics are on the order of $6n\pm1$, where n is any positive integer.

In a 12-pulse bridge, there are two 6-pulse bridges with two transformers, one with Y-Y connection and the other with Y-Δ connection (see Figure 10.23). The harmonics of odd values of n cancel out. Hence,

$$i = \frac{2\sqrt{3}}{\pi} 2I_d \left(\sin\omega t + \frac{1}{11}\sin 11\omega t + \frac{1}{13}\sin 13\omega t + \frac{1}{23}\sin 23\omega t + \frac{1}{25}\sin 25\omega t + \cdots\right) \quad (10.43)$$

The remaining harmonics which have the order $12n\pm1$ (i.e., 11^{th}, 13^{th}, 23^{th}, 25^{th}, etc.) flow into the ac system. Their magnitudes decrease with increasing order; an h^{th} order harmonic has magnitude $1/h$ times the fundamental.

When the commutating reactance is considered, the overlap angle during commutation rounds off the square edges of the current waves, and this reduces the magnitude of harmonic components. The reduction factor of the harmonic components is given by [3]

$$\frac{i_h}{i_{ho}} = \frac{\sqrt{H^2+K^2-2HK\cos(2\alpha+\mu)}}{\cos\alpha-\cos(\alpha+\mu)} \quad (10.44)$$

where

i_h = harmonic current
i_{h0} = harmonic current with no overlap
h = harmonic order
$H = [\sin(h+1)\mu/2]/(h+1)$
$K = [\sin(h-1)\mu/2]/(h-1)$

It is apparent that the harmonics produced on the ac system are a function of the operating conditions. As μ increases, the harmonic component decreases, with the reduction being more pronounced at higher harmonics. Under typical full load conditions, μ is about 20° and α is about 15°; the 11^{th} and 13^{th} harmonics are about 30 to 40% of those shown in the basic equations, which neglected overlap. During faults, however, α reaches nearly 90°, the overlap angle is reduced, and for a given line current the ac harmonics will increase.

The above discussions consider only balanced conditions. The harmonics produced under such ideal conditions are referred to as "characteristic harmonics."

Various unbalances, such as non-equally spaced firing pulses, bus voltage unbalances and unbalances in the commutating reactance between phases will produce additional harmonics which are referred to as "non-characteristic harmonics." Transformer excitation current also contributes to these harmonics.

The converter manufacturers attempt to minimize these harmonics in the design of the terminals. With modern day equal-spaced firing, the biggest sources of non-characteristic harmonics are bus voltage unbalance, transformer impedance unbalance and the transformer excitation current. Unbalances in ac system voltages depend on the operating conditions and are determined by the design and operating practices of the system. Unbalances in the reactances between the phases of the transformer are

usually less than 1% of the phase values. With bus voltage unbalance of less than 1% and normal excitation current levels, non-characteristic harmonics are not significant, unless a resonant condition exists at a particular harmonic frequency.

AC harmonic filters

Harmonics have to be filtered out sufficiently at the terminal so that the harmonics entering the ac system are small and distortion of the ac voltage caused by the harmonic currents is within limits. Harmonics, if not reduced by filters, can produce undesirable effects such as telephone interference, higher losses and heating in ac equipment (machines, capacitors, etc.), or resonance problems which could produce overvoltages and/or overcurrents.

The penetration of the harmonics into the ac system and resonance conditions depends on the harmonic impedance of the ac network, which is difficult to determine. It is constantly varying as the circuits are being added or switched out and the system operating conditions are varying. In filter design, quite elaborate studies are undertaken that consider various factors including possible system resonance conditions.

A typical filter system for a 12-pulse converter terminal is shown in Figure 10.44. The filter impedance is minimum at the 11^{th} and 13^{th} harmonics resulting from the two series-resonant tuned branches. The high pass filter maintains a low impedance for higher harmonic frequencies.

Part of the capacitors required for reactive power compensation is provided by filters. The additional cost of converting the required reactive power capacitors to filters is not very high. Of the 50% reactive power compensation required, about 30% would be in filter form divided among the eleventh, thirteenth, and high pass filters.

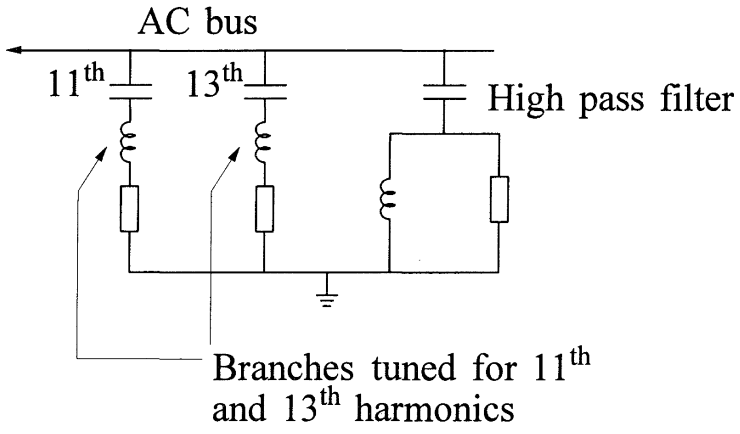

Figure 10.44 Typical filter system configuration

10.5.2 DC Side Harmonics

An ideal 6-pulse bridge converter, with repetitive switching every 60°, produces a direct voltage waveform as shown in Figure 10.19. Fourier analysis of the voltage waveform shows that it contains harmonics of order $6n$ (i.e., 6^{th}, 12^{th}, 18^{th}, etc.). The magnitude of the effective harmonic voltage varies widely over the operating range of α; operation at α near 90° produces higher levels of harmonics than at smaller values of α. The overlap angle μ also has a significant impact on the magnitude of the harmonics.

In a bipole system consisting of two 6-pulse bridges (one in each pole), the transformers would be connected Y-Y and Δ-Y because the 30° phase shift produces cancellation of low order harmonic on the ac bus. This would also have a beneficial effect on the dc side. The 6^{th}, 18^{th}, 30^{th}, ... harmonics are out-of-phase in the two bridges, while the 12^{th}, 24^{th}, 36^{th}, ... harmonics are in phase. The out-of-phase harmonic voltages produce ground return mode currents in the dc line, whereas the in-phase components of harmonic voltages produce line-to-line mode currents.

In the case of a 12-pulse bridge, the out-of-phase components of harmonic voltages will cancel within a 12-pulse bridge; only the in-phase components will produce harmonic currents in the line. For a balanced condition, the significant harmonics in the voltage produced by a dc terminal are therefore of order 12 and its integral multiples.

The non-characteristic harmonics due to unbalances would be small in a well designed system. The dc side harmonics are reduced by the smoothing reactor and filters. Most of the harmonic voltages are dropped across the smoothing reactor. The dc filters are designed to shunt a major portion of the direct harmonic currents so that harmonic currents flowing into the dc line are within the permissible limits.

The smoothing reactor and the rest of the dc system beyond the reactor (dc filters, dc line and remote terminals) act as voltage dividers for the harmonic voltages. In general, a larger value of smoothing reactor will require less dc filtering. However, the smoothing reactor size is influenced by other considerations associated with converter terminal design.

The following are some of the considerations influencing the selection of the smoothing reactor size:

1. The size of the smoothing reactor has a dominant effect on the ripple in the bridge current; the ripple current is less for higher values of the reactor. As discussed in Section 10.4.1, the ripple current determines the minimum current operating point for the terminal.

2. The smoothing reactor, filters, and dc lines combine to produce an impedance to the dc bridge which can be resonant at some generated voltage harmonics. Generally, this is not a problem for the higher harmonics (12^{th}, 24^{th}, ...), but the non-characteristic harmonics generated at low frequency (2^{nd}, 4^{th}, 6^{th}, ...) can produce high harmonic currents if the effective impedance is low at these

frequencies. The high harmonic currents at low frequencies can cause problems with control circuitry and interference with communication circuits. Therefore, the smoothing reactor is selected to avoid a low impedance at 2nd or 4th harmonic frequency. In addition, low frequency harmonic resonance must be avoided for other reasons. Repeated commutation failures on an inverter may introduce fundamental frequency pulses on the dc line (see Section 10.3.2). If the input impedance affecting the bridge were near resonance at the fundamental frequency, high transient voltages would occur.

3. The smoothing reactor size has an influence on the likelihood of commutation failures during a dip in ac voltages and on the likelihood of consequent commutation failure.

4. A higher smoothing reactor limits the fault current near the rectifier.

10.6 INFLUENCE OF AC SYSTEM STRENGTH ON AC/DC SYSTEM INTERACTION

The nature of ac/dc system interactions and the associated problems are very much dependent on the strength of the ac system relative to the capacity of the dc link. The ac system can be considered as "weak" from two aspects: (a) ac system impedance may be high, (b) ac system mechanical inertia may be low [18]. In this section we will discuss problems associated with dc systems connected to weak ac systems and methods of dealing with such problems.

10.6.1 Short-Circuit Ratio

Since the ac system strength has a very significant impact in the ac/dc system interactions, it is useful to have a simple means of measuring and comparing relative strengths of ac systems. The *short-circuit ratio* (SCR) has evolved as such a measure. It is defined as

$$\text{SCR} = \frac{\text{short-circuit MVA of ac system}}{\text{dc converter MW rating}}$$

The short-circuit MVA is given by

$$\text{SC MVA} = \frac{E_{ac}^2}{Z_{th}}$$

where E_{ac} is the commutation bus voltage at rated dc power and Z_{th} is the Thevenin

equivalent impedance of the ac system.

The basic SCR gives the inherent strength of the ac system. From the viewpoint of the HVDC system performance, it is more meaningful to consider the *effective short-circuit ratio* (ESCR), which includes the effects of ac side equipment associated with the dc link: filters, shunt capacitors, synchronous condensers, etc.

HVDC controls play an important role in most ac/dc system interaction phenomena, and must be taken into consideration in assessing acceptable levels of ac system strength. Traditionally, the ac system strength has been classified as follows [16]:

- High, if ESCR is greater than 5;
- Moderate, if ESCR is between 3 and 5; and
- Low, if ESCR is less than 3

With refinements in dc and ac system controls, these classifications change. Reference 18 recommends the following classification:

- High, if ESCR is greater than 3;
- Low, if ESCR is between 2 and 3; and
- Very low, if ESCR is less than 2.

The above classification of ac system strength provides a means for preliminary assessment of potential ac/dc interaction problems. Detailed studies are, however, necessary for proper evaluation of the problems. In addition to the short-circuit ratio, the phase angle of the Thevenin equivalent impedance Z_{th} has an impact on the ac/dc system interaction. It is termed the "damping angle" and has an impact on the dc system control stability. Local resistive loads, while not having a significant effect on ESCR, improve damping of the system. Typical values of the damping angle are in the range of 75° to 85°.

10.6.2 Reactive Power and AC System Strength

From Equations 10.12 and 10.25, we have

$$\cos\phi \approx \cos\alpha - \frac{I_d}{V_{d0}}\frac{3}{\pi}X_c$$

Therefore, each converter consumes reactive power which increases with increased power. With normally accepted rectifier ignition delay angle (α) and inverter

extinction advance angle (γ) of 15° to 18° and commutating reactance (X_c) of 15%, a converter consumes 50 to 60% reactive power (i.e., if P_{dc}=1.0 pu, Q absorbed by each converter is 0.5 to 0.6 pu). Generally, this has to be provided at the converter site to prevent large reactive power flow through ac lines. Part of the reactive power required is provided by the capacitors associated with the ac filter banks.

The least expensive way to provide the required reactive power is to use shunt capacitor banks. Since the reactive power varies with the dc power transmitted, capacitors must be provided in appropriate sizes of switchable banks, so that steady-state ac voltage is held within an acceptable range (usually ±5%) at all load levels. This is also influenced by the strength of the ac system. The stronger the ac system, the larger the switchable bank size can be for an acceptable voltage change.

Generators, if present near the dc terminal, can be very helpful in handling some of the reactive power demands and in maintaining steady-state voltage within an acceptable range. For weak ac systems, it may be necessary to provide reactive compensation in the form of *static var compensators* (SVCs) or synchronous condensers.

10.6.3 Problems with Low ESCR Systems [16-18]

The following are the problems associated with the operation of a dc system when connected to a weak ac system:

- High dynamic overvoltages,
- Voltage instability,
- Harmonic resonance, and
- Objectionable voltage flicker.

Dynamic overvoltage

When there is an interruption to the dc power transfer, the reactive power absorption of the HVDC converters drops to zero. With a low ESCR system, the resulting increase in alternating voltage due to shunt capacitors and harmonic filters could be excessive. This will require a high insulation level of terminal equipment, thus imposing an economic penalty. It may also cause damage of local customer equipment. Special schemes may be necessary to protect the thyristors in case of restart delays [17].

Voltage stability [16]

With dc systems connected to weak ac systems, particularly on the inverter side, the alternating as well as direct voltages are very sensitive to changes in loading.

An increase in direct current is accompanied by a fall of alternating voltage. Consequently, the actual increase in power may be small or negligible. Control of voltage and recovery from disturbances become difficult. The dc system response may even contribute to collapse of the ac system. The sensitivities increase with large amounts of shunt capacitors.

In such a system, the dc system controls may contribute to voltage instability by responding to a reduction in alternating voltage as follows:

- Power control increases direct current to restore power.
- Inverter γ may increase to maintain volt-second commutation margin.
- Inverter draws more VARs; with reduced voltage, shunt capacitors, however, produce fewer VARs.
- The alternating voltage is reduced, further aggravating the situation.

The process thus leads to progressive fall of voltage.

Harmonic resonance

Most of the problems of harmonic resonance are due to parallel resonance between ac capacitors, filters, and the ac system at lower harmonics.

Capacitors tend to lower the natural resonant frequencies of the ac system, while inductive elements (machines and lines) tend to increase the frequencies. If large numbers of capacitors are added, the natural frequency seen by the commutation bus may drop to 4^{th}, 3^{rd} or even 2^{nd} harmonic. If a resonance at one of these frequencies occurs, there can be a high impedance parallel resonance between the inductive elements and capacitive elements on the commutation bus. A low-impedance series resonance condition could arise in remote points in the system. Harmonic voltages from remote points would tend to be amplified. The avoidance of low-order harmonic resonance is extremely important to reduce transient overvoltages.

Voltage flicker

Another characteristic of a weak ac system is that switching of shunt capacitors and reactors causes unacceptably large voltage changes in the vicinity of compensation equipment. The transient voltage flicker due to frequently switched reactive devices increases with higher levels of dc power transfer.

10.6.4 Solutions to Problems Associated with Weak Systems

The traditional approach to the solution of weak system ac/dc interaction problems is to use synchronous condensers or SVCs. In addition, HVDC controls

which switch to current control from power control and reduce direct current for low alternating voltage (for example, VDCOL) will help the situation.

The use of synchronous condensers also reduces the effective system impedance and hence shifts the parallel resonance frequency to higher frequencies at which the system damping is usually better. With 12-pulse bridge circuits, there are no large filters below 11^{th} harmonic; the possibility of excitation of parallel resonance at lower harmonics is therefore low.

An alternative solution to the reactive power and voltage problem is to control the dc converter itself so that the reactive power is modulated in response to voltage variations in a manner similar to an SVC. The shunt capacitors and filters provide the required reactive power; the converter firing angle control stabilizes the ac voltage. Artificial or forced commutation, discussed in Section 10.6.6, provides considerably more freedom in controlling reactive power.

Reference 17 describes five dc links (all back-to-back) connected to weak ac systems, and special techniques used to achieve their satisfactory performance.

10.6.5 Effective Inertia Constant

The ability of the ac system to maintain the required voltage and frequency depends on the rotational inertia of the ac system. For satisfactory performance, the ac system should have a minimum inertia relative to the size of the dc links. A measure of the relative rotational inertia is the effective dc inertia constant, defined as follows [18]:

$$H_{dc} = \frac{\text{total rotational inertia of ac system, MW·s}}{\text{MW rating of dc link}}$$

An effective inertia constant, H_{dc}, of at least 2.0 to 3.0 s is required for satisfactory operation.

For ac systems with very low or no generation, synchronous condensers have to be used to increase the inertia and assist in satisfactory operation of line commutated inverters.

10.6.6 Forced Commutation

The converter bridge circuits we have discussed so far rely on the natural voltage of the ac system for commutation. Such a commutation is known as "natural commutation," and requires the ignition angle (α) to be in the range of 0° to 180° (2° to 165° in practice for reliable turn-on and turn-off of the valves) for successful commutation. As a consequence, the converter absorbs reactive power from the ac system, while operating as a rectifier as well as an inverter.

If our objective is to have the converters supply reactive power to the ac system when so desired, we need to be able to force commutation at any desired point on the ac cycle. This can be achieved by superimposing harmonics or by use of

special capacitor circuits to modify the voltages across the valves appropriately in relation to ac system voltages. Such a commutation is called "forced commutation." A system using this form of commutation will also allow feeding into a system without any generation.

A converter bridge circuit with a forced commutation scheme is shown in Figure 10.45 [3,5]. Forced commutation is initiated at the desired times by firing the auxiliary valves (A1 to A6) with the associated capacitors pre-charged. Such capacitive commutations, however, cause considerable stress on the valves and other converter equipment.

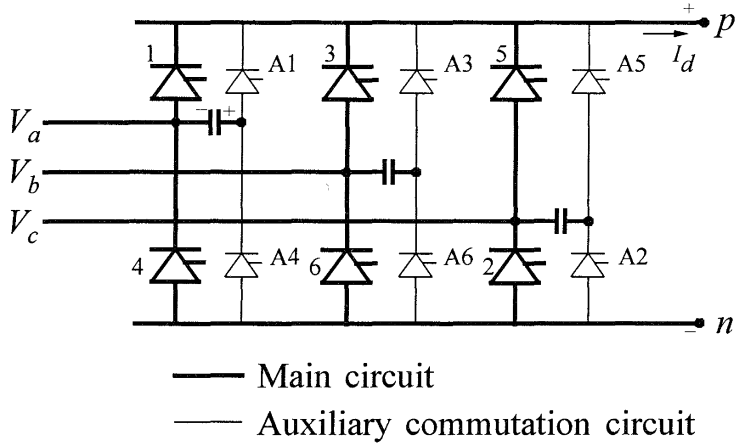

Figure 10.45 Bridge circuit with forced commutation

While converter circuits with forced commutation are feasible, they are very expensive. To date they have not found application in commercial HVDC converters.

Self-commutated voltage sourced inverters using gate turn-off (GTO) thyristors have been used in industrial applications, for example, variable speed drives, uninterruptible power supplies, and battery systems. The voltage and current ratings of these devices are increasing. It is likely that their application for HVDC transmission will become economically practical in the future.

10.7 RESPONSES TO DC AND AC SYSTEM FAULTS

The operation of HVDC transmission is affected by faults on the dc line, converters, or the ac system. The impact of the fault is reflected through the action of converter controls. In ac systems, relays and circuit-breakers are used to detect and remove faults. In contrast, most faults associated with dc systems either are self-clearing or are cleared through action of converter controls. Only in some cases is it necessary to take a bridge or an entire pole out of service. The converter controls thus play a vital role in the satisfactory response of HVDC systems to faults on the dc as well as the ac systems.

10.7.1 DC Line Faults

Faults on dc lines are almost always pole-to-ground faults. A pole-to-pole fault is uncommon since it requires considerable physical damage to bring conductors of two poles together. Lightning never causes a bipolar fault [7].

A pole-to-ground fault blocks power transfer on that pole; the remaining pole is virtually unaffected. As discussed below, the impact of a dc line fault on the connected ac systems is not as disruptive as that of ac faults.

Response of normal control action [2]

A short-circuit momentarily causes the rectifier current to increase (since the rectifier is feeding a low impedance fault rather than the high back voltage of the inverter) and the inverter current to decrease.

The current control of the rectifier acts to reduce the direct voltage and bring back the current to its normal set value (I_{ord}). At the inverter, the current becomes less than its current controller reference setting (I_{ord}-I_m). Consequently, the inverter mode of operation changes from CEA control to CC control. This causes the inverter voltage to run down to zero and then reverse polarity as shown by curve 2 of Figure 10.46. The voltages are equal to the RI drop in the line from each converter to the fault. The rectifier current is I_{ord} and inverter current is I_{ord}-I_m in the opposite direction. The steady-state fault current is thus equal to the current margin I_m, which is only about 15% of the rated current.

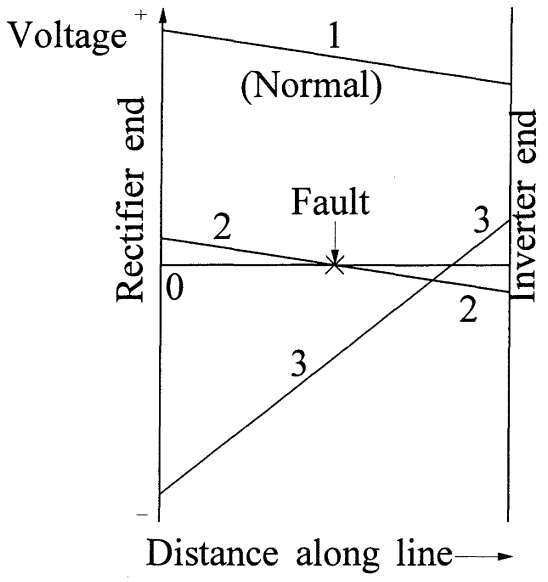

Figure 10.46 Voltage profile of a dc line:
1. Under normal operation
2. With dc line fault and normal control
3. With fast-acting line protection

Fast-acting line protection [7]

The normal control action of the converters, while limiting the fault current to I_m, does not extinguish the fault arc. Therefore, additional control is used to reduce the fault current and recovery voltage across the fault path to zero.

The fault is detected by a collapse in dc voltage usually at the rectifier and by a decrease in the current at the inverter. Both magnitude of voltage drop and rate of change of voltage may be used to detect the fault. Faults on the ac system beyond the dc link do not produce such rapid voltage changes.

To clear the fault, the inverter is kept in inversion and the rectifier is also driven to inversion. To establish terminal voltages of correct polarity for fault clearing, angle β of the inverter is given a maximum limit of about 80° (which allows the inverter voltage to run down to low value but not to reverse) and the rectifier ignition delay angle α is shifted considerably beyond 90°, to about 140°. The resulting voltage profile is as indicated by curve 3 in Figure 10.46. The current in the pole attempts to reverse direction. However, the current in the rectifier cannot reverse because of the unidirectional current characteristic of the valves. Therefore, the current is reduced to zero rapidly (in about 10 ms). This fault clearing process is called "forced retard."

DC overhead lines are restarted after allowing for de-ionization of the air surrounding the arc (60 to 200 ms). If the fault is temporary and the restart is successful, the voltage and current are ramped up. Typically, the total time for fault clearing and return to rated power transfer is on the order of 200 to 300 ms. The recovery time is higher for dc links connected to weak ac systems.

Automatic restarts are not attempted for wholly cable systems because cable faults are nearly always permanent faults.

10.7.2 Converter Faults

Most dc power circuit faults in the converter station will require either the valve group or the pole to be shut down.

A valve group fault, unless it is of a minor nature, will require the entire pole to cease transmission of power. Usually a very fast current reduction to zero is ordered. Coincidentally, the firing angle at the rectifier is shifted to at least 90° and possibly well into the inverter region. The current in the pole can be brought to zero in less than 30 ms.

An isolation sequence will follow which may take several seconds to execute, depending on the type of valve group isolators used. Then the remaining valve groups in the pole may be restarted in the normal manner.

10.7.3 AC System Faults

For ac system transient disturbances, the dc system's response is generally very much faster than that of the ac system. The dc system either rides through the disturbance with temporary reduction of power or shuts down until the ac system

recovers sufficiently to allow restarting and restoration of power. Commutation failures and recovery from ac system faults represent important aspects of dc system operation.

Rectifier side ac system faults

For remote three-phase faults, the rectifier commutation voltage drops slightly. This results in a reduction of rectifier direct voltage and hence the current. The current regulator decreases α to restore current by increasing voltage. If α hits the α_{min} limit, the rectifier switches to CIA mode of control. This transfers current control to the inverter whose current order is less than that of the rectifier by an amount equal to the current margin (I_m). If the low voltage persists, the tap changers will operate to restore the direct voltage and current to normal. Depending on how low the voltage drops, the VDCOL may regulate current and power transfers. For close-in three-phase faults, the rectifier commutation voltage drops significantly. The dc system shuts down under VDCOL control until the fault is cleared.

In theory, dc power may be transferred at very low rectifier voltages. This would require the inverter to assume current control by lowering its voltage and greatly increasing β. The resulting increased consumption of reactive power may be more detrimental to the ac system performance than briefly shutting down the dc system.

Remote single-phase and phase-to-phase faults do not usually result in shutting down of the dc link. The average of the alternating voltages is higher than that for three-phase faults. If the resulting direct voltage is sufficiently high, the dc system is likely to ride through the disturbance without any noticeable effect. If, on the other hand, the reduction in direct voltage is significant, the response is similar to that for remote three-phase faults.

For close-in unbalanced faults, the harmonic ripple in the direct voltage may be higher than normal. This may produce ripples in the direct current with a large second harmonic component. The line reactors and filters, designed for smoothing out normal characteristic harmonics, are not effective in reducing the second harmonics. The high ripple current could result in current extinction. Depending on the type of valve-firing system used, this may require blocking of the dc link [7].

Inverter side ac system faults

For remote three-phase faults resulting in small voltage dips at the inverter, an increase in direct current occurs. The rectifier CC and the inverter CEA (or constant voltage) controls respond to the changes. Tap changes will occur to restore converter firing angle and direct voltage, if the low alternating voltage persists.

If the voltage dip is significant, the reduction in commutating voltages may lead to temporary commutation failure at the inverter, prior to any corrective control action. With inverter operation at a γ of 18°, it is likely that a voltage reduction by 10% to 15% will cause commutation failure. It takes about 1 or 2 cycles to clear the commutation failure. Following this, some power may be transmitted with the rectifier

direct voltage reduced to match the reduction in inverter direct voltage. The resulting increase in reactive power may necessitate reduction of direct current. The VDCOL function (see Section 10.4.1) normally provided by the dc control system will cause this reduction of direct current. During extremely low voltage conditions, repeated commutation failures cannot be avoided. Therefore, it may be necessary to block and bypass the valves until the ac voltage recovers.

Unbalanced faults (both remote and close-in) may lead to commutation failure, partly due to phase shifts in the timing of the phase voltage crossings. For a severe contingency, it may be necessary to block and then restart the inverter.

When the fault has cleared, the allowable rate of restoration is dependent on the strength of the ac system. The controls are adjusted to provide the desired rate of power buildup. The performance of the overall power system following any system disturbance depends largely on the ac/dc system interaction as discussed below. It is also influenced by the subtle design features and response adjustments associated with the converter controls. These tend to vary with manufacturers. Special control strategies may be helpful in specific cases.

Recovery from ac system faults [18]

The post-fault system performance for ac system faults is far more sensitive to system parameters than for dc system faults. Recovery after an ac system fault is easier and can be more rapid with a strong ac system. Weak ac systems may have difficulty providing sufficient reactive power at the rate required for fast dc system restoration. Such systems also exhibit high temporary overvoltages and severe voltage distortion due to harmonics caused by inrushing magnetizing currents. These may cause subsequent commutation failures. Consequently the rate of recovery has to be slow.

The time for the dc system to recover to 90% of its pre-fault power is typically in the range of 100 ms to 500 ms, depending on the dc and ac system characteristics and the control strategy used. The dc system characteristics which influence the allowable rate of recovery are the line inductance and capacitance (particularly for cables), size of dc reactor, resonant harmonic frequencies of the line, converter transformer and filter characteristics. The significant ac system characteristics are ESCR, impedance at low order (2^{nd} to 4^{th}) harmonics, damping characteristics of loads near the dc system, system inertia, and method of voltage control near the converter bus.

Control strategies that assist in satisfactory dc system recovery (without post-fault commutation failures) include delayed or slow ramp recovery, and at reduced current level during recovery.

The VDCOL function can play a significant role in determining the recovery from faults. It limits the current order as a function of either the direct voltage or the alternating voltage. Consequently, reactive power demand is reduced during periods of depressed voltage. This helps prevent further deterioration of ac system voltage. Following fault clearing, the current order limit imposed by the VDCOL may be removed after a delay and gradually increased at a desired ramping rate.

From the viewpoint of ac system stability and minimization of dc power interruption, too slow a recovery is undesirable. The control strategies must therefore be tailored to meet specific needs of an application so as to maximize the recovery rate without compromising secure recovery of the dc system. Such strategies should be based on a detailed study of the individual system.

Special measures to assist recovery

Special measures may be used to assist HVDC system recovery from disturbances and to protect the valves. These measures act on either the firing angle directly or the current order. They depend on the requirements of a specific installation. The following are examples of such measures:

- Circuits that increase α_{min} from approximately 5° to over 30° during ac undervoltage conditions.
- Circuits in the inverter which transiently increase γ should γ slip below the γ_{min} limit. Then γ is increased on all succeeding firings for a prescribed period of time.
- Circuits that advance the firing angle limits by about 10° during start-up of the second valve group in a pole to prevent commutation failures.
- Circuits that increase β immediately following commutation failure so that the next valve is fired early to aid the recovery and to lessen the likelihood of subsequent commutation failure. Typically, β might be moved to 40°, 60°, and 70° on successive commutation failures. Should commutation failure cease, β would gradually retreat to its original value over a few hundred milliseconds. However, if it does not cease, a temporary bypass is usually ordered.

10.8 MULTITERMINAL HVDC SYSTEMS

In the previous sections, we considered the performance and application of point-to-point dc links, i.e., two-terminal dc systems. Successful application of such systems worldwide has led power system planners to consider the use of dc systems with more than two terminals. It is increasingly being realized that multiterminal dc (MTDC) systems may be more attractive in many cases to fully exploit the economic and technical advantages of HVDC technology.

The first MTDC system designed for continuous operation is the Sardinia-Corsica-Italy scheme. This is an expansion of the Sardinia-Italy two-terminal dc system built in 1967; a third terminal tap was added at Corsica in 1991. The two-terminal dc system between Des Cantons in Quebec and Comerford in New Hampshire built in 1986 is being extended to a three-terminal and then possibly to a five-terminal scheme [22]. Similarly, other MTDC systems are likely to evolve from the expansion of existing two-terminal schemes.

In this section, we will describe alternative MTDC system configurations and basic principles of controlling such systems. References 8, 23, 24, and 25 are recommended for further reading.

10.8.1 MTDC Network Configurations

There are two possible connection schemes for MTDC systems:

- Constant voltage parallel scheme
- Constant current series scheme

In the parallel scheme, the converters are connected in parallel and operate at a common voltage. The connections can be either radial or mesh. Figures 10.47 and 10.48 depict the two types of connections.

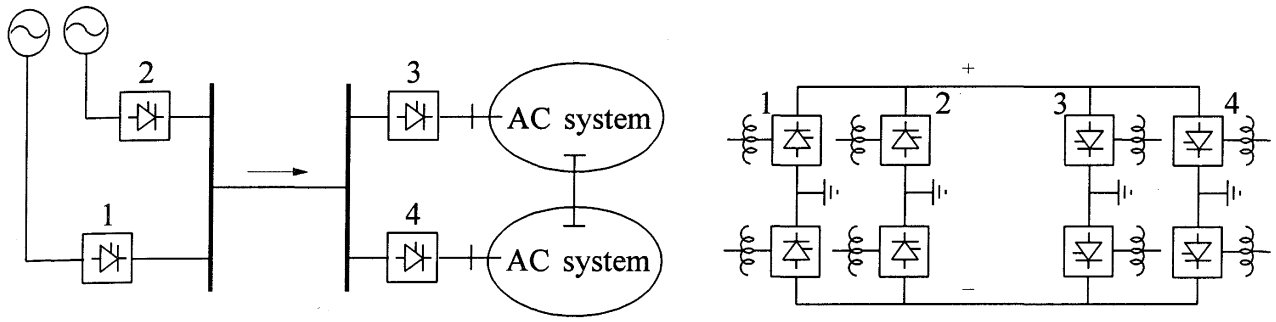

(a) System diagram (b) Converter stations' connection

Figure 10.47 Parallel MTDC bipolar scheme with radial dc network

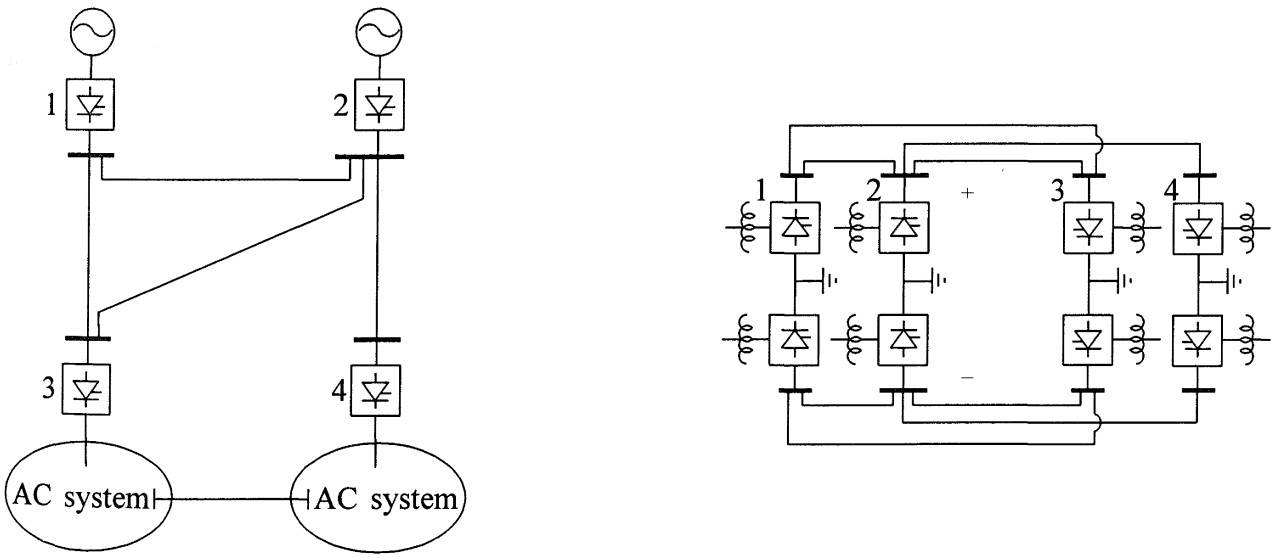

(a) System diagram (b) Converter stations' connection

Figure 10.48 Parallel MTDC bipolar scheme with mesh type connection

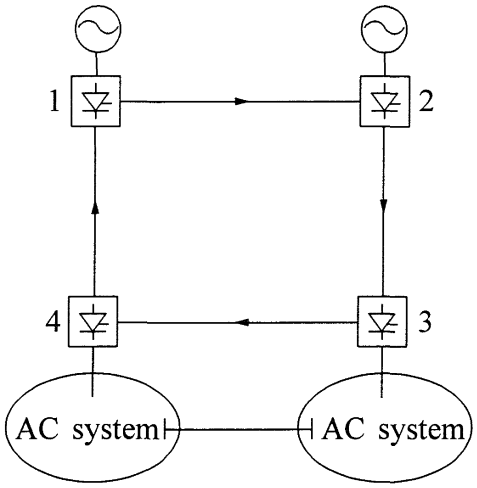

(a) System diagram

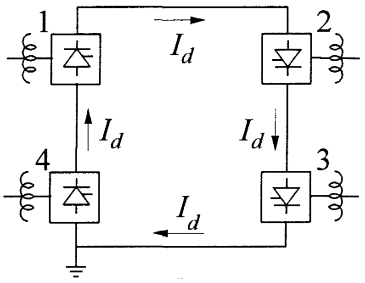

(b) Converter stations' connection

Figure 10.49 Series MTDC scheme

In the series scheme, the converters are connected in series with a common direct current flowing through all terminals. The dc line is grounded at one location. Figure 10.49 illustrates the series connection.

It is also conceivable to have a hybrid MTDC system involving both series and parallel-connected converter stations. The availability of dc circuit breakers [25] will add to the flexibility of MTDC systems and influence their selection.

The majority of studies and proposed applications of MTDC have considered parallel configuration with radial-type connection. The mesh connection, although offering more redundancy, requires greater length of dc lines.

Consideration of series connected schemes has been generally confined to applications with small power taps (less than 20%) where it may be more economical to operate at a higher current and lower voltage than for a full voltage tap at full voltage and reduced current. In a series tap, the voltage rating is proportional to the power capacity of the tap. However, the converter transformer must have full dc network voltage insulation. Flexibility of the power transfer could require a wide range for the transformer taps of the series stations.

In any specific MTDC system application, its special needs will determine the preferred network configuration. In general, the parallel scheme is widely accepted as the most practical scheme with fewest operational problems. Compared to the series-connected scheme, it results in fewer line losses, is easier to control, and offers more flexibility for future extension.

10.8.2 Control of MTDC Systems

The basic control principle for MTDC systems is a generalization of that for two-terminal systems. The control characteristic for each converter is composed of segments representing constant-current control and constant-firing angle control (CEA

for inverter and CIA for rectifier). In addition, an optional constant-voltage segment may be included.

The converter characteristics, together with the dc network conditions, establish the operating point of the system. For a common point to exist, converter control characteristics must intersect.

For MTDC systems, there is considerable room for providing flexibility of options to meet the requirements of individual systems. References 23 and 25 discuss different proposed control strategies.

The following is a general discussion of significant aspects related to control of parallel- and series-connected systems.

Parallel-connected systems

In a parallel-connected system, one of the terminals establishes the operating voltage of the dc system, and all other terminals operate on constant-current (CC) control. The voltage setting terminal is the one with the smallest ceiling voltage. This may be either a rectifier on CIA control or an inverter on CEA control.

The *V-I* characteristics for a four-terminal dc system are shown in Figure 10.50. The individual converter characteristics are shown in Figure 10.50(a), and the combined characteristics are shown in Figure 10.50(b). It is assumed that two of the terminals are operating as rectifiers and the other two terminals as inverters. The characteristics shown are for one pole. For the sake of simplicity, VDCOLs are not shown. It is assumed that each terminal has only two modes of control (CC, and CEA or CIA); the voltage control option is not considered.

In Figure 10.50, it is assumed that rectifier 1 is the voltage-setting terminal (CIA mode). Tap changers keep angles within the desired range. To maintain stable control operation, a positive-current margin must be maintained.

If an inverter is the voltage-controlling station, it is vulnerable to inadvertent overloading. It is unable to control the current at its terminals in the event of a system disturbance or load change. Disconnection of a current-controlled inverter will require reallocation of rectifier current settings to prevent overloading the voltage-controlled inverter.

On the other hand, if a rectifier defines the system voltage, the operation is more stable. All inverters control current, thereby avoiding operation in the less stable CEA control mode. The voltage-controlling rectifier is capable of protecting itself without causing overloading of other stations. The system is less dependent on high-speed communication and hence is more secure. In general, voltage control at a large rectifier terminal should provide better performance.

The following are the main drawbacks of parallel-connected MTDC systems:

- Any disturbance on the dc system (line fault or commutation failure) affects the entire dc system.

- Reversal of power at any terminal requires mechanical switch operation.

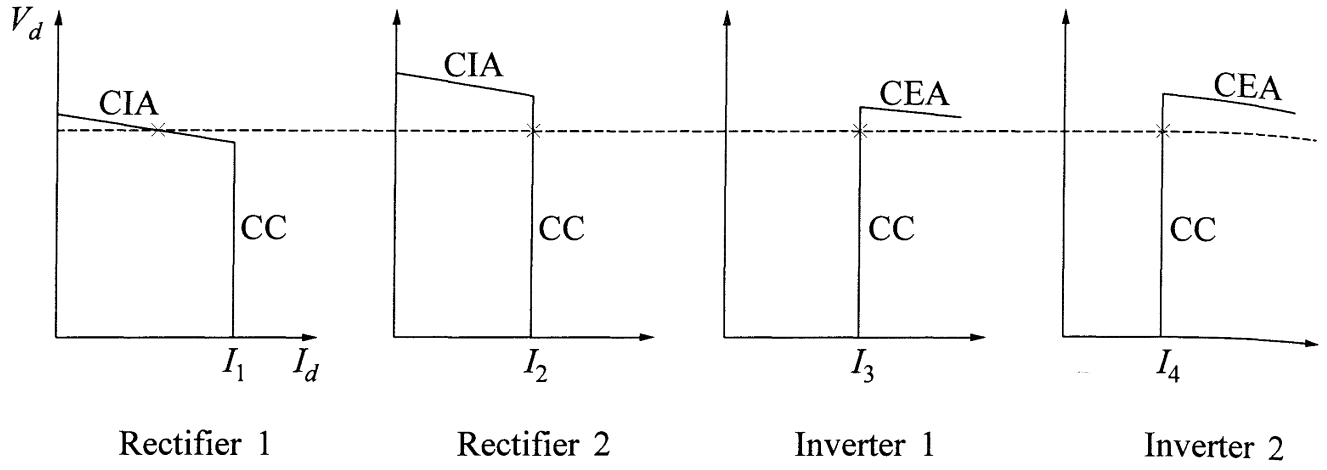

(a) Individual converter characteristics

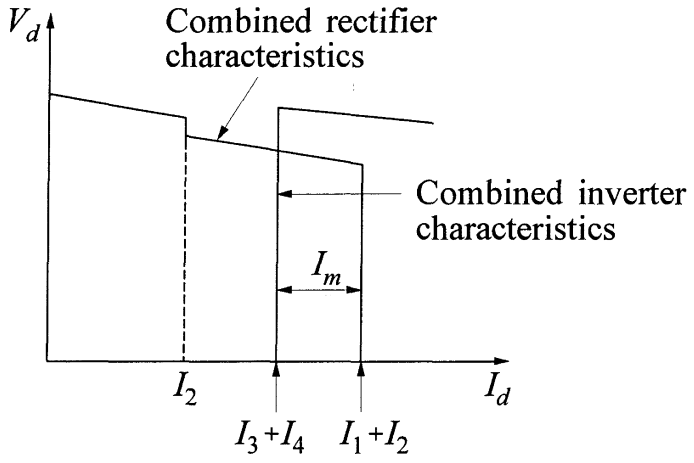

(b) Overall characteristics

Figure 10.50 Control characteristics of parallel-connected MTDC systems

- Blocking of a single bridge, in a converter station consisting of two or more series-connected bridges, requires either operation of the whole system at reduced voltage or disconnection of the affected station.

- Commutation failure at an inverter can draw current from other terminals and this may affect recovery.

Series-connected systems

In a series-connected system, current is controlled by one terminal, and all other terminals either operate at constant-angle (α or γ) control or regulate voltage. Figure 10.51 illustrates the control strategy usually considered for series systems.

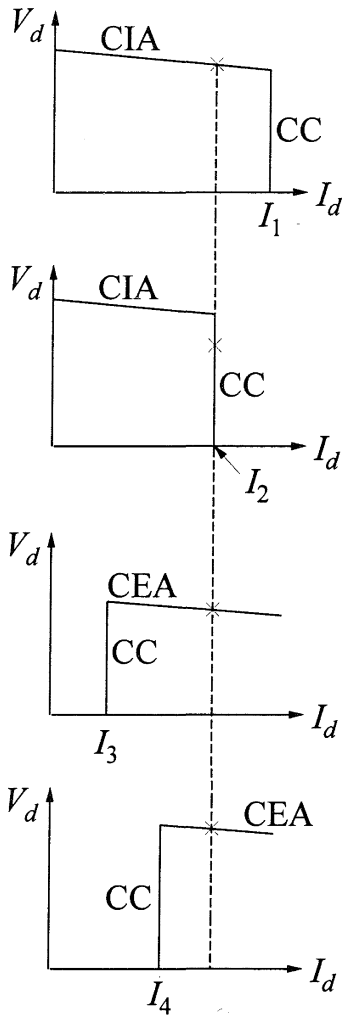

(a) Individual characteristics

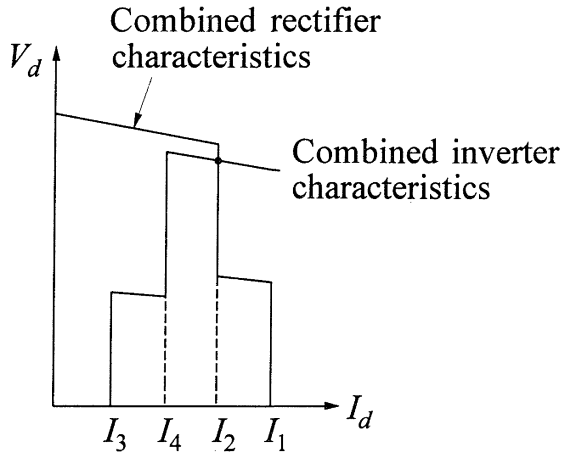

(b) Combined characteristics

Figure 10.51 Control characteristics of series systems

Current control is assumed by a rectifier if the sum of the rectifier voltages at the ordered current is greater than the sum of the inverter voltages; the rectifier with the lowest current order assumes the current control. On the other hand, if the sum of the inverter voltages is greater, the inverter with higher current order assumes current control.

For series systems, the voltage references must be balanced, whereas for parallel systems current references must be coordinated. However, for series systems the coordination problem is not as critical as it could be with parallel systems.

The series systems allow high-speed reversal of power at any terminal without the need for switching operations. Bridges and terminals can be taken out of service without affecting the rest of the system. Communication between terminals is required for controlling line loadings to minimize losses; this can be achieved with a relatively slow communication.

The operation of converters in series requires converter operation with high firing angles. This can be minimized by tap-changer control and backing off one bridge against another.

The following are the main drawbacks of the series-connected systems:

- As the voltage to ground is different in various parts of the system, insulation coordination is complex and expensive. Losses are higher in portions with lower voltage.
- A permanent line fault causes interruption of the entire system.
- Flexibility for future extension is limited.

10.9 MODELLING OF HVDC SYSTEMS

In this section, we will discuss the modelling of HVDC systems in power-flow and stability studies. The representation of the dc systems requires consideration of the following:

- Converter model
- DC transmission line/network model
- Interface between ac and dc systems
- DC system controls model

The representation of the converters is based on the following basic assumptions:

(a) The direct current I_d is ripple-free.

(b) The ac systems at the inverter and the rectifier consist of perfectly sinusoidal, constant frequency, balanced voltage sources behind balanced impedances. This assumes that all harmonic currents and voltages introduced by the commutation system do not propagate into the ac system because of filtering.

(c) The converter transformers do not saturate.

The validity of making the first two assumptions for power-flow and stability studies has been demonstrated in reference 27.

10.9.1 Representation for Power-Flow Solution

From the analysis presented in Section 10.2, the converter equations may be summarized as follows:

$$V_{do} = \frac{3\sqrt{2}}{\pi} BTE_{ac}$$

$$V_d = V_{do}\cos\alpha - \frac{3}{\pi} X_c I_d B$$

or

$$V_d = V_{do}\cos\gamma - \frac{3}{\pi} X_c I_d B$$

$$\phi \approx \cos^{-1}(V_d/V_{do}) \qquad (10.45)$$

$$P = V_d I_d = P_{ac}$$

$$Q = P\tan\phi$$

where

E_{ac} = RMS line-to-line voltage on HT bus
T = transformer turns ratio
B = no. of bridges in series
P = active power
Q = reactive power
$X_c = \omega L_c$ = commutating reactance per bridge/phase
V_d, I_d = direct voltage and current per pole

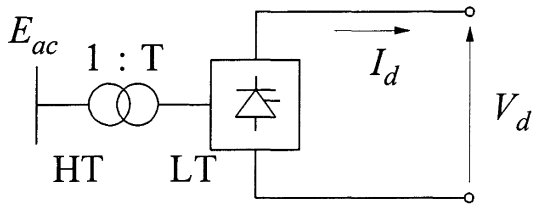

The equation used above for determining the power factor angle (ϕ) is approximate. It simplifies analysis significantly and gives results of acceptable accuracy, consistent with the level of accuracy associated with iterative solution techniques used for power-flow analysis. For specific applications requiring greater accuracy, exact relationships between ac and dc quantities derived in Section 10.2.2 may be used.

For the purpose of illustration, we will consider a two-terminal dc link. Using the subscripts r and i to denote rectifier and inverter quantities, respectively, the equation for a dc line having a resistance R_L is given by

$$V_{dr} = V_{di} + R_L I_d \qquad (10.46)$$

(a) AC/DC interface at the HT bus

Power-flow analysis requires joint solution of the dc and ac system equations. One approach is to solve the two sets of equations iteratively, as illustrated in Figure 10.52, with the converter transformer HT bus (ac side) providing the interface between the ac and dc equations.

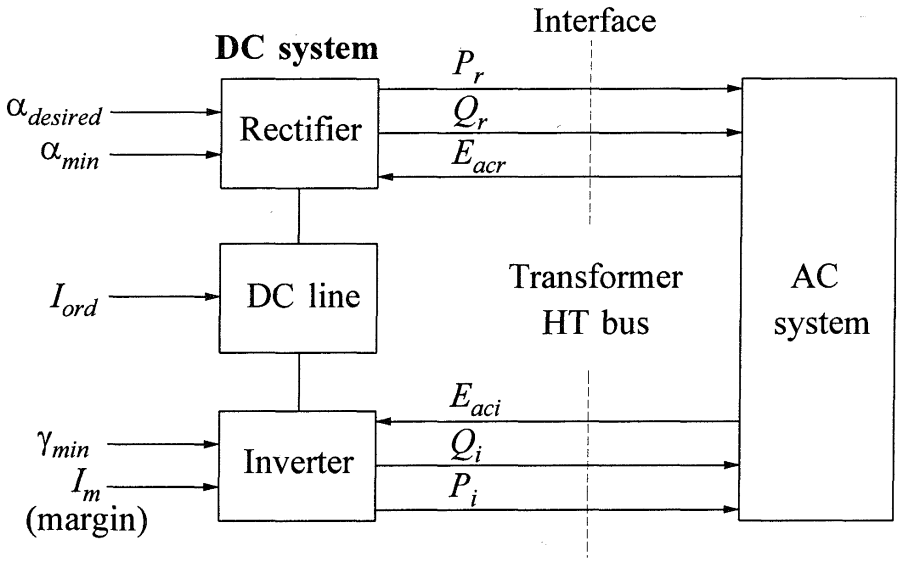

Figure 10.52

Here E_{acr} and E_{aci} are considered to be input quantities for the solution of dc system equations. They are known from the previous step in ac solution.

Variables P_r, Q_r, P_i and Q_i are considered to be the outputs from the solution of the dc system equations. They are used in the next iteration for solving the ac system equations.

The dependent and independent variables in the solution of dc equations depend on rectifier and inverter control modes. The three possible modes of operation are:

Mode 1: Rectifier on CC control; inverter on CEA control
Mode 2: Inverter on CC control; rectifier on CIA control
Mode 3: Rectifier on CIA control; inverter on modified characteristic

In mode 1, alternative inverter control functions are constant voltage control and constant-β control (see Section 10.4.1). For purposes of illustration we will consider here only the CEA control mode.

(1) Mode 1: rectifier on CC control and inverter on CEA control:

In mode 1, we have

- Inverter firing angle adjusted to give $\gamma=\gamma_{min}$.
- Rectifier firing angle adjusted to give $I_d=I_{ord}$.
- Rectifier transformer tap adjusted to give α within a desired range.
- Inverter transformer tap adjusted to give desired voltage.

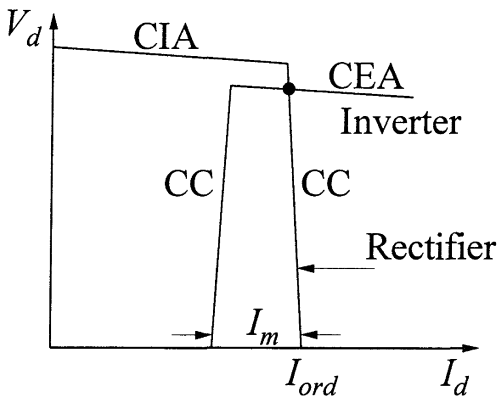

Figure 10.53

From Equation 10.45, with $I_d=I_{ord}$, we may write inverter equations as follows:

$$\begin{aligned} V_{doi} &= \frac{3\sqrt{2}}{\pi} B_i T_i E_{aci} \\ V_{di} &= V_{doi}(\cos\gamma_{min}) - \frac{3}{\pi} X_{ci} B_i I_{ord} \\ \phi_i &= \cos^{-1}(V_{di}/V_{doi}) \\ P_i &= V_{di} I_{ord} \\ Q_i &= P_i \tan\phi_i \end{aligned} \tag{10.47}$$

Since γ_{min} and I_{ord} are known and E_{aci} is given by the previous ac solution, V_{di}, P_i and Q_i can be computed. The transformer tap can be adjusted to give V_{di} within the desired range.

The rectifier equations are

$$\begin{aligned} V_{dr} &= V_{di} + R_L I_{ord} \\ V_{dor} &= \frac{3\sqrt{2}}{\pi} E_{acr} B_r T_r \\ \alpha &= \cos^{-1}\left(\frac{V_{dr}}{V_{dor}} + \frac{X_{cr} I_{ord}}{\sqrt{2} E_{acr} T_r}\right) \end{aligned} \tag{10.48}$$

In the above equations voltage E_{acr} is known from the previous ac solution. The turns ratio T_r is adjusted to give α within the desired range.

$$\begin{aligned} \phi_r &= \cos^{-1}(V_{dr}/V_{dor}) \\ P_r &= V_{dr} I_{ord} \\ Q_r &= P_r \tan\phi_r \end{aligned} \tag{10.49}$$

Here P_i, P_r, Q_i and Q_r are outputs to be used in the next iteration of the ac solution.

(2) Mode 2: inverter on CC control and rectifier on CIA control

In mode 2, we have

- Rectifier firing angle $\alpha=\alpha_{min}$.
- Inverter firing angle adjusted to give $I_d=I_{ord}-I_m$.
- Rectifier transformer tap adjusted to maximize dc voltage.
- Inverter transformer tap adjusted so that $\gamma>\gamma_{min}$ and var consumption is minimized.

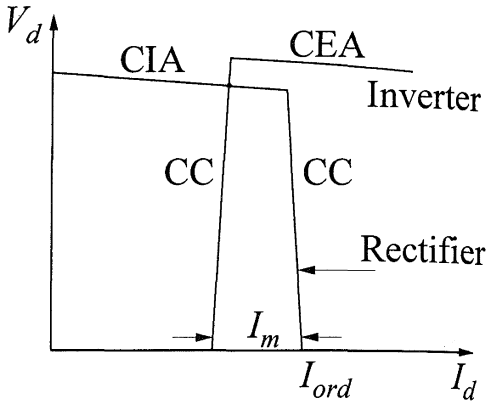

Figure 10.54

With $I_d = I_{ord}-I_m$, the rectifier equations are

$$\begin{aligned} V_{dor} &= \frac{3\sqrt{2}}{\pi} B_r T_r E_{acr} \\ V_{dr} &= V_{dor}\cos\alpha_{min} - \frac{3}{\pi} X_{cr}(I_{ord}-I_m) B_r \\ \phi_r &= \cos^{-1}(V_{dr}/V_{dor}) \\ P_r &= V_{dr}(I_{ord}-I_m) \\ Q_r &= P_r \tan\phi_r \end{aligned} \tag{10.50}$$

In the above equations, E_{acr} is known from the previous ac solution, and I_d is held at $I_{ord}-I_m$ by the inverter. Turns ratio T_r may be adjusted to maximize V_{dr}.

With E_{aci} known from the ac solution, the inverter equations may be solved as follows:

$$V_{doi} = \frac{3\sqrt{2}}{\pi} E_{aci} B_i T_i$$

$$V_{di} = V_{dr} - R_L I_d$$

$$= V_{dr} - R_L (I_{ord} - I_m)$$

$$\gamma = \cos^{-1}\left[\frac{V_{di}}{V_{doi}} + \frac{X_{ci}(I_{ord} - I_m)}{\sqrt{2} E_{aci} T_i}\right] \tag{10.51}$$

$$\phi_i = \cos^{-1}(V_{di}/V_{doi})$$

$$p_i = V_{di} I_d = V_{di}(I_{ord} - I_m)$$

$$Q_i = P_i \tan\phi_i$$

Turns ratio T_i may be adjusted to ensure $\gamma > \gamma_{min}$ and minimize var consumption. Variables P_r, P_i, Q_r and Q_i are outputs of the above calculations to be used for the next iteration of the ac solution.

(3) Mode 3: rectifier on CIA control and inverter on modified characteristic

For power-flow studies, it is usually sufficient to consider modes 1 and 2. However, for power-flow solutions (solution of network algebraic equations) associated with stability studies, it is necessary to consider the transition between modes 1 and 2. For reasons given in Section 10.4.1, the inverter characteristic is modified as shown in Figure 10.55. The segment JK, with a positive slope, provides a more stable control mode than the segment FK. One method of realizing this modified characteristic is to operate the inverter in the constant-β mode.

In mode 3, we have

- Rectifier ignition delay angle = α_{min}.
- Inverter ignition advance angle = β_c.
- $I_d = I'_d$ such that $I_{ord} > I'_d > (I_{ord} - I_m)$.

The dc system equations are solved as follows to compute the line current.

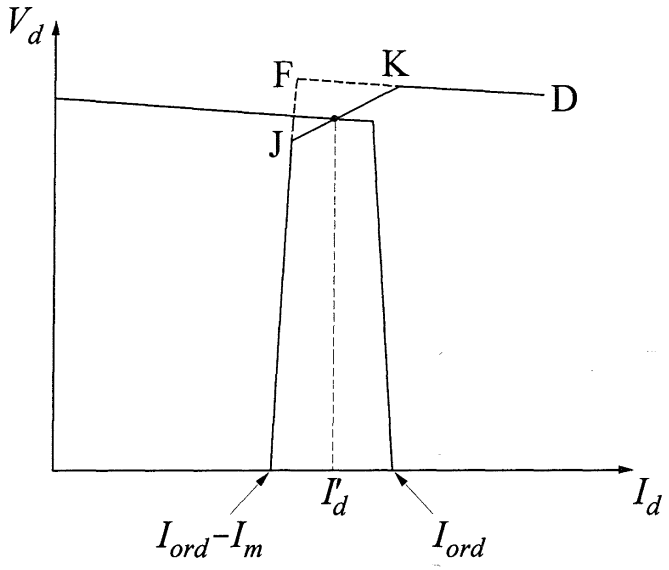

Figure 10.55

$$V_{dor} = \frac{3\sqrt{2}}{\pi} B_r T_r E_{acr}$$
$$V_{doi} = \frac{3\sqrt{2}}{\pi} B_i T_i E_{aci} \tag{10.52A}$$

Variables E_{acr} and E_{aci} are known from the previous ac solution.

$$V_{dr} = V_{dor}\cos\alpha_{min} - \frac{3}{\pi} I_d' X_{cr} B_r$$
$$V_{di} = V_{doi}\cos\beta_c + \frac{3}{\pi} I_d' X_{ci} B_i \tag{10.52B}$$

From line equation, we have

$$V_{dr} = V_{di} + R_L I_d'$$

Hence,

$$I_d' = \frac{V_{dr} - V_{di}}{R_L}$$
$$= \frac{1}{R_L}\left[V_{dor}\cos\alpha_{min} - V_{doi}\cos\beta_c - \frac{3}{\pi} I_d' (X_{cr} B_r + X_{ci} B_i)\right]$$

Rearranging, we have the following expression for I'_d in terms of V_{dor}, V_{doi}, α_{min} and β_c, whose values are known.

$$I'_d = \frac{V_{dor}\cos\alpha_{min} - V_{doi}\cos\beta_c}{R_L + \frac{3}{\pi}X_{cr}B_r + \frac{3}{\pi}X_{ci}B_i} \tag{10.53}$$

With the value of I'_d known, V_{dr} and V_{di} are calculated by using Equation 10.52B. The ac quantities can then be calculated as follows:

$$\begin{aligned} \phi_r &= \cos^{-1}(V_{dr}/V_{dor}) \\ \phi_i &= \cos^{-1}(V_{di}/V_{doi}) \\ P_r &= V_{dr}I'_d\,, \quad Q_r = P_r\tan\phi_r \\ P_i &= V_{di}I'_d\,, \quad Q_i = P_i\tan\phi_i \end{aligned} \tag{10.54}$$

For transient stability simulations, the tap-changer action is too slow and hence not considered.

For any given system condition, the rectifier and inverter modes of operation may not be known prior to the solution of system equations. Therefore, the following procedure may be used to establish operating modes and solve the ac and dc equations.

1. Solve for ac equations; output E_{acr}, E_{aci}.

2. (a) Solve mode 1 dc equations.
   If $\alpha>\alpha_{min}$, mode 1 condition is satisfied; go to step 3.

   (b) If $\alpha\leq\alpha_{min}$, solve for mode 2 dc equations.
   If $\gamma>\gamma_{min}$, mode 2 condition is satisfied; go to step 3.

   (c) If $\gamma\leq\gamma_{min}$, solve for mode 3 equations.

3. Calculate P_i, Q_i, P_r and Q_r. If mismatch is greater than tolerance, go back to step 1 and solve ac equations.

4. If mismatch is less than tolerance, solution is complete.

(b) AC/DC interface at the LT bus

In the representation discussed above, the ac/dc interface is at the HT side of the commutating transformer. An alternative representation is to have the ac/dc interface at the LT side (the valve side) of the commutating transformer.

An advantage of using the ac/dc interface at the LT bus is that it allows the commutation reactance to be different from the leakage reactance of the commutating transformer. Ideally, it should be the leakage reactance plus the equivalent system reactance at the HT bus. In most cases, the system reactance is small compared to the transformer reactance and, therefore, the LT bus representation may not be essential. In weak systems, this may not be true and the flexibility offered by the so-called LT representation is useful. The LT bus representation also offers flexibility in modelling SVCs, synchronous condensers, and filters connected to the tertiary winding of the converter transformers.

In the LT bus interface approach, the ac system representation includes converter transformers, and the ac solution includes computation of LT bus voltages. The LT voltages are used as input to the solution of dc equations. The HT bus voltage (or more precisely the commutating voltage) is computed from the LT voltage, and used in the solution of dc equations, which are essentially the same as those for the HT bus interface approach. The output of the solution of dc equations, for use in the next iteration of ac solution, is P and Q at the LT bus.

The following are the details of the calculations. Since an equivalent HT bus is used, there is no need for a transformer tap ratio in the dc equations.

Calculation of equivalent HT bus line voltage:

Let

E_{LT} = RMS line-to-line voltage at LT bus
E_{ac} = RMS line-to-line voltage behind X_c
X_c = equivalent commutating reactance per phase
ϕ_{LT} = angle between LT bus phase voltage and line current

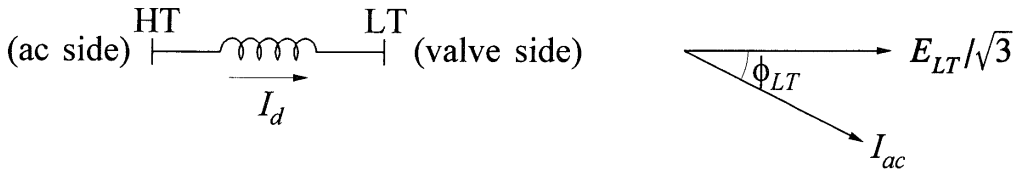

Using the LT bus line-to-neutral voltage ($E_{LT}/\sqrt{3}$) as reference phasor, we have

$$\frac{E_{ac}}{\sqrt{3}} = \frac{E_{LT}}{\sqrt{3}} + j\frac{X_c}{B} I_{ac}(\cos\phi_{LT} - j\sin\phi_{LT})$$

$$E_{ac} = E_{LT} + j\sqrt{3}\frac{X_c}{B}\frac{\sqrt{6} I_d B}{\pi}(\cos\phi_{LT} - j\sin\phi_{LT}) \tag{10.55}$$

$$= \left(E_{LT} + \frac{6X_c}{\sqrt{2}\pi} I_d \sin\phi_{LT}\right) + j\frac{6X_c}{\sqrt{2}\pi} I_d \cos\phi_{LT}$$

Calculation of reactive power at the LT bus:

As before, active power is

$$P = V_d I_d = P_{ac}$$

and the reactive power at the equivalent HT bus is

$$Q_{HT} = P\tan\phi_{HT}$$

where

$$\phi_{HT} = \cos^{-1}(V_d/V_{do})$$

To find the reactive power at the LT bus, Q_{HT} is reduced by the three-phase $X_c I^2$ loss. Since there are B bridges in parallel,

$$Q_{LT} = Q_{HT} - 3\frac{X_c}{B} I_{ac}^2$$

$$= Q_{HT} - 3\frac{X_c}{B}\left(\frac{\sqrt{6}}{\pi} I_d B\right)^2 \tag{10.56}$$

$$= Q_{HT} - BX_c\frac{18}{\pi^2} I_d^2$$

Reference 28 uses the above approach.

Inclusion of converter station losses

The dc system equations used so far did not consider converter station losses. There are several losses associated with a converter station such as those of converter transformers, filters, valves and valve auxiliaries, and smoothing reactors. The transformer copper loss may be represented by a series resistance, while other ac side losses are neglected. Inclusion of this resistance in the commutation overlap equation, however, results in considerable complexity in the converter equations; this is not usually justified.

The losses associated with the valves and their auxiliaries may be combined with the smoothing reactor and explicitly represented as equivalent series resistance (R_{eq}) on the dc side. There is also a small valve forward voltage drop (V_{drop}) due to arc drop in mercury-arc valves or forward voltage drop in thyristors. Their effects may be included by modifying the converter equations as follows:

$$V_d = V_{do}\cos\alpha - R_c I_d - R_{eq} I_d - V_{drop} \tag{10.57}$$

where

R_c = equivalent commutating resistance = $(3/\pi)X_c$
R_{eq} = equivalent resistance representing the losses in the valves and auxiliaries
V_{drop} = voltage drop across the valve

The above equation is applicable to a rectifier as well as an inverter. However, for inverter calculations we prefer to write the equations in terms of γ:

$$V_d = V_{do}\cos\gamma - R_c I_d + R_{eq} I_d + V_{drop} \tag{10.58}$$

Figure 10.56 shows the corresponding equivalent circuits. These modifications to the original equations present little complexity and are easy to incorporate.

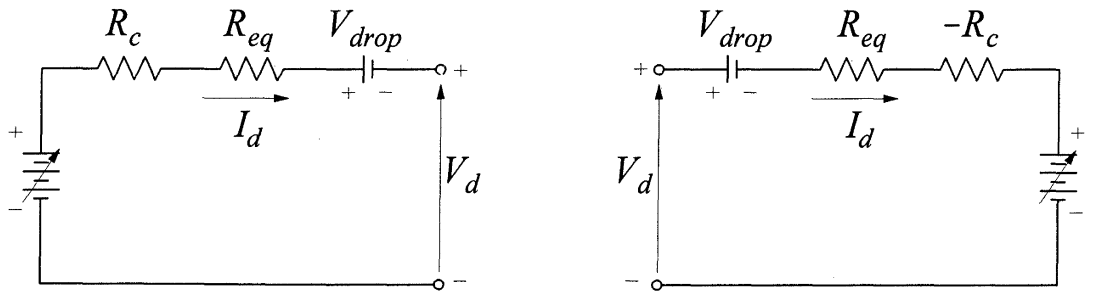

(a) Rectifier (b) Inverter

Figure 10.56 Converter equivalent circuits

The effect of neglecting losses is to introduce a small error in the computed value of active power and a relatively significant error in the value of reactive power [27]. These effects could be important for the case of back-to-back links.

Multiterminal DC systems

The formulation of power-flow equations developed above applies to two-terminal dc systems. The method can be readily extended to multiterminal systems.

Two approaches have evolved for the solution of power-flow equations. One is the sequential solution approach [29] in which the ac and dc equations are solved separately at each iteration. The other is the unified solution approach [30] in which the ac and dc systems are combined and solved as one set of equations during each iteration.

Example 10.2

Figure E10.2 shows a bipolar dc link with a rating of 1,000 MW, ±250 kV. The line resistance is 10 Ω/line. Each converter has a 12-pulse bridge with $R_c=(3/\pi)X_c=12$ Ω (6 Ω for each of the 6-pulse bridges).

The performance of the bipolar link is to be analyzed by considering it to be a monopolar link of +500 kV. The rectifier ignition delay angle limit (α_{min}) is equal to 5°. The effects of converter station losses and forward voltage drop across the valves may be neglected.

The dc link is initially operating with the rectifier on CC control with $\alpha_0=18°10'$, and the inverter on CEA control with $\gamma_0=18°10'$. The current margin I_m is set at 15%, and the transformer turns ratio at each converter is 0.5. At the inverter, the dc power is 1,000 MW, and the dc voltage is 500 kV (for the equivalent monopolar link).

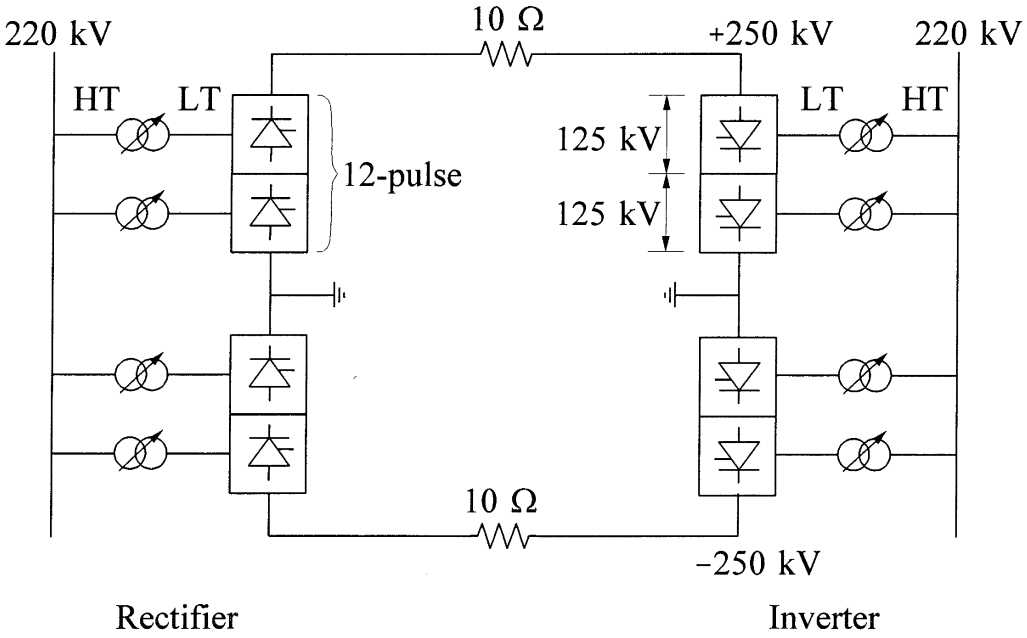

Figure E10.2

(a) For the above operating condition, compute the following:

(i) Power factor and the reactive power at the inverter HT bus.

(ii) Inverter commutation overlap angle μ.

(iii) RMS values of the line-to-line alternating voltage, fundamental component of the line current and the reactive power at rectifier HT bus.

(b) If the rectifier side HT bus ac voltage drops by 20%, compute the following:

(i) DC voltages at the rectifier and inverter terminals.

(ii) Rectifier angle α, and inverter angles γ and μ.

(iii) Active and reactive power at the inverter and rectifier HT buses.

Assume that the transformer taps have not changed and that the inverter side ac voltage is maintained constant.

(c) If the inverter side HT bus ac voltage drops by 15% and the rectifier side ac voltage remains at its initial value, determine the following after the tap changer action:

(i) The dc voltage at the rectifier and inverter terminals.

(ii) Rectifier angle α and the inverter angle γ.

(iii) Active and reactive power at the rectifier and inverter terminals.

The rectifier transformer control action attempts to hold α between 15° and 20°, and the inverter transformer control action attempts to hold the inverter dc voltage within the range of 500 to 510 kV. Assume that the maximum and minimum tap positions are 1.2 pu and 0.8 pu (corresponding to turns ratios of 0.6 and 0.4) respectively, with a tap step size of 0.01 pu.

Solution

Figure E10.3 shows the equivalent circuit of the bipolar link represented as a monopolar link of +500 kV.

(a) The initial operating condition is as follows:

$\alpha_0 = \gamma_0 = 18.167°$ $\quad P_i = 1{,}000$ MW

$T_r = T_i = 0.5$ $\quad V_{di} = 500$ kV

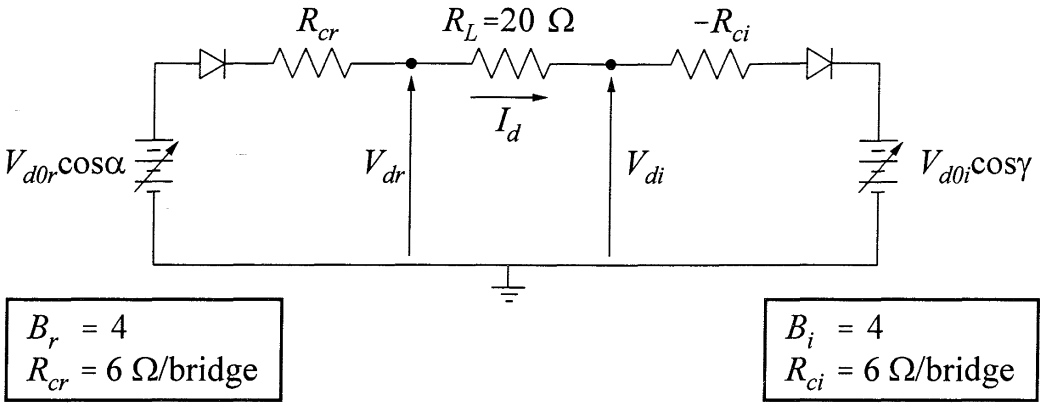

Figure E10.3 Equivalent circuit

The direct current is

$$I_d = \frac{P_i}{V_d} = \frac{1000}{500} = 2 \quad \text{kA}$$

The inverter ideal no-load voltage is

$$V_{d0i} = \frac{V_{di} + B_i R_{ci} I_d}{\cos\gamma_0}$$

$$= \frac{500 + 4 \times 6 \times 2}{\cos 18.167^\circ}$$

$$= 576.75 \quad \text{kA}$$

(i) The power factor at the inverter HT bus is

$$\cos\phi_i \approx \frac{V_{di}}{V_{doi}} = \frac{500}{576.75} = 0.8669$$

and

$$\phi_i = 29.896^\circ$$

The reactive power at the inverter HT bus is

$$Q_i = P_i \tan\phi_i = 1000 \tan 29.896^\circ = 574.94 \quad \text{MVAr}$$

(ii) Since $V_{di} = V_{d0i}(\cos\gamma + \cos\beta)/2$,

$$\cos\beta = 2\frac{V_{di}}{V_{d0i}} - \cos\gamma_0$$

$$= 2\times\frac{500}{576.75} - \cos 18.167^\circ$$

$$= 0.7837$$

and

$$\beta = 38.399^\circ$$

Hence, the inverter commutation angle is

$$\mu_i = \beta - \gamma_0 = 38.399^\circ - 18.167^\circ = 20.232^\circ$$

(iii) At the rectifier, we have

$$V_{dr} = V_{di} + R_L I_d = 500 + 2\times 20 = 540 \quad \text{kV}$$

and

$$V_{d0r} = \frac{V_{dr} + B_r R_{cr} I_d}{\cos\alpha_0}$$

$$= \frac{540 + 4\times 6\times 2}{\cos 18.167^\circ}$$

$$= 618.85 \quad \text{kV}$$

The RMS line-to-line ac voltage at the HT bus is

$$E_{acr} = \frac{V_{dor}}{1.3505 B_r T_r}$$

$$= \frac{618.85}{1.3505\times 4\times 0.5}$$

$$= 229.12 \quad \text{kV}$$

The sum of the RMS fundamental line currents in the four transformers is

$$I_{L1r} \approx \frac{\sqrt{6}}{\pi} B_r T_r I_d$$

$$= 0.7797\times 4\times 0.5\times 2$$

$$= 3.119 \quad \text{kA}$$

The dc power at the rectifier is

$$P_r = V_{dr} I_d = 540 \times 2 = 1080 \quad \text{MW}$$

The power factor at the rectifier HT bus is

$$\cos\phi_r \approx \frac{V_{dr}}{V_{d0r}} = \frac{540}{618.85} = 0.8726$$

and

$$\phi_r = 29.24°$$

The reactive power at the rectifier HT bus is

$$Q_r = P_r \tan\phi_r = 1080 \tan 29.24° = 604.57 \quad \text{MVAr}$$

(b) With the transformer taps unchanged, V_{d0} is directly proportional to E_{ac}. Therefore, when the rectifier HT bus voltage drops by 20%, we have

$$V_{d0r} = 0.8 \times 618.85 = 495.08 \quad \text{kV}$$

We will first assume that the dc link continues to operate in mode 1: rectifier on CC control with $I_d = I_{ord} = 2$ kA, and the inverter on CEA control with $V_{di} = 500$ kV. The corresponding direct voltage at the rectifier is

$$V_{dr} = V_{di} + R_L I_d = 500 + 20 \times 2 = 540 \quad \text{kV}$$

Therefore,

$$\cos\alpha = \frac{V_{dr} + B_r R_{cr} I_d}{V_{dor}}$$

$$= \frac{540 + 4 \times 6 \times 2}{495.08} > 1.0$$

Therefore, mode 1 condition is not satisfied. The controls switch to mode 2: rectifier on CIA control with $\alpha = \alpha_{min} = 5°$, and the inverter on CC control with

$$I_d = I_{ord} - I_m = (1.0 - 0.15) \times 2 = 1.7 \quad \text{kA}$$

(i) The rectifier and inverter direct voltages now are

$$V_{dr} = V_{d0r} \cos\alpha - B_r R_{cr} I_d$$

$$= 495.08 \cos 5° - 4 \times 6 \times 1.7$$

$$= 452.39 \quad \text{kV}$$

$$V_{di} = V_{dr} - R_L I_d$$
$$= 452.39 - 20 \times 1.7$$
$$= 418.39 \text{ kV}$$

(ii) Since the inverter ac bus voltage has not changed, $V_{d0i} = 576.75$ kV. With $I_d = 1.7$ kA, we have

$$\cos\gamma = \frac{V_{di} + B_i R_{ci} I_d}{V_{d0i}}$$
$$= \frac{418.39 + 4 \times 6 \times 1.7}{576.75}$$
$$= 0.796$$

and

$$\gamma = 37.23°$$

Now,

$$V_{di} = V_{d0i} \frac{\cos\gamma + \cos\beta}{2}$$

Hence,

$$\cos\beta = \frac{2V_{di}}{V_{d0i}} - \cos\gamma$$
$$= \frac{2 \times 418.39}{576.75} - 0.796$$
$$= 0.655$$

and

$$\beta = 49.10°$$

The inverter commutation angle is

$$\mu_i = \beta - \gamma = 49.10° - 37.23° = 11.87°$$

(iii) The dc power at the inverter is

$$P_i = V_{di} I_d = 418.39 \times 1.7 = 711.26 \text{ MW}$$

The power factor at the inverter HT bus is

$$\cos\phi_i \approx \frac{V_{di}}{V_{d0i}} = \frac{418.39}{576.75} = 0.725$$

and

$$\phi_i = 43.49°$$

The reactive power at the inverter HT bus is

$$Q_i = P_i \tan\phi_i = 711.26\tan 43.49° = 674.85 \quad \text{MVAr}$$

The dc power at the rectifier is

$$P_r = V_{dr} I_d = 452.39 \times 1.7 = 769.06 \quad \text{MW}$$

The power factor at the rectifier HT bus is

$$\cos\phi_r \approx \frac{V_{dr}}{V_{d0r}} = \frac{452.39}{495.08} = 0.914$$

and

$$\phi_r = 23.97°$$

The reactive power at the rectifier HT bus is

$$Q_r = P_r \tan\phi_r = 769.06\tan 23.97° = 341.87 \quad \text{MVAr}$$

(c) When the inverter side ac voltage drops by 15% and the rectifier voltage remains at its normal value, mode 1 operation is possible. Hence, the rectifier is on CC control with

$$I_d = I_{ord} = 2 \quad \text{kA}$$

and the inverter is on CEA control with

$$\gamma = 18.167°$$

Due to the reduction in ac voltage, the inverter dc voltage drops. The rectifier α increases and the dc voltage decreases so that I_d is maintained constant. The rectifier transformer tap changer acts to hold α between 15° and 20°, and the inverter transformer tap changer acts to hold V_{di} between 500 kV and 510 kV.

The ideal no-load voltage of a converter is directly proportional to the ac voltage and the transformer turns ratio. In (a), we computed the rectifier and inverter ideal no-load voltages under normal ac voltages and 1.0 pu tap position (turns ratio of 0.5) to be

$$V_{d0r} = 618.85 \quad \text{kV}$$

and

$$V_{d0i} = 576.75 \quad \text{kV}$$

With normal ac voltage and tap changer action, for the rectifier, we have

$$V_{d0r} = 618.85 T_r'$$

where T_r' is the pu tap position.

Similarly, for the inverter with ac voltage reduced by 15%, we have

$$V_{d0i} = 576.75(0.85) T_i' = 490.24 T_i'$$

Hence, the inverter dc voltage is

$$\begin{aligned} V_{di} &= V_{d0i}\cos\gamma - B_i R_{ci} I_d \\ &= 490.24 T_i' \cos 18.167° - 4\times 6\times 2 \\ &= 465.72 T_i' - 48 \quad \text{kV} \end{aligned} \tag{E10.1}$$

The rectifier direct voltage required to maintain I_d at 2 kA is

$$V_{dr} = V_{di} + R_L I_d = V_{di} + 20\times 2 = V_{di} + 40 \quad \text{kV} \tag{E10.2}$$

This should be equal to

$$\begin{aligned} V_{dr} &= V_{d0r}\cos\alpha - B_r R_{cr} I_d \\ &= 618.85 T_r' \cos\alpha - 48 \end{aligned} \tag{E10.3}$$

From Equations E10.2 and E10.3 we have

$$\cos\alpha = \frac{V_{di} + 88}{618.85 T_r'} \tag{E10.4}$$

Table E10.1 shows the variations in V_{di} and α as T_i' and T_r' change from their initial values to satisfy the control requirements.

Table E10.1

T_i'	T_r'	V_{di} (kV)	α (degrees)
1.0	1.0	417.7	35.2
1.01	0.99	422.4	33.6
⋮	⋮	⋮	⋮
1.07	0.93	450.3	20.7
1.08	0.93	455.0	19.4
⋮	⋮	⋮	⋮
1.10	0.93	464.3	16.3
1.11	0.93	468.9	14.6
1.12	0.94	473.6	15.1
1.13	0.95	478.3	15.6
⋮	⋮	⋮	⋮
1.17	0.98	496.9	15.3
1.18	0.99	501.5	15.8

Notes: V_{di} computed using Equation E10.1
α computed using Equation E10.4

From the table we see that the inverter tap position increases until T_i' =1.18 pu (corresponding to a turns ratio of 0.59) which results in a V_{di} of 501.55 kV.

The rectifier pu tap position T_r' which meets the control requirements is 0.99 (turns ratio of 0.495); the corresponding α is 15.8° and the direct voltage from Equation E10.3 is

$$V_{dr} = 618.85 \times 0.99 \times \cos 15.8° - 48 = 541.51 \quad \text{kV}$$

At the rectifier we have

$$P_r = V_{dr} I_d = 541.51 \times 2 = 1083.02 \quad \text{MW}$$

$$\cos\phi_r \approx \frac{V_{dr}}{V_{d0r}} = \frac{541.51}{618.85 \times 0.99} = 0.884$$

$$Q_r = P_r \tan\phi_r = 1083.02 \tan\phi_r = 573.2 \quad \text{MVAr}$$

At the inverter we have

$$P_i = V_{di} I_d = 501.55 \times 2 = 1003.1 \quad \text{MW}$$

$$\cos\phi_i \approx \frac{V_{di}}{V_{d0i}} = \frac{501.55}{490.24 \times 1.18} = 0.867$$

$$Q_i = P_i \tan\phi_i = 1003.1 \tan\phi_i = 576.7 \quad \text{MVAr}$$

■

10.9.2 Per Unit System for DC Quantities

A convenient per unit system for the dc quantities has the following base values:

$$\begin{aligned} V_{dc\,base} &= B\frac{3\sqrt{2}}{\pi} V_{ac\,base} = V_{do} \\ I_{dc\,base} &= I_{dc\,rated} \\ Z_{dc\,base} &= V_{dc\,base}/I_{dc\,base} \\ P_{dc\,base} &= V_{dc\,base} I_{dc\,base} \end{aligned} \tag{10.59}$$

where

B = number of bridges in series in the dc converter
$V_{ac\,base}$ = line-to-line ac base voltage referred to the LT side of the commutating transformer

If the commutating reactance per bridge expressed in ohms is X, then the per unit total commutating reactance for the B bridges in series is

$$\bar{X}_{dc} = \frac{BX}{Z_{dc\,base}} \tag{10.60}$$

Relationship between per unit quantities in the dc and ac systems

The base power and base impedance for the ac system are

$$P_{ac\,base} = \text{MVA}_{base} = \sqrt{3} V_{ac\,base} I_{ac\,base}$$
$$Z_{ac\,base} = V_{ac\,base}/(\sqrt{3} I_{ac\,base})$$

In the ac solution, the commutating reactance is represented by the parallel combination of B individual transformer reactances. The per unit value of X_c in the ac per unit system is

$$\bar{X}_{ac} = \frac{X}{BZ_{ac\,base}}$$

Therefore, the ratio of the per unit values of X_c in the two systems is

$$\begin{aligned}\frac{\bar{X}_{dc}}{\bar{X}_{ac}} &= \frac{BX}{Z_{dc\,base}} \times \frac{BZ_{ac\,base}}{X} \\ &= B^2\left(\frac{Z_{ac\,base}}{Z_{dc\,base}}\right) = B^2\left(\frac{V_{ac\,base}}{V_{dc\,base}}\right)^2 \frac{P_{dc\,base}}{P_{ac\,base}} \\ &= \left(\frac{3\sqrt{2}}{\pi}\right)^2 \frac{P_{dc\,base}}{P_{ac\,base}} \\ &= \frac{18}{\pi^2}\frac{P_{dc\,base}}{P_{ac\,base}}\end{aligned} \tag{10.61}$$

$$\begin{aligned}\frac{\bar{I}_{dc}}{\bar{I}_{ac}} &= \frac{I_{dc}}{I_{dc\,base}}\frac{I_{ac\,base}}{I_{ac}} = \frac{I_{dc}}{B\frac{\sqrt{6}}{\pi}I_{dc}}\frac{I_{ac\,base}}{I_{dc\,base}} \\ &= \frac{\pi}{B\sqrt{6}}\frac{P_{ac\,base}}{P_{dc\,base}}\frac{V_{dc\,base}}{\sqrt{3}V_{ac\,base}} = \frac{P_{ac\,base}}{P_{dc\,base}}\frac{\pi}{\sqrt{6}}\frac{B3\sqrt{2}}{B\pi\sqrt{3}} \\ &= \frac{P_{ac\,base}}{P_{dc\,base}}\end{aligned} \tag{10.62}$$

Usually, $P_{dc\,base}$ is chosen to be equal to $P_{ac\,base}$. Alternatively, $P_{dc\,base}$ may be chosen to be the nominal rating of the dc line. It is obvious that the use of the per unit system for the dc quantities offers no particular advantage. The dc quantities may in fact be handled in terms of their natural units, and many computer programs do so.

10.9.3 Representation for Stability Studies

In a stability program, the ac network equations are represented in terms of positive-sequence quantities. This imposes a fundamental limitation on the modelling of the dc systems. In particular, commutation failures cannot be accurately predicted. Commutation failure may result from a severe three-phase fault near the inverter, unbalanced faults on the inverter side ac system, or saturation of converter transformers during dynamic overvoltage conditions.

Notwithstanding the above limitation, models of various degrees of detail have been effectively used to represent dc systems in stability studies [28,31-37]. A general functional block diagram model of dc systems is shown in Figure 10.57.

Some of the early efforts to incorporate HVDC system models into stability programs used detailed representation which accounted for the dynamics of the line and the converter controls [28,31,32]. In recent years, the trend has been toward simpler models [33]. Such models are adequate for general purpose stability studies of systems in which the dc link is connected to strong parts of the ac system. However, for weak ac system applications requiring complex dc system controls and for multiterminal dc systems, detailed models are required. Therefore, the trend is reversing and the preference is to have flexible modelling capability with a wide range of detail [8,34,35,36]. The required degree of detail depends on the purpose of the study and the particular dc system.

Each dc system tends to have unique characteristics tailored to meet the specific needs of its application. Therefore, standard models of fixed structures have not been developed for representation of dc systems in stability studies. Instead, three categories of models have evolved: (a) simple model, (b) response or performance model, and (c) detailed model with flexible modelling capability.

(a) Simple models

For remote dc links, which do not have a significant impact on the results of the stability analysis, very simple models are usually adequate. The dc links may be represented as constant active and reactive power injections at the ac terminals of the converters. Where more realistic models are required, the dc link is represented by the static converter equations and functional effects of the controls. The models appear as algebraic equations and the interface between ac and dc systems is treated in a manner similar to that described for power-flow analysis in Section 10.9.1.

(b) Response models

For general purpose stability studies the dynamics of the dc line and pole controls may be neglected. The pole control action is assumed to be instantaneous and the lines are represented by their resistances.

Many of the control functions are represented in terms of their net effects, rather than actual characteristics of the hardware. The following are the features included in a typical response type model.

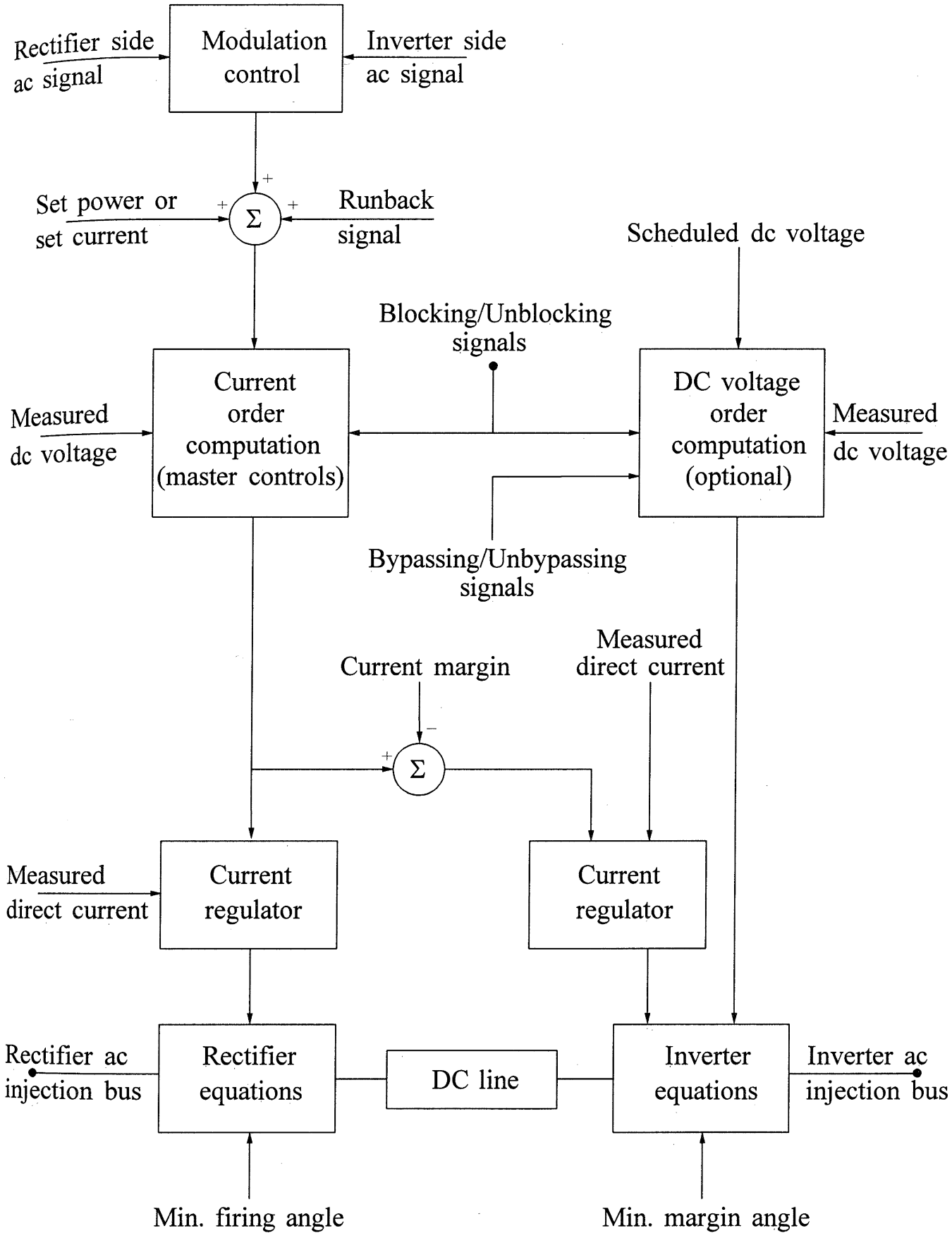

Figure 10.57 Functional block diagram of an HVDC system model

Converter and line equations:

The three modes of control, as identified before, are

- Rectifier on CC and inverter on CEA control
- Rectifier on CIA and inverter on CC control
- Rectifier on CIA and inverter on constant-β control (transition mode)

The control logic associated with the three modes of control may be incorporated into the stability solution as described in Section 10.9.1. In this case, however, transformer taps are not adjusted as they are not fast enough to be effective during the period of interest.

Current-control order with limits:

The current order is determined so as to provide either current control or power control as desired. Constraints are imposed on the current-order level to keep the current within maximum and minimum limits. The maximum current is determined by the voltage-dependent current-order limit (VDCOL) as shown in Figure 10.58. The VDCOL may be given a time delay to assist in riding through ac system faults (see Section 10.7).

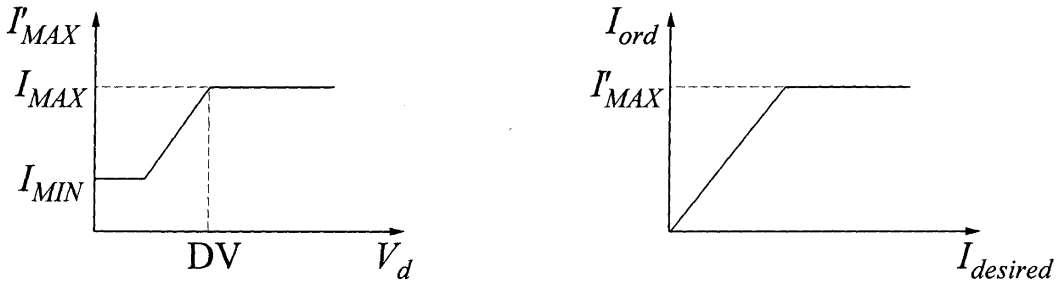

Figure 10.58 Voltage-dependent current-order limits

Control actions during ac faults:

It is necessary to have adequate representation of the actions of controls during ac faults. The following is an example of the logic that may be used to account for the control actions.

If the ac voltage on either side falls below a certain value for longer than a specified time, the direct-current order is set to zero. A ramp limit restricts the rate of decrease of direct current. The line is shut off when the current falls below a specified minimum value.

The direct line current is restored after the ac voltage recovers to an acceptable level. If the voltage recovers before the direct line current has reached its minimum value, the desired current is immediately restored to its original value. The line current increases at a specified maximum rate. If the voltage recovery occurs after the line has been shut down, the recovery is delayed by a specified time. After this, the direct line current is restored to its original value at a specified maximum rate.

The following are examples of two alternative types of recovery procedures:

(i) The current is increased by controlling rectifier α, with the inverter firing angle fixed at 90°. When the current reaches the desired value minus the current margin, the inverter extinction angle is ramped down to a specified value (normally original value) at a specified rate.

(ii) The current is increased with the maximum possible dc voltage (with $\gamma=\gamma_0$ or with $\alpha=\alpha_{min}$).

Option (i) ensures that during recovery the maximum reactive power is drawn from the ac system and may be used to control the overvoltages. Option (ii) ensures that maximum possible power is transmitted through the dc link.

The mode of operation and dc blocking and deblocking sequences are system dependent. The optimum sequence is established by experimentation.

A typical dc controller representation is shown in Figure 10.59. The dc shutoff recovery sequence for ac system faults is illustrated in Figure 10.60.

Commutation failure checks:

The dc model usually includes a logic for shutting off the dc line for commutation failure, detected by monitoring commutation voltage or converter margin angle.

Power/Current order modulation:

Dynamics of controls used for ac system stabilization are represented accurately, consistent with the representation used for other forms of stability controls (for example, power system stabilizers).

(c) Detailed flexible model

A wide range of dc system-modelling detail is required in stability studies. Either separate models each representing a dc link in detail or a single detailed model with facilities for simplification should be provided to achieve this flexibility. Because of the variety of controls associated with dc links, "user-defined" control models are likely to be required in addition to the basic ac/dc interface model.

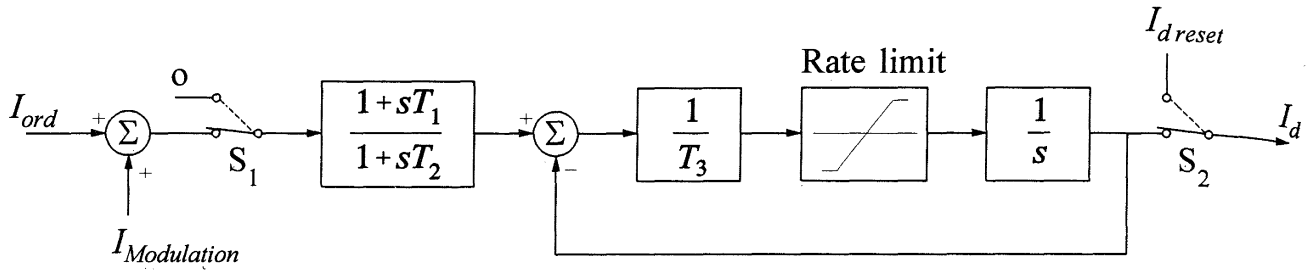

Note: 1. S_1 is switched to o if $E_{acr}<E_{min\,r}$ or $E_{aci}<E_{min\,i}$ for a period $\Delta T>T_{D1}$
2. S_2 is switched to $I_{d\,reset}$ if line shuts off and E_{acr} and E_{aci} are greater than $E_{recovery}$ and $\Delta T>T_{D2}$
3. T_3 is the response time of current control loop

Figure 10.59 Current-control block diagram

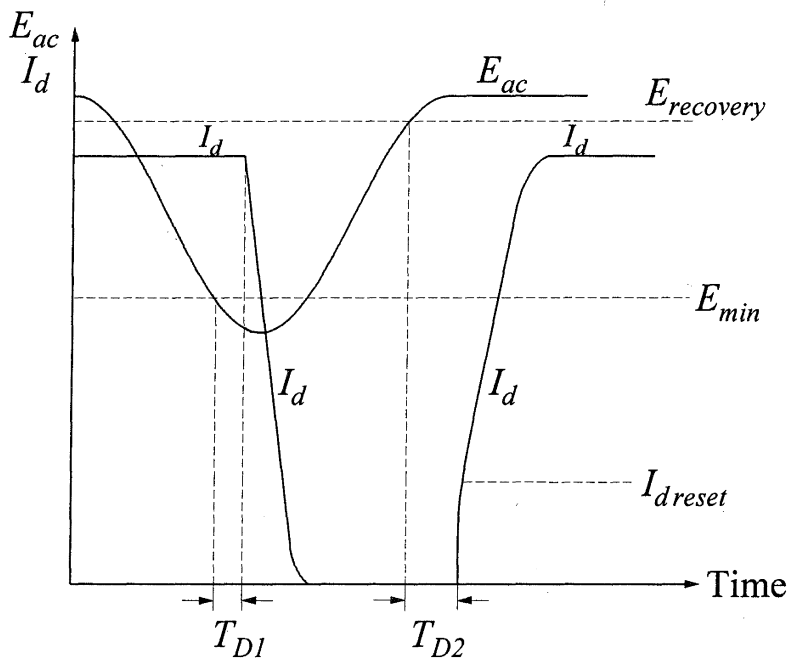

Figure 10.60 Shutoff and recovery sequence

At the highest level of detail, the following modelling features should be provided:

- DC line — a dynamic model which represents the resistance, inductive and capacitive effects of the dc line. The capacitive effects may be particularly important for cables.

- Converter controls represented by appropriate dynamic models for

- Master controls
- VDCOL including dynamics
- Current/power modulation
- Fast power change logic, including blocking/deblocking
- Pole controls capable of representing different control options such as CC, CEA, constant ac voltage, constant dc voltage, etc.
- Commutation failure simulation logic
- Special controls used to assist HVDC system recovery from disturbances, prevent commutation failure, etc.

- AC/DC interface — correct representation of the commutating voltage, commutating reactance, and transformer tertiary bus to which SVCs and synchronous condensers and other devices are connected.

In such models, the converter angle limits are embedded in the dc controls so that no special mode shift algorithm is required. However, the converter characteristics are still represented by equations relating average values of dc quantities and RMS values of ac fundamental components. This model may be referred to as "quasi steady-state model." It would accurately represent the HVDC system performance in stability studies for analysis of balanced operation, consistent with the representation used for other elements of the power system.

Since the waveforms of the voltages and currents are not represented in the model, only some general predictions regarding commutation failure can be made. These can be based on the magnitude of commutating voltage or inverter margin (extinction) angle.

A flexible quasi steady-state model should have facilities for simplifications so that models with a level of detail that is appropriate for the purpose and scope of the stability study may be used.

Detailed HVDC system models include dynamics which are usually much faster than those associated with the ac system models. In stability studies involving time-domain simulations, very small integration time steps are required to solve the dc equations. Hence, care should be exercised in integrating the ac and dc system equations. One approach often used in such situations is to solve dc equations by using time steps which are submultiples of time steps used for ac equations.

Detailed three-phase representation:

The detailed model described above, based on positive-sequence phasor representation of ac system quantities, is not accurate for analysis of unbalanced faults and for prediction of commutation failure. Accurate simulation of such conditions requires a detailed three-phase, cycle-by-cycle representation including dynamics of the ac line, filters and converter controls, during the disturbance and initial recovery. Thus, the two types of simulation, one using detailed three-phase representation of a small part of the system near the dc link and the other a single-phase quasi steady-

state representation of the complete power system, are used in a complementary manner. The first type of simulation can be performed by using an electromagnetic transients program (EMTP) [38] or a dc simulator. It is conceivable that in the future this type of simulation could be incorporated into a transient stability program [6,39].

An example of detailed model

A converter control model used by some early stability programs [28, 31] with detailed representation of dc links is shown in Figure 10.61. It represents controls used for the Pacific DC Intertie and other similar systems.

In these systems, *individual phase control* is used to generate the converter firing pulses (see Section 10.4.3). This is reflected in the model. The heart of the control system is the "delay angle computer," which is represented by block 7 of Figure 10.61. It is based on Equations 10.39 and 10.40. As discussed in Section 10.4.3, the control system consists of three units: the first provides an output proportional to direct current I_d, the second provides an output proportional to $E_m\cos\gamma_c$, and the third provides an alternating voltage proportional to $E_m\cos\omega t$ [12].

The control system uses the ac voltage to establish zero firing point reference. It then adds a direct voltage proportional to the error current to establish the proper firing point. The delay angle computer adds a bias signal $E_0\cos\gamma_{min}$ to the ac voltage. The input E_0, the commutating voltage, in reality consists of three sinusoidal voltages, one for each pair of elements connected to an ac terminal. The output $\cos\alpha$ actually is a signal suitable for producing a firing pulse at the proper time, i.e., delayed by an angle α. The following is the basis for the "delay angle computer" block shown in Figure 10.61.

From Equation 10.39, the instant of firing $\alpha=\omega t_1$ is given by

$$\sqrt{3}E_m\cos\omega t_1 = 2I_dX_c - \sqrt{3}E_m\cos\gamma$$

Hence,

$$\begin{aligned}\cos\alpha &= \cos\omega t_1 \\ &= \frac{2X_cI_d}{\sqrt{3}E_m} - \cos\gamma \\ &= \frac{2R_cI_d}{\sqrt{3}E_m}\frac{\pi}{3} - \cos\gamma \\ &= \frac{V_c}{E_0} - \cos\gamma\end{aligned} \tag{10.63}$$

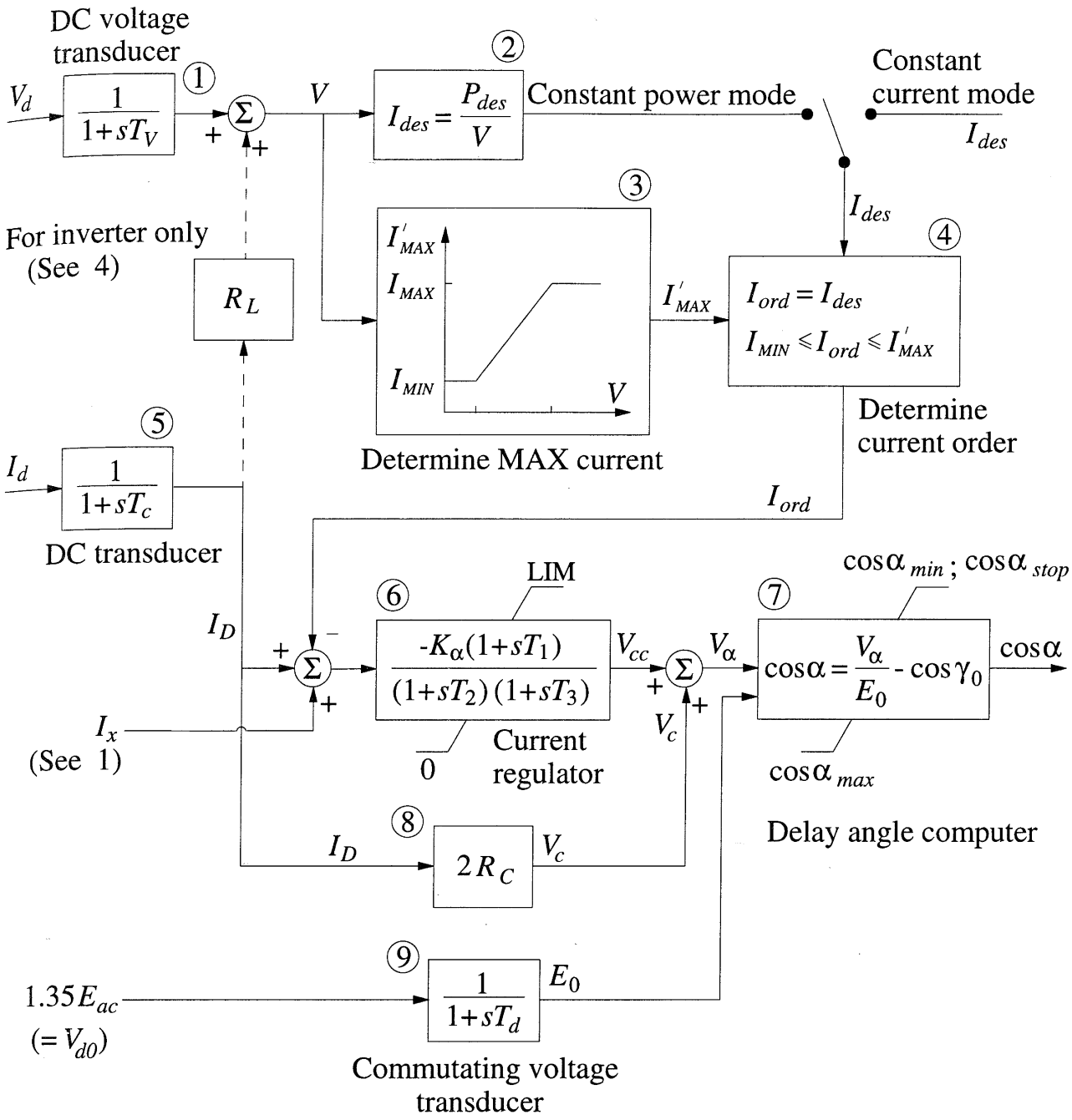

Notes:

1. $I_x = I_{ref} - I_{mod}$ for rectifier; $I_x = I_{margin}$ for inverter,

   where I_{mod} is modulating signal if used, and I_{ref} is computed to give required $\cos\alpha$ under steady state.

2. Limit on current regulator output: LIM = $E_0(\cos\gamma_0 + \cos\alpha_{min}) - V_c$

3. γ_0 = initial inverter extinction angle.

4. P_{des} is specified at rectifier end. Therefore, to determine I_{ord} for inverter, the voltage drop due to line resistance has to be taken into consideration.

Figure 10.61 A detailed HVDC converter model

where

$V_c = 2R_cI_d$

E_0 = output of commutating voltage transducer

$$= V_{d0} = \frac{3\sqrt{3}E_m}{\pi} = \frac{3\sqrt{2}E_{ac}}{\pi} = 1.35E_{ac}$$

To include current control, an additional signal V_{cc} is added so that

$$\begin{aligned} \cos\alpha &= \frac{V_c}{E_0} + \frac{V_{cc}}{E_0} - \cos\gamma \\ &= \frac{V_\alpha}{E_0} - \cos\gamma \end{aligned} \tag{10.64}$$

The upper part of Figure 10.61 shows how the current order is determined. Either constant power mode or constant current mode may be specified. The current order is limited by the maximum and minimum current limits. The maximum limit is voltage dependent (VDCOL).

There are three possible modes of operation:

- Constant ignition angle, with $\alpha = \alpha_{min}$;
- Constant current; and
- Constant extinction angle, with $\gamma = \gamma_0$.

(a) CIA mode:

The mode of operation exists when V_{cc} = LIM. The corresponding V_α is

$$\begin{aligned} V_\alpha &= V_{cc} + V_c = \text{LIM} + V_c \\ &= [E_0(\cos\gamma_0 + \cos\alpha_{min}) - V_c] + V_c \end{aligned}$$

Hence,

$$\cos\alpha = \frac{V_\alpha}{E_0} - \cos\gamma_0 = \frac{E_0}{E_0}(\cos\gamma_0 + \cos\alpha_{min}) - \cos\gamma_0$$

$$= \cos\alpha_{min}$$

(b) CC mode:

This is the normal mode for the rectifier. In this mode V_{cc} lies between 0 and LIM. Initially I_{ref} is computed so as to give the required cosα to satisfy steady-state conditions.

(c) CEA mode:

This is the normal mode for the inverter. For this mode, V_{cc} is equal to its lower limit of zero. From Figure 10.61 and Equation 10.64, with V_{cc}=0 and $\gamma=\gamma_0$, we have

$$\cos\alpha = \frac{V_\alpha}{E_0} - \cos\gamma_0 = \frac{2R_c I_d}{E_0} - \cos\gamma_0$$

Therefore, the control will ensure that cosα corresponds to a condition with $\gamma=\gamma_0$.

Limits on the output block:

The limits ensure that the firing angle is limited to the desired values. Usually, α_{min}=5° and α_{stop}=110°.

We see that the above model reflects the dynamic performance of the converter control hardware closely. In contrast, a response model uses logic to represent many of the functions.

Chapter 17 (Section 17.2.3) gives an additional example of a dc link model with a detailed representation of pole and master controls.

Guidelines for selection of modelling detail

The modelling requirements of dc systems are influenced by the following factors:

- Nature and scope of the study,
- Type of disturbance considered, and
- Strength of the associated ac systems.

The following provide general guidelines for selection of modelling detail.

1. For studies involving disturbances remote from dc links, simple algebraic models may be used unless very low frequency interarea oscillations are excited by the fault. In such a case, response models which include the dc link

modulation controls should be used.

2. For studies associated with preliminary planning of a dc link, response models are usually adequate.

3. For studies involving dc links connected to weak ac systems, response models may be used for initial planning studies provided that they represent the relevant control action adequately. Detailed models are necessary if special dc link controls are to be studied.

4. For studies associated with planning and design specifications of equipment close to dc links, detailed models are required.

5. For studies involving multiterminal HVDC systems, detailed models are required to ensure that the coordination of the converter controls is correct. Convergence difficulties are often experienced with the use of response models for such systems. In initial studies, simple pole controls may be used to minimize the modelling requirement. Special controls necessary for multiterminal systems such as current balances must be modelled.

6. For determination of the effects of dc modulation controls, a response model is usually adequate.

7. For studies involving worst-case disturbances specified by planning/operating criteria, the modelling requirements depend on the disturbance as follows:

   (a) Bipolar outage with no restart (say, due to high-level control malfunction) or with unsuccessful restart on both poles — A simple model could be used, since the dc power would be either zero or relatively low.

   (b) Rectifier side single-line-ground ac fault with breaker and pole outage (the remaining pole would be ramped to cover the loss, subject to overload limits) — A response model is normally adequate. The zero sequence impedance of the Y-Δ converter transformer should be included in the fault shunt.

   (c) Three-phase ac faults at critical locations near the rectifier, in which case either some dc power can be transmitted during the fault, or the dc shuts down and must be restarted rapidly — The restart or recovery characteristic is important. For example, a very fast recovery could be counterproductive if the ac system is weak. Generally, a detailed model is required. In early planning stages, however, a response model including restart may be used.

(d) Inverter side single-phase ac faults which block dc power during the fault because of commutation failure — A detailed model is required since recovery time and characteristic can be critical (and multiple dc links may be affected).

(e) Various ac disturbances where dc special stability controls (modulation or fast power changes) are used — A response model is normally needed. More detailed representation of controls would be required in the case of weak ac systems. Normal power modulation can be counter-productive, and it may be necessary to model controls which decrease dc power during voltage dips (desynchronizing effect).

8. For studies involving unbalanced ac disturbances and unbalances caused by the dc system, depending on the purpose of the study, an EMTP/transient stability combination model may be desirable.

REFERENCES

[1] "Compendium of HVDC Schemes throughout the World," International Conference on Large High Voltage Electric Systems, CIGRE WG 04 of SC 14, 1987.

[2] E.W. Kimbark, *Direct Current Transmission*, Wiley-Interscience, 1971.

[3] E.Uhlmann, *Power Transmission by Direct Current*, Springer-Verlag, 1975.

[4] C. Adamson and N.G. Hingorani, *High Voltage Direct Current Power Transmission*, Garraway Limited, London, 1960.

[5] B.J. Cory (editor), *High Voltage Direct Current Converters and Systems*, Macdonald, London, 1965.

[6] J. Arrillaga, *High Voltage Direct Current Transmission*, IEE Power Engineering Series 6, Peter Peregrinus Ltd., 1983.

[7] EPRI Report EL-3004, "Methodology for Integration of HVDC Links in Large AC Systems - Phase 1: Reference Manual," Prepared by Ebasco Services Inc., March 1983.

[8] EPRI Report EL-4365, "Methodology for the Integration of HVDC Links in Large AC Systems - Phase 2: Advanced Concepts," Prepared by Institut de Recherche d'Hydro-Quebec, April 1987.

[9] ANSI/IEEE Standard 1030-1987, *IEEE Guide for Specification of High-Voltage Direct Current Systems - Part I Steady-State Performance.*

[10] A. Ekstrom and G. Liss, "A Refined HVDC Control System," *IEEE Trans.*, Vol. PAS-89, pp. 723-732, May/June 1970.

[11] N.G. Hingorani and P. Chadwick, "A New Constant Extinction Angle Control for AC/DC/AC Static Converters," *IEEE Trans.*, Vol. PAS-87, pp. 866-872, March 1968.

[12] P.G. Engstrom, "Operation and Control of HVDC Transmission," *IEEE Trans.*, Vol. PAS-83, pp. 71-77, January 1964.

[13] J.D. Ainsworth, "The Phase-Locked Oscillator: A New Control System for Controlled Static Convertors," *IEEE Trans.*, Vol. PAS-87, pp. 857-865, March 1968.

[14] E. Rumpf and S. Ranade, "Comparison of Suitable Control Systems for HVDC Stations Connected to Weak AC Systems, Parts I and II," *IEEE Trans.*, Vol. PAS-91, pp. 549-564, March/April 1972.

[15] "High Voltage Direct Current Controls Guide," prepared by the HVDC Controls Committee, Canadian Electrical Association, October 1984.

[16] C.W. Taylor, *Power System Voltage Stability*, McGraw-Hill, 1993.

[17] IEEE Committee Report, "DC Transmission Terminating at Low Short Circuit Ratio Locations," *IEEE Trans.*, Vol. PWRD-1, No. 3, pp. 308-318, July 1986.

[18] CIGRE and IEEE Joint Task Force Report, "Guide for Planning DC Links Terminating at AC Locations Having Low Short-Circuit Capacities, Part I: AC/DC Interaction Phenomena," CIGRE Publication 68, June 1992.

[19] IEEE Committee Report, "Dynamic Performance Characteristics of North American HVDC Systems for Transient and Dynamic Stability Evaluations," *IEEE Trans.*, Vol. PAS-100, pp. 3356-3364, July 1981.

[20] IEEE Committee Report, "HVDC Controls for System Dynamic Performance," *IEEE Trans.*, Vol. PWRS-6, No. 2, pp. 743-752, May 1991.

[21] R. Jötten, J.P. Bowles, G. Liss, C.J.B. Martin, and E. Rumpf, "Control in HVDC Systems, The State of the Art, Part I: Two Terminal Systems," CIGRE Paper 14-10, 1978.

[22] J. Hegi, M. Bahrman, G. Scott, and G. Liss, "Control of the Quebec-New England Multi-Terminal HVDC System," CIGRE Paper 14-04, Paris 1988.

[23] J. Reeve, "Multiterminal HVDC Power Systems," *IEEE Trans.*, Vol. PAS-99, pp. 729-737, March/April 1980.

[24] W.F. Long, J. Reeve, J.R. McNicol, R.E. Harrison, and J.P. Bowels, "Considerations for Implementing Multiterminal DC Systems," *IEEE Trans.*, Vol. PAS-104, pp. 2521-2530, September 1985.

[25] F. Nozari, C.E. Grund, and R.L. Hauth, "Current Order Coordination in Multiterminal DC Systems," *IEEE Trans.*, Vol. PAS-100, pp. 4629-4636, November 1981.

[26] J.J. Vithayathil, A.L. Courts, W.G. Peterson, N.G. Hingorani, S. Nilsson, and J.W. Porter, "HVDC Circuit Breaker Development and Field Tests," *IEEE Trans.*, Vol. PAS-104, pp. 2693-2705, October 1985.

[27] B.K. Johnson, F.P. DeMello, and J.M. Undrill, "Comparing Fundamental Frequency and Differential Equation Representation of AC/DC," *IEEE Trans.*, Vol. PAS-101, pp. 3379-3384, September 1982.

[28] G.D. Breuer, J.F. Luini, and C.C. Young, "Studies of Large AC/DC Systems on the Digital Computer," *IEEE Trans.*, Vol. PAS-85, pp. 1107-1115, November 1966.

[29] J. Reeve, G. Fahmy, and B. Stott, "Versatile Load Flow Method for Multiterminal HVDC Systems," *IEEE Trans.*, Vol. PAS-96, pp. 925-933, May/June 1977.

[30] M.M. El Marsafawy and R.M. Mathur, "A New, Fast Technique for Load Flow Solution of Integrated Multiterminal DC/AC Systems," *IEEE Trans.*, Vol. PAS-99, pp. 246-255, January/February 1980.

[31] J.F. Clifford and A.H. Schmidt, "Digital Representation of a DC Transmission System and Its Controls," *IEEE Trans.*, Vol. PAS-89, pp. 97-105, January 1970.

[32] N. Sato, N.V. Dravid, S.M. Chan, A.L. Burns, and J.J. Vithayathil, "Multiterminal HVDC System Representation in a Transient Stability Program," *IEEE Trans.*, Vol. PAS-99, pp. 1927-1936, September/October 1980.

[33] G.K. Carter, C.E. Grund, H.H. Happ, and R.V. Pohl, "The Dynamics of

AC/DC Systems with Controlled Multiterminal HVDC Transmission," *IEEE Trans.*, Vol. PAS-96, pp. 402-413, March/April 1977.

[34] R. Proulx, S. Lefebvre, A. Valette, D. Soulier, and A. Venne, "DC Control Modelling in a Transient Stability Program," *Proceedings of International Conference on DC Power Transmission*, Montreal, Canada, pp. 16-22, June 4-8, 1984.

[35] T. Adielson, "Modelling of an HVDC System for Digital Simulation of AC/DC Transmission Interactions," Paper 100-02, *CIGRE Symposium on AC/DC Interactions and Comparisons*, Boston, September 28-30, 1987.

[36] D.G. Chapman, J.B. Davies, F.L. Alvarado, R.H. Lasseter, S. Lefebvre, P. Krishnayya, J. Reeve, and N.J. Balu, "Programs for the Study of HVDC Systems," *IEEE Trans.*, Vol. PWRD-3, pp. 1182-1188, July 1988.

[37] S. Arabi, G.J. Rogers, D.Y. Wong, P. Kundur, and M.G. Lauby, "Small Signal Stability Program Analysis of SVC and HVDC in AC Power Systems," *IEEE Trans.*, Vol. PWRS-6, No. 3, pp. 1147-1153, August 1991.

[38] H.W. Dommel, "Digital Computer Solution of Electromagnetic Transients in Single- and Multi-Phase Networks," *IEEE Trans.*, Vol. PAS-88, pp. 388-399, April 1969.

[39] J. Reeve and R. Adapa, "Advances in AC Transient Stability Studies Including DC Modelling," Fourth International Conference on AC and DC Transmission, London, September 23-26, 1985.